

LONDON  
SCHOOL *of*  
HYGIENE  
& TROPICAL  
MEDICINE



***The development of a mathematical modelling  
framework to translate TB vaccine responses between  
species and predict the most immunogenic dose in  
humans using animal data***

Sophie Rhodes

Thesis submitted in accordance with the requirements for the degree of

Doctor of Philosophy

University of London

July 2017

Department of Infectious Disease Epidemiology  
Faculty of Epidemiology and Population Health  
London School of Hygiene & Tropical Medicine

Funded by a studentship from Aeras

## **Declaration**

**I, Sophie Rhodes, confirm that the work presented in this thesis is my own. Where information has been derived from other sources, I confirm that this has been indicated in the thesis.**



Sophie Rhodes

July 2017

## Abstract

### Background:

Preclinical animal experiments measuring vaccine immunogenicity and safety are essential, not only to establish if the vaccine should progress further, but to generate information on how the vaccine should be administered in humans. Animal models that represent human vaccine responses well are vital to translate information about vaccine dose to clinical phases. Vaccine dose is a key aspect in creating an effective vaccine. However, if the wrong dose is chosen, vaccine candidates may be mistakenly discarded and considerable resources wasted. Current methods of finding optimal vaccine dose are mostly empirically based, which may be leading to sub-optimal doses progressing into later clinical trials. A current example of this is in the tuberculosis (TB) vaccine developmental pipeline, where a series of adjuvanted subunit vaccines, the H-series, have progressed through to later stages of clinical development with a high dose that has been shown to *less* immunogenic than lower doses. In drug development, mathematical model-based methods are routinely used alongside empirical evaluations, to inform dose-finding. I hypothesised that vaccine development may benefit from the application of similar quantitative methods. As such, I launched the new field of vaccine immunostimulation/immunodynamic (IS/ID) mathematical modelling. My aims for this thesis were 1) to establish differences in Bacillus Calmette–Guérin (BCG) Interferon-Gamma (IFN- $\gamma$ ) response by human subpopulation, then develop a IS/ID model to represent these response dynamics and identify the most representative macaque subpopulation for human BCG responses. Aim 2) was to predict human H-series vaccine IFN- $\gamma$  response using IS/ID model calibrated to mouse multi-dose IFN- $\gamma$  data and allometric scaling.

**Methods:** For aim 1, longitudinal data on IFN- $\gamma$  emitting CD4+ T cells following vaccination BCG were available in humans and macaques. Human (sub)population covariates were: baseline BCG vaccination status, time since BCG vaccination, gender and monocyte/lymphocyte cell count ratio. The macaque (sub)population covariate was colony of origin. I developed a two-compartmental mathematical model describing the post-BCG IFN- $\gamma$  immune response dynamics. The model was calibrated to the human and macaque data using

Nonlinear Mixed Effects Modelling (NLMEM) to establish if there were differences in IFN- $\gamma$  dynamics for both species subpopulations. I then established which macaque subpopulation best described human data. For aim 2, longitudinal data on IFN- $\gamma$  emitting CD4+ T cells following two vaccinations with five doses of novel TB vaccine H56+IC31 in mice were generated. I then assessed the shape of the dose response curve at early and late time points. I calibrated the T cell model to the mouse data and established the change in key model parameters across dose. Using the change in model parameters across dose found in the mice, I predicted the immune response dynamics in humans for different doses and which dose was most immunogenic.

**Results:** In aim 1, I found that BCG status in humans (baseline BCG-naïve or baseline BCG-vaccinated) was associated with differences in the peak and end IFN- $\gamma$  response after vaccination with BCG. When the mathematical model was calibrated to the BCG data for both macaques and humans, significant differences ( $p < 0.05$ ) in key model parameters were found after stratification by macaque colony and human baseline-BCG status. Indonesian cynomolgus macaques had the closest immune response dynamics to the baseline BCG-naïve humans. In aim 2, a peaked curve was the best description of the mouse H56+IC31 dose response curve for early and late time points. Calibrating a revaccination model to the data and mapping changes in the estimated mouse model parameters across dose group to the estimated human model parameters, I found at day 224 (a latest time point), the model-predicted median number of human IFN- $\gamma$  secreting CD4+ T cells were the highest for the dose group in the range 1-10 $\mu$ g H56/H1+500 nmol IC31. This suggests a dose of 1-10 $\mu$ g may be the most immunogenic in humans.

**Discussion:** Finding the most predictive animal model and optimal vaccine dose is essential for efficiently accelerating the development of new, effective, TB vaccines. I demonstrated that mathematical modelling was a useful tool to quantify BCG immune response dynamics in macaques and humans. I established which macaque subpopulation should be used to represent a human BCG (or potentially new TB vaccine) induced IFN- $\gamma$  response in future clinical trials. Using IFN- $\gamma$  as marker of vaccine immunogenicity, mathematical modelling predictions using preclinical data suggested that doses in current novel TB vaccines clinical

trials on healthy BCG-vaccinated participants should be between 1-10 $\mu$ g H56/H1+500 nmol IC31, a result which has been recently corroborated in an empirical H56+IC31 dose-ranging trial. This project has demonstrated the potential utility of mathematical modelling in vaccine development. I believe future work on IS/ID modelling should include data on more complex immune response networks and different animal and human subpopulations. This future work is entirely feasible and would establish IS/ID modelling as a legitimate tool to accelerate vaccine development.

## Contents

Abstract .....	3
Acknowledgements .....	9
Abbreviations .....	11
List of Tables .....	13
List of Figures .....	16
Chapter 1. Background and Thesis Overview .....	21
Vaccine Development .....	21
<i>Animal models</i> .....	21
<i>Dose selection</i> .....	23
Tuberculosis .....	24
<i>The burden of tuberculosis disease</i> .....	24
<i>Natural history of Mtb. infection</i> .....	26
<i>TB immune response</i> .....	26
<i>Risk factors for Mtb. infection and progression to TB disease</i> .....	28
<i>Correlates of protection against TB disease</i> .....	30
<i>TB vaccines</i> .....	32
<i>H-series TB vaccine performance and dose escalation</i> .....	40
Potential issues with current vaccine dose-finding methods .....	42
Model-based drug development: Pharmacokinetic/Pharmacodynamic Modelling .....	43
<i>Model-based drug development (MBDD) methods</i> .....	47
Thesis Rationale: Model-based vaccine development – Vaccine Immunostimulation/Immunodynamic modelling .....	49
<i>Vaccine Immunostimulation/Immunodynamic modelling</i> .....	49
<i>TB immune response mathematical modelling: literature review</i> .....	50
<i>Summary of thesis data, IS/ID model and model calibration</i> .....	57
Thesis Aims and Objectives .....	58
Thesis overview .....	59
Author contributions .....	64
Funding .....	65
Chapter 2. Exploration into the immune response to BCG vaccination in a heterogeneous human population: Paper 1 .....	66
Chapter 2 introduction .....	66
Paper 1 title: Individual-level factors associated with variation in mycobacterial-specific immune response: Gender and previous BCG vaccination status .....	70

Supplementary Material for paper 1 .....	78
<i>Additional Results</i> .....	78
<b>Chapter 3. Exploration into the immune response to BCG vaccination in a heterogeneous human and macaque population using a vaccine Immunostimulation/Immunodynamic (IS/ID) mathematical model and the predictive power between macaque and human subpopulation data: paper 2 .....</b>	<b>81</b>
Chapter 3 introduction.....	81
Paper 2 title: Using Data from Macaques to Predict Gamma Interferon Responses after Mycobacterium bovis BCG Vaccination in Humans: A Proof-of-Concept Study of Immunostimulation/Immunodynamic Modeling Methods .....	85
Supplementary Material for paper 2 .....	98
<i>Additional Methods</i> .....	98
<i>Additional Results</i> .....	106
<i>Additional Discussion</i> .....	130
<b>Chapter 4. Generation of immune response data to multi-dose of H56+IC31 in mice for the application of vaccine Immunostimulation/Immunodynamic (IS/ID) modelling: paper 3 .....</b>	<b>133</b>
Chapter 4 introduction.....	133
Paper 3 title: The TB vaccine H56+IC31 dose-response curve is peaked not saturating: Data generation for new mathematical modelling methods to inform vaccine dose decisions .....	138
Supplementary material for paper 3 .....	147
<i>Additional Methods</i> .....	147
<i>Additional Results</i> .....	151
<b>Chapter 5. Predicting human multi-dose immune responses to H-series vaccination using multi-dose data in mice and vaccine Immunostimulation/Immunodynamic (IS/ID) modelling: paper 4</b>	<b>160</b>
Chapter 5 introduction.....	160
Paper 4 title: Animal dose response curve predicts lower optimal tuberculosis vaccine dose in humans: Using vaccine Immunostimulation/Immunodynamic modelling methods to inform vaccine dose decision-making .....	163
Supplementary material for paper 4 .....	185
<i>Additional Methods</i> .....	185
Additional Results .....	194
Additional Discussion .....	218
<b>Chapter 6. Discussion &amp; Conclusion .....</b>	<b>222</b>
Summary of findings .....	222
Strengths.....	223
Weaknesses & Challenges.....	230
Implications .....	235
Future work .....	237

<b>Conclusion .....</b>	<b>244</b>
<b>References .....</b>	<b>246</b>
<b>Appendices .....</b>	<b>265</b>
<b>Appendix A. Paper 5: Dose finding for new vaccines: the role for immunostimulation/immunodynamic modelling.....</b>	<b>265</b>
<b>Appendix B. Additional Background.....</b>	<b>287</b>
<b>Appendix C. Supplementary Material for paper 2 (chapter 3) .....</b>	<b>325</b>
<b>Appendix D. Supplementary Material for paper 3 (chapter 4).....</b>	<b>340</b>
<b>Appendix E. Additional Discussion .....</b>	<b>353</b>
<b>Appendix References .....</b>	<b>358</b>

## Acknowledgements

Firstly, I would like to thank my advisory committee Dr Tom Evans, Dr Steve Kern, Dr Jeremie Guedj, Dr Thomas Lindenstrøm and Prof Denise Kirschner. Their expertise and guidance throughout the PhD project has been invaluable in publishing the papers and completing this thesis.

Secondly, I would like to thank Dr Andrea Zelmer, Satria Arief Prabowo, Lisa Stockdale and members of the Dr Helen Fletcher's laboratory team at LSHTM for working tirelessly to complete the rather large mouse experiment for my third and fourth papers. I appreciate the time taken out of their own work to help me complete mine and without the mouse data, this PhD project would not have been possible. I would like to thank my colleagues who provided the human data (BCG and H-series), those involved with the MVA-85A trial and those at Aeras, and for their helpfulness in answering any (basic) immunology questions I had! Similarly, I would like to thank my colleagues at Public Health England, Dr Sally Sharpe, Charlotte Sarfas and Andrew White for providing the macaque data for my second paper.

Thirdly, the TB modelling group at LSHTM have been a reliable support group throughout the project and the regular group meetings always lifted my Tuesday afternoon (with the exceptions of the days when I had to present...). I feel honoured to be part of a smart, driven, happy and generally cool group of people. Specifically, I would like to mention the PPM group who I have always been a source of good company, good fun and good wine!

My family and partner Alex have supported me throughout the project, listening to various random facts about TB or vaccines or mice experiments with interest. More importantly they have been there when things have seemed tough.

Last, but in no way, least I would like to thank my supervisors, Prof Richard White, Dr Helen Fletcher and Dr Gwenan Knight. They have supported and encouraged me, given me guidance and direction and tolerated my terrible spelling. There has been a fair amount of head-

scratching during this project and they have always been there to work through potential hurdles. I very much look to working with them in the very near future.

## Abbreviations

WHO	World Health Organisation
MBDD	Model-based drug development
PK	Pharmacokinetics
PD	Pharmacodynamics
PK/PD	Pharmacokinetic/Pharmacodynamic
FDA	Food and Drug Administration
MSWG	Modelling and Simulation Working Group
ISOP	International Society of Pharmacovigilance
IS	Immunostimulation
ID	Immunodynamic
IS/ID	Immunostimulation/Immunodynamic
TB	tuberculosis
<i>Mtb.</i>	<i>Mycobacterium tuberculosis</i>
MHC	Major histocompatibility complex
IFN- $\gamma$	Interferon gamma
IL-2	Interleukin 2
IL-12	Interleukin 12
TNF- $\alpha$	Tumour Necrosis factor alpha
ML ratio	Monocyte/Lymphocyte ratio
NK	Natural killer
T cell	T lymphocyte
B cell	B lymphocyte
BCG	Bacillus Calmette–Guérin
NTM	Non-tuberculous mycobacteria
HIV	Human immunodeficiency virus
SSI	Statens Serum Institut
Ag85B	Antigen 85b
ESAT-6	6 kDa early secretory antigenic target

NHP	Nonhuman primate
AUC	Area Under the Curve
LTR	Long-term retrospective
STP	Short-term prospective
PPD	Purified protein derivative
ELISPOT	<i>ex vivo</i> IFN- $\gamma$ Enzyme-Linked ImmunoSpot
SFU	Spot forming unit
PBMC	Peripheral blood mononuclear cells
ANOVA	Analysis of variance
IQR	Interquartile range
PHE	Public Health England
NLMEM	Nonlinear mixed effects modelling
MLE	Maximum likelihood estimate
RSE	Relative standard error
RE	Residual error
-2LL	-2 log likelihood
BIC	Bayesian information criterion
AIC	Akiake information criteria
AICc	Corrected Akiake information criteria
LRT	Likelihood ratio test
VPC	Visual predictive check
TEM	Transitional effector memory
CM	Central memory
PDF	Probability density function
ODE	Ordinary differential equation
LTBI	Latent TB infection
SS	Sum of squares

## List of Tables

The tables in this thesis follow three numbering systems, those written into the thesis body (which are numbered following the chapter they feature in), and tables in the main papers and supplementary material (labelled with S preceding the number) referenced in the papers.

No.	Title	Page
<b>Chapter 2</b>		
Paper 1 Tables		
1	Demographic and trial information for participants included in Long-term retrospective (LTR) and Short-term prospective (STP) analyses.	73
2	Long-term Retrospective (LTR) analysis: Results of the linear regression analysis on baseline IFN- $\gamma$ responses (SFU/mill cells) against individual-level covariates.	73
3	Short-term prospective (STP) analysis: Results of the linear regression analysis on AUC	75
4	Short-term prospective (STP) analysis: Results of the linear regression analysis on 24 week IFN- $\gamma$ response	75
5	Short-term prospective (STP) analysis: Results of the linear regression analysis on peak IFN- $\gamma$ response	75
Paper 1 Supplementary Tables		
S1	Participant demographics	78
S2	ANOVA test results comparing M1 to M2 for LTR and STP outcome measures	80
<b>Chapter 3</b>		
Paper 2 Tables		
1	Population mean parameter estimates for analysis 1 and 2 for macaques and humans	90
Paper 2 Supplementary Tables		
S1	Human demographics	98
S2	Macaque demographics	99
S3	Scenario analysis for parameter $\mu_{TEM}$ in macaques and humans	103
S4	Results of comparing residual error models using Monolix in-built tool	103
S5	Tests for random effects correlations for macaques and humans	104
S6	Residual error model estimated parameters for a combined residual error model for macaques and humans	107

S7	p-value results of applying the non-parametric Kruskal-Wallis and post-hoc Dunn test (for more than two groups) with a Bonferroni correction on individual macaque estimated parameters from analysis 1 with colony as the predictor	109
S8	Forward stepwise addition method for selecting a subpopulation-model for colony in macaques	111
S9	Results of applying the Wilcoxon test on individual human estimated parameters from analysis 1 with gender as the predictor	112
S10	Results of applying linear regression on individual human estimated parameters from analysis 1 with ML ratio as the predictor	114
S11	p-value results of applying the non-parametric Kruskal-Wallis and post-hoc Dunn test (for more than two groups) with a Bonferroni correction on individual human estimated parameters from analysis 1 with BCG history as the predictor	116
S12	Results of applying the Wilcoxon test on individual human estimated parameters from analysis 1 with BCG status as the predictor	118
S13	Forward stepwise addition method for selecting a covariate model for BCG status in humans. -2LL values are taken from running in Monolix with BCG status applied to the parameter	120
S14	Main assumptions of the model and implications on challenging these assumptions	132
<b>Chapter 4</b>		
Paper 3 Tables		
1	Median (IQR) values for the summary measures day 56 response, peak between first and second vaccination and post-second vaccination IFN- $\gamma$ responses by dose	144
Paper 3 Supplementary Tables		
S1	Table outlining Burnham and Anderson's criteria for support for models using AICc difference	150
S2	Median values and p-values using the Wilcox test to compare the five IFN- $\gamma$ responses between consecutive time points for each dose	152
S3	Frequency of significantly (with a Bonferroni correction for multiple groups) different AUC comparisons over 200 samples of possible AUC values	153
S4	Summary of nonlinear regression analysis of the Gamma and Sigmoidal curve fitting for the responses pre-second vaccination	156
S5	Summary of nonlinear regression analysis of the Gamma and Sigmoidal curve fitting for the responses post-second vaccination	157
S6	Summary of nonlinear regression analysis of the Gamma and Sigmoidal curve fitting for the responses at day 56	158
S7	Testing initial parameter estimates	159
<b>Chapter 5</b>		
Paper 4 Tables		
1	Population parameter estimates for analysis 1 and 2 for mice and humans	179

Paper 4 Supplementary Tables

S1	Outline of the H56+IC31 and H1+IC31 phase i clinical trials and human demographics for each	188
S2	Results of calibrating the model to the pooled mouse data for the three forms of $\delta$	194
S3	Residual error model estimated parameters for a combined residual error model for mice	195
S4	Tests for random effects correlations for mice	195
S5	Results of indexing the dose group covariate on all combinations of estimated parameters in the mouse pooled model	201
S6	Residual error model estimated parameters for a combined residual error model for human	205
S7	Tests for random effects correlations for humans	206
S8	Results of indexing the vaccine type covariate on all combinations of estimated parameters in the human pooled model	214
S9	Population parameters for mice and humans from model calibration (analysis 1&2) and prediction (analysis 3). All estimated model parameter standard deviations were fixed at 0.5.	216
S10	Main assumptions of the model and implications on challenging these assumption	221

## List of Figures

The Figures in this thesis follow two numbering systems, those written into the thesis body (which are numbered following the chapter they feature in), and Figures in the main papers and supplementary material (labelled with S preceding the number) referenced in the papers.

No.	Title	Page
<b>Chapter 1</b>		
1.1	Estimated TB incidence rates by country, 2015	25
1.2	2015 developmental pipeline for new TB vaccines by Aeras, TB vaccine developers	35
1.3	Flowchart of the literature review process using the search terms	51
1.4	Aim 1 of the thesis with corresponding objectives thesis chapters, papers, data requirements and methods	60
1.5	Aim 2 of the thesis with corresponding objectives thesis chapters, papers, data requirements and methods	61
<b>Chapter 2</b>		
Paper 1 Figures		
1	Longitudinal BCG induced IFN- $\gamma$ responses for the Short-term prospective (STP) analysis for 55 participants	74
Paper 1 Supplementary Figures		
S1	Distribution of ML ratios of participants included in Short-term prospective (STP) analysis.	79
<b>Chapter 3</b>		
Paper 2 Figures		
1	Schematic of A) the mathematical model representing the immune response dynamics of two CD4+ T cell populations secreting IFN- $\gamma$ , B) depiction of how the recruitment rate of transitional effector memory cells ( $\delta$ ) changes over time and C) key model parameters. Equations can be found in the supplementary material.	89
2	Visual Predictive Check (VPC) plot showing number of IFN- $\gamma$ SFU/million PMBC, by time (days) for A) all macaques and B) all humans.	91
3	Data (black points) and model predicted (black lines) total number of T cells secreting IFN- $\gamma$ (sum of the number of Transitional effector memory cells and resting central memory cells), over time.	92

4	Data (black Points and red triangles) and model predicted (lines) mean immune responses for the four macaque colonies and human BCG: Y (left) and BCG: N (right) with the human empirical responses and mean empirical responses.	93
5	: Data (black points), predicted total number of T cells secreting IFN- $\gamma$ (black line), predicted number of transitional effector memory (TEM) cells (green line), and predicted number of resting central memory (CM) cells (orange line), over time.	94
<b>Paper 2 Supplementary Figures</b>		
S1	Longitudinal BCG induced IFN- $\gamma$ responses for the Short-term prospective (STP) analysis for 55 participants	100
S2	Number of IFN- $\gamma$ secreting CD4+ T cells per million PBMCs over time as measured by the ELISPOT assay in macaques	101
S3	Data (black points), predicted total number of T cells secreting IFN- $\gamma$ (black line), predicted number of transitional effector memory (TEM) cells (blue line), and predicted number of resting central memory (CM) cells (orange line), over time.	108
S4	Residual (difference between data and total cells as predicted by the model) plots for macaque predicted total responses ( <b>Appendix C</b> )	326
S5	Residual (difference between data and total cells as predicted by the model) plots for human predicted total responses ( <b>Appendix C</b> )	327
S6	Empirical data versus predicted total IFN- $\gamma$ responses for A. macaques and B. humans ( <b>Appendix C</b> )	328
S7	Prediction distribution plot for A. macaques and B. humans ( <b>Appendix C</b> )	329
S8	Boxplot of individual macaque estimated parameters from analysis 1 by macaque colony	110
S9	Boxplot of individual human estimated parameters from analysis 1 by gender, F=Female, M=Male	113
S10	Scatterplots of individual human estimated parameters from analysis 1 against ML ratio	115
S11	Boxplot of individual human estimated parameters from analysis 1 by BCG history	117
S12	Boxplot of individual human estimated parameters from analysis 1 by BCG status	119
S13	Visual predictive check plots for all colonies of macaque.	122
S14	Visual predictive check plots for BCG: N and BCG: Y humans	123
S15	Residual (difference between data and total cells as predicted by the model) plots for macaque predicted total responses stratified by colony ( <b>Appendix C</b> )	331
S16	Macaque observed versus predicted IFN- $\gamma$ total responses stratified by colony ( <b>Appendix C</b> )	332
S17	Residual (difference between data and total cells as predicted by the model) plots for human predicted total responses stratified by BCG status ( <b>Appendix C</b> )	333
S18	Human observed versus predicted IFN- $\gamma$ responses stratified by BCG status ( <b>Appendix C</b> )	334
S19	Prediction distribution plot for all colonies of macaque.	124
S20	Prediction distribution plot for humans by BCG status subpopulation.	125
S21	VPC plots for macaque estimated subpopulation-model parameters fit to the human BCG: Y data (top) and BCG: N data (bottom) for <u>Chinese cynomolgus macaques</u>	126
S22	VPC plot for macaque estimated subpopulation-model parameters fit to the human BCG: Y data (top) and BCG: N data (bottom) for <u>Mauritian cynomolgus macaques</u> .	127
S23	VPC plot for macaque estimated subpopulation-model parameters fit to the human BCG: Y data (top) and BCG: N data (bottom) for <u>Indonesian cynomolgus macaques</u> .	128
S24	VPC plot for macaque estimated subpopulation-model parameters fit to the human BCG: Y data (top) and BCG: N data (bottom) for <u>Indian rhesus macaques</u> .	129

<b>Chapter 4</b>		
Paper 3 Figures		
1	Median IFN- $\gamma$ responses (horizontal black bars) and responses of individual mice per time point (blue points) for each dose.	143
2	AUC calculated from number of IFN- $\gamma$ secreting CD4+ T cells after two vaccinations with H56 + IC31 from individual mice spleens, number of IFN- $\gamma$ secreting CD4+ T cells between first and second vaccination, after second vaccination and day 56 by dose ( $\mu\text{g}$ H56 + 100nmol IC31). Dose 0 equates to the control group.	144
3	Results of the dose-response curve fitting analysis for the time ranges A. between first and second vaccination (aggregated responses from days 2, 7, 9 and 14), B. post-second vaccination (days 21, 28 and 56) and C. Day 56 (last time point).	145
Paper 3 Supplementary Figures		
S1	Example representation of the possible combinations of AUC calculations.	148
S2	Number of IFN- $\gamma$ secreting CD4+ T cells after two vaccinations with H56+IC31 from individual mice spleens (pooled over time and dose) for the two ELISPOT assay incubation times (24 and 48 hour). There was no significant difference between the two incubation times.	151
S3	Plot showing the effect of changing parameter $p$ in the sigmoidal curve equation the dashed line corresponds to a $p=50$ , the dotted line, $p=100$ and the solid line, $p=200$ on the day 56 data.	155
<b>Chapter 5</b>		
Paper 4 Figures		
1	Modelling overview. A) Schematic of the mathematical model representing the immune response dynamics of two IFN- $\gamma$ secreting CD4+ T cell populations after primary and re-vaccination. Dashed arrows correspond to T cell dynamics as a result of only revaccination. B) Table of key model parameters. Model parameters are either fixed to a value from literature ( $\mu_{\text{TEM}}$ and $R_{\text{CM}}$ ), to an assumed value ( $\beta_{\text{CM}}$ ) or free to be estimated using NLMEM ( $\beta_{\text{TEM}}$ , $\tau$ , and the parameters that comprise $\delta$ ).	178
2	Empirical and model predicted number of IFN- $\gamma$ secreting CD4+ T cells over time for A. pooled <u>mouse</u> data, B. low dose group (0.1-1 $\mu\text{g}$ H56+IC31), C. middle dose group (5 $\mu\text{g}$ H56+IC31) and D. high dose group (15 $\mu\text{g}$ H56+IC31). Grey points correspond to number of IFN- $\gamma$ secreting CD4+ T cells measured over time by ELISPOT assay in <u>mouse</u> splenocytes for each mouse after receiving vaccination of H56+IC31 at day 0 and day 15. Median responses over time are marked by a blue triangle, the 75 <sup>th</sup> percentile responses by an orange triangle and the 25 <sup>th</sup> percentile responses by a purple triangle. The model prediction (total cells) calibrated to the data in the calibration framework (parameters in Table 1) is plotted against the median data (blue line). The orange and purple dashed lines are the model prediction (total cells) of the 75 <sup>th</sup> and 25 <sup>th</sup> percentiles of the data, a result of the variation in the estimated parameters (standard deviation fixed to 0.5 for all parameters (Table 1)).	180

3	Empirical and model predicted number of IFN- $\gamma$ secreting CD4+ T cells over time for A. pooled <u>human</u> data (all data, pooled over vaccine type) (50 $\mu$ g H56/H1+IC31), and the predicted human immune responses following a B. low (mouse-data mapped dose of 1-10 $\mu$ g H56/H1+IC31) or C. high dose vaccination (mouse-data mapped dose of 150 $\mu$ g H56/H1+IC31). A. Grey points correspond to number of IFN- $\gamma$ secreting CD4+ T cells measured over time by ELISPOT assay in <u>human PBMC</u> after receiving vaccination of H56/H1+IC31 at day 0 and day 56. Median responses over time are marked by blue triangles, the 75 <sup>th</sup> percentile responses by an orange triangle and the 25 <sup>th</sup> percentile responses by a purple triangle. The model prediction (total cells) (parameters in Table 1) is plotted against the median data (blue line). The orange and purple dashed lines are the model prediction (total cells) of the 75 <sup>th</sup> and 25 <sup>th</sup> percentiles of the data, a result of the variation in the estimated parameters (standard deviation fixed to 0.5 for all parameters (Table 1)). In B. and C. Median (blue dashed), 75 <sup>th</sup> (orange dots) and 25 <sup>th</sup> (purple dots) of the model predicted human responses after mapping from the mouse dose group model calibration (predicted parameters in Table 1) are shown.	181
<b>Paper 4 Supplementary Figures</b>		
S1	Median IFN- $\gamma$ responses (horizontal black bars) and responses of individual mice per time point (blue points) for each dose.	187
S2	Number of IFN- $\gamma$ secreting CD4+ T cells in humans in H56+IC31 phase I trial (ClinicalTrials.gov no NCT01967134) and H1+IC31 phase I trial (ClinicalTrials.gov no NCT00929396) over time measured using an ELISPOT assay	189
S3	Visual Predictive Check (VPC) plot for the pooled mouse model (parameters from Table 1 using the Gaussian equation for $\delta$ Table S2).	197
S4	Prediction distribution plot for the calibration to the mouse data (parameters from Table 1 using the Gaussian equation for $\delta$ Table S2)	198
S5	Mouse observed data versus model predicted IFN- $\gamma$ responses (parameters from Table 1 using the Gaussian equation for $\delta$ Table S2)	199
S6	Visual Predictive Check (VPC) plot for the covariate mouse model (dose group indexed on parameter $\beta_{TEM}$ , see Table S5, estimated parameters in Table 1)	202
S7	Prediction distribution plot for the calibration to the mouse data stratified by dosing group (dose group indexed on parameter $\beta_{TEM}$ , see Table S5, estimated parameters in Table 1).	203
S8	Mouse observed data versus model predicted IFN- $\gamma$ responses stratified by dose group (dose group indexed on parameter $\beta_{TEM}$ , see Table S5, estimated parameters in Table 1).	204
S9	Visual Predictive Check (VPC) plot for the pooled human model (model parameters Table 1).	208
S10	Prediction distribution plot for the calibration to the human data.	209
S11	Human observed data versus model predicted IFN- $\gamma$ responses	210
S12	Model predictions for each participant of the human data set. Plot 1 of 2.	211
S13	Model predictions for each participant of the human data set. Plot 2 of 2.	212
S14	Empirical and model predicted number of IFN- $\gamma$ secreting CD4+ T cells over time for A. pooled human data (all data, pooled over vaccine type) (50 $\mu$ g H56/H1+IC31), and the predicted human immune responses following a B. low (mouse-data mapped dose of 0.3-3.33 $\mu$ g H56/H1+IC31) or C. middle dose vaccination (mouse-data mapped dose of 16.7 $\mu$ g H56/H1+IC31) assuming a dose allometric scaling factor of 3.3. A. Grey points correspond to number of IFN- $\gamma$ secreting CD4+ T cells measured over time by ELISPOT assay in <u>human PBMC</u> after receiving vaccination of H56/H1+IC31 at day 0 and day 56. Median responses over time are marked by blue triangles, the 75 <sup>th</sup> percentile responses by an orange triangle and the 25 <sup>th</sup> percentile responses by a purple triangle. The model	217

	prediction (total cells) (parameters in Table S9) is plotted against the median data (blue line). The orange and purple dashed lines are the model prediction (total cells) of the 75 <sup>th</sup> and 25 <sup>th</sup> percentiles of the data, a result of the variation in the estimated parameters (standard deviation fixed to 0.5 for all parameters (Table S9)). In B. and C. Median (blue dashed), 75 <sup>th</sup> (orange dots) and 25 <sup>th</sup> (purple dots) of the model predicted human responses after mapping from the mouse dose group model calibration (predicted parameters in Table S9).	
<b>Chapter 6</b>		
6.1	Schema depicting the steps required to incorporate vaccine Immunostimulation (IS) /Immunodynamic (ID) modeling into vaccine development	245

## **Chapter 1. Background and Thesis Overview**

### **Vaccine Development**

Vaccines are one of the most important public health discoveries and are the most cost-efficient intervention known in medicine [1]. The physician Edward Jenner has been widely recognised as the pioneer of vaccination when he made a breakthrough discovery against smallpox, a deadly disease with a high fatality rate in infants and adults (80% and 20-60%, respectively) in the 18<sup>th</sup> century [2]. In 1798, he observed that dairymaids who were exposed to cowpox, were protected from smallpox, and thus inoculation with cowpox pathogen could protect against smallpox disease [3]. This was the first recorded vaccine and led to the eradication of smallpox [2]. Since then vaccines have been developed and licensed for multiple diseases [4]. Currently, both the pipeline and business rationale for new vaccines are strong [5].

The vaccine development process follows a progression of phases to produce a safe and effective vaccine which can take up to 10-15 years to complete [1]. After initial discovery, vaccine immunogenicity and safety bounds are identified in animals (pre-clinical experiments) before the vaccine can be given to humans in clinical trials for further safety and immunogenicity testing (phases 1 and 2). Finally, large efficacy trials (phase 3) are conducted to assess the vaccine performance in the chosen population and if successful, the vaccine will be licensed [6]. Taking a vaccine from discovery to licensure can cost in the region of US\$0.8 billion [7]; the later stage is the most expensive, with phase 3 trials costing in the region of US\$0.5 billion [1]. With these enormous costs, there is intense pressure to make well-informed decisions at each stage of the development process; mistakes are expensive and delays can waste precious time that could save lives. As such, it is vital that key developmental decisions are thoroughly investigated.

### ***Animal models***

Ideally, the most accurate information regarding vaccine performance would be gained if vaccines were tested directly in humans; however, developers are constrained by clinical, ethical, and financial concerns. As such, in the early stages of vaccine development animal models are employed to help understand the safety, immunogenicity and efficacy (amongst other aspects) of a vaccine before administration in humans [8, 9]. Animal models are essential to the vaccine development process as developers are able to test a wide range of developmental factors quickly at a relatively reduced cost. It is vital that a representative animal model is found to enable translation of the findings in pre-clinical experiments to clinical trials, as accurately as possible [10].

Nonhuman primates (NHP) are used to represent human vaccine responses as they are physiologically and immunologically closer to humans than other animals [9, 11, 12]. In many cases NHPs have been shown to be a valuable model for vaccine development, for example, in the study of vaccines for HIV [13, 14], measles [15] and yellow fever/dengue [16]. Despite their obvious value in vaccine development, the use of NHPs for vaccine research is expensive and requires specialist expertise, care and laboratory facilities. Other larger animals have proved successful animal models for vaccine development including pigs [17], cattle [18, 19] and sheep [20].

Smaller animals (e.g. rodents) are regularly used in the earliest phases of development as they are cheaper, easier to house and monitor. In-bred animals with varying susceptibility to numerous diseases allow the testing of specific immunological pathways [21]. However, unless genetically modified to be “humanised”, in many cases, smaller animals are less predictive of human vaccine responses [22-24].

The key challenge is to accurately translate vaccine responses from these animal studies to humans, as the relationships are still not fully characterized, and fraught with issues of not only scale, but physiological differences between species. Many vaccines are still searching for the most representative animal model to accelerate vaccine development [25, 26].

## ***Dose selection***

A key consideration in developing a vaccine is establishing an optimal vaccine dose concentration. Throughout the thesis, I refer primarily to vaccine dose concentration (hereafter dose) to mean the amount of *antigen* in the vaccine that promotes the intended immune response [21]. Additionally, vaccine delivery systems, i.e. adjuvants are considered a separate component of the vaccine construct and not included in my definition of dose.

Once a representative animal model is identified, a key aim of preclinical experiments is to establish a vaccine dose that is safe and a range of doses that are safe and likely to provide the highest protection when tested in humans. In the case of a pre-exposure vaccine (a vaccine given to prevent infection), the optimal vaccine dose will promote an immune response in the host that is sufficient to protect against subsequent infection, whilst remaining non-toxic. Further to this, from a cost-effectiveness perspective, the optimal dose may be the lowest dose that achieves both of these criteria.

In current vaccine development, effective human doses are estimated based on pre-clinical experiments in which developers are able to test large dose ranges over short timeframes. Methods for finding optimal vaccine dose are purely empirical [27] and based on the long-standing assumption that the relationship between dose and host response is saturating. This assumes a minimum vaccine dose can be found that gives no host response, followed by a window of vaccine doses where the selected immune response rapidly escalates then a clear response plateau above a certain dose threshold [28, 29]. The goal of vaccine development has then been to increase the dose until the response plateau is reached and assume the highest, safe dose is optimal (with some margin of error to allow for host variation). Typically, following toxicology tests to establish a safety bounds of the vaccine [30], a “low” dose in mice or other small animals is chosen and increased by half log increments until the maximum plateau in response is met. This dose range is then scaled up to be applied in larger animals and humans using a proposed allometric dose scaling factor. Allometric scaling is the quantifiable relationship between animal body size and characteristic, e.g. the physiological relationship between animal size and metabolism or life span [31]. The allometric dose scaling

factor is a value by which the developer believes the vaccine dose that is equivalent across species (i.e. small to large animal to human. Once the starting dose has been established in humans, it is then increased incrementally until a “maximal” safe dose, which is defined by predetermined safety criteria, is achieved.

However, this “classic” saturating dose response curve is now being challenged by data from newer vaccine platforms. Recent immune data for tuberculosis disease (TB) has highlighted the shortcomings of this vaccine dose selection assumption.

## **Tuberculosis**

### ***The burden of tuberculosis disease***

Tuberculosis disease (TB) caused by the bacteria *Mycobacterium tuberculosis* (*Mtb.*), remains a substantial global health problem as one of the top 10 causes of death worldwide [32]. There were approximately 10.4 million new cases (11% of which were in people living with HIV) and 1.4 million deaths from disease (with an additional 0.4 million deaths from TB disease in people living with HIV) worldwide in 2015 [32]. In 2015, there were 480,000 new cases of multi-drug resistant TB [32]. Countries with the highest incidence of TB (those that account for 60% of new cases) include: India, Indonesia, China, Nigeria, Pakistan and South Africa (Figure 1.1).

The Sustainable Development Goals put forward by the United Nations in 2015, have the goal to “end TB epidemic by 2030” [33] and the WHO End TB Strategy aims for a 95% reduction in TB deaths and 90% reduction in TB incidence (approximately 10 per 100,000 population) compared to 2015 by 2035 [34]. TB incidence has declined worldwide by 1.5% between 2014 and 2015 [32], but to achieve the WHO targets, this rate of decline will have to increase to 4-5%. Major new technologies will be required to achieve this goal [35].

## Estimated TB incidence rates, 2015

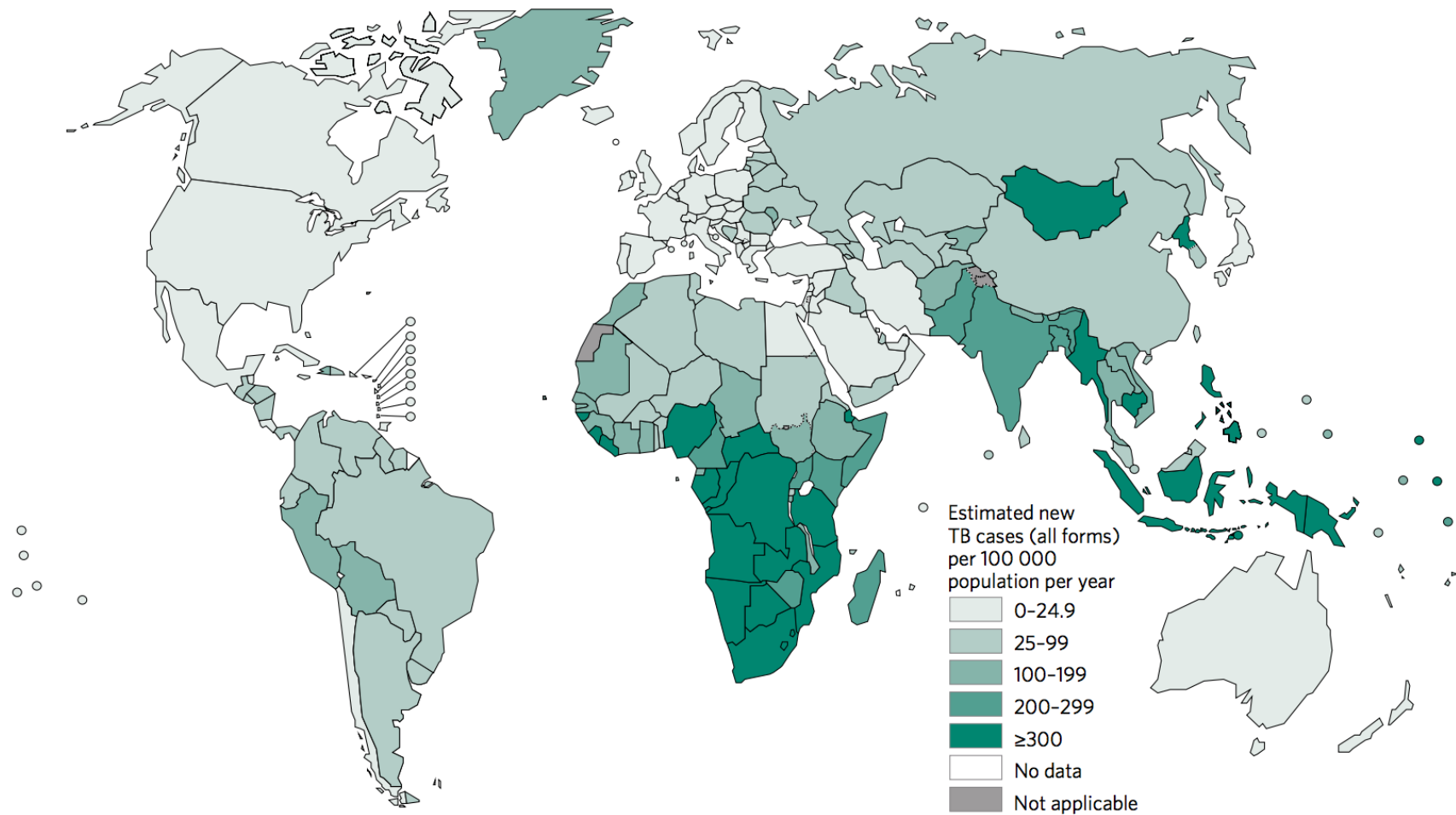


Figure 1.1 Estimated TB incidence rates by country, 2015 (WHO, 2016 TB report – permission to use granted 26/6/17 see appendix B for e-mail correspondence)

### ***Natural history of *Mtb.* infection***

Once an infection with *Mtb.* has been established, approximately 10% of individuals will progress straight onto active TB disease [36, 37]. In the classic paradigm of tuberculosis disease, the remaining individuals will clear the infection or develop latent *Mtb.* infection whereby no TB disease symptoms are observed and it is assumed their infection is in a quiescent state [37]. In this case, progression from latency to active is possible and approximately 3-10% of those latently infected will progress on to active TB disease in their lifetime [36, 37]. This rate is considerably increased to >10% per life-year by factors such as age and HIV infection that compromise the immune system [38].

### ***TB immune response***

Transmission of *Mtb.* occurs after an individual with active disease aerosolizes bacilli by coughing, sneezing [39]. There is data to suggest a great amount of variability around the infectiousness of an aerosol produced when an actively infected person coughs [40] and some people with active disease may be more infectious than others [41]. TB disease can disseminate to other organs within the host (extra-pulmonary TB disease) or remain in the lungs (pulmonary TB disease), here I focus on the latter.

### ***The innate response to *Mtb.* infection***

The first line of defence against *Mtb.* infection is the innate immune response. The innate or “natural” immune system is present at birth and does not fundamentally change throughout the host’s lifetime [42]. Additionally, the innate immune response is thought not to possess memory to previous interaction with pathogens [43, 44].

In *Mtb.* infection, the primary innate response is respiratory mucosa located in the hosts airways [45]. Respiratory mucosa acts to create a physical barrier that prevents invasion and a first-line introduction of *Mtb.* to key innate immune response cells [46]. Evading this, the bacilli will eventually establish in the lung alveoli [40]. Here, the bacilli is phagocytosed by alveolar macrophages [47] and taken up by neutrophils [48] and antigen presenting dendritic

cells [49]. Once internalized by the macrophage, the *Mtb.* bacilli are chemically destroyed via a process of autophagy, which is activated by cytokines emitted by the adaptive response [50, 51]. Alternatively, macrophage apoptosis (or cell “suicide”) acts to destroy the internalized bacilli, and halt further bacteria replication [52]. Simultaneously, antigen presenting cells, dendritic cells process *Mtb.* and migrate to the draining lymph node for presentation to naïve T cells [53, 54]. Naïve T cells then differentiate into the appropriate adaptive cell type.

### *The adaptive response to Mtb. infection*

The adaptive immune system is comprised of B and T lymphocytes, whose role is to stimulate (and activate) the innate immune system and store information on invading pathogens in order to recognise and immobilize the pathogen more quickly if a repeat infection occurs. In the case of infection with *Mtb.*, an intracellular bacteria, it is assumed that a cellular (Th1) defence is required. The adaptive immune cells widely acknowledged to be most associated with *Mtb.* infection are Th1-phenotype CD4<sup>+</sup> and CD8<sup>+</sup> T-cells [55-62] as research has shown that both Major Histocompatibility Complex (MHC)-I and MHC-II pathways can be stimulated by *Mtb.* antigens. Once stimulated by an antigen-presenting cell, CD4<sup>+</sup> T-cells secrete the cytokines IFN- $\gamma$ , IL-12 and TNF- $\alpha$ , which are known to be essential to the immune response to *Mtb.* infection by facilitating interactions between the innate and adaptive immune response cells [63-68]. Cytotoxic CD8<sup>+</sup> T cells are known to increase in the later stages of infection as bacterial burden increases to kill infected cells [60], although the role of CD8<sup>+</sup> T cells in *Mtb.* infection is complex and still an area of research [69]. Regulation of these responses during infection are also vital to avoid causing damage to host tissue, as such regulatory T cells secreting cytokines such as IL-10 [70] control pro-inflammatory responses [71, 72]. There is also emerging evidence to suggest the importance of Th17,  $\gamma\delta$ - T cells, B-cells, MAIT and NK cells in *Mtb.* infection [73-78].

### *Immunological memory*

CD4<sup>+</sup> T cells in early adaptive response to *Mtb.* infection are known as effector phenotype [79, 80]. Once the pathogen has been cleared, effector cells “contract” by apoptosis or cell death [4]. Here it is approximated that up to 95% of the cells die to avoid over-inflammation

in the host [81, 82]. The remaining 5% of cells migrate to the lymph nodes and remain in the hosts system as long-lived memory cells or “central” memory cells [83]. These cells have the ability to rapidly proliferate when the same pathogen is encountered, providing protective response to infection [44, 81, 84]. Studies have shown that in the case of *Mtb.* infection, a large pool of central memory T cells is indicative of protection [79, 85, 86] and vaccination against the disease should aim to induce these T cells above any other memory type [87, 88] (see review in [89] of other memory cells).

### *Granuloma Formation*

A key immune mechanism to slow the progression to active disease is the formation of the granuloma in the lung. Following an activated adaptive immune response, macrophages, neutrophils and lymphocyte cells gather in the lung to form a physical containment of *Mtb.* bacilli [90]. Inside the granuloma, cells maintain a hypoxic environment encourage a state of dormancy in the bacteria [37]. There is still unknown whether an individual will effectively sterilize the bacteria as granuloma have been shown to be variable within the host [91]. However recent evidence has shown that a balance of pro- and anti-inflammatory cytokines inside the granuloma is key to sterilization of the bacteria [92]. Factors such as age and HIV infection that compromise the immune system can cause break down of the granuloma construct [38].

### ***Risk factors for Mtb. infection and progression to TB disease***

Risk factors associated with increased risk of *Mtb.* infection are mainly external to the host [93], for example, the infectiousness of a TB index case [94], contact patterns with infectious individuals [95-97], residence (e.g. confined spaces such as prisons [98]) or behavioural risk factors (e.g. visiting enclosed bars with little ventilation [99, 100]).

Risk factors of progression from *Mtb.* infection to TB disease are mainly driven by endogenous host factors. Human Immunodeficiency virus (HIV) is a major risk factor for TB disease and HIV-TB co-infection is highly prevalent in South Africa, a major contributor to global TB disease incidence [32]. HIV infection suppresses the cell-mediated response believed to be important

for prevention of TB disease progression [101]. For example, HIV infection disrupts the ability for *Mtb.* infected phagocytic cells, such as macrophages to apoptosis providing the bacteria more opportunity to replicate [102]. TB disease is also known to exacerbate HIV infection [101]. Elimination of TB disease is heavily dependent on addressing this co-epidemic [32]. Co-infection with other diseases also cause immunosuppression that can lead to TB disease. In diabetes infection cell-mediated immune responses are depleted [103], including IFN- $\gamma$  production [104] and impaired movement of innate cells such as neutrophils [105]. Additionally, in Helminth-TB coinfection, regulatory cytokines IL-10 are upregulated which dampens immune response to protect against TB [106, 107].

There has been recent research into the importance of the monocyte (innate cells) to lymphocyte (adaptive cells) (ML ratio) in the risk of TB disease. Recent evidence has shown that the ratio of host monocyte to lymphocytes cells (ML ratio) was associated with risk of TB disease [108-110]. "Naranbhai et. al. observed that in HIV positive, South African adults on combination antiretroviral therapy, this relationship was nonlinear, i.e. low and high, compared to moderate, ML ratios were associated with a higher risk of TB disease [108]. Little investigation has been made into how ML ratio may affect mycobacterial-specific immune responses and further insight into this relationship could potentially inform targeted TB interventions." (*quoted text taken from my paper 1 [111]*).

Age of an individual plays an important role in the likelihood of progression to disease. There is potentially a non-linear relationship between age and risk of disease progression, where infants (< 3 years) [112] and the elderly [113] are at a higher risk than adolescents and adults. In both groups, the immune system is compromised leading to higher risk of TB disease progression. In infants, increased risk is due to an immature immune system, which struggles to contain *Mtb.* infection [112]. In the elderly, TB disease is more likely due to reactivation as the immune system declines and fails to contain latent *Mtb.* infection [114].

Socio-economic and behavioural related factors can also increase the risk of disease progression [93]. Country of residence is associated with a higher risk of TB disease, where the poorest, developing countries experiencing the highest burden of TB [93, 115]. Risk factors including poorly ventilated accommodation leading to indoor air pollution and

crowding increase the likelihood of exposure to *Mtb*. Malnutrition [116], high alcohol intake [117] and smoking [118, 119], which are also associated with socio-economic status, have been shown to increase risk of TB disease progression. In the case of malnutrition risk of TB disease progression is increased by between 6 to 10-fold [116], due to reduced cell-mediated immunity [120, 121]. However, the authors acknowledge further research is required as TB disease itself can lead to malnourishment [122, 123]. The risk of progression to active TB is almost three times as high for those who consume above average alcohol [100]; this is due to reduced production of the cytokine, TNF- $\alpha$  from T cells [124]. Smoking tobacco causes damage to lung mucosa [125], a first line defence against *Mtb*. infection in the lung and reduced CD4+ function due to nicotine intake [126].

### ***Correlates of protection against TB disease***

Despite extensive research into the immune response to *Mtb*. infection, there is currently no definitive correlate of protection against TB disease [127]. A candidate for such a correlate is IFN- $\gamma$ ; a key cytokine produced by CD4+ and CD8+ cells, which primarily acts to stimulate phagocytic cells, such as macrophages, to clear intracellular pathogens [37, 55]. IFN- $\gamma$  has been shown to be essential in the control of such pathogens as *Leishmania major* [128]. Cooper et al. [129] show that mice with a disrupted IFN- $\gamma$  gene, failed to control their infection and succumbed to tuberculosis disease more frequently than that of a control group [129]. Similarly, Chakerian et al. [57] demonstrated that mice that could induce an early IFN- $\gamma$  producing T-cell response were better protected than an alternative strain of mouse that could not provoke such a response. These results are supported by many other animal studies [64, 130, 131]. Human studies have demonstrated that individuals deficient in the IFN- $\gamma$  receptor gene are more susceptible to infection with *Mtb*. [66, 132, 133]. For example, Newport et al. show that defects in the IFN- $\gamma$  receptor gene (IFN- $\gamma$  R1) in four children with severe *Mtb*. infection led to an absence of IFN- $\gamma$  receptors on innate cell surfaces. Consequently, a failure in the up-regulation of a key inflammatory cytokine, TNF- $\alpha$ , by macrophages usually provoked by IFN- $\gamma$  response [133]. As such, IFN- $\gamma$  has long been regarded as one of the best measures of immune response against *Mtb*. infection [37, 64, 134]. Despite this, there is mixed evidence as to whether levels of IFN- $\gamma$  correlate with protection against disease in humans [135, 136]. Most notably, a study by Kagina et al [136]

on a group of infants in South Africa, showed that there was no difference in T-cell responses, including the secretion of IFN- $\gamma$  between the TB cases and non-TB infected controls. However, in research relating to the recent TB vaccine, MVA-85A, T cells secreting IFN- $\gamma$  were shown to be associated with reduced risk of TB disease in infants, amongst other T cell activation markers [137].

As such, IFN- $\gamma$  has long been regarded as one of the best measures of immune response against *Mtb.* infection [37, 64, 134]. Despite this, there is mixed evidence as to whether levels of IFN- $\gamma$  correlate with protection against disease in humans [135, 136]. A study by Kagina et al [136] on a group of infants in South Africa, showed that there was no difference in T-cell responses, including the secretion of IFN- $\gamma$  between the TB cases and non-TB infected controls. However, in research relating to the recent TB vaccine, MVA-85A, T cells secreting IFN- $\gamma$  were shown to be associated with reduced risk of TB disease in a large sample of infants who were more intensively screened for LTBI and HIV infection, than in the study by Kagina et. al. [137]. Surprisingly, Ag85A IgG was also found to be associated with reduced risk of TB disease, indicating a potential role for antibodies in addition to IFN- $\gamma$  in protection from disease [137].

It has been widely acknowledged in the TB community that increased IFN- $\gamma$  responses are necessary but not sufficient to provide a protective response against TB disease [138]. Polyfunctionality of T cells (i.e. secreting IFN- $\gamma$ , TNF- $\alpha$  and IL-2) may be a stronger correlate of protection, as has been shown for other pathogens [139]. In addition, as both antibodies and other T-cell populations may contribute to the protective immune response against *Mtb.* infection, such as CD8+ T-cells and Natural Killer (NK) cells [59, 62, 74, 140, 141], it is likely that a correlate of protection for TB is a complex network of innate, humoral and Th1 immune responses [138, 142, 143]. Not only cell types, but the balance of T cell phenotypes which, through measurement of T cell differentiation markers are thought to be indicative of bacterial load within the host [144, 145]. Host factors may also play a vital role in correlate discovery, including age, biology and HIV status, etc. [138]. Finding a correlate of protection for TB disease is a priority, and is especially important for TB vaccine development [142]. Hanekom et al. [127] suggest IFN- $\gamma$  and other cytokines should be a reading of “vaccine take” until a comprehensive surrogate of protection is established. As such, IFN- $\gamma$  secreting T cells

(measured by ELISPOT assay) and IFN- $\gamma$  levels (measured by ELISA assay) are the markers of choice for the majority of TB immunological studies and the association of IFN- $\gamma$  with reduced risk of TB disease in BCG immunised South African infants supports the continued use of IFN- $\gamma$  as a marker of vaccine take [146, 147].

### ***TB vaccines***

The WHO Stop TB strategy has outlined the goal of 90% reduction in TB incidence (approximately 10 per 100,000 population) compared to 2015 by 2035 [34]. To reach this goal, more effective employment of current treatments and development of new TB control technology is paramount [32, 148, 149]. A recent systematic review by Harris et. al. on studies that assessed the impact of a new TB vaccine on TB disease using epidemiological mathematical models found the incidence rate ratio (IRR) of a new pre-exposure vaccine 25 years after vaccination was approximately 80% if given to all ages [150, 151]. The IRR for a pre-exposure vaccine given only to neonates 40 years after vaccination was approximately 33% [150, 152]. Similar modelling studies also showed the IRR of a post-exposure vaccine 25-35 years after vaccination given to all ages was approximately 80-85% [148, 151] and given only to neonates was 25-39% [148, 151]. A new vaccine could therefore be key to meeting the 2035 targets [153, 154].

#### *Existing TB vaccine: Bacillus Calmette–Guérin (BCG)*

There is currently only one licensed TB vaccine, Bacillus Calmette–Guérin (BCG), a live attenuated vaccine, which has been in use for nearly 100 years. BCG is a strain of *Mycobacterium bovis* that went through more than 230 round of attenuation (passage of the organism in culture) when developed by Albert Calmette and Camille Guérin in 1908 [155]. Since then, attenuation of BCG continued and was distributed globally, resulting in more than 16 strains of BCG worldwide [156]. So far, BCG has been administered over 4 billion times [153] and shows strong efficacy against tuberculous meningitis in children [157]. BCG efficacy against adult pulmonary TB is variable [87, 158]. Studies have shown BCG vaccine to exhibit high levels of protection from pulmonary TB, with efficacy as high as 80% [159-161], however in other studies it showed little to no protection at all [162-164].

The reason as to exactly why BCG exhibits such variable efficacy is still a prominent question in TB vaccine research. It has been shown that one of the major factors contributing to higher efficacy was the latitude at which the trial was conducted [165, 166]. One hypothesis to explain this trend lies in the observation that latitude is associated with varying levels of exposure to non-tuberculous mycobacteria (NTM) [167] and it is thought that lower levels of exposure occur in more Northern regions [168]. Regular exposure to NTM is presumed to “mask” the effects of BCG vaccination against TB disease by priming the immune system and thus introducing a level of protection for the host [169]. Age at vaccination has also been suggested as a factor influencing BCG efficacy [166]. As a possible explanation for this, Ottenhoff et al. suggest that vaccination of infants/neonates could be detrimental to the immune memory required for protection by BCG as very early immune responses are not as fully developed as adolescents [153]. Immunosenescence can also affect the efficacy of BCG; two of the most common forms are age and infections that target the immune system, such as HIV [170-172]. Other factors such as BCG strain have been suggested to influence to efficacy of BCG [173].

Despite widespread use of BCG, tuberculosis continues to be the leading infectious disease killer globally [174] as such, a new TB vaccine is required [175].

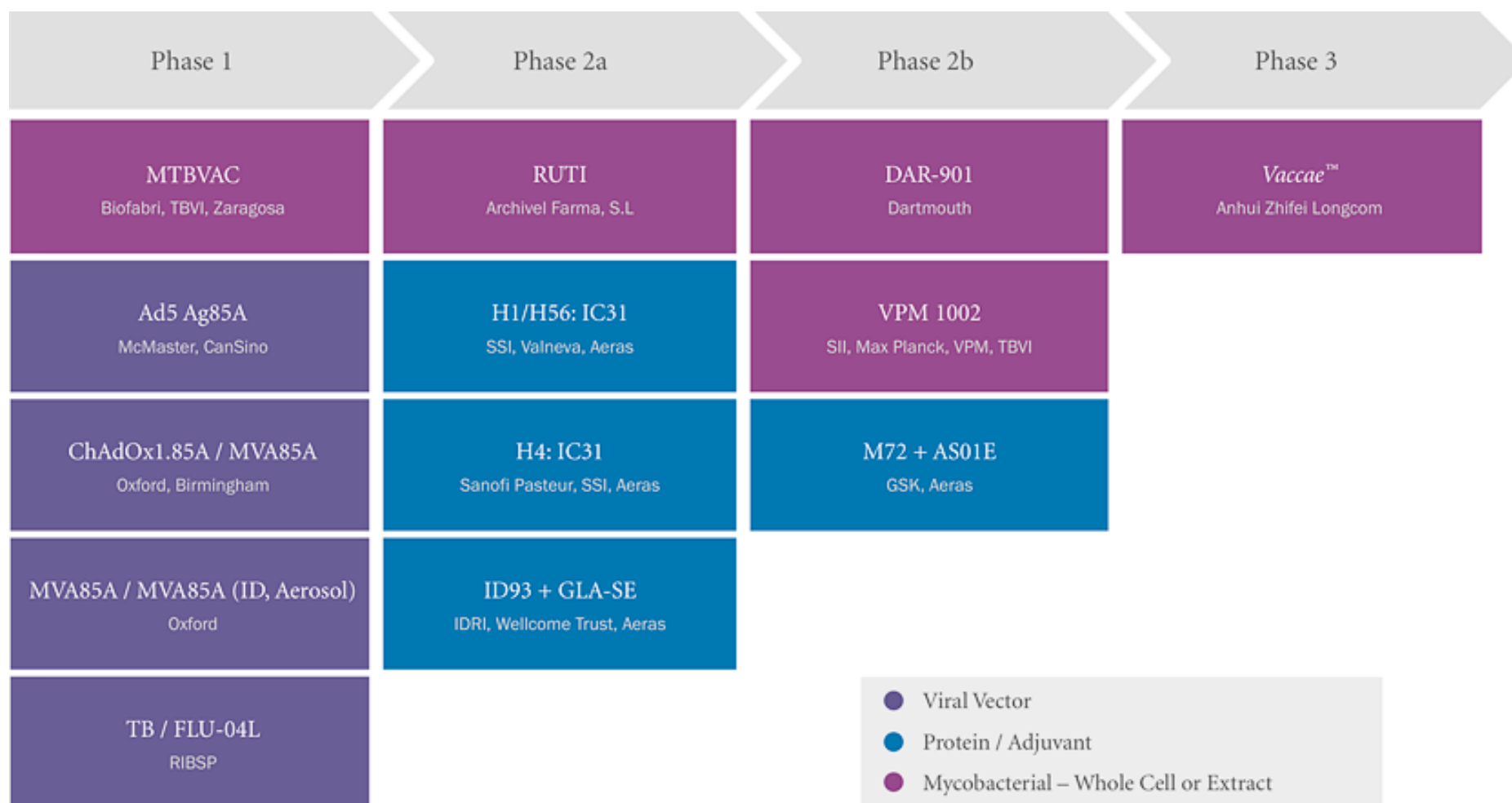
### *New TB vaccines*

There are currently 13 candidate TB vaccines in development, with the majority in phase 2 and 3 (Figure 1.2) [32]. As outlined above, the Th1 type response is important in inducing a protective response to *Mtb.* challenge in animals [129] and in observational human genetic studies [66, 133]. The majority of new TB vaccines aim to induce a strong Th1 immune response, predominantly CD4+ T cell mediated [35, 88, 155]. Only those candidates that are safer, more immunogenic and provide better efficacy than BCG are likely to proceed in the vaccine development process [58, 153].

TB vaccines can be classified into three types [35]: whole cell vaccine, viral vectored subunit vaccine and adjuvant protein subunit vaccine. New candidate TB vaccines can also be

categorised into two strategies: to replace BCG or to boost on previous BCG immune responses [176]. A booster vaccine works by building upon the immunity induced by previous vaccination [177]. A BCG booster vaccine would be administered following BCG vaccination either during infancy or adolescence [174]. In the current pipeline, most of the whole cell vaccines are designed to replace BCG and the subunit vaccines are predominantly used as BCG boosters.

A brief description of each vaccine candidate can be found in Appendix B.



Please note: Information is self-reported by vaccine sponsors.

*Revised on October 7, 2016*

**Figure 1.2 2015 developmental pipeline for new TB vaccines by Aeras, TB vaccine developers (permission to use granted 15/6/17 see appendix B for e-mail correspondence)**

## H-series

In this thesis, I use data on the H-series subunit, BCG booster vaccines. These vaccines are currently in Phase 2 of development (Figure 1.2). The H-series vaccines are protein adjuvant vaccines developed by Statens Serum Institut (SSI, Denmark), Aeras and Sanofi Pasteur. Three subunit protein vaccines from the H-series, designed to boost BCG vaccination, are currently in the vaccine development pipeline: Hybrid-1 (H1), HyVac-4 (H4) and Hybrid-56 (H56). H1 is comprised of the antigens Ag85b and ESAT-6 and H56 is comprised of Ag85b, ESAT-6 and Rv2660c (see Table B.1 in Appendix B). To address the complication of misdiagnosis of TB disease, due to the reliance of an immune response to ESAT-6 in current TB disease diagnostic tools [178], the vaccine H4 was developed, comprised of antigens Ag85B and TB10.4. H4, H1 and H56 have been adjuvanted with, IC31 [179, 180](Table B.1, Appendix B) has been used in the majority of preclinical and clinical trials with the H-series vaccines, however animal early experimentation also utilised proprietary liposomal adjuvant CAF01 [181, 182]. As I use data on H-series vaccines in this thesis, a more detailed outline of the pre-clinical and clinical performance can be found below.

### *Developing new TB vaccines*

To test the immunogenicity of new TB vaccines, IFN- $\gamma$  is commonly chosen as an indicator of the induction of vaccine mediated antigen specific immune response, although as mentioned, on its own it is necessary but not sufficient for a protective response against TB disease [138]. ELISA assays are used to measure IFN- $\gamma$  concentrations in whole blood by stimulating cells using a specific antigen [183]. To measure the number of cells producing IFN- $\gamma$  in peripheral blood mononuclear cells (PBMCs), an enzyme-linked immunosorbent spot (ELISPOT) assay is commonly used [184]. Flow cytometric analysis is also used to stain cells for multiple cytokine secretion as well as determining cell surface markers which would indicate CD4+ or CD8 T cell types and effector or memory cell type [58, 83]. Due to the additional complexity involved in flow cytometry, the assay is more expensive than ELISA or ELISPOT so the latter are more frequently used.

Just as with many vaccines, animal models are exploited in an effort to aid the development of TB vaccines. Due to the complex natural history of TB disease, multiple animal models have been developed with the aim of representing the different stages of disease progression as well as different settings or populations (infant versus adolescent, latently TB infected versus *Mtb.* naïve) [185].

Pre-clinical TB vaccine development is predominantly conducted in the mouse and the availability of inbred mouse strains enables reproducible and direct comparison between animals and across laboratories [185]. Comparisons of mouse and human immune responses have been made extensively due to the large body of data that exists in both species and is an active area of research [185-191]. The infection model in mice is thought to reflect the early stages of human infection (preceding granuloma formation) as the commonly used mouse strains do not make granulomas [188]. While there are established differences in mouse and human immunology [23], the fundamental mechanisms of cytokine responses secreted by Th1 T cells are thought to be similar [189]. However, broadly speaking, the ability of mice to form lesions (granuloma) after *Mtb.* infection, that reflect the pathology in humans is lacking [190] and variable amongst mouse strains [191].

Guinea pigs are also used to model TB disease as post-infection. Guinea pigs experience heightened inflammatory responses leading to lesions in the lung, which reflects the pathology observed in human *Mtb.* infection [192]. As a result of the similarities between guinea pig and human *Mtb.* response, it is a promising animal model to use once a vaccine has been “screened” in the mouse model [185].

The nonhuman primate (NHP) model is, arguably, the most appropriate TB animal model to represent human *Mtb.* infection and disease pathology as they are genetically and physiologically more like humans than small animals [193, 194]. This means direct comparison of NHP vaccination studies (immunology and efficacy) can be applied to clinical trials [185]. PET-CT imaging in macaques has provided valuable insight into the dynamics of TB lesions [91]. “Historically, rhesus (*Macaca mulatta*) [195] and cynomolgus (*Macaca fascicularis*) [196] macaque species have been used as the primary NHP-model in TB vaccine research [197-200]. Both species have been shown to respond to, and be partially protected from, TB by BCG

vaccination [147, 201-204]; however, it has been shown that the same experimental conditions (infection with *Mycobacterium tuberculosis* (*Mtb*) following vaccination or vaccine immune response) may lead to divergent outcomes between the two species [193, 205-207]. Furthermore, the colony (country of origin) of macaque, even within the same species, has been shown to affect the level of protection to infection and response after vaccination [208]. For example, differing levels of protection between Chinese and Mauritian cynomolgus macaques have been observed, whereby Mauritian cynomolgus macaques developed end stage progressive TB in 7 weeks, while the Chinese cynomolgus macaques remained well past the end of the study (12 weeks)[209]. Additionally, the cost and expertise required to facilitate an NHP study far exceeds that of any small animal studies. Despite this, in 2014, the Bill and Melinda Gates Foundation adopted a new strategy for the up-selection of new TB vaccine candidates for clinical testing selecting vaccines on immune response and challenge results in NHPs [210].” (*quoted text taken from my paper 2 [200]*)

After pre-clinical evaluation, TB vaccines are progressed into clinical stages to establish efficacy in humans. Due to a lack of correlate of protection, this requires large efficacy trials that must be carried out in high incidence settings and as TB is a slow progressing disease, large numbers and long follow up times are required [88]. Additionally, due to differing immunogenicity and levels of susceptibility, there are three distinct populations to target with a new TB vaccine [88]: infants, adolescents and HIV infected [38, 175]. In the latter two, latent *Mtb.* infection may be an added complication that new TB vaccines will have to accommodate. Depending on the BCG policy of the country where the trial is held, it is likely that participants in efficacy trials may already have BCG vaccination, potentially at birth. If the vaccine under consideration is a BCG booster then measures may have to be taken to prime participants with BCG before enrolment (with sufficient time to build an adequate immune response). To establish if a new TB vaccine is an improvement on BCG, BCG vaccination may be included in vaccine trials as a control arm [211, 212].

#### *Recent TB vaccine clinical trials*

To date, there has only been one TB vaccine that has progressed through to efficacy trials with published results. The first efficacy trial for MVA85A, developed at Oxford university,

was conducted in 2,794 BCG-vaccinated infants in South Africa [213]. The purpose of the trial was, primarily, to investigate safety of the vaccine, followed by efficacy against TB disease and infection [158]. None of the serious adverse events were associated with the vaccine and elevated immune responses were recorded [213]. However, the efficacy of the vaccine against TB disease (measured using microbiological and clinical criteria) was calculated at 17.3% (95% CI: -31.9% to 48.2%) and the efficacy of the vaccine for protection against *Mtb.* infection (measured using the Quantiferon-TB Gold assay) was -3.8% (95% CI: -28.1% to 15.9%) suggesting this vaccine was not efficacious in this population [213]. The investigators of the trial speculated that immature immune systems and low immune responses to MVA85A may have affected the MVA85A efficacy in the infants [213]. It is also speculated that the high incidence rates of TB in South Africa may be a challenge for any TB vaccine to protect the population, especially those with underdeveloped immune systems [158]. Despite this, this study demonstrated that a large TB vaccine efficacy trial could be successfully conducted that produced meaningful results; a first for the TB vaccine community. A further MVA85A efficacy trial was conducted in adults with HIV infection in South Africa and Senegal, although following the infant result the study was down-graded to a safety study and had insufficient statistical power to assess vaccine efficacy [214]. Similar results were found in this trial: the vaccine was safe, however there was no efficacy against *Mtb.* infection (efficacy of 11.7% (95% CI: -41.3% to 44.9%)) or against TB disease (efficacy of 32.8% (95% CI: -111.5% to 80.3%)) [214]. This study marks an important breakthrough in establishing a safe TB vaccine in an HIV infected population [214].

The lack of MVA85A efficacy in the infant trial (efficacy wasn't tested in the HIV trial) was potentially attributed to inadequate understanding of the necessary immune response needed for protection against TB disease [214]; new TB vaccines may have to shift focus to induce wider immune responses including non-classical T cells, innate and humoral immunity [35, 175]. Additionally, it has been suggested that for future TB vaccines to be successful, a broader range of *Mtb.* antigens maybe required [35, 215]. Data from the MVA85A vaccine trials have helped in moving forward the correlate of protection work [137] and new TB vaccines [216]. As more TB vaccines progress through efficacy trials (M72+AS01E, VPM1002 and Vaccae are currently in phase 2b and 3 efficacy trials (Figure 1.2, and Appendix B)) more data on the responses required for protection against TB disease will become available.

### ***H-series TB vaccine performance and dose escalation***

In animal studies, HyVac-4 (H4) adjuvanted with IC31 (H4+IC31) administered as a BCG boost, was shown to be safe, immunogenic and protective when compared to BCG alone [217, 218]. Similarly, when administered with the CAF01 adjuvant, the vaccine was protective in mice as a pre-exposure vaccine [219, 220]. Following this pre-clinical investigation, a phase I clinical trial in South Africa, where a two vaccination regimen, given two months apart, of H4+IC31 was administered in BCG vaccinated healthy participants in varying antigen dose was conducted [221]. Adverse events to the vaccine were minimal and multifunctional (IFN- $\gamma$ , TNF- $\alpha$  and IL-2 or TNF- $\alpha$  and IL-2 producing) CD4+ T cell expansion was long lasting. A similar result was found when a two vaccination regimen, given two months apart, of H4+IC31 was administered in BCG vaccinated healthy participants in two Scandinavian countries in a phase 1 trial [222]. The trial escalated both antigen and adjuvant dose. Similarly, small animal studies showed that the vaccination with Hybrid-1 (H1) adjuvanted with CAF01 (H1+CAF01) induced key polyfunctional immune responses that were long lasting [223, 224] and protection against challenge [224, 225]. Nonhuman primate (NHP) studies with H1+IC31 also showed reduced bacteria numbers in the lungs and lung pathology after challenge with *Mtb*. [226]. Phase I clinical studies showed that in BCG-naïve, BCG-vaccinated participants and latently TB infected participants, a two vaccination regimen, given two months apart, of H1+IC31 promotes strong and long lasting T cell (measured by IFN- $\gamma$  secreting CD4+ + T cells) response [227, 228]. The same strong immune response was shown when a two vaccination regimen, given two months apart, of H1 was administered with CAF01 adjuvant [181]. The effect of HIV infection on T cell responses to H1+IC31 were investigated and showed mixed results [229, 230]. The effects of vaccination with Hybrid-56 (H56) adjuvanted with IC31 (H56+IC31) in BCG-vaccinated NHP's was effective containment of infection and reduced rate of clinical disease. Additionally, strong responses to ESAT-6 and Rv2660c were recorded in NHPs [231]. Of note, macaques in this study who received BCG and H56+IC31 did not reactivate latent infection after anti-TNF antibody was administered. H56+IC31 was administered in a first-in-man study where three vaccinations, two months apart, were given to latently infected and healthy participants [232]. Results showed that both groups (latently

infected and healthy participants) expressed Th1 CD4+ T cells. The frequency of T cell responses following vaccination were higher in latently infected than in healthy participants.

The dose escalation studies of the H-series vaccines are as follows. Initial dose response testing with the H4+IC31 candidate revealed Th1 immunogenicity as low as 0.005 µg of the H4 antigen, the highest responses were observed at doses of 0.05 to 1 µg [217]. Here, the adjuvant dose was kept constant. The best protection in a challenge model in mice was observed with the lowest dose tested, 0.5 µg H4 [217]. The protection and measured immunogenicity then decreased at 5 µg and was minimal at 15 µg. A similar dose response was shown in an accompanying guinea pig challenge study [217]. However, in further animal studies, 20 µg of H4 + IC31 was chosen for a pivotal guinea pig study [218], 5 µg chosen for studies of murine post-TB intervention [219, 220, 233], and 100 µg used in cynomolgus challenge studies [226]. A potentially important cynomolgus challenge study used H56 + IC31 at the likely high dose of 50 µg, and whether the results may have been improved with a lower dose [231] is unknown. Following this pre-clinical investigation, a “classic” method was employed to the clinical environment. The current hypothesis in TB protein vaccine developers is that the allometric dose scaling factor of dose between small animals and humans is in the range of one to ten (personal communication, Thomas Evans MD), and for H56+IC31 a factor of ten has been assumed from mice to human and NHP [230, 234, 235].

However, the lowest dose tested in a human was 5 µg, despite evidence of protection at 0.1 µg in the guinea pig (where the scaling factor between small animal and human is believed to be less than 50 – see above). The dose escalation went from 5 µg to 15, 50, and 150 µg of the H4 + IC31 vaccine in two trials performed in Scandinavia [222]. In those studies, there was no difference in response at the 5 and 15 µg doses, the immune response began to drop at 50 µg and was markedly lessened by 150 µg. This study was then repeated in a BCG vaccinated, non-latently infected tuberculosis endemic population in South Africa [221] and the same dose response pattern was seen. 15 and 50 µg alone were studied in small numbers in the First in Man (FIM) trial of the H56 + IC31 vaccine [232], 50 µg was chosen as a single dose in the FIM study of H1 + CAF01 [227, 228] and for the H1 + IC31 studies [229, 230]. To note, different dose-response curves may be observed between the H-series vaccine constructs,

however H56 and H1 adjuvanted with IC31, result in similar immunological profiles at varying doses [236].

### **Potential issues with current vaccine dose-finding methods**

H-series vaccine development has benefitted from robust dose escalation testing. However, the dose ranging data in the animals suggested that the lower doses were the most (Th1) immunogenic compared to higher doses, but a comparatively high dose range was chosen to be tested in humans. Thus, despite numerous human published studies on the H-series vaccines, the lower end of the dose response curve in man has not been established.

These unconventional dose response curves present important evidence that long-standing vaccine development assumptions (that the dose response curve is saturating) are flawed and as such, suboptimal doses could be progressing to later clinical stages. Similar instances of non-saturating dose response curves have also been seen in HIV [237], malaria [238] and Influenza [239] vaccines. As an added complication, vaccine responses may differ across human subpopulation (e.g. all current TB vaccine clinical trials are stratified by HIV status [32]), highlighting the possibility that dose response curves may differ *within* the human population [240].

Preclinical dose data has potential as an effective predictive tool for human dose decision making. However, in TB vaccine development, there is a wide range of scaling factors between species; as previously mentioned, a scaling factor is assumed to be ten has been used for H56 from mice to human and NHP [230, 234, 235], ten times from mouse to human for BCG [241, 242], 100 times for MVA 85A [213, 241] and 0.5 for VPM1002 [241, 243] (recombinant BCG vaccine, currently in phase 2, see vaccine pipeline Figure 1.2). There is little evidence as to why these differ so widely. The yellow fever vaccine presents another example of mistakes in dose decision making. In this case, due to vaccine shortages, yellow fever vaccine dose fractionation studies were carried out and a lower dose was found to be as effective (measured using a known correlate) as the current higher licensed dose [244-246].

These errors in vaccine dose decision making may be occurring partly because translating vaccine responses from animal studies to humans is challenging and a representative animal model is required. The relationships between species are still not fully characterized; there are issues of not only scale, but physiological differences. Additionally, within human differences in vaccine response may require *multiple* animal models to develop a vaccine for a broad population. To my knowledge, no formal assessment of vaccine allometric scaling has been undertaken for vaccine development.

It is clear that mistakes are being made in vaccine development concerned with dose-finding. The consequences of which could mean wasted resources (e.g. animals), money and potentially, lives. Surprisingly, the definitive text on vaccine development does not include strategies for dose finding [27] and there is limited regulatory guidance on vaccine dose-finding methodologies from licensing organizations such as the FDA [147].

### **Model-based drug development: Pharmacokinetic/Pharmacodynamic Modelling**

Drug development faces similar pressures to those experienced in vaccine development; translating evidence from pre-clinical experiments and finding the optimal drug dose is paramount for effective, safe treatment. Yet, the drug development decision-making process is far more advanced than in vaccine development, mostly due the use of systematic, quantitative methods for drug optimization.

Model-based drug development (MBDD) combines data on drug responses and biological mechanism through mathematical modelling to quantify within-host drug effects [247] and has become an essential tool in developing safe drugs. The main goals of MBDD are to use mathematical based simulation to; focus in on promising candidates and develop the right dose(s) early on, decrease probability of failed or useless trials, reduce animal resources in developmental phases, decrease time to market and avoid post-marketing changes in dose or regimen or withdrawals [248].

MBDD is commonly split in to two components:

1. **Pharmacokinetics (PK):** What the body does to the drug, i.e. the concentration of drug in the body (as it is absorbed and eliminated) over time [249],
2. **Pharmacodynamics (PD):** What the drug does to the body, i.e. how the “effect” of the drug (e.g. in the blood) changes with the concentration of the drug in the body [249].

These are collectively known as pharmacometrics or PK/PD modelling [250].

Finding an appropriate model to represent the drug course can aid in development of safe and optimal drug dose and regimen. PK/PD modelling commonly combines compartmental ordinary differential equation models to represent drug dynamics within the host (PK) and a continuous nonlinear relationship between drug concentration and clinical effect (PD). In PK modelling, ordinary differential equations are used to describe the movement of drug concentration between model compartments which represents biological region of the host. The parameters of the model dictate the rate of drug movement. These models can either represent defined organs (e.g. the stomach or liver) known to be relevant to the drug (physiological-based models) or more abstract in that they do not represent a specific part of the body [250]. The integration of PK and PD models provides a vital link between drug dynamics and the desired effect. See Figures B.1, B.2 for a simple PK example.

Population characteristics such as age, weight or renal function can affect drug response. In order to find safe drugs for a target population, it is essential MBDD can incorporate these differences [251]. Population PK/PD modelling describes population typical response dynamics and how those dynamics vary across a population to gain information on appropriate drug dose or regimen for a given sub-population [250, 252].

While it is feasible to assume the biological mechanisms in response to drug (i.e. the model) do not change across a heterogeneous population, the magnitude of key mechanistic parameters might. Hence, the aim of population PK/PD modelling is to establish differences in model parameters associated with population covariates. To achieve this, models are calibrated to the response data and the parameters and parameter variation, estimated which requires a robust statistical framework. Nonlinear Mixed Effects Modelling is commonly used in pharmacometric modelling as it enables simultaneous estimation of both the population average responses, the variation in responses across individuals in the

population and the effect of population covariates on this variation [252]. Due to the nonlinearity of the model-predicted response dynamics advanced computational software are required to execute parameter estimation. These methods are outlined in more detail in the proposed methods section and appendix B.

MBDD has been in use for approximately 40/50 years. Drawing upon existing modelling practises in fields such as economics, meteorology and engineering [251], modelling to inform drug trials was first recognised in the late 1990's [253]. Pivotal work by Sheiner et al. to encourage "learning and confirming" [254] using mathematical models in clinical drug trials meant MBDD came to the forefront as an innovative and efficient tool to aid drug development. MBDD soon began to filter into the drug development community, featuring in influential pharmacological conferences [255] industry [256-258] and gained support from regulatory agencies such as the Food and Drug Administration (FDA) [259, 260]. Currently there are many consortiums and work groups dedicated to MBDD (e.g. Modelling and Simulation Working Group (MSWG) [261], International Society of Pharmacovigilance (ISOP)) and the large pharmaceutical industry has decades of effort applying quantitative analysis to improve drug dose and regimen selection for small molecule drugs.

The main applications of PK/PD modelling to drug development are in the following areas.

#### *Translation of drug dynamics between species and "first-in-man" dose selection*

Animal experiments are first conducted to understand the concentration and toxicology of the active drug components in the relevant regions of the body. This data is used to parameterise PK/PD models and establish differences in response dynamics by dose or regimen. Here, model simulation can be used to optimise the design of animal experiments to gain the most information with the least use of resources, thus improving the efficiency of pre-clinical testing phase. By applying allometric scaling (based on information on physiological scaling due to body mass, variation in metabolic pathway across species or major anatomical differences [262-264]), of the model parameters an estimation of the doses needed to obtain similar exposure in humans is then derived. For examples see [265, 266]. Allometric scaling is also used within species, for example in humans allometry is applied to

common PK parameters such as volume of distribution, absorption and clearance of the drug by the host's weight, (e.g. for the drug Isoniazid e.g.[267]).

### *Clinical Trial Simulation*

Model-based trial simulation is an important tool in drug development to explore drug effects without empirical testing. In drug trials, simulation studies can help determine key aspects such as the bounds of the dose response curve in a dose escalation simulation [268], important for proof-of-concept studies and regimen of drug administration. In the later stages of development, confirmatory studies can be fully simulated [256, 269]. As more data becomes available, PK/PD models can be used iteratively to refine these simulation estimates, aiding in a reduction of the total number of subjects required to establish the desired confidence intervals, thus minimizing potential harm. As an example, modelling was able to systematically assess the different doses and protocols to derive optimal values for TB drug treatments, which previously had never been formally compared [270-272].

### *Identifying important subpopulations and personalised medicine*

Identification of which population covariates cause substantial variability in model parameters can help drug developers to adapt dose or dose regimen to maintain safe, effective responses in those populations [251, 273-275]. Personalised medicine is an extension to this. Personalised medicine aims to provide individuals with drug dose and regimen optimised based on their characteristics [276]. It is thought, by personalizing medicine to fit an individual would increase adherence rates as the drug is more likely to be safe and effective [277]. Predictions from large scale individual-based PK/PD models have been shown to improve treatment in individual cancer patients [278, 279].

In summary, model based drug development is used to explore drug host interaction; test and confirm ranges of safe drug doses by directly translating information from animal experiments to first-in-human trials; modify regimens to specific subpopulations of individuals and evaluate appropriate study design to reduce numbers of required participants and thus exposure to the drug.

## ***Model-based drug development (MBDD) methods***

### *Statistical curve models*

Statistical curves are regularly used in MBDD to describe drug simple pharmacokinetics [280] and pharmacodynamics [281] (e.g. Emax equations). These parametric, analytical models have the benefit of being potentially simple (minimal parameters). However, these curves focus entirely on describing the *shape* of the response data over time with no consideration of underlying biological mechanism. This presents limitations if the aim is to make inferences on the differences in response biology by subpopulation, for example.

### *Mechanistic models*

The second method is to use a mechanistic compartmental differential equation model to represent drug pharmacokinetics [250]. This approach provides biological, mechanistic understanding of the longitudinal response to drug exposure by using model compartments and differential equations to describe the change in response over time [282]. The method seeks to establish how population covariates effects the model parameters and the potential biological reasons for this. More complex drug responses could be incorporated in a network mechanistic model (with separate models to represent different organs or cells, e.g.). Integrating complex interdependent responses would be less intuitive with a statistical curve model. However, the complexity involved in representation of biological mechanism could potentially be a disadvantage. A mechanistic model may require additional model parameters (and thus, degrees of freedom) compared to the simpler statistical curve model.

### *Nonlinear Mixed Effects Modelling*

To calibrate mathematical models representing PK and PD of a drug course, the method of nonlinear mixed effects modelling (NLMEM) is regularly employed [283]. NLMEM is used to estimate the parameters of mathematical models designed to represent the drug dynamics at individual and (sub)population level'. Quantifying the variance of drug dynamics in a

population is essential to avoid either sub-therapeutic or toxic exposure to the drug to those individuals with widely varying responses.

A brief description of the aims of NLMEM are outlined here, methods and implementation of NLMEM employed in this thesis are outlined in appendix B. For a more general and technically in-depth explanation of NLMEM and its implementation see [250, 252, 280, 284].

#### *Nonlinear Mixed Effects Modelling (NLMEM) aims*

Nonlinear Mixed Effects Modelling (NLMEM) is a statistical framework which combines a mathematical or statistical model to describe the longitudinal response data over time and statistical models to capture variation in the mathematical model parameters due to multiple individual responses in a population. Using NLMEM inferences can be made about the variation in response across a population when population covariate analysis is conducted [284, 285].

The main aims of NLMEM are [252]:

1. To estimate the parameters of the mathematical model that describe the population typical response dynamics over time
2. Estimate the variation around the population average dynamics as a result of individuals in the population (inter-individual variation) as thus estimate the individual responses
3. Establish residual variation between model prediction and response data (intra-individual variation)
4. Assess the effect of population covariates on the population typical dynamics (mathematical model parameters) and associated variation (statistical model parameters)

Due to the nested levels of variation (intra-individual and inter-individual variation), NLMEM is also known as hierarchical nonlinear modelling or nested hierarchical nonlinear modelling [284]. Nonlinear refers to the nonlinearity in the relationship of the host response to the drug (or vaccine), represented by the mathematical model. Mould et. al. give the following

definition of fixed and random-effects: “‘Mixed-effects’ refers to the [model] parameterization: parameters that do not vary across individuals are referred to as ‘fixed effects’, parameters that vary across individuals are called ‘random effects.’” The term ‘mixed effects’ refers to the combination of fixed and random effects in the NLMEM framework.

NLMEM employs maximum likelihood based methods to estimate the population and individual parameters; further details on these methods and implementation in available software are outlined in Appendix B.

### **Thesis Rationale: Model-based vaccine development – Vaccine Immunostimulation/Immunodynamic modelling**

There are valid reasons as to why current empirical vaccine development methods might be leading to mistakes in dose decision making. For example, thorough evaluation of the dose-dependent immune response dynamics is not currently undertaken in current vaccine development and as a result, is not fully understood. This is leading to unexpected dose response relationships such as the H-series TB vaccine highlighted above, essentially being missed. These errors in vaccine dose decision making may be occurring partly because translating vaccine responses from animal studies to humans is challenging as response dynamics are not fully understood and a tool to translate responses from a representative animal model is required. More systematic approaches to vaccine development should be used to avoid these mistakes.

#### ***Vaccine Immunostimulation/Immunodynamic modelling***

I intend to develop mechanistic mathematical models to represent vaccine immune response dynamics, translate vaccine responses between the animal and human to make better predictions for human vaccine dosage.

To reflect the similarities in my methods to that of PK/PD modelling, I introduce this type of modelling as vaccine *Immunostimulation/Immunodynamic (IS/ID) modelling*. Analogous to population PK/PD modelling, population vaccine IS/ID modelling uses mathematical models

in a statistical framework to explore population typical vaccine responses and the variation in response due to individuals. Vaccine IS/ID models describe the immune response stimulation (IS) that produce the measured immune response dynamics (ID) following vaccination. Mathematical models representing the immune response to infection and vaccination, that could be considered suitable IS/ID models exist (e.g. [286, 287] and see literature review for TB specific models), but as far as I am aware, no such models have been incorporated into a PK/PD style framework to inform vaccine species translation and dose prediction.

To demonstrate the potential utility of IS/ID methods, I apply them to IFN- $\gamma$  immunogenicity data from the H-series TB vaccine. As discussed, these vaccines are currently in the pipeline and previous mistakes may have been made in dosing, therefore the implementation of mathematical modelling to TB vaccine dosing data could have an immediate impact on further development.

### ***TB immune response mathematical modelling: literature review***

To investigate the current work on TB immune response modelling, a literature review in the Pubmed database was conducted on the topic. I did not confine the search to “vaccine immune response to TB” as this search yielded limited results. Instead, I used the search terms “Tuberculosis” or “TB” and “mathematical model\*” and “immun\*” in all fields. The flowchart in Figure 1.3 depicts the literature review process in which 30 publications were found, 5 of which were excluded for reasons outlined in Figure 1.3, leaving 25 publications for the review.

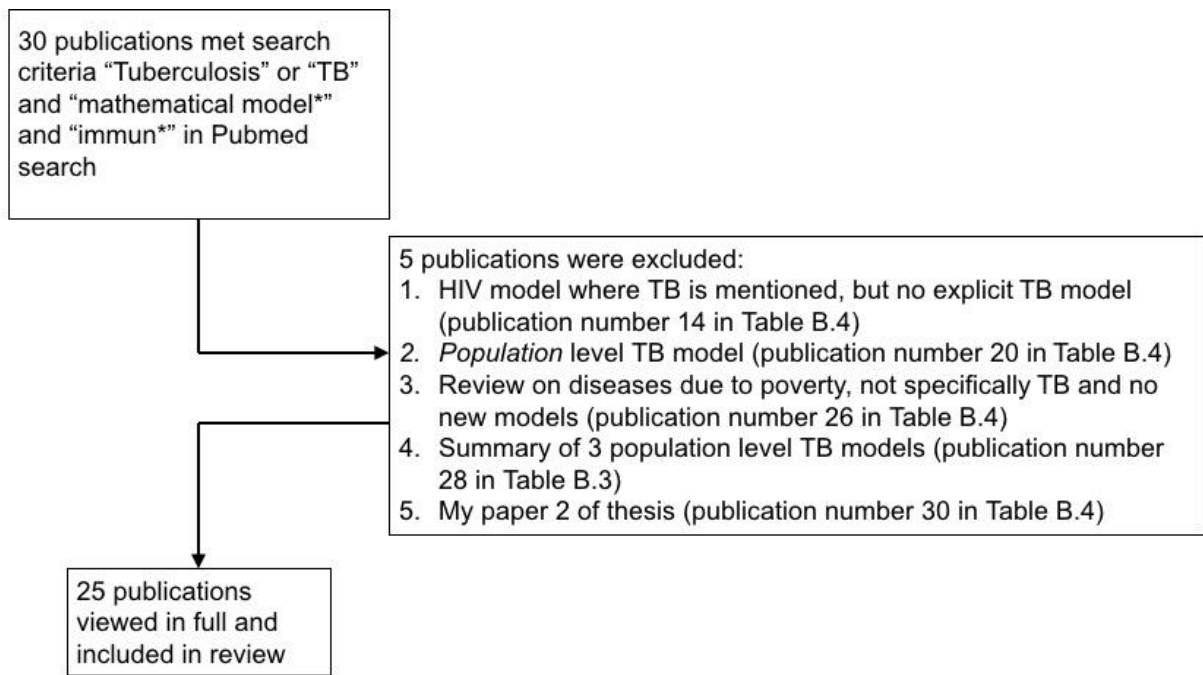


**Figure 1.3** Flowchart of the literature review process using the search terms

Table B.4 in appendix B outlines the aims, model structure, interventions (e.g. initiation of TB drug treatment) and main findings.

#### *Aims of previous TB immune response modelling publications*

For 18/25 publications, the primary aim was to build models to simulate an immune response to *Mtb.* infection [53, 60, 288-303]. In 11 of these, the secondary aims were to detect the parameters within the model that influence the state of TB disease (latent or active) by sensitivity analysis or virtual experiments [53, 60, 288-296]. Five of these publications (the majority authored by Marino and Kirschner) focussed specifically on developing models of the lung and lymph node then extending these models to investigate specific elements of the immune response and their influence on disease state [53, 291, 292, 296, 297]. A further five publications focussed on the immune response in a granuloma formation and the conditions in which *Mtb.* infection can be successfully contained [297-301]. An early work by Denise Kirschner focussed on the interplay of immune response between HIV and *Mtb.* infection [302] and Ray et. al. aimed to investigate the intracellular mechanisms of macrophage activation [303].

5/25 publications aimed to model the dynamics of *Mtb.* itself; the dynamics of bacteria replication and death, the conditions required for bacteria transition between active and latent states and the effect of TB drugs on drug sensitive and resistant strains [304-308].

2/25 publications used a PK/PD model to establish regimen of the TB drug, Rifampin, in mice [309, 310].

### *Data*

In the majority of publications, data were used to aid parameterisation of the models. Six publications calibrated models to longitudinal immune response data [292, 296, 299, 308-310]. Calibration methods included nonlinear least squares with Latin Hypercube Sampling (LHS) of the model parameters [292], multiple linear regressions to data for different time ranges [308] and Bayesian Markov chain Monte Carlo (MCMC) procedures [309, 310]. Six publications used experimental data from mice [53, 292, 299, 305, 308-310] and Datta et. al. used data from experiments in rabbits to parameterize the model [301]. In the remaining publications, parameterisation of the models was conducted using published experimental data, weighted towards those conducted in humans where possible.

### *Methods*

The majority of the publications used compartmental deterministic ordinary differential equation (ODE) models (19/25) [53, 60, 288, 289, 291-293, 295, 296, 300, 302-310], with the remaining incorporating two other types: Agent Based Models (ABMs) (2/25) [298, 299] and Spatio-temporal reaction-diffusion partial differential equation models (4/25) [290, 294, 297, 301]. Two publications used both ABMs and ODE models [300, 307].

14/18 publications whose aim it was to model the host immune response to *Mtb.* infection ([53, 60, 288-303]), included T cells, eight of those were CD4+ specific and four were CD4+ and CD8 specific. Macrophage cell populations featured in 16/18 publications, six of those included dendritic cells also. 9/18 included cytokine populations, all of which included IFN- $\gamma$  and three include chemokines. 17/18 of the publications investigating immune responses to *Mtb.* infection included a bacteria population(s), with all but one making the distinction between intra- (within macrophages) and extracellular bacteria. One publication did not

include any cells or bacteria and focussed that only on the oxygen concentration dispersion subject to different boundary conditions across varying layers of a granuloma [301].

In the publications that aimed to model the dynamics of *Mtb.* [304-308], all defined an “active” state of the *Mtb.* bacilli, whereby the bacteria were able to replicate. 4/5 also defined a “latent” state where replication was considerably slowed and three out of these had models for the concentrations of nutrients, iron, oxygen and/or Nitrous Oxide (NO) to explore the effects changes in host biochemistry on bacteria transition between the active and latent states.

Both publications who aimed to quantify Rifampin PK in mice, included a physiological based model of the concentration of Rifampin in 12 compartments of the mouse body (e.g. lung, brain, gut, etc.) (Lyons et. al. 2013, 2015) [309, 310]. The later publication by these authors added an immune response model including CD4+ and CD8 T cells, macrophages and bacteria and a PD model [310].

#### *Model outcomes representing TB disease*

For those models that included extracellular bacteria, active TB disease was defined as when the extracellular bacteria increased to high levels and did not appear to be saturating or controlled by the immune response [53, 60, 288-300, 302, 310]. Conversely, latent TB disease was established when intracellular bacteria counts reached a constant low level over time and extracellular bacteria was eliminated or remained at a very low level. Ray et. al. represented bacteria killing that results in elimination of disease by monitoring NO levels producing by macrophages in the model [303]. Granuloma outcomes associated with control of *Mtb.* infection included; bacteria count with the granuloma [297-300], granuloma size and amount of diseased tissue or necrosis [297, 298, 300], absence of infected macrophages [298], TNF- $\alpha$  [300] and oxygen concentration [301]. Persistence of the active *Mtb.* bacteria versus latent state bacteria was considered indicative of TB disease in models by Pedruzzi et. al., Magombedze et. al., Chisholm et. al. and McDaniel et. al. [305-308]. Alavez-Ramirez et. al. focus more on the progression of bacteria toward antibiotic resistance [304].

#### *Interventions*

Six publications used cytokine “depletion and deletion” experiments. These can be thought of as virtual experiment, designed to mimic “knock-out” experiments in laboratory settings. They are useful in suggesting which immune response elements are the strongest predictors of latency or active disease [60, 289, 291-293, 303]. Model parameter perturbations featured in ten of the publications [290, 294-299, 305, 306, 308] with the aim of assessing the effect on disease outcome of interest due to; changes in bacteria growth or kill (by macrophages) rate [290, 308], infection rate of macrophages [295] or increased immune response “strength”, which was considered to be; differing concentrations of nutrients, oxygen and NO produced by immune cells and the environment surrounding the bacteria [305] and changes in chemokine signalling strength [297, 299]. Additionally, perturbation of multiple key (or all) parameters using LHS was conducted to systematically explore the parameter space and its correlation with disease outcome [294, 298, 306]. Seven publications introduced TB drug interventions [291, 293, 296, 297, 300, 302, 304] by manipulating appropriate parameters such as; decreasing growth rate or increasing kill rate of bacteria [302, 304], increasing innate cell recruitment [291], decreasing the rate pro-inflammatory cytokine production [297, 300] or decreasing the rate of TNF- $\alpha$  production (to assess stability of granuloma formation after anti-TNF treatment) [293]. Two publications looked at TB drug dose fractionation. Experimental Rifampin concentration data at different doses in mice from [311-313] was used to calibrate models in the two PK/PD publications [309, 310]. Finally, vaccination as an intervention was considered by Sud et al. [60] by increasing memory T-cells (defined as T-cells with extended half-life) as an initial condition (when bacteria is introduced to the immune system in the model).

## Results

The main findings of the publications are summarised here:

- In all publications that modelled the immune response to *Mtb.* infection, both latent and active disease states were effectively established (using outcomes outlined above).
- Decreasing inflammatory cytokines (e.g. IFN- $\gamma$ ) led to less effective innate immune response performance and increased extracellular-bacterial load indicating active disease [289-291, 294, 295, 298].

- Inclusion of broader adaptive immune responses (e.g. CD8 helper and cytotoxic cells) contributed to more effective protection against active disease [60, 290].
- Interactions between innate and adaptive immune response timings between organs, i.e. cell trafficking were influential in the state of disease [53].

#### Granuloma specific results:

- A balance between inflammatory and regulatory cytokines led to avoidance of tissue damage and unstable granuloma formation [292, 293, 297, 300].
- Chemokine levels and distribution determine the formation of the granuloma, the stronger the signals, the more successful the granuloma [299].
- Only large granulomas can achieve a necrotic core [297, 301].

#### Bacteria specific results

- Persistence of bacteria is a result of latent state (where the gain from latency and therefore survival against immune responses outweighs the loss of transmission opportunities [307]) and slow replication [288, 299, 308].
- Level of Nitrus oxide was most influential on the stability of the system (i.e. controlled bacterial growth) [306] and the ability of the bacteria to disrupt iron production by the host ensured its survival and persistence [306].

#### Intervention specific results:

- HIV infection exacerbates *Mtb.* load, however, treatment of TB can have a profound effect on HIV as T cell counts improve after TB treatment initiation [302].
- By varying combinations of Th1 CD4+ and CD8+ T-cells, the model showed that a vaccine that jointly increased CD4+ and cytotoxic CD8+ memory T-cells was most effective at clearing bacteria once challenged [60].
- Early treatment and a less aggressive adaptive immune response is most affective to kill bacteria in the granuloma [297, 300].
- When drugs administered, a biphasic bacteria kill curve observed, firstly due to drug, secondly to macrophage activation. This reflects clinical data [296].

- PK/PD simulations agreed with Rifampin concentrations and bacteria killing in mice. Area under the concentration-time curve most correlated with Rifampin efficacy [310].

### *Publication Conclusions*

Each publication drew specific conclusions that reflected their own results, here I outline the overarching, common conclusions drawn by all publications.

It was acknowledged by many of the publications that aimed to model the immune response to *Mtb.* infection, that a balance between inflammatory and regulatory immune responses was vital to contain bacteria, avoid TB disease and damage to host lung tissue [60, 289, 292-295, 302]. Further to this, Clarelli et. al. and Ibarguen-Mondragon et. al. emphasized that threshold values in the parameter space that pushed the system from latency to active disease needed to be empirically verified [294, 295]. Three publications suggest that strategies for the development of more effective therapeutics, i.e. drugs that stimulate innate processes [53, 291, 303]. Finally, although all publications use mathematical models to explore their aims a few authors highlight explicitly the use of models as tools to; understand the immunology of *Mtb.* infection [290], optimize drug treatment [296, 297, 301, 310], understand granulomas (specifically the spatial models) [298, 299] and understand bacteria progression from active to latent states [305, 308].

In conclusion, Wigginton and Sud [60, 289] suggest that “executable models enable manipulation of the immune system elements to mimic treatment, vaccine or the immune system becoming compromised”. The outcome of the immune response models helps us understand the complex interactions involved in the immune response and has implications for further research [289, 314].

### *Literature review summary*

The models covered in this literature review had three main aims, to investigate; the host immune response to *Mtb.* infection, bacteria transition between states and pharmacometrics of TB drugs. All models that included immune response processes were Th1 based, i.e. B cell and antibody populations were not included in any publication. Assumptions about the

immune response to *Mtb.* infection vary between the models in the review, generating a wide range of model complexity from highly parameterised ABM's [300] to ODE's with minimal compartments [295]. However, the main constituents were T cells, innate cells and bacteria. Publications concerned with only the dynamics of cells/cytokines over time were represented using ODE models, whereas, ABMs and spatial models were used to represent spatial-temporal constructs, i.e. the granuloma. In most cases, data were mostly used to parameterise the model, not to calibrate the model. The conclusions of the papers acknowledge modelling as an effective tool to accelerate knowledge around the TB immune response, the effect of intervention or immunosenescence. While I agree with this statement, I believe, especially in the case of modelling the effect of vaccination on the TB immune response (my focus in this thesis), these dynamics are still largely not understood, therefore results of this modelling should be further scrutinized.

### ***Summary of thesis data, IS/ID model and model calibration***

I use data on immune responses following vaccination with existing TB vaccine, BCG (aim 1) and candidate vaccines h-series, adjuvanted with IC31 (aim 2). The immune response I focussed on was the number of IFN- $\gamma$  secreting CD4+ T cells following. As mentioned previously, IFN- $\gamma$  secreted by CD4+ T cells are believed to be fundamental to a TB vaccine immune response [83]. As such, these responses are the current immunogenicity marker of choice in TB vaccine development. It is important to note from the outset that in aim 2 where my aim was to predict dose response curves, I use the terminology "most immunogenic", not "optimal" dose to make the distinction between a dose that elicits a high IFN- $\gamma$  response versus a dose that is the most protective. For specific information regarding the source of the data and laboratory methods used to generate it, see individual chapters. Only data from animals and humans who are not latently infected are included, as such we consider the two TB vaccines to be pre-exposure vaccines in this thesis. BCG is used in this way, as it is routinely given at birth in endemic countries [315]. However, H56 was originally designed as a post-exposure vaccine [232], nevertheless, it was tested in healthy adults with no latent infection, the data of which we use here. Data sample sizes, demographic data as well as vaccine dose and regimen (timing of vaccinations) are outlined in the relevant chapters.

The T cell mathematical IS/ID model structure used in this thesis represents the dynamics of these responses. The models in the above review concerned with immune cell dynamics, specifically those including T cells were used to inform the structure of the IS/ID model used here. However, as I only had data on number of CD4+ T cells secreting IFN- $\gamma$ , my model was simpler than the majority of models outlined above, despite this, the fundamental dynamics are the same. Alongside the literature review, I took expert advice from supervisory and advisory panel members (Dr. Helen Fletcher, Prof Richard White, Dr Thomas Evans, Dr. Gwenan Knight and Prof. Denise Kirschner) as well as influential publications on T cell mechanism (focusing on CD4+) [81, 286, 287, 316, 317].

To calibrate the mathematical model to longitudinal vaccine response data and establish differences in model predictions due to subpopulations, I used the method of Nonlinear Mixed Effects Modelling (NLMEM) outlined above and in Appendix B. I implemented NLMEM in the software Monolix, a software commonly used in PK/PD modelling, developed by Lixoft, Paris [318], the implementation requirements for Monolix are also outlined in Appendix B.

### **Thesis Aims and Objectives**

**The overall purpose of this thesis was to develop a mathematical modelling framework to translate TB vaccine response between species and predict the most immunogenic dose in humans using animal data.**

There were two aims of the thesis.

1. Establish individual human response differences to the TB vaccine Bacillus Calmette–Guérin (BCG) Interferon-Gamma (IFN- $\gamma$ ) then develop an IS/ID model to represent these response dynamics and identify the most representative macaque subpopulation for human BCG responses
2. Predict the human H-series vaccine IFN- $\gamma$  response using an IS/ID model calibrated to mouse multi-dose IFN- $\gamma$  data using an allometric scaling assumption.

The aims of the thesis were achieved using the following objectives:

Aim 1:

1. Preliminary data analysis of differences in human IFN- $\gamma$  response to BCG
2. Development of the mechanistic IS/ID model to describe IFN- $\gamma$  response dynamics and application of the model to human BCG data to establish differences in IFN- $\gamma$  response dynamics (if any) by human subpopulation
3. Application of the mechanistic model to macaque BCG IFN- $\gamma$  response data to establish differences in IFN- $\gamma$  response dynamics by subpopulation
4. Comparison of the IS/ID modelling results between macaque and human to establish most representative macaque for humans in terms of IFN- $\gamma$  responses

Aim 2:

5. Generation of IFN- $\gamma$  response data to multi-dose of the TB vaccine, H56+IC31, in mice and assessment of dose response curve in mice for varying time points
6. Development of a revaccination model and calibration of the IS/ID model to mouse IFN- $\gamma$  response data (stratified by dose) and human H56/H1+IC31 IFN- $\gamma$  response data
7. Mapping of the changes in IFN- $\gamma$  response dynamics across the doses in H56+IC31 in mice
8. Prediction of the human immune response to other H56/H1+IC31 doses using a proposed mouse to human allometric dose scaling factor and mapping in objective 7

**Thesis overview**

Figures 1.4 and 1.5 outline aim 1 and 2 of the thesis, respectively, the objectives to achieving these aims, how the objectives align with the thesis chapters, research papers, and the data and methods required to completing the objectives.

## Aim 1

Aim: Develop a mathematical model to represent the T cell dynamics following BCG vaccination to establish differences in BCG immune response dynamics in humans and macaques and compare model predictions between human and macaque subpopulation

## Objectives

**Objective 1**  
Preliminary data analysis of differences in human immune response to BCG

**Objective 2**  
Development of the mechanistic model to describe the BCG immune response and application to human BCG data to establish differences in response dynamics by subpopulation

**Objective 3**  
Application of the mechanistic model to the macaque BCG data to establish differences dynamics by subpopulation

**Objective 4**  
Comparison of the mathematical modelling results between macaque and human

## Chapters

**Chapter 2**  
Exploration into the immune response to BCG vaccination in a heterogeneous human population

**Chapter 3**  
Exploration into the immune response to BCG vaccination in a heterogeneous human and macaque population using an Immunostimulation/Immunodynamic (IS/ID) mathematical model and the predictive power between macaque and human data

## Papers

**Paper 1**  
Individual-level factors associated with variation in Mycobacterial-specific immune response: gender and previous BCG vaccination status

**Paper 2**  
Using Data from Macaques to Predict Gamma Interferon Responses after Mycobacterium bovis BCG Vaccination in Humans: A Proof-of-Concept Study of Immunostimulation/Immunodynamic Modeling Methods

## Data

Longitudinal BCG IFN- $\gamma$  responses (number of CD4 T cells, ELISPOT) in humans after one dose and one vaccination and human population covariates (secondary data)

Longitudinal BCG IFN- $\gamma$  responses (number of CD4 T cells, ELISPOT) in macaques after one dose and one vaccination and macaque population covariates (secondary data)

No additional data required

## Methods

Linear regression models to determine which population covariates significantly correlated with key immune response estimates

Mathematical model to the T cell dynamics following vaccination calibrated to the human and macaque data using Nonlinear Mixed Effects Modelling to determine model parameter estimates for human and macaque subpopulations

Calibration of the macaque subpopulation model predictions to the human data and assessment of best fit using goodness of fit measures

Figure 1.4. Aim 1 of the thesis with corresponding objectives thesis chapters, papers, data requirements and methods

## Aim 2

Aim: Adapt the mathematical model to represent the T cell dynamics following two vaccinations with H-series vaccine and calibrate to multi-dose data in mice to establish differences in the immune response dynamics by dose and predict the human multi-dose immune response dynamics using the mouse model predictions.

### Objectives

#### Objective 5

Generation of immune response data to multi-dose of H56+IC31 in mice and assessment of dose response curve in mice for varying time points

#### Objective 6

Development of a revaccination model and calibration of the model to mouse immune response data (stratified by dose) and human H56/H1+IC31 immune response data

#### Objective 7

Mapping of the immune response using allometric scaling from one dose of H56+IC31 in mouse to human

#### Objective 8

Prediction of the human immune response to other H56/H1+IC31 doses using mapping and assessment of most immunogenic dose at late time point

### Chapters

#### Chapter 4

Generation of immune response data to multi-dose of H56+IC31 in mice for the application of Immunostimulation/Immunodynamic (IS/ID) modelling

#### Chapter 5

Predicting human multi-dose immune responses to H series vaccination using multi-dose data in mice and an Immunostimulation/Immunodynamic (IS/ID) modelling

### Papers

#### Paper 3

The TB vaccine H56+IC31 dose-response curve is peaked not saturating: data generation for new mathematical modelling methods to inform vaccine dose decisions

#### Paper 4

Animal dose response curve predicts lower optimal TB vaccine dose in humans: A proof-of-concept study of Immunostimulation/Immunodynamic modelling methods to inform vaccine dose decision-making

### Data

Longitudinal H56+IC31 IFN- $\gamma$  responses (number of CD4 T cells, ELISPOT) in mice after five dose (plus 0 dose) and two vaccinations (primary data – results of objective 5)  
Longitudinal H56 and H1+IC31 (pooled) IFN- $\gamma$  responses (number of CD4 T cells, ELISPOT) in humans after one dose and two vaccinations (secondary data)

Data on allometric scaling for H series vaccine

No additional data required

### Methods

ELISPOT assay on mouse splenocytes after two vaccinations (day 0 and 15) with H56+IC31 for 5 different doses (plus 0 dose). Sampled over eight time points from day 0 to 56 (5 mice per dose per time point)

Mathematical model to the T cell dynamics following two vaccinations calibrated to the mouse multi-dose and human single-dose data using Nonlinear Mixed Effects Modelling.

Comparison of model parameter estimates for each dose in mice and using allometric scaling data, mapping model parameter estimates from one dose in mice to the equivalent dose in humans

Prediction of human immune responses to multi doses using mapping in objective 7.

Figure 1.5. Aim 2 of the thesis with corresponding objectives thesis chapters, papers, data requirements and methods

There are six chapters in this thesis. Chapter one provides a detailed background to the thesis. Issues arising in the qualitative nature of current vaccine development are outlined and an example of a current vaccine for TB, whose dose choice could be misinformed, is presented. I then contrast vaccine development methods to the quantitative methods employed in drug development. The new field of quantitative IS/ID modelling for vaccine development is then presented. The final sections of chapter one is a literature review on current TB immune response models, proposed aims for the thesis and this review.

Chapters two to five are research papers, three of which are published and one is under review at the time of writing. Research paper chapters include firstly an introduction, then the paper, followed by the corresponding supplementary material which is referenced throughout the paper. Any other unpublished work that is relevant to the thesis is included in the chapter introduction. The thesis concludes with a discussion of the findings and future areas of research. A final perspective article was written, but was not included in the thesis as a specific chapter; instead the contents were included in the background and discussion chapters.

I would like the reader to be aware that each paper was written as a standalone article, and as such, there is some repetition of information. I have endeavoured to keep terminology consistent throughout the papers, but due to variation in journal specifications differences in terminology may exist. The papers are presented in an order conducive to the two aims of the thesis (Figures 1.4 and 1.5), which may not be in temporal order of publication. References for the thesis body and supplementary material for each chapter are at the end of the thesis main body. Each paper has its own set of references as does the appendix.

Chapter 2 is a **research paper** (paper 1) exploring the immune response to BCG vaccination in a heterogeneous human population.

Main objectives of the paper:

- To consider how individual-level factors affect BCG immunogenicity as measured by tuberculin purified protein derivative (PPD) stimulated interferon gamma (IFN- $\gamma$ ) response following vaccination, focusing on long-term responses and short-term dynamics.

This chapter corresponds to aim 1 and objective 1 of the thesis (see Figure 1.4).

Citation: **Rhodes SJ, Knight GM, Fielding K, Scriba TJ, Pathan AA, McShane H, Fletcher H, White RG. 2016.** *Individual-level factors associated with variation in mycobacterial-specific immune response: Gender and previous BCG vaccination status.* Tuberculosis (Edinb) **96**:37-43.

Chapter 3 is a **research paper** (paper 2) exploring the immune response to BCG vaccination in a heterogeneous human and macaque population using a mathematical model. Further, it considers and which macaque subpopulation best predicts human IFN- $\gamma$  response.

Main objectives of the paper:

- Develop a model of post-BCG vaccination, IFN- $\gamma$  producing CD4+ T cell dynamics, and assess the suitability of the model structure to predict responses by calibrating to data.
- Investigate the impact of the human and macaque population covariates to explain the within-population variation in responses.
- Test which macaque subpopulation best predicts human IFN- $\gamma$  response

This chapter corresponds to aim 1 and objectives 2-4 of the thesis (see Figure 1.4).

Citation: **Rhodes SJ, Sarfas C, Knight GM, White A, Pathan AA, McShane H, Evans TG, Fletcher H, Sharpe S, White RG. 2017.** *Using Data from Macaques to Predict Gamma Interferon Responses after Mycobacterium bovis BCG Vaccination in Humans: A Proof-of-Concept Study of Immunostimulation/Immunodynamic Modeling Methods.* Clin Vaccine Immunol doi:10.1128/CVI.00525-16.

Chapter 4 is a **research paper** (paper 3) outlining the generation of immune response data to multi-dose of H56+IC31 in mice for the application of mathematical modelling.

Main objectives of the paper:

- Generate longitudinal response data in mice for a wide range of H56+IC31 doses for use in future mathematical modelling
- Test whether a 'saturating' or 'peaked' dose-response curve, better fit the empirical data.

This chapter corresponds to aim 2 and objective 5 of the thesis (see Figure 1.4).

Citation: **Rhodes SJ, Zelmer A, Knight GM, Prabowo SA, Stockdale L, Evans TG, Lindenstrom T, White RG, Fletcher H.** 2016. *The TB vaccine H56+IC31 dose-response curve is peaked not saturating: Data generation for new mathematical modelling methods to inform vaccine dose decisions.* *Vaccine* **34**:6285-6291.

Chapter 5 is a **research paper** (paper 4) predicting human multi-dose immune responses to H-series vaccination using multi-dose data in mice and mathematical modelling.

Main objectives:

- Develop a mathematical model of the IFN- $\gamma$  producing CD4+ T cell dynamics following primary and revaccination with the H56+IC31 vaccine
- Calibrate the model to the mouse H56+IC31 multi-dose data
- Calibrate the model to the human H-series (H56/H1+IC31 pooled) data
- Predict the human immune response dynamics and establish the most immunogenic dose in humans.

This chapter corresponds to aim 2 and objectives 6-8 of the thesis (see Figure 1.4).

Citation: **Rhodes SJ, Guedj J, Lindenstrom T, Fletcher H, Evans TG, Knight GM White RG.** *Animal dose response curve predicts lower optimal TB vaccine dose in humans: A proof-of-concept study of Immunostimulation/Immunodynamic modelling methods to inform vaccine dose decision-making* (submitted)

A perspective article with the citation: **Rhodes SJ, Knight GM, Kirschner D, White RG, Evans TG.** *Dose finding for new vaccines: the role for immunostimulation/immunodynamic modelling* (in review at *Vaccine*), was written during the thesis (paper 5). Contents from this paper are included in the background and discussion of the thesis. I would like to acknowledge Dr Steven Kern for his input to this paper. The paper and description of author contributions can be found in Appendix A.

### **Author contributions**

The overall idea for the PhD project to apply mathematical modelling to vaccine development was generated by Dr Thomas Evans and Prof Richard White. Author contributions for papers 1-4 (as well as the supplementary material) are outlined in the associated chapters.

## **Funding**

This PhD project was funded through a studentship granted by Aeras (a tuberculosis vaccine development organisation) awarded before I started working on the PhD project. The mouse experiment in chapter 4 was funded by a separate grant from the Bill and Melinda Gates Foundation, on which I was co-applicant.

## Chapter 2. Exploration into the immune response to BCG vaccination in a heterogeneous human population: Paper 1

### Chapter 2 introduction

The objective of paper 1 was to conduct a preliminary exploration into the differences in BCG-induced IFN- $\gamma$  immune responses across human subpopulations to account for differences in BCG across individuals. This work addresses aim 1, objective 1 of the thesis (Figure 1.4).

I chose BCG to study as, not only is it the only licensed vaccine against TB disease, it is the basis for booster vaccines now in the developmental pipeline (see Figure 1.2). Data were readily available to my group as supervisory member Dr Helen Fletcher and colleagues (McShane et al.) at the Jenner Institute (Oxford university) had recently conducted immunogenicity trials on TB viral vector vaccine expressing *Mtb.* antigen 85A (MVA-85A) [319] where BCG was regularly used as a control arm. As such, I was able to combine BCG data from multiple MVA-85A trials (referenced in paper 1) to create a BCG longitudinal dataset. As all BCG data included in my dataset were generated by the Jenner Institute, lab assays and protocols were standardized across all trial sites (in UK and Africa).

I analysed the effect of population covariates on BCG-induced IFN- $\gamma$  responses retrospectively, using trial baseline responses as an indicator of long-term responses before BCG was administered in the trials (analysis 1) and prospectively using short-term longitudinal data after BCG vaccination in the trials (analysis 2). I used methods of summarising the data that are conventional in vaccine development when assessing longitudinal responses, i.e. summary measures (Area Under the Curve (AUC)) or point estimates of interest (peak responses, late responses) and applied regression to account for differences by population covariate. This preliminary analysis on differences in IFN- $\gamma$  immune responses was conducted in preparation for the calibration of an IS/ID model to the data.

I presented the work in paper 1 in poster form at the following conference:

- Keystone Symposium: **Host Response in Tuberculosis**, Santa Fe, USA, January 2015.  
“Impacts of key individual-level factors on the variation in Mycobacterium

tuberculosis-specific immune response” **S. J. Rhodes**, G. M. Knight, K. L. Fielding, T. J. Scriba, A. A. Pathan, H. McShane, H. A. Fletcher, R. G. White

Registry  
T: +44(0)20 7299 4646  
F: +44(0)20 7299 4656  
E: registry@lshtm.ac.uk

## RESEARCH PAPER COVER SHEET

PLEASE NOTE THAT A COVER SHEET MUST BE COMPLETED FOR EACH RESEARCH PAPER INCLUDED IN A THESIS.

### SECTION A – Student Details

Student	Sophie Rhodes
Principal Supervisor	Richard White
Thesis Title	The development of a mathematical modelling framework to translate TB vaccine response between species and predict the most immunogenic dose in humans using animal data

If the Research Paper has previously been published please complete Section B, if not please move to Section C

### SECTION B – Paper already published

Where was the work published?	Tuberculosis Journal		
When was the work published?	January 2016		
If the work was published prior to registration for your research degree, give a brief rationale for its inclusion			
Have you retained the copyright for the work?*	No	Was the work subject to academic peer review?	Yes

\*If yes, please attach evidence of retention. If no, or if the work is being included in its published format, please attach evidence of permission from the copyright holder (publisher or other author) to include this work.

### SECTION C – Prepared for publication, but not yet published

Where is the work intended to be published?	
Please list the paper's authors in the intended authorship order:	
Stage of publication	Choose an item.

### SECTION D – Multi-authored work

For multi-authored work, give full details of your role in the research included in the paper and in the preparation of the paper. (Attach a further sheet if necessary)	See next page
--	---------------

Student Signature: \_\_\_\_\_

Date: 13/6/17

Supervisor Signature:  \_\_\_\_\_

Date: 13/6/17 \_\_\_\_\_

**Paper 1 title: Individual-level factors associated with variation in mycobacterial-specific immune response: Gender and previous BCG vaccination status**

**Authors: Sophie J Rhodes, Gwenan M. Knight, Katherine Fielding, Thomas J. Scriba, Ansar A. Pathan, Helen McShane, Helen Fletcher\*, Richard G. White\***

**Author contribution:**

The human BCG data used in paper 1 were provided by Dr. Helen Fletcher, Prof. Helen Mcshane, Dr. Thomas Scriba and Dr. Ansar Pathan. These data were the control arms of clinical trials for the TB vaccine MVA-85A. Statistical analysis was conducted by myself with guidance from my supervisor committee members, modellers Prof. Richard White and Dr. Gwenan Knight and advisory panel member Dr. Katherine Fielding. All authors reviewed the paper. The interpretation of the results was my own work.

**Permission from copyright holder to include this work:**

ELSEVIER

SEARCH CART MENU

## Personal use

Authors can use their articles, in full or in part, for a wide range of scholarly, non-commercial purposes as outlined below:

- Use by an author in the author's classroom teaching (including distribution of copies, paper or electronic)
- Distribution of copies (including through e-mail) to known research colleagues for their personal use (but not for Commercial Use)
- Inclusion in a thesis or dissertation (provided that this is not to be published commercially)
- Use in a subsequent compilation of the author's works
- Extending the Article to book-length form
- Preparation of other derivative works (but not for Commercial Use)
- Otherwise using or re-using portions or excerpts in other works

These rights apply for all Elsevier authors who publish their article as either a subscription article or an open access article. In all cases we require that all Elsevier authors always include a full acknowledgement and, if appropriate, a link to the final published version hosted on Science Direct.

<https://www.elsevier.com/about/our-business/policies/copyright>



## IMMUNOLOGICAL ASPECTS

# Individual-level factors associated with variation in mycobacterial-specific immune response: Gender and previous BCG vaccination status



Sophie J. Rhodes <sup>a,\*</sup>, Gwenan M. Knight <sup>b</sup>, Katherine Fielding <sup>c</sup>, Thomas J. Scriba <sup>d</sup>, Ansar A. Pathan <sup>e</sup>, Helen McShane <sup>f</sup>, Helen Fletcher <sup>g,1</sup>, Richard G. White <sup>a,1</sup>

<sup>a</sup> TB Modelling Group, CMMID, TB Centre, London School of Hygiene and Tropical Medicine, UK

<sup>b</sup> National Institute for Health Research Health Protection Research Unit in Healthcare Associated Infection and Antimicrobial Resistance, Imperial College London, UK

<sup>c</sup> Infectious Disease Epidemiology Department, London School of Hygiene and Tropical Medicine, UK

<sup>d</sup> South African Tuberculosis Vaccine Initiative, Institute of Infectious Disease and Molecular Medicine and School of Child and Adolescent Health, University of Cape Town, Cape Town, South Africa

<sup>e</sup> College of Health and Life Sciences, Department of Life Sciences, Brunel University, UK

<sup>f</sup> The Jenner Institute, UK University, UK

<sup>g</sup> Immunology and Infection Department, London School of Hygiene and Tropical Medicine, UK

## ARTICLE INFO

## Article history:

Received 15 April 2015

Received in revised form

1 October 2015

Accepted 6 October 2015

## Keywords:

Tuberculosis

BCG

IFN- $\gamma$

Immune response

## SUMMARY

**Introduction:** A more effective tuberculosis (TB) vaccine is needed to eliminate TB disease. Many new vaccine candidates enhance the immunogenicity of the existing vaccine, Bacillus Calmette–Guérin (BCG). Understanding BCG induced immune variation is key to developing a new vaccine.

**Aims:** We aimed to establish if individual-level covariates were associated with cell-mediated immune response (interferon gamma (IFN- $\gamma$ )) at vaccine trial enrolment (baseline) in a long-term retrospective analysis (LTR) and after BCG vaccination in a short-term prospective analysis (STP).

**Methods:** Four covariates were analysed: gender, country, BCG vaccination history and monocyte/lymphocyte cell count ratio. Univariable and multivariable linear regression were conducted on IFN- $\gamma$  response at baseline for LTR, and area under the curve (AUC), 24 week and peak IFN- $\gamma$  response for STP.

**Results:** Previous BCG vaccination was strongly associated with higher IFN- $\gamma$  response at baseline (LTR analysis) ( $p$ -values < 0.05). Being male showed a weak association with higher baseline response ( $p$ -value = 0.1). BCG revaccination was strongly associated with a larger response increase than primary-vaccination (AUC & peak  $p$ -values < 0.01), but did not differ at 24 weeks (STP analysis). All other covariates were non-significant ( $p$ -values > 0.1).

**Conclusion:** This analysis suggests that previous BCG vaccination and gender are associated with durable IFN- $\gamma$  responses. Vaccine trials may need to stratify by BCG vaccination history and gender.

© 2015 The Authors. Published by Elsevier Ltd. This is an open access article under the CC BY-NC-ND license (<http://creativecommons.org/licenses/by-nc-nd/4.0/>).

## 1. Introduction

Tuberculosis disease (TB) caused by the organism *Mycobacterium tuberculosis* (*M.tb*), remains a substantial global health problem with approximately 9 million people developing active disease and 1.5 million TB-related deaths in 2013 [1]. This is despite nearly

70 years of widespread use of the only licensed TB vaccine, Bacillus Calmette–Guérin (BCG), a live attenuated strain of *Mycobacterium bovis*, which has exhibited variable efficacy [2]. Novel TB vaccines are considered an essential tool to meet the WHO goal of TB elimination by 2050 [3,4], and many candidates utilise a BCG prime-boost strategy.

It has been proposed that the observed variation in BCG efficacy could be attributed to individual-level factors that influence host mycobacterial-specific immune responses [5,6]. Factors that have been shown to be consistent in their influence of such responses include: latitude, which is known to be associated with varying

\* Corresponding author.

E-mail address: [sophie.rhodes@lshtm.ac.uk](mailto:sophie.rhodes@lshtm.ac.uk) (S.J. Rhodes).

<sup>1</sup> Joint senior authors.

exposure to non-tuberculous mycobacteria (NTM) [7], and *M.tb*-specific sensitization of the immune system through previous BCG vaccination [8]. Additional factors that have shown consistent influence include age at vaccination and BCG strain [5].

Another factor that may influence the mycobacterial-specific immune response is gender. TB prevalence surveys report a higher occurrence of disease in males than females [9], which is thought in part to be due to differences in the immune response between the sexes [10], in addition to social aspects [11]. However, so far, investigations into the effects of gender on the mycobacterial immune response have shown equivocal results [12,13] and few TB vaccine immunogenicity or efficacy trials have reported results stratified by gender.

In addition, recent evidence has shown that the ratio of host monocyte to lymphocytes cells (ML ratio) was associated with risk of TB disease [14–16]. Naranbhai et al. observed that in HIV positive, South African adults on combination antiretroviral therapy, this relationship was nonlinear, i.e. low and high, compared to moderate, ML ratios were associated with a higher risk of TB [14]. Little investigation has been made into how ML ratio may affect mycobacterial-specific immune responses and further insight into this relationship could potentially inform targeted TB vaccine strategies.

New detailed longitudinal immune response data to BCG vaccination has recently become available due to an increase in research into new TB vaccines in which BCG vaccination was used as a control [17]. These detailed data have the potential to give new insights into how individual-level factors alter the immune response to BCG.

Our aim was to consider how individual-level factors affect BCG immunogenicity as measured by tuberculin purified protein derivative (PPD) stimulated interferon gamma (IFN- $\gamma$ ) response following vaccination. Utilizing new immunological data allowed us to provide a more detailed analyses of the immune response than previous studies, which have focused on long-term responses with less detail of short-term dynamics.

## 2. Methods

In this study, two analyses were performed on data from participants included in new TB vaccine (BCG-booster) trials in which participants were given a new TB vaccine or BCG as a control measure. The data from the BCG control arms were used in this analysis.

Our first analysis aimed to determine which individual level covariates were associated with increased PPD antigen-specific IFN- $\gamma$  immune response at enrolment to the trials. In this analysis, IFN- $\gamma$  responses measured at enrolment to the trial (and before BCG vaccination was administered) is referred to as the 'baseline response'. This was a cross-sectional analysis of previously BCG vaccinated or BCG-naïve trial participants, and is referred to as the 'long-term retrospective' or 'LTR' analysis.

The second analysis aimed to determine which covariates were associated with IFN- $\gamma$  immune response over a short period, following BCG vaccination. This analysis was conducted using data from the prospective follow-up of study participants, who had either been revaccinated or primary-vaccinated with BCG immediately following baseline screening and were followed up for 24 weeks post vaccination. This is referred to as the 'short-term prospective' or 'STP' analysis.

### 2.1. Data and materials

In this study we used data from seven vaccine trials involving BCG (Table 1). The available data were on HIV negative and *M.tb*

naïve participants (see references in Table 1 for HIV and *M.tb* latency testing procedures). Data on haematological parameters were based on routine laboratory haematology testing at baseline and only those participants with values within normal limits were included in clinical trials.

IFN- $\gamma$  response was measured using a standardized ex vivo IFN- $\gamma$  Enzyme-Linked ImmunoSpot (ELISPOT) assay which quantifies IFN- $\gamma$  secreting CD4+ T cells as spot forming units (SFU) per million peripheral blood mononuclear cells (PBMCs) using PPD as a stimulant. The same ELISPOT method including plates, antibody kits, antigens, developing reagents, washing method, ELISPOT reader and ELISPOT counting method were used across all UK trials and all South African trials. South African researchers visited the UK laboratory for ELISPOT training and reagents for the ELISPOT assay were shipped from UK to South Africa for these studies. As these BCG studies were conducted as part of a series of Phase I clinical trials with MVA85A all lab protocols and lab reagents were harmonized as far as possible between UK trials and between UK and South African trial. For the exact laboratory methodology see [17–20].

### 2.2. Covariates

The four individual-level factors (covariates) included in this analysis were country (UK or South Africa), gender, BCG vaccination history at baseline and baseline ML ratio. ML ratio data were not available for three of the studies (two UK trials and the South African trial, Table 1). For details on how BCG-vaccination history was determined see original trial methods [17–20]. BCG vaccination history was categorised into "never" and 10 year time-periods since vaccination with the reference group as 1–9 years since BCG vaccination. Age was not included as a covariate as it was colinear with BCG vaccination history.

### 2.3. Statistical analysis

The analyses were performed using linear regression. Firstly, a univariable model analyses was conducted referred to as the 'unadjusted' analysis, followed by multivariable model; the 'fully adjusted' analysis. Analysis was conducted using R [21]. A  $p$ -value of  $\leq 0.05$  was considered as strong evidence for an association with the outcome.

All outcomes were log transformed (natural log) as data were right-skewed and the residuals verified to justify this transformation. The effect measures are the anti-logged regression slope parameters, the associated 95% confidence interval (CI) and  $p$ -value. For the categorical covariates (country, gender and BCG vaccination history), these represent the ratio of the geometric means (GM) of the IFN- $\gamma$  response outcome variable compared to the reference group. For the continuous covariate, ML ratio, the effect measure represents the increase in GM of the IFN- $\gamma$  response outcome variable for an increase in 0.1 ML ratio (as ML ratio is bound by zero and one), assuming a linear trend in ML ratio.

Additionally, due to previous research that found a nonlinear relationship to exist between ML ratio and risk of TB disease [14], both linear and quadratic regression models were fitted to establish if a similar relationship existed between IFN- $\gamma$  response and ML ratio (see Supplementary Material for example, Table S2). Analysis of variance (ANOVA) was used to assess if a non-linear relationship more adequately described this association.

#### 2.3.1. Long-term retrospective (LTR) outcome variables

Baseline IFN- $\gamma$  responses were used as the outcome variable in the long-term analysis. All four individual-level covariates were considered in the analysis. In the BCG vaccination history covariate,

**Table 1**

Demographic and trial information for participants included in long-term retrospective (LTR) and short-term prospective (STP) analyses. Trial information was split by BCG vaccine history where possible.

Vaccine trials no.	No. of participants	Country	Male (%)	Median age (IQR) years	Previous BCG vaccination (median years since (IQR))	Blood haematological: median (IQR) % of cells in whole blood		Median ML ratio (IQR)	Included in LTR/STP analysis	Reference
						Monocytes	Lymphocytes			
NCT00480688	11	UK	3 (27%)	25 (8.5)	None (NA)	0.30 (0.15)	1.76 (0.43)	0.20 (0.05)	LTR/STP	[17]
NCT00480714	6	UK	2 (33%)	25 (0)	None (NA)	0.36 (0.21)	1.90 (0.32)	0.19 (0.16)	LTR/STP	[17]
NA*	14	UK	4 (29%)	23.5 (9)	None (NA)	0.56 (0.18)	1.89 (0.41)	0.31 (0.18)	LTR/STP	[36]
	14		7 (50%)	23 (8.5)	Yes (15 (0.6))	0.57 (0.18)	1.66 (0.34)	0.29 (0.07)		
NCT00654316	13	UK	4 (29%)	25 (11)	Yes (12 (11))	0.34 (0.17)	1.53 (0.42)	0.24 (0.10)	LTR/STP	[18]
NCT00427453	10	UK	3 (30%)	24 (7.3)	None (NA)	NA	NA	NA	LTR	[19]
NCT00427830	15	UK	7 (47%)	27 (10.5)	Yes (21 (7))	NA	NA	NA	LTR	[17]
NCT00460590	4	South Africa	2 (50%)	40.5 (4.8)	None (NA)	NA	NA	NA	LTR	[20]
	14	Africa	3 (21%)	33.5 (12)	Yes (33.5 (12))	NA	NA	NA		
Aggregated	101	–	35 (35%)	26 (11)	21 (17.3)	0.41 (0.24)	1.70 (0.51)	0.22 (0.11)	–	–

\* Trial number was not available for this trial at time of analysis. Three participants from the first four trials (those included in both the LTR and STP analyses) did not have full STP data, so were only included in the LTR. NA = not available. IQR = Interquartile range; ML = Monocyte/lymphocyte.

the groups represent time since previous BCG vaccination with the group “never” representing those who were BCG naïve at baseline.

### 2.3.2. Short-term prospective (STP) outcome variables

To investigate the short-term response, IFN- $\gamma$  responses at baseline and 4, 8 and 24 weeks post BCG vaccination were used and summarized using the following three statistics as outcome variable: area under the curve (AUC), peak and the 24 week (referred to as ‘sustained’) IFN- $\gamma$  responses. The AUC summarises the total change in IFN- $\gamma$  response over 24 weeks post BCG vaccination and was calculated using the R package “Kulife” [22].

For the STP analysis, unadjusted and fully adjusted regression was conducted separately for the three outcomes. For the STP analysis, an additional analysis was also carried out for peak and 24 week response, whereby adjustment for baseline IFN- $\gamma$  responses was conducted, known as the ‘partially adjusted’ analysis. This was not adopted for the AUC outcome variable, as the AUC calculation is standardized by the baseline value, so adjustment for the effect is not necessary.

In the STP analysis, the categories defined for the BCG vaccination history covariate correspond to years since previous BCG vaccination before receiving BCG at enrolment into the trial. The group ‘never’, corresponds to being ‘primary vaccinated’ at

enrolment. As all trials used in the STP analysis were UK based, all individual-level covariates except country were included.

## 3. Results

101 participants were included in this analysis (Table 1). Seven vaccine clinical trials were used in the LTR analysis; four of those also had data available for the STP analysis (Table 1 and Table S1). Participants were either vaccinated with BCG (56 participants), at a median of 21 years (interquartile range (IQR) = 17.3) before baseline or BCG naïve at baseline (45 participants). The median of the ML ratio was 0.22 (IQR = 0.11). The distribution of ML ratio amongst the population can be found in Figure S1.

### 3.1. Long-term retrospective (LTR) analysis

All 101 participants were included in the LTR analysis. All covariates were included in the fully adjusted analysis, except for ML ratio as data on this measure were not available for some of the trials (data were only available for 58 participants (Table 1)).

For male participants, the unadjusted GM ratio of the IFN- $\gamma$  response at baseline was nearly twice that of females (GM ratio 1.97, 95% CI (1.03, 3.77)) (Table 2), and remained weakly associated

**Table 2**

Long-term retrospective (LTR) analysis: results of the linear regression analysis on baseline IFN- $\gamma$  responses (SFU/mill cells) against individual-level covariates.

Covariates (n)	Geometric mean of IFN- $\gamma$ response	Unadjusted GM ratio (95% CI), <i>p</i> -value	Fully adjusted* GM ratio (95% CI), <i>p</i> -value
Country			
South Africa (18)	65.62	1	1
UK (83)	47.56	0.73	1.02
		(0.32, 1.65), 0.63	(0.41, 2.55), 0.97
Gender			
Female (66)	39.82	1	1
Male (35)	78.45	1.97	1.76
		(1.03, 3.77), 0.04	(0.96, 3.25), 0.07
BCG vacc history			
1–9 yrs (8)	133.54	1	1
10–19 yrs (13)	121.28	0.91	0.74
		(0.25, 3.28)	(0.20, 2.70)
20–29 yrs (19)	80.58	0.60	0.57
		(0.18, 2.01)	(0.17, 1.93)
30 + yrs (12)	94.93	0.71	0.72
		(0.19, 2.62)	(0.17, 3.13)
Never (49)	24.27	0.18	0.18
		(0.06, 0.54), <0.001†	(0.06, 0.52), <0.001†
ML ratio (58)		0.89‡	–
		(0.58, 1.38), 0.61	–

As an example of the GM of the IFN- $\gamma$  response by ML ratio two values were chosen from the range of ML ratio (Table 1) to represent high and low values and the GM calculated using the unadjusted GM ratio value in the above table. As such, the GM for the IFN- $\gamma$  response for a ML ratio of 0.1 and 0.3 were 52.03 and 50.88, respectively. Abbreviations: IFN- $\gamma$  = Interferon gamma; vacc = vaccination; GM = geometric mean; yrs = years; ML = Monocyte/lymphocyte.

\* Adjusted for all variables in the model except ML ratio.

† *p*-value for all categories of BCG vaccination history covariate using an ANOVA summary.

‡ Represents the value of the change in GM of the IFN- $\gamma$  response for an increase in 0.1 of ML ratio.

after adjustment for country and years since BCG vaccination (GM ratio 1.76, 95% CI (0.96, 3.25)).

For BCG-naïve participants ('never'), a GM ratio of their IFN- $\gamma$  response at baseline of 0.18 (95% CI (0.06, 0.54)) was found, compared to that of the reference group of 1–9 years since BCG vaccination (Table 2) and remained strongly associated after full adjustment (GM ratio 0.18, 95% CI (0.06, 0.52)). GM IFN- $\gamma$  response was similar for 10–19, 20–29 and 30+ years since BCG vaccination, compared to 1–9 years since BCG vaccination (Table 2).

There was no evidence of an association between IFN- $\gamma$  response at baseline and ML ratio in the linear or quadratic analyses (Table 2, Table S2). Neither was there an association between IFN- $\gamma$  response and country (Table 2).

### 3.2. Short-term prospective (STP) analysis

Data from 55 participants, all UK adults, were available for the STP analysis. The IFN- $\gamma$  responses over the 24 week follow-up period, by primary or revaccination status, are shown in Figure 1.

All analyses (unadjusted, partially and fully adjusted) suggested there was no association between gender or ML ratio and AUC (Table 3), 24 week response (Table 4) or peak response (Table 5).

Being primary-vaccinated ('never' in Table 3) was strongly associated with a lower AUC in the unadjusted analysis with a GM ratio of 0.16 (95% CI (0.06, 0.44)) (Table 3 and Figure 1). This association remained strong after adjustment for baseline IFN- $\gamma$  response, gender and ML ratio (GM ratio 0.22, 95% CI (0.07, 0.68)). No other groups in the BCG vaccination history covariate were associated with AUC.

BCG vaccination history was strongly associated with 24 week response in the unadjusted analysis, specifically: primary-vaccinated participants had lower 24 week responses (GM ratio 0.14, 95% CI (0.06, 0.36)) ('never' in Table 4) compared to the reference group. After full adjustment, this association remained but was weaker (GM ratio 0.29, 95% CI (0.07, 1.12)). The partially adjusted analysis showed changes in the GM ratio for all covariates (Table 4). Most notably, the GM ratio for those who were primary

vaccinated increased from 0.14 (95% CI (0.06, 0.36)) to 0.25 (95% CI (0.09, 0.69)) compared to the reference group in the unadjusted and partially adjusted analyses, respectively.

Primary-vaccinated participants had lower peak IFN- $\gamma$  response compared to the reference group in the unadjusted analysis (GM ratio 0.24, 95% CI (0.14, 0.39)) (Table 5). This remained after full adjustment for all covariates (GM ratio 0.32, 95% CI (0.15, 0.68)) (Table 5). The partially adjusted analysis did not significantly change this value (GM ratio 0.29, 95% CI (0.16, 0.51)), indicating a minimal affect of baseline response on the association between BCG vaccination history and peak response (Table 5).

## 4. Discussion

We investigated the impact of multiple individual-level covariates on the mycobacterial-specific immune response pre- and post- BCG vaccination. Being male or previously BCG vaccinated was associated with higher IFN- $\gamma$  response at baseline. BCG revaccination resulted in a larger initial increase in immune response than primary-vaccinated participants, but response was not significantly different at 24 weeks. All other covariates (country and ML ratio) were non-significant.

Differences in TB disease notification rates between the genders have been well documented and are thought to be a result of both social and biological factors [10]. In our analysis we found a weak association between male gender and higher IFN- $\gamma$  levels at baseline in the long term retrospective (LTR) analysis. This could be linked to sex hormones causing differences in gender-associated immune responsiveness, specifically those of IFN- $\gamma$  [10,23]. Our results are consistent with previous studies that show women have significantly lower IFN- $\gamma$  response after PPD stimulation than men (after adjustment for age, BMI and *M.tb* infection) [13] as well as less strong tuberculin skin testing results [24]. However, these results remain somewhat surprising as reported disease incidence tends to be higher in men [9]. This could imply that disease burden differences may be due to behavioural, rather than biological, reasons or that a balanced immune response is

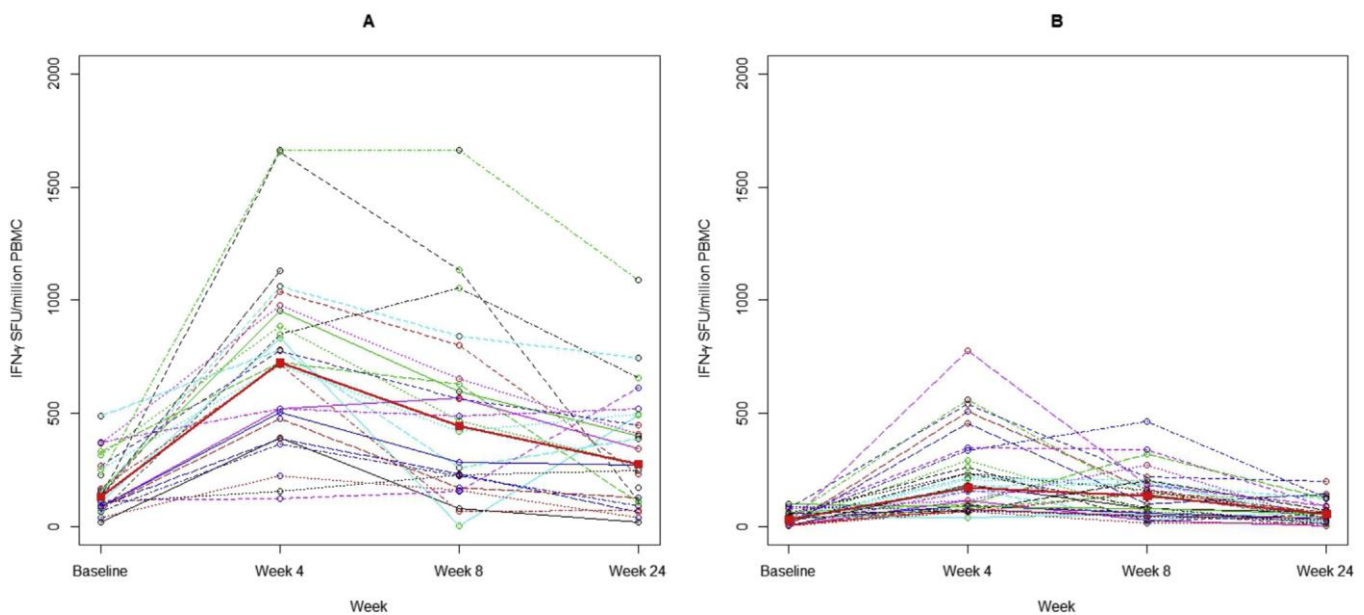


**Figure 1.** Longitudinal IFN- $\gamma$  responses for the Short-term prospective (STP) analysis for 55 participants. BCG revaccinated (A) and primary-vaccinated (B). The bold red line represents the median values of each group at each time point. X-axis is not to scale. Abbreviations: IFN- $\gamma$  = Interferon gamma; SFU = spot forming unit; PBMC = peripheral blood mononuclear cells. (For interpretation of the references to colour in this figure legend, the reader is referred to the web version of this article.)

**Table 3**  
Short-term prospective (STP) analysis: results of the linear regression analysis on AUC.

Area under the curve (AUC)					
Covariates (n)	Geometric mean of AUC	Unadjusted GM ratio (95% CI), <i>p</i> -value		Fully adjusted* GM ratio (95% CI), <i>p</i> -value (n = 43 <sup>†</sup> )	
Baseline IFN- $\gamma$ response (55)	329.03	1.00	(0.99, 1.01), 0.49	1.00	(0.99, 1.01), 0.76
Gender					
Female (36)	280.13	1	—	1	—
Male (19)	446.30	1.59	(0.73, 3.49), 0.24	1.04	(0.55, 1.96), 0.91
BCG vacc history <sup>‡</sup>					
1–9 yrs (8)	1156.66	1	—	1	—
10–19 yrs (10)	579.88	0.50	(0.15, 1.63)	0.45	(0.16, 1.27)
20–29 yrs (7)	384.62	0.33	(0.09, 1.21)	0.70	(0.19, 2.50)
Never (30)	187.84	0.16	(0.06, 0.44), 0.002 <sup>§</sup>	0.22	(0.07, 0.68), 0.01
ML ratio (43)		1.16 <sup>¶</sup>	(0.85, 1.58), 0.33	1.09 <sup>¶</sup>	(0.82, 1.45), 0.53

Using a similar analysis of GM of IFN- $\gamma$  response by ML ratio as in Table 2; GM for the AUC for a ML ratio of 0.1 and 0.3 were 111.57 and 115.01, respectively. Abbreviations: IFN- $\gamma$  = Interferon gamma; vacc = vaccination; GM = geometric mean; yrs = years; ML = Monocyte/lymphocyte.

\* Adjusted for all variables in the model.

<sup>†</sup> Due to missing ML ratio data.

<sup>‡</sup> Prior to BCG vaccination in trial.

<sup>§</sup> *p*-value for all categories of BCG vaccination history covariate using an ANOVA summary.

<sup>¶</sup> The value of the change in GM of the AUC for an increase in 0.1 of ML ratio.

**Table 4**  
Short-term prospective (STP) analysis: results of the linear regression analysis on 24 week IFN- $\gamma$  response.

24 week IFN- $\gamma$ response							
Covariates (n)	Geometric mean of 24 week IFN- $\gamma$ response	Unadjusted GM ratio (95% CI), <i>p</i> -value		Partially adjusted (for baseline IFN- $\gamma$ response) GM ratio (95% CI), <i>p</i> -value		Fully adjusted* GM ratio (95% CI), <i>p</i> -value (n = 43 <sup>†</sup> )	
Baseline IFN- $\gamma$ response (55)	87.44	1.01	(1.01, 1.01), <0.001	—	—	1.00	(0.99, 1.01), 0.17
Gender							
Female (36)	83.11	1	—	1	—	1	—
Male (19)	96.29	1.16	(0.51, 2.64), 0.72	1.12	(0.57, 2.21), 0.74	0.69	(0.32, 1.51), 0.35
BCG vacc history <sup>‡</sup>							
1–9 yrs (8)	274.13	1	—	1	—	1	—
10–19 yrs (10)	212.37	0.78	(0.26, 2.32)	0.84	(0.29, 2.42)	1.05	(0.30, 3.73)
20–29 yrs (7)	214.43	0.78	(0.24, 2.59)	0.68	(0.21, 2.16)	1.55	(0.32, 7.35)
Never (30)	38.91	0.14	(0.06, 0.36), <0.001 <sup>§</sup>	0.25	(0.09, 0.69), <0.001 <sup>§</sup>	0.29	(0.07, 1.12), >0.05 <sup>§</sup>
ML ratio (43)		1.08 <sup>¶</sup>	(0.71, 1.65), 0.72	1.14 <sup>¶</sup>	(0.81, 1.59), 0.45	1.04 <sup>¶</sup>	(0.73, 1.47), 0.83

Using a similar analysis of GM of the IFN- $\gamma$  response by ML ratio as in Table 2; GM for the 24 week response for a ML ratio of 0.1 and 0.3 were 125.08 and 126.01, respectively. The GM ratio for the baseline IFN- $\gamma$  response covariate in the partially adjusted analysis is not included here, but all were similar to the unadjusted analysis value (approximately 1 and *p*-value < 0.05). Abbreviations: IFN- $\gamma$  = Interferon gamma; vacc = vaccination; GM = geometric mean; yrs = years; ML = Monocyte/lymphocyte.

\* Adjusted for all variables in the model.

<sup>†</sup> Due to missing ML ratio data.

<sup>‡</sup> Prior to BCG vaccination.

<sup>§</sup> *p*-value for all categories of BCG vaccination history covariate using an ANOVA summary.

<sup>¶</sup> The value of the change in GM of the 24 week response for an increase in 0.1 of ML ratio.

**Table 5**  
Short-term prospective (STP) analysis: results of the linear regression analysis on peak IFN- $\gamma$  response.

Peak IFN- $\gamma$ response measured over 24 week follow-up							
Covariates (n)	Geometric mean of peak IFN- $\gamma$ response	Unadjusted GM ratio (95% CI), <i>p</i> -value		Partially adjusted (for baseline IFN- $\gamma$ response) GM ratio (95% CI), <i>p</i> -value		Fully adjusted* GM ratio (95% CI), <i>p</i> -value (n = 43 <sup>†</sup> )	
Baseline IFN- $\gamma$ response (55)	343.08	1.00	(1.00, 1.01), <0.001	—	—	1.00	(0.99, 1.01), 0.14
Gender							
Female (36)	336.38	1	—	1	—	1	—
Male (19)	356.90	1.06	(0.64, 1.76), 0.81	1.05	(0.68, 1.59), 0.83	0.89	(0.58, 1.36), 0.57
BCG vacc history <sup>‡</sup>							
1–9 yrs (8)	853.93	1	—	1	—	1	—
10–19 yrs (10)	595.42	0.70	(0.38, 1.28)	0.71	(0.39, 1.30)	0.72	(0.35, 1.45)
20–29 yrs (7)	588.23	0.70	(0.36, 1.32)	0.65	(0.34, 1.24)	0.75	(0.32, 1.76)
Never (30)	201.06	0.24	(0.14, 0.39), <0.001 <sup>§</sup>	0.29	(0.16, 0.51), <0.001 <sup>§</sup>	0.32	(0.15, 0.68), <0.001 <sup>§</sup>
ML ratio (43)		1.05 <sup>¶</sup>	(0.82, 1.35), 0.70	1.09 <sup>¶</sup>	(0.89, 1.32), 0.38	1.01	(0.84, 1.22), 0.89

Using a similar analysis of GM of the IFN- $\gamma$  response by ML ratio as in Table 2; GM for the peak response for a ML ratio of 0.1 and 0.3 were 536.34 and 564.72, respectively. The GM ratio for the baseline IFN- $\gamma$  response covariate in the partially adjusted analysis is not included here, but all were similar to the unadjusted analysis value (approximately 1 and *p*-value < 0.05). Abbreviations: IFN- $\gamma$  = Interferon gamma; vacc = vaccination; GM = geometric mean; yrs = years; ML = Monocyte/lymphocyte.

\* Adjusted for all variables in the model.

<sup>†</sup> Due to missing ML ratio data.

<sup>‡</sup> Prior to BCG vaccination.

<sup>§</sup> *p*-value for all categories of BCG vaccination history covariate using an ANOVA summary.

<sup>¶</sup> The value of the change in GM of the peak response for an increase in 0.1 of ML ratio.

required to protect against TB disease and in males, a higher immune response may lead to detrimental exaggerated inflammatory responses [25].

There is uncertainty in the duration of protection of efficacy following BCG vaccination. In our Long-term retrospective (LTR) analysis, we found previous BCG vaccination was associated with a higher IFN- $\gamma$  response at baseline, which supports results from several previous studies [8,26]. We also found, in both LTR analysis and short-term prospective (STP) analysis, no difference between any IFN- $\gamma$  response if vaccinated any time between 10 and 30 years ago versus less than 10 years ago, suggesting that there may be no difference in the immune response generated at one year and up to 30 years after primary vaccination. These results suggest that BCG vaccination induces a durable memory response. However, previous studies have shown that IFN- $\gamma$  responses following BCG vaccination can wane [27]. In order to more precisely assess the possibility of a waning response in our data, the BCG vaccination history covariate could be stratified into smaller groupings. However, with the current dataset size, this would impact on the statistical power of the analysis. The duration of a BCG immune response is complex and currently, not fully understood. As such, more trials to measure this specific immune response may be necessary.

In our STP analysis, we found that revaccination with BCG was associated with an increase in total (AUC) over 24 weeks and peak (taking into account baseline levels) IFN- $\gamma$  response. However, it was not associated with higher IFN- $\gamma$  response (when baseline responses were taken into account) at 24 weeks. Our in-depth characterization of this short term effect is supported by previous work at single time points that showed initial increases following revaccination with BCG [25–27] that were not sustained at 24 [28] or 52 weeks [29,30]. This suggests that revaccination with BCG has an impact on overall IFN- $\gamma$  levels in the short term (<24 weeks) but may have little effect on IFN- $\gamma$  levels long term (>24 weeks).

All other covariates were non-significant. This may be due to small numbers of participants or no association.

Recent evidence has revealed a complex relationship between ML ratio and risk of TB disease [14]. We explored if this could be explained by a link between ML ratio and IFN- $\gamma$  responses. However, our results showed that ML ratio had no association on IFN- $\gamma$  response in the LTR or STP analyses. This difference could be explained by HIV status amongst our participant population compared to previous work [14].

There are a number of limitations of our work. Most importantly, we chose to use IFN- $\gamma$ -expressing cells as our marker of immune response. Whilst the presence of IFN- $\gamma$  has been shown to be important in protection against *M.tb* infection [31], it has not proven to be a correlate of protection for TB disease [32,33]. It is, however, one of the most commonly used measures of TB vaccine immunogenicity we have [34]. The use of IFN- $\gamma$ -expressing cells as our sole indicator of immunogenicity has benefits in its simplicity, and was the only outcome for which data was available to us. Other studies are being carried out that may give a more in depth view of the immune response to BCG in which a more complex “biosignature” is being investigated [34]. Secondly, our work was limited to the data available from the seven TB vaccine trials, which restricted the covariates available and the size of the participant cohorts. For example, HIV positive and latently infected individuals were excluded. Thirdly, in the outlined laboratory procedure [17–20] a 16-h ELISPOT assay was chosen, which may have potentially missed central memory CD4+ T-cells as they require a longer period of antigen re-stimulation to generate IFN- $\gamma$  [35]. As such, our responses may underestimate the true “memory” cell presence, specifically at the later time point of 24 weeks.

The implications of our results are as follows. Our results show that previous BCG vaccination generates a higher immune response and this may complicate the interpretation of immunological results of new TB vaccine clinical trials, and support stratification of vaccine trial results by previous TB vaccination status, as is carried out previously [17,26]. In addition, if replicated in future analysis, our results also suggest that future TB vaccine trials may need to also stratify their analysis by gender. Moreover, to potentially capitalize on the impact of higher immune response due to previous vaccination and to improve upon the variable efficacy of BCG, it has recently been suggested that revaccination with BCG may increase efficacy [36]. Our findings showed that revaccination with BCG, whilst providing a higher IFN- $\gamma$  peak response, did not increase IFN- $\gamma$  at 24 weeks over the levels measure in primary-vaccinated participants. This provides more evidence to support the WHO policy not to revaccinate with BCG [37].

As an extension to our analysis, the time between the long-term retrospective (LTR) and short-term prospective (STP) analysis could be considered (for example, a number of years via a phase II/III clinical trial), which is not addressed here. Knowledge of this may indicate why we see a gender effect in the long term and not in the short-term and give further insight into the duration of BCG immunogenicity. Moreover, the link between ML ratio and TB disease is an exciting development in the search for informative TB risk factors and further work with additional detailed datasets should be conducted on the immunology driving this relationship. To improve upon the methods used in our STP analysis, mathematical models could be adopted to explore the underlying mechanisms behind the dynamics. The impact of the covariates on key immune system parameters would then be analysed.

## 5. Conclusion

The research conducted in this analysis aimed to establish, using new detailed mycobacterial-specific immune response data, which, if any, individual level covariates alter the immune response over the long term or shortly after BCG vaccination. This analysis suggests that previous BCG vaccination and gender are associated with durable IFN- $\gamma$  responses. The results of this analysis imply that future vaccine trials should consider stratifying the trial population for analysis by gender and BCG vaccination history.

**Funding:** SJR is funded by a PhD studentship from Aeras. HMCS is a Wellcome Trust Senior Clinical Research Fellow. RGW is funded the Medical Research Council (UK) (MR/J005088/1), the Bill and Melinda Gates Foundation (TB Modelling and Analysis Consortium: OPP1084276), CDC/PEPFAR via the Aurum Institute (U2GPO008111), and USAID/IUTLD/The Union North America (TREAT TB: Technology, Research, Education, and Technical Assistance for Tuberculosis; GHN-A-OO-08-00004-00). The funders had no involvement in the design, collection, analysis or interpretation of the data, in writing the report or in the decision to submit.

**Competing interests:** None Declared.

**Ethical approval:** Not required.

## Appendix A. Supplementary data

Supplementary data related to this article can be found at <http://dx.doi.org/10.1016/j.tube.2015.10.002>.

## References

- [1] WHO. Global tuberculosis report 2014. World Health Organization; 2014. p. 1–171.
- [2] McShane H. Tuberculosis vaccines: beyond bacille Calmette-Guerin. *Philos Trans R Soc Lond B Biol Sci* 2011;366(1579):2782–9.
- [3] Dye C, Glaziou P, Floyd K, Raviglione M. Prospects for tuberculosis elimination. *Annu Rev Public Health* 2013;34:271–86.
- [4] Knight GM, Griffiths UK, Sumner T, Laurence YV, Gheorghie A, Vassall A, Glaziou P, White RG. Impact and cost-effectiveness of new tuberculosis vaccines in low- and middle-income countries. *Proc Natl Acad Sci U S A* 2014;111(43):15520–5.
- [5] Mangtani P, Abubakar I, Ariti C, Beynon R, Pimpin L, Fine PE, Rodrigues LC, Smith PG, Lipman M, Whiting PF, Sterne JA. Protection by BCG vaccine against tuberculosis: a systematic review of randomized controlled trials. *Clin Infect Dis* 2014;58(4):470–80.
- [6] Colditz GA, Brewer TF, Berkey CS, Wilson ME, Burdick E, Fineberg HV, Mosteller F. Efficacy of BCG vaccine in the prevention of tuberculosis. Meta-analysis of the published literature. *J Am Med Assoc* 1994;271(9):698–702.
- [7] Hoefsloot W, van Ingen J, Andrejak C, Angeby K, Bauriaud R, Bemer P, Beylis N, Boeree MJ, Cacho J, Chihota V, Chimara E, Churchyard G, Cias R, Daza R, Daley CL, Dekhuijzen PN, Domingo D, Drobniowski F, Esteban J, Fauville-Dufaux M, Folkvardsen DB, Gibbons N, Gomez-Mampaso E, Gonzalez R, Hoffmann H, Hsueh PR, Indra A, Jagielski T, Jamieson F, Jankovic M, Jong E, Keane J, Koh WJ, Lange B, Leao S, Macedo R, Mannsaker T, Marras TK, Maugein J, Milburn HJ, Mlisko T, Morcillo N, Morimoto K, Papaventsis D, Palenque E, Paez-Pena M, Piersimoni C, Polanova M, Rastogi N, Richter E, Ruiz-Serrano MJ, Silva A, da Silva MP, Simek H, van Soolingen D, Szabo N, Thomson R, Tortola Fernandez T, Tortoli E, Totten SE, Tyrrell G, Vasankari T, Villar M, Walkiewicz R, Winthrop KL, Wagner D, G. Nontuberculous Mycobacteria Network European Trials. The geographic diversity of nontuberculous mycobacteria isolated from pulmonary samples: an NTM-NET collaborative study. *Eur Respir J* 2013;42(6):1604–13.
- [8] Black GF, Weir RE, Floyd S, Bliss L, Warndorff DK, Crampin AC, Ngwira B, Sichali L, Nazareth B, Blackwell JM, Branson K, Chaguluka SD, Donovan L, Jarman E, King E, Fine PE, Dockrell HM. BCG-induced increase in interferon-gamma response to mycobacterial antigens and efficacy of BCG vaccination in Malawi and the UK: two randomised controlled studies. *Lancet* 2002;359(9315):1393–401.
- [9] Borgdorff MW, Nagelkerke NJ, Dye C, Nunn P. Gender and tuberculosis: a comparison of prevalence surveys with notification data to explore sex differences in case detection. *Int J Tuberc Lung Dis* 2000;4(2):123–32.
- [10] Nhamoyebonde S, Leslie A. Biological differences between the sexes and susceptibility to tuberculosis. *J Infect Dis* 2014;209(Suppl. 3):S100–6.
- [11] Allotey P, Gyapong M. Gender in tuberculosis research. *Int J Tuberc Lung Dis* 2008;12(7):831–6.
- [12] Aronson NE, Santosham M, Comstock GW, Howard RS, Moulton LH, Rhoades ER, Harrison LH. Long-term efficacy of BCG vaccine in American Indians and Alaska Natives: a 60-year follow-up study. *J Am Med Assoc* 2004;291(17):2086–91.
- [13] Nielsen NO, Soborg B, Borresen M, Andersson M, Koch A. Cytokine responses in relation to age, gender, body mass index, *Mycobacterium tuberculosis* infection, and otitis media among Inuit in Greenland. *Am J Hum Biol* 2013;25(1):20–8.
- [14] Naranbhai V, Hill AV, Abdool Karim SS, Naidoo K, Abdool Karim Q, Warimwe GM, McShane H, Fletcher H. Ratio of monocytes to lymphocytes in peripheral blood identifies adults at risk of incident tuberculosis among HIV-infected adults initiating antiretroviral therapy. *J Infect Dis* 2014;209(4):500–9.
- [15] Naranbhai V, Kim S, Fletcher H, Cotton MF, Violari A, Mitchell C, Nachman S, McSherry G, McShane H, Hill AV, Madhi SA. The association between the ratio of monocytes:lymphocytes at age 3 months and risk of tuberculosis (TB) in the first two years of life. *BMC Med* 2014;12(120):1–6.
- [16] Naranbhai V, Moodley D, Chipato T, Stranix-Chibanda L, Nakabaiiti C, Kamateeka M, Musoke P, Manji K, George K, Emel LM, Richardson P, Andrew P, Fowler M, Fletcher H, McShane H, Coovadia HM, Hill AV, Team HP. The association between the ratio of monocytes: lymphocytes and risk of tuberculosis among HIV-infected postpartum women. *J Acquir Immune Defic Syndr* 2014;67(5):573–5.
- [17] McShane H, Pathan AA, Sander CR, Keating SM, Gilbert SC, Huygen K, Fletcher HA, Hill AV. Recombinant modified vaccinia virus Ankara expressing antigen 85A boosts BCG-primed and naturally acquired antimycobacterial immunity in humans. *Nat Med* 2004;10(11):1240–4.
- [18] Whelan KT, Pathan AA, Sander CR, Fletcher HA, Poulton I, Alder NC, Hill AV, McShane H. Safety and immunogenicity of boosting BCG vaccinated subjects with BCG: comparison with boosting with a new TB vaccine, MVA85A. *PLoS One* 2009;4(6):e5934.
- [19] Pathan AA, Sander CR, Fletcher HA, Poulton I, Alder NC, Beveridge NE, Whelan KT, Hill AV, McShane H. Boosting BCG with recombinant modified vaccinia ankara expressing antigen 85A: different boosting intervals and implications for efficacy trials. *PLoS One* 2007;2(10):e1052.
- [20] Hawkrigde T, Scriba TJ, Gelderbloem S, Smit E, Tameris M, Moyo S, Lang T, Veldsman A, Hatherill M, Merwe L, Fletcher HA, Mahomed H, Hill AV, Hanekom WA, Hussey GD, McShane H. Safety and immunogenicity of a new tuberculosis vaccine, MVA85A, in healthy adults in South Africa. *J Infect Dis* 2008;198(4):544–52.
- [21] R, R: A Language and Environment, D.C. Team, Editor. R Foundation for Statistical Computing. 2005. Vienna, Austria. <http://www.r-project.org/>.
- [22] Ekstrom C, Skovgaard IM, Martinussen T. kulife: datasets and functions from the (now non-existing). Faculty of Life Sciences, University of Copenhagen; 2013. R package version 0.1-14. Available from: <http://CRAN.R-project.org/package=kulife>.
- [23] Pernis AB. Estrogen and CD4+ T cells. *Curr Opin Rheumatol* 2007;19(5):414–20.
- [24] Kurasawa T. Tuberculin skin test of patients with active pulmonary tuberculosis and non-tuberculous pulmonary diseases. *Kekkaku* 1990;65(1):47–52.
- [25] Kaufmann SH, Dorhoi A. Inflammation in tuberculosis: interactions, imbalances and interventions. *Curr Opin Immunol* 2013;25(4):441–9.
- [26] Harris SA, Meyer J, Satti I, Marsay L, Poulton ID, Tanner R, Minassian AM, Fletcher HA, McShane H. Evaluation of a human BCG Challenge model to assess antimycobacterial immunity induced by BCG and a candidate tuberculosis vaccine, MVA85A, alone and in combination. *J Infect Dis* 2013;209(8):1259–68.
- [27] Weir RE, Gorak-Stolinska P, Floyd S, Lalor MK, Stenson S, Branson K, Blitz R, Ben-Smith A, Fine PE, Dockrell HM. Persistence of the immune response induced by BCG vaccination. *BMC Infect Dis* 2008;8(9).
- [28] Hoft DF, Worku S, Kampmann B, Whalen CC, Ellner JJ, Hirsch CS, Brown RB, Larkin R, Li Q, Yun H, Silver RF. Investigation of the relationships between immune-mediated inhibition of mycobacterial growth and other potential surrogate markers of protective *Mycobacterium tuberculosis* immunity. *J Infect Dis* 2002;186(10):1448–57.
- [29] Oliveira ES, Marinho JM, Barbosa T, Study G. Interferon-gamma production by mononuclear cells in Bacille Calmette-Guerin-revaccinated healthy volunteers predicted long-term antimycobacterial responses in a randomized controlled trial. *Vaccine* 2013;31(37):3778–82.
- [30] Fjallbrant H, Ridell M, Larsson LO. Primary vaccination and revaccination of young adults with BCG: a study using immunological markers. *Scand J Infect Dis* 2007;39(9):792–8.
- [31] Flynn JL, Chan J, Triebold KJ, Dalton DK, Stewart TA, Bloom BR. An essential role for interferon gamma in resistance to *Mycobacterium tuberculosis* infection. *J Exp Med* 1993;178(6):2249–54.
- [32] Kagina BM, Abel B, Scriba TJ, Hughes EJ, Keyser A, Soares A, Gamielidien H, Sidibana M, Hatherill M, Gelderbloem S, Mahomed H, Hawkrigde A, Hussey G, Kaplan G, Hanekom WA, I. other members of the South African Tuberculosis Vaccine. Specific T cell frequency and cytokine expression profile do not correlate with protection against tuberculosis after bacillus Calmette-Guerin vaccination of newborns. *Am J Respir Crit Care Med* 2010;182(8):1073–9.
- [33] Caruso AM, Serbina N, Klein E, Triebold K, Bloom BR, Flynn JL. Mice deficient in CD4 T cells have only transiently diminished levels of IFN-gamma, yet succumb to tuberculosis. *J Immunol* 1999;162(9):5407–16.
- [34] Hanekom WA, Dockrell HM, Ottenhoff TH, Doherty TM, Fletcher H, McShane H, Weichold FF, Hoft DF, Parida SK, Fruth UJ. Immunological outcomes of new tuberculosis vaccine trials: WHO panel recommendations. *PLoS Med* 2008;5(7):e145.
- [35] Calarota SA, Baldanti F. Enumeration and characterization of human memory T cells by enzyme-linked immunosorbent assays. *Clin Dev Immunol* 2013;2013:1–8.
- [36] Dye C. Making wider use of the world's most widely used vaccine: bacille Calmette-Guerin revaccination reconsidered. *J R Soc Interface* 2013;10(87):20130365.
- [37] Global tuberculosis programme and global programme on vaccines. Statement on BCG revaccination for the prevention of tuberculosis. *Wkly Epidemiol Rec* 1995;70(32):229–31.

## Supplementary Material for paper 1

The following is the published supplementary material referenced in paper 1. All references to the below tables and Figures are preceded with the suffix “S” in the paper.

### **Additional Results**

The demographics of the participants used in the long-term retrospective (LTR) and short-term prospective (STP) analyses can be found in S1. The distribution of the ML ratios in the participants (measured at baseline) is shown in Figure S1.

	Long-term retrospective (LTR) (n=101) (M = 35)	Short-term prospective (STP) (n=55) (M = 19)
Geography: UK	83 (M = 30)	55 (M = 19)
Time since BCG vaccination		
1 to 9	8 (M = 2)	7 (M = 2)
10 to 19	13 (M = 8)	10 (M = 6)
20 to 29	19 (M = 7)	8 (M = 3)
30+	12 (M = 3)	-
Never	49 (M = 15)	30 (M = 8)

**Table S1. Participant demographics. M = males**

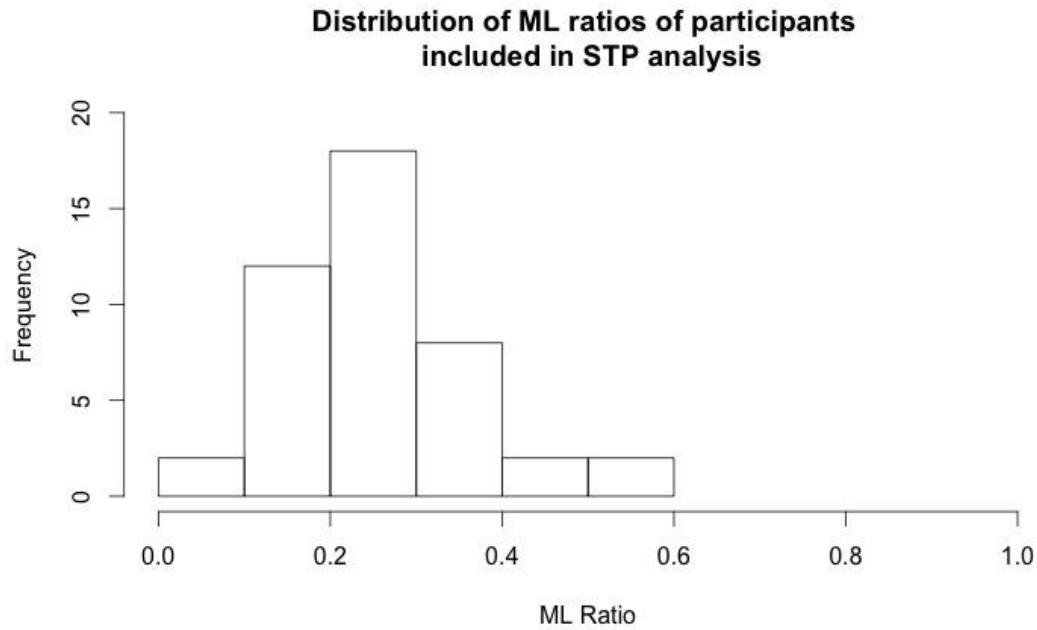


**Figure S1. Distribution of ML ratios of participants included in STP analysis.**

Nonlinear regression model for ML ratio on LTR and STP outcome measures

Both linear and quadratic regression models were fitted to establish if a similar relationship existed between the LTR and STP outcome measures and ML ratio. Below is an outline of these models.

Linear model (M1)

$$\log(\text{Outcome}) = a + b_1 * (\text{ML})$$

Nonlinear model (M2)

$$\log(\text{Outcome}) = a + b_1 * (\text{ML}) + b_2 * (\text{ML}^2)$$

A model comparison test (ANOVA) was conducted to establish if a non-linear relationship more adequately described this association, the F-score and p-value of which are displayed in Table S2.

LTR	STP		
Outcome: Baseline IFN- $\gamma$	Outcome: AUC	Outcome: 24 week	Outcome: Peak
F-score (p-value)	F-score (p-value)	F-score (p-value)	F-score (p-value)
0.41 (0.53)	0.01 (0.94)	0.27 (0.60)	0.05 (0.82)

**Table S2. ANOVA test results comparing M1 to M2 for LTR and STP outcome measures. This was an unadjusted analysis, therefore, no other covariates were included here.**

As none of the p-values were below 0.05 I concluded that the quadratic model did not improve upon the description of the relationship between ML ratio and the LTR and STP outcome variables provided by the linear regression analysis. Therefore, there was no evidence of a nonlinear relationship between ML ratio and the LTR and STP outcome variables as stated in the main text.

## **Chapter 3. Exploration into the immune response to BCG vaccination in a heterogeneous human and macaque population using a vaccine Immunostimulation/Immunodynamic (IS/ID) mathematical model and the predictive power between macaque and human subpopulation data: paper 2**

### **Chapter 3 introduction**

The objectives of this paper were three-fold:

1. Design and implement a model representing the CD4+ T cell mechanisms producing the IFN- $\gamma$  immune response dynamics in the data and validate this model by calibrating it to the human IFN- $\gamma$  data (paper 1) and longitudinal IFN- $\gamma$  data in macaques.
2. Establish which model parameters (if any) are statistically different for different subpopulations in both species separately.
3. Use the model predictions for the macaque subpopulations (if any) to fit to the human data and establish which macaque subpopulation model best represents human IFN- $\gamma$  immune response dynamics.

This chapter aims fulfil the remainder of aim 1 of the thesis and objective 2-4 (Figure 1.4).

This is my first application of IS/ID modelling to vaccine response data for the purpose of immune response translation between species.

Drawing on the results of paper 1, I hypothesized that there would be differences in IFN- $\gamma$  immune response dynamics in humans due to BCG status (baseline BCG-naïve or baseline BCG-vaccinated). As there was a weak significant effect on baseline IFN- $\gamma$  responses by gender (long-term retrospective analysis in paper 1), but not in the IFN- $\gamma$  dynamics after BCG vaccination (short-term prospective analysis in paper 1), I hypothesized I would not find a difference in model predicted immune response dynamics stratified by gender. As both time since BCG vaccination and ML ratio were not significantly associated with differences in either baseline or IFN- $\gamma$  response dynamics after BCG vaccination, I hypothesized I would find no differences in model predicted immune response dynamics due to either of these covariates.

The macaque BCG data was provided by colleagues at Public Health England (Sally Sharpe, et. al.). Data were combined from pre-clinical immunogenicity experiments for the MVA-85A vaccine, which preceded the clinical data used here and in paper 1. Preliminary analysis (equivalent to my analysis in paper 1) of the macaque subpopulation data was conducted prior to my work by Charlotte Sarfas (PHE) who had shown that there were significant differences in peak and AUC response by macaque colony of origin (personal communication, publication in review). As such, in paper 2 I focused only on investigating the differences in the mathematical model parameters to the macaque subpopulation data and not the preliminary analysis methods of paper 1. From Charlotte's work I hypothesized there would be differences in mathematical modelling parameters due to macaque colony of origin.

I presented the work in paper 2 in poster form at the following conference:

- **Population Approach Group Europe (PAGE) meeting 2016**, Lisbon, Portugal, June 2016. "Previous BCG vaccination associated with variation in Mycobacterial-specific immune response: a modelling study" **S. J. Rhodes**, G. M. Knight, J. Guedj, H. A. Fletcher, R. G. White

I also presented this work as an oral abstract at the following conference:

- **The 47<sup>th</sup> Union World Conference on Lung Health**, Liverpool, UK, October 2016. "Previous BCG vaccination associated with variation in Mycobacterial-specific immune response: a modelling study". **S. J. Rhodes**, G. M. Knight, J. Guedj, H. A. Fletcher, R. G. White

Registry  
 T: +44(0)20 7299 4646  
 F: +44(0)20 7299 4656  
 E: registry@lshtm.ac.uk

## RESEARCH PAPER COVER SHEET

PLEASE NOTE THAT A COVER SHEET MUST BE COMPLETED FOR EACH RESEARCH PAPER INCLUDED IN A THESIS.

### SECTION A – Student Details

Student	Sophie Rhodes
Principal Supervisor	Richard White
Thesis Title	The development of a mathematical modelling framework to translate TB vaccine response between species and predict the most immunogenic dose in humans using animal data

*If the Research Paper has previously been published please complete Section B, if not please move to Section C*

### SECTION B – Paper already published

Where was the work published?	Clinical and Vaccine Immunology Journal		
When was the work published?	January 2017		
If the work was published prior to registration for your research degree, give a brief rationale for its inclusion			
Have you retained the copyright for the work?*	No	Was the work subject to academic peer review?	Yes

*\*If yes, please attach evidence of retention. If no, or if the work is being included in its published format, please attach evidence of permission from the copyright holder (publisher or other author) to include this work.*

### SECTION C – Prepared for publication, but not yet published

Where is the work intended to be published?	
Please list the paper's authors in the intended authorship order.	
Stage of publication	Choose an item.

### SECTION D – Multi-authored work

For multi-authored work, give full details of your role in the research included in the paper and in the preparation of the paper. (Attach a further sheet if necessary)	See next page
--	---------------

Student Signature: 

Date: 13/6/17

Supervisor Signature: \_\_\_\_\_



Date: \_\_\_\_\_

13/6/12

**Paper 2 title: Using Data from Macaques to Predict Gamma Interferon Responses after Mycobacterium bovis BCG Vaccination in Humans: A Proof-of-Concept Study of Immunostimulation/Immunodynamic Modeling Methods**

**Authors: Sophie J. Rhodes\*, Charlotte Sarfas\*, Gwenan M. Knight, Andrew White, Ansar A. Pathan, Helen McShane, Thomas G. Evans, Helen Fletcher, Sally Sharpe\*\*, Richard G. White\*\***

**\*Joint first author**

**\*\*Joint senior author**

**Author contribution:**

The human BCG data was the same dataset used in paper 1. The macaque BCG data were provided by Dr. Sally Sharpe, Charlotte Sarfas and Andrew White at PHE. The data were collated over multiple experiments by Charlotte Sarfas. The mathematical model of the IFN- $\gamma$  secreting T cell response was developed by myself with guidance from Prof. Richard White and Dr. Gwenan Knight and advisory panel members, immunological expert Dr. Thomas Evans and TB immune response modeller, Prof. Denise Kirschner. The calibration method, Nonlinear Mixed Effects Modelling in the software Monolix was implemented solely by myself, however training in the program was undertaken with the guidance of advisory panel member Dr. Jeremie Guedj. The design of methods to translate responses between species was exclusively my own work. All authors reviewed the paper. Joint first authorship was granted to myself for developing and applying the mathematical model to the data and writing the paper and Charlotte Sarfas for aggregation of the macaque data and reviewing the paper. The interpretation of the results was my own work.

**Permission from copyright holder to include this work:**

**Received** 14 November 2016 **Returned for modification** 2 December 2016 **Accepted** 4 January 2017

**Accepted manuscript posted online** 11 January 2017

**Citation** Rhodes SJ, Sarfas C, Knight GM, White A, Pathan AA, McShane H, Evans TG, Fletcher H, Sharpe S, White RG. 2017. Using data from macaques to predict gamma interferon responses after *Mycobacterium bovis* BCG vaccination in humans: a proof-of-concept study of immunostimulation/immunodynamic modeling methods. Clin Vaccine Immunol 24: e00525-16. <https://doi.org/10.1128/CI.00525-16>.

**Editor** Helene F. Rosenberg, IIS/LAD/NIAID/NIH

**Copyright** © 2017 Rhodes et al. This is an open-access article distributed under the terms of the [Creative Commons Attribution 4.0 International license](#).

Address correspondence to Sophie J. Rhodes, [Sophie.rhodes@ishtm.ac.uk](mailto:Sophie.rhodes@ishtm.ac.uk).

S.J.R. and C.S. are joint first authors. S.S. and R.G.W. are joint senior authors.



**Attribution 4.0 International (CC BY 4.0)**

This is a human-readable summary of (and not a substitute for) the [license](#).

[Disclaimer](#)



**You are free to:**

- Share** — copy and redistribute the material in any medium or format
- Adapt** — remix, transform, and build upon the material for any purpose, even commercially.

The licensor cannot revoke these freedoms as long as you follow the license terms.

**Under the following terms:**

-  **Attribution** — You must give **appropriate credit**, provide a link to the license, and **indicate if changes were made**. You may do so in any reasonable manner, but not in any way that suggests the licensor endorses you or your use.

**No additional restrictions** — You may not apply legal terms or **technological measures** that legally restrict others from doing anything the license permits.



# Using Data from Macaques To Predict Gamma Interferon Responses after *Mycobacterium bovis* BCG Vaccination in Humans: a Proof-of-Concept Study of Immunostimulation/Immunodynamic Modeling Methods

Sophie J. Rhodes,<sup>a</sup> Charlotte Sarfas,<sup>b</sup> Gwenan M. Knight,<sup>a,c</sup> Andrew White,<sup>b</sup> Ansar A. Pathan,<sup>d</sup> Helen McShane,<sup>e</sup> Thomas G. Evans,<sup>f</sup>  Helen Fletcher,<sup>g</sup> Sally Sharpe,<sup>b</sup> Richard G. White<sup>a</sup>

TB Modelling Group, CMMID, TB Centre, London School of Hygiene and Tropical Medicine, London, United Kingdom<sup>a</sup>; Public Health England, Porton Down, United Kingdom<sup>b</sup>; Imperial College, London, United Kingdom<sup>c</sup>; College of Health and Life Sciences, Department of Life Sciences, Brunel University, London, United Kingdom<sup>d</sup>; The Jenner Institute, University of Oxford, Oxford, United Kingdom<sup>e</sup>; TomegaVax, Portland, Oregon, USA<sup>f</sup>; Immunology and Infection Department, London School of Hygiene and Tropical Medicine, London, United Kingdom<sup>g</sup>

**ABSTRACT** Macaques play a central role in the development of human tuberculosis (TB) vaccines. Immune and challenge responses differ across macaque and human subpopulations. We used novel immunostimulation/immunodynamic modeling methods in a proof-of-concept study to determine which macaque subpopulations best predicted immune responses in different human subpopulations. Data on gamma interferon (IFN- $\gamma$ )-secreting CD4<sup>+</sup> T cells over time after recent *Mycobacterium bovis* BCG vaccination were available for 55 humans and 81 macaques. Human population covariates were baseline BCG vaccination status, time since BCG vaccination, gender, and the monocyte/lymphocyte cell count ratio. The macaque population covariate was the colony of origin. A two-compartment mathematical model describing the dynamics of the IFN- $\gamma$  T cell response after BCG vaccination was calibrated to these data using nonlinear mixed-effects methods. The model was calibrated to macaque and human data separately. The association between subpopulations and the BCG immune response in each species was assessed. The macaque subpopulations that best predicted immune responses in different human subpopulations were identified using Bayesian information criteria. We found that the macaque colony and the human baseline BCG status were significantly ( $P < 0.05$ ) associated with the BCG-induced immune response. For humans who were BCG naïve at baseline, Indonesian cynomolgus macaques and Indian rhesus macaques best predicted the immune response. For humans who had already been BCG vaccinated at baseline, Mauritian cynomolgus macaques best predicted the immune response. This work suggests that the immune responses of different human populations may be best modeled by different macaque colonies, and it demonstrates the potential utility of immunostimulation/immunodynamic modeling to accelerate TB vaccine development.

**KEYWORDS** nonhuman primates, T-cell immunity, bacillus Calmette-Guérin, interferons, mathematical modeling, tuberculosis, tuberculosis vaccines

Tuberculosis (TB) disease remains a major global health problem (1), and *Mycobacterium tuberculosis* bacillus Calmette-Guérin (BCG), the only licensed TB vaccine, exhibits variable efficacy (2, 3). In order to reach WHO TB control goals, a new, effective

**Received** 14 November 2016 **Returned for modification** 2 December 2016 **Accepted** 4 January 2017

**Accepted manuscript posted online** 11 January 2017

**Citation** Rhodes SJ, Sarfas C, Knight GM, White A, Pathan AA, McShane H, Evans TG, Fletcher H, Sharpe S, White RG. 2017. Using data from macaques to predict gamma interferon responses after *Mycobacterium bovis* BCG vaccination in humans: a proof-of-concept study of immunostimulation/immunodynamic modeling methods. *Clin Vaccine Immunol* 24:e00525-16. <https://doi.org/10.1128/CVI.00525-16>.

**Editor** Helene F. Rosenberg, IIS/LAD/NIAID/NIH

**Copyright** © 2017 Rhodes et al. This is an open-access article distributed under the terms of the [Creative Commons Attribution 4.0 International license](https://creativecommons.org/licenses/by/4.0/).

Address correspondence to Sophie J. Rhodes, [Sophie.rhodes@lshtm.ac.uk](mailto:Sophie.rhodes@lshtm.ac.uk).

S.J.R. and C.S. are joint first authors. S.S. and R.G.W. are joint senior authors.

vaccine is vital (4). Animal models are used in almost every aspect of vaccine development, including helping to understand the transmission dynamics of the disease and the immunogenicity and efficacy of vaccines (5). They are therefore a vital and efficient tool in vaccine development (6). In preclinical TB vaccine research, nonhuman primates (NHPs) are a valuable animal model (7, 8) and are genetically and physiologically more similar to humans than small animals with respect to TB disease and immune response (7, 9).

Historically, rhesus (*Macaca mulatta*) (10) and cynomolgus (*Macaca fascicularis*) (11) macaque species have been used as the primary NHP models in TB vaccine research (12–14). Both species have been shown to respond to BCG vaccination, which affords them partial protection from TB (15–19); however, it has been shown that the same experimental conditions (infection with *Mycobacterium tuberculosis* following vaccination or a vaccine immune response) may lead to divergent outcomes for the two species (7, 20–22). Furthermore, the colony (country of origin) of macaque, even within the same species, has been shown to affect the level of protection against infection and the level of response after vaccination. For example, differing levels of protection have been observed for Chinese and Mauritian cynomolgus macaques: Mauritian cynomolgus macaques developed end-stage progressive TB in 7 weeks, while Chinese cynomolgus macaques remained healthy past the end of the study (12 weeks) (23).

These differences suggest that the immune responses of different human populations (e.g., those with previous BCG vaccination or those who are BCG naïve) may be best modeled by different macaque colonies. In 2014, the Bill and Melinda Gates Foundation adopted a new strategy for the selection of new TB vaccine candidates for clinical testing based on immune response and challenge results in NHPs (24). Therefore, in order to increase the likelihood of developing an effective vaccine, it is critical to identify and understand differences between macaque populations.

Here we focus on establishing the most representative NHP model for modeling the gamma interferon (IFN- $\gamma$ ) immune responses of adult humans in the UK following recent BCG vaccination, as one example of the prediction of vaccine immune responses in humans from a macaque animal model.

For this purpose, we conduct a proof-of-concept study to evaluate the potential use of novel immunostimulation/immunodynamic (IS/ID) modeling methods in vaccine immune response translation between species. A mechanistic mathematically based approach is used to quantify the dynamics of the immune response. By building the mathematical models on the basis of quantitative immunological data, it is possible to describe how these mechanisms may differ within and between species and to draw quantitative comparisons. Such modeling techniques are commonly used in drug development (pharmacokinetic/pharmacodynamic modeling) to translate drug responses between species (25–27) but have yet to be used in vaccine development.

First, we develop a model of IFN- $\gamma$ -producing CD4<sup>+</sup> T cell dynamics after BCG vaccination and assess the suitability of the model structure for predicting responses by calibrating the model to the data (analysis 1). We investigate the impact of the human and macaque population covariates to explain the within-population variation in responses, which our previous analysis on humans (28) showed can have a substantial impact on the magnitude of the response (analysis 2). We then test which calibrated macaque models best predict human IFN- $\gamma$  responses (analysis 3). Finally, we use the calibrated mathematical models for macaque and human subpopulations to predict the dynamics of the constituent T cell populations over time (analysis 4).

## RESULTS

**Analysis 1. Calibration of the model to IFN- $\gamma$  data and exploration of model predictions for macaques and humans separately.** Our mathematical model representing the immune response dynamics of two CD4<sup>+</sup> T cell populations secreting IFN- $\gamma$  is diagrammed in Fig. 1. The estimated parameter values for both macaques and humans can be found in Table 1. The visual predictive check (VPC) plots in Fig. 2 show that the ranges for macaques and humans in the model simulation cover the empirical data,

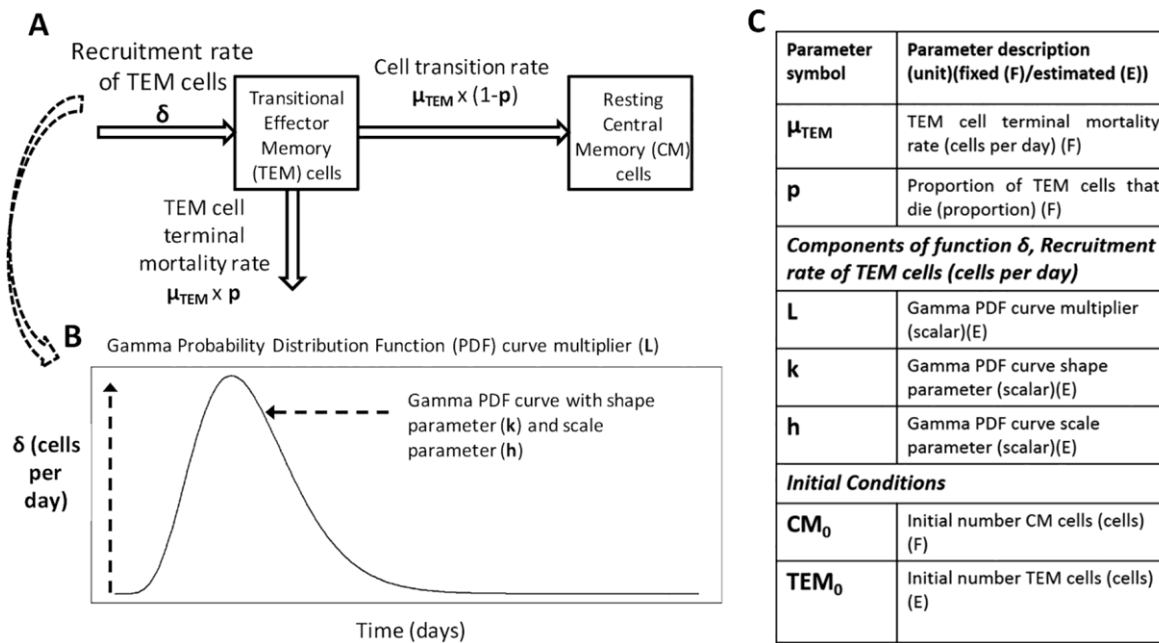


**FIG 1** (A) Schematic of the mathematical model representing the immune response dynamics of two CD4<sup>+</sup> T cell populations secreting IFN- $\gamma$ . (B) Depiction of the changes in the recruitment rate of transitional effector memory cells ( $\delta$ ) over time. (C) Key model parameters. Equations may be found in the supplemental material.

indicating that our model yields a good representation of the empirical data. Further diagnostic plots and model prediction plots can be found in Fig. S3 to S7 in the supplemental material.

**Analysis 2. Population covariate impact on within-population variation in model parameter estimates.** We found two covariates to be important: stratifying macaques by colony and humans by baseline BCG status reduced the within-population variation in the initial transitional effector memory cell count ( $TEM_0$ ) for macaques,  $TEM_0$  for humans, and the human gamma probability density function (PDF) multiplier and scale parameters (parameters  $L$  and  $h$ ) (Table 1; see also Tables S7 to S13 and Fig. S8 to S12 in the supplemental material). The VPC and further diagnostic plots for the subpopulation models show that the model describes the data adequately (see Fig. S13 to S18 in the supplemental material). Accounting for the population covariates reduced the Bayesian information criterion (BIC) value significantly, by 73, for humans from that in analysis 1 (BIC values, 2,779 in analysis 1 and 2,706 in analysis 2 [Table 1]) and decreased it by 2 for macaques (BIC values, 7,253 in analysis 1 and 7,251 in analysis 2 [Table 1]). The model-predicted total mean number of IFN- $\gamma$ -secreting cells (transitional effector memory [TEM] cells plus central memory [CM] cells) over time is shown in Fig. 3 as a visual assessment of the goodness of fit of the model to the mean empirical data. Also, Fig. S19 and S20 in the supplemental material show the 10th to 90th percentiles of model predictions after accounting for within-population variation.

**Analysis 3. Which macaque subpopulations best predicted immune responses in different human subpopulations?** The calibrated model for Indonesian cynomolgus macaques from analysis 2 provided the lowest BIC values for the human population that was BCG naïve at baseline (BCG: N), and that for Indian rhesus macaques provided the second lowest BIC value (1,357 and 1,391, respectively [Fig. 4; see also Fig. S20 to S27 in the supplemental material]). The calibrated model for Mauritian cynomolgus macaques best represented the human population that had already been BCG vaccinated prior to baseline (BCG: Y) (BIC value, 1,608 [Fig. 4; also Fig. S21 to S28]).

**Analysis 4. Predicted numbers of TEM and resting CM cells over time.** Figure 5 shows the model-predicted numbers of total (transitional effector memory and central memory) cells secreting IFN- $\gamma$ , over time, for the mean macaque and human subpop-

**TABLE 1** Population mean parameter estimates for analyses 1 and 2 for macaques and humans<sup>a</sup>

Parameter or statistic	Macaques					Humans				
	All (analysis 1)		Covariates (analysis 2)			All (analysis 1)		Covariates (analysis 2)		
	Value	RSE (%)	Subpop.	Value	RSE (%)	Value	RSE (%)	Subpop.	Value	RSE (%)
Parameter (unit)										
Initial no. of TEM cells (TEM <sub>0</sub> ) (cells) (E)	20.7	29	Chi	0.29	39*	59.9	17	BCG: Y	149	15
			Maur	65.1	24			BCG: N	30.6	14
			Indo	23.2	41*					
			R: Ind	15.7	20					
Gamma PDF curve multiplier (L) (scalar) (E)	1,170	13	Chi	617	43*	1,490	14	BCG: Y	3,240	14
			Maur	1,460	28			BCG: N	747	14
			Indo	1,100	45*					
			R: Ind	1,250	14					
Gamma PDF curve shape parameter (k) (scalar) (E)	3.31	5	Chi	4.3	11	1.45	9		1.55	16
			Maur	3.15	10					
			Indo	3	20					
			R: Ind	3.53	6					
Gamma PDF curve scale parameter (h) (scalar) (E)	15	8		13.8	7	18.4	18	BCG: Y	21.7	24
								BCG: N	15.2	34*
Initial no. of CM cells (CM <sub>0</sub> ) (cells) (F)	0			0		0			0	
TEM cell terminal mortality rate ( $\mu_{\text{TEM}}$ ) (/day) (F)	0.1			0.1		0.083			0.083	
Proportion of TEM cells that die (p) (proportion) (F)	0.925			0.925		0.925			0.925	
Within-population variation (WPV) (%)										
Initial TEM cell population (TEM <sub>0</sub> )	130	25		41	27	107	15		52	19
Gamma PDF curve multiplier (L)	96	13		90	13	95	10		61	12
Gamma PDF curve shape parameter (k)	24	24		23	24	25	28		32	33*
Gamma PDF curve scale parameter (h)	19	21		21	20	58	25		43	37*
Goodness-of-fit statistics										
-2LL	7,209			7,183		2,738			2,653	
BIC	7,253			7,251		2,779			2,706	

<sup>a</sup>For details on the parameter-covariate relationship, see the supplemental material. F, fixed; E, estimate; TEM, transitional effector memory; CM, central memory; PDF, probability density function; RSE, relative standard error; subpop., subpopulation; Chi, Chinese cynomolgus macaques; Maur, Mauritian cynomolgus macaques; Indo, Indonesian cynomolgus macaques; R: Ind, Indian rhesus macaques; BCG: Y, human participants who were BCG vaccinated at baseline; BCG: N, human participants who were BCG naïve at baseline; -2LL, -2 log likelihood; BIC, Bayesian information criteria. RSEs of  $\geq 30\%$  are marked with asterisks.

ulation data. These model dynamics present a prediction for the phenotypic behavior of CD4<sup>+</sup> T cells and the ways in which they differ between species and subpopulations, which can be validated experimentally.

## DISCUSSION

In our proof-of-concept study, we applied novel immunostimulation/immunodynamic (IS/ID) modeling to BCG immune response data and found that the macaque colony and the human baseline BCG status were significantly ( $P < 0.05$ ) associated with the BCG-induced IFN- $\gamma$  immune response. No other population covariates were significantly associated. For baseline BCG-naïve humans, Indonesian cynomolgus macaques and Indian rhesus macaques best predicted the immune response. For baseline BCG-vaccinated humans, Mauritian cynomolgus macaques best predicted the immune response.

A key strength of this proof-of-concept study was the application of mathematical modeling techniques to vaccine data that are rarely explored quantitatively. We used established robust quantitative and statistical frameworks (compartmental mathematical models with nonlinear mixed-effects modeling [NLMEM] [29]) to explore the complex biological dynamics, giving an early example of the utility of IS/ID modeling. The biological data we used were standardized between species, with respect to time points and laboratory techniques, which allowed a direct comparison of the immune responses to BCG vaccination.

Although our model was a highly simplified version of the complexities of the immune system (see the discussion in the supplemental material for the main assumptions and their impact [Table S14]), analysis 1 showed that the model described the

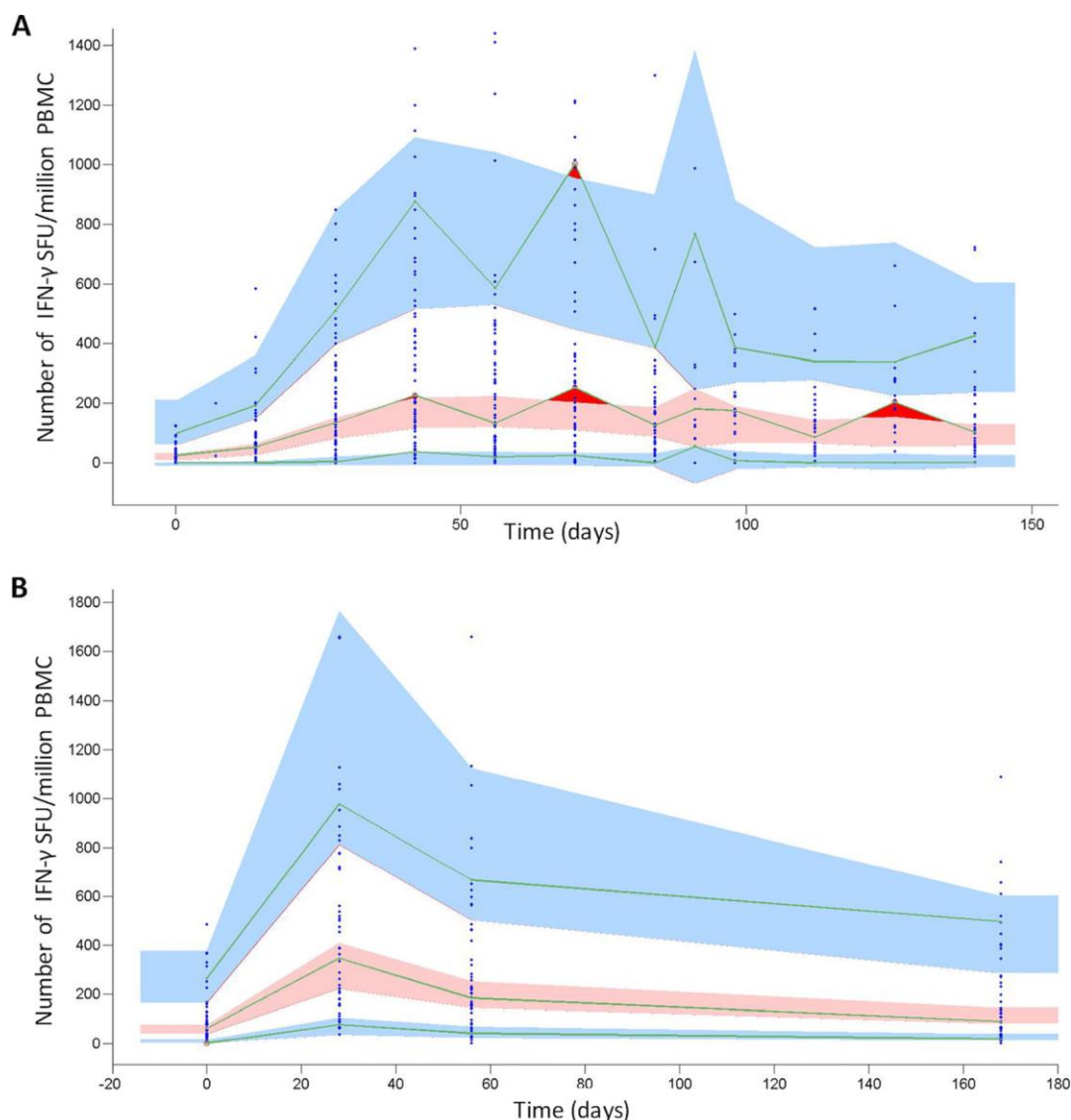


**FIG 2** VPC plots showing the number of IFN- $\gamma$  SFU per million PMBC, by time (days) for all macaques (A) and all humans (B). The VPC plot assesses the appropriateness of the proposed mathematical model (Fig. 1) for describing the empirical data by comparing the data simulated using the model, the population mean parameters, and associated variances (Table 1) to the empirical data distribution (see the supplemental material for more details). Blue points show empirical data. Pink regions represent the ranges of the medians of the simulated data for 500 simulations. Blue regions represent the ranges of the 90th and 10th percentiles of the simulated population data. The green lines link the empirical percentiles (10th, 50th, and 90th). Dark red regions show where the empirical data fall outside the ranges of the simulated percentiles. The lack of dark red regions (aside from cases in which data are variable between time points in macaques) indicates that our proposed mathematical model (Fig. 1) adequately represents the empirical data.

data well. The model was also a good description of the subpopulation data in analysis 2. However, when the model was calibrated to smaller subpopulation sizes (especially for the Chinese and Indonesian cynomolgus macaques), the estimated model parameters were more uncertain than for the larger populations (see the relative standard error [RSE] values in Table 1). Access to larger data sets on these populations would increase the certainty of the parameter estimates. Additionally, in analysis 2, our aim was to establish how population covariates affect the model parameters using a stepwise addition method. However, as Whittingham et al. point out, there are inherent drawbacks with such a method, despite its widespread use (30).

By modeling the recruitment rate of transitional effector memory cells by the function  $\delta$ , we were able to represent the nonlinear stimulation of the CD4 T cell response following BCG vaccination, allowing comparison of the dynamics of the response

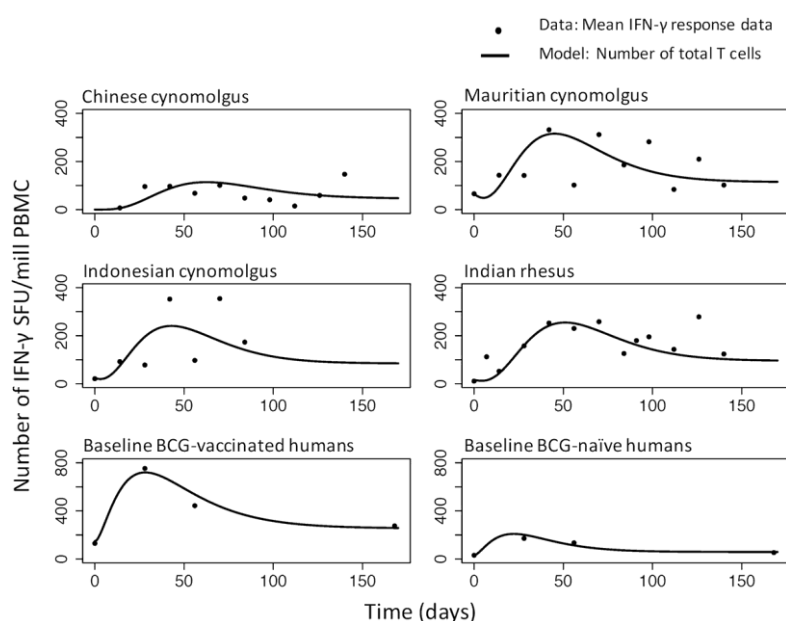


**FIG 3** Total number of T cells secreting IFN- $\gamma$  (the sum of the number of transitional effector memory cells and resting central memory cells) over time. Each point represents the mean of the data at a particular time point. Lines represent model predictions. Model predictions use the estimated subpopulation model parameters from Table 1 for the four macaque colonies and the two human subpopulations with different BCG statuses. (Note the differences in scale between macaques and humans.)

between subpopulations. However, since the recruitment rate of transitional effector memory cells was not based on biological data and was characterized by a theoretical shape, it is difficult to make direct biological interpretations of the parameters. To incorporate a mechanistic stimulation curve in future work, data on the cells involved in the stimulation response would be required.

The results in this analysis were consistent with previous work, in which we applied descriptive statistics to the human data (28). In that study, men experienced a higher baseline IFN- $\gamma$  response ( $P < 0.1$ ) than women. A similar pattern can be seen in the current work: the median initial number of transitional effector memory cells ( $TEM_0$ ) for men is higher than that of women (Fig. S8 in the supplemental material). Additionally, the model in analysis 2 is consistent with our previous findings (28) for humans, in which immune responses were higher in magnitude and were sustained longer for baseline BCG-vaccinated humans than for baseline BCG-naïve humans. Therefore, our results suggest that BCG revaccination provides a higher and more sustained IFN- $\gamma$  response than primary vaccination in humans. Finally, our results suggest that there are differences in BCG response between different colonies of macaques. This is consistent with work by Langermans et al., who show that rhesus macaques experience a higher IFN- $\gamma$  response 13 weeks after BCG vaccination than cynomolgus macaques (22), although the potential effect of the colony on IFN- $\gamma$  response was not highlighted in that work. Differences in responses across macaque colonies have also been found in *M. tuberculosis* challenge studies: Sharpe et al. showed that the  $AUC_{12Week}$  (area under the concentration-time curve at 12 weeks) values for IFN- $\gamma$ -secreting CD4 T cells were significantly higher for Indian rhesus macaques than for Indonesian cynomolgus (21). Although we do not consider *M. tuberculosis* challenge in our analysis, these differences may be important to consider when one is selecting an NHP model for human mycobacterial immune response.

Our results imply that responses in Indonesian cynomolgus macaques, followed by those in Indian rhesus macaques, most closely resembled the response in primary-vaccinated humans determined by enzyme-linked immunospot (ELISPOT) assays. However, we approach this conclusion with caution, since the sample sizes of the macaque

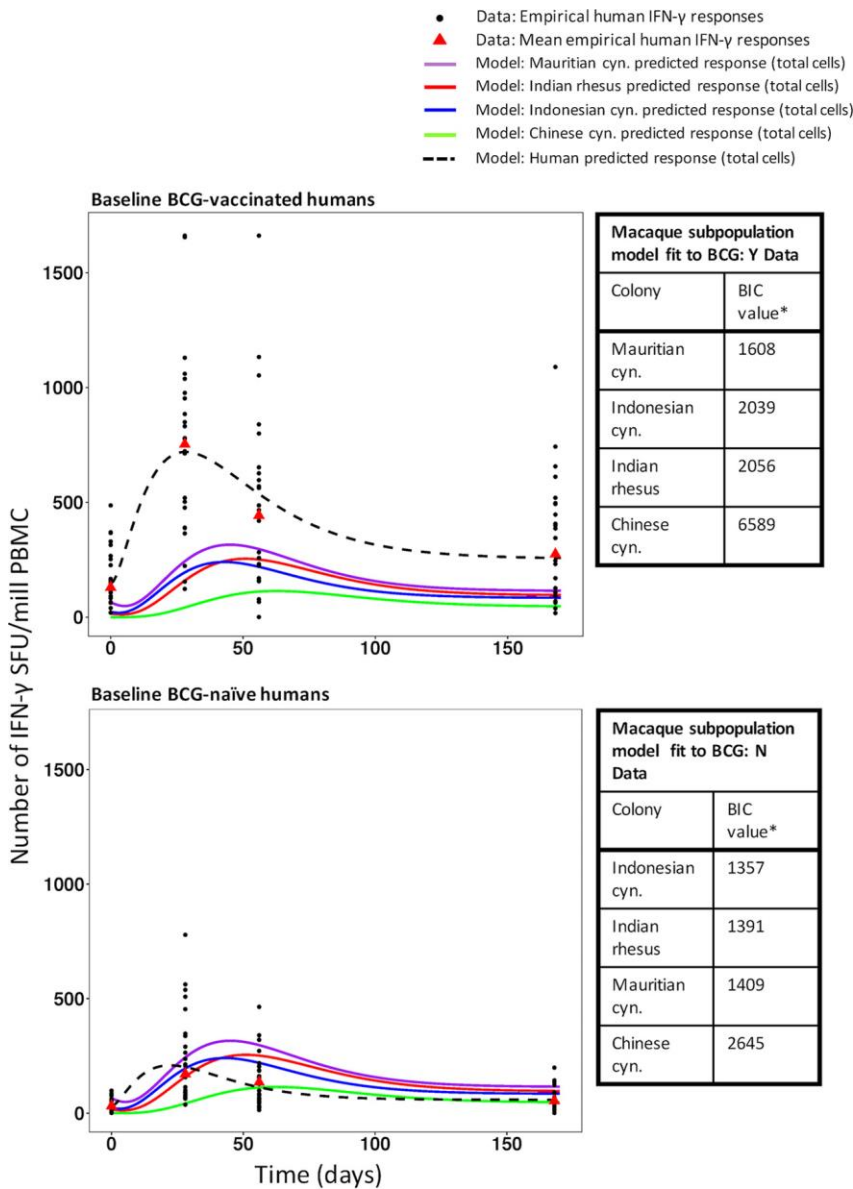


**FIG 4** Mean immune responses of the four macaque colonies and of human subpopulations that were BCG vaccinated (BCG: Y) or BCG naïve (BCG: N) at baseline. Empirical data for human responses are represented by black points (individual data) and red triangles (means). Lines show model predictions. The tables show the results of assessments of the ability of the calibrated macaque colony mathematical model parameters (Table 1, analysis 2) to describe the data for the human BCG: Y and BCG: N subpopulations. Bayesian information criterion (BIC) values are listed in ranked order, from lowest to highest. Asterisks indicate that all differences in BIC values are significant (a BIC value difference of >6 is considered significant [46]). cyn., cynomolgus.

colony subpopulations were variable. With these smaller sample sizes, model parameterization and validation are less reliable than for larger groups. More data on the colonies with small sample sizes should be collected and remodeled to verify our results. Nevertheless, the large sample size obtained for the Indian rhesus macaques was collated over decades of experimentation. Conventional vaccine studies in macaques are often limited to 6 to 9 animals per group due to space and cost. These smaller macaque experiments are then used to inform clinical vaccine trials, making our small sample sizes more representative of current vaccine development than the large rhesus macaque data set.

It should be noted that in terms of BCG vaccination history, the baseline BCG-naïve human subpopulation is the most comparable to all of the macaque subpopulations.

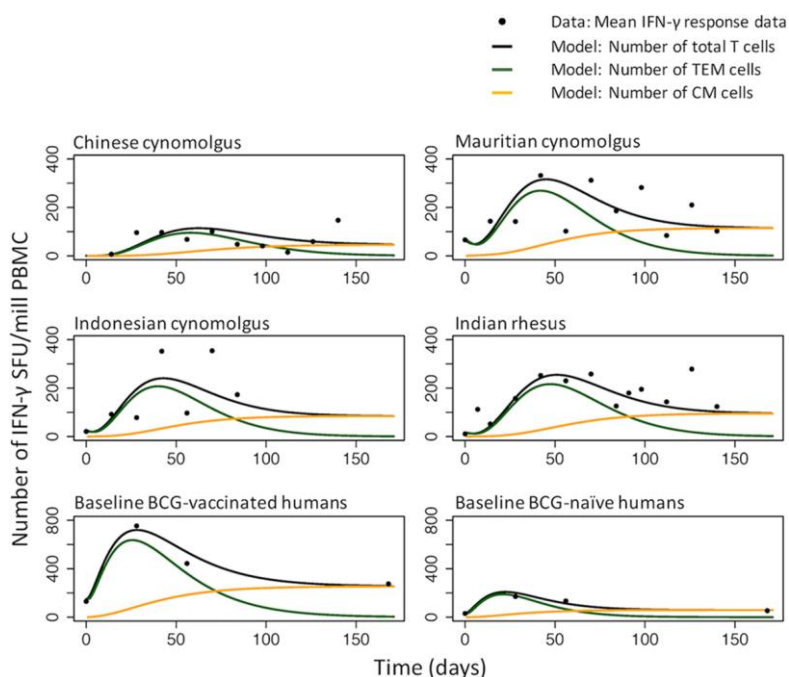


**FIG 5** Mean IFN- $\gamma$  response data (black points) and model predictions for the total number of T cells secreting IFN- $\gamma$  (black lines), the number of transitional effector memory (TEM) cells (green lines), and the number of resting central memory (CM) cells (orange lines) over time. Model predictions use the estimated subpopulation model parameters from Table 1 for the four macaque colonies and the two human subpopulations with different BCG statuses. (Note the differences in scale between macaques and humans.)

Mauritian cynomolgus macaques mounted the highest response to a primary BCG vaccination, and therefore, their data most closely resemble those for revaccination in humans. However, it is apparent from Fig. 4 that the BCG-vaccinated humans experienced a considerably higher magnitude of responses than all of the macaque subpopulations (which were BCG naïve at baseline). This suggests that the immune response to an antigen encountered for the first time is lower and slower than the response induced to the same antigen on subsequent occasions (31). Our results therefore suggest that a revaccinated macaque animal model may be most appropriate for revaccinated humans. This should be considered in further IS/ID translational analysis between macaques and humans.

In our analyses, we consider only a UK-based human population. In future evaluations, an analysis similar to that presented here could be carried out on populations from various geographical locations, since BCG responses have been shown to differ by geographic location (32). Other population covariates, such as age, may also be important (8). Additionally, the question of whether this analysis will be appropriate for other candidate vaccines would benefit from further scrutiny.

Figure 5 explores the dynamics of the constituent T cell populations and provides insights into how and when memory may be developed—an important consideration in vaccine regimen design, i.e., the timing of revaccination and differences between subpopulations. However, we do not currently have data to support these dynamics, so future work could be undertaken using flow cytometry to characterize the relative numbers of complex phenotypic cell types over time and thus to inform models that can provide a better understanding of T-cell dynamics.

In this analysis, we used solely IFN- $\gamma$  as a proxy for BCG vaccine immunogenicity (33) and did not consider BCG efficacy measures explicitly. We understand that in order to develop a vaccine, both immunogenicity and efficacy are vital considerations. Therefore, in predicting which macaque model best represents the human vaccine response, vaccine efficacy cannot be ignored. However, to incorporate efficacy would require

more-complex models and data than those we present here. As more immunological information or functional parameters become available, IS/ID modeling methods will allow us to easily integrate new information, e.g., on cytokines, cells, or (for efficacy measures) bacterial counts. Thus, we will be able to make decisions on the best NHP model to use based on a more complete vaccine performance framework.

**Conclusion.** This work suggests that the immune responses of different human subpopulations may be best modeled by different macaque colonies, and it demonstrates the potential utility of immunostimulation/immunodynamic modeling to accelerate the development of TB vaccines.

## MATERIALS AND METHODS

**Data.** Data on the number of purified protein derivative (PPD)-stimulated CD4<sup>+</sup> T cells secreting IFN- $\gamma$  (in spot forming units [SFU] per 1 million peripheral blood mononuclear cells [PBMC]), measured by an *ex vivo* IFN- $\gamma$  ELISPOT assay, were available for 55 humans and 81 macaques. BCG vaccination was given on day zero, and ELISPOT measurements were performed up to 140 days after vaccination. The details of the human data set and laboratory techniques have been published previously (28). Briefly, healthy UK volunteers aged 18 to 55 years, either with no history of BCG vaccination or previously immunized with BCG, were given 100  $\mu$ l of BCG, administered intradermally in the upper arm. Immune responses to BCG were measured using an IFN- $\gamma$  ELISPOT assay at weeks 1, 4, 8, and 24. For demographics and laboratory details, see the supplemental material (Table S1; Fig. S1). All macaque studies were conducted in accordance with the Home Office (UK) Code of Practice for the Housing and Care of Animals Used in Scientific Procedures (1989) and the Guidelines on Primate Accommodation, Care and Use of the National Committee for Refinement, Reduction and Replacement (NC3Rs), issued in August 2006. All animal procedures were approved by the Public Health England, Porton Down Ethical Review Committee, and were authorized under an appropriate UK Home Office project license. Vaccination, sample collection procedures, and immunological methods are described in full in references 19, 23, 34, and 35). All macaques were demonstrated to be mycobacterially naïve prior to BCG vaccination and were between the ages of 3 and 14 years. The human population covariates were baseline (before vaccination at time zero) BCG vaccination status (either BCG vaccinated [BCG: Y] or BCG naïve [BCG: N] at baseline), years since BCG vaccination (grouped as 1 to 9, 10 to 19, or 20 to 29 years, or “never”), gender, and monocyte-to-lymphocyte cell count ratio (ML ratio). The macaque population covariate was the colony of origin (Indian rhesus macaques; for cynomolgus macaques, Chinese, Mauritian, or Indonesian [see Table S2 and Fig. S2 in the supplemental material]). Rhesus macaques and cynomolgus macaques of the Indonesian and Mauritian genotypes were obtained from established UK breeding colonies. Chinese cynomolgus macaques were imported from a Home Office-approved breeding colony in China.

**Mathematical IS/ID model.** An ordinary differential-equation model was used to describe the IFN- $\gamma$  response dynamics of two CD4<sup>+</sup> T cell populations, transitional effector memory (36) and resting “central” memory cells, which are short- and long-lived, respectively (37–39) (Fig. 1). Briefly, cells were recruited into the transitional effector memory compartment at rate  $\delta$ . A proportion ( $p$ ) of transitional effector memory cells underwent apoptosis at rate  $\mu_{TEM}$ , and the remaining proportion ( $1 - p$ ) transitioned to a central memory phenotype, where they stayed for the duration of the model run (170 days) (Fig. 1). Central memory cells are quiescent in the host until stimulated by an antigen (31); however, we considered them here to contribute to IFN- $\gamma$  production, since the ELISPOT assay uses PPD to stimulate all potentially IFN- $\gamma$ -secreting CD4<sup>+</sup> T cells. To reflect this, the IFN- $\gamma$  immune response predicted by the mathematical model was the sum of the number of transitional effector memory and central memory cell populations over time. We assumed that any nonzero responses at baseline were existing memory responses that had immediately reverted to the transitional effector memory phenotype in the presence of an antigen. Therefore, the initial transitional effector memory population ( $TEM_0$ ) was positive for those subjects. We assumed that the increases in the number of transitional effector memory and central memory cells did not occur immediately after vaccination but gradually increased over time due to immune processes such as vaccine antigen trafficking and presentation (31, 40). This increase then subsided, as T cell stimulation was assumed not to last indefinitely (31, 40–43). The recruitment of transitional effector memory cells over time was controlled in the model using the recruitment rate  $\delta$ , which was a peaked curve specified using a gamma probability density function (PDF) distribution with parameters  $L$ ,  $k$ , and  $h$  (Fig. 1).

**Analyses. (i) Analysis 1. Calibration of the model to IFN- $\gamma$  data and exploration of model predictions for macaques and humans separately.** In analysis 1, the model was calibrated to the macaque and human data separately to quantify the dynamics of the IFN- $\gamma$  response for each species. To do this, three parameters (the components of function  $\delta$ :  $L$ ,  $k$ , and  $h$  [Fig. 1]) and  $TEM_0$ , the initial number of transitional effector memory cells, were estimated using the established method of nonlinear mixed effects modeling (NLMEM) (29) using the software *Monolix* v. 4.3.3 (44). Briefly, NLMEM uses maximum likelihood methods to estimate the model parameters that best describe the population mean response and the associated parameter variance which accounts for the within-population variation (for more details see reference 45). Evaluation of the model’s ability to describe the data was conducted primarily by simulation-based, visual predictive check (VPC) plots (see the supplemental material for details); assessment of the precision of the estimated parameters using the relative standard error (RSE) and a goodness of fit measure (Bayesian Information Criteria [BIC]). A difference in BIC of  $>6$  was considered a significant ( $P$  value  $< 0.05$ ) effect (46) and a parameter RSE of  $<30\%$  was considered a

well-estimated parameter. The proportion of transitional effector memory cells that die ( $p$ ) was assumed to be 0.925, as supported by literature (38) (Fig. 1; Table 1) and the parameter governing the mortality rate of transitional effector memory cells,  $\mu_E$ , was fixed after a scenario analysis was conducted (Table S3). Further tests required to establish the NLMEM framework are outlined in Tables S4 to S6.

**(ii) Analysis 2. Population covariate impact on within-population variation in model parameter estimates.** In analysis 2, we explored whether population covariates (i.e., subpopulations, such as different colonies) could reduce the within-population variation of the estimated parameters from that in analysis 1, and we thus established subpopulation models for macaques and humans separately. To do this, covariate-parameter relationships were tested and selected based on a forward-addition strategy and likelihood ratio test method (see the supplemental material for details). Once the appropriate covariate-parameter relationship was found, the subpopulation model was calibrated to the data and the subpopulation parameters estimated. We observed the change in the BIC values and within-population variation of model parameters from analysis 1 to analysis 2 as a result of accounting for the population covariates.

**(iii) Analysis 3. Which macaque subpopulations best predicted immune responses in different human subpopulations?** To evaluate which macaque subpopulations best predicted the immune responses in different human subpopulations, estimated parameters and parameter variances from the macaque subpopulation model (analysis 2) were fit to the human data (or human subpopulation data [analysis 2]). The subpopulation of macaques that best described the human data was defined as the model with the lowest BIC.

**(iv) Analysis 4. Predicted numbers of TEM and resting CM cells over time.** The calibrated mathematical model was then used to predict the number of transitional effector memory (36) and resting central memory cells over time. These dynamics were not measured empirically.

## SUPPLEMENTAL MATERIAL

Supplemental material for this article may be found at <https://doi.org/10.1128/CVI.00525-16>.

**SUPPLEMENTAL FILE 1**, PDF file, 3.6 MB.

## ACKNOWLEDGMENTS

We thank our colleagues at INSERM (J. Guedj and F. Mentre), Paris, France, who provided training on NLMEM methods.

S.J.R. is supported by a LSHTM studentship funded by Aeras. G.M.K. is funded by the National Institute for Health Research Health Protection Research Unit (NIHR HPRU) in Healthcare Associated Infection and Antimicrobial Resistance at Imperial College London in partnership with Public Health England (PHE). The views expressed are those of the authors and not necessarily those of the NHS, the NIHR, the Department of Health, or Public Health England. R.G.W. is funded by the UK Medical Research Council (MRC) and the UK Department for International Development (DFID) under the MRC/DFID Concordat agreement, which is also part of the EDCTP2 program supported by the European Union (MR/P002404/1), the Bill and Melinda Gates Foundation (TB Modeling and Analysis Consortium: OPP1084276/OPP1135288, SA Modeling for Policy: OPP1110334, CORTIS: OPP1137034, Vaccines: OPP1160830), and UNITAID (4214-LSHTM-Sept15; PO 8477-0-600).

We declare no competing financial interests.

## REFERENCES

1. WHO. 2015. Global tuberculosis report 2015. World Health Organization, Geneva, Switzerland.
2. Mangtani P, Abubakar I, Ariti C, Beynon R, Pimpin L, Fine PE, Rodrigues LC, Smith PG, Lipman M, Whiting PF, Sterne JA. 2014. Protection by BCG vaccine against tuberculosis: a systematic review of randomized controlled trials. *Clin Infect Dis* 58:470–480. <https://doi.org/10.1093/cid/cit790>.
3. Dye C. 2013. Making wider use of the world's most widely used vaccine: Bacille Calmette-Guerin revaccination reconsidered. *J R Soc Interface* 10:20130365. <https://doi.org/10.1098/rsif.2013.0365>.
4. Dye C, Glaziou P, Floyd K, Raviglione M. 2013. Prospects for tuberculosis elimination. *Annu Rev Public Health* 34:271–286. <https://doi.org/10.1146/annurev-publhealth-031912-114431>.
5. Acosta A, Norazmi MN, Hernandez-Pando R, Alvarez N, Borrero R, Infante JF, Sarmiento ME. 2011. The importance of animal models in tuberculosis vaccine development. *Malays J Med Sci* 18:5–12.
6. Tanner R, McShane H. 26 September 2016. Replacing, reducing and refining the use of animals in tuberculosis vaccine research. *ALTEX* <https://doi.org/10.14573/altex.1607281>.
7. Flynn JL, Gideon HP, Mattila JT, Lin PL. 2015. Immunology studies in non-human primate models of tuberculosis. *Immunol Rev* 264:60–73. <https://doi.org/10.1111/imr.12258>.
8. McShane H, Williams A. 2014. A review of preclinical animal models utilised for TB vaccine evaluation in the context of recent human efficacy data. *Tuberculosis (Edinb)* 94:105–110. <https://doi.org/10.1016/j.tube.2013.11.003>.
9. Carlsson HE, Schapiro SJ, Farah I, Hau J. 2004. Use of primates in research: a global overview. *Am J Primatol* 63:225–237. <https://doi.org/10.1002/ajp.20054>.
10. Gormus BJ, Blanchard JL, Alvarez XH, Didier PJ. 2004. Evidence for a rhesus monkey model of asymptomatic tuberculosis. *J Med Primatol* 33:134–145. <https://doi.org/10.1111/j.1600-0684.2004.00062.x>.
11. Capuano SV, III, Croix DA, Pawar S, Zinovik A, Myers A, Lin PL, Bissel S, Fuhrman C, Klein E, Flynn JL. 2003. Experimental *Mycobacterium tuber-*

- culosis infection of cynomolgus macaques closely resembles the various manifestations of human *M. tuberculosis* infection. *Infect Immun* 71: 5831–5844. <https://doi.org/10.1128/IAI.71.10.5831-5844.2003>.
12. Pena JC, Ho WZ. 2015. Monkey models of tuberculosis: lessons learned. *Infect Immun* 83:852–862. <https://doi.org/10.1128/IAI.02850-14>.
  13. Kaushal D, Mehra S, Didier PJ, Lackner AA. 2012. The non-human primate model of tuberculosis. *J Med Primatol* 41:191–201. <https://doi.org/10.1111/j.1600-0684.2012.00536.x>.
  14. Scanga CA, Flynn JL. 2014. Modeling tuberculosis in nonhuman primates. *Cold Spring Harb Perspect Med* 4:a018564. <https://doi.org/10.1101/cshperspect.a018564>.
  15. Barclay WR, Anacker RL, Brehmer W, Leif W, Ribí E. 1970. Aerosol-induced tuberculosis in subhuman primates and the course of the disease after intravenous BCG vaccination. *Infect Immun* 2:574–582.
  16. Janicki BW, Good RC, Minden P, Affronti LF, Hymes WF. 1973. Immune responses in rhesus monkeys after bacillus Calmette-Guerin vaccination and aerosol challenge with *Mycobacterium tuberculosis*. *Am Rev Respir Dis* 107:359–366.
  17. Reed SG, Coler RN, Dalemans W, Tan EV, De La Cruz EC, Basaraba RJ, Orme IM, Skeiky YA, Alderson MR, Cowgill KD, Prieels JP, Abalos RM, Dubois MC, Cohen J, Mettens P, Lobet Y. 2009. Defined tuberculosis vaccine, Mtb72F/AS02A, evidence of protection in cynomolgus monkeys. *Proc Natl Acad Sci U S A* 106:2301–2306. <https://doi.org/10.1073/pnas.0712077106>.
  18. Kaushal D, Foreman TW, Gautam US, Alvarez X, Adekambi T, Rangel-Moreno J, Golden NA, Johnson AM, Phillips BL, Ahsan MH, Russell-Lodrigue KE, Doyle LA, Roy CJ, Didier PJ, Blanchard JL, Rengarajan J, Lackner AA, Khader SA, Mehra S. 2015. Mucosal vaccination with attenuated *Mycobacterium tuberculosis* induces strong central memory responses and protects against tuberculosis. *Nat Commun* 6:8533. <https://doi.org/10.1038/ncomms9533>.
  19. White AD, Sarfas C, West K, Sibley LS, Wareham AS, Clark S, Dennis MJ, Williams A, Marsh PD, Sharpe SA. 2015. Evaluation of the immunogenicity of *Mycobacterium bovis* BCG delivered by aerosol to the lungs of macaques. *Clin Vaccine Immunol* 22:992–1003. <https://doi.org/10.1128/CI.00289-15>.
  20. Sharpe SA, Eschelbach E, Basaraba RJ, Gleeson F, Hall GA, McIntyre A, Williams A, Kraft SL, Clark S, Gooch K, Hatch G, Orme IM, Marsh PD, Dennis MJ. 2009. Determination of lesion volume by MRI and stereology in a macaque model of tuberculosis. *Tuberculosis (Edinb)* 89:405–416. <https://doi.org/10.1016/j.tube.2009.09.002>.
  21. Sharpe S, White A, Gleeson F, McIntyre A, Smyth D, Clark S, Sarfas C, Laddy D, Rayner E, Hall G, Williams A, Dennis M. 2016. Ultra low dose aerosol challenge with *Mycobacterium tuberculosis* leads to divergent outcomes in rhesus and cynomolgus macaques. *Tuberculosis (Edinb)* 96:1–12. <https://doi.org/10.1016/j.tube.2015.10.004>.
  22. Langermans JA, Andersen P, van Soelingen D, Vervenne RA, Frost PA, van der Laan T, van Pinxteren LA, van den Hombergh J, Kroon S, Peekel I, Florquin S, Thomas AW. 2001. Divergent effect of bacillus Calmette-Guerin (BCG) vaccination on *Mycobacterium tuberculosis* infection in highly related macaque species: implications for primate models in tuberculosis vaccine research. *Proc Natl Acad Sci U S A* 98:11497–11502. <https://doi.org/10.1073/pnas.201404898>.
  23. Javed S, Marsay L, Wareham A, Lewandowski KS, Williams A, Dennis MJ, Sharpe S, Vipond R, Silman N, Ball G, Kempell KE. 2016. Temporal expression of peripheral blood leukocyte biomarkers in a *Macaca fascicularis* infection model of tuberculosis; comparison with human datasets and analysis with parametric/non-parametric tools for improved diagnostic biomarker identification. *PLoS One* 11:e0154320. <https://doi.org/10.1371/journal.pone.0154320>.
  24. The Collaboration for TB Vaccine Discovery (CVTD). 2014. BMGF TB vaccine strategy. <https://www.ctvd.co/Pages/Strategy.aspx>. Accessed January 2017.
  25. Knibbe CA, Zuideveld KP, Aarts LP, Kuks PF, Danhof M. 2005. Allometric relationships between the pharmacokinetics of propofol in rats, children and adults. *Br J Clin Pharmacol* 59:705–711. <https://doi.org/10.1111/j.1365-2125.2005.02239.x>.
  26. Dubois VF, de Witte WE, Visser SA, Danhof M, Della Pasqua O, Cardiovascular Safety Project Team, TI Pharma PKPD Platform. 2016. Assessment of interspecies differences in drug-induced QTc interval prolongation in cynomolgus monkeys, dogs and humans. *Pharm Res* 33:40–51. <https://doi.org/10.1007/s11095-015-1760-9>.
  27. Mould DR, Upton RN. 2012. Basic concepts in population modeling, simulation, and model-based drug development. *CPT Pharmacometrics Syst Pharmacol* 1:e6. <https://doi.org/10.1038/psp.2012.4>.
  28. Rhodes SJ, Knight GM, Fielding K, Scriba TJ, Pathan AA, McShane H, Fletcher H, White RG. 2016. Individual-level factors associated with variation in mycobacterial-specific immune response: gender and previous BCG vaccination status. *Tuberculosis (Edinb)* 96:37–43. <https://doi.org/10.1016/j.tube.2015.10.002>.
  29. Lavielle M. 2015. Mixed effects models for the population approach: models, tasks, methods and tools. CRC Press, Boca Raton, FL.
  30. Whittingham MJ, Stephens PA, Bradbury RB, Freckleton RP. 2006. Why do we still use stepwise modelling in ecology and behaviour? *J Anim Ecol* 75:1182–1189. <https://doi.org/10.1111/j.1365-2656.2006.01141.x>.
  31. Abbas A, Lichtman A, Pillai S. 2015. Cellular and molecular immunology, 8th ed. Elsevier Saunders, Philadelphia, PA.
  32. Weir RE, Black GF, Nazareth B, Floyd S, Stenson S, Stanley C, Branson K, Sichali L, Chaguluka SD, Donovan L, Crampin AC, Fine PE, Dockrell HM. 2006. The influence of previous exposure to environmental mycobacteria on the interferon-gamma response to bacille Calmette-Guerin vaccination in southern England and northern Malawi. *Clin Exp Immunol* 146:390–399. <https://doi.org/10.1111/j.1365-2249.2006.03222.x>.
  33. Fletcher HA. 2007. Correlates of immune protection from tuberculosis. *Curr Mol Med* 7:319–325. <https://doi.org/10.2174/156652407780598520>.
  34. White AD, Sibley L, Dennis MJ, Gooch K, Betts G, Edwards N, Reyes-Sandoval A, Carroll MW, Williams A, Marsh PD, McShane H, Sharpe SA. 2013. Evaluation of the safety and immunogenicity of a candidate tuberculosis vaccine, MVA85A, delivered by aerosol to the lungs of macaques. *Clin Vaccine Immunol* 20:663–672. <https://doi.org/10.1128/CI.00690-12>.
  35. Sharpe SA, McShane H, Dennis MJ, Basaraba RJ, Gleeson F, Hall G, McIntyre A, Gooch K, Clark S, Beveridge NE, Nuth E, White A, Marriott A, Dowall S, Hill AV, Williams A, Marsh PD. 2010. Establishment of an aerosol challenge model of tuberculosis in rhesus macaques and an evaluation of endpoints for vaccine testing. *Clin Vaccine Immunol* 17: 1170–1182. <https://doi.org/10.1128/CI.00079-10>.
  36. Seder RA, Darrah PA, Roederer M. 2008. T-cell quality in memory and protection: implications for vaccine design. *Nat Rev Immunol* 8:247–258. <https://doi.org/10.1038/nri2274>.
  37. Pepper M, Jenkins MK. 2011. Origins of CD4(+) effector and central memory T cells. *Nat Immunol* 12:467–471. <https://doi.org/10.1038/nrm3166>.
  38. Kaech SM, Wherry EJ, Ahmed R. 2002. Effector and memory T-cell differentiation: implications for vaccine development. *Nat Rev Immunol* 2:251–262. <https://doi.org/10.1038/nri778>.
  39. McKinstry KK, Strutt TM, Swain SL. 2010. The potential of CD4 T-cell memory. *Immunology* 130:1–9. <https://doi.org/10.1111/j.1365-2567.2010.03259.x>.
  40. Urdahl KB, Shafiani S, Ernst JD. 2011. Initiation and regulation of T-cell responses in tuberculosis. *Mucosal Immunol* 4:288–293. <https://doi.org/10.1038/mi.2011.10>.
  41. Chackerian AA, Alt JM, Perera TV, Dascher CC, Behar SM. 2002. Dissemination of *Mycobacterium tuberculosis* is influenced by host factors and precedes the initiation of T-cell immunity. *Infect Immun* 70:4501–4509. <https://doi.org/10.1128/IAI.70.8.4501-4509.2002>.
  42. Cooper AM. 2009. Cell-mediated immune responses in tuberculosis. *Annu Rev Immunol* 27:393–422. <https://doi.org/10.1146/annurev.immunol.021908.132703>.
  43. De Rosa SC. 2004. Multicolor immunophenotyping: human mature immune system. *Methods Cell Biol* 75:577–594. [https://doi.org/10.1016/S0091-679X\(04\)75024-4](https://doi.org/10.1016/S0091-679X(04)75024-4).
  44. Lixoft. 2014. Monolix: user guide, version 4.3.3. Lixoft, Antony, France. <http://lixoft.com/ressources/legacy-documentation/>.
  45. Lavielle M, Mentre F. 2007. Estimation of population pharmacokinetic parameters of saquinavir in HIV patients with the MONOLIX software. *J Pharmacokinet Pharmacodyn* 34:229–249. <https://doi.org/10.1007/s10928-006-9043-z>.
  46. Raftery A. 1995. Bayesian model selection in social research. *Sociolog Methodol* 25:111–163. <https://doi.org/10.2307/271063>.

## Supplementary Material for paper 2

The following is the published supplementary material referenced in paper 2. All references to the below tables and Figures are preceded with the suffix “S” in the paper.

### **Additional Methods**

#### Human and macaque demographics and IFN- $\gamma$ response data longitudinal plots

*(The following text on human data and laboratory methods are text taken from my paper 1 [111])*

Human demographic data and IFN- $\gamma$  longitudinal plot stratified by BCG status can be found in Table S1 and Figure S1, respectively.

Total population	55
Age; median (range)	25 (18, 55)
Baseline-BCG status	BCG: N= 30, BCG: Y=25
Gender	M=19, F=36
Time since BCG vaccination	
1 to 9	7 (M = 2)
10 to 19	10 (M = 6)
20 to 29	8 (M = 3)
Never	30 (M = 8)
ML ratio; median (range)	0.26 (0.07, 0.56)

**Table S1. Human demographics**

The available data were on HIV negative and *Mtb.* naïve participants (see [242, 319, 320] for HIV and *Mtb.* latency testing procedures). Data on haematological parameters were based on routine laboratory haematology testing at baseline and only those participants with values within normal limits were included in clinical trials. IFN- $\gamma$  response was measured using a standardized ELISPOT assay which quantifies IFN- $\gamma$  secreting CD4+ T cells as spot forming units (SFU) per million PBMCs using PPD as a stimulant. The same ELISPOT method including plates, antibody kits, antigens, developing reagents, washing method, ELISPOT reader and ELISPOT

counting method were used in all the data collection. As these BCG studies were conducted as part of a series of Phase I clinical trials with MVA85A all lab protocols and lab reagents were harmonized as far as possible. For the IFN- $\gamma$  ELISPOT assay 300,000 PMBC per well were performed in duplicate and the results were averaged. Incubation time was 18 hours. For the exact laboratory methodology see [242, 319, 320].

The covariates included in this analysis were gender, BCG vaccination history at baseline and baseline ML ratio. For details on how BCG-vaccination history was determined see original trial methods [242, 319, 320]. BCG vaccination history was categorised into “never” and 10-year time-periods since vaccination with the reference group as 1 to 9 years since BCG vaccination. Age was not included as a covariate as it was colinear with BCG vaccination history.

For macaques, colony demographics can be found in Table S2 and the IFN- $\gamma$  longitudinal plot stratified by colony can be found in Figure S2.

<b>Species (% of total animals)</b>	<b>Colony (% of total animals)</b>
Rhesus, n= 58 (72%)	India, n= 58 (72%)
Cynomolgus, n= 23 (28%)	Mauritian, n=12 (15%)
	Chinese, n=6 (8%)
	Indonesian, n= 5 (6%)

**Table S2. Macaque demographics**

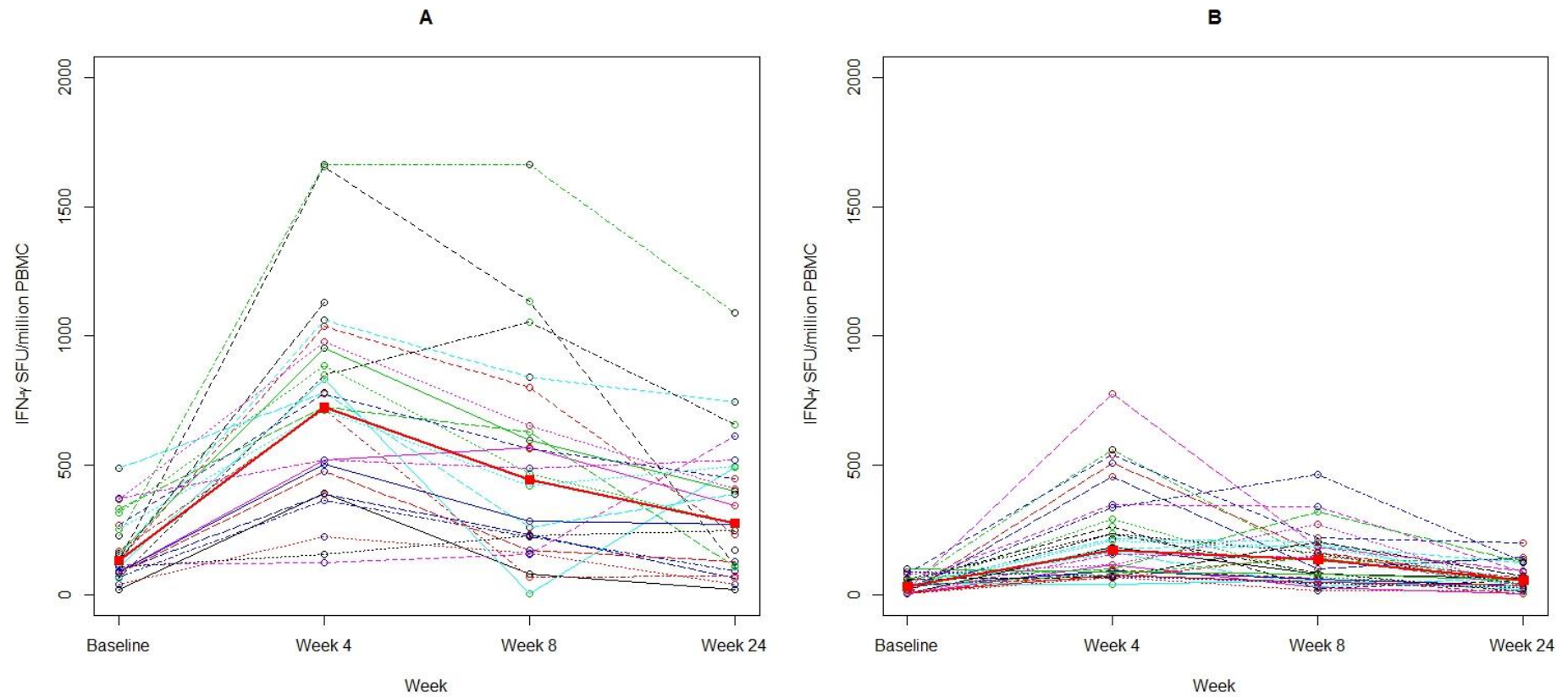


**Figure S1. Longitudinal IFN- $\gamma$  responses for analysis for 55 human participants. Baseline-BCG vaccinated (A) and baseline-BCG naive (B). The bold line represents the median values of each group at each time point. X-axis is not to scale. Abbreviations: IFN- $\gamma$  = Interferon gamma ; SFU = spot forming unit ; PBMC = peripheral blood mononuclear cells**

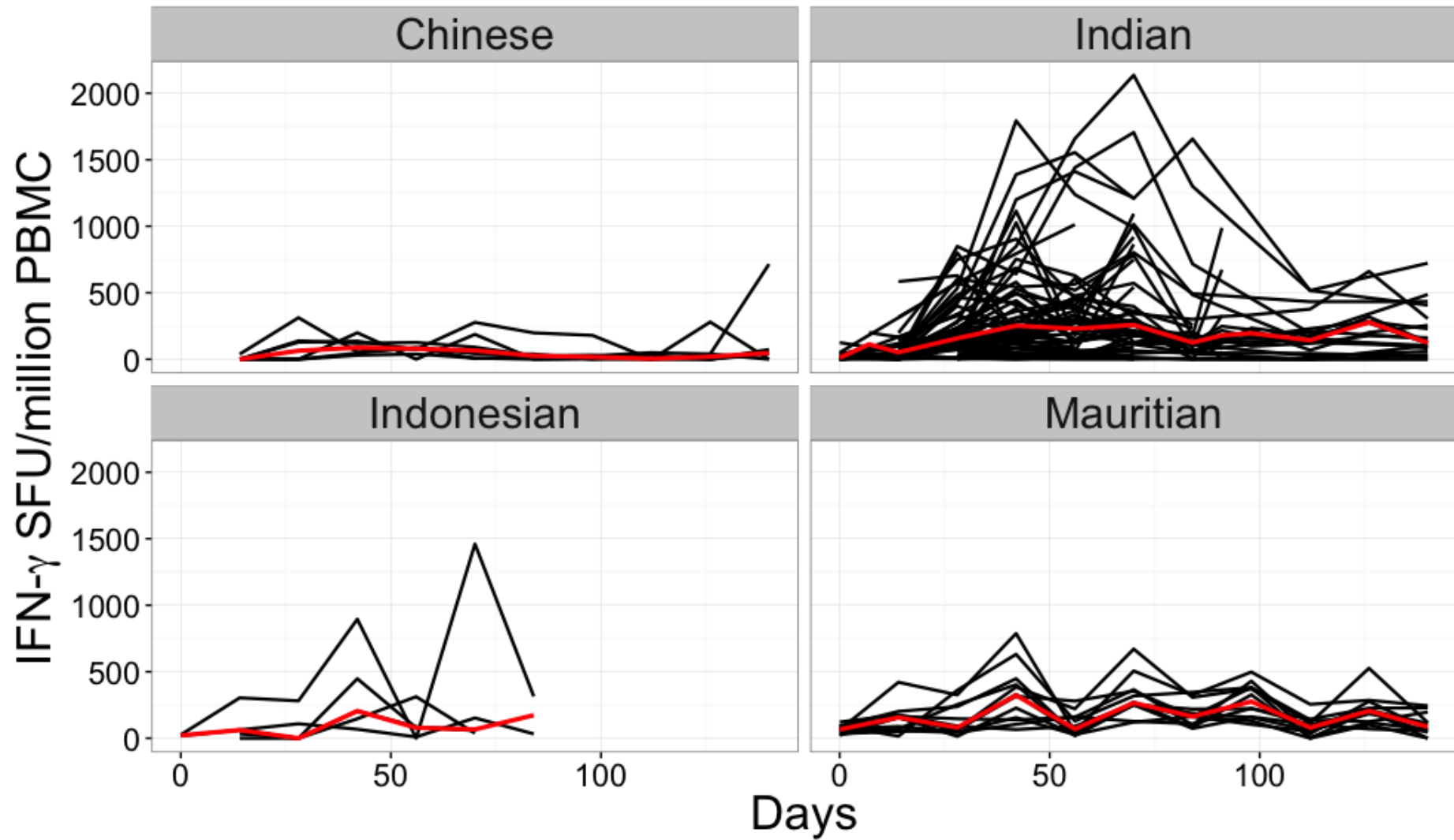


Figure S2. Number of IFN- $\gamma$  secreting CD4+ T cells per million PBMCs over time as measured by the ELISPOT assay in macaques. Data is shown for each colony separately, Chinese, Indonesian and Mauritian cynomolgus macaques and Indian rhesus macaques. The red line indicates median responses.

## Mathematical vaccine Immunostimulation/Immunodynamic (IS/ID) Model Equations

The equations for the IS/ID two-compartmental in Figure 1 in paper 2 were as follows:

$$\frac{dTEM}{dt} = \delta - p\mu_{TEM}TEM - (1-p)\mu_{TEM}TEM \quad (1)$$

$$\frac{dCM}{dt} = (1-p)\mu_{TEM}TEM \quad (2)$$

Where TEM represents the transitional effector memory (TEM) cell population, CM, the resting central memory (CM) cell population, t, the time in days and parameters outlined in Figure 1. The equation for the recruitment of the TEM cell population,  $\delta$ , is:

$$\delta = L * \frac{\left(\frac{1}{h}\right)^k}{\Gamma(k)} * time^{(k-1)} * e^{-\left(\frac{1}{h}*time\right)} \quad (3)$$

Where L, h and k are the gamma PDF parameters outlined in Figure 1.

### Analyses

Analysis 1: Model calibration to IFN- $\gamma$  data and exploration of model predictions for macaque and humans, separately

#### *Scenario analysis for parameter $\mu_{TEM}$ (per day)*

Table S3 summarises the scenario analysis of parameter  $\mu_{TEM}$  in macaques and humans.

	Macaque	Human
Param $\mu_{TEM}$ (per day)	BIC	BIC
0.5	7269.01	2825.22
0.25	7259.65	2803.31
0.167	7254.20	2791.84
0.125	<b>7248.89</b>	2783.49
0.1	7251.55	<b>2778.53</b>
0.083	7254.49	2780.97

0.071	7259.81	2780.80
0.063	7263.44	2782.09
0.056	7264.81	2785.31
0.05	7271.37	2792.95
0.045	7276.46	2798.21

**Table S3. Scenario analysis for parameter  $\mu_{TEM}$  in macaques and humans**

In macaques the value of 0.13 for  $\mu_{TEM}$  resulted in the lowest BIC value, however there was no significant difference in the BIC for the values  $\mu_{TEM}$  from 0.167 to 0.083 (shaded) (see [321] for significance associated with difference of BIC values). Similarly, in humans the value of 0.1 for  $\mu_{TEM}$  resulted in the lowest BIC value, with no significant difference between values of 0.1 to 0.0625 (shaded).

#### *Residual Error (RE) Model*

Table S4 outlines the results of the RE model comparison for macaques and humans separately using BIC as an assessment of fit. For a detailed description of the residual error in NLMEM and how it is incorporated in Monolix, see Appendix B.

Error model	Model Description	Macaque	Human
		BIC	BIC
Constant	$Y = f+a*e$	7753.10	2895.72
Proportional	$Y = f+b*f*e$	-	2780.65
Combined	$Y = f+(a+b*f)*e$	7248.89	2776.66

**Table S4. Results of comparing residual error models using Monolix in-built tool. Definitions: Y = observation, f = model prediction, a,b= scalars to be determined during parameter estimation process, e = Normally distributed random variable N(0,1).**

The BIC for the human residual error model indicate that a combined model best represented the residual error in the data (as the BIC value was lower), however the proportional or combined model were not significantly different with respect to calibration to the data (the difference between the BIC value was <6, which according to Raftery [321], is a non-significant difference).

The same comparisons were made for the macaque dataset, however when a proportional RE model (i.e. without an additive term) was applied, the parameter  $TEM_0$  was poorly estimated, potentially due to a lack of data at time=0. Therefore, the BIC was compared between only the constant and combined RE models. As the BIC value as a result of calibration of the model to the macaque data with a combined RE model was considerably lower than the BIC value with the additive model (7248 vs. 7753), the combined RE model was chosen.

The estimated values for the residual error model for macaque and human can be found in Table S6.

#### *Test for random effects correlations*

It is important to test if the random effects (the variation) of the model parameters are co-dependent, i.e. correlated. I tested if any combination of parameters were correlated across the population with the inbuilt Monolix tool. Results for the pairwise test for random effects correlations for human and macaques are shown in Table S5.

Combination tested	Macaque			Human		
	BIC	Diff to "none" (BIC)	Decision to include	BIC	Diff to "none" (BIC)	Decision to include
None	7253	-	-	2779	-	-
$TEM_0$ & L	7252	0.94	No	2788	8.81 (higher)	No
$TEM_0$ & k	7256	3.21 (higher)	No	2782	2.62 (higher)	No
$TEM_0$ & h	7258	5.1 (higher)	No	2778	0.95	No
L & k	7256	2.2	No	2784	5.37 (higher)	No
L & h	7257	3.73 (higher)	No	2778	1.05	No
k & h	7218	35.6	No*	2787	8.17 (higher)	No

**Table S5. Tests for random effects correlations for macaques and humans**

All BIC values in Table S5 were non-significantly different from no random effects correlations in the macaque population except for when parameters k and h were correlated. \*However, applying this correlation meant that some parameters could not be accurately estimated (RSE% was NA) so it was not included. In the human population, all BIC values were either non-significantly lower, or higher than the model with no random effects correlations, so no correlations were considered necessary to apply in further analyses.

Analysis 2: Population covariate impact on within-population variation in model parameter estimates

To establish if there were significant differences in response dynamics by population covariate, I ran regression analysis on the individual model parameter estimates (resulting from analysis 1) with population covariates as the predictors. This was conducted in R [322] using graphical plots and non-parametric rank tests for each species separately. The non-parametric rank tests conducted to establish parameter-covariate relationships are as follows. For categorical covariates with 2 levels (BCG status and gender in humans) the Wilcoxon test was applied. For categorical covariates with 2+ categories (BCG vaccination history in human and colony in macaques) a kruskal-Wallis followed by a Dunn post-hoc test with a Bonferroni correction was applied. For continuous covariate, ML ratio, linear regression was applied. If a significant association ( $p\text{-value} < 0.05$ ) was found between model parameters and a covariate, a forward stepwise addition strategy was used in Monolix to establish a subpopulation-model. Here, parameter-covariate relationships were added to the subpopulation -model one at a time and the likelihood ratio test (LRT) was used to assess if the addition improved the fit. The parameter-covariate relationship that provided the best fit (a significant decrease in the -2LL using the LRT) provided the subpopulation model for the results of analysis 2. The resulting subpopulation model estimated parameter values were reported in the results for analysis 2, in paper 2.

The parameter-covariate relationship was multiplicative, for example, the population estimation of the initial transitional effector memory cells ( $TEM_0$ ) in accounting for BCG status was modelled by  $TEM_{0BCG:N} = TEM_{0BCG:Y} * e^\alpha$ , where  $TEM_{0BCG:Y}$  is the value for  $TEM_0$  for those in

the BCG:Y subpopulation (the reference subpopulation) and  $\alpha$  is the exponentiated scalar of this value to represent changes in  $TEM_0$  for those in the BCG:Y subpopulation. The covariate effects ( $\alpha$ 's) are estimated in the NLMEM analysis alongside the associated p-values, but the value for the subpopulation parameter (left hand side of above equation) is reported in the results of paper 2.

Analysis 3: Which macaque subpopulations best predicted immune responses in different human subpopulations?

In analysis 3, my aim was to calibrate the macaque estimated model parameters stratified by colony (analysis 2, Table 1) to the human subpopulation (stratified by BCG status) response data to establish which macaque subpopulation model parameters were the best description of the human subpopulation data. Here, the resulting BIC value was used to assess the goodness of fit of the calibration of the macaque subpopulation estimated model parameter values and to compare between macaque subpopulations. To achieve the calibration, my aim was to fix all parameter values to those macaque subpopulation values in analysis 2, Table 1 and record the resulting BIC value. However, to achieve the calibration in Monolix, it was necessary to provide one parameter to estimate (as NLMEM needs something to estimate!). To get around this, all macaque subpopulation model parameters were fixed at their estimated value (table 1) except for parameter L, which was allowed to vary within the range  $[(\text{estimated value of } L)-1, (\text{estimated value of } L)+1]$ , which is small compared to the magnitude of the estimated values of parameter L and thus, would not be considered substantially different from the estimated value of L for each macaque subpopulation in Table 1. The BIC values for this analysis are reported in Figure 4 in paper 2.

### ***Additional Results***

Analysis 1: Model calibration to IFN- $\gamma$  data and exploration of model predictions for macaque and humans, separately

*Estimates for the residual error model parameters*

	Macaque				Human			
	All (analysis 1)		Covariate (analysis 2)		All (analysis 1)		Covariate (analysis 2)	
	Estimated Value	RSE (%)	Estimated Value	RSE (%)	Estimated Value	RSE (%)	Estimated Value	RSE (%)
Additive contribution (cells)	5.37	90	5.51	17	3.79	65	6.04	23
Proportional contribution (% of predicted response)	61	10	61	9	42	10	39	10

**Table S6. Residual error model estimated parameters for a combined residual error model for macaques and humans.**

The estimates for the combined residual error model parameters for both macaques and humans for analysis 1 and 2 are in Table S6.

#### *Diagnostic plots*

Key diagnostic plots were used to assess the model's ability to accurately represent the data. These were the Visual Predictive Check (VPC) plot and model prediction distribution plots. For a description of these diagnostic plots, see Appendix B.

The VPC plot in paper 2 (Figure 2) showed a good fit of the model to the data for humans and macaques separately (analysis 1). Model prediction versus response data were also plotted to show how the model predictions compare to the empirical data. Figure S3 below shows that model predicted (total) cells secreting IFN- $\gamma$  fits through the population median data well. Additional diagnostic plots for analysis 1 can be found in Appendix C Figures S4-S7.

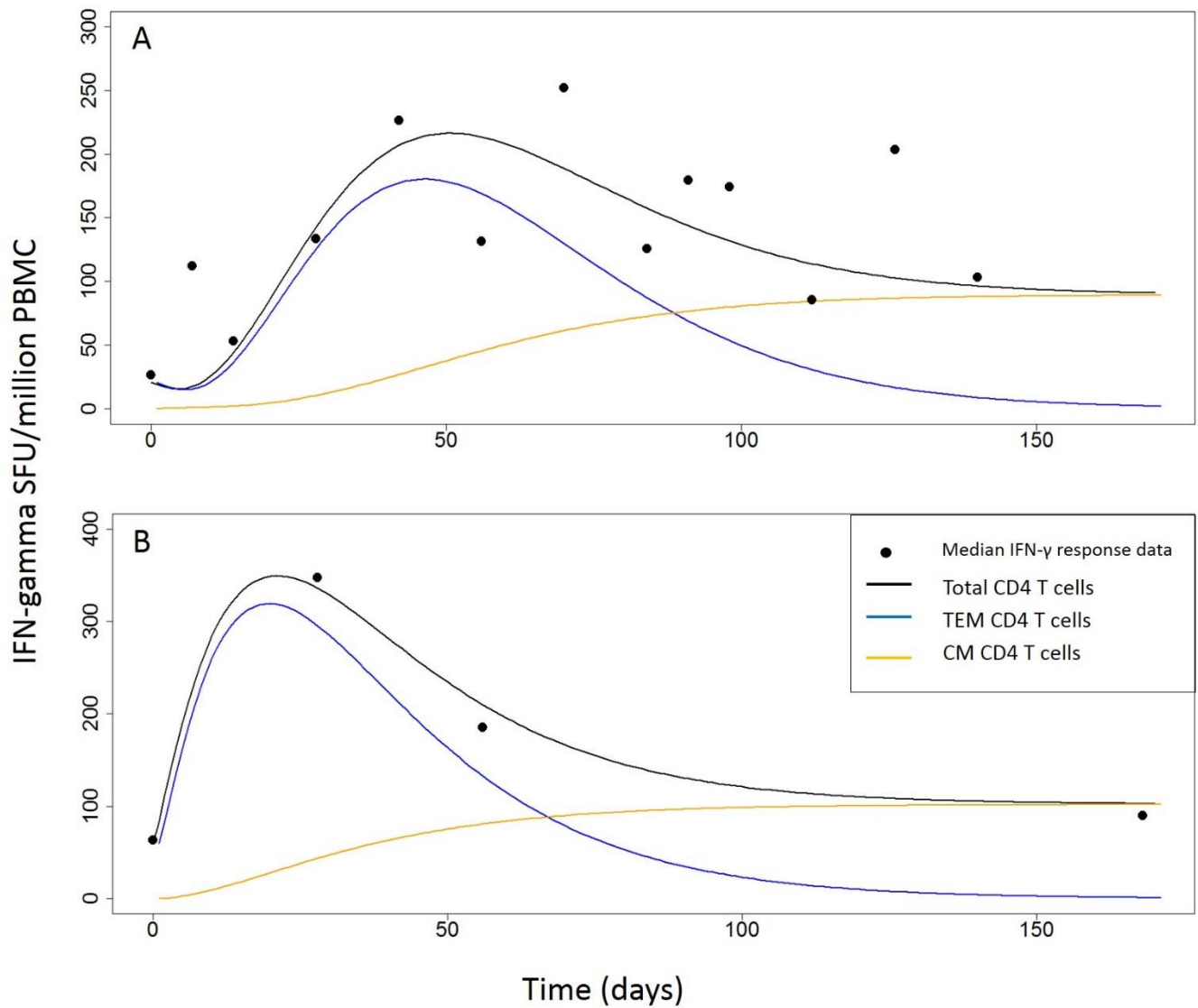


Figure S3. Data (black points), predicted total number of T cells secreting IFN- $\gamma$  (black line), predicted number of transitional effector memory (TEM) cells (blue line), and predicted number of resting central memory (CM) cells (orange line), over time. Model predictions use the estimated parameters from Table 1 for the A) macaque and B) human populations.

Analysis 2: Population covariate impact on within-population variation in model parameter estimates

*Non-parametric rank test in R on potential differences on the individual macaque estimated model parameter values (from Analysis 1) by macaque population covariate*

**Macaque population covariate: Colony**

Table S7 and Figure S8 show significant differences on the individual macaque estimated parameters (estimated in analysis 1) TEM<sub>0</sub>, L and k between the Chinese, Mauritian, Indonesian cynomolgus and Indian rhesus macaques. The colony covariate will be added to the covariate model for macaques in analysis 2.

TEM <sub>0</sub>				L			
	Cyn: Chi	Rhe: Ind	Cyn: Indo		Cyn: Chi	Rhe: Ind	Cyn: Indo
Rhe: Ind	NS			Rhe: Ind	NS		
Cyn: Indo	<b>S</b>	NS		Cyn: Indo	NS	NS	
Cyn: Maur	<b>S</b>	<b>S</b>	<b>S</b>	Cyn: Maur	NS	NS	<b>S</b>
k				h			
	Cyn: Chi	Rhe: Ind	Cyn: Indo		Cyn: Chi	Rhe: Ind	Cyn: Indo
Rhe: Ind	NS			Rhe: Ind	NS		
Cyn: Indo	NS	NS		Cyn: Indo	NS	NS	
Cyn: Maur	<b>S</b>	NS	NS	Cyn: Maur	NS	NS	NS

Table S7. p-value results of applying the non-parametric Kruskal-Wallis and post-hoc Dunn test (for more than two groups) with a Bonferroni correction on individual macaque estimated parameters from analysis 1 with colony as the predictor. Abbreviations: Cyn: chi = cynomolgus macaques of Chinese origin, Cyn: Maur = cynomolgus macaques of Mauritian origin, Cyn: Indo= cynomolgus macaques of Indonesian origin, Rhe: Ind = Rhesus macaques of Indian origin. NS equates to non-significant (adjusted p-value>0.008=0.05/6), S equates to significant (adjusted p-value<0.008=0.05/6).

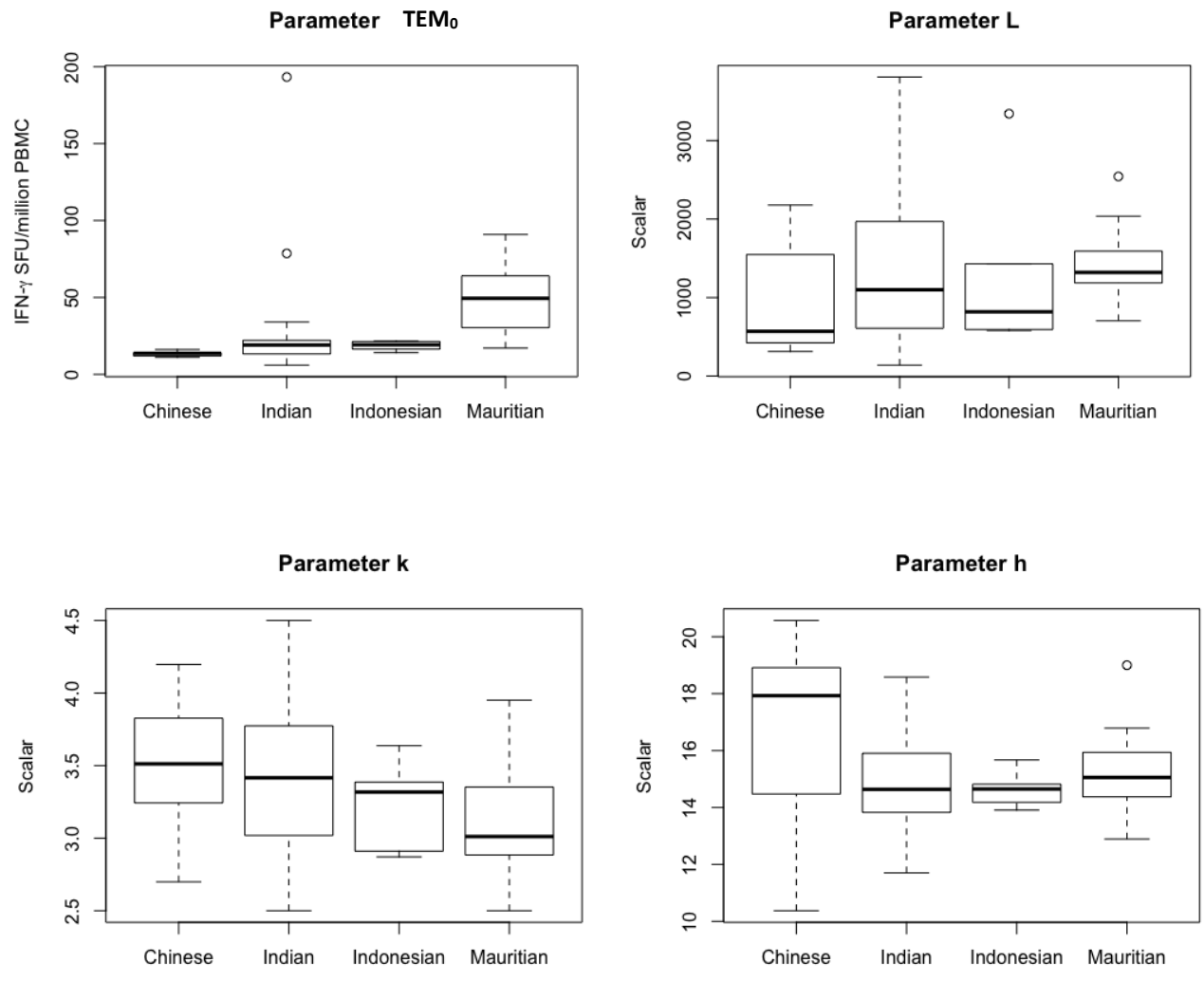


Figure S8. Boxplot of individual macaque estimated parameters from analysis 1 by macaque colony

*Forward stepwise addition method for selecting macaque covariate model*

To select which parameters in the model should be indexed by macaque colony covariate, a forward selection method was adopted. Here, the covariate was added to one model parameter separately and the -2LL recorded (for example, in Table S8, parameter TEM<sub>0</sub>). The parameter which provides the lowest -2LL is this indexed alongside a second model parameter (e.g. TEM<sub>0</sub>+L and all other pairwise parameters, separately, e.g. TEM<sub>0</sub>+k and TEM<sub>0</sub>+h) and the resulting -2LL compared using the likelihood ratio test (chi<sup>2</sup> distribution with the appropriate degrees of freedom). This is continued until the model with the most parameters indexed on the colony covariate, with significantly lower -2LL is found. The results of Table S8 show that indexing parameters TEM<sub>0</sub>, L and k on macaque colony provide the lowest -2LL. The estimated values for each of these parameters for each macaque colony can be found in Table 1 of paper 2.

Model #	Parameter(s) indexed on colony covariate	-2LL	Diff in -2LL (*from Model # 0)	0.05 level significant? (Chi <sup>2</sup> test 4 d.f.: crit val = 9.48, 8 d.f. crit val = 15.5, 12 d.f: crit. Val = 19.68)
0	None	7209		
1	TEM <sub>0</sub>	7189.96	19.04	Yes (4 d.f.)
2	L	7206.53	3	No (4 d.f.)
3	k	7209.26	+0.26	No (4 d.f.)
4	h	7222.45	+13.45	No (4 d.f.)
<hr/>				
3	TEM <sub>0</sub> +L	7183.75	25.25	Yes (8 d.f.)
4	TEM <sub>0</sub> +k	7183.89	25.11	Yes (8 d.f.)
5	TEM <sub>0</sub> +h	7199.01	9.99	No (8 d.f.)
<hr/>				
<b>5</b>	<b>TEM<sub>0</sub>+L+k</b>	<b>7177.55</b>	<b>31.45</b>	<b>Yes (12 d.f.)</b>

**Table S8. Forward stepwise addition method for selecting a subpopulation-model for colony in macaques. -2LL values are taken from running in Monolix with colony applied to the parameter. Difference in -2LL from the full model (model number 0) is calculated and significance is assessed by a chi squared distribution for the appropriate degree of freedom.**

*Non-parametric rank test in R on potential differences on the individual human estimated model parameter values (from Analysis 1) by human population covariate*

***Human population covariate: Gender***

Table S9 and Figure S9 show no significant differences on the individual humans estimated parameters (estimated in analysis 1) associated with gender. As a result, stratification of model parameters by gender was not considered further in this work.

Parameter	Wilcoxon test p-value
TEM <sub>0</sub>	0.45
L	0.26
k	0.31
h	0.14

**Table S9. Results of applying the Wilcoxon test on individual human estimated parameters from analysis 1 with gender as the predictor**

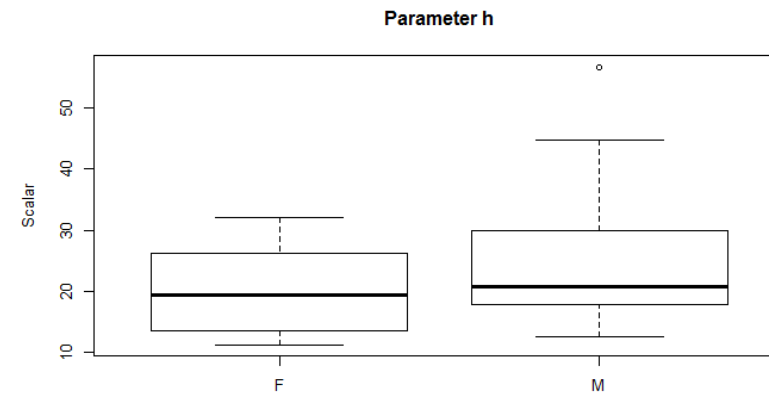
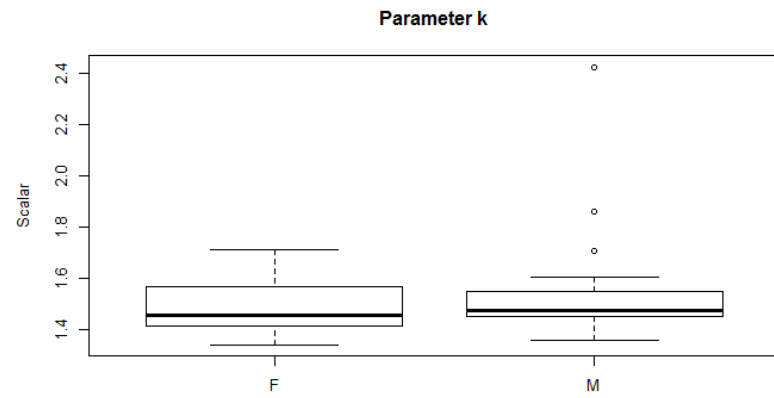
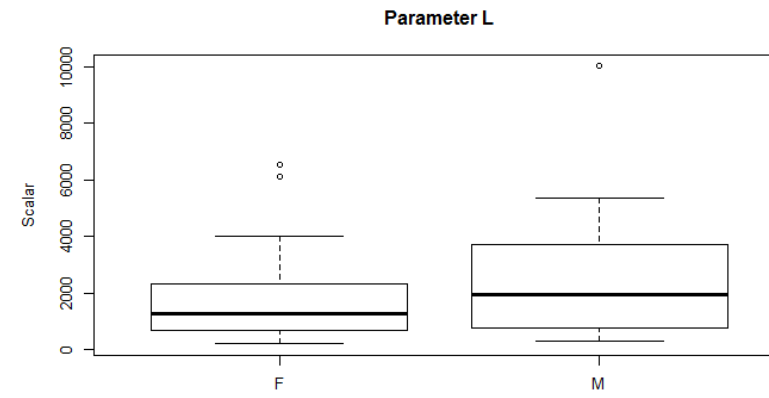
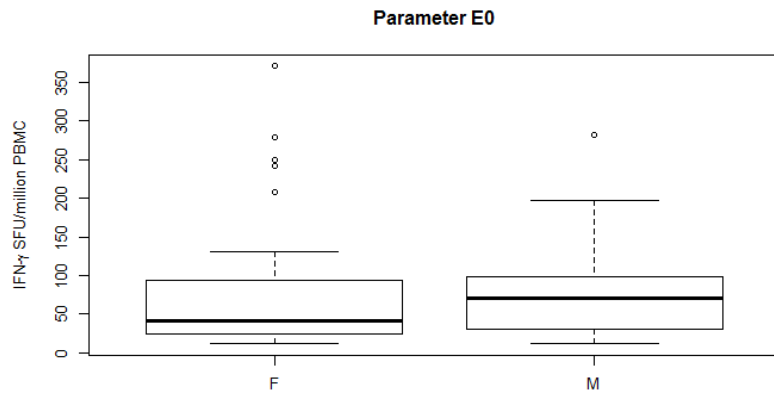


**Figure S9. Boxplot of individual human estimated parameters from analysis 1 by gender, F=Female, M=Male**

**Human population covariate: ML Ratio**

Table S10 and Figure S10 show no significant differences on the individual humans estimated parameters (estimated in analysis 1) associated with ML ratio. As a result, stratification of model parameters by ML ratio was not considered further in this work.

Parameter	Linear regression slope parameter p-value
TEM <sub>0</sub>	0.70
L	0.69
k	0.33
h	0.24

**Table S10. Results of applying linear regression on individual human estimated parameters from analysis 1 with ML ratio as the predictor**

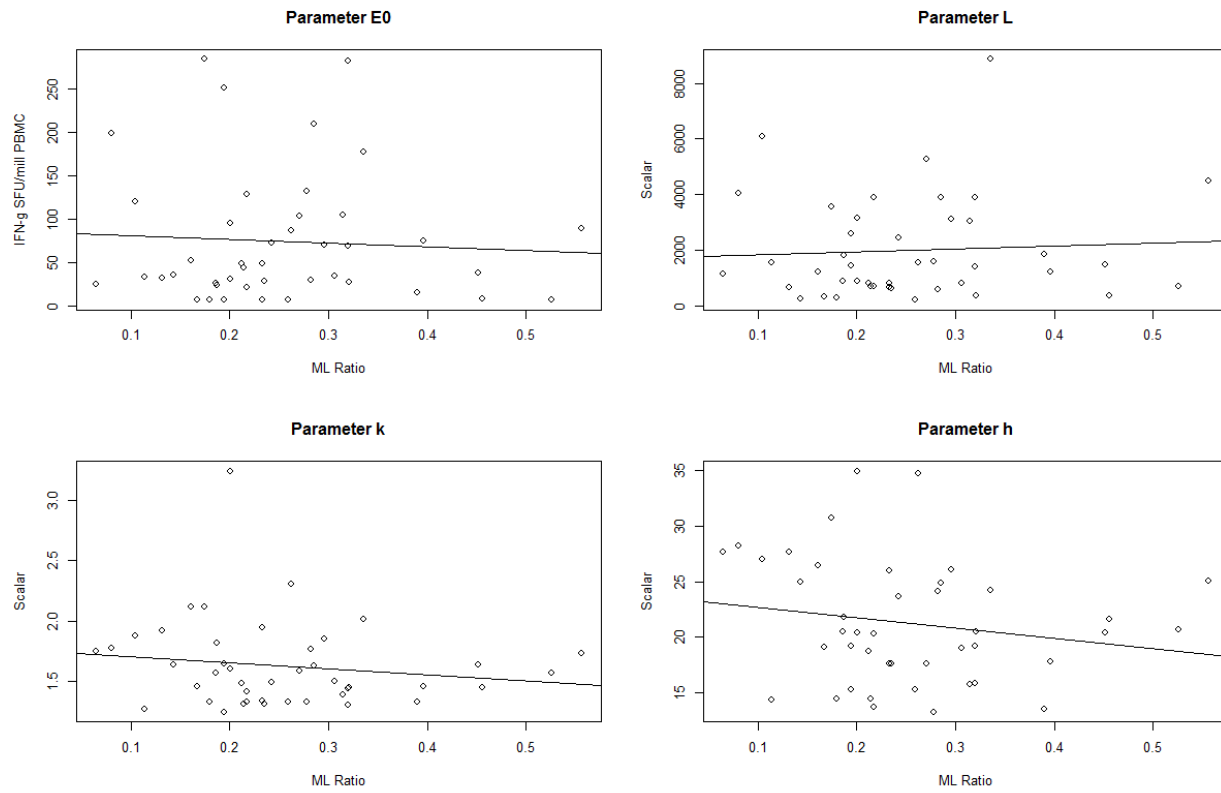


Figure S10. Scatterplots of individual human estimated parameters from analysis 1 against ML ratio

**Human population covariate: BCG History**

Table S11 and Figure S11 show that there is a significant difference on the individual estimated parameters between the “never” group, and the 1-9, 10-19 and 20-29 years since BCG vaccination groups, but not between the 1-9, 10-19 and 20-29 years since BCG vaccination groups. As such, these groups are considered as “BCG status”, where 1+ years since BCG vaccination groups are aggregated into a BCG:Y group and the “never”, BCG:N.

TEM <sub>0</sub>				L			
	Never	10-19 yrs	1-9yrs		Never	10-19 yrs	1-9yrs
10-19 yrs	S			10-19 yrs	S		
1-9yrs	S	NS		1-9yrs	S	NS	
20-29 yrs	S	NS	NS	20-29 yrs	S	NS	NS
k				h			
	Never	10-19 yrs	1-9yrs		Never	10-19 yrs	1-9yrs
10-19 yrs	NS			10-19 yrs	NS		
1-9yrs	NS	NS		1-9yrs	NS	NS	
20-29 yrs	NS	NS	NS	20-29 yrs	NS	NS	NS

**Table S11. p-value results of applying the non-parametric Kruskal-Wallis and post-hoc Dunn test (for more than two groups) with a Bonferroni correction on individual human estimated parameters from analysis 1 with BCG history as the predictor. NS equates to non-significant (adjusted p-value>0.008=0.05/6), S equates to significant (adjusted p-value<0.008=0.05/6).**

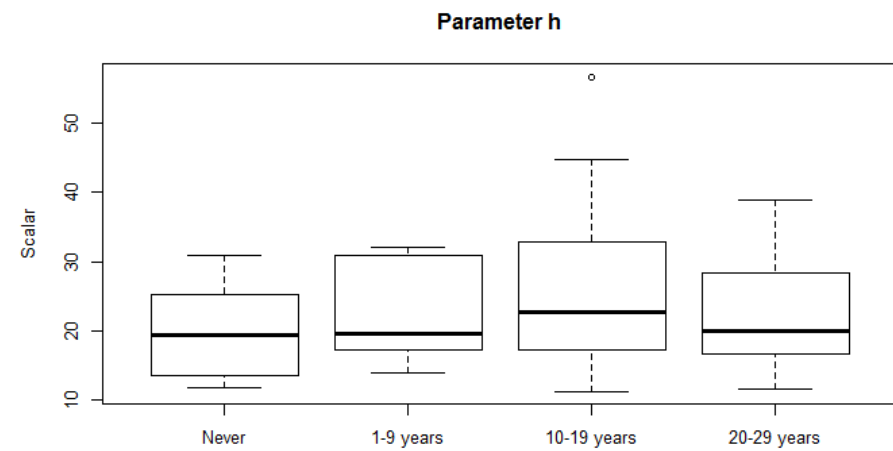
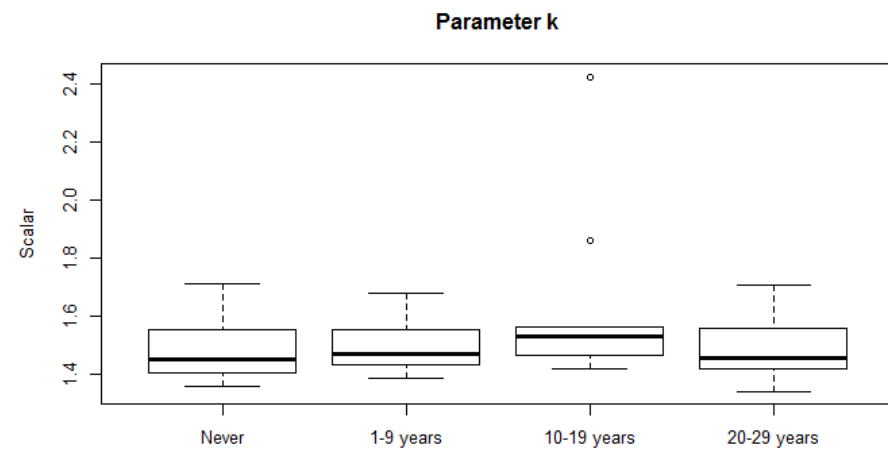
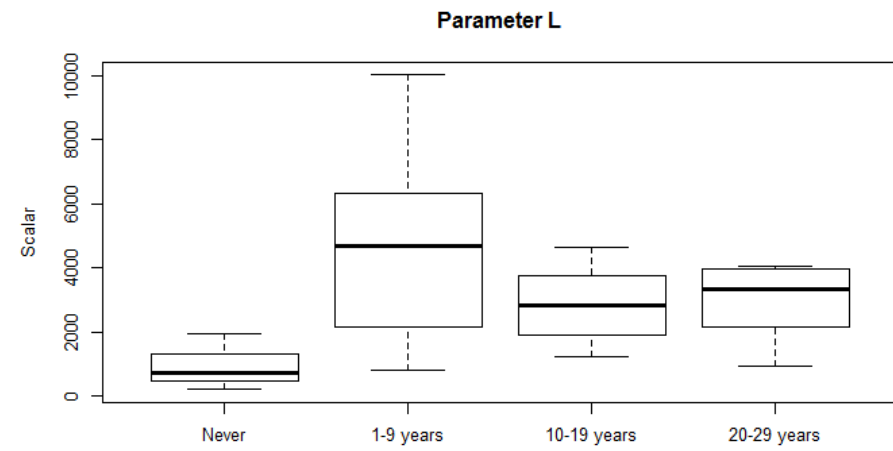
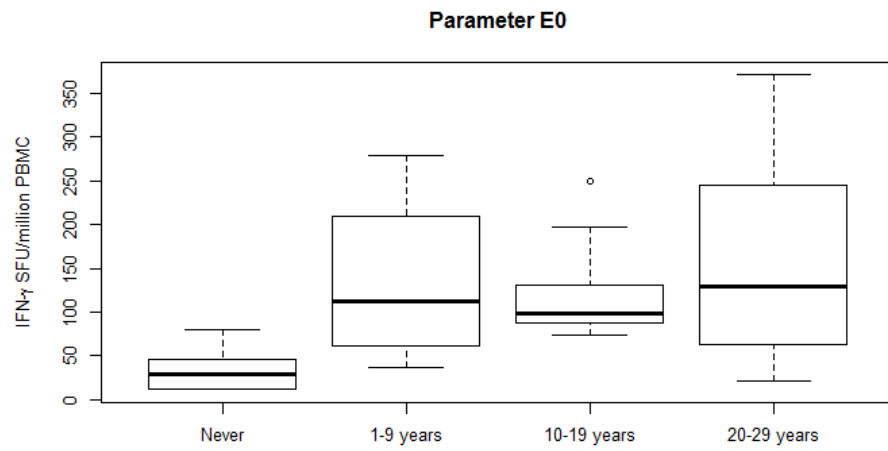


Figure S11. Boxplot of individual human estimated parameters from analysis 1 by BCG history

**Human population covariate: BCG Status**

As BCG status significantly impacted the individual human estimated parameters (Table S12 and Figure S12), it will be used to stratify estimated model parameters (Table S12, Figure S12).

Parameter	Wilcoxon test p-value
TEM <sub>0</sub>	2x10 <sup>-10</sup>
L	9.6x10 <sup>-9</sup>
k	0.31
h	0.13

**Table S12. Results of applying the Wilcoxon test on individual human estimated parameters from analysis 1 with BCG status as the predictor**

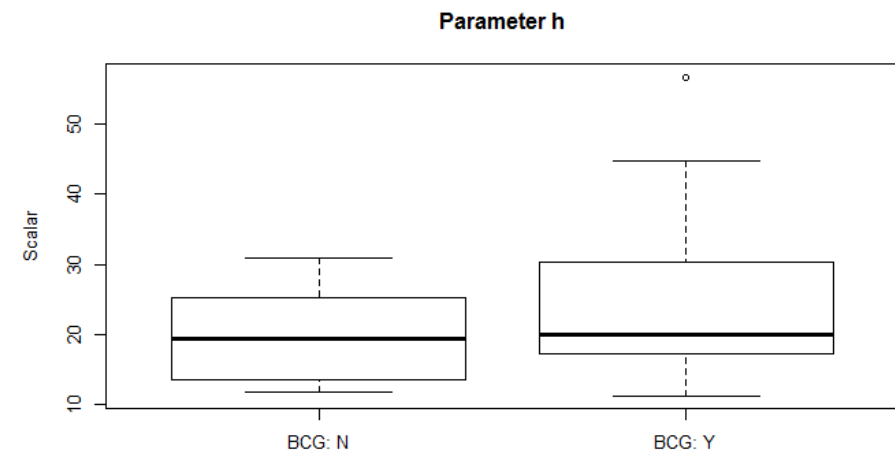
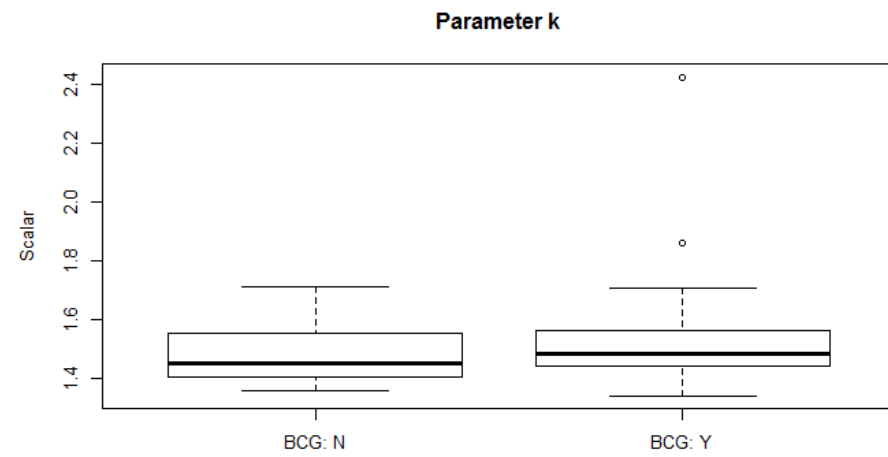
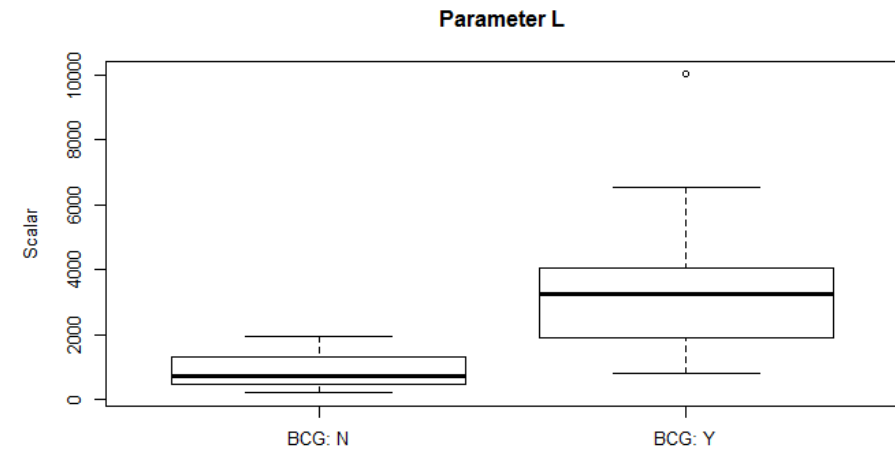
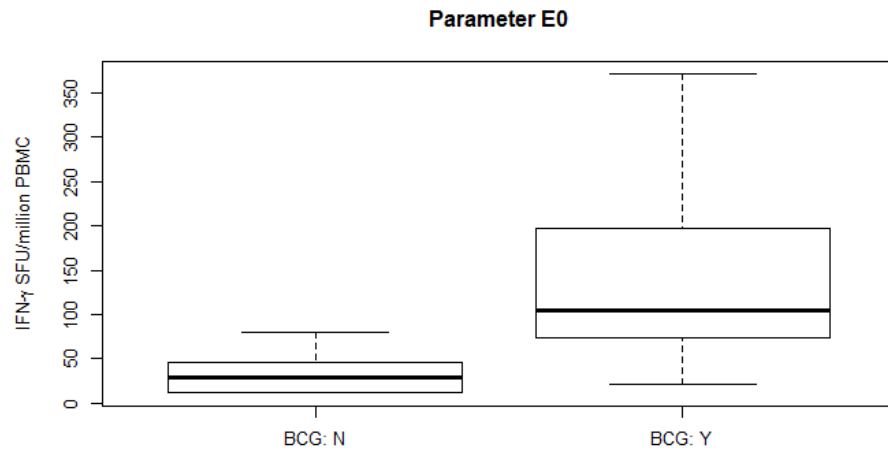


Figure S12. Boxplot of individual human estimated parameters from analysis 1 by BCG status

*Forward stepwise addition method for selecting human covariate model*

The results of Table S13 show that indexing parameters TEM<sub>0</sub>, L and h on human BCG status provides the lowest significant -2LL. The estimated values for each of these parameters for baseline BCG-vaccinated and baseline BCG-naive can be found in Table 1 of paper 2.

Model #	Parameter(s)	-2LL	Diff in -2LL (*from Model # 0)	0.05 level significant? (Chi <sup>2</sup> test 2 d.f.: crit val = 5.99, 4 d.f.: crit val = 9.49, 6 d.f. crit val = 12.59, 8 d.f. crit val = 15.5)
0	None	2738		
1	TEM <sub>0</sub>	2698.00	40	Yes (2 d.f.)
2	L	2697.36	40.64	Yes (2 d.f.)
3	k	2739.45	+1.45	No (2 d.f.)
4	h	2737.22	0.78	No (2 d.f.)
5	L + TEM <sub>0</sub>	2665.75	72.25	Yes (4 d.f.)
6	L + h	2694.01	43.99	Yes (4 d.f.)
7	L + k	2696.85	41.15	Yes (4 d.f.)
8	L+TEM <sub>0</sub> +k	2657.75	80.25	Yes (6 d.f.)
<b>9</b>	<b>L+TEM<sub>0</sub>+h</b>	<b>2653.96</b>	<b>84.04</b>	<b>Yes (6 d.f.)</b>
10	L+TEM <sub>0</sub> +h+k	2723.54	14.5	No (8 d.f.)

**Table S13.** Forward stepwise addition method for selecting a covariate model for BCG status in humans. -2LL values are taken from running in Monolix with BCG status applied to the parameter. Difference in -2LL from the full model (model number 0) is calculated and significance is assessed by a chi squared distribution for the appropriate degree of freedom.

*Diagnostic plots*

Using the estimated model parameter values for the subpopulation models for macaque and humans outlined in Table 1 (i.e. the estimated model parameters TEM<sub>0</sub>, L and k, stratified by macaque colony covariate and TEM<sub>0</sub>, L and h stratified by human BCG status, provided by the subpopulation model analysis in Table S8 and S13), the VPC in Figure S13 and S14 show the model fits well to the macaque and human

subpopulations, respectively. Additional diagnostic plots for the macaque and human subpopulation-models can be found in Appendix C, Figures S15-S18. The model prediction distribution for the macaque and human subpopulations can be found in Figures S19 and S20, respectively.

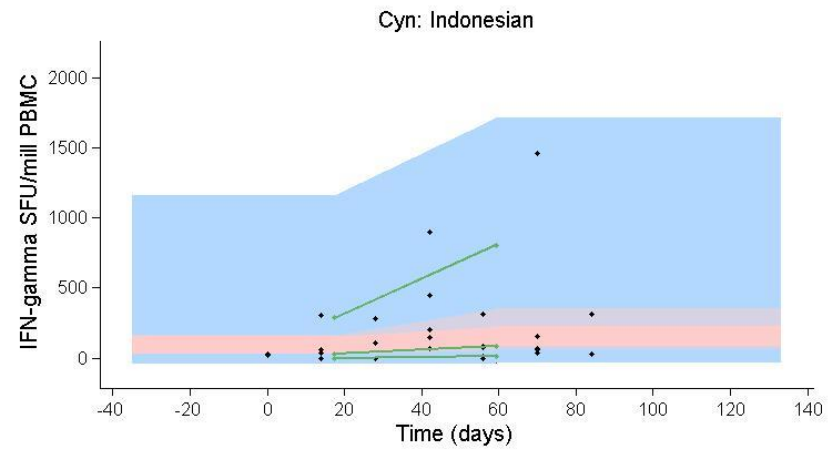
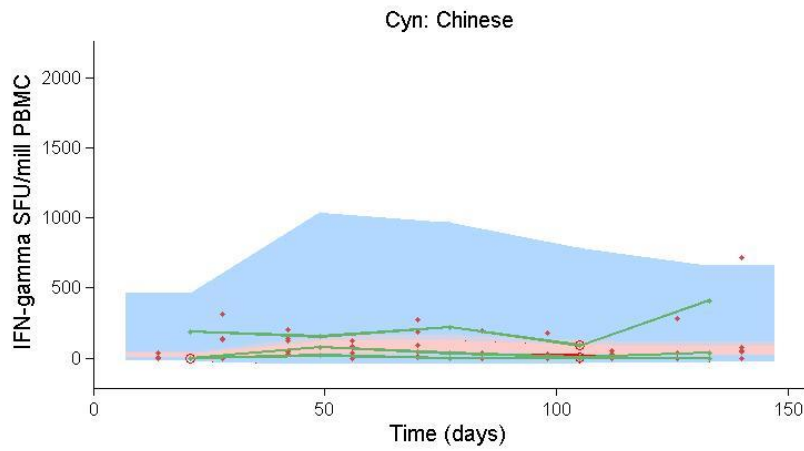
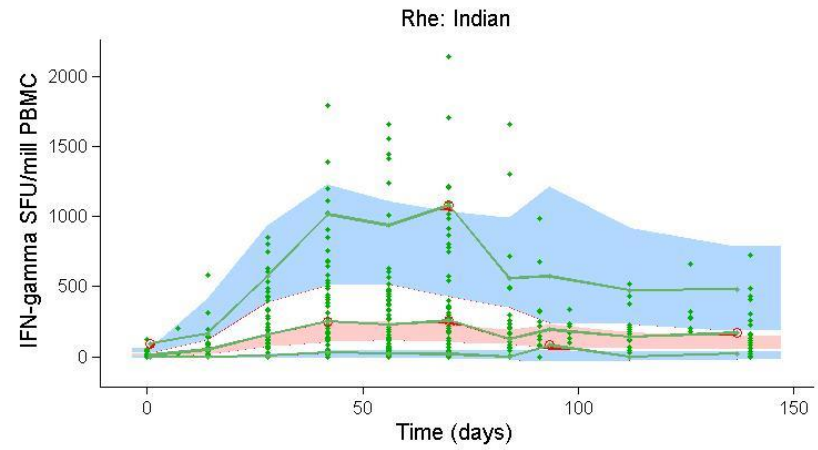
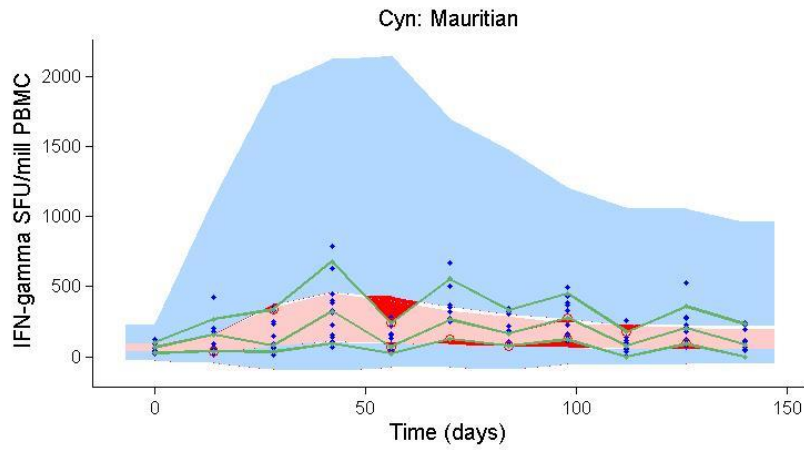


Figure S13. Visual predictive check plots for all colonies of macaque. Points represent the empirical data. Blue regions represent the ranges of the 90<sup>th</sup> and 10<sup>th</sup> percentiles of the simulated populations. The pink region represents the range of the 50<sup>th</sup> percentile. The green line links the observed percentiles (10<sup>th</sup>, 50<sup>th</sup> and 90<sup>th</sup>) for each time point. Red regions represent where the observed data falls outside the ranges of the simulated percentiles.

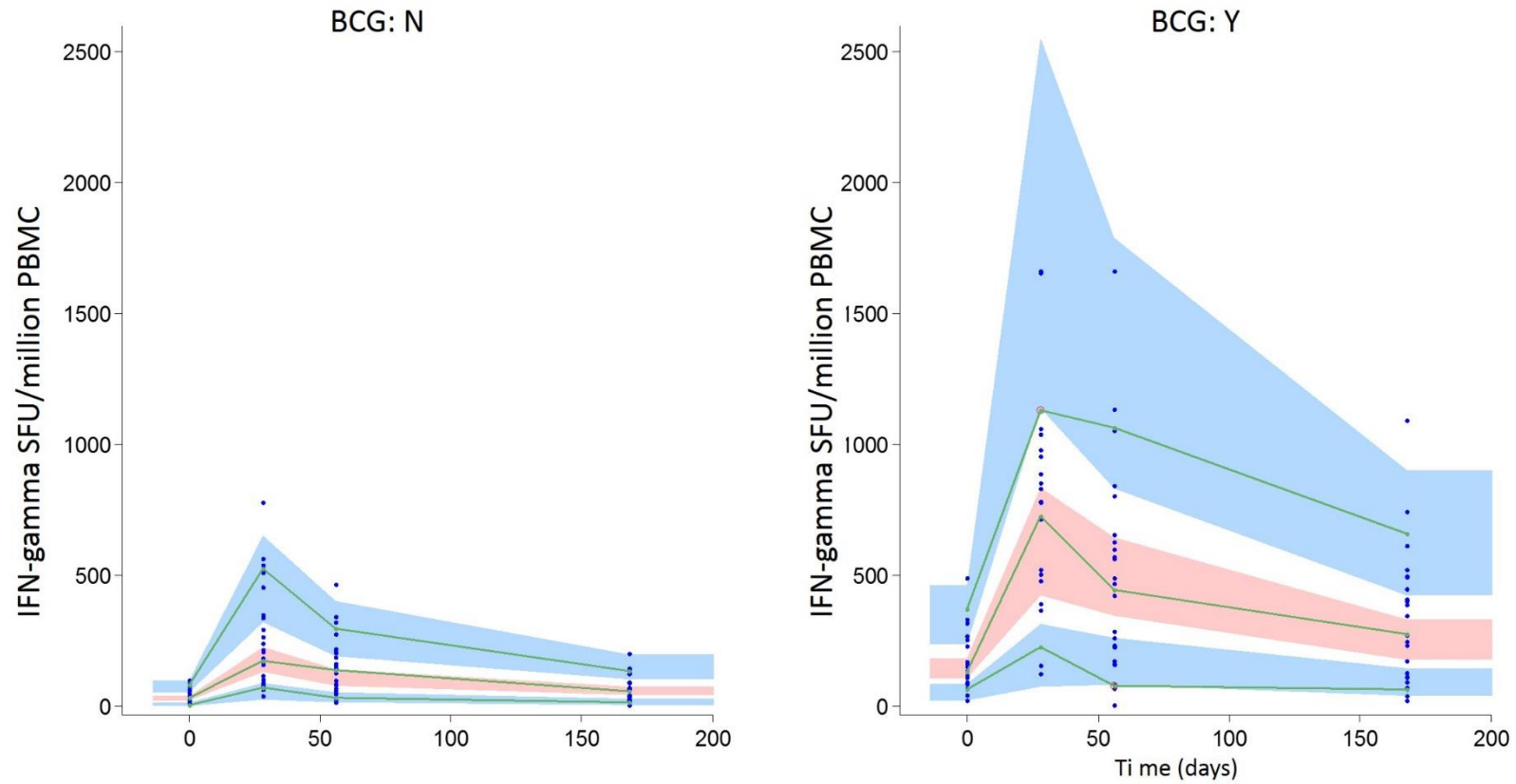
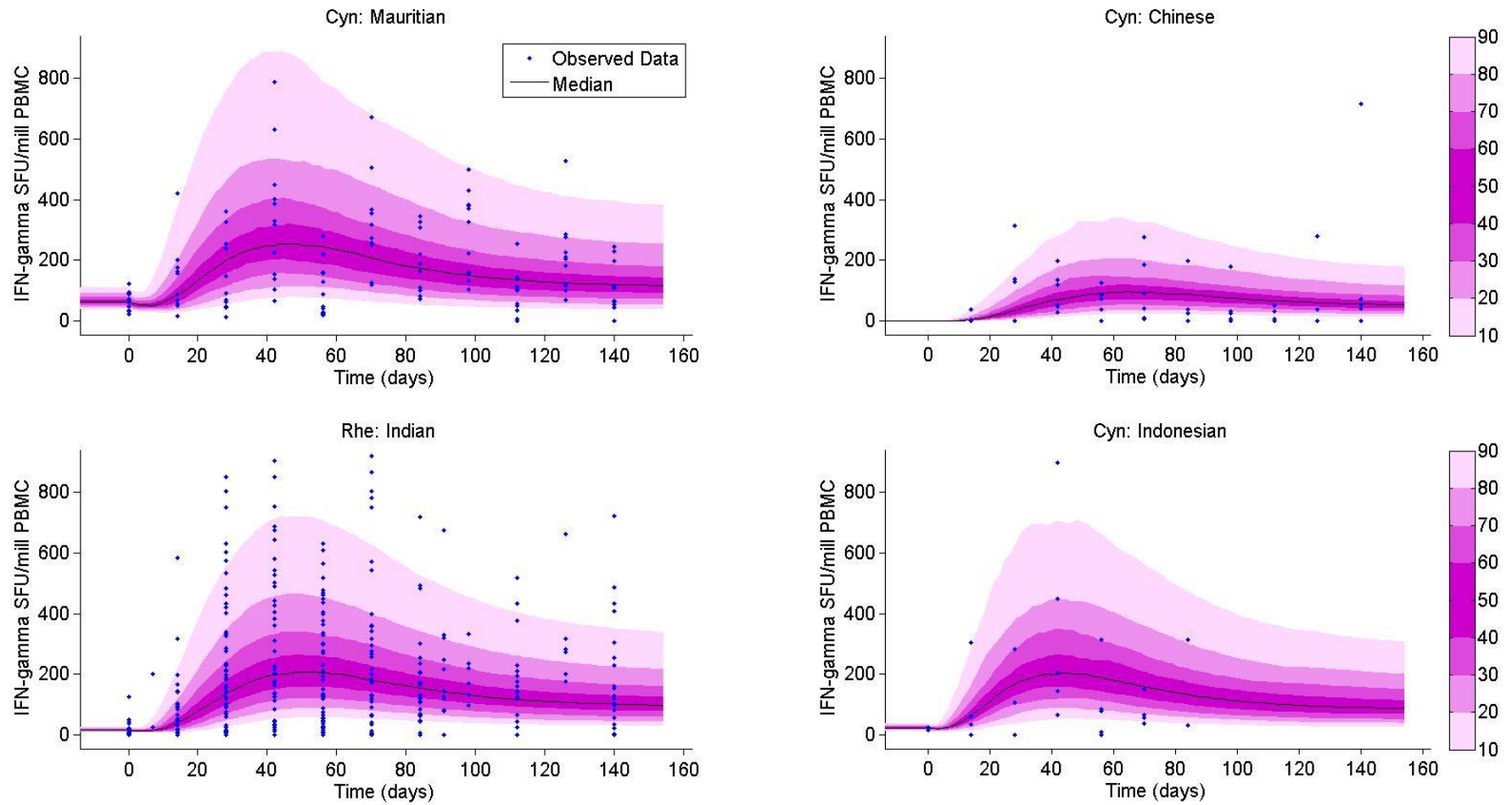


Figure S14. Visual predictive check plots for BCG: N and BCG: Y humans. Points represent the observed data. Blue regions represent the ranges of the 90<sup>th</sup> and 10<sup>th</sup> percentiles of the simulated populations. The pink region represents the range of the 50<sup>th</sup> percentile. The green line links the observed percentiles (10<sup>th</sup>, 50<sup>th</sup> and 90<sup>th</sup>) for each time point. Red regions represent where the observed data falls outside the ranges of the simulated percentiles.



**Figure S19. Prediction distribution plot for all colonies of macaque. Points represent the empirical data. The bands represent the 10<sup>th</sup> to 90<sup>th</sup> percentiles of the theoretical predictions using the predicted population parameters and associated variation for analysis 2 (Table 1). The black line shows the median total response prediction.**

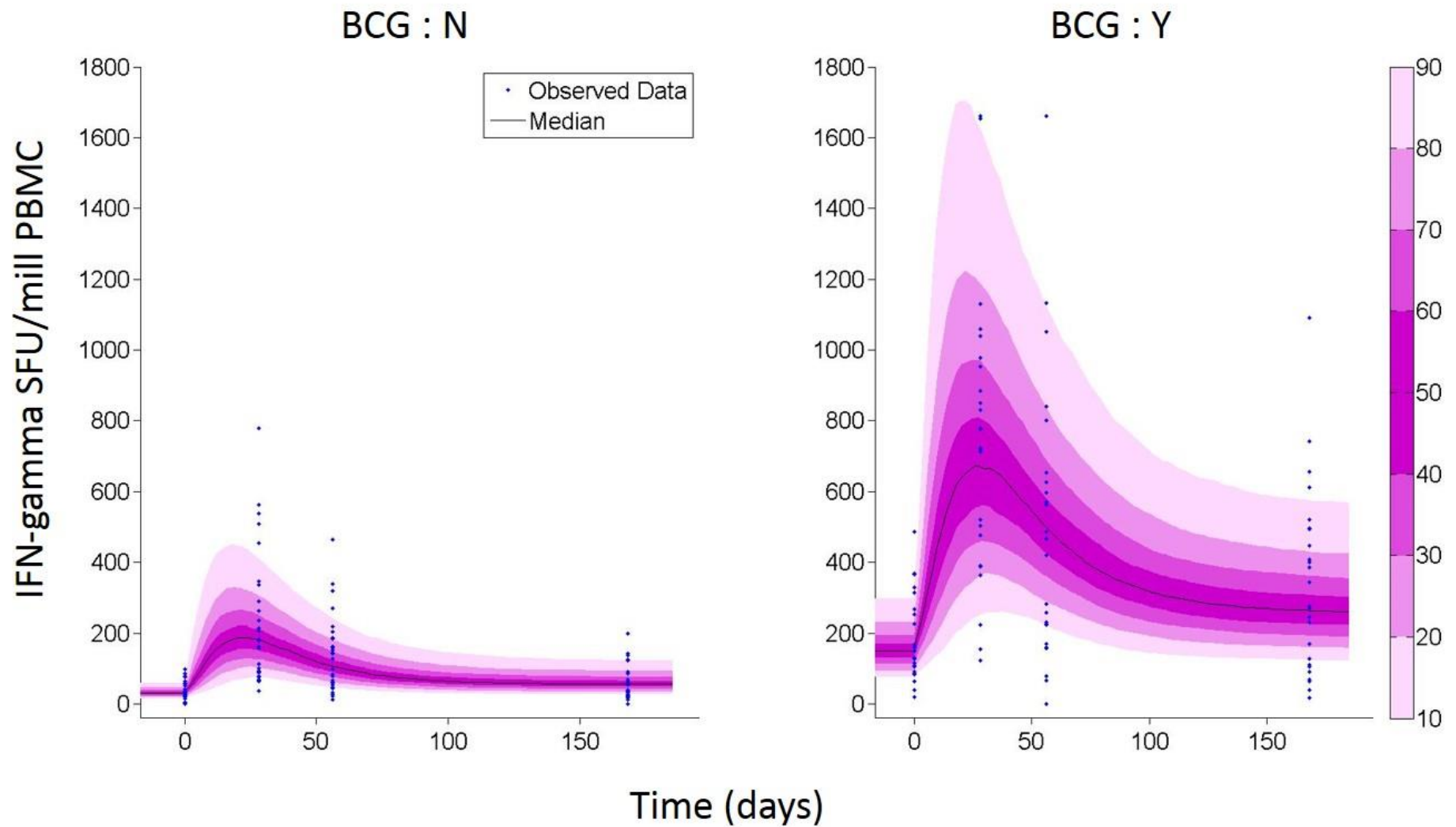
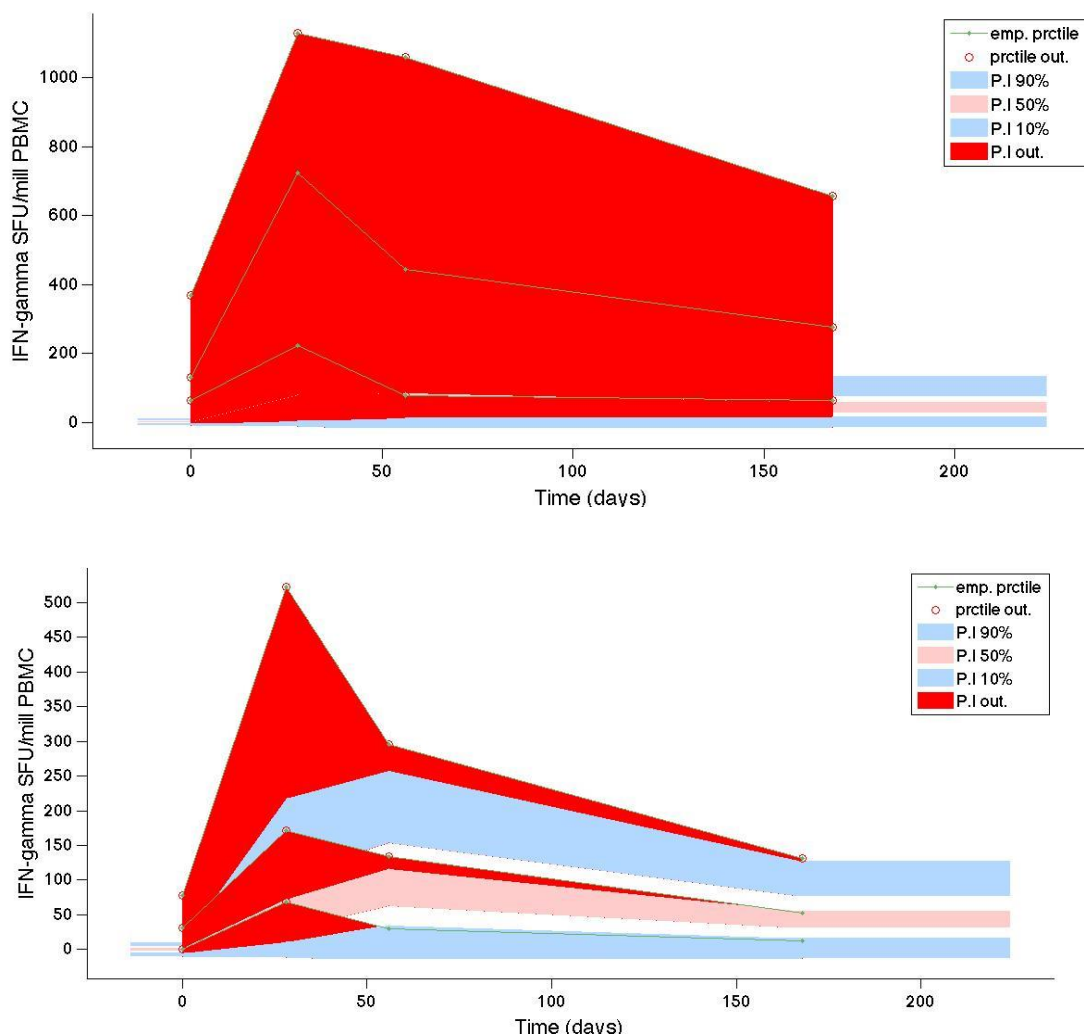


Figure S20. Prediction distribution plot for humans by BCG status subpopulation. Points represent the empirical data. The bands represent the 10<sup>th</sup> to 90<sup>th</sup> percentiles of the theoretical predictions using the predicted population parameters and associated variation for analysis 2 (Table 1). The black line shows the median total response prediction.

Analysis 3: Which macaque subpopulations best predicted immune responses in different human subpopulations?

The results of calibrating the macaque subpopulation estimated model parameter values to the human subpopulation data are in Figure 4, paper 2. The VPC plots for these calibrations can be found in Figure S21-S24. Further diagnostic plots can be found in Appendix C Figures S25-S28



**Figure S21.** VPC plots for macaque estimated subpopulation-model parameters fit to the human BCG: Y data (top) and BCG: N data (bottom) for Chinese cynomolgus macaques. The green line links the observed percentiles (10<sup>th</sup>, 50<sup>th</sup> and 90<sup>th</sup>) for each time point for the human BCG: Y data (top) and BCG: N data (bottom). Blue regions represent the ranges of the 90<sup>th</sup> and 10<sup>th</sup> percentiles of the simulated populations time-matched to the observed data points. The pink region represents the range of the 50<sup>th</sup> percentile. Red regions represent where the observed data falls outside the ranges of the simulated percentiles.

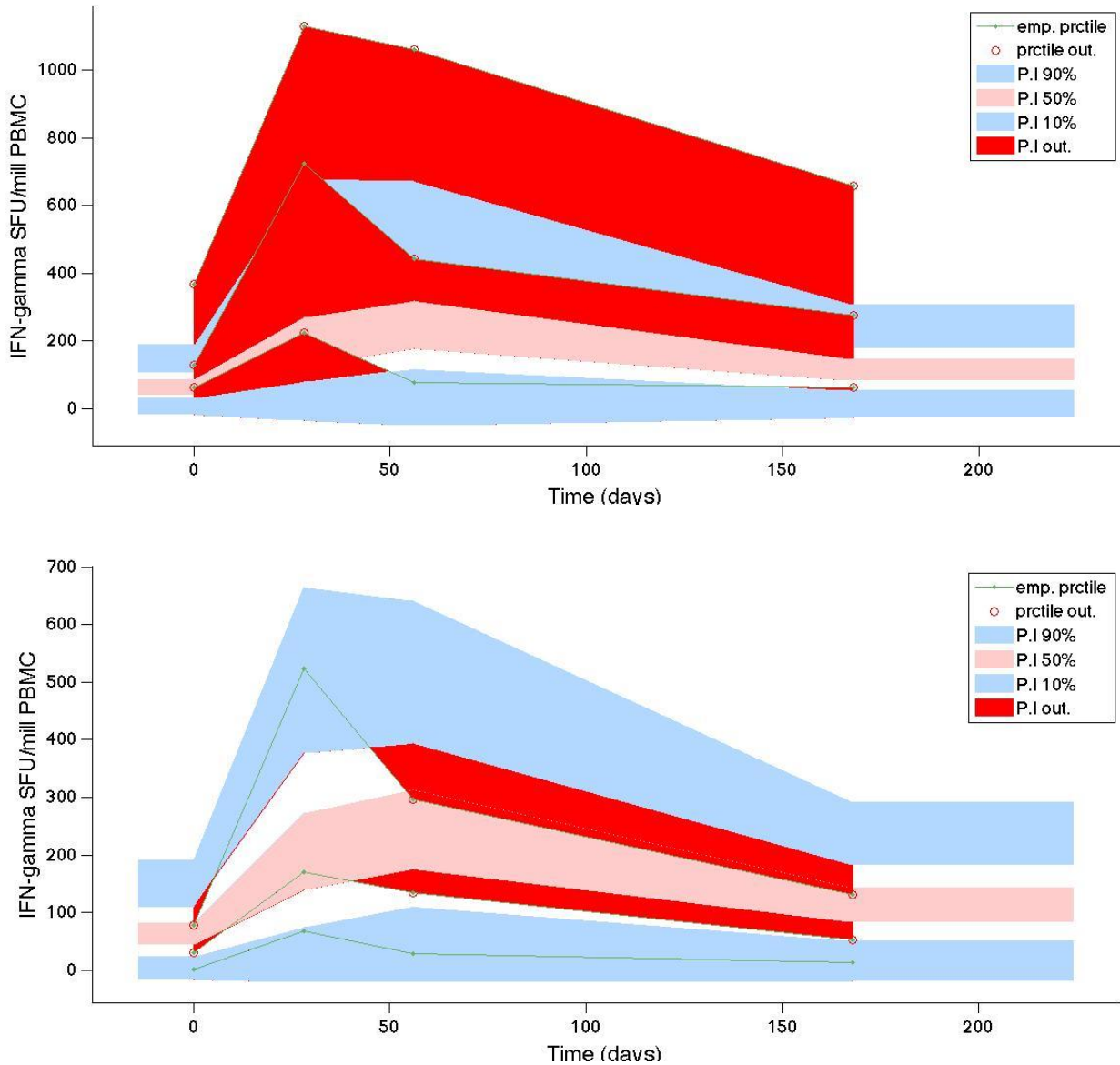
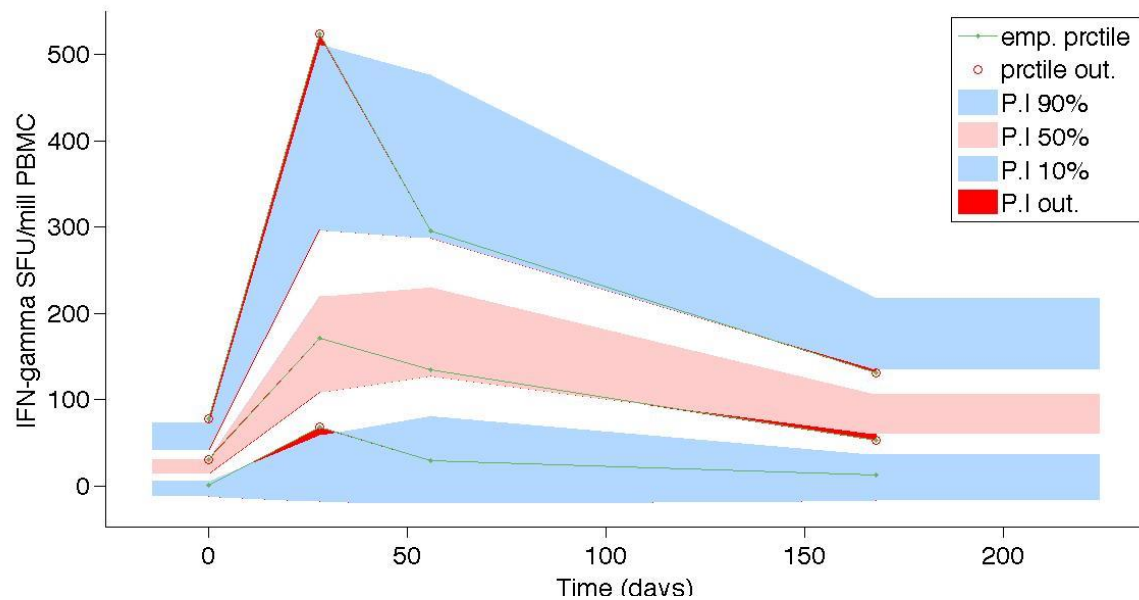
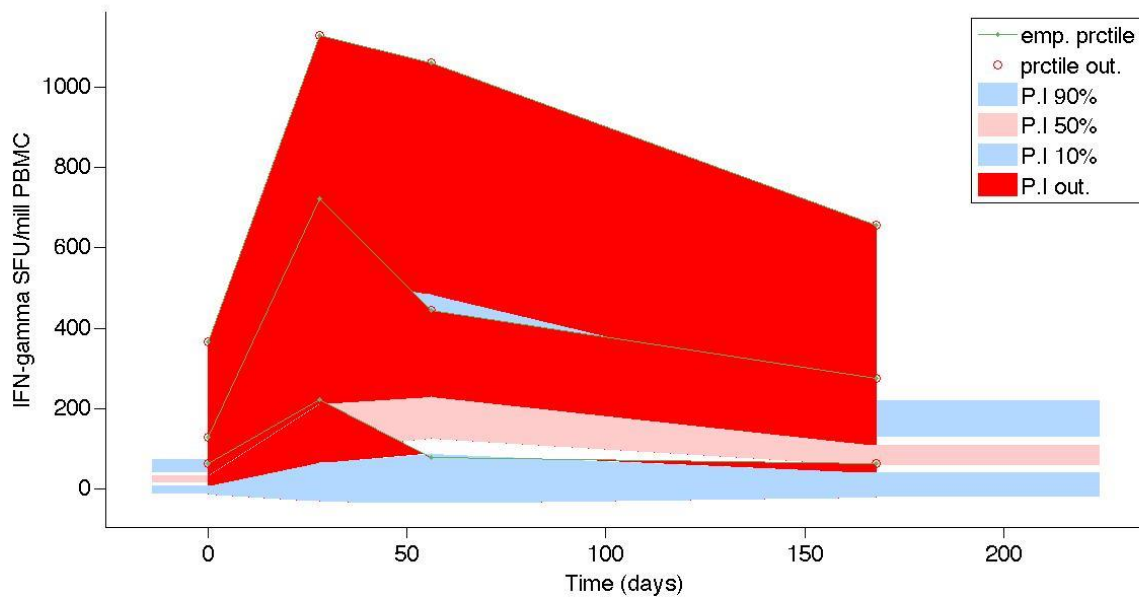


Figure S22. VPC plot for macaque estimated subpopulation-model parameters fit to the human BCG: Y data (top) and BCG: N data (bottom) for Mauritian cynomolgus macaques. The green line links the observed percentiles (10<sup>th</sup>, 50<sup>th</sup> and 90<sup>th</sup>) for each time point for the human BCG: Y data (top) and BCG: N data (bottom). Blue regions represent the ranges of the 90<sup>th</sup> and 10<sup>th</sup> percentiles of the simulated populations time-matched to the observed data points. The pink region represents the range of the 50<sup>th</sup> percentile. Red regions represent where the observed data falls outside the ranges of the simulated percentiles.



**Figure S23. VPC plot for macaque estimated subpopulation-model parameters fit to the human BCG: Y data (top) and BCG: N data (bottom) for Indonesian cynomolgus macaques.** The green line links the observed percentiles (10<sup>th</sup>, 50<sup>th</sup> and 90<sup>th</sup>) for each time point for the human BCG: Y data (top) and BCG: N data (bottom). Blue regions represent the ranges of the 90<sup>th</sup> and 10<sup>th</sup> percentiles of the simulated populations time-matched to the observed data points. The pink region represents the range of the 50<sup>th</sup> percentile. Red regions represent where the observed data falls outside the ranges of the simulated percentiles.

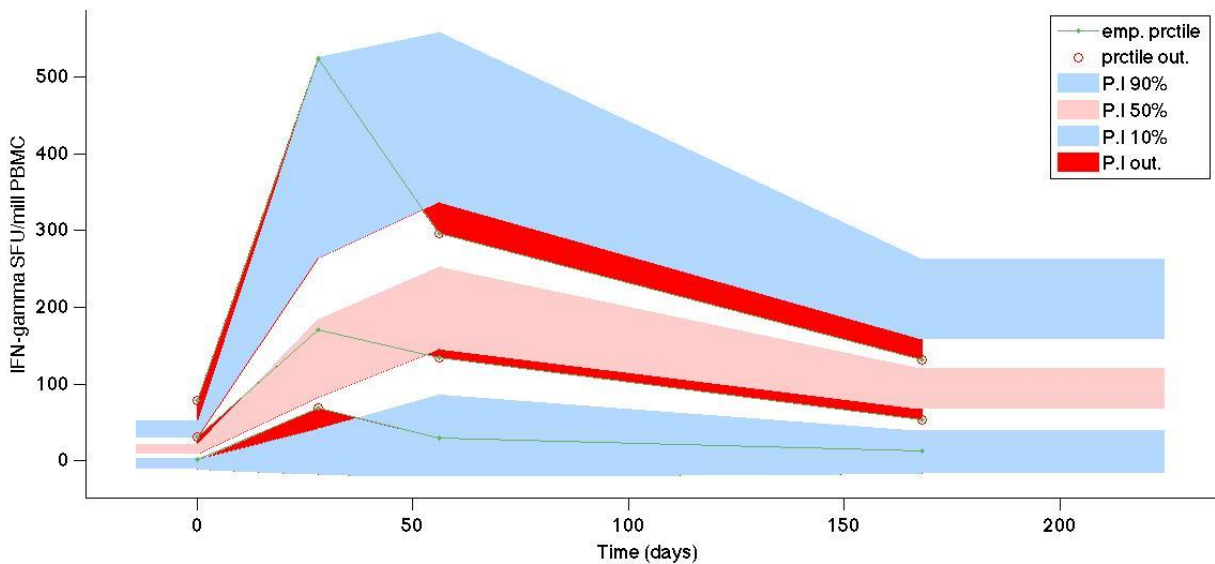
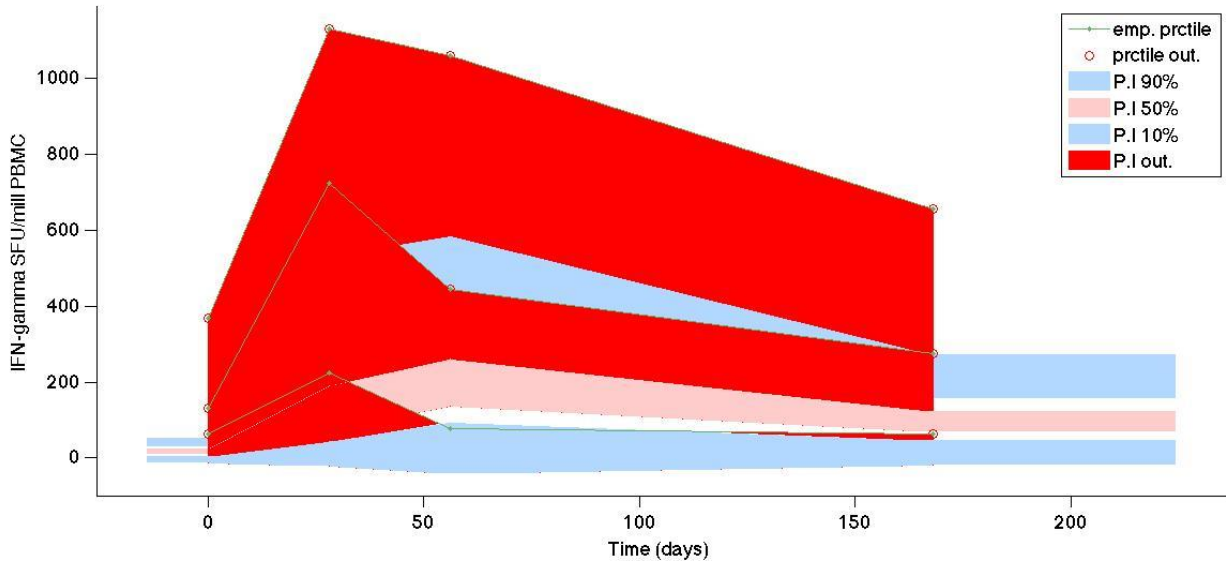


Figure S24. VPC plot for macaque estimated subpopulation-model parameters fit to the human BCG: Y data (top) and BCG: N data (bottom) for Indian rhesus macaques. The green line links the observed percentiles (10<sup>th</sup>, 50<sup>th</sup> and 90<sup>th</sup>) for each time point for the human BCG: Y data (top) and BCG: N data (bottom). Blue regions represent the ranges of the 90<sup>th</sup> and 10<sup>th</sup> percentiles of the simulated populations time-matched to the observed data points. The pink region represents the range of the 50<sup>th</sup> percentile. Red regions represent where the observed data falls outside the ranges of the simulated percentiles.

### ***Additional Discussion***

The main assumptions for the IS/ID model structure used in paper 2 are outlined in Table S14.

<b>IS/ID model assumption</b>	<b>Implications for model</b>
<p><b><u>IFN-<math>\gamma</math> responses are not scaled to host body size</u></b></p> <p>The ELISPOT assay readout is conventionally measured per million cells in all species and as the model represents a systemic response regardless of host blood volume, it was not necessary to scale the ELISPOT readout to reflect body size. This was an important assumption in this work, where I translate dynamics directly onto the ELISPOT data in humans from macaques, however, following from conventional macaque to human vaccine translation, scaling by body size is not regularly conducted.</p>	
<p><b><u>CD4+ T cell stimulation greatly simplified</u></b></p> <p>The immune response to vaccination is a complex network of cells and cytokines behaving nonlinearly over time. In the Th1 response to <i>Mtb.</i> infection (or vaccination), innate and adaptive cells interact to optimise and maintain a protective response [37]. Very simply, cytokines secreted by innate cells after infection or vaccination, such as IL-12, work to stimulate adaptive cells to produce IFN-<math>\gamma</math> that both encourages innate cells to phagocytose bacteria and produce more IL-12 [66, 323]. As such, a feedback stimulation loop is established. In addition, to avoid an over-inflammatory response (which is harmful to the host) cytokines such as IL-10 are produced to regulate and dampen the immune response [324]. In the model, function <math>\delta</math> is used to represent the delay of T cell initiation due to</p>	<p>If data were available on IL-12 or other cytokines believed to be important to an immune response to BCG, It is possible that <math>\delta</math> could be modelled as a parallel “innate response” compartmental model. Incorporating such a model would provide insight into the innate cell mechanisms and thus strengthen the conclusions drawn on the T cell dynamics.</p>

<p>processes such as antigen processing and presentation and the decline of T cell responses due to depreciation of the required stimulation (creating a “n-shaped” curve). However, <math>\delta</math> neglects the influence of stimulation amplification as a result of cytokine feedback loops, amongst other co-stimulation factors. As such, <math>\delta</math> is a generalization of the complex networks required to protect against infection or vaccination and may not be as prolonged as required to generate a response to vaccination.</p>	
<p><b><u>Shape of stimulation curve, <math>\delta</math></u></b></p> <p>The Gamma pdf distribution function fit well for <math>\delta</math> for the BCG data in the analysis, so no other functional forms were tested. Although an abstract concept, it is possible that a different shape may be required if the model was to be applied to different type of vaccine (i.e. viral vector vaccines (e.g. novel TB vaccine MVA-85A) deliver a rapid “burst” of transitional effector cells compared to a live replicating vaccines (BCG) [communication, H. Fletcher]).</p>	
<p><b><u>Central Memory (CM) cells do not die</u></b></p> <p>The central memory cell population is assumed to be maintained by a constant turnover, the death rate was omitted from both the human and mouse model [316]. Although there is evidence to suggest CD4+ long-term memory cells turnover may diminish with time [325, 326], this is assumed not affect the time frame of the model.</p>	
<p><b><u>No initial recruitment into resting memory compartment</u></b></p> <p>The model assumes a linear progression from effector cell to resting memory cell phenotype [327-329]. However, an alternative model has been suggested, whereby</p>	<p>To incorporate a nonlinear effector-memory pathway into the model, a recruitment term like <math>\delta</math> would be added to the memory compartment.</p>

<p>effector and central memory cells are initiated simultaneously after vaccination [81, 83, 330]. This could be another possibility for the model. The determining factor as to which pathway is optimal is still not fully understood [44].</p>	
<p><b><u>Transition and replication of transitional effector cells happens in Lymph node before entering the blood</u></b></p> <p>The model assumes that the recruited transitional effector cells are former <i>Mtb.</i>-specific naïve CD4+ T cells that have clonally expanded within the <i>lymph node</i> and exited into the blood stream. Under this assumption, transitional effector cells do not replicate in this model. The rate of naïve CD4+ T cell clonal expansion changes with time dependent on stimulation from innate processes and antigen presence [44] so could be considered to be incorporated into <math>\delta</math>.</p>	<p>To incorporate replication of transitional effector cells into the model, a parameter <math>R_E</math> would be applied which would determine the rate at which replication occurs, dependent on the current transitional effector cell count.</p>

**Table S14. Main assumptions of the model and implications on challenging these assumptions**

## **Chapter 4. Generation of immune response data to multi-dose of H56+IC31 in mice for the application of vaccine Immunostimulation/Immunodynamic (IS/ID) modelling: paper 3**

### **Chapter 4 introduction**

The second aim of the thesis was to predict human H-series vaccine IFN- $\gamma$  response using IS/ID model calibrated to mouse multi-dose IFN- $\gamma$  data and allometric scaling. In order to achieve this, extensive longitudinal data in mice was required.

Mouse data was used in this chapter as I wanted to be able to translate responses over time between animal and humans on multiple doses and the majority of H-series dose escalation work was conducted in mice as is common in vaccine development. However, a review of the existing H56+IC31 data (generated by SSI), showed a lack of extensive time sampling in healthy mice, with most data sets measuring immune responses at most three time points after vaccination, e.g. [217]. This was sufficient for the purpose of testing immunogenicity in the experiments they were designed for, but would not provide enough information to provide identifiable model predictions. As a result, we generated the data at LSHTM (see author contributions below for details of persons involved in the experiment and to what degree). Again, we chose to use mice as the IFN- $\gamma$  response mechanics are thought not to differ between mouse and human [189] and they could be housed at LSHTM for the experiment at a cheaper cost than an alternative animal model (e.g. macaque). The design of the experiment was developed to provide adequate temporal information on the IFN- $\gamma$  response dynamics to provide an identifiable calibration of the IS/ID model. The logistics and resources required to carry out the experiment were managed by experimental PI, Dr. Helen Fletcher. The experiment was designed to match a subset of the data from human clinical trials outlined in [222, 232] where H56+IC31 or H1+IC31 was given in a two-vaccination regimen to healthy, BCG-vaccinated participants (see chapter 5, paper 4). As such, two vaccinations of H56+IC31 were given to healthy mice, however the mice did not receive BCG vaccination. This was due to evidence that suggests the time course required to generate a sufficient BCG immune response in mice equivalent to humans, was too long to complete in

the time scale of the thesis (personal communication, Dr Thomas Evans). Whilst it is possible that this omission might alter the magnitude of response in mice, we hypothesized it would not affect the response dynamics. The time scale used for the vaccinations was taken from previous pre-clinical experiments conducted by colleagues at SSI [217, 220, 223, 331]. The dose range was chosen to be wide (0.1-15 mg H56 (over 2 log increase)) based on previous work on H-series dose response curves which resulted in notable “bounds” in IFN- $\gamma$  immunogenicity [217, 224]. We used the IC31 adjuvant in this experiment in order to mirror the human data. However, for the existing H56 pre-clinical mouse experiments, the adjuvant CAF01 was predominantly used. We used the dose of IC31 in previous H4 pre-clinical trials (100nmol) [217], which was kept constant over antigen dose. For further details on experiment design and logistics, see Appendix D.

In summary, the purpose of this chapter was to outline the generation of longitudinal IFN- $\gamma$  immune response data in mice after receiving 5 different doses (and 0 dose) of H56+IC31 (aim 2, objective 5, Figure 1.5). This data was generated in order to complete aim 2 of the thesis, i.e. for the application of an IS/ID model to predict human multi-dose responses (see chapter 5, paper 4).

Additionally, I wanted to investigate the shape of the H56+IC31 dose response curve in mice over time. As stated previously, vaccine development regularly employs the assumption of a sigmoidal dose response curve. Based on previous work on H-series vaccine dose response which showed a clear peaked (or n-shaped) dose response curve shape [217], I hypothesized that the mouse IFN- $\gamma$  data would show a peaked dose response relationship. To show definitively that this was the case, I applied statistical curve fitting to the data and compared a saturating (described using a sigmoidal or “Emax” equation [332]) and peaked curve shape (described by a gamma PDF equation). It is important to note that I did not aim here to find a curve that provided the “best” fit, but only to show which curve shape out of the two (saturating or peaked) was a better representation of the data.

I presented the work in paper 3 in poster form and as a presentation at the following conference:

- Keystone Symposium: **Translational Vaccinology for Global Health**, London, UK, October 2017 (invited speaker). “Use of mathematical modelling for dose finding in T cell mediated vaccines”. **S. J. Rhodes**, G. M. Knight, A. Zelmer, T. G. Evans, P. Andersen, H. Fletcher, R. G. White

Registry  
 T: +44(0)20 7299 4646  
 F: +44(0)20 7299 4656  
 E: registry@lshtm.ac.uk

## RESEARCH PAPER COVER SHEET

**PLEASE NOTE THAT A COVER SHEET MUST BE COMPLETED FOR EACH RESEARCH PAPER INCLUDED IN A THESIS.**

### SECTION A – Student Details

Student	Sophie Rhodes
Principal Supervisor	Richard White
Thesis Title	The development of a mathematical modelling framework to translate TB vaccine response between species and predict the most immunogenic dose in humans using animal data

**If the Research Paper has previously been published please complete Section B, if not please move to Section C**

### SECTION B – Paper already published

Where was the work published?	Vaccine Journal		
When was the work published?	November 2016		
If the work was published prior to registration for your research degree, give a brief rationale for its inclusion			
Have you retained the copyright for the work?*	No	Was the work subject to academic peer review?	Yes

*\*If yes, please attach evidence of retention. If no, or if the work is being included in its published format, please attach evidence of permission from the copyright holder (publisher or other author) to include this work.*

### SECTION C – Prepared for publication, but not yet published

Where is the work intended to be published?	
Please list the paper's authors in the intended authorship order:	
Stage of publication	Choose an item.

### SECTION D – Multi-authored work

For multi-authored work, give full details of your role in the research included in the paper and in the preparation of the paper. (Attach a further sheet if necessary)	See next page
--	---------------

Student Signature: 

Date: 13/6/17

Supervisor Signature:  \_\_\_\_\_

Date: 13/6/17

**Paper 3 title: The TB vaccine H56+IC31 dose-response curve is peaked not saturating:  
Data generation for new mathematical modelling methods to inform vaccine dose  
decisions**

**Authors: Sophie J. Rhodes\*, Andrea Zelmer\*, Gwenan M. Knight, Satria Arief Prabowo,  
Lisa Stockdale, Thomas G. Evans, Thomas Lindenstrøm, Richard G. White\*\*, Helen  
Fletcher\*\***

**\*Joint first author**

**\*\*Joint senior author**

**Author contributions:**

The mouse H56+IC31 data in paper 3 were generated at LSHTM by Dr. Helen Fletcher, Dr. Andrea Zelmer, Satria Arief Prabowo and Lisa Stockdale. The vaccine and adjuvant were provided by colleagues at Statens Serum Institut (SSI), Dr. Thomas Lindenstrøm. Animal vaccination, sacrifice and splenocyte harvest was conducted by Dr. Andrea Zelmer, Satria Arief Prabowo and Lisa Stockdale. My contribution to the data generation was to conduct the last stages in the ELISPOT develop protocol for all time points. I was solely responsible for designing the experiment, with advice from Dr. Helen Fletcher and Dr. Thomas Evans. The methods of statistical curve fitting to establish dose response was conceived and executed by myself, with the guidance of Prof. Richard White and Dr. Gwenan Knight. All authors reviewed the paper. Joint first authorship was granted to myself for designing the experiment, applying statistical modelling methods to the data and writing the paper and Dr. Andrea Zelmer for organizing and executing the mouse experiment, writing the laboratory ELISPOT methods and reviewing the paper. The interpretation of the results was my own work.

**Permission from copyright holder to include this work:**

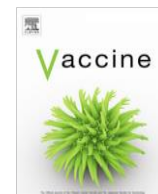
## Personal use

Authors can use their articles, in full or in part, for a wide range of scholarly, non-commercial purposes as outlined below:

- \* Use by an author in the author's classroom teaching (including distribution of copies, paper or electronic)
- \* Distribution of copies (including through e-mail) to known research colleagues for their personal use (but not for Commercial Use)
- \* Inclusion in a thesis or dissertation (provided that this is not to be published commercially)
- \* Use in a subsequent compilation of the author's works
- \* Extending the Article to book-length form
- \* Preparation of other derivative works (but not for Commercial Use)
- \* Otherwise using or re-using portions or excerpts in other works

These rights apply for all Elsevier authors who publish their article as either a subscription article or an open access article. In all cases we require that all Elsevier authors always include a full acknowledgement and, if appropriate, a link to the final published version hosted on Science Direct.

<https://www.elsevier.com/about/our-business/policies/copyright>



# The TB vaccine H56 + IC31 dose-response curve is peaked not saturating: Data generation for new mathematical modelling methods to inform vaccine dose decisions



Sophie J. Rhodes<sup>a,\*,1</sup>, Andrea Zelmer<sup>b,1</sup>, Gwenan M. Knight<sup>a,c</sup>, Satria Arief Prabowo<sup>b</sup>, Lisa Stockdale<sup>b</sup>, Thomas G. Evans<sup>d</sup>, Thomas Lindenstrøm<sup>e</sup>, Richard G. White<sup>a,2</sup>, Helen Fletcher<sup>b,2</sup>

<sup>a</sup> TB Modelling Group, CMMID, TB Centre, London School of Hygiene and Tropical Medicine, UK

<sup>b</sup> Immunology and Infection Department, London School of Hygiene and Tropical Medicine, UK

<sup>c</sup> National Institute for Health Research Health Protection Research Unit in Healthcare Associated Infection and Antimicrobial Resistance, Imperial College London, UK

<sup>d</sup> TomegaVax, Portland, OR, United States

<sup>e</sup> Statens Serum Institut, Copenhagen, Denmark

## ARTICLE INFO

### Article history:

Received 12 July 2016

Received in revised form 4 October 2016

Accepted 22 October 2016

Available online 2 November 2016

## ABSTRACT

**Introduction:** In vaccine development, dose-response curves are commonly assumed to be saturating. Evidence from tuberculosis (TB) vaccine, H56 + IC31 shows this may be incorrect. Mathematical modelling techniques may be useful in efficiently identifying the most immunogenic dose, but model calibration requires longitudinal data across multiple doses and time points.

**Aims:** We aimed to (i) generate longitudinal response data in mice for a wide range of H56 + IC31 doses for use in future mathematical modelling and (ii) test whether a ‘saturating’ or ‘peaked’ dose-response curve, better fit the empirical data.

**Methods:** We measured IFN- $\gamma$  secretion using an ELISPOT assay in the splenocytes of mice who had received doses of 0, 0.1, 0.5, 1, 5 or 15  $\mu$ g H56 + IC31. Mice were vaccinated twice (at day 0 and 15) and responses measured for each dose at 8 time points over a 56-day period following first vaccination. Summary measures Area Under the Curve (AUC), peak and day 56 responses were compared between dose groups. Corrected Akaike Information Criteria was used to test which dose-response curve best fitted empirical data, at different time ranges.

**Results:** (i) All summary measures for dose groups 0.1 and 0.5  $\mu$ g were higher than the control group ( $p < 0.05$ ). The AUC was higher for 0.1 than 15  $\mu$ g dose. (ii) There was strong evidence that the dose-response curve was peaked for all time ranges, and the best dose is likely to be lower than previous empirical experiments have evaluated.

**Conclusion:** These results suggest that the highest, safe dose may not always optimal in terms of immunogenicity, as the dose-response curve may not saturate. Detailed longitudinal dose range data for TB vaccine H56 + IC31 reveals response dynamics in mice that should now be used to identify optimal doses for humans using clinical data, using new data collection and mathematical modelling.

© 2016 The Authors. Published by Elsevier Ltd. This is an open access article under the CC BY-NC-ND license (<http://creativecommons.org/licenses/by-nc-nd/4.0/>).

## 1. Introduction

Vaccines are one of the most important and cost-effective interventions in public health [1]. However, development from vaccine discovery to licensure is costly; in the region of US\$0.8 billion [2]. Mistakes in vaccine development may cause not only a waste of resources (both financial and experimental) but also ultimately,

delay licensure of an effective vaccine. A key decision in development is vaccine dose amount (hereafter dose), which, if chosen optimally would achieve maximum vaccine efficacy, with minimal side effects.

It is common practise in pre-clinical and clinical trials that vaccine dose is increased incrementally until a maximum safe dose that promotes an effective response (usually an antibody response) is achieved; it is assumed that this response will then saturate [3]. This saturating relationship between dose and host response has been the standard assumption in vaccine development and many vaccines have proceeded through to the late stages of development with this method as a basis for dose choice [4,5].

\* Corresponding author.

E-mail address: [sophie.rhodes@lshtm.ac.uk](mailto:sophie.rhodes@lshtm.ac.uk) (S.J. Rhodes).

<sup>1</sup> Joint first authors.

<sup>2</sup> Joint senior authors.

However, in tuberculosis (TB) vaccine development, early pre-clinical studies in mice with the IC31 adjuvanted fusion protein TB10.4 /Ag85B (H4) revealed that low antigen doses were both more immunogenic and provided increased protection relative to high doses [6]. In accordance, a clinical study showed that responses after vaccination with the same H4 + IC31 vaccine were not different between the 5 and 15 µg doses, decreased at 50 µg and were minimal for the 150 µg dose [7]. In a latently infected target population, vaccination with an analogous vaccine H56 (an ESAT-6/Ag85B/Rv2620 fusion protein vaccine) also adjuvanted with IC31 (H56 + IC31) showed that out of two doses tested in Quantiferon-positive (QTF+) individuals, the lowest dose (15 µg H56 + IC31) was more effective at inducing polyfunctional CD4+ T cell responses than the higher dose (50 µg H56 + IC31) [8]. Of note, the higher dose (50 µg) of the related first-generation Hybrid vaccine H1 + IC31 was taken forward to a First-in-man study, which may have led to suboptimal vaccine evaluation [9]. Although immunogenicity not only depends on antigen dose, but indeed also on the type and nature of the adjuvant employed, the incorrect assumption that a higher dose is preferred per se for protein vaccines (or other platforms) has further been brought into question by vaccines using other types of adjuvants [10].

Translational quantitative analysis methods to inform dose decision-making already exist in the drug development world. Pharmacokinetic/Pharmacodynamic (PK/PD) modelling uses mechanistic mathematical methods to describe how dose influences drug dynamics over time [11,12]. Translational modelling to predict human PK/PD parameters based on animal data is a key stage in model-based drug dose decision-making [12–14], and is often required by regulators during development. Although pharmacokinetic data is often not available for vaccines, pharmacokinetics is dependent on dose and regimen, and thus analogies to dose finding for vaccines are relevant. No translational quantitative methods are applied in vaccine development, as the chosen vaccine dose to be tested in a clinical environment is usually based on qualitative assessment of the pre-clinical data [15], which has the potential to ignore or underutilise dose-response information.

To address this gap, we are proposing the new field of *Immuno stimulation/Immunodynamic (IS/ID) modelling*, analogous to that of PK/PD modelling, to make more informed human vaccine dosing decisions based on animal response data. In this field, models will be created to describe the underlying mechanisms that determine the immune response dynamics (immunodynamics) following vaccination, e.g. the influence of the innate and regulatory systems for T cell expansion and contraction (immunostimulation). These models will then be calibrated to dose ranging data from animals and model parameters “mapped” to known human response data. Subsequently, dose-response curve in humans can be predicted, providing information on the most effective range of doses to be first evaluated in clinical trials. In this larger body of work, we will apply these methods on the aforementioned TB vaccine, H56 + IC31 by measuring IFN-γ after vaccination over time.

As in model-based drug development, extensive longitudinal data are required. Published data on a wide dynamic range of doses and time points do not exist for H56 + IC31, where dose-ranging studies have only ever been conducted on minimal pre-specified time points [6]. As such, we conducted and report here an experiment in which we vaccinated mice with a wide range of doses of H56 + IC31 and measured responses extensively over time. These data outlined in this paper will be used in future IS/ID modelling to further our knowledge in mice, non-human primates and humans. In this paper, we aim to (i) generate longitudinal response data in mice for a wide range of H56 + IC31 doses for use in future mathematical modelling and (ii) test whether a ‘saturating’ or ‘peaked’ dose-response curve, better fit the empirical data.

## 2. Materials and methods

### 2.1. Ethics statement

All animal work was carried out in accordance with the Animals (Scientific Procedures) Act 1986 under a license granted by the UK Home Office (PPL 70/8043), and approved by the LSHTM Animal Welfare and Ethics Review Body.

### 2.2. Animals

Female CB6F1 mice were acquired from Charles River UK at 6–8 weeks of age. Animals were housed in specific pathogen-free individually vented cages, were fed ad libitum, and were allowed to acclimatize for at least 5 days before the start of any experimental procedure.

### 2.3. Vaccination

The experimental vaccine H56 (comprising *Mycobacterium tuberculosis* antigens Ag85B-ESAT-6-Rv2660c [16], provided by Statens Serum Institute (SSI), Copenhagen, Denmark) was formulated in IC31<sup>®</sup> adjuvant (provided by SSI on behalf of Valneva Technologies) and 10 mM Tris-HCl buffer (pH 7.4) as described in [17] to obtain a final volume of 200 µl/mouse. The adjuvant IC31<sup>®</sup> consists of a mixture of the cationic peptide KLK (NH<sub>2</sub>-KLK15KLK-COOH) and the oligodeoxynucleotide ODN1a (oligo-(dIdC)<sub>13</sub>). Adjuvant doses were 100 nmol peptide and 4 nmol oligonucleotide for every vaccine (H56) dose. Antigen doses of 0.1, 0.5, 1, 5 or 15 µg of H56 + 100/4 nmol IC31 (hereafter, H56 + IC31) were administered per animal at day 0 and 15, the same dose was used at both vaccination times within a group. Control animals received no vaccination. The vaccine was administered subcutaneously into the left or right leg flap.

### 2.4. IFN-γ ELISPOT

IFN-γ secreting CD4+ T cells were measured using the ELISPOT assay. Single cell suspensions of mouse splenocytes were prepared by mechanical disruption of spleens through a 100 µm cell strainer on the day of sacrifice. After lysis of red blood cells, single cell suspensions were made up in antibiotic-free media [RPMI-1640 (Sigma-Aldrich, Dorset, UK) + 10% heat-inactivated FBS (Labtech International Ltd, Uckfield, UK) + 2 mM L-Glutamine (Fisher Scientific, Loughborough, UK)]. 96-well microtiter ELISPOT plates (MAIPS4510, Millipore, Watford, UK) were coated with 10 µg/ml rat anti-mouse IFN-γ (clone AN18, Mabtech, Nacka Strand, Sweden). Free binding sites were blocked with RPMI 1640 supplemented as described above.  $2.5 \times 10^5$  of total splenocytes were added and incubated in duplicate with H56 (10 µg/ml), supplemented RPMI as a negative control, or Phorbol myristate acetate (PMA) (50 µg/ml, Sigma-Aldrich) and Phytohemagglutinin (PHA) (10 µg/ml, Sigma-Aldrich) as a positive control. After 24 or 48 h of incubation at 37 °C in 5% CO<sub>2</sub>, IFN-γ was detected with 1 µg/ml biotin labelled rat anti-mouse antibody (clone R4-6A2, Mabtech) and 1 µg/ml alkaline phosphatase-conjugated streptavidin (Mabtech). The enzyme reaction was developed with BCIP/NBT substrate (5-Bromo-4-chloro-3-indolyl phosphate/Nitro blue tetrazolium) (MP Biochemicals, UK) and stopped by washing the plates with tap water when individual spots could be visually detected (up to 5 min). ELISPOT plates were analysed using an automatic plate reader. IFN-γ-specific cells are expressed as number of spot-forming units (SFU) per million spleen cells after non-specific background was subtracted using negative control wells.

## 2.5. Experimental schedule

ELISPOTs were carried out at 2, 7, 9, 14, 16, 21, 28, and 56 days after the first vaccination for all doses. Five mice were used per time point per dose group (equating to 40 mice in a dose group from initiation to conclusion of the experiment). This schedule was designed to reflect the H56 + IC31 phase I clinical trial schedule [8] and previous experimental schedules in mice using the H-series vaccines by SSI in CB6F1 mice [6,16,18,19].

## 2.6. Statistical methods

### 2.6.1. Summary of IFN- $\gamma$ response data after two vaccinations with TB vaccine H56+IC31 for future mathematical modelling

The Wilcoxon test was used to test for differences in IFN- $\gamma$  responses generated as a result of the two ELISPOT incubation times (on data pooled across dose groups and time points). The following summary measures were used to quantify responses over time: Area Under the Curve (AUC), day 56 response, peak response between first and second vaccination and peak response post-second vaccination (peaks may occur at different times as they were defined as the highest median response measured in the respective time period). As IFN- $\gamma$  responses over time within a dose group were not dependent (each taken from an individual mouse spleen), AUC was calculated using 200 samples of the possible combinations of the five mice per dose group over time. Full details of this method are outlined in [Supplementary material and Fig. S1](#). The non-parametric Dunn test was used to compare the summary measures between the dose groups and a Bonferroni correction applied to account for comparisons across multiple groups. A  $p$ -value < 0.05 was considered significant.

### 2.6.2. Determine the shape of dose-response curve when examined at varying sample times and the best dose predicted by fitted curves

To assess the shape of the dose-response curve (IFN- $\gamma$  SFU per million splenocytes versus dose), a saturating or peaked curve was fitted to all IFN- $\gamma$  responses against the ( $\log_{10}$  transformed) doses using nonlinear regression, in the software Prism (v 7 for Mac, GraphPad Software, California USA, [www.graphpad.com](http://www.graphpad.com)). Briefly, the aim of nonlinear regression is to find the parameters that minimise the sum of the squared residuals from all data points to the curve (see [Supplementary material for description](#)). We choose a sigmoidal equation as the saturating curve and the gamma probability density function (pdf) as the peaked curve (see [Supplementary for equations](#)). The choice of the gamma pdf was due to the hypothesis that the dose response, once peaked, will not increase again and will never decrease to a zero response. To establish which of the shapes best described the dose-response curves the goodness-of-fit measure, the corrected Akaike information criteria (AICc) was compared, where a lower AICc indicates a better fit. A difference in AICc value between curve fits of greater than seven was considered strong evidence of a better fit and a difference in AICc of greater than ten was considered absolute evidence of a better fit [20] ([Table S1](#)). To assess how the dose-response curve changed with time, the response data was pooled into three time ranges: between the first and second vaccination (day 2, 7, 9, 14 aggregated), post-second vaccination (day 21, 28 and 56 aggregated) and day 56 responses. The best dose was defined as the dose that produced the maximum IFN- $\gamma$  response as predicted by the fitted curves.

## 3. Results

### 3.1. Summary of IFN- $\gamma$ response data after two vaccinations with TB vaccine H56+IC31 for future mathematical modelling

Splenocyte-derived IFN- $\gamma$  responses did not differ for the 24 versus the 48 h ELISPOT incubation times when responses were pooled over all dose groups and time points ( $p$ -value = 0.67, [Fig. S2](#)). Therefore, an incubation time of 24 h was used in the following analyses.

The IFN- $\gamma$  responses over time for each dose group are shown in [Fig. 1](#) (significance of the changes in dynamics over time are in [Table S2](#)). Out of the samples taken to calculate the AUC, the common significance trend showed that dose groups 0.1, 0.5 and 1  $\mu$ g had significantly higher AUC than the control group, and the dose group 0.1  $\mu$ g had significantly higher AUC than dose group 15  $\mu$ g ([Fig. 2, Table S3](#)). Peak responses between first and second vaccination were significantly higher in the dose groups 0.1, 1, 5  $\mu$ g than in the control group and for post-second vaccination, dose groups 0.1, 0.5 and 5  $\mu$ g were significantly higher than the control group ([Figs. 1 and 2, Table 1](#)). Similarly, day 56 responses were significantly higher for the dose groups 0.1, 0.5 and 1  $\mu$ g than the control group and the dose group 0.5  $\mu$ g was higher than 15  $\mu$ g. However, this did not reach statistical significance ([Figs. 1 and 2, Table 1](#)). For all summary measures, no other comparisons between dose groups were statistically significantly different ([Fig. 2, Table 1](#)).

### 3.2. Determine the shape of dose-response curve when examined at varying sample times and the best dose predicted by fitted curves

To establish the shape of the dose-response curve (IFN- $\gamma$  SFU per million splenocytes versus dose), we fitted either a saturating or peaked function for three time ranges. There was strong evidence that the peaked curve was a better fit to the response data between first and second vaccination ([Fig. 3A, Table S4](#)) with a AICc difference of 7.5 favouring the peaked (gamma) curve. The AICc difference was 18.8 and 10.9 for the post-second vaccination ([Fig. 3B, Table S5](#)) and day 56 ([Fig. 3C, Table S6](#)) response data, suggesting absolute support for the peaked curve for both these time ranges. The best dose predicted by the peaked fitted curve for the time ranges; between first and second vaccination, post-second vaccination and day 56 were 0.026, 0.11 and 0.25  $\mu$ g, respectively (transformed from  $\log_{10}$  scale, [Fig. 3](#)). Due to the right-skewed nature of the responses the best saturation curve had an almost immediate increase followed by immediate plateau for all time ranges ([Fig. 3](#)). As such it was not possible to obtain a best predicted dose using the saturation model as, in this case, all doses generated the same response.

## 4. Discussion

Our future aim is to apply the new field of Immunostimulation/immunodynamic (IS/ID) modelling to translate vaccine dose-response information between animals and humans and thus quantitatively inform vaccine dose decision-making. To begin initial examination of such methods, we conducted a longitudinal dose-ranging experiment of the novel TB vaccine H56 + IC31 in mice, and a mathematical analysis of the dose-response curve over time.

We successfully generated an intensive time course of IFN- $\gamma$  response data to vaccination where AUC and peak analysis showed a trend toward higher responses over time in the lower doses than in the higher doses. By using mathematical curve fitting, we showed that the IFN- $\gamma$  dose-response follows a peaked shape instead of the commonly assumed saturation shape for all time

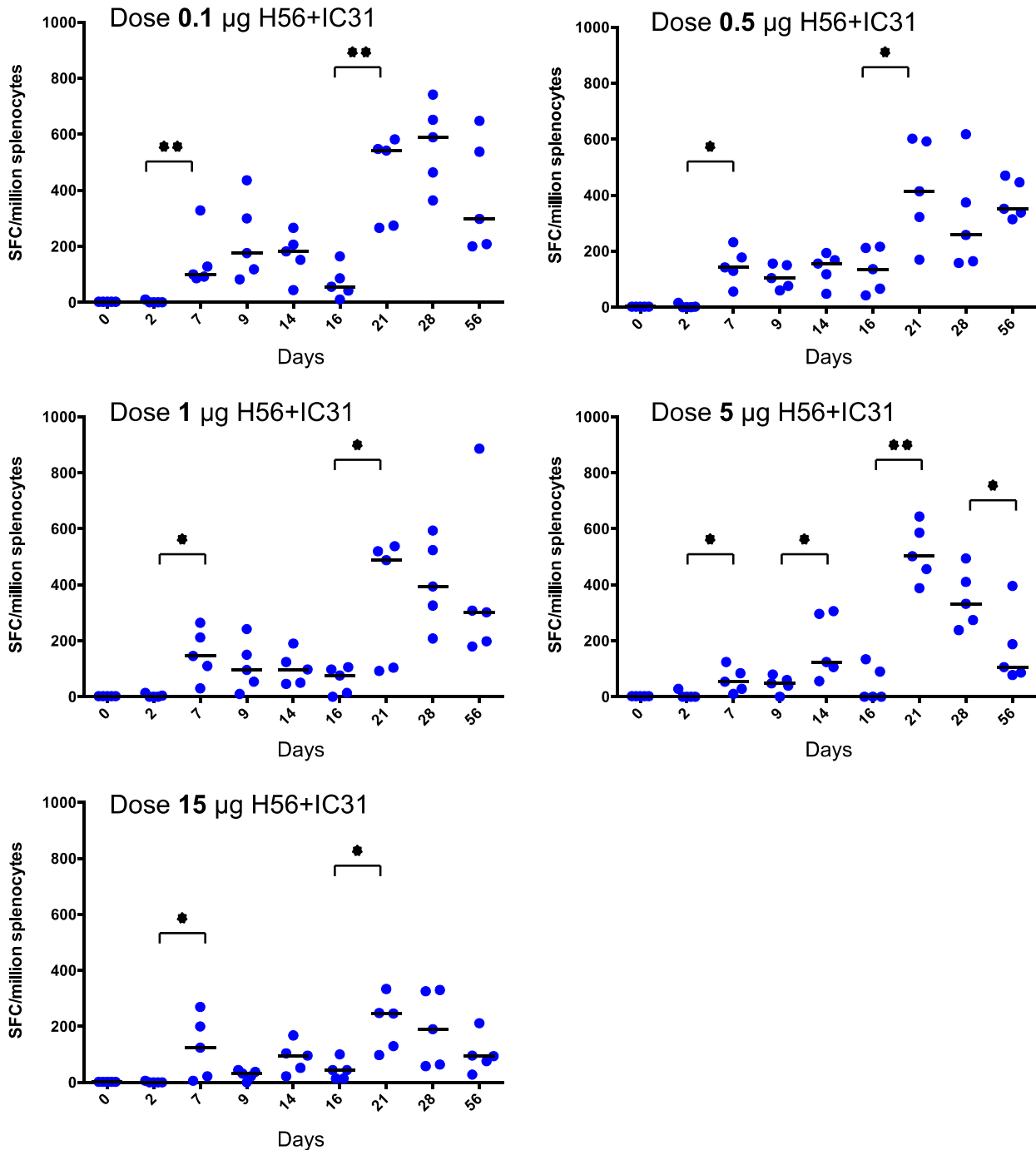


**Fig. 1.** Median IFN- $\gamma$  responses (horizontal black bars) and responses of individual mice per time point (blue points) for each dose. As the control group did not receive H56 + IC31, the median of all responses from the control group (which did not significantly change throughout the experiment) was used to represent all mice at baseline. The Wilcoxon test was used to compare consecutive time points, where \*equates to p-value < 0.05 and \*\*p-value < 0.01 (Table S2). (For interpretation of the references to colour in this figure legend, the reader is referred to the web version of this article.)

ranges. This was most apparent post-second vaccination, and trended toward that curve shape after the first dose. Using the peaked fitted curve, we were able to determine which dose may provide the maximal predicted IFN- $\gamma$  response in mice. Our results indicate this was at a low range; between 0.02 and 0.25  $\mu\text{g}$  H56 + IC31. It must be noted that, there is uncertainty associated with our predictions for best dose which is apparent in Tables S4–S6, where the standard error was high for some gamma distribution function parameters, particularly for the time ranges between first and second vaccination and post-second vaccination. This is poten-

tially due to a lack of response information between dose 0 and 0.1  $\mu\text{g}$ , which would provide information on the increase of the peaked curve. Despite this, as we show a definitive decline in the dose-response at the higher dose range (approximately after dose 1  $\mu\text{g}$  H56 + IC31), our predicted best dose range show compelling evidence that lower doses than previously explored in mice using very similar vaccines [6,16,18,21,22], would be preferential. Importantly, as previous evidence suggest the human dose-response may be of a similar shape for the H-series of vaccines from SSI [7,8] (although higher in magnitude), this implies that previously tested

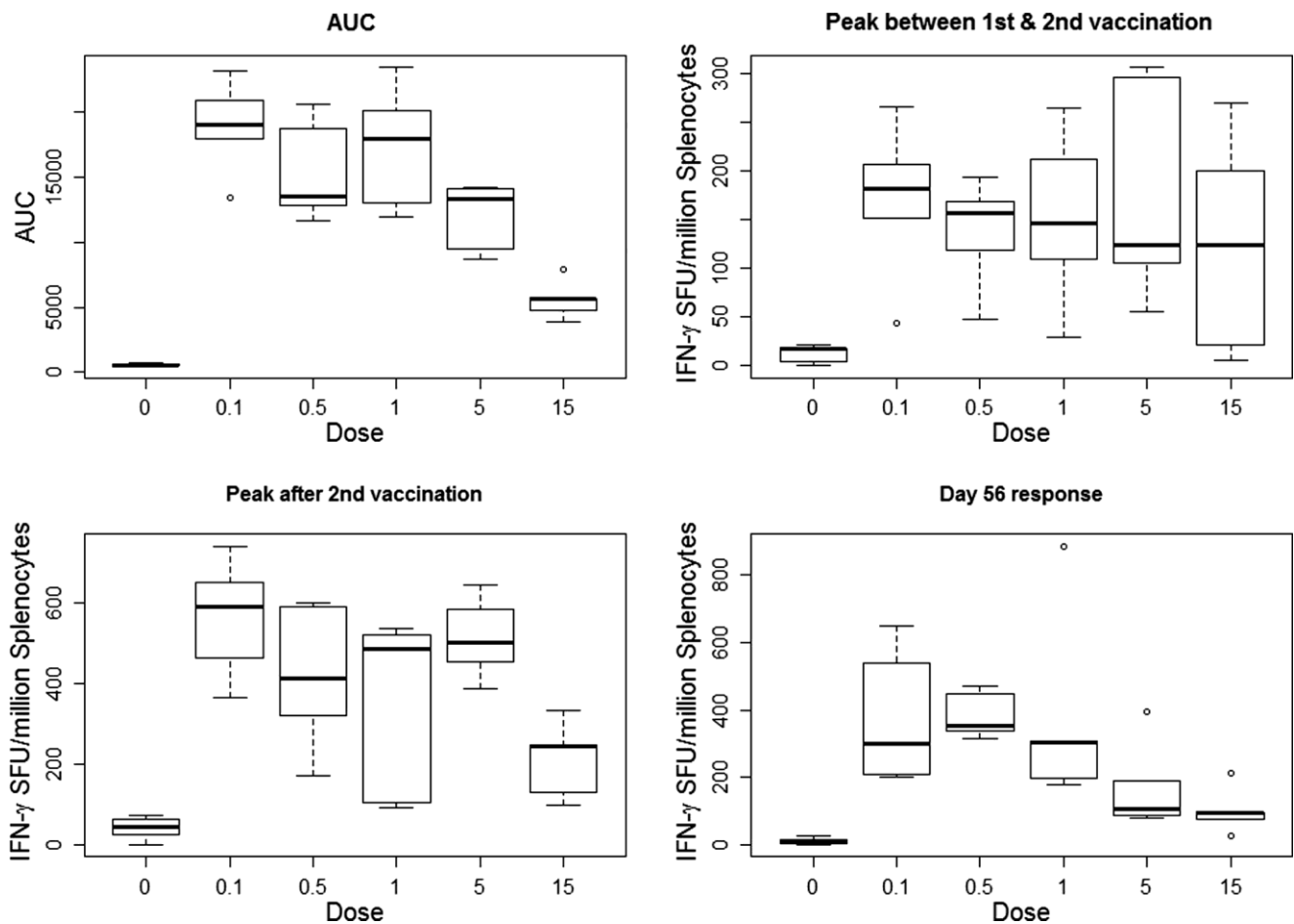


**Fig. 2.** AUC calculated from number of IFN- $\gamma$  secreting CD4+ T cells after two vaccinations with H56 + IC31 from individual mice spleens, number of IFN- $\gamma$  secreting CD4+ T cells between first and second vaccination, after second vaccination and day 56 by dose ( $\mu\text{g}$  H56 + 100 nmol IC31). Dose 0 equates to the control group. The plot for AUC is representative of the 200 samples taken to establish statistical differences in AUC by dose (see methods). X axis not to scale.

**Table 1**

Median (IQR) values for the summary measures day 56 response, peak between first and second vaccination and post-second vaccination IFN- $\gamma$  responses by dose. Significance in the summary measures was tested between dose groups using the non-parametric Dunn test with a Bonferroni correction. Those comparisons between dose groups with a p-value < 0.05 or 0.05 < p-value < 0.1 (starred) are displayed. Abbreviations: IQR = interquartile range, vacc = vaccination.

Dose group ( $\mu\text{g}$ H56 + IC31)	Median day 56 response (IQR)	Significantly different from dose	Median Peak between 1st and 2nd vacc (IQR)	Significantly different from dose	Median Peak post 2nd vacc (IQR)	Significantly different from dose
Control	10 (2–14)	0.1, 0.5, 1	18 (4–18)	0.1, 1, 5	44 (26–64)	0.1, 0.5, 5
0.1	298 (208–538)	Control	182 (152–206)	Control	590 (464–652)	Control
0.5	352 (338–446)	Control, 15*	156 (118–168)	–	414 (322–592)	Control
1	302 (198–308)	Control	146 (110–212)	Control	488 (104–520)	–
5	106 (86–188)	–	124 (106–296)	Control	502 (456–586)	Control
15	94 (76–96)	0.5*	124 (22–200)	–	246 (130–248)	–

clinical dose ranges may also have been too high to capture the optimal response in terms of immunogenicity.

We use the frequency of IFN- $\gamma$  secreting CD4+ T cells measured using the ELISPOT assay as our chosen immune response readout to reflect the current convention in TB vaccine development for dose selection. IFN- $\gamma$  is a cytokine shown to be associated with control of infection or decreased risk of TB disease [23], however these findings have been a topic of controversy in TB vaccine development [24]. In previous work by Aagaard et al. in the vaccine H4 + IC31, results showed that mice vaccinated with a lower dose (0.5  $\mu\text{g}$  H4) experienced significantly higher IFN- $\gamma$  responses than higher doses (5 and 15  $\mu\text{g}$  H4) and, significantly stronger protection against *Mtb.* infection (measured by *Mtb.* colony forming units) than the higher doses, in two independent challenge exper-

iments [6]. These results support our choice of IFN- $\gamma$  as a readout. We also compliment Aagaard et al.'s study by measuring the IFN- $\gamma$  response at *multiple* time points, thus assessing trends in the dose-response curve over time.

It is possible that varying dose may alter the function or type of CD4 T cell secreting IFN- $\gamma$ , which the ELISPOT assay will not detect. Further lab assays such as flow cytometry should be used in the future work to determine the function or type of cell produced as a result of varying dose, which may then be used in clinical trials for human dose selection.

Dose concentration feasibility and animal cost and overall numbers limited the size of our study. By testing in larger groups of mice at potentially fewer time points, we may have gained greater certainty in response differences and fitted dose-response curves.

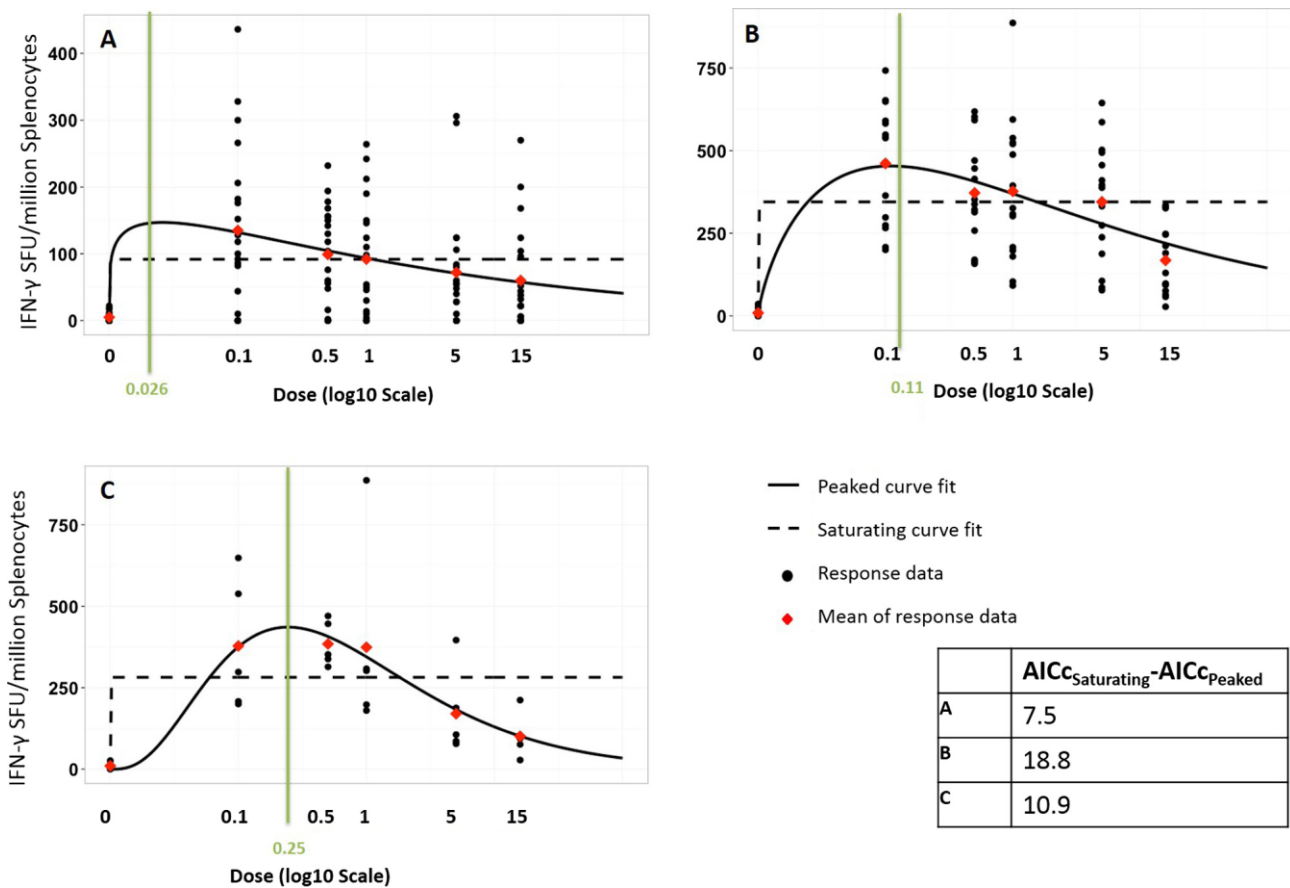


**Fig. 3.** Results of the dose-response curve fitting analysis for the time ranges (A) between first and second vaccination (aggregated responses from days 2, 7, 9 and 14), (B) post-second vaccination (days 21, 28 and 56) and C. Day 56 (last time point). Black points correspond to the number of IFN- $\gamma$  secreting CD4+ T cells from one mouse spleen in response to vaccination for the relevant time range, red diamonds show the mean of the responses, the black solid lines are the peaked (gamma) fit, the black dashed line show the saturating (sigmoidal) curve fit and the vertical green line indicated the best dose as predicted by the peaked curve fit. The table shows the differences in AICc for A,B and C between the saturating and peaked curve fits. The x-axis is  $\log_{10}(\text{dose: } \mu\text{g H56 + IC31}) + 2$  to transform the dose to a log scale and to ensure positivity, but x-axis labels show the non-logged value for clarity (to avoid infinite values, control (dose 0) is not logged).

However, we chose the extensive time course to determine detailed dynamics of the vaccine response and dose-response curves over time, since this has been performed infrequently in the past. We believe a higher maximum dose may have better defined the decline in the dose-response curve. As the size of the study was limited, we concentrated efforts on the lower doses, where previous exploration is lacking; however, we found that the probable best dose is still lower than the minimum dose used here.

We have identified the following areas for further research. The mathematical curve fitting we conducted has provided the basis for further optimised studies in animals, i.e. we now know that the dose range that captures the probable best dose should be 0–0.3  $\mu\text{g H56 + IC31}$  (based on our predicted best dose values) not the initial 0–15  $\mu\text{g H56 + IC31}$  (a reduction of 98% in the range). Expanding the dose range in the lower end between 0 and 0.1  $\mu\text{g}$  will further increase our best dose predictions, as the peaked curve parameters will be estimated with greater certainty. This warrants further animal studies to investigate in greater detail the host response to low dose vaccination.

Additionally, we used AUC to quantify the magnitude of the immune response for the duration of the experiment and compared AUC between dose groups. However, we do not interpret this measure as the cumulative immune response over time, as would be appropriate in drug AUC measures, but an indication of overall higher immune response magnitude. In vaccine development, dose

decisions are made based on the dose response curve at one time point (usually a long-term time point) and as such it would be advantageous to know how dose effects the dynamics of the immune response that may lead to higher average response in the long-term. As such, our future aim is to apply the new field of Immunostimulation/immunodynamic (IS/ID) modelling, where by a mechanistic mathematical model incorporating the fundamental T cell subsets involved in a Th1 immune response will be calibrated to the ELISPOT or another given measure over time. The IS/ID model will allow us to quantify how the dynamics of the immune response differ between dose groups (and across the entire mouse population) by assessing the change in model parameters by dose. To achieve this, we will use the robust statistical framework, Nonlinear Mixed Effects Modelling to calibrate the model to the data and characterise the parameters and associated parameter variation. IS/ID modelling will also be used to translate vaccine dose-response information between animals and humans. To achieve this we will utilise known allometric scaling factors for H56 + IC31 between mouse and human we aim to “map” IS/ID model parameters from one dose of the outlined experiment to existing human H56 + IC31 dose data (one dose 50  $\mu\text{g H56 + 500 nmol IC31}$ ). The effect of heterogeneity in target human populations (due to HIV status, existing latent infection, etc.) on IS/ID modelling parameters will be taken into account. Following this mapping, we can then use the remaining doses to predict the dose response curve in humans. This predicted human dose-response

curve will be used as a guide to select further doses to test in clinical trials.

Additionally, as the antigen dose-response may also vary with the adjuvant dose and type of adjuvant, in order to fully characterise and optimise complete vaccine (H56 + IC31) dose it would be necessary to perform a checkerboard interaction pattern, the design of which could be informed by IS/JID modelling through optimal design analysis [25].

## 5. Conclusion

Our results suggest that the highest, safe dose is not always optimal in terms of host response as the dose-response curve is not saturating, which may also be true for vaccines against diseases other than TB. Mathematical modelling can be used on the detailed longitudinal dose range data for TB vaccine H56 + IC31 to simulate responses to optimise further experiments in mice and help to identify optimal doses for humans.

## Funding

Funding for the experiment was provided by the Bill and Melinda Gates Foundation. SR is supported by a LSHTM studentship funded by Aeras. The views expressed are those of the author(s) and not necessarily those of the SSI, the NHS, the NIHR, the Department of Health or Public Health England. RGW is funded the UK Medical Research Council (MRC) and the UK Department for International Development (DFID) under the MRC/DFID Concordat agreement that is also part of the EDCTP2 programme supported by the European Union (MR/J005088/1), the Bill and Melinda Gates Foundation (TB Modelling and Analysis Consortium: OPP1084276) and UNITAID (4214-LSHTM-Sept15; PO #8477-0-600).

## Conflicts of interest

There are no conflicts of interest.

## Acknowledgements

We would like to thank our collaborators at Staten Serum Institute Peter Andersen and Else Marie Agger (now at Novo Nordisk) for advising the mouse experiment schedule and Steven Kern at the Bill and Melinda Gates Foundation for facilitating experiment funding.

## Appendix A. Supplementary material

Supplementary data associated with this article can be found, in the online version, at <http://dx.doi.org/10.1016/j.vaccine.2016.10.060>.

## References

- [1] Han S. Clinical vaccine development. *Clin Exp Vaccine Res* 2015;4:46–53.
- [2] Dickson M, Gagnon JP. The cost of new drug discovery and development. *Discovery Med* 2004;4:172–9.
- [3] Quinn CP, Sabourin CL, Niemuth NA, Li H, Semenova VA, Rudge TL, et al. A three-dose intramuscular injection schedule of anthrax vaccine adsorbed generates sustained humoral and cellular immune responses to protective antigen and provides long-term protection against inhalation anthrax in rhesus macaques. *Clin Vaccine Immunol*: CVI 2012;19:1730–45.
- [4] Little SF, Webster WM, Norris SL, Andrews GP. Evaluation of an anti-rPA IgG ELISA for measuring the antibody response in mice. *Biol: J Int Assoc Biol Standardization* 2004;32:62–9.
- [5] Semenova VA, Schiffer J, Steward-Clark E, Soroka S, Schmidt DS, Brawner MM, et al. Validation and long term performance characteristics of a quantitative enzyme linked immunosorbent assay (ELISA) for human anti-PA IgG. *J Immunol Methods* 2012;376:97–107.
- [6] Aagaard C, Hoang TT, Izzo A, Billeskov R, Troudt J, Arnett K, et al. Protection and polyfunctional T cells induced by Ag85B-TB10.4/IC31 against Mycobacterium tuberculosis is highly dependent on the antigen dose. *PLoS ONE* 2009;4:e5930.
- [7] Geldenhuys H, Mearns H, Miles DJ, Tameris M, Hokey D, Shi Z, et al. The tuberculosis vaccine H4:IC31 is safe and induces a persistent polyfunctional CD4 T cell response in South African adults: a randomized controlled trial. *Vaccine* 2015;33:3592–9.
- [8] Luabeya AK, Kagina BM, Tameris MD, Geldenhuys H, Hoff ST, Shi Z, et al. First-in-human trial of the post-exposure tuberculosis vaccine H56:IC31 in Mycobacterium tuberculosis infected and non-infected healthy adults. *Vaccine* 2015;33:4130–40.
- [9] van Dissel JT, Arend SM, Prins C, Bang P, Tingskov PN, Lingnau K, et al. Ag85B-ESAT-6 adjuvanted with IC31 promotes strong and long-lived Mycobacterium tuberculosis specific T cell responses in naive human volunteers. *Vaccine* 2010;28:3571–81.
- [10] Evans TG, McElrath MJ, Matthews T, Montefiori D, Weinhold K, Wolff M, et al. QS-21 promotes an adjuvant effect allowing for reduced antigen dose during HIV-1 envelope subunit immunization in humans. *Vaccine* 2001;19:2080–91.
- [11] Wright DF, Winter HR, Duffull SB. Understanding the time course of pharmacological effect: a PKPD approach. *Br J Clin Pharmacol* 2011;71:815–23.
- [12] Mould DR, Upton RN. Basic concepts in population modeling, simulation, and model-based drug development. *CPT: Pharmacometrics Syst Pharmacol* 2012;1:e6.
- [13] Knibbe CA, Zuideveld KP, Aarts LP, Kuks PF, Danhof M. Allometric relationships between the pharmacokinetics of propofol in rats, children and adults. *Br J Clin Pharmacol* 2005;59:705–11.
- [14] Dubois VF, de Witte WE, Visser SA, Danhof M, Della Pasqua O, Cardiovascular Safety Project T, et al. Assessment of interspecies differences in drug-induced QTc interval prolongation in cynomolgus monkeys, dogs and humans. *Pharm Res* 2016;33:40–51.
- [15] Plotkin SA, Orenstein WA, Offit PA. Vaccines. 6th ed. Saunders; 2013.
- [16] Aagaard C, Hoang T, Dietrich J, Cardona PJ, Izzo A, Dolganov G, et al. A multistage tuberculosis vaccine that confers efficient protection before and after exposure. *Nat Med* 2011;17:189–94.
- [17] Lalvani A, Pathan AA, McShane H, Wilkinson RJ, Latif M, Conlon CP, et al. Rapid detection of Mycobacterium tuberculosis infection by enumeration of antigen-specific T cells. *Am J Respir Crit Care Med* 2001;163:824–8.
- [18] Hoang T, Aagaard C, Dietrich J, Cassidy JP, Dolganov G, Schoolnik GK, et al. ESAT-6 (EsxH) and TB10.4 (EsxH) based vaccines for pre- and post-exposure tuberculosis vaccination. *PLoS ONE* 2013;8:e80579.
- [19] Christensen D, Lindstrom T, van de Wijdeven G, Andersen P, Agger EM. Syringe free vaccination with CAF01 Adjuvanted Ag85B-ESAT-6 in bioneedles provides strong and prolonged protection against tuberculosis. *PLoS ONE* 2010;5:e15043.
- [20] Burnham KP, Anderson DR. Multimodel inference: understanding AIC and BIC in model selection. *Sociol. Methods Res.* 2004;33:261–304.
- [21] Ciabattini A, Prota G, Christensen D, Andersen P, Pozzi G, Medaglini D. Characterization of the antigen-specific CD4(+) T Cell response induced by prime-boost strategies with CAF01 and CpG adjuvants administered by the intranasal and subcutaneous routes. *Front Immunol* 2015;6:430.
- [22] Elvang T, Christensen JP, Billeskov R, Thi Kim Thanh Hoang T, Holst P, Thomsen AR, et al. CD4 and CD8 T cell responses to the M. tuberculosis Ag85B-TB10.4 promoted by adjuvanted subunit, adenovector or heterologous prime boost vaccination. *PLoS ONE* 2009;4:e5139.
- [23] Fletcher HA, Snowden MA, Landry B, Rida W, Satti I, Harris SA, et al. T-cell activation is an immune correlate of risk in BCG vaccinated infants. *Nature Commun* 2016;7:11290.
- [24] Kagina BM, Abel B, Scriba TJ, Hughes EJ, Keyser A, Soares A, et al. Specific T cell frequency and cytokine expression profile do not correlate with protection against tuberculosis after bacillus Calmette-Guerin vaccination of newborns. *Am J Respir Crit Care Med* 2010;182:1073–9.
- [25] Chien JY, Friedrich S, Heathman MA, de Alwis DP, Sinha V. Pharmacokinetics/pharmacodynamics and the stages of drug development: role of modeling and simulation. *AAPS J* 2005;7:E544–59.

## **Supplementary material for paper 3**

The following is the supplementary material referenced in paper 3. All references to the below tables and Figures are preceded with the suffix “S” in the paper.

### ***Additional Methods***

#### **Statistical methods**

##### **Analysis (i) Summary of IFN- $\gamma$ response data after two vaccinations with TB vaccine H56+IC31 for future mathematical modelling**

To compare the magnitude of the IFN- $\gamma$  response over time between dose grouping, I calculated the Area Under the Curve (AUC) from day 0 to 56 for each dose grouping. Conventional AUC calculations are conducted on repeated measures data; the area of the curve created by connecting responses over time for one host make the AUC value for that host. Responses in our experiment are not repeated measures as each IFN- $\gamma$  response measured was taken from a spleen of one euthanized mouse. To account for this in the AUC calculation I take samples of all possible AUC's in one dosing group and compare across groups. The procedure for this is as follows. As there are five mice per time point and eight time points per dosing group (excluding day 0), there are  $5^8$  possible combinations of AUC values for each dose grouping (i.e. by linking mouse one at time point one to mouse one at time point two, etc. until time point eight. Or mouse one at time point one to mouse two at time point two, etc. and calculating the AUC from these combinations of responses over time, see Figure S1). I sample 5 (to reflect the use of five mice per time point) out of the total possible AUC values ( $5^8$ ) for one dose group. I do this for each dosing group. I then compare these AUC values across the dosing groups and note the significant differences (using the Dunn test with a Bonferroni correction for multiple group comparisons and adjusted p-value<0.003). I re-sample five AUC values (repeating the procedure above) for each dosing group and compare across dosing groups. I sample a total of 200 times. Results are presented in Table S3 showing the frequency of observed significantly different AUC's between dosing groups for all 200 samples.

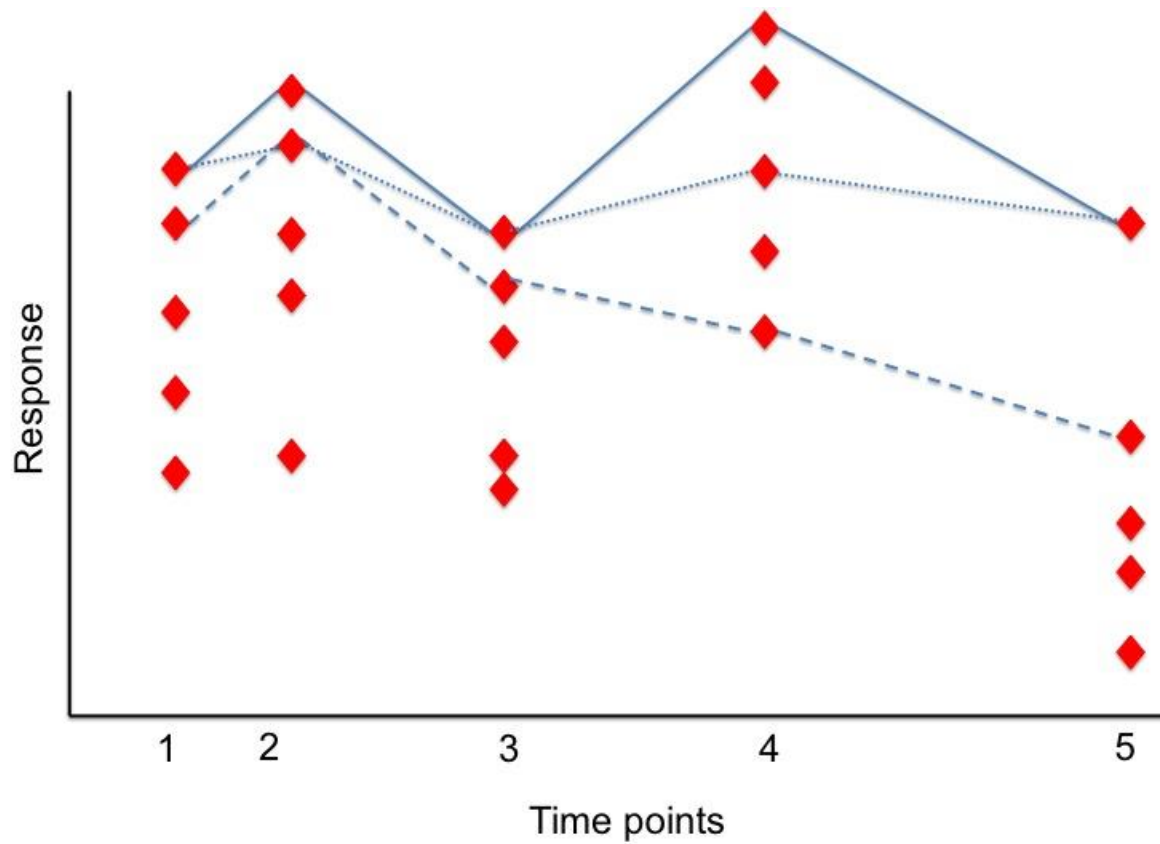


Figure S1. Example representation of the possible combinations of AUC calculations. In this example, there are 5 times points and 5 data points (diamonds) per time point. Three lines are shown (solid, dotted and dashed) which AUC would be calculated from. These are 3 random combinations out of the possible  $5^5$  combinations that could be drawn.

**Analysis (ii) Determine the shape of dose-response curve when examined at varying sample times and the best dose predicted by fitted curves**

In this analysis, I conducted nonlinear regression using the functional forms gamma pdf and sigmoidal in the software Prism. The functional form for the sigmoidal curve is:

$$Response = Baseline + \frac{Rmax * Dose^p}{R50 + Dose^p}$$

Where Dose is the Dose(log10), Rmax is the saturation maximum, R50 is the value where the response is 50% of the saturation maximum. Baseline is the value of the curve when dose is 0. As I assume that the response at dose 0 is very low (almost zero) due to the lack of exposure to the vaccine, I fix this value to the mean response at dose 0 for the different time ranges. The functional form for the gamma pdf curve is:

$$Response = Baseline + \left( S * \frac{r^{sh}}{\Gamma(sh)} * Dose^{(sh-1)} * e^{-r*Dose} \right)$$

S is a scalar multiplying the gamma pdf, r is the gamma rate parameter, and sh, the gamma shape parameter.

In the Prism software, nonlinear regression is conducted by minimizing the sum of the squares of the residuals (SS), under the assumption that the residuals are normally distributed. Thus I used a maximum likelihood method. I fit the curves to all data points in the time range, hence, the SS is calculated by summing all squared residuals from all data points. Prism uses the derivative-based, Levenberg-Marquardt method to perform the parameter optimization (for an in-depth mathematical description see [333]).

To assess the precision of the parameter best-fit estimates I used the standard error of the estimates produced by Prism. See [334] for a brief explanation into their calculation. I used relative standard error, which is expressed as the percentage of the standard error of the

parameter to the best-fit estimate parameter and can give an indication of the relative magnitude of the standard error.

To measure the goodness of fit of each model to the data, I used the corrected Akaike Information Criteria (AICc). AICc is a recommended criterion to compare the fit of non-nested models in nonlinear regression on data from small studies. It is in-built to nonlinear regression analysis in Prism. The AICc is calculated using the following formula:

$$AICc = N * \ln\left(\frac{SS}{N}\right) + 2K + \frac{2K(K + 1)}{N - K - 1}$$

where N is the number of data points, K is the number of fitted model parameters (+1) and SS is the sum of the squared residuals. To find the “best” model to describe the data, I used the in-built model comparison tool in prism, which calculates the probability that the model is “correct”, also known as the Akaike weight (see [334-336]) using the model AICc. I also used the criteria for model selection using the difference in AICc outlined by Burnham & Anderson [336] in Table S1 :

Difference in AICc between model with lowest AICc (MLow) and model being compared (MCom)	Conclusion
0-2	Substantial support for MCom
4-7	Considerably less support for MCom
>10	Essentially no support for MCom

**Table S1. Table outlining Burnham and Anderson’s criteria for support for models using AICc difference**

To assess for homoscedasticity of the data (i.e. the variance of the data around the mean response is not dependent on the magnitude of the response), I ran the in-built test in Prism [334] (see Tables S4-S6). If this test failed, this would indicate weighing the data by response could be necessary. Additionally, to establish if the estimated parameters were global minimums, I ran the regression with varying initial parameter estimates (see Table S7).

## Additional Results

### Statistical results

#### Analysis (i) Summary of IFN- $\gamma$ response data after two vaccinations with TB vaccine H56+IC31 for future mathematical modelling

The Wilcoxon test was used to test for differences in IFN- $\gamma$  responses generated as a result of the two ELISPOT incubation times (on data pooled across dose groups and time points). IFN- $\gamma$  responses did not differ for the 24 versus the 48 hour ELISPOT incubation times ( $p$ -value = 0.67). Figure S2 shows a comparison between all mouse IFN- $\gamma$  responses (over all dose groupings and all time points) for the two ELISPOT incubation times. Therefore, an incubation time of 24 hours was used in paper 3.

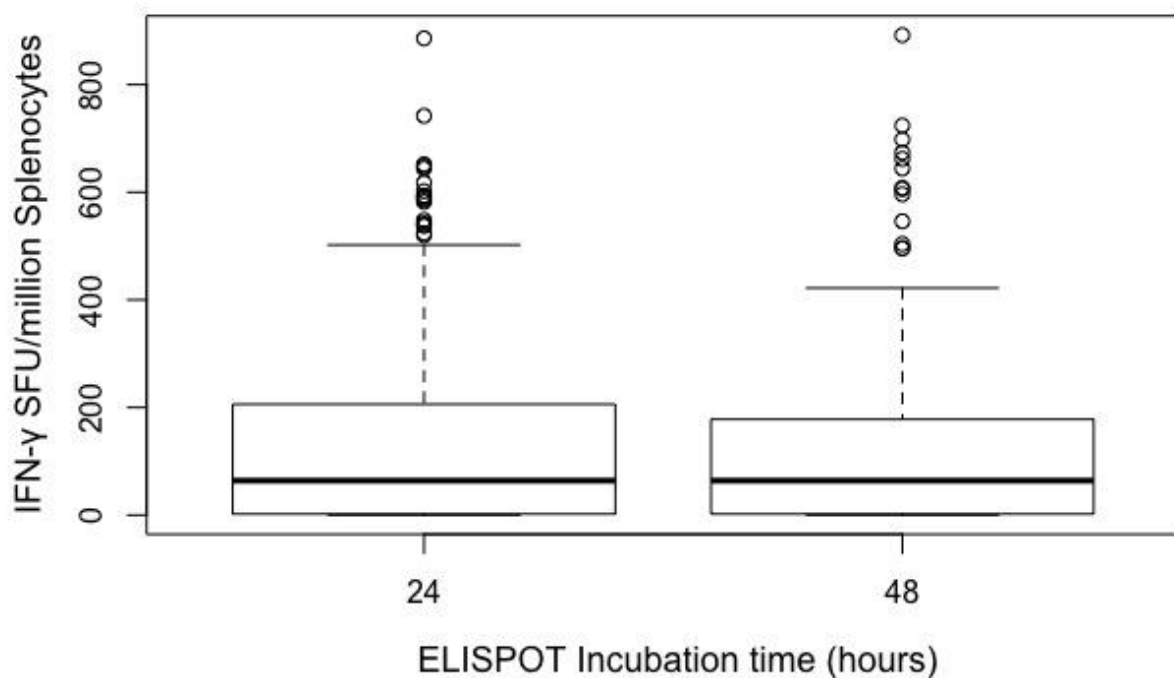


Figure S2. Number of IFN- $\gamma$  secreting CD4+ T cells after two vaccinations with H56+IC31 from individual mice spleens (pooled over time and dose) for the two ELISPOT assay incubation times (24 and 48 hour). There was no significant difference between the two incubation times.

Table S2 outlines significant changes in median IFN- $\gamma$  responses between consecutive time points by dosing group (highlighted grey in Table S2). For each dose grouping (except the control group) there was a significant difference in median response between the day 2 and day 7 and between day 16 and day 21. In both cases (and for all dose groupings) this was a significant increase in median IFN- $\gamma$  response over time. This is presumably because the IFN- $\gamma$  response increases significantly due to primary vaccination between day 2 and 7 and also increases significantly due to revaccination between day 16 and 21. For the dose grouping receiving 5  $\mu$ g of H56, there were further instances of significant differences between time points, namely between day 9 and 14 (an increase) and day 28 and 56 (a decrease). The decrease in response for this dosing group is potentially interesting as it suggests the mice receiving 5  $\mu$ g of H56 experience a significant drop off of immunity in the long term.

		Dose group ( $\mu$ g H56+IC31)					
		Median SFU per million cells for two timepoints ( <i>p</i> -value for difference)					
		control	0.1	0.5	1	5	15
Significant difference in response between days:	0 & 2	2 & 0 (0.65)	2 & 0 (0.11)	2 & 0 (0.28)	2 & 0 (0.65)	2 & 0 (0.11)	2 & 0 (0.1)
	2 & 7	0 & 0 (0.72)	<b>0 &amp; 100 (0.009)</b>	<b>0 &amp; 142 (0.01)</b>	<b>0 &amp; 146 (0.02)</b>	<b>0 &amp; 54 (0.02)</b>	<b>0 &amp; 124 (0.01)</b>
	7 & 9	0 & 2 (0.5)	100 & 176 (0.55)	142 & 104 (0.55)	146 & 96 (0.55)	54 & 48 (0.69)	124 & 32 (0.35)
	9 & 14	2 & 18 (0.2)	176 & 182 (0.84)	104 & 156 (0.35)	96 & 98 (1)	<b>48 &amp; 124 (0.047)</b>	32 & 96 (0.07)
	14 & 16	18 & 44 (0.12)	182 & 56 (0.1)	156 & 136 (1)	98 & 76 (0.35)	124 & 0 (0.07)	96 & 44 (0.14)
	16 & 21	44 & 6 (0.14)	<b>56 &amp; 542 (0.008)</b>	<b>136 &amp; 414 (0.03)</b>	<b>76 &amp; 488 (0.047)</b>	<b>0 &amp; 502 (0.009)</b>	<b>44 &amp; 246 (0.02)</b>
	21 & 28	6 & 8 (0.26)	542 & 590 (0.22)	414 & 258 (0.42)	488 & 394 (0.69)	502 & 332 (0.06)	246 & 190 (0.69)
	28 & 56	8 & 10 (0.83)	590 & 298 (0.15)	258 & 351 (0.42)	394 & 302 (0.31)	<b>332 &amp; 106 (0.049)</b>	190 & 94 (0.55)

Table S2. Median values and *p*-values using the Wilcoxon test to compare the five IFN- $\gamma$  responses between consecutive time points for each dose. Bold and highlighted values are below 0.05.

Table S3 shows the frequency of significant differences in sampled AUC values across dosing groups after 200 samples of 5 AUC values per dosing group (see additional methods, analysis (i)). Out of the samples taken to calculate the AUC, the common significance trend showed that dose groups 0.1, 0.5 and 1 µg had significantly higher AUC than the control group, and the dose group 0.1 µg had significantly higher AUC than dose group 15 µg (Figure 2, Table S3).

Dose (µg H56+IC31) grouping comparison	Frequency of significantly different (adjusted p-value < 0.003) AUC values* out of the 200 samples (% of the 200 samples)
control – 0.1	179 (89.5%)
control – 0.5	167 (83.5%)
control - 1	164 (82%)
control - 5	18 (9%)
control - 15	0 (0%)
0.1 – 0.5	0 (0%)
0.1 - 1	0 (0%)
0.1 - 5	0 (0%)
0.1 -15	86 (43%)
0.5 - 1	0 (0%)
0.5 - 5	0 (0%)
0.5 - 15	7 (4%)
1 - 5	0 (0%)
1 - 15	18 (9%)
5 - 15	0 (0%)

**Table S3. Frequency of significantly (with a Bonferroni correction for multiple groups) different AUC comparisons over 200 samples of possible AUC values. \*Five AUC values for each dose grouping per sample.**

## Statistical results

### **Analysis (ii) Determine the shape of dose-response curve when examined at varying sample times and the best dose predicted by fitted curves**

In this analysis, I conducted nonlinear regression using the functional forms gamma pdf and sigmoidal in the software Prism. In order to obtain a reasonable nonlinear curve fit to the dose response data, constraints on the fitting algorithm were required. I have outlined above that the baseline parameter was fixed to 0 for both curves (see above). Additionally, for the Gamma curve, I applied the constraint of 1.2 to the shape parameter (sh). This was to avoid an exponential shape curve (which violates my peaked curve shape hypothesis), which occurs when the shape parameter is equal to 1. For the sigmoidal curve, the parameter E50 was constrained to be >0 as a negative E50 would not produce a saturating curve shape. Additionally, in preliminary fits where the parameter p was estimated, Prism reported an “ambiguous” value. I believe this was due to the right skew of the data which forced the sigmoidal curve to increase immediately to the Rmax value. As such, the effect of changing parameter p will shift the sigmoidal curve to the right (see Figure S3 for demonstration), but does not change the AICc value of the overall fit. As such I fixed the value at p=1.

Test for value of Sigmoidal curve value p on day 56  
response data

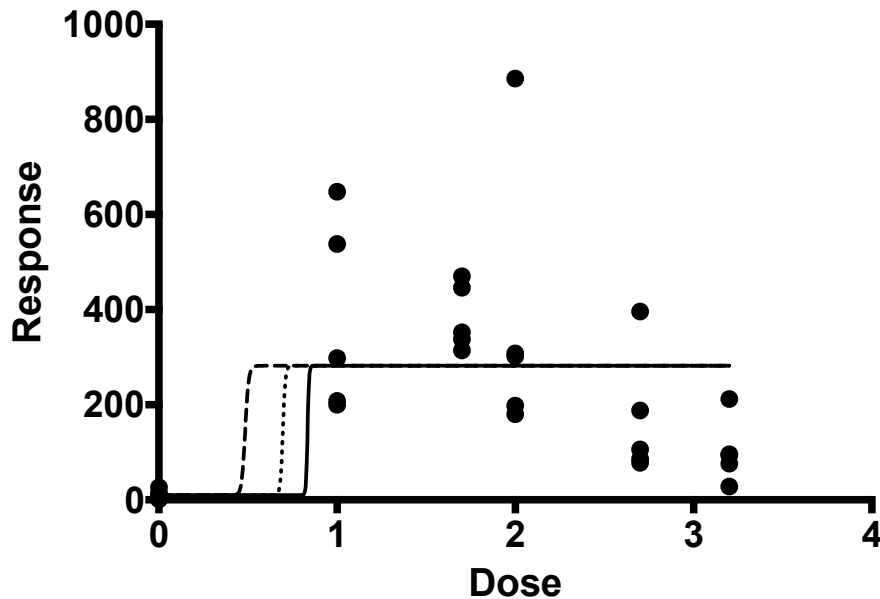


Figure S3. Plot showing the effect of changing parameter p in the sigmoidal curve equation the dashed line corresponds to a p=50, the dotted line, p=100 and the solid line, p=200 on the day 56 data. If values are increased further (to approximately p=700), Prism reports a “bad initial value” error.

Tables S4-S6 outlines the results of the regression analysis on responses for the time ranges pre-second vaccination (between first and second vaccination), post-second vaccination and day 56. Tables S4-S6 show that the Sigmoidal Rmax parameter was well estimated (low relative standard error), except for the day 56 data, which is due to small sample size. For every fit, the R50 parameter hit the low bound (very close to zero). This was due to the right skew of the data, which forced the sigmoidal curve to increase immediately to the Rmax value, and as such, R50 to be very small. A value of absolute zero here would cause an inflection point which and the derivative-based fitting algorithm to fail.

The Gamma parameters were not well estimated for in any of the fits. I believed this is due to a lack of data in the range between dose 0 and 0.1 (log10) which would provide information on the nature increase of the peaked curve. This was most apparent in the pre-second data set where the shape parameter (sh) hit the constraint value and as such produced a heavily right-skewed curve (Figure 3A). The day 56 data do provide information on the increase of

the peaked curve, but the sample size is small, so the relative standard error of the parameters is high.

Pre-second vaccination Gamma curve fit		Pre-second vaccination Sigmoidal curve fit	
Best-fit parameter values		Best-fit parameter values	
Baseline	5 (fixed)	Baseline	5 (fixed)
S	440.5	Rmax	87.02
r	0.5047	p	1 (fixed)
sh	1.2	R50	$1.8 \times 10^{-16}$
Standard Error (% relative SE)		Standard Error (% relative SE)	
Baseline	-	Baseline	-
S	255.1 (58%)	Rmax	21.16 (24%)
r	0.7405 (150%)	p	-
sh	Hit constraint	R50	Hit constraint
Goodness of Fit		Goodness of Fit	
Degrees of Freedom	117	Degrees of Freedom	118
Absolute Sum of Squares	786326	Absolute Sum of Squares	851795
AICc	1063	AICc	1070
Test for homoscedasticity	Passed	Test for homoscedasticity	Passed
<b>Comparison of Gamma and Sigmoidal curve fit</b>			
Simpler model		Sigmoidal	
Probability it is correct		2.35%	
Alternative model		Gamma	
Probability it is correct		97.65%	
Ratio of probabilities		41.59	
Preferred model		Gamma	
Difference in AICc		7.456	
Strength of evidence for model with higher AICc (according to [336])		Between “considerably less” and “Essentially no” support for Sigmoidal – strong support for Gamma	

**Table S4. Summary of nonlinear regression analysis of the Gamma and Sigmoidal curve fitting for the responses pre-second vaccination.**

Post-second vaccination Gamma curve fit		Post-second vaccination Sigmoidal curve fit	
Best-fit parameter values		Best-fit parameter values	
Baseline	9 (fixed)	Baseline	9 (fixed)
S	1451	Rmax	336
r	0.7535	p	1 (fixed)
sh	1.787	R50	1.8x10 <sup>-16</sup>
Standard Error (% relative SE)		Standard Error (% relative SE)	
Baseline	-	Baseline	-
S	309.7 (21%)	Rmax	50.73 (15%)
r	0.4175 (55%)	p	-
sh	0.7283 (40%)	R50	Hit constraint
Goodness of Fit		Goodness of Fit	
Degrees of Freedom	87	Degrees of Freedom	88
Absolute Sum of Squares	2167842	Absolute Sum of Squares	2737663
AICc	916.5	AICc	935.3
Test for homoscedasticity	Passed	Test for homoscedasticity	Passed
<b>Comparison of Gamma and Sigmoidal curve fit</b>			
Simpler model		Sigmoidal	
Probability it is correct		<0.01%	
Alternative model		Gamma	
Probability it is correct		>99.99%	
Ratio of probabilities			
Preferred model		Gamma	
Difference in AICc		18.81	
Strength of evidence for model with higher AICc (according to [336])		"Essentially no support" for Sigmoidal	

**Table S5. Summary of nonlinear regression analysis of the Gamma and Sigmoidal curve fitting for the responses post-second vaccination.**

<b>Day 56 Gamma curve fit</b>		<b>Day 56 Sigmoidal curve fit</b>	
Best-fit parameter values		Best-fit parameter values	
Baseline	10 (fixed)	Baseline	10 (fixed)
S	846.3	Rmax	271.8
r	2.336	p	1 (fixed)
sh	4.242	R50	1.8x10 <sup>-16</sup>
Standard Error (% relative SE)		Standard Error (% relative SE)	
Baseline	-	Baseline	-
S	140.4 (17%)	Rmax	93.28 (34%)
r	1.048 (45%)	p	-
sh	1.687 (40%)	R50	Hit constraint
Goodness of Fit		Goodness of Fit	
Degrees of Freedom	27	Degrees of Freedom	28
Absolute Sum of Squares	623052	Absolute Sum of Squares	981648
AICc	307.8	AICc	318.8
Test for homoscedasticity	Passed	Test for homoscedasticity	Passed
<b>Comparison of Gamma and Sigmoidal curve fit</b>			
Simpler model		Sigmoidal	
Probability it is correct		0.41%	
Alternative model		Gamma	
Probability it is correct		99.59%	
Ratio of probabilities		239.99	
Preferred model		Gamma	
Difference in AICc		10.96	
Strength of evidence for model with higher AICc (according to [336])		“Essentially no support” for Sigmoidal – absolute support for Gamma	

**Table S6. Summary of nonlinear regression analysis of the Gamma and Sigmoidal curve fitting for the responses at day 56.**

To establish if the estimated parameters were global minimums, I ran the regression with varying initial parameter estimates. Table S7 shows varying the initial parameter estimates did not impact the best-fit estimates in the regression analysis for any time range.

Time range	Curve	Initial parameter estimates	Best-fit parameter values
Pre-second vaccination	Gamma	S=600, r=3, sh=3	S=440.5, r=0.5047, sh=1.2
		S=100, r=1, sh=1.2	S=440.5, r=0.5047, sh=1.2
		S=2000, r=6, sh=5	S=440.5, r=0.5047, sh=1.2
	Sigmoidal	Rmax=300, R50=0.001	Rmax=87.02, R50=1.8x10 <sup>-16</sup>
		Rmax=10,R50=0.000001	Rmax=87.02, R50=1.8x10 <sup>-16</sup>
		Rmax=2000,R50=2	Rmax=87.02, R50=1.8x10 <sup>-16</sup>
Post-second vaccination	Gamma	S=600, r=3, sh=3	S=1451, r=0.7535, sh=1.787
		S=100, r=1, sh=1.2	S=1451, r=0.7535, sh=1.787
		S=2000, r=6, sh=5	S=1451, r=0.7535, sh=1.787
	Sigmoidal	Rmax=300, R50=0.001	Rmax=336, R50=1.8x10 <sup>-16</sup>
		Rmax=10,R50=0.000001	Rmax=336, R50=1.8x10 <sup>-16</sup>
		Rmax=2000,R50=2	Rmax=336, R50=1.8x10 <sup>-16</sup>
Day 56	Gamma	S=600, r=3, sh=3	S=846.3, r=2.336, sh=4.242
		S=100, r=1, sh=1.2	S=846.3, r=2.336, sh=4.242
		S=2000, r=6, sh=5	S=846.3, r=2.336, sh=4.242
	Sigmoidal	Rmax=300, R50=0.001	Rmax=271.8, R50=1.8x10 <sup>-16</sup>
		Rmax=10,R50=0.000001	Rmax=271.8, R50=1.8x10 <sup>-16</sup>
		Rmax=2000,R50=2	Rmax=271.8, R50=1.8x10 <sup>-16</sup>

Table S7. Testing initial parameter estimates

## **Chapter 5. Predicting human multi-dose immune responses to H-series vaccination using multi-dose data in mice and vaccine Immunostimulation/Immunodynamic (IS/ID) modelling: paper 4**

### **Chapter 5 introduction**

In paper 3, I showed that vaccine dose affects the immune response and to achieve a higher IFN- $\gamma$  response, a lower dose of H56+IC31 may be required. In paper 4, I aimed to identify which of the immune response mechanisms in the IS/ID model were affected by dose. This was achieved by calibrating the IS/ID model to the longitudinal multi-dose IFN- $\gamma$  data in mice outlined in paper 3. The model was then calibrated to H56/H1+ IC31 response data after one dose in humans. I mapped the change in model parameters by dose in mice and used this mapping alongside a proposed mouse to human dose scaling factor to predict the human immune response to remaining H56/H1+IC31 doses. The work in this chapter falls in line with aim 2 and objective 6-8 of the thesis (Figure 1.5).

The human data used in this paper were pooled from two phase 1 clinical trials (see Appendix Table D.1) where non-HIV and non-latent TB infected, BCG vaccinated participants were given either 50  $\mu$ g H56 + 500nmol IC31 (n=8) or 50  $\mu$ g H1 + 500nmol IC31 (n=10). The data were pooled as it has been shown that H56 and H1 induce similar IFN- $\gamma$  immune responses in humans [236]. Demographic data was not available for the H1 data, so the differences in model predicted IFN- $\gamma$  responses in humans by demographics is not considered in this work. Further data on H-series clinical trials was not available to me at the time of this work.

The IS/ID model used in paper 4 is based on the T cell mathematical model used in paper 2. However, by incorporating advice from advisory and supervisory panel members (Prof. White, Dr. Knight, Dr Fletcher, Dr Evans, Dr Guedj) the model was evolved to incorporate the T cell dynamics following revaccination. Key differences in the one vaccination and re vaccination models are discussed in the paper supplementary material.

Registry  
T: +44(0)20 7299 4646  
F: +44(0)20 7299 4656  
E: registry@lshtm.ac.uk

## RESEARCH PAPER COVER SHEET

**PLEASE NOTE THAT A COVER SHEET MUST BE COMPLETED FOR EACH RESEARCH PAPER INCLUDED IN A THESIS.**

### SECTION A – Student Details

Student	Sophie Rhodes
Principal Supervisor	Richard White
Thesis Title	The development of a mathematical modelling framework to translate TB vaccine response between species and predict the most immunogenic dose in humans using animal data

**If the Research Paper has previously been published please complete Section B. If not please move to Section C**

### SECTION B – Paper already published

Where was the work published?	
When was the work published?	
If the work was published prior to registration for your research degree, give a brief rationale for its inclusion	
Have you retained the copyright for the work?*	Choose an item. Was the work subject to academic peer review? Choose an item.

*\*If yes, please attach evidence of retention. If no, or if the work is being included in its published format, please attach evidence of permission from the copyright holder (publisher or other author) to include this work.*

### SECTION C – Prepared for publication, but not yet published

Where is the work intended to be published?	npj Vaccines
Please list the paper's authors in the intended authorship order:	Sophie J Rhodes, Jeremie Guedj, Helen Fletcher, Thomas Lindenstrøm, Thomas J. Scriba, Thomas G. Evans, Gwenan M Knight, Richard G White
Stage of publication	Submitted

### SECTION D – Multi-authored work

For multi-authored work, give full details of your role in the research included in the paper and in the preparation of the paper. (Attach a further sheet if necessary)	See next page
--	---------------

Student Signature: \_\_\_\_\_

Date: 3/1/18 \_\_\_\_\_

Supervisor Signature: \_\_\_\_\_



Date: 13/6/17

**Paper 4 title: Animal dose response curve predicts lower optimal tuberculosis vaccine dose in humans: Using vaccine Immunostimulation/Immunodynamic modelling methods to inform vaccine dose decision-making**

**Authors**

Authors: Sophie J Rhodes, Jeremie Guedj, Helen Fletcher, Thomas Lindenstrøm, Thomas J. Scriba, Thomas G. Evans, Gwenan M Knight, Richard G White

**Author contributions:**

The mouse H56+IC31 data are the same as in paper 3 (Dr. Thomas Lindenstrøm reviewed both paper 3 and 4 as vaccine developer of H56 and H1 vaccines). The human H56/H1+IC31 data in paper 4 were provided by Aeras, PI on the H56+IC31 clinical trial data was Dr. Thomas Scriba. The mathematical model to represent the IFN- $\gamma$  immune response to two vaccinations of H-series vaccine was adapted from paper 2 with help from advice Dr. Helen Fletcher and Dr. Thomas Evans. The calibration method was the same as in paper 2, and conducted by myself with advice from Dr. Jeremie Guedj. The framework to calibrate the model to the data was my own work with guidance from Prof. Richard White and Dr Gwenan Knight.

**Animal dose response curve predicts lower optimal tuberculosis vaccine dose in humans:  
Using vaccine Immunostimulation/Immunodynamic modelling methods to inform vaccine  
dose decision-making**

**Authors**

Authors: Sophie J Rhodes<sup>a</sup>, Jeremie Guedj<sup>b</sup>, Helen Fletcher<sup>c</sup>, Thomas Lindenstrøm<sup>d</sup>, Thomas J. Scriba<sup>e</sup>, Thomas G. Evans<sup>f</sup>, Gwenan M Knight<sup>a,g\*</sup>, Richard G White<sup>a\*</sup>

\*Joint senior authors

<sup>a</sup> TB Modelling Group, CMMID, TB Centre, London School of Hygiene and Tropical Medicine, UK

<sup>b</sup> IAME, UMR 1137, INSERM, F-75018 Paris, France; Univ Paris Diderot, Sorbonne Paris Cité, F-75018 Paris, France

<sup>c</sup> Immunology and Infection Department, London School of Hygiene and Tropical Medicine, UK

<sup>d</sup> Statens Serum Institut, Copenhagen, Denmark

<sup>e</sup> South African Tuberculosis Vaccine Initiative, Institute of Infectious Disease and Molecular Medicine and Division of Immunology, Department of Pathology, University of Cape Town, South Africa

<sup>f</sup> Vaccitech, Oxford, UK

<sup>g</sup> Imperial College, London, UK

## Abstract

**Introduction:** Unlike drug dose optimisation, mathematical modelling has not been applied to vaccine dose finding. We applied a novel Immunostimulation/Immunodynamic mathematical model to translate multi-dose TB vaccine immune responses from mice, to predict most immunogenic dose in humans.

**Methods:** Data were available on IFN- $\gamma$  secreting CD4+ T cells over time for novel TB vaccines H56 and H1 adjuvanted with IC31 in mice (3 dose groups (0.1-1,5 and 15  $\mu$ g H56+IC31), 45 mice) and humans (1 dose (50  $\mu$ g H56/H1+IC31), 18 humans). A two-compartment mathematical model, describing the dynamics of the post-vaccination IFN- $\gamma$  T cell response, was calibrated to mouse and human data, separately, using nonlinear mixed effects methods. We used these calibrated models and a vaccine dose allometric scaling assumption, to predict the most immunogenic human dose.

**Results:** At day 224, the model-predicted median number of human IFN- $\gamma$  secreting CD4+ T cells for the 1-10 $\mu$ g, 50 $\mu$ g and 150 $\mu$ g H56/H1+IC31 dose groups were 374, 188, and 118 SFU/mill PBMC, respectively, suggesting the 1-10 $\mu$ g dose may be the most immunogenic in humans, based on the mouse data.

**Conclusion:** A 1-10 $\mu$ g of H-series TB vaccines in humans, may be as, or more, immunogenic, as larger doses. Mathematical modelling is a novel, and potentially revolutionary tool, to predict most immunogenic vaccine doses, and accelerate vaccine development.

## Introduction

Vaccines are one of the most effective interventions in public health [1]. However, to progress a vaccine from discovery to licensure can take decades and cost up to US\$0.8 billion [2]. With costs so high, it is vital that development is made more efficient. A primary goal in vaccine development is to establish optimal vaccine efficacy, and vaccine dose amount (hereafter 'dose') is a crucial factor in achieving this. The consequences of selecting the wrong dose can lead to inadequate protection against disease, and ultimately wasted resources and lives.

In humans, vaccine dose decisions are made based on dose escalation trials, the dose range of which is based on experiments in animals. In classical pre-clinical experiments, an initial dose is tested and incrementally increased until the dose is no longer considered safe. The resulting maximum safe dose is then scaled-up to be applied in a clinical setting. Historically, pre-clinical dose escalation experiments assume the response 'saturates', i.e. increases, then plateaus, as vaccine dose is increased. Many vaccines have progressed through developmental phases with doses selected under this assumption [3, 4].

However, recent pre-clinical data suggest that this 'saturating' assumption may not always be correct. Studies in mice [5], and humans [6], using the potential tuberculosis (TB) vaccine H4 adjuvanted with IC31<sup>®</sup> (H4+IC31) have shown that lower vaccine doses have higher immunogenicity and protective efficacy than higher doses. We have recently shown that the IFN- $\gamma$  dose-response curve in mice, for the novel TB vaccine H56+IC31, was peaked, not saturating [7], and an ongoing phase 1/2a H56+IC31 dose-ranging clinical trial will test this prediction in humans (ClinicalTrials.gov No. NCT01865487). Similar non-saturating dose-response curves have been observed in clinical trials in HIV and Malaria vaccines using other adjuvants [8, 9]. These data suggest that developing vaccines based on a 'saturating dose' response curve assumption is likely to lead to sub-immunogenic doses being selected for later stage vaccine development, and risk efficacious vaccine discovery.

In contrast to vaccine development, drug development benefits from systematic, quantitative analysis through the application of Pharmacokinetic/Pharmacodynamic (PK/PD)

modelling. PK/PD modelling employs mechanistic mathematical models to quantify drug concentration dynamics in the host over time (PK) and drug effect as the concentration varies (PD) [10]. Model-Based Drug Development (MBDD) is recognized as an efficient tool to accelerate and streamline drug development, by minimizing developmental time and resources [11]. MBDD has been established for decades in the pharmaceutical industry [12] and is often required by regulatory agencies in all stages of drug development. As such, MBDD is regularly used to establish optimal drug dose [13] and translate drug response dynamics between species [14].

PK/PD model-based methods have not been applied in vaccine development for dose decision making [1]. The application of quantitative methods similar to that of MBDD, could lead to better evaluation and translation of the vaccine dose-response data from animals to humans, and accelerate vaccine development.

Consequently, we propose the new field of vaccine *Immunostimulation/Immunodynamic (IS/ID) modelling* as a method to inform vaccine dose decision making. Analogous to PK/PD modelling, IS/ID modelling applies mathematical models to describe the underlying mechanisms, the immune response stimulation (IS) that produce the measured immune response dynamics following vaccination (ID).

In anticipation of the release of the dose-ranging clinical trial data (NCT01865487), the aim of this work was to employ a novel IS/ID model to translate H56+IC31 TB vaccine immune responses from mice to predict the most immunogenic dose in humans. We calibrated our model to IFN- $\gamma$  data following two vaccinations with TB vaccine H56 adjuvanted with IC31 (H56+IC31) in mice and humans, and H1+IC31 data in humans. The model was used to describe the IFN- $\gamma$  response dynamics of two CD4+ T cell populations, and predict the most immunogenic dose in humans.

Our analysis was in three stages. In analysis 1, the model was calibrated to the mouse data. In analysis 2, the model was calibrated to the limited dose data on humans. In analysis 3, we used our calibrated models to predict the most immunological dose in humans.

## Methods

### Data

Full details of mouse IFN- $\gamma$  response data are in [7]. Briefly, female CB6F1 mice were given five doses, 0.1, 0.5, 1, 5, or 15  $\mu\text{g}$  H56 adjuvanted with 100 nmol IC31<sup>®</sup> (supplied by SSI on behalf of Valneva Austria GmbH; hereafter designated H56+IC31) plus a control dose of 0  $\mu\text{g}$  H56+IC31, at day 0 and 15. Data on the number of H56 antigen stimulated IFN- $\gamma$  secreting CD4+ T cells (in spot forming units (SFU)) per 1 million splenocytes measured by an *ex vivo* IFN- $\gamma$  Enzyme-Linked ImmunoSpot (ELISPOT) assay, were taken at eight time points over 56 days (Figure S1 and supplementary methods). Mouse dose groups were: low (0.1, 0.5 and 1  $\mu\text{g}$  H56+IC31), middle (5  $\mu\text{g}$  H56+IC31) and high (15  $\mu\text{g}$  H56+IC31).

Human IFN- $\gamma$  response data was pooled from phase I clinical trials for the vaccines H56+IC31 ([15], ClinicalTrials.gov no. NCT01967134) (N=8) and H1+IC31 ([16] ClinicalTrials.gov no. NCT00929396) (N=10). H1 is comprised of a subset of the H56 antigens [17]. For both vaccine trials, primary vaccination was administered intramuscularly on day 0 and revaccination, day 56, both at a dose of 50  $\mu\text{g}$  of the vaccine antigen (H1 or H56) and 500 nmol IC31 in healthy, BCG vaccinated participants (hereafter, H56/H1+IC31). IFN- $\gamma$  responses were measured using ELISPOT in SFU per 1 million Peripheral Blood Mononuclear Cells (PBMC), taken until day 224 (Figure S2). Further trial information can be found in Table S1.

The adjuvant dose remained constant across antigen dose for both species (100 nmol and 500 nmol IC31 in mice and humans, respectively).

### Mathematical vaccine Immunostimulation/Immunodynamic (IS/ID) Model

An ordinary differential equations mathematical model was used to describe the IFN- $\gamma$  response dynamics of two CD4+ T cell populations induced following vaccination: transitional effector memory [18] which had effector functionality (activated to produce IFN- $\gamma$  [19]) and were short-lived and resting “central” memory (Figure 1). Here, we assumed following primary

vaccination, cells were recruited as transitional cells and entered the transitional effector memory cells population (TEM) at rate  $\delta$ . TEM cells then either died, at rate  $\mu_{\text{TEM}}$ , or transitioned into central memory cells (CM) at rate  $\beta_{\text{TEM}}$ . CM cells were assumed not to die over the short duration modelled (60 and 250 days in mice and humans, respectively). Following revaccination, transitional cells entering the TEM population were again recruited at rate  $\delta$ , and central memory cells replicated at a rate  $R_{\text{CM}}$  for  $\tau$  days. The time that replication occurred for,  $\tau$ , was dependent on the CM population size at time of revaccination. Following replication, CM cells were recruited back to the TEM pool at rate  $\beta_{\text{CM}}$ . As with primary vaccination, TEM cells transition to CM cells at rate  $\beta_{\text{TEM}}$  following revaccination. As stimulation of T cell responses is delayed following vaccination (due to immune processes such as vaccine antigen trafficking and presentation [20, 21]) and does not last indefinitely [21], we assumed the TEM cell recruitment rate,  $\delta$ , was nonlinear.  $\delta$  was initiated at time of primary and re- vaccination and was assumed to be the same at both vaccination points.

The death rate of the TEM cells ( $\mu_{\text{TEM}}$ ) was fixed to values found in literature for mice [22] and humans [23], separately. For both species, the replication rate of the CM cells,  $R_{\text{CM}}$ , was fixed to one replicate every 10 hours [24] and the transition rate to TEM pool following replication post revaccination,  $\beta_{\text{CM}}$ , was assumed to be instantaneous. All other parameters were free to be estimated. For parameter value description, see Figure 1.

As central memory cells are known to be essentially non-proliferating in the host until stimulated by antigen [24]; we assumed they contributed to IFN- $\gamma$  production, because the ELISPOT assay uses the vaccine antigens to stimulate all potentially IFN- $\gamma$  secreting CD4+ T-cells. To reflect this, the IFN- $\gamma$  immune response predicted by the mathematical model was assumed equal to the sum of the number of TEM and CM cell populations over time. To account for the potential non-zero baseline responses, the initial TEM cell count was fixed at the median cell count for mice and humans, separately.

## **Analyses**

*Analysis 1: Calibration of the IS/ID model to the mouse data, pooled and stratified by dose group*

In analysis 1, the model was calibrated (i) to all mouse ELISPOT data, pooled over dose groups, and (ii) to the data stratified by dose group, to quantify the IFN- $\gamma$  response dynamics. Calibration of the model to the data was achieved using nonlinear mixed effects modelling (NLMEM) [25] and the SAEM algorithm implemented in the software Monolix v. 4.3.3 [26]. SAEM uses maximum likelihood methods to estimate the free model parameters that best describe the population typical IFN- $\gamma$  response and the inter-individual variability [25]. For further description of the NLMEM statistical framework see supplementary methods.

Calibrated model parameters were considered well estimated if their relative standard error (RSE) was less than 30% [27]. Model selection was carried out using Bayesian Information Criteria (BIC) value assessment, where a lower BIC value was indicative of a better fit. Evaluation of the model's ability to describe the data was assessed primarily using the Visual Predictive Check (VPC) and further diagnostic plots (see supplementary methods for description).

For analysis 1i, we tested two nonlinear equations for the recruitment of TEM cells (parameter  $\delta$ , Figure 1); a Gaussian equation and a gamma Probability Density Function (PDF) equation. We also tested the replacement of rate  $\delta$  with a naïve T cell compartment, whereby naïve cells replicate for  $\tau_N$  days before transitioning to TEM at rate  $\beta_N$ . (for mathematical description of the forms, see supplementary). All parameters within the forms of  $\delta$  were free to be estimated. The form of  $\delta$  that resulted in the lowest BIC value when calibrated to the pooled mouse data was chosen. This form was then used when the model was calibrated to the mouse data stratified by dose group (analysis 1ii) and the human data (analysis 2).

For analysis 1ii, we used the likelihood ratio test (LRT) to identify which model parameters should be stratified by dose to improve the model fit, compared to analysis 1i.

*Analysis 2: Calibration of the IS/ID model to the pooled human data*

In analysis 2, the model was calibrated to the human data using the same methods as analysis 1. We calibrated the model to the pooled human data set (across vaccine H1+IC31 and H56+IC31) as the two vaccines are known to have a similar immunological profile [28] (see supplementary material for analysis on the human data stratified by vaccine type to validate this assumption).

*Analysis 3: Use calibrated mathematical models in analysis 1 & 2, and a vaccine dose allometric scaling assumption, to predict the human immune response dynamics and predict the most immunogenic dose in humans*

In analysis 3, the estimated model parameters identified for the dose groups in mice (analysis 1ii) and for the one dose in humans (analysis 2) were used to predict the IFN- $\gamma$  response in humans for a range of doses. As the current (antigen) dose allometric scaling factor between mouse and humans for the H-series vaccines is assumed to be approximately ten [29-31], we initially assumed the 50  $\mu\text{g}$  H56/H1+IC31 dose given to humans was equivalent to the middle (5  $\mu\text{g}$  H56+IC31) dose group in the mice. Under this assumption, the low and high doses in humans were estimated to be 1-10 and 150  $\mu\text{g}$  H56/H1+IC31, respectively.

Firstly, we calculated the percentage change between the mouse-data-estimated model parameters from the middle dose group vs the low and high dose groups (found in analysis 1ii). Then we applied these percentage changes to the human estimated model parameters found in analysis 2 (the human middle dose group) to predict the model parameters for the low and high dose groups in humans. To establish the 'most immunogenic' human dose we compared long term (day 224) model-predicted responses for the three human dose groups. We conducted a sensitivity analysis on the dose allometric scaling factor by assuming the human dose was equivalent to the high (15 $\mu\text{g}$  H56 + IC31) dose group in the mice, giving a scaling factor of 3.33.

## Results

### *Analysis 1: Calibration of the IS/ID model to the mouse data, pooled and stratified by dose group*

The best (lowest BIC value) form for the TEM recruitment parameter,  $\delta$ , for primary and revaccination was the Gaussian equation (Table S2):

$$a * \left( e^{\frac{-(time-b)^2}{2c^2}} + e^{\frac{-(time-(b+revaccination\ time))^2}{2c^2}} \right)$$

where  $a$  is a scalar,  $b$ , the Gaussian equation mean,  $c$ , the variance and time is measured in days. Using this  $\delta$ , all free model parameters (including Gaussian equation  $\delta$ ,  $N=5$ , Figure 1) were well estimated ( $RSE < 30\%$ ) (Table 1). The model predicted IFN- $\gamma$  responses for this parameter set (Table 1) are plotted in Figure 2A. The VPC showed the model predictions represented the median pooled data well (Figure S3, further diagnostic plots Figure S4-S5).

Using the LRT and lowest BIC value, the best parameter set of the model for analysis 1ii, was when the Transitional Effector Memory (TEM) to Central Memory (CM) cell transition rate ( $\beta_{TEM}$ ) differed by dose group (Table 1, Table S5). Figure 2 shows the model predicted IFN- $\gamma$  response for the low (Fig 2B), middle (Fig 2C) and high (Fig 2D) dose groups (VPC and diagnostic plots in Figures S6-S8). In Figure 2A-D, model predictions for the 25<sup>th</sup> and 75<sup>th</sup> percentiles of the data were not as well estimated as the medians because the parameter standard deviations were fixed at 0.5 throughout.

### *Analysis 2: Calibration of the IS/ID model to the pooled human data*

Parameter estimates for all free parameters (including Gaussian equation  $\delta$ ,  $N=5$ , Figure 1) for analysis 2 can be found in Table 1. Due to the smaller sample size of the human data, parameters  $\beta_{TEM}$  and  $\tau$  were not identifiably estimated ( $RSE > 30\%$ ). Model parameter standard deviations were fixed at 0.5.

Figure 3A and the VPC (Figure S9) shows that the model predicted IFN- $\gamma$  responses from this parameter set (Table 1) was a good description of the median data, despite the wide variability

over time of the human responses. See Figures S10-S13 for further diagnostic plots and model predictions for each participant.

*Analysis 3: Use calibrated mathematical models in analysis 1 & 2, and a vaccine dose allometric scaling assumption, to predict the human immune response dynamics and predict the most immunogenic dose in humans*

In analysis 1ii, the estimated parameter  $\beta_{\text{TEM}}$  increased by 53% (0.15 to 0.23) from the middle to low dose group and decreased by 63% (0.15 to 0.056) from the middle to high dose group. Applying these changes to parameter  $\beta_{\text{TEM}}$  in the human model parameter set (Table 1), resulted in a value of 0.032 and 0.0074 for the low and high dose group, respectively (Table 1). Using these values for  $\beta_{\text{TEM}}$  in humans, the model predicted median number of IFN- $\gamma$  secreting CD4+ T cells at day 224 were 374, 188, and 118 (SFU per million PBMC) for the low, middle and high (1-10, 50 and 150 $\mu$ g H56/H1+IC31, respectively) dose groups, suggesting the low dose (1-10  $\mu$ g H56/H1+IC31) may be most immunogenic in humans (Figure 3). In the sensitivity analysis, using a vaccine dose allometric scaling factor of 3.33, the low dose range (now 0.3-3.3  $\mu$ g H56/H1+IC31) was also the most immunogenic (Table S9, Figure S14).

## Discussion

In this work, mathematical models were successfully calibrated to animal and human TB vaccine IFN- $\gamma$  data. At day 224 post primary vaccination the model-predicted median number of human IFN- $\gamma$  secreting CD4+ T cells were 374, 188, and 118 (SFU per million PBMC) for the low, middle and high dose groups (1-10, 50 and 150  $\mu$ g H56/H1+IC31, respectively). This indicated that lower doses (1-10  $\mu$ g H56/H1+IC31) may be the most immunogenic in humans.

A key strength of this work was the application of mathematical modelling techniques to vaccine data that are rarely explored quantitatively. We used established, robust quantitative and statistical frameworks (compartmental mathematical models with NLMEM [25]) to explore and translate the complex biological dynamics between species, giving an early example of the utility of Immunostimulation/Immunodynamic modelling. We present here the first example of the allometric mapping between vaccine immune dynamics between mice and humans through the mapping of estimated model parameters between the two species. This mirrors established techniques incorporated in PK/PD modelling for drug development. Using diagnostic tests and goodness of fit measures, we showed our IS/ID mathematical model was a good description of the mouse dose group and human data and produced potentially biological meaningful results.

We made the following key assumptions in this work. Our model was a highly simplified version of the complexities of the T cell response following vaccination. Our model assumes a linear progression from TEM to CM memory cell phenotype [32, 33]. However, an alternative model has been suggested, whereby TEM and CM cells are initiated simultaneously after vaccination [18, 19, 24]. Additionally, the death rate of TEM cells may also be affected by antigen dose. Both of these assumptions were necessary to avoid over-parameterisation given the data sample sizes available to us. See supplementary discussion for further model structure assumptions and their impact (Table S3). The IFN- $\gamma$  secreting CD4+ T cell dynamics we incorporate in the IS/ID model was used to describe both the mouse and human response to H-series vaccination. This was justified as the fundamental mechanisms of Th1 response induction by vaccination are thought not to differ between these two species [34].

There were weaknesses in our work. Small data sample sizes meant we had to firstly, group the mouse dose data in analysis 1ii, limiting our conclusions on the full range of doses we tested. Secondly, due to the small human dataset (N=18), two of the model parameters were not identifiably estimated, therefore the results of the model fit to the human data should be approached with caution. Additionally, due to small sample sizes, we constrained the model parameter standard deviations to 0.5 throughout, which restricted the conclusions we could make around the inter-individual variability. The geographical location of the clinical trials was correlated with vaccine type (H1 or H56), so this was not included as a human population covariate. However, as immune response to the current TB vaccine, BCG, are known to vary by geographic location [35], this covariate may also influence H-series vaccine responses. We did not consider participants with latent TB infection (LTBI) in this analysis, as vaccine take has been shown to differ markedly in non-exposed versus LTBI participants [36]. As such, predicting the optimal vaccine dose for this population, would require new IS/ID modelling efforts to account for these effects.

Previous work on the H4+IC31 vaccine [6, 37] showed that after vaccination with a dose of 50 µg H4+500 nmol IC31, the median H4-stimulated IFN-γ response measured with the ELISPOT assay at day 182 (latest time point) was 222 IFN-γ secreting CD4+ T cells. This is close to our model prediction for the equivalent dose with H56/H1+IC31 (a median of 188 total cells). The dose response relationship showed a similar trend to our results also, i.e. the lower doses (5, 15 µg H4+IC31) perform better than the higher doses (50, 150 µg H4+IC31) [6, 37].

Preliminary empirical results from the phase 1/2a clinical dose ranging study of H56 + 500 nmol IC31 (ClinicalTrials.gov no. NCT01865487) may support our model predictions (unpublished, personal communication, Thomas Scriba). These preliminary trial findings from NCT01865487 suggest that doses 5, 15 and 50 µg H56+IC31 were equally immunogenic in healthy, BCG vaccinated participants, and therefore developers have decided to use 5 µg H56+IC31 in future clinical trials, rather than 50 µg in previous trials. If these preliminary findings are confirmed, they may support the utility of IS/ID modelling. It must be noted, that these results are preliminary, and empirical sample sizes were small.

There are several areas for future research. In analysis 3, our vaccine dose allometric assumption; that a dose of 5 µg H56+IC31 (middle dose group) in mice was equivalent to a 50 µg H56/H1+IC31 in humans, is in line with the current hypothesis in TB protein vaccine developers [29-31]. However, to our knowledge, no formal assessment of this scaling factor has been extensively undertaken and it is possible that this scaling factor could range between zero and ten. It is vital that further empirical data are collected to support these allometric scaling assumptions for a given antigen-adjuvant combination. Additionally, the effects of changing adjuvant dose on the dose-dependent dynamics should be explored.

Further lab assays such as flow cytometry could be conducted to characterise the relative number of complex phenotypic cell types (TEM or CM) over time to further parameterize this model. Additionally, we use the frequency of IFN-γ secreting CD4+ T cells measured using the ELISPOT assay as our chosen immune response readout to reflect the current convention in TB vaccine development for dose selection. IFN-γ is a cytokine shown to be associated with control of infection or decreased risk of TB disease [38], however these findings have been a topic of controversy in TB vaccine development [39]. Despite this, Aagaard et al. showed in two independent studies that higher IFN-γ responses in mice correlated with stronger protection against Mtb. infection (measured by Mtb. colony forming units) [5]. Additionally, it is possible that varying dose may alter the function or type of IFN-γ secreting CD4+ T cells, which the ELISPOT assay will not detect. Flow cytometry could provide information on other cytokine types which could be incorporated into a more complex network model which can provide better understanding of T-cell dynamics.

The clinical data used in this work were from a two vaccination regimen. However, in the H56 trial [15] an additional vaccination was given after two months (data after third vaccination was excluded). Current methods to determine regimen are conducted empirically in early clinical phases (1/2a) in vaccine development [40-43]. In contrast, drug regimen is regularly explored and optimised using model-based simulation based on early response data. With this in mind, IS/ID modelling could be used to explore the effects of timing of a third vaccination, providing insight into the opportune time to boost vaccine responses, which can then be empirically verified.

In summary, using a mathematical model within a new IS/ID framework, we predicted that low doses of H-series TB vaccine may increase immune response in humans based on animal data. Forthcoming empirical clinical evaluations may support this prediction. We have illustrated that mathematical modelling may be a novel and potentially revolutionary tool to predict most immunogenic vaccine dose, and accelerate vaccine development.

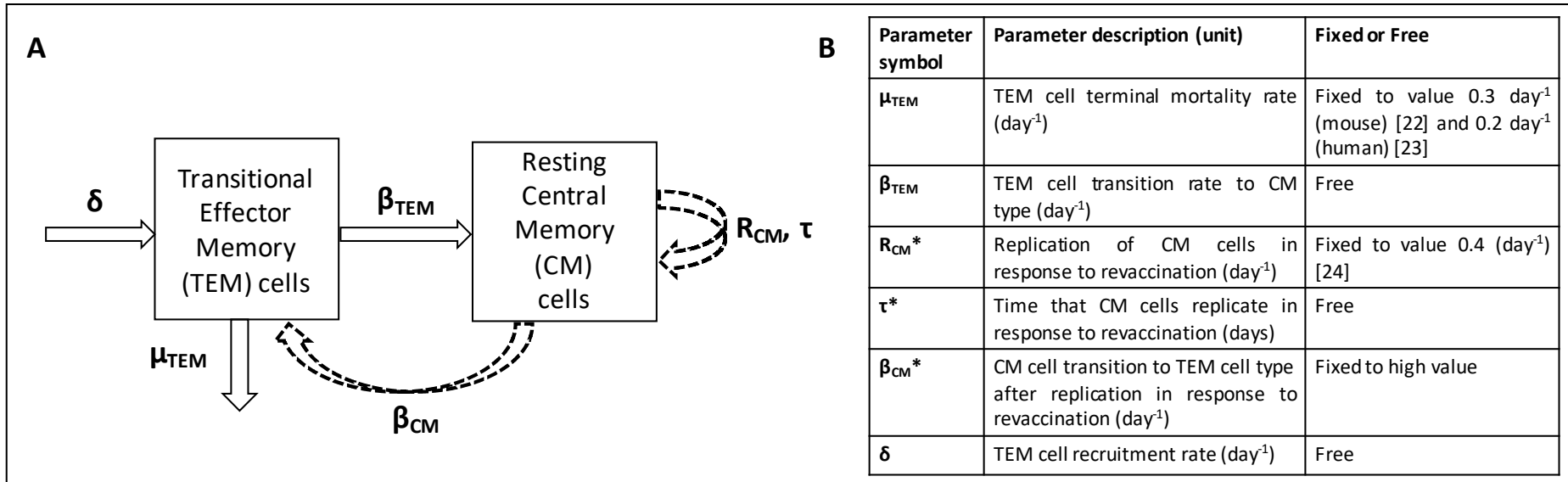


**Figure 1. Modelling overview.** A) Schematic of the mathematical model representing the immune response dynamics of two IFN- $\gamma$  secreting CD4+ T cell populations after primary and re- vaccination. Dashed arrows correspond to T cell dynamics as a result of only revaccination. B) Table of key model parameters. Model parameters are either fixed to a value from literature ( $\mu_{TEM}$  and  $R_{CM}$ ), to an assumed value ( $\beta_{CM}$ ) or free to be estimated using NLMEM ( $\beta_{TEM}$ ,  $\tau$ , and the parameters that comprise  $\delta$ ). Asterisked parameter symbols correspond to those resulting from only revaccination. Equations can be found in the supplementary material. The form of  $\delta$  to be identified in analysis 1i.

	Mouse					Human			
	Pooled (analysis 1i)		Dose covariate (analysis 1ii)			Pooled (analysis 2)		Predicting dose (analysis 3)	
Parameter (unit)	Value	RSE (%)	Dose group	Value	RSE (%)	Value	RSE (%)	Dose group	Value
Death rate of Transitional effector memory cells, $\mu_{TEM}$ (per day)	0.3 (F)*	-		0.3 (F)*	-	0.2 (F)**	-		0.2 (F)**
Transition rate from Transitional Effector to Central Memory cell type, $\beta_{TEM}$ (per day)	5.5 (E)	17	Low	0.23 (E)	14	0.022 (E)	31	Low	0.032 (P)
			Middle	0.15 (E)	23			Middle	0.022 (F')
			High	0.056 (E)	26			High	0.0074 (P)
Replication rate of Central Memory cells (per day), $R_{CM}$	0.4 (F)***	-		0.4 (F)***	-	0.4 (F)***	-		0.4 (F)***
Central Memory cell replication time, $\tau$ (days)	1.1 (E)	2		1.1 (E)	7	0.34 (E)	35		0.34 (F')
Transition rate from Central Memory to Transitional Effector type, $\beta_{CM}$ (per day)	10 (F) <sup>§</sup>	-		10 (F) <sup>§</sup>	-	10 (F) <sup>§</sup>	-		10 (F) <sup>§</sup>
Recruitment of Transitional Effector rate $\delta$ : Gaussian equation scalar, a (# cells)	92.9 (E)	14		103 (E)	13	51 (E)	23		51 (F')
Recruitment of Transitional Effector rate $\delta$ : Gaussian equation mean, b (days)	6 (E)	8		6.2 (E)	10	16.6 (E)	20		16.6 (F')
Recruitment of Transitional Effector rate $\delta$ : Gaussian equation variance, c (days)	0.91 (E)	15		0.89 (E)	7	5.7 (E)	13		5.7 (F')

**Table 1. Population parameters for mice and humans from model calibration (analysis 1&2) and prediction (analysis 3). All estimated model parameter standard deviations were fixed at 0.5. Abbreviations: RSE = relative standard error, F=Fixed, E=Free parameters that were Estimated using NLMEM, F' = fixed to value found in analysis 2, P=predicted, fixed to value in literature: \*[22],\*\*[23], \*\*\*[24]. § Fixed to be high.**

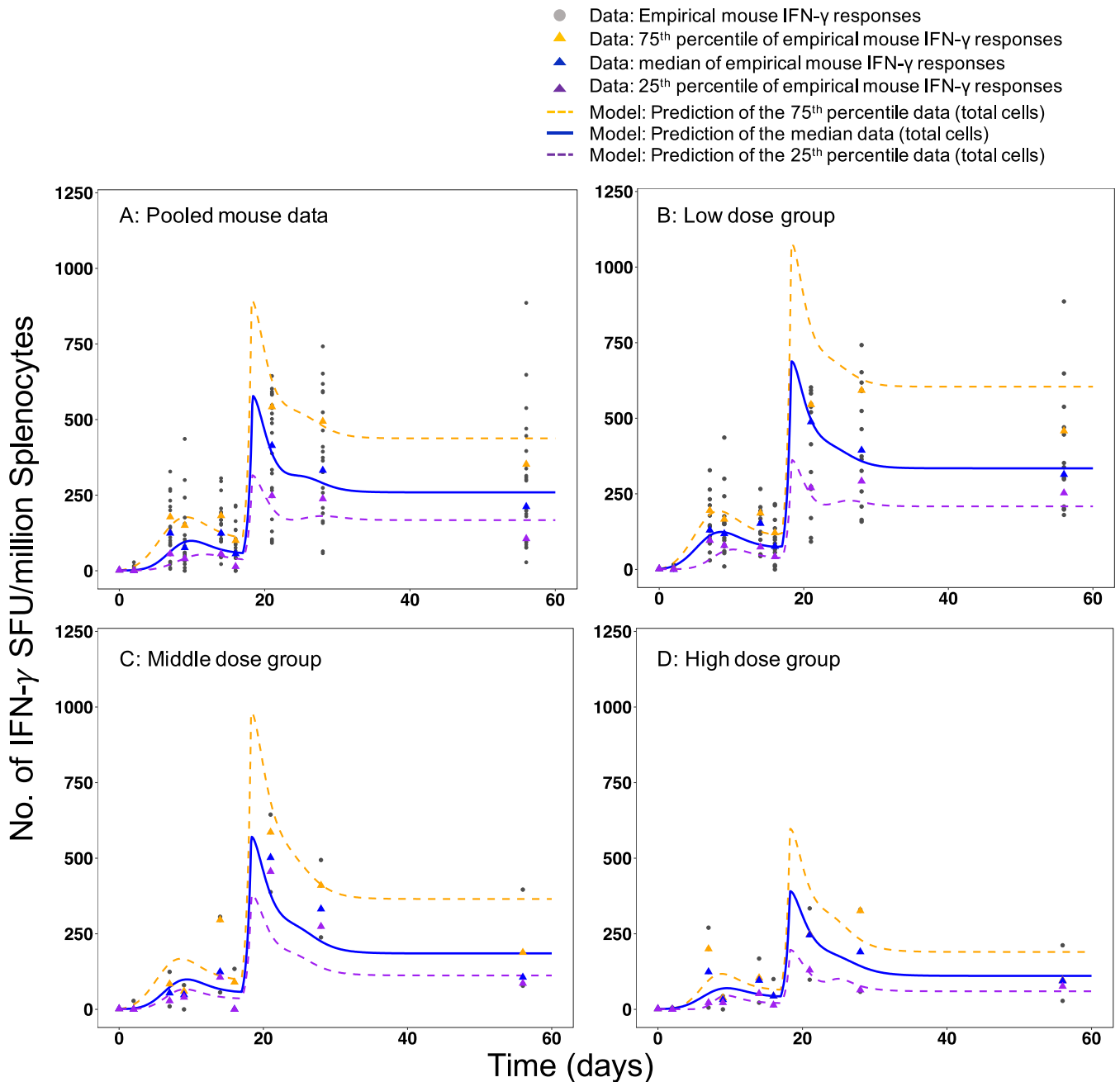


Figure 2. Empirical and model predicted number of IFN- $\gamma$  secreting CD4<sup>+</sup> T cells over time for A. pooled mouse data, B. low dose group (0.1-1  $\mu$ g H56+IC31), C. middle dose group (5  $\mu$ g H56+IC31) and D. high dose group (15  $\mu$ g H56+IC31). Grey points correspond to number of IFN- $\gamma$  secreting CD4<sup>+</sup> T cells measured over time by ELISPOT assay in mouse splenocytes for each mouse after receiving vaccination of H56+IC31 at day 0 and day 15. Median responses over time are marked by a blue triangle, the 75<sup>th</sup> percentile responses by an orange triangle and the 25<sup>th</sup> percentile responses by a purple triangle. The model prediction (total cells) calibrated to the data in the calibration framework (parameters in Table 1) is plotted against the median data (blue line). The orange and purple dashed lines are the model prediction (total cells) of the 75<sup>th</sup> and 25<sup>th</sup> percentiles of the data, a result of the variation in the estimated parameters (standard deviation fixed to 0.5 for all parameters (Table 1)).

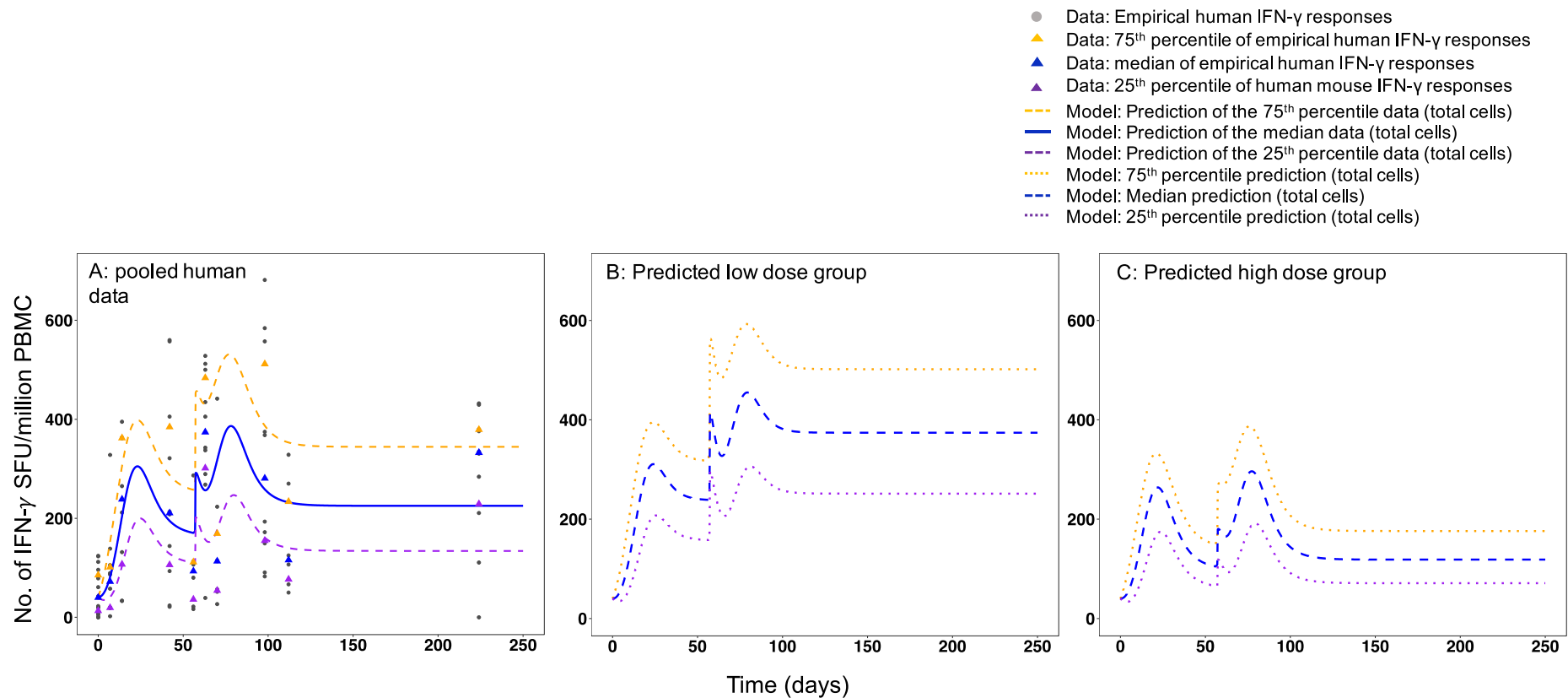


Figure 3. Empirical and model predicted number of IFN- $\gamma$  secreting CD4+ T cells over time for A. pooled human data (all data, pooled over vaccine type) (50  $\mu$ g H56/H1+IC31), and the predicted human immune responses following a B. low (mouse-data mapped dose of 1-10  $\mu$ g H56/H1+IC31) or C. high dose vaccination (mouse-data mapped dose of 150  $\mu$ g H56/H1+IC31). A. Grey points correspond to number of IFN- $\gamma$  secreting CD4+ T cells measured over time by ELISPOT assay in human PBMC after receiving vaccination of H56/H1+IC31 at day 0 and day 56. Median responses over time are marked by blue triangles, the 75<sup>th</sup> percentile responses by an orange triangle and the 25<sup>th</sup> percentile responses by a purple triangle. The model prediction (total cells) (parameters in Table 1) is plotted against the median data (blue line). The orange and purple dashed lines are the model prediction (total cells) of the 75<sup>th</sup> and 25<sup>th</sup> percentiles of the data, a result of the variation in the estimated parameters (standard deviation fixed to 0.5 for all parameters (Table 1)). In B. and C. Median (blue dashed), 75<sup>th</sup> (orange dots) and 25<sup>th</sup> (purple dots) of the model predicted human responses after mapping from the mouse dose group model calibration (predicted parameters in Table 1) are shown.

## References

- [1] Plotkin SA, Orenstein WA, Offit PA. *Vaccines*. 6 ed: Saunders; 2013.
- [2] Dickson M, Gagnon JP. The cost of new drug discovery and development. *Discovery medicine*. 2004;4:172-9.
- [3] Little SF, Webster WM, Norris SL, Andrews GP. Evaluation of an anti-rPA IgG ELISA for measuring the antibody response in mice. *Biologicals : journal of the International Association of Biological Standardization*. 2004;32:62-9.
- [4] Semenova VA, Schiffer J, Steward-Clark E, Soroka S, Schmidt DS, Brawner MM, et al. Validation and long term performance characteristics of a quantitative enzyme linked immunosorbent assay (ELISA) for human anti-PA IgG. *Journal of immunological methods*. 2012;376:97-107.
- [5] Aagaard C, Hoang TT, Izzo A, Billeskov R, Troudt J, Arnett K, et al. Protection and polyfunctional T cells induced by Ag85B-TB10.4/IC31 against *Mycobacterium tuberculosis* is highly dependent on the antigen dose. *PloS one*. 2009;4:e5930.
- [6] Geldenhuys H, Mearns H, Miles DJ, Tameris M, Hokey D, Shi Z, et al. The tuberculosis vaccine H4:IC31 is safe and induces a persistent polyfunctional CD4 T cell response in South African adults: A randomized controlled trial. *Vaccine*. 2015;33:3592-9.
- [7] Rhodes SJ, Zelmer A, Knight GM, Prabowo SA, Stockdale L, Evans TG, et al. The TB vaccine H56+IC31 dose-response curve is peaked not saturating: Data generation for new mathematical modelling methods to inform vaccine dose decisions. *Vaccine*. 2016;34:6285-91.
- [8] Evans TG, McElrath MJ, Matthews T, Montefiori D, Weinhold K, Wolff M, et al. QS-21 promotes an adjuvant effect allowing for reduced antigen dose during HIV-1 envelope subunit immunization in humans. *Vaccine*. 2001;19:2080-91.
- [9] Regules JA, Cicatelli SB, Bennett JW, Paolino KM, Twomey PS, Moon JE, et al. Fractional Third and Fourth Dose of RTS,S/AS01 Malaria Candidate Vaccine: A Phase 2a Controlled Human Malaria Parasite Infection and Immunogenicity Study. *The Journal of infectious diseases*. 2016;214:762-71.
- [10] Upton RN, Mould DR. Basic concepts in population modeling, simulation, and model-based drug development: part 3-introduction to pharmacodynamic modeling methods. *CPT: pharmacometrics & systems pharmacology*. 2014;3:e88.
- [11] Milligan PA, Brown MJ, Marchant B, Martin SW, van der Graaf PH, Benson N, et al. Model-based drug development: a rational approach to efficiently accelerate drug development. *Clinical pharmacology and therapeutics*. 2013;93:502-14.
- [12] Kimko H, Pinheiro J. Model-Based Clinical Drug Development in the Past, Present & Future: a Commentary. *British journal of clinical pharmacology*. 2014.
- [13] Sherwin CM, Zobell JT, Stockmann C, McCrory BE, Wisdom M, Young DC, et al. Pharmacokinetic and pharmacodynamic optimisation of intravenous tobramycin dosing among children with cystic fibrosis. *Journal of pharmacokinetics and pharmacodynamics*. 2014;41:71-9.
- [14] Dubois VF, de Witte WE, Visser SA, Danhof M, Della Pasqua O, Cardiovascular Safety Project T, et al. Assessment of Interspecies Differences in Drug-Induced QTc Interval Prolongation in *Cynomolgus* Monkeys, Dogs and Humans. *Pharmaceutical research*. 2016;33:40-51.
- [15] Luabeya AK, Kagina BM, Tameris MD, Geldenhuys H, Hoff ST, Shi Z, et al. First-in-human trial of the post-exposure tuberculosis vaccine H56:IC31 in *Mycobacterium tuberculosis* infected and non-infected healthy adults. *Vaccine*. 2015;33:4130-40.
- [16] van Dissel JT, Soonawala D, Joosten SA, Prins C, Arend SM, Bang P, et al. Ag85B-ESAT-6 adjuvanted with IC31(R) promotes strong and long-lived *Mycobacterium tuberculosis* specific T cell responses in volunteers with previous BCG vaccination or tuberculosis infection. *Vaccine*. 2011;29:2100-9.
- [17] Agger EM, Rosenkrands I, Olsen AW, Hatch G, Williams A, Kritsch C, et al. Protective immunity to tuberculosis with Ag85B-ESAT-6 in a synthetic cationic adjuvant system IC31. *Vaccine*. 2006;24:5452-60.
- [18] Seder RA, Darrah PA, Roederer M. T-cell quality in memory and protection: implications for vaccine design. *Nature reviews Immunology*. 2008;8:247-58.

- [19] Restifo NP, Gattinoni L. Lineage relationship of effector and memory T cells. *Current opinion in immunology*. 2013;25:556-63.
- [20] Abbas A, Lichtman A, Pillai S. *Cellular and Molecular Immunology*. 8 ed: Elsevier Saunders; 2015.
- [21] Urdahl KB, Shafiani S, Ernst JD. Initiation and regulation of T-cell responses in tuberculosis. *Mucosal immunology*. 2011;4:288-93.
- [22] Sprent J, Basten A. Circulating T and B lymphocytes of the mouse. II. Lifespan. *Cellular immunology*. 1973;7:40-59.
- [23] Hao W, Crouser ED, Friedman A. Mathematical model of sarcoidosis. *Proceedings of the National Academy of Sciences of the United States of America*. 2014;111:16065-70.
- [24] Kaech SM, Wherry EJ, Ahmed R. Effector and memory T-cell differentiation: implications for vaccine development. *Nature reviews Immunology*. 2002;2:251-62.
- [25] Lavielle M. *Mixed Effects Models for the Population Approach: Models, Tasks, Methods and Tools*: Chapman & Hall; 2015.
- [26] Monolix: Users Guide. 4.3.3 ed2014.
- [27] Mould DR, Upton RN. Basic concepts in population modeling, simulation, and model-based drug development-part 2: introduction to pharmacokinetic modeling methods. *CPT: pharmacometrics & systems pharmacology*. 2013;2:e38.
- [28] Ruhwald M, Agger EM, Hoff ST, Andersen P. H1- and H56- subunit vaccines against TB - an overview of the clinical development. *The European respiratory journal*. 2014;44.
- [29] Knudsen NP, Olsen A, Buonsanti C, Follmann F, Zhang Y, Coler RN, et al. Different human vaccine adjuvants promote distinct antigen-independent immunological signatures tailored to different pathogens. *Sci Rep*. 2016;6:19570.
- [30] Billeskov R, Tan EV, Cang M, Abalos RM, Burgos J, Pedersen BV, et al. Testing the H56 Vaccine Delivered in 4 Different Adjuvants as a BCG-Booster in a Non-Human Primate Model of Tuberculosis. *PloS one*. 2016;11:e0161217.
- [31] Reither K, Katsoulis L, Beattie T, Gardiner N, Lenz N, Said K, et al. Safety and Immunogenicity of H1/IC31(R), an Adjuvanted TB Subunit Vaccine, in HIV-Infected Adults with CD4+ Lymphocyte Counts Greater than 350 cells/mm<sup>3</sup>: A Phase II, Multi-Centre, Double-Blind, Randomized, Placebo-Controlled Trial. *PloS one*. 2014;9:e114602.
- [32] Soares AP, Kwong Chung CK, Choice T, Hughes EJ, Jacobs G, van Rensburg EJ, et al. Longitudinal changes in CD4(+) T-cell memory responses induced by BCG vaccination of newborns. *The Journal of infectious diseases*. 2013;207:1084-94.
- [33] Harrington LE, Janowski KM, Oliver JR, Zajac AJ, Weaver CT. Memory CD4 T cells emerge from effector T-cell progenitors. *Nature*. 2008;452:356-60.
- [34] Apt A, Kramnik I. Man and mouse TB: contradictions and solutions. *Tuberculosis*. 2009;89:195-8.
- [35] Weir RE, Black GF, Nazareth B, Floyd S, Stenson S, Stanley C, et al. The influence of previous exposure to environmental mycobacteria on the interferon-gamma response to bacille Calmette-Guerin vaccination in southern England and northern Malawi. *Clinical and experimental immunology*. 2006;146:390-9.
- [36] Mogueche AO, Musvosvi M, Penn-Nicholson A, Plumlee CR, Mearns H, Geldenhuys H, et al. Antigen Availability Shapes T Cell Differentiation and Function during Tuberculosis. *Cell Host Microbe*. 2017;21:695-706 e5.
- [37] Norrby M, Vesikari T, Lindqvist L, Maeurer M, Ahmed R, Mahdavi S, et al. Safety and immunogenicity of the novel H4:IC31 tuberculosis vaccine candidate in BCG-vaccinated adults: Two phase I dose escalation trials. *Vaccine*. 2017.
- [38] Fletcher HA, Snowden MA, Landry B, Rida W, Satti I, Harris SA, et al. T-cell activation is an immune correlate of risk in BCG vaccinated infants. *Nature communications*. 2016;7:11290.
- [39] Kagina BM, Abel B, Scriba TJ, Hughes EJ, Keyser A, Soares A, et al. Specific T cell frequency and cytokine expression profile do not correlate with protection against tuberculosis after bacillus Calmette-Guerin vaccination of newborns. *American journal of respiratory and critical care medicine*. 2010;182:1073-9.

- [40] Kester KE, McKinney DA, Tornieporth N, Ockenhouse CF, Heppner DG, Hall T, et al. Efficacy of recombinant circumsporozoite protein vaccine regimens against experimental *Plasmodium falciparum* malaria. *The Journal of infectious diseases*. 2001;183:640-7.
- [41] Hadler SC, de Monzon MA, Lugo DR, Perez M. Effect of timing of hepatitis B vaccine doses on response to vaccine in Yucpa Indians. *Vaccine*. 1989;7:106-10.
- [42] Belshe RB, Frey SE, Graham I, Mulligan MJ, Edupuganti S, Jackson LA, et al. Safety and immunogenicity of influenza A H5 subunit vaccines: effect of vaccine schedule and antigenic variant. *The Journal of infectious diseases*. 2011;203:666-73.
- [43] Nassim C, Christensen S, Henry D, Holmes S, Hohenboken M, Kanesa-Thasan N. Identification of Antigen and Adjuvant Doses Resulting in Optimal Immunogenicity and Antibody Persistence up to One Year After Immunization with a Pandemic A/H1N1 Influenza Vaccine in Children 3 to < 9 Years of Age. *The Pediatric infectious disease journal*. 2012.

## **Supplementary material for paper 4**

The following is the supplementary material referenced in paper 4. All references to the below tables and Figures are preceded with the suffix “S” in the paper.

### ***Additional Methods***

#### **Data**

*(The following text on the mouse data and laboratory methods is taken from my paper 3 [337])*

#### Mouse IFN- $\gamma$ ELISPOT data

The methods and materials used to generate the mouse IFN- $\gamma$  response data following H56+IC31 vaccination are outlined below. These methods are outlined in chapter 4 [337].

#### *Ethics Statement*

All animal work was carried out in accordance with the Animals (Scientific Procedures) Act 1986 under a license granted by the UK Home Office (PPL 70/8043), and approved by the LSHTM Animal Welfare and Ethics Review Body.

#### *Animals*

Female CB6F1 mice were acquired from Charles River UK at 6-8 weeks of age. Animals were housed in specific pathogen-free individually vented cages, were fed ad libitum, and were allowed to acclimatize for at least 5 days before the start of any experimental procedure.

#### *Vaccination*

The experimental vaccine H56 (comprising *Mycobacterium tuberculosis* antigens Ag85B-ESAT-6-Rv2660c [338], provided by Statens Serum Institute (SSI), Copenhagen, Denmark) was formulated in IC31<sup>®</sup> adjuvant (provided by SSI on behalf of Valneva Technologies) and 10 mM Tris-HCL buffer (pH 7.4) as described in [339] to obtain a final volume of 200  $\mu$ l/mouse. The adjuvant IC31<sup>®</sup> consists of a mixture of the cationic peptide KLK (NH<sub>2</sub>-KLKL5KLK-COOH) and the oligodeoxynucleotide ODN1a (oligo-(dIdC)<sub>13</sub>). Adjuvant doses were 100 nmol peptide

and 4 nmol oligonucleotide for every vaccine (H56) dose. Antigen doses of 0.1, 0.5, 1, 5 or 15 µg of H56 + 100/4 nmol IC31 (hereafter, H56+IC31) were administered per animal at day 0 and 15, the same dose was used at both vaccination times within a group. Control animals received no vaccination. The vaccine was administered subcutaneously into the left or right leg flap.

#### *IFN-γ ELISPOT*

IFN-γ secreting CD4<sup>+</sup> T cells were measured using the ELISPOT assay. Single cell suspensions of mouse splenocytes were prepared by mechanical disruption of spleens through a 100µm cell strainer on the day of sacrifice. After lysis of red blood cells, single cell suspensions were made up in antibiotic-free media [RPMI-1640 (Sigma-Aldrich, Dorset, UK) + 10% heat-inactivated FBS (Labtech International Ltd, Uckfield, UK) + 2 mM L-Glutamine (Fisher Scientific, Loughborough, UK)]. 96-well microtiter ELISPOT plates (MAIPS4510, Millipore, Watford, UK) were coated with 10 µg/ml rat anti-mouse IFN-γ (clone AN18, Mabtech, Nacka Strand, Sweden). Free binding sites were blocked with RPMI 1640 supplemented as described above.  $2.5 \times 10^5$  of total splenocytes were added and incubated in duplicate with H56 (10 µg/ml), supplemented RPMI as a negative control, or Phorbol myristate acetate (PMA) (50 µg/ml, Sigma-Aldrich) and Phytohemagglutinin (PHA) (10 µg/ml, Sigma-Aldrich) as a positive control. After 24 or 48 hrs of incubation at 37°C in 5% CO<sub>2</sub>, IFN-γ was detected with 1 µg/ml biotin labelled rat anti-mouse antibody (clone R4-6A2, Mabtech) and 1 µg/ml alkaline phosphatase-conjugated streptavidin (Mabtech). The enzyme reaction was developed with BCIP/NBT substrate (5-Bromo-4-chloro-3-indolyl phosphate/Nitro blue tetrazolium) (MP Biochemicals, UK) and stopped by washing the plates with tap water when individual spots could be visually detected (up to 5min). ELISPOT plates were analysed using an automatic plate reader. IFN-γ-specific cells are expressed as number of spot-forming units (SFU) per million spleen cells after non-specific background was subtracted using negative control wells.

#### *Experimental Schedule*

ELISPOTs were carried out at 2, 7, 9, 14, 16, 21, 28, and 56 days after the first vaccination for all doses. Five mice were used per time point per dose group (equating to 40 mice in a dose group from initiation to conclusion of the experiment). This schedule was designed to reflect

the H56+IC31 phase I clinical trial schedule [232] and previous experimental schedules in mice using the H-series vaccines by SSI in CB6F1 mice [217, 219, 338, 340].

Figure S1 shows the ELISPOT results using the 24 hour incubation time for each dosing group. Each blue dot represents the responses of one mouse, the black horizontal lines indicate the median responses. This Figure is a replication of Figure 1 in [337], chapter 4.

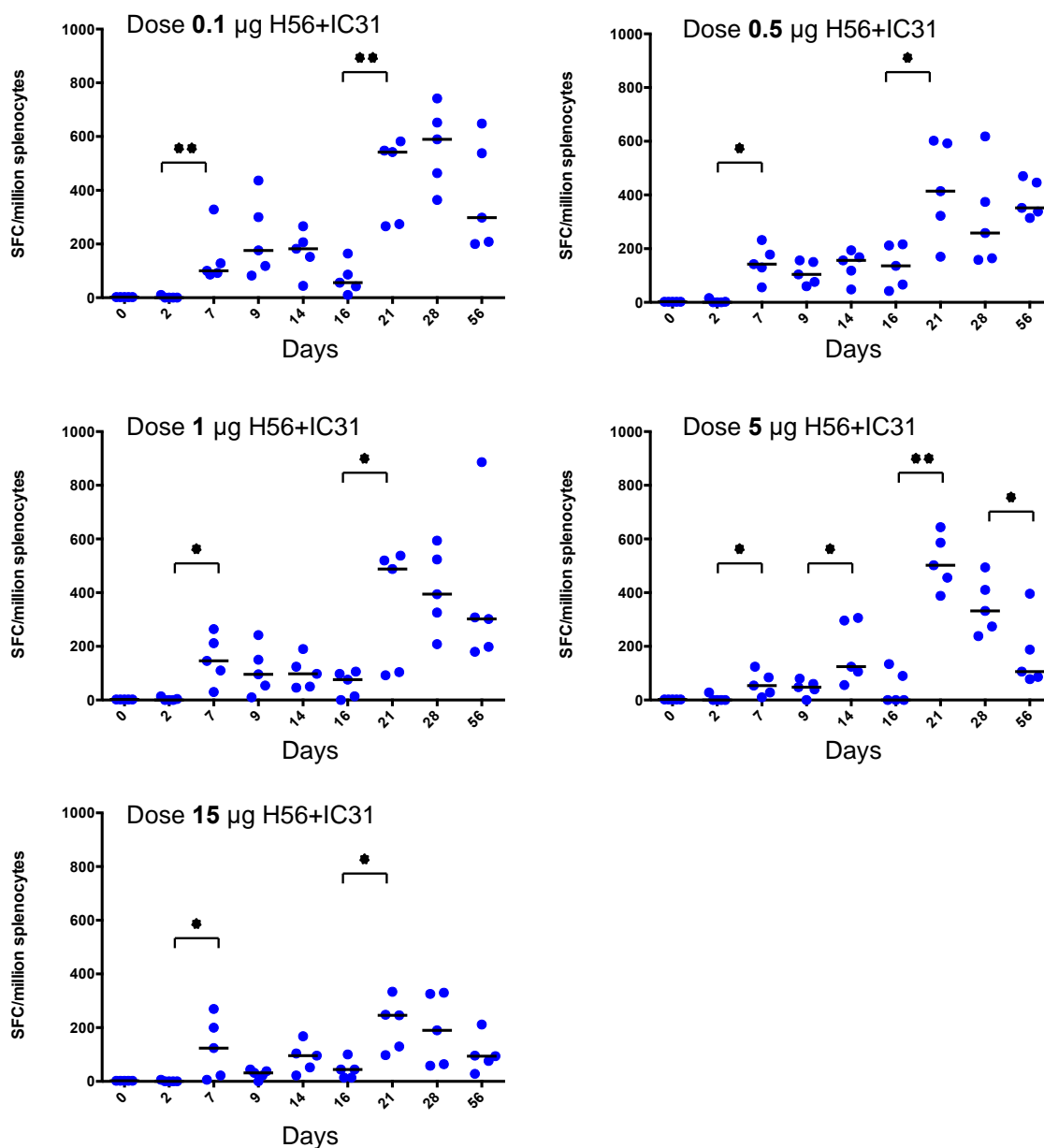


Figure S1. Median IFN- $\gamma$  responses (horizontal black bars) and responses of individual mice per time point (blue points) for each dose. As the control group did not receive H56+IC31, the median of all responses from the control group (which did not significantly change throughout the experiment) was used to represent all mice at baseline. The Wilcoxon test was used to compare consecutive time points, where \*equates to p-value<0.05 and \*\*p-value<0.01 (Table S2 in [337]). This Figure is duplicated from [337] here as a reminder of the data generated in chapter 4.

Human IFN- $\gamma$  ELISPOT data

Table S1 summarizes the two H-series trials from which the human ELISPOT data was taken. Figure S2 shows the individual IFN- $\gamma$  responses (measured using ELISPOT assay) over time for both trials and the pooled median response across both trials.

Clinical trial Information						Data from Clinical trial used in the analysis					
Vaccine	ClinicalTrials.gov ID/publication	Phase	Purpose of trial (taken from ClinicalTrials.gov)	Country conducted	Study arms	Study arm used	N	Response measurement times (days)	Median age (IQR)	Gender	Years since BCG
H56+IC31	NCT01967134/[232]	i	Evaluation of the Safety and immunogenicity profile of H56+IC31 administered to HIV-negative adults and without LTBI and no history or evidence of tuberculosis (TB) disease.	South Africa	<ol style="list-style-type: none"> <li>N=8, LTBI negative, dose = 50 <math>\mu</math>g H56(+500nmol IC31), two vaccinations (day 0, 56)</li> <li>N=8, LTBI positive, dose = 15 <math>\mu</math>g H56(+500nmol IC31), two vaccinations (day 0, 56)</li> <li>N=9, LTBI positive, dose = 50 <math>\mu</math>g H56(+500nmol IC31), two vaccinations (day 0, 56)</li> </ol>	1	8	0, 14, 56, 70, 112	32 (19–38)	M=4, F=4	>10 (assumed to be vaccinated at birth)
H1+IC31	NCT00929396/[227]	i	A safety and immunogenicity Phase 1 Trial with an adjuvanted TB subunit vaccine H1+IC31 (Ag85B-ESAT-6 + IC31) administered in PPD positive volunteers at 0 and 2 months	Netherlands	<ol style="list-style-type: none"> <li>N=10, LTBI negative, BCG positive, dose= 50 <math>\mu</math>g H1(+500nmol IC31), two vaccinations (day 0, 56)</li> <li>N=10, LTBI positive, dose= 50 <math>\mu</math>g H1(+500nmol IC31), two vaccinations (day 0, 56)</li> </ol>	1	10	0, 7, 42, 63, 98, 224	49 (24–54)	M=7, F=3	>2

**Table S1. Outline of the H56+IC31 and H1+IC31 phase i clinical trials and human demographics for each. Abbreviations: LTBI = Latent Tuberculosis Infection, IQR= Inter quartile range.**

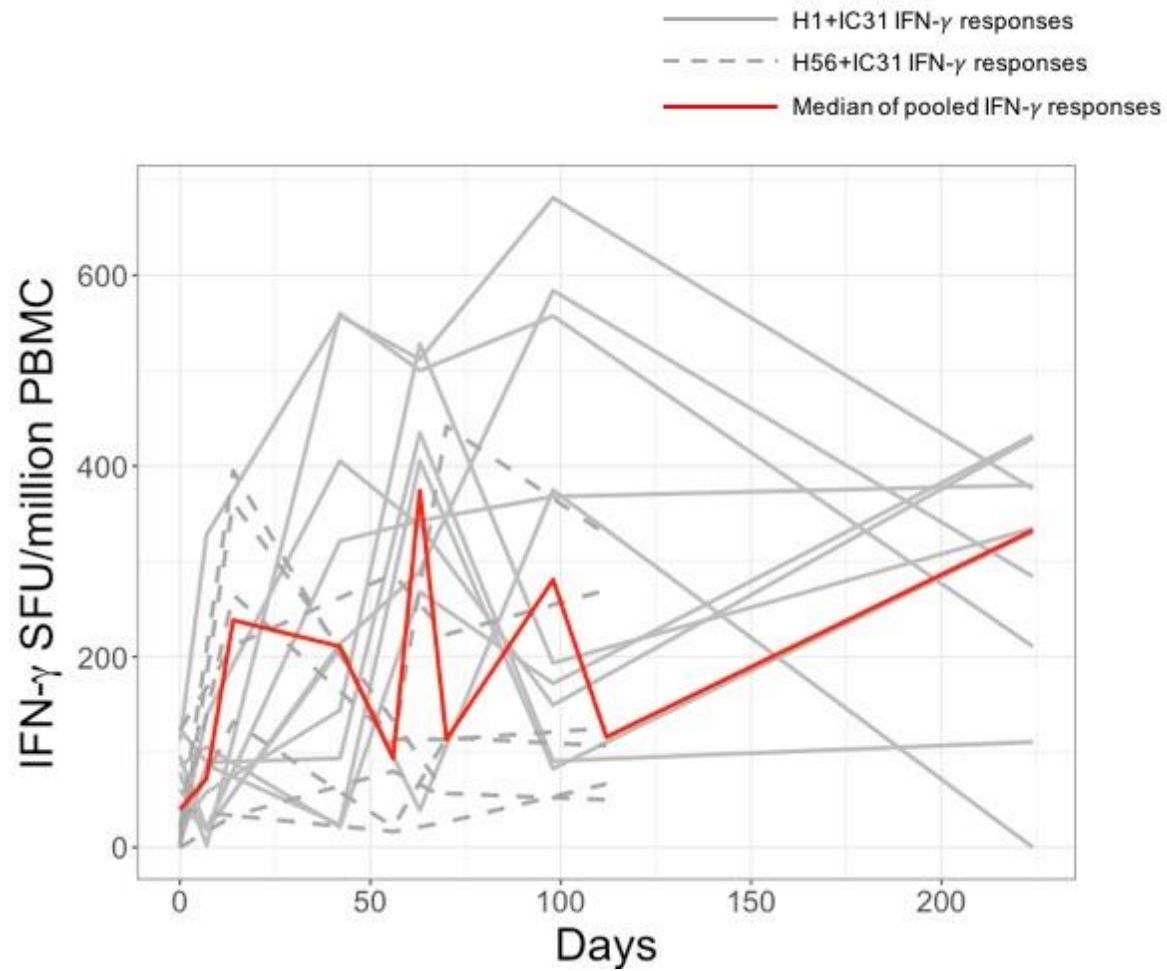


Figure S2. Number of IFN- $\gamma$  secreting CD4+ T cells in humans in H56+IC31 phase I trial [232] (ClinicalTrials.gov no NCT01967134) and H1+IC31 phase I trial [227] (ClinicalTrials.gov no NCT00929396) over time measured using an ELISPOT assay. Vaccinations of the respective vaccines were given at day 0 and day 56. The median of the pooled data is shown in red and the responses in those that received H1+IC31 are shown in solid grey and for those that received H56+IC31 are shown in dashed grey.

### *Laboratory procedures for the human IFN- $\gamma$ data*

#### *H56+IC31 phase I trial [232]: ClinicalTrials.gov no NCT01967134*

Screening procedures for HIV status included a medical history and blood collection for baseline chemistry. QuantiFERON<sup>®</sup>-TB Gold In Tube test (qft, cellestis limited) was used to determine latent TB infection (LTBI) status.

#### *H1+IC31 phase I trial [227]: ClinicalTrials.gov no NCT00929396*

The ELISPOT methods for the H1+IC31 clinical trial are outlined in [227]. I summarise the methods below.

Frozen cells were pre-stimulated for 16-18 hours, followed by 24 hours in the ELISPOT plate.  $1 \times 10^6$  thawed cells/well were stimulated in 24 well plates with H1 antigens (Ag85B and ESAT-6 proteins) as well as PPD, separate peptide pools and positive and negative controls (see [227]). All samples were assayed in triplicate. Incubation was done overnight in a fully humidified incubator at 37 °C, 5% CO<sub>2</sub>. Subsequently, cells were resuspended and divided over 3 wells (250,000 cells/well) of a mixed cellulose ester-backed 96 well plate (MAHAS45, Millipore) which had been pre-coated with anti-IFN- $\gamma$ -antibody (mAb1-D1K, Mabtech, Sweden) and blocked with AIMV medium. The next day biotinylated detector antibody (mAb 7-B6-1, Mabtech) was added and spots colored with alkaline phosphatase conjugated streptavidin (Mabtech, Sweden) and FastTMNBT/BCIP (Sigma–Aldrich, The Netherlands). Substrate incubation was done at room temperature for 10 min and stopped by rinsing the plates with tap water. Plates were dried and spots were counted in the Bioreader 3000 pro (BioSys, Germany) using calibrated parameters.

BCG vaccination status was determined by tuberculin-skin-test (TST), whereby a reaction range 6–15mm or any documented value between 6 and 15mm on medical file in the past, indicated the participant was BCG vaccinated. To determine LTBI status, a QuantiFERON<sup>®</sup>-TB Gold In Tube test and a 6-day lymphocyte stimulation test (as described in [228]) in addition

to chest X-rays, were conducted at screening. HIV status was determined by reviewing recorded medical history and conducting standard blood tests.

### Mathematical vaccine Immunostimulation/Immunodynamic (IS/ID) Model

The equations for the IS/ID two-compartmental in Figure 1 are as follows:

$$\frac{dTEM}{dt} = \delta - \beta_{TEM}TEM - \mu_{TEM}TEM + \beta_{CM}CM \quad (1)$$

$$\frac{dCM}{dt} = \beta_{TEM}TEM + RCM - \beta_{CM}CM \quad (2)$$

Where TEM represents the transitional effector memory (TEM) cell population, CM, the resting central memory (CM) cell population, t, the time in days and the parameters are those outlined in Figure 1. The parameters in the model follow the rules:

- $\delta$  initiated at time=0 and time=revaccination and has the same value at both times.
- $RCM = 0$  until time = time of revaccination then 0 after time = time of revaccination +  $\tau$
- $\beta_{CM} = 0$  until time = time of revaccination +  $\tau$  then is 0 shortly after (once 95% of CM cells have transitioned) time = time of revaccination +  $\tau$  to ensure there is no flow back into the TEM compartment other than that due to revaccination. The value of  $\beta_{CM}$  is fixed arbitrarily high, at a value of 10 cells per day.
- $\mu_{TEM}$  is fixed to values found in literature: 0.3 per day for mice [341] and 0.2 per day for humans [297, 317, 342].

### Analysis 1: Calibration of the IS/ID model to the mouse data, pooled and stratified by dose group

*Testing the structural model for parameter  $\delta$*

Three different mathematical forms were used to represent parameter  $\delta$ :

1. Gamma Probability Density Function (PDF) equation:

$$\delta = L * \frac{\left(\frac{1}{h}\right)^k}{\Gamma(k)} * time^{(k-1)} * e^{-\left(\frac{1}{h}*time\right)}$$

the parameters were: L=multiplier to scale up the gamma PDF, k= Gamma PDF shape parameter, h=Gamma PDF scale parameter.

2. Gaussian function equation:

$$\delta = a * \exp\frac{-(time - b)^2}{2c^2}$$

the parameters were: a=height of Gaussian function, b=mean of Gaussian function, c=variance of Gaussian function.

3. Naïve T cell compartment: A naïve T cell compartment was added to the model which introduced cells to the Transitional Effector Memory (TEM) compartment. There were initially 10 cells in the naïve compartment, which replicated every 10 hours for  $\tau_N$  days. After this, they left the Naïve compartment and enter the TEM compartment at rate  $\beta_N$ . As naïve cells do not express cytokines until they are differentiated [44], they do not contribute to IFN- $\gamma$  output of the model. They were also long-lived cells [343], so do not die.

### *Statistical (NLMEM) model*

The residual error model and potential random effects correlations were tested in the analyses (see chapter 3 and Appendix B for description of the statistical NLMEM model).

**Analysis 3: Use calibrated mathematical models in analysis 1 & 2, and a vaccine dose allometric scaling assumption, to predict the human immune response dynamics and predict the most immunogenic dose in humans**

### *Sensitivity analysis of vaccine dose allometric scaling factor*

I assumed a scaling factor of 3.33 instead of 10, so the 50 µg H56/H1 + 500 nmol IC31 dose given to humans was now equivalent to the high (15 µg H56 + 100 nmol IC31) dose group in the mice. Under this assumption, the low and middle doses in humans were estimated to be 0.3-3.3 and 16.7 µg H56/H1 + 500 nmol IC31, respectively.

Like in the main analysis, I calculated the percentage change between the mouse-data-estimated model parameters from the high dose group vs the low and middle dose groups (identified in analysis 1ii). Then I applied these percentage changes to the human estimated model parameters found in analysis 2 (now assumed to be the human high dose group) to predict the model parameters for the low and middle dose groups in humans. To establish the 'most immunogenic' human dose group I compared long term (day 224) model-predicted responses for the three human dose groups.

## Additional Results

### Analysis 1: Calibration of the IS/ID model to the mouse data, pooled and stratified by dose group

Analysis 1i: Calibration of the IS/ID model to the pooled mouse data: Mouse pooled model

Table S2 shows the result of the calibration of the model to the pooled mouse data for each form of  $\delta$  in the model (Figure 1). The Gaussian equation provided the best fit according to the BIC value and all parameters were well estimated (RSE<30%). The estimated parameter values for the Gaussian equation calibration are in Table 1.

Form of $\delta$	Model parameters (fixed or to be estimated in Monolix)		Results after calibration to pooled mouse data		
	Fixed (value)	To be estimated	Parameters with RSE >30%	BIC value	-2LL value
Gamma PDF		L, k, h, $\beta_{TEM}$ , $\tau$	None	2453	2415
Gaussian equation	$\mu_{TEM}$ (0.3 day <sup>-1</sup> )*, $\beta_{CM}$ (10 per day <sup>-1</sup> )&	a, b, c, $\beta_{TEM}$ , $\tau$	None	2379	2341
Naïve compartment		$\tau_N$ , $\beta_N$ , $\beta_{TEM}$ , $\tau$	None	2503	2471

Table S2. Results of calibrating the model to the pooled mouse data for the three forms of  $\delta$ . \*Fixed to value found in literature, &Fixed to assumed high value

### Residual Error (RE) Model

The following residual error models were tested on the pooled mouse data with the Gaussian  $\delta$  function: additive, proportional and combined (additive and proportional). An additive model resulted in a BIC value of 2732, the proportional; 2430 and the combined 2379 (as in table S2). The combined residual error model was therefore used throughout analysis 1. The estimated values for the combined residual error model for analysis 1 can be found in Table S3. All are well estimated (RSE<30%).

	Pooled (analysis 1i)	Dose covariate (analysis 1ii)
--	----------------------	-------------------------------

	Estimated Value	RSE (%)	Estimated Value	RSE (%)
Additive contribution (cells)	0.63	18	0.63	14
Proportional contribution (% of predicted response)	22	25	21	24

**Table S3. Residual error model estimated parameters for a combined residual error model for mice.**

### Test for random effects correlations

Results for the pairwise test for random effects correlations for mice are shown in Table S4.

Combinati on tested	Mice		
	BIC	Diff to "none" (BIC)	Decisio n to include
None	2379	-	-
a & b	2401	22	No
a & c	2402	23	No
a & $\beta_{TEM}$	2405	26	No
a & $\tau$	2395	16	No
b & c	2399	20	No
b & $\beta_{TEM}$	2398	19	No
b & $\tau$	2416	37	No
c & $\beta_{TEM}$	2397	18	No
c & $\tau$	2413	34	No
$\beta_{TEM}$ & $\tau$	2432	53	No

**Table S4. Tests for random effects correlations for mice**

All BIC values in Table S4 were non-significantly different from no random effects correlations in the mice population. No correlations were considered necessary to apply in further analyses.

## Diagnostic Plots

The VPC plot, model prediction distribution plot and the observed versus predicted (for the population and individual mice) for the pooled mouse model can be found in Figures S3-S5.

The VPC plot shows that the simulated model predictions cover the data well and there are little red areas (red areas indicate the simulated model predictions did not adequately cover the observed data) (Figure S3). The red areas in the early response stages may be due to variable responses at this stage. The red area for the 25<sup>th</sup> percentile prediction indicates the model is under predicting the data. This could be due to the 0.5 value constraint placed on the standard deviation of the parameters which limit the degree to which the predictions can vary to cover the data. The model prediction distribution plot suggests the percentiles of the data are adequately covered (Figure S4), however, as all parameter standard deviations are fixed at 0.5, this may be underestimating the responses in some cases (as the observed versus predicted individual responses suggests (Figure S5)). Figure 2A in the main paper reflects these results.

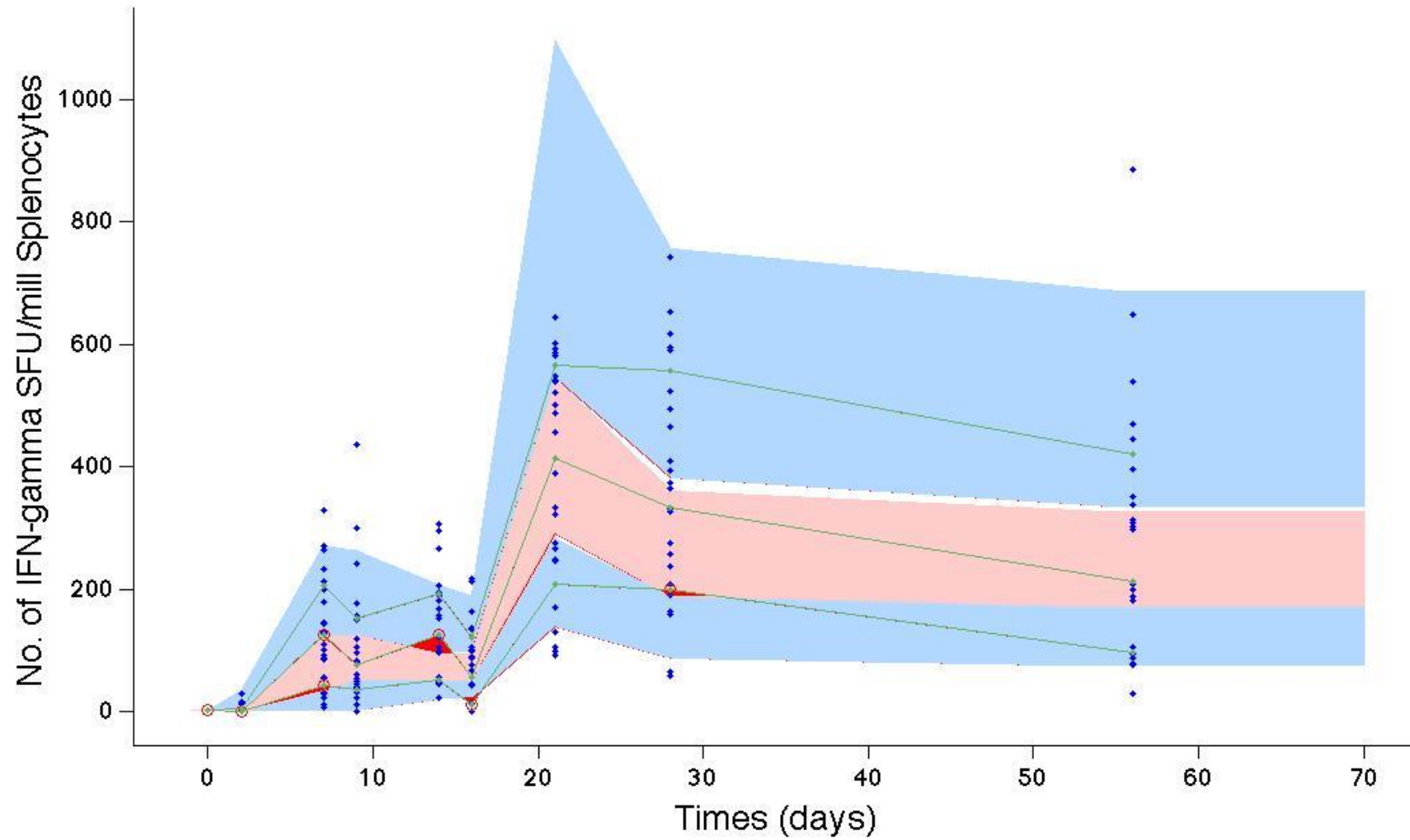


Figure S3. Visual Predictive Check (VPC) plot for the pooled mouse model (parameters from Table 1 using the Gaussian equation for  $\delta$  Table S2). Blue points represent the observed data. Blue regions represent the ranges of the 75<sup>th</sup> and 25<sup>th</sup> percentiles of the simulated populations. The pink region represents the range of the 50<sup>th</sup> percentile. The green line links the observed percentiles (25<sup>th</sup>, 50<sup>th</sup> and 75<sup>th</sup>) for each time point. Red regions represent where the observed data falls outside the ranges of the simulated percentiles.

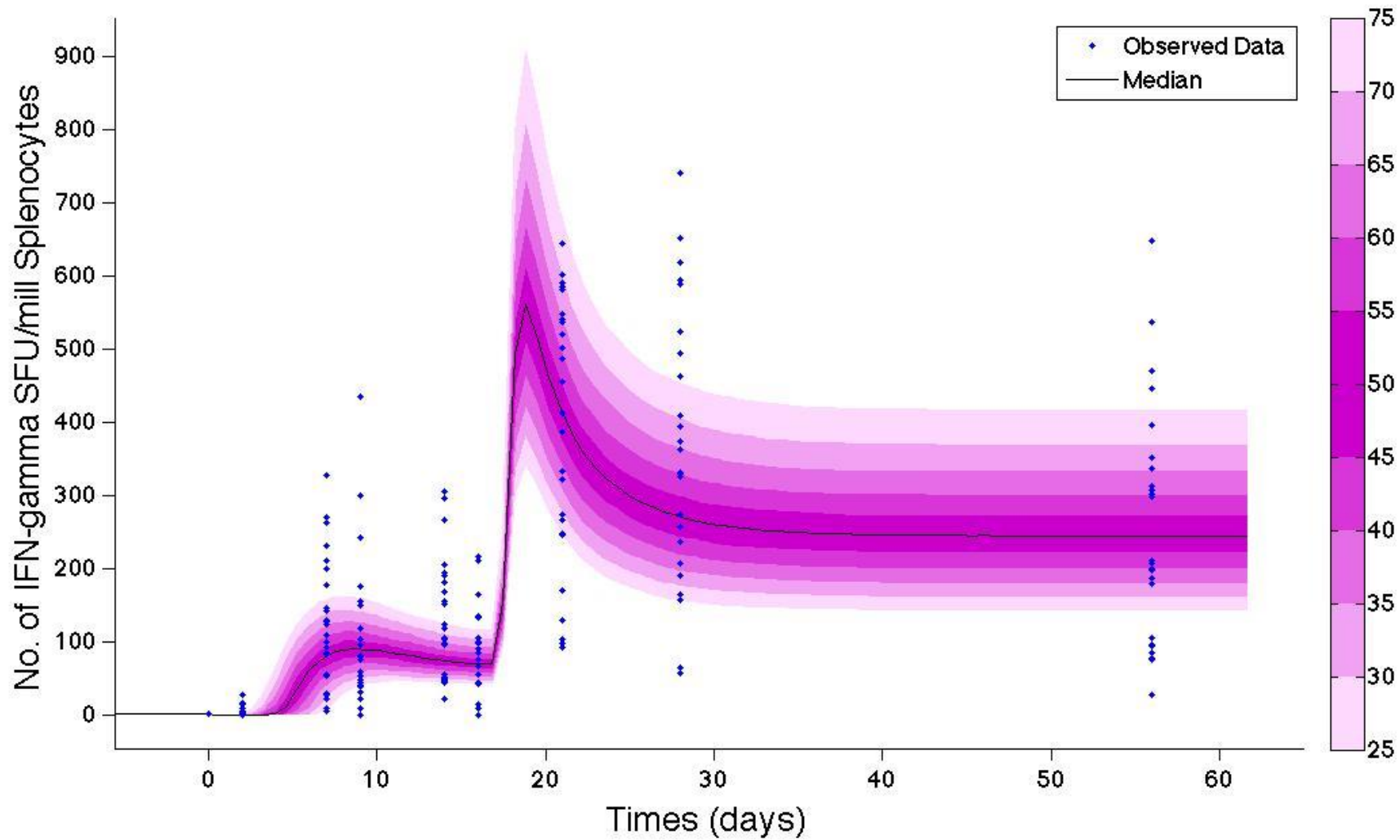


Figure S4. Prediction distribution plot for the calibration to the mouse data (parameters from Table 1 using the Gaussian equation for  $\delta$  Table S2). The blue points represent the data. The bands represent the 25<sup>th</sup> to 75<sup>th</sup> percentiles of the theoretical predictions using the estimated population parameters and associated variation for analysis 1i (Table 1). The black line shows the median total cell response prediction

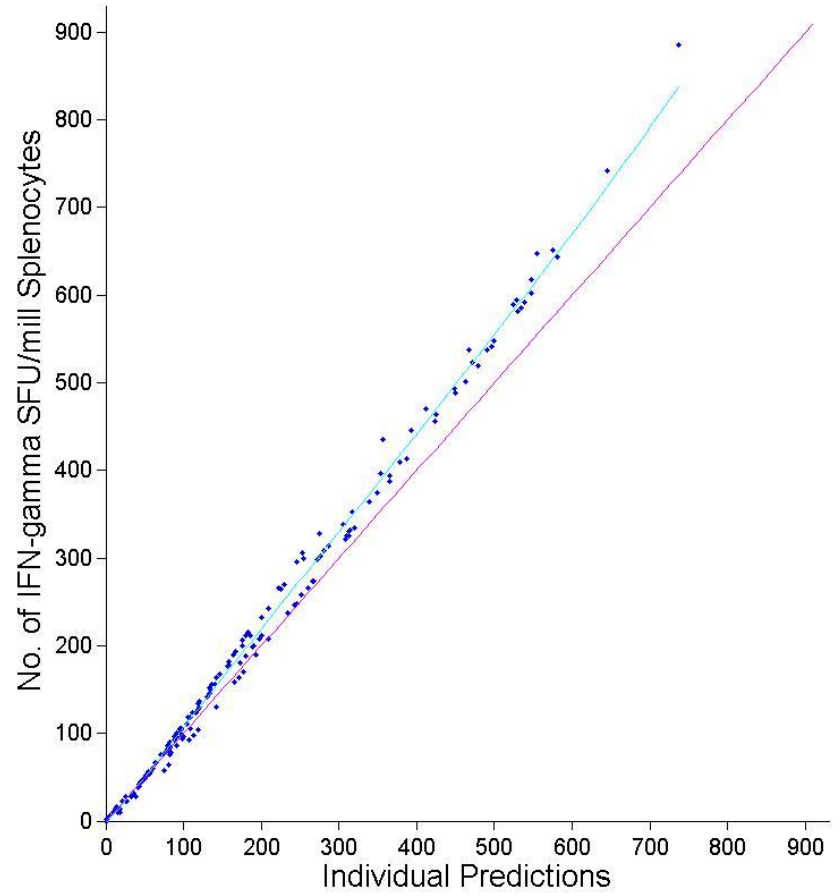
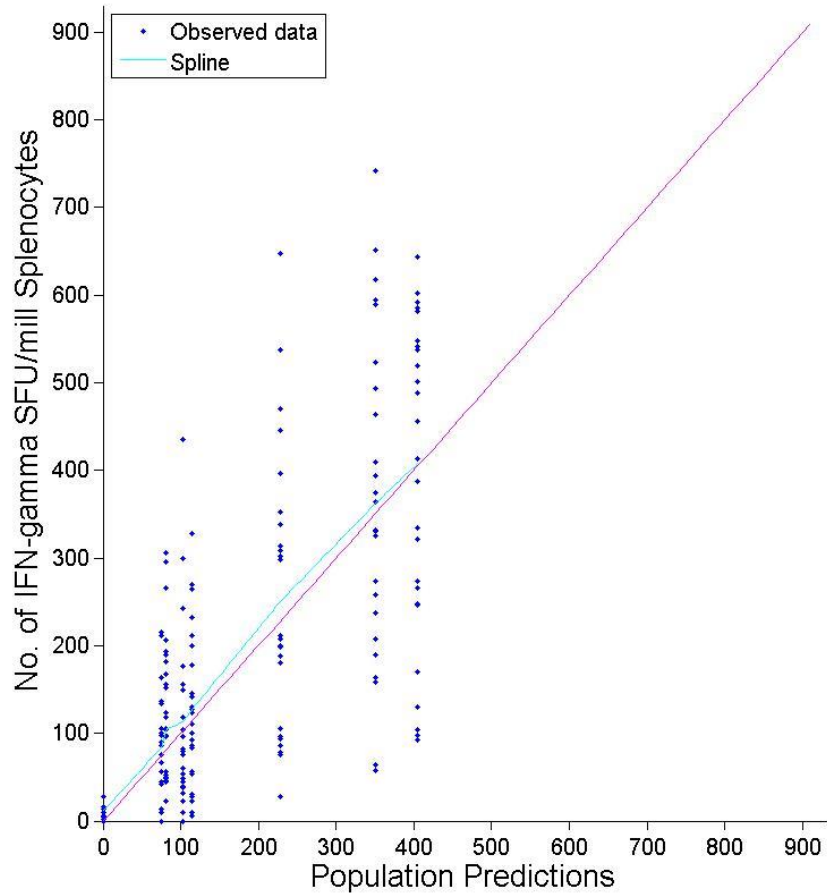


Figure S5. Mouse observed data versus model predicted IFN- $\gamma$  responses (parameters from Table 1 using the Gaussian equation for  $\delta$  Table S2)

Analysis 1ii: Calibration of the IS/ID model to the mouse data stratified by dose group: Mouse covariate model

As described, the LRT was used to establish the mouse covariate model. The selected model for analysis 1ii was the one which satisfied the LRT against the pooled model, had all estimated model parameters RSE <30%, and had the lowest -2LL. Table S5 shows the result of indexing dose group on the estimated model parameters from the pooled model (model parameter standard deviations were all 0.5).

-2LL value for pooled model	Dose group indexed on parameter(s)	Results		Difference in -2LL from pooled model (pooled-dose group)	0.01 level significant? (Chi <sup>2</sup> test 3 d.f.: crit val = 11.34, 6 d.f.: crit val = 16.81, 9 d.f.: crit val = 21.67, 12 d.f.: crit val = 26.22, 15 d.f.: crit val = 30.58)
		Parameters with RSE >30%	-2LL		
2341	a	None	2322	19	(3 d.f.) Yes
	b	None	2333	8	(3 d.f.) No
	c	None	2322	19	(3 d.f.) Yes
	$\beta_{TEM}$	None	2315	26	(3 d.f.) Yes
	$\tau$	None	2335	6	(3 d.f.) No
	a, b	a	2314	27	(6 d.f.) Yes
	a, c	a	2323	18	(6 d.f.) Yes
	a, $\beta_{TEM}$	c	2318	23	(6 d.f.) Yes
	a, $\tau$	None	2322	19	(6 d.f.) Yes
	b, c	None	2315	26	(6 d.f.) Yes
	b, $\beta_{TEM}$	None	2319	22	(6 d.f.) Yes
	b, $\tau$	None	2329	12	(6 d.f.) No
	c, $\beta_{TEM}$	c	2320	21	(6 d.f.) Yes
	c, $\tau$	c	2320	21	(6 d.f.) Yes
	$\beta_{TEM}, \tau$	c	2316	25	(6 d.f.) Yes
	a, b, c	a, b, c, $b_{TEM}$	2313	28	(9 d.f.) Yes
	a, b, $\beta_{TEM}$	a, $b_{TEM}$	2312	29	(9 d.f.) Yes
	a, b, $\tau$	a, b, $\tau$	2316	25	(9 d.f.) Yes
	a, c, $\beta_{TEM}$	a, c, $b_{TEM}$	2322	19	(9 d.f.) No
	a, c, $\tau$	a, c, $t$	2325	16	(9 d.f.) No
	a, $\beta_{TEM}, \tau$	a, c, $b_{TEM}$	2319	22	(9 d.f.) Yes
	b, c, $\beta_{TEM}$	$b_{TEM}$	2317	24	(9 d.f.) Yes
	b, c, $\tau$	b, c	2316	25	(9 d.f.) Yes
b, $\beta_{TEM}, \tau$	$\beta_{TEM}$	2312	29	(9 d.f.) Yes	

	c, $\beta_{TEM}$ , $\tau$	$b_{TEM}$	2322	19	(9 d.f.) No
	a, b, c, $\beta_{TEM}$	a, b, c, $b_{TEM}$	2317	24	(12 d.f.) No
	a, b, c, $\tau$	None	2317	24	(12 d.f.) No
	a, b, $\beta_{TEM}$ , $\tau$	a, $b_{TEM}$	2315	26	(12 d.f.) No
	a, c, $\beta_{TEM}$ , $\tau$	a, c, $b_{TEM}$	2321	20	(12 d.f.) No
	b, c, $\beta_{TEM}$ , $\tau$	All	2310	31	(12 d.f.) Yes
	a, b, c, $\beta_{TEM}$ , $\tau$	All	2320	21	(15 d.f.) No

**Table S5. Results of indexing the dose group covariate on all combinations of estimated parameters in the mouse pooled model**

Table S5 shows that the best covariate model is when dose group was indexed on model parameter  $\beta_{TEM}$  with all model parameter standard deviations fixed to 0.5 (highlighted)(allowing the standard deviations to be estimated led to RSE of one or more parameters >30%).

### Diagnostic Plots

The VPC plot, prediction distribution and observed versus predicted response plots can be found in S6-S8.

The VPC shows that for each dosing group (low, middle and high), the model predicts the data well (Figure S6), although with less data per group the VPC is not as definitive as for in the mouse pooled model (Figure S3). This is due to the small sample size for the high and middle dose groups, as the VPC plot does not summarise all responses, either observed data (green line) and model simulations (blue and orange regions) for all times points which is why the green line, blue and orange regions do not reflect the expected shape of the model prediction, i.e. there is no clear peak after primary and revaccination as would be expected from the design of the IS/ID model. This is not a reflection of an unidentifiable model calibration, but an artefact of the default settings for the VPC plot in Monolix, where model predictions for small sample sizes are misrepresented. Figure 2B-D is a better depiction of the model prediction versus the observed data. The observed versus predicted response plots in Figure S8 suggest that the model predictions fall in line with the observed data for the dose groups on a population and individual level.

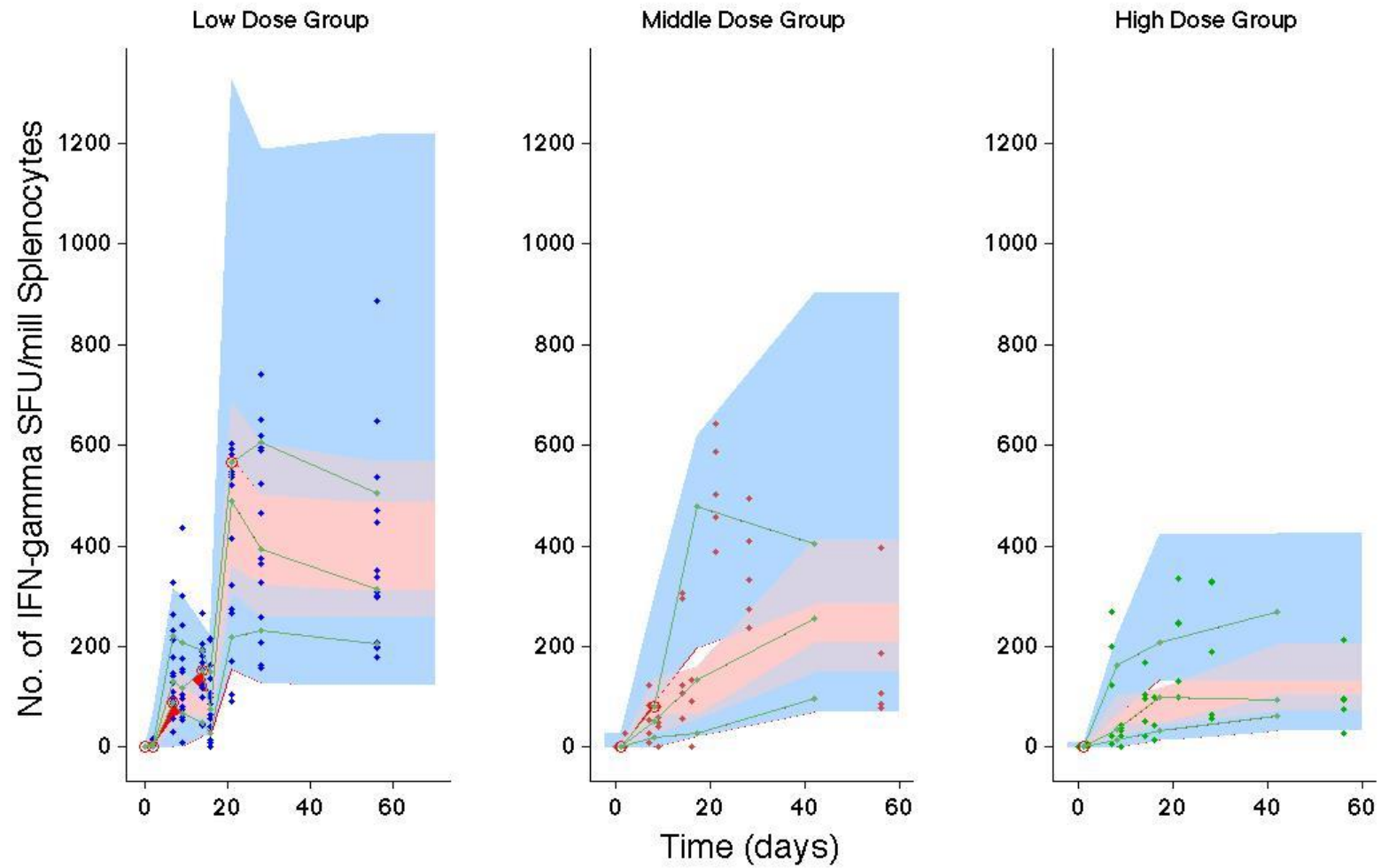


Figure S6. Visual Predictive Check (VPC) plot for the covariate mouse model (dose group indexed on parameter  $\beta_{TEM}$ , see Table S5, estimated parameters in Table 1). Blue points represent the observed data. Blue regions represent the ranges of the 75<sup>th</sup> and 25<sup>th</sup> percentiles of the simulated populations. The pink region represents the range of the 50<sup>th</sup> percentile. The green line links the observed percentiles (25<sup>th</sup>, 50<sup>th</sup> and 75<sup>th</sup>) for each time point. Red regions represent where the observed data falls outside the ranges of the simulated percentiles

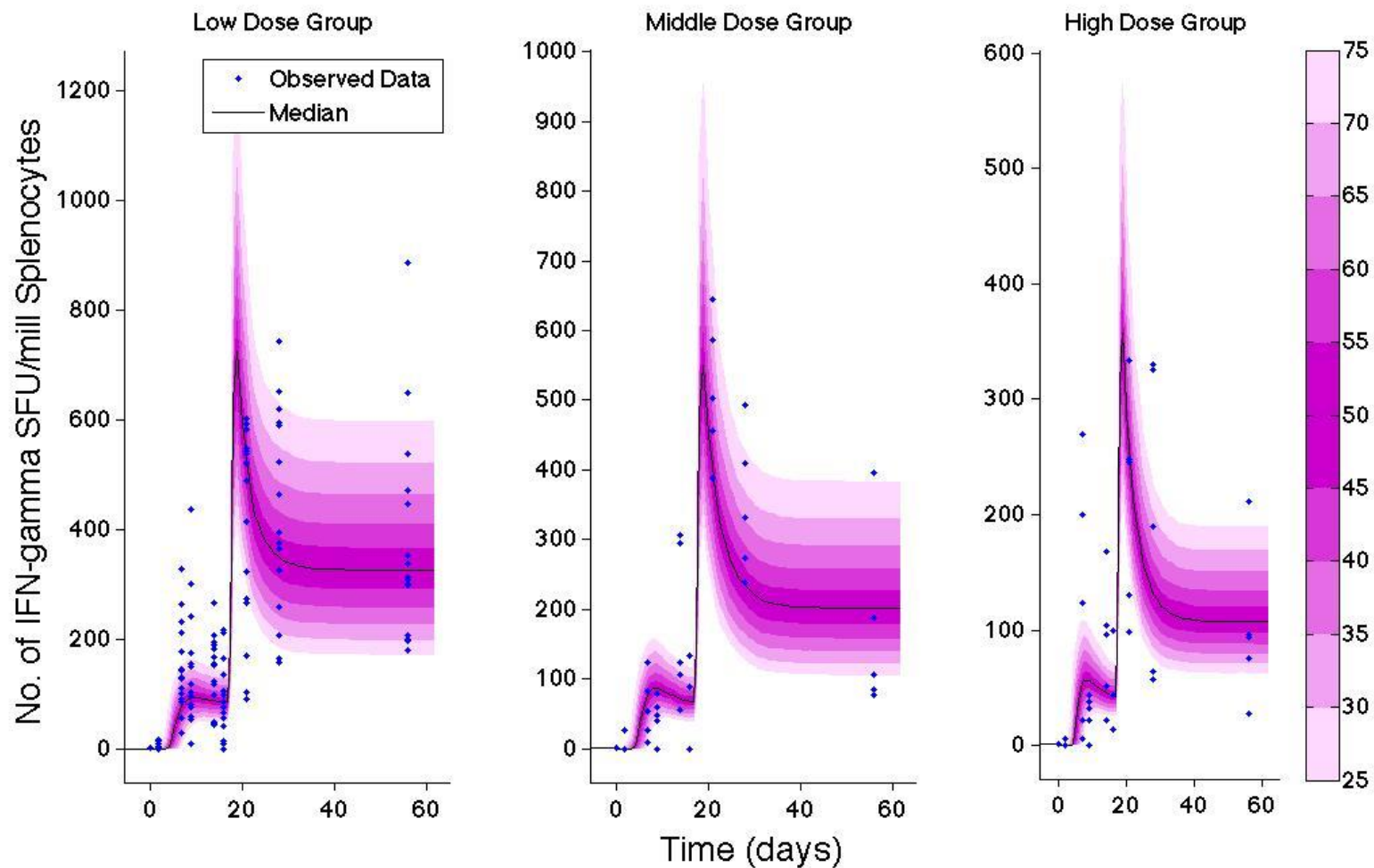


Figure S7. Prediction distribution plot for the calibration to the mouse data stratified by dosing group (dose group indexed on parameter  $\beta_{TEM}$ , see Table S5, estimated parameters in Table 1). The blue points represent the data. The bands represent the 25<sup>th</sup> to 75<sup>th</sup> percentiles of the theoretical predictions using the estimated population parameters and associated variation for analysis 1i (Table 1). The black line shows the median total cell response prediction. Note, Y-axis not on the same scale.

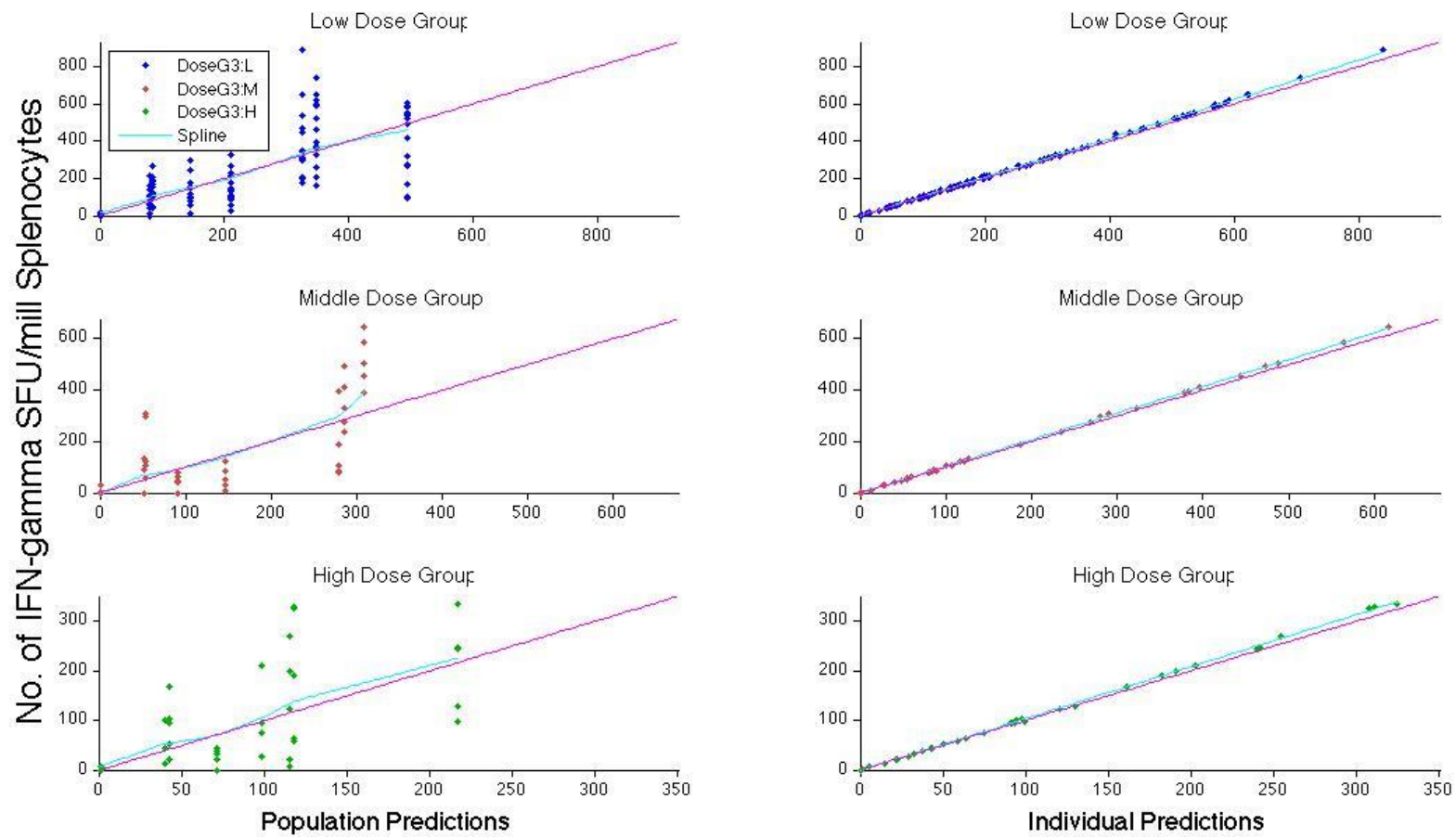


Figure S8. Mouse observed data versus model predicted IFN- $\gamma$  responses stratified by dose group (dose group indexed on parameter  $\beta_{TEM}$ , see Table S5, estimated parameters in Table 1).

## Analysis 2: Calibration of the IS/ID model to the pooled human data

Analysis 2: Calibration of the IS/ID model to the pooled human data: Human pooled model

The results of the model calibration to the human data can be found in Table 1. As two of the parameters were not identifiably estimated, I did not test the effects of estimating model parameter standard deviations as it was clear there was not enough data to estimate further parameters.

### Residual Error (RE) Model

The following residual error models were tested on the pooled human data with the Gaussian  $\delta$  function: additive, proportional and combined (additive and proportional). An additive model resulted in a BIC value of 1277, the proportional; 1270 and the combined 1248. The combined residual error model was therefore used throughout analysis 2. The estimated values for the combined residual error model for analysis 2 can be found in Table S6. All are well estimated (RSE<30%).

	Pooled (analysis 1i)	
	Estimated Value	RSE (%)
Additive contribution (cells)	24.7	29
Proportional contribution (% of predicted response)	37	23

Table S6. Residual error model estimated parameters for a combined residual error model for human.

### Test for random effects correlations

Results for the pairwise test for random effects correlations for humans are shown in Table S7.

	Humans
--	--------

Combinati on tested	BIC	Diff to "none" (BIC)	Decision to include
None	1248	-	-
b & c	1308	60	No
b & $\beta_{\text{TEM}}$	1362	114	No
b & $\tau$	1390	142	No
c & $\beta_{\text{TEM}}$	1275	27	No
c & $\tau$	1410	162	No
$\beta_{\text{TEM}}$ & $\tau$	1274	26	No

**Table S7. Tests for random effects correlations for humans**

All BIC values in Table S7 were non-significantly different from no random effects correlations in the human population. No correlations were considered necessary to apply in further analyses.

### **Diagnostic Plots**

The VPC plot, model prediction distribution plot and the observed versus predicted (for the population and individual participants) for the pooled human model can be found in S9-S11.

The VPC plot shows that the simulated model cover the data well and there are no red areas (indicating the simulated model predictions did adequately cover the observed data) (Figure S9). However, the model prediction is trending toward under estimating the median response at latest time point. Again, due to the small sample size, this VPC plot does not summarise all responses, either observed data (green line) and model simulations (blue and orange regions) for all times points which is why the green line, blue and orange regions do not reflect the shape of the model prediction in Figure 3 of the main paper. Similarly, this is not a reflection of the calibration of the model, but an artefact of the default settings for the VPC plot in Monolix, where model predictions for small sample sizes are misrepresented. However, the expected profile from the IS/ID model can be seen better in the model prediction distribution

plot, which suggest the percentiles of the data are adequately covered (Figure S10) despite widely variable responses over time in the human data set. Figure 3 in the main paper shows how the model predictions follow the trend of this variable data. However, similar to the mouse pooled model, as all parameter standard deviations are fixed at 0.5, this may be underestimating the responses in some cases (although the observed versus predicted individual responses suggests the model is a good fit (Figure S11)). Figure 3A in the main paper reflects these results.

The individual plots for each human participant can be found in Figure S12 and S13.

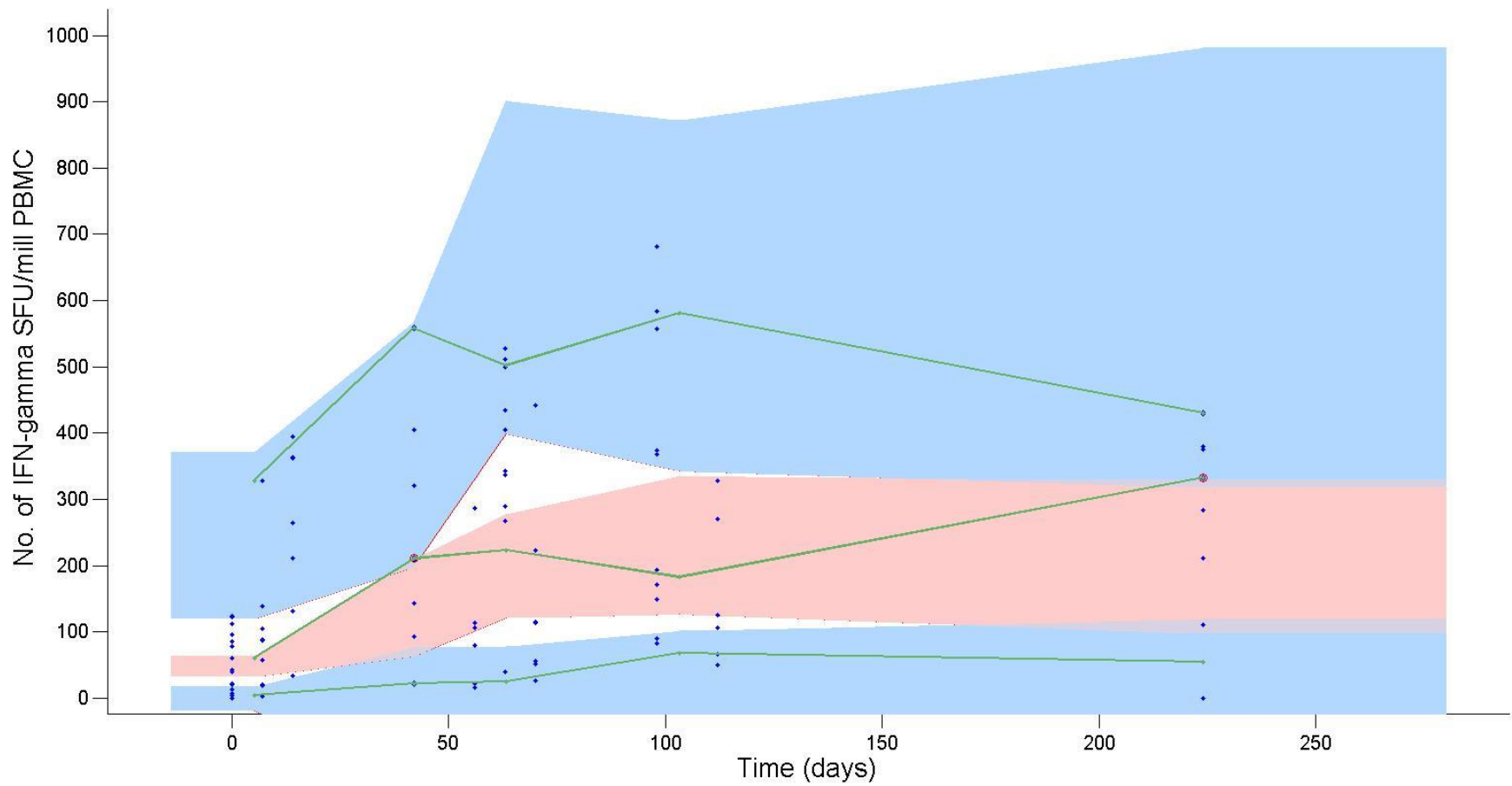


Figure S9. Visual Predictive Check (VPC) plot for the pooled human model (model parameters Table 1). Points represent the observed data. Blue regions represent the ranges of the 75<sup>th</sup> and 25<sup>th</sup> percentiles of the simulated populations. The pink region represents the range of the 50<sup>th</sup> percentile. The green line links the observed percentiles (25<sup>th</sup>, 50<sup>th</sup> and 75<sup>th</sup>) for each time point. Red regions represent where the observed data falls outside the ranges of the simulated percentiles.

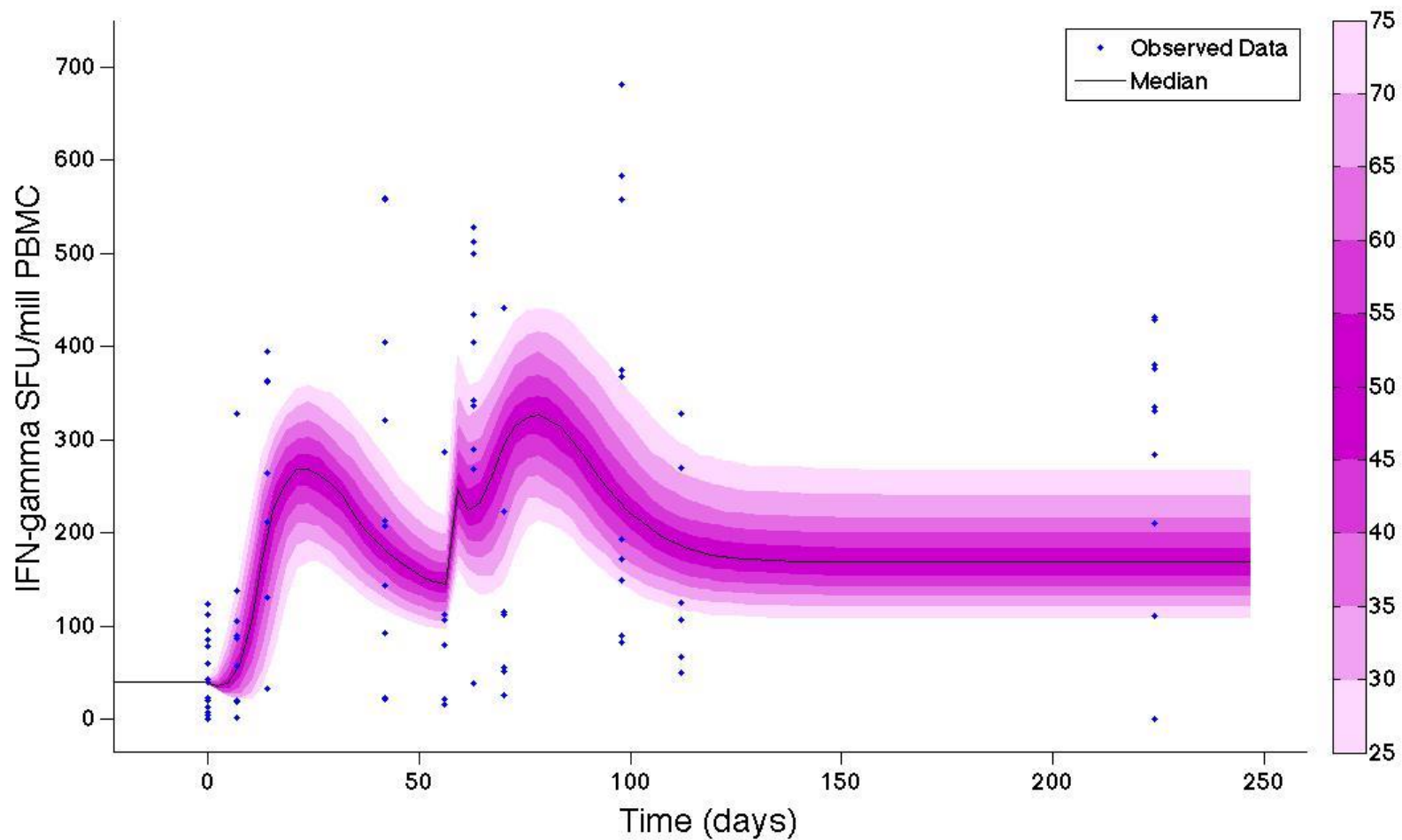


Figure S10. Prediction distribution plot for the calibration to the human data. The black points represent the data. The bands represent the 25<sup>th</sup> to 75<sup>th</sup> percentiles of the theoretical predictions using the estimated population parameters and associated variation for analysis 2 (Table 1). The black line shows the median total cell response prediction

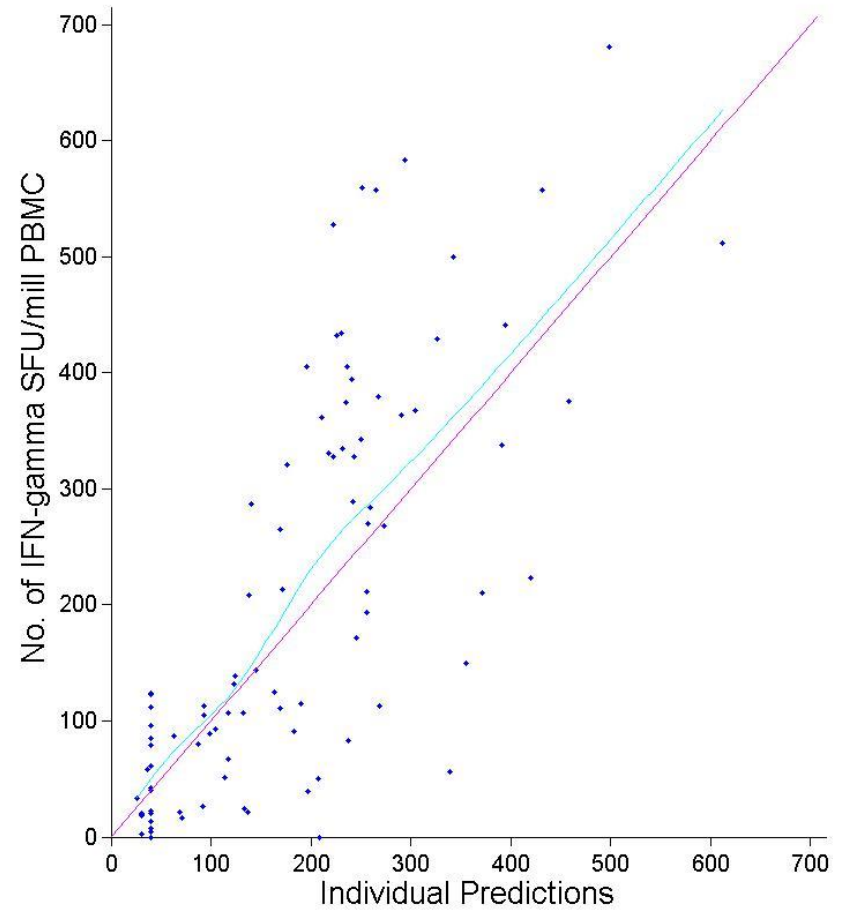
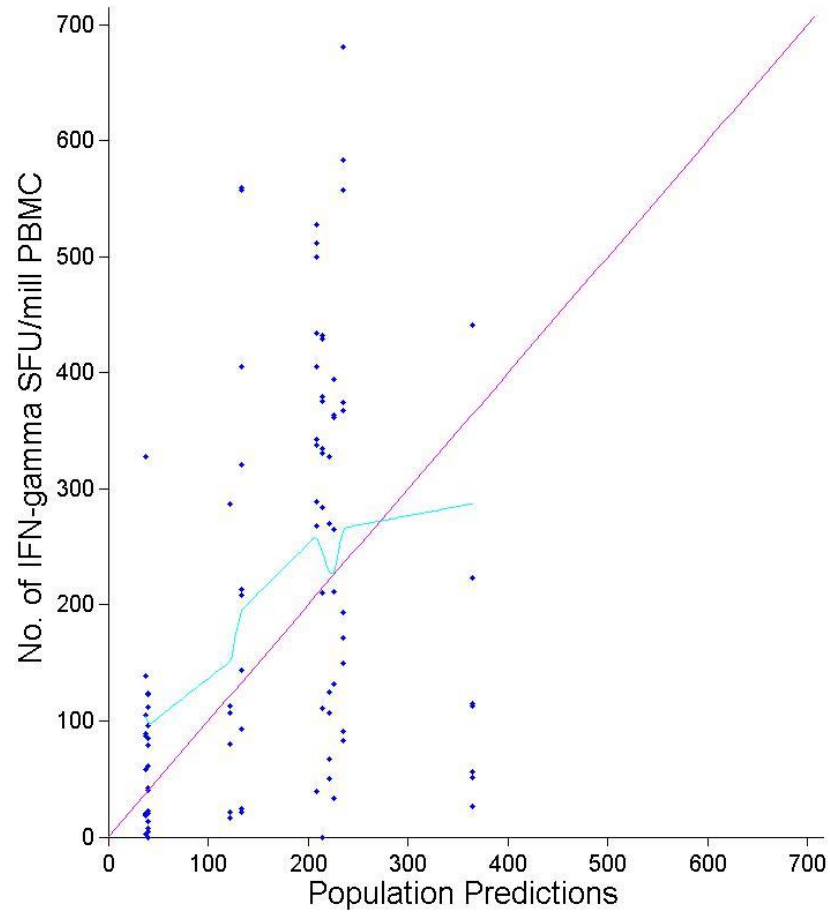


Figure S11. Human observed data versus model predicted IFN- $\gamma$  responses

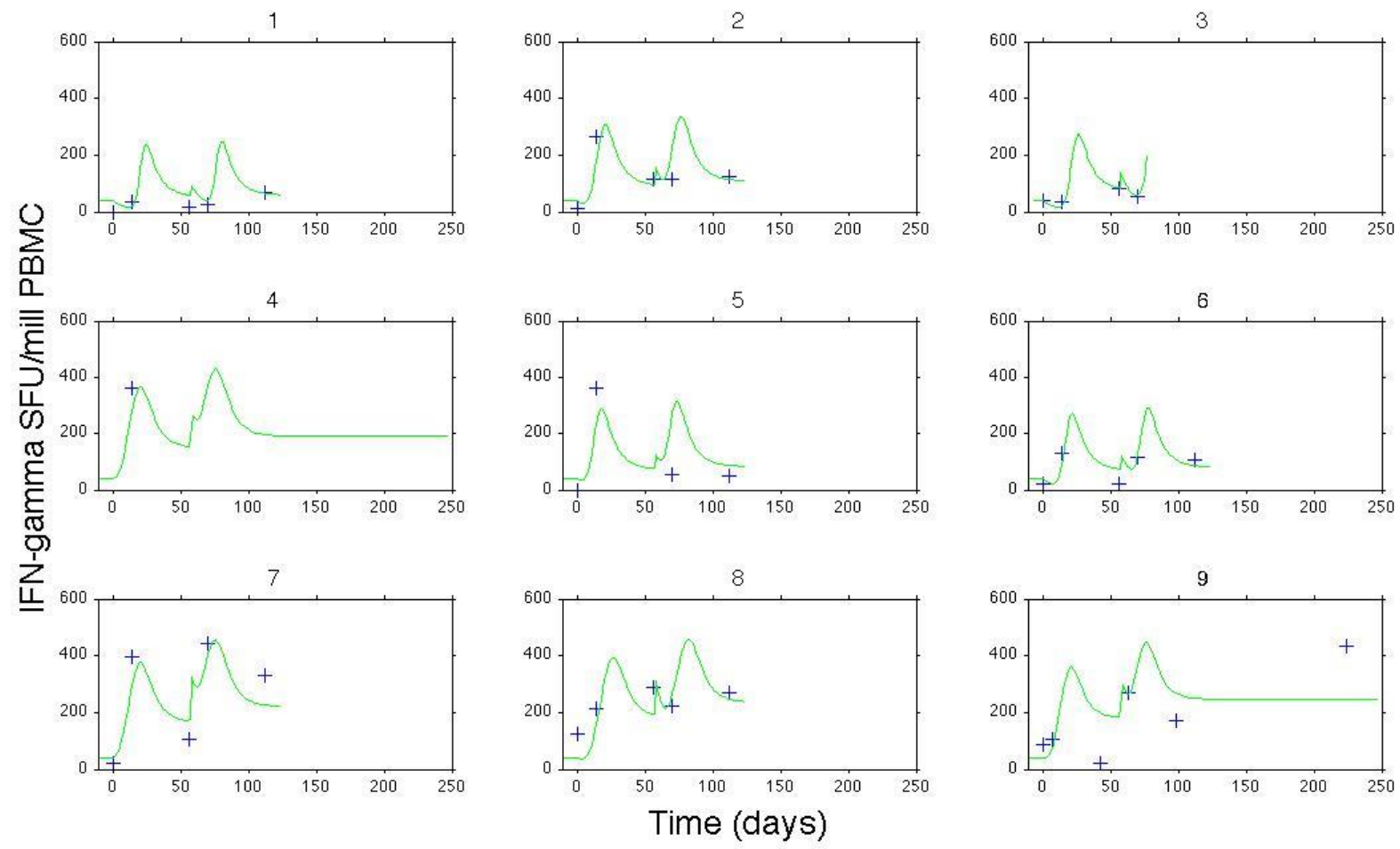


Figure S12. Model predictions for each participant of the human data set. Plot 1 of 2.

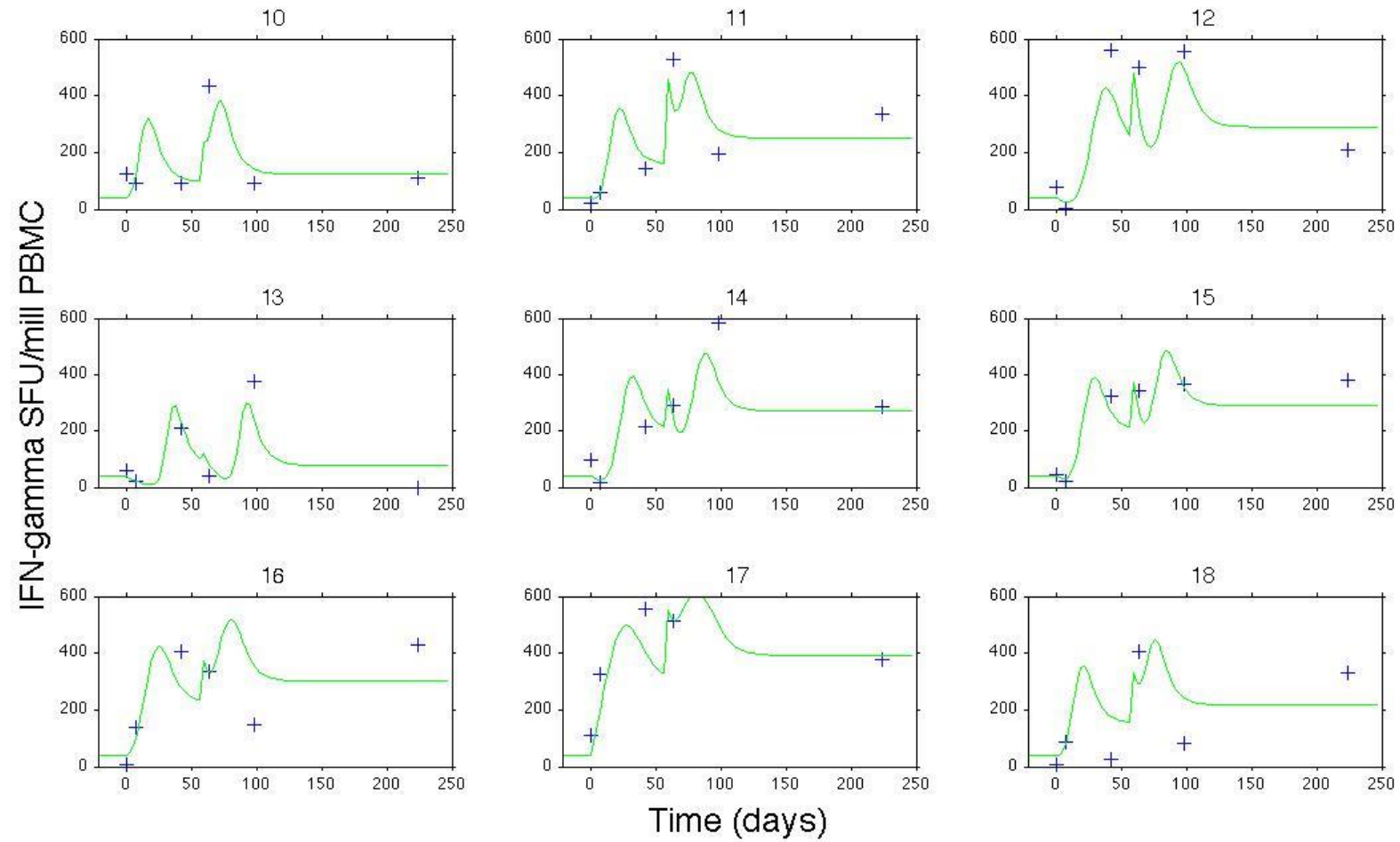


Figure S13. Model predictions for each participant of the human data set. Plot 2 of 2.

### Validation of Pooling Human data across Vaccine Type

Table S8 shows the result of indexing vaccine type on the estimated model parameters from the human pooled model.

-2LL value for pooled model	Vaccine type indexed on parameter(s)	Results		Difference in -2LL from pooled model (pooled model-covariate model)	0.01 level significant? (2 or 4 d.f.) (Chi <sup>2</sup> test 2 d.f.: crit val = 9.21, 4 d.f.: crit val = 13.28)
		Parameters with RSE >30%	-2LL		
1231	b	$\beta_{TEM}, \tau$	1281	-50	(2 d.f.) No -2LL larger
	c	b, $\beta_{TEM}, \tau$	1241	-10	(2 d.f.) No -2LL larger
	$\beta_{TEM}$	None	1292	-61	(2 d.f.) No -2LL larger
	$\tau$	b, c, $\beta_{TEM}$	1326	-95	(2 d.f.) No -2LL larger

	b, c	c, $\tau$	1262	-31	(4 d.f.) No -2LL larger
	b, $\beta_{\text{TEM}}$	$\beta_{\text{TEM}}$	1346	-115	(4 d.f.) No -2LL larger
	b, $\tau$	All	1363	-132	(4 d.f.) No -2LL larger
	c, $\beta_{\text{TEM}}$	All	1271	-40	(4 d.f.) No -2LL larger
	c, $\tau$	$\tau$	1308	-77	(4 d.f.) No -2LL larger
	$\beta_{\text{TEM}}, \tau$	All	1518	-287	(4 d.f.) No -2LL larger

**Table S8. Results of indexing the vaccine type covariate on all combinations of estimated parameters in the human pooled model**

Table S8 shows that the vaccine type covariate was not associated with a significant improvement in model fit from the model fit to the pooled human data. This result was not surprising as H56 and H1 have been shown to have a similar immunogenicity profile [236]. As indexing on two model parameters on vaccine type resulted in unidentifiable model fits (for all), we did not analyse the effect of indexing all combinations of three or more model parameters on vaccine type.

**Analysis 3: Use calibrated mathematical models in analysis 1 & 2, and a vaccine dose allometric scaling assumption, to predict the human immune response dynamics and predict the most immunogenic dose in humans**

*Sensitivity analysis of vaccine dose allometric scaling factor*

In analysis 1ii, the estimated parameter  $\beta_{\text{TEM}}$  increased by 168% (0.056 to 0.15) from the high to middle dose group and by 311% (0.056 to 0.23) from the high to low dose group. Applying these changes to parameter  $\beta_{\text{TEM}}$  in the human model parameter set (Table S9), resulted in a value of 0.091 and 0.059 for the low and middle dose group, respectively (Table S9). Using these values for  $\beta_{\text{TEM}}$  in humans, the predicted median number of IFN- $\gamma$  secreting CD4+ T cells at day 224 were 757, 542, and 188 (SFU per million PBMC) for the low, middle and high (0.3-3.3  $\mu\text{g}$ , 16.7 $\mu\text{g}$  and 50 $\mu\text{g}$  H56/H1+IC31, respectively) dose groups, suggesting the low dose (0.3-3.3  $\mu\text{g}$  H56/H1+IC31) may be most immunogenic in humans (Figure S14). This result which supports the findings using a scaling factor of 10. Using both scaling factors, a range of 1-3.3  $\mu\text{g}$  H56/H1+IC31 may be most immunogenic dose in humans.

	Mouse					Human			
	Pooled (analysis 1i)		Dose covariate (analysis 1ii)			Pooled (analysis 2)		Predicting dose (analysis 3)	
Parameter (unit)	Value	RSE (%)	Dose group	Value	RSE (%)	Value	RSE (%)	Dose group	Value
Death rate of Transitional effector memory cells, $\mu_{TEM}$ (per day)	0.3 (F)*	-		0.3 (F)*	-	0.2 (F)**	-		0.2 (F)**
Transition rate from Transitional Effector to Central Memory cell type, $\beta_{TEM}$ (per day)	5.5 (E)	17	Low	0.23 (E)	14	0.022 (E)	31	Low	0.091 (P)
			Middle	0.15 (E)	23			Middle	0.059 (P)
			High	0.056 (E)	26			High	0.022 (F')
Replication rate of Central Memory cells (per day)	0.4 (F)***	-		0.4 (F)***	-	0.4 (F)***	-		0.4 (F)***
Central Memory cell replication time, $\tau$ (days)	1.1 (E)	2		1.1 (E)	7	0.34 (E)	35		0.34 (F')
Transition rate from Central Memory to Transitional Effector type, $\beta_{CM}$ (per day)	10 (F) <sup>§</sup>	-		10 (F) <sup>§</sup>	-	10 (F) <sup>§</sup>	-		10 (F) <sup>§</sup>
Recruitment of Transitional Effector rate $\delta$ : Gaussian equation scalar, a (# cells)	92.9 (E)	14		103 (E)	13	51 (E)	23		51 (F')
Recruitment of Transitional Effector rate $\delta$ : Gaussian equation mean, b (days)	6 (E)	8		6.2 (E)	10	16.6 (E)	20		16.6 (F')
Recruitment of Transitional Effector rate $\delta$ : Gaussian equation variance, c (days)	0.91 (E)	15		0.89 (E)	7	5.7 (E)	13		5.7 (F')

Table S9. Population parameters for mice and humans from model calibration (analysis 1&2) and prediction (analysis 3). All estimated model parameter standard deviations were fixed at 0.5. Abbreviations: RSE = relative standard error, F=Fixed, E=Free parameters that were Estimated using NLMEM, F' = fixed to value found in analysis 2, P=predicted (using scaling factor 3.33), fixed to value in literature: \* [341], \*\*[342], \*\*\*[81]. <sup>§</sup> Fixed to be very fast.

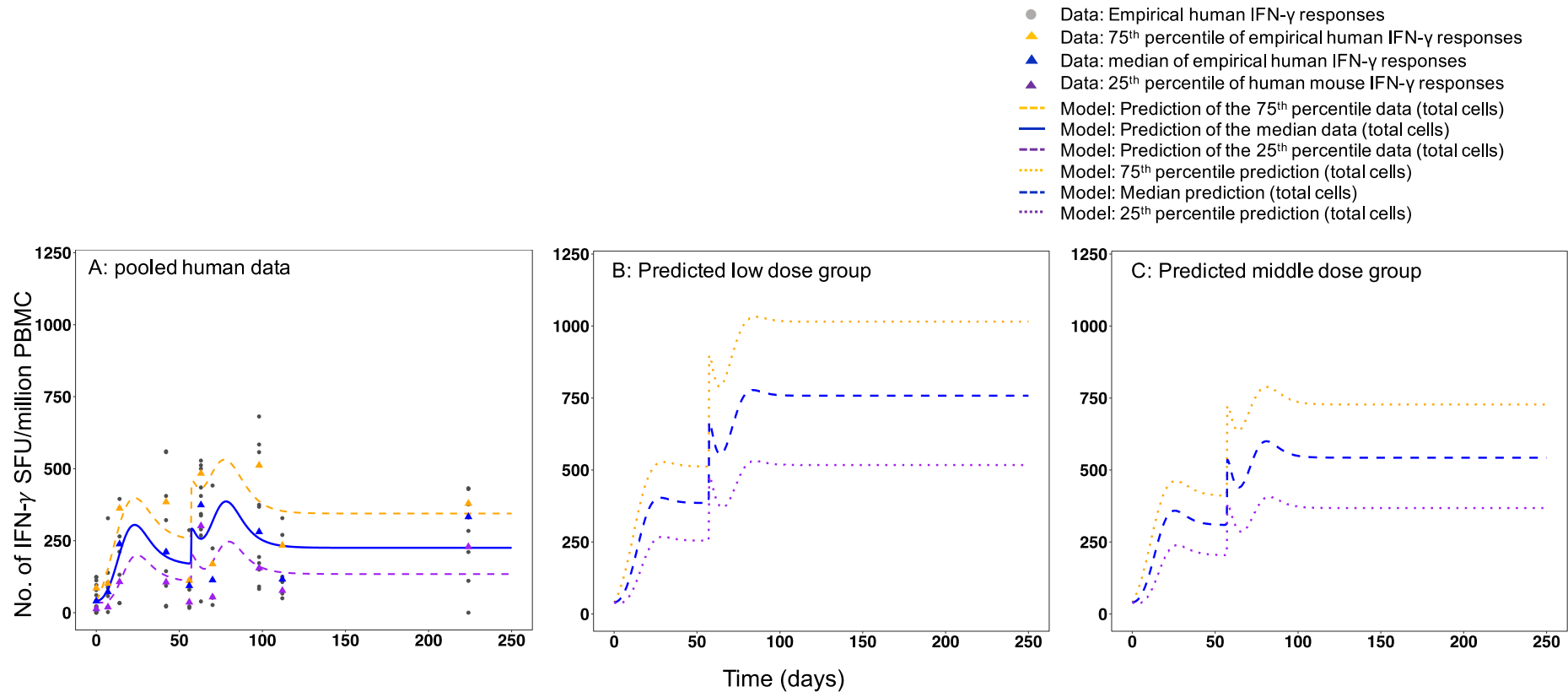


**Figure S14.** Empirical and model predicted number of IFN- $\gamma$  secreting CD4+ T cells over time for A. pooled human data (all data, pooled over vaccine type) ( $50 \mu\text{g}$  H56/H1+IC31), and the predicted human immune responses following a B. low (mouse-data mapped dose of  $0.3\text{-}3.33 \mu\text{g}$  H56/H1+IC31) or C. middle dose vaccination (mouse-data mapped dose of  $16.7 \mu\text{g}$  H56/H1+IC31) assuming a dose allometric scaling factor of 3.3. A. Grey points correspond to number of IFN- $\gamma$  secreting CD4+ T cells measured over time by ELISPOT assay in human PBMC after receiving vaccination of H56/H1+IC31 at day 0 and day 56. Median responses over time are marked by blue triangles, the 75<sup>th</sup> percentile responses by an orange triangle and the 25<sup>th</sup> percentile responses by a purple triangle. The model prediction (total cells) (parameters in Table S9) is plotted against the median data (blue line). The orange and purple dashed lines are the model prediction (total cells) of the 75<sup>th</sup> and 25<sup>th</sup> percentiles of the data, a result of the variation in the estimated parameters (standard deviation fixed to 0.5 for all parameters (Table S9)). In B. and C. Median (blue dashed), 75<sup>th</sup> (orange dots) and 25<sup>th</sup> (purple dots) of the model predicted human responses after mapping from the mouse dose group model calibration (predicted parameters in Table S9).

## Additional Discussion

### Model Assumptions

Key model assumptions from the IS/ID model are outlined in Table S10.

Assumption	Implications for model
<p><b><u>Baseline responses were fixed at the median value</u></b></p> <p>In this model, the initial values for the Transitional Effector Memory cells (TEM<sub>0</sub>) were not estimated. This is due to the fact that all mice IFN-<math>\gamma</math> responses at baseline were based on measurements from one unvaccinated mouse and therefore were all zero. As all human participants in the clinical trials were previously BCG vaccinated and no other human covariates were considered that could impact on a baseline response, the baseline responses were fixed to the median value. This also aided in avoiding over parameterisation compared to the small sample size of the human data.</p>	
<p><b><u>Central Memory (CM) cells do not die</u></b></p> <p>The central memory cell population is assumed to be maintained by a constant turnover, so we assumed the death rate could be omitted from both the human and mouse model [316]. Although there is evidence to suggest CD4<sup>+</sup> long-term memory cells turnover may diminish with time [325, 326], we assumed this does not affect the time frame of the model.</p>	<p>Introducing a death rate of memory cells would result in a decline of the long-term responses.</p>
<p><b><u>Replication followed by transition of CM cells after revaccination and rate of transition, <math>\beta_{CM}</math></u></b></p>	

<p>In the model, after revaccination, the CM cells replicated at a fixed rate for time <math>\tau</math>, which was estimated in the model calibration stage. Only after replication had occurred, the cells transitioned back to TEM cell type at a rate <math>\beta_{CM}</math>, which was assumed to be fast. Although this may be a simplification of the host immune response dynamics, it was necessary to assume as we did not have information on <math>\beta_{CM}</math>. We therefore considered the transition of CM cells to TEM cells as a result of revaccination to be a proliferation followed by a “burst” as opposed to a slower gradual transition (where proliferation and transition occur simultaneously). We believe this assumption is justified as the purpose of CM cells are to mount an immune (in our case, IFN-<math>\gamma</math>) response faster than a primary response as a result of re-exposure to the antigen (revaccination) [44] and a “burst” response is an effective method to represent this dynamic.</p>	
<p><b><u>IFN-<math>\gamma</math> responses are not scaled to host body size</u></b></p> <p>The ELISPOT assay readout is conventionally measured per million cells in all species and we considered the model to represent a systemic response regardless of host blood volume, it was not necessary to scale the ELISPOT readout to reflect body size. As our focus was on translating the <i>change</i> in dynamics due to change in dose between mouse and human, therefore this scaling the ELISPOT readout was not essential.</p>	
<p><b><u>CD4+ T cell stimulation greatly simplified</u></b></p> <p>The immune response to vaccination is a complex network of cells and cytokines behaving nonlinearly over time. In the Th1 response to <i>Mtb.</i> infection (or</p>	<p>If data were available on IL-12 or other cytokines believed to be important to an immune response to BCG, It is possible that <math>\delta</math> could be modelled as a</p>

<p>vaccination), innate and adaptive cells interact to optimise and maintain a protective response [37]. Very simply, cytokines secreted by innate cells after infection or vaccination, such as IL-12, work to stimulate adaptive cells to produce IFN-<math>\gamma</math> that both encourages innate cells to phagocytose bacteria and produce more IL-12 [66, 323]. As such, a feedback stimulation loop is established. In addition, to avoid an over-inflammatory response (which is harmful to the host) cytokines such as IL-10 are produced to regulate and dampen the immune response [324]. In the model, function <math>\delta</math> is used to represent the delay of T cell initiation due to processes such as antigen processing and presentation and the decline of T cell responses due to depreciation of the required stimulation (creating a “n-shaped” curve). However, <math>\delta</math> neglects the influence of stimulation amplification as a result of cytokine feedback loops, amongst other co-stimulation factors. As such, <math>\delta</math> is a generalization of the complex networks required to protect against infection or vaccination and may not be as prolonged as required to generate a response to vaccination.</p>	<p>parallel “innate response” compartmental model. Incorporating such a model would provide insight into the innate cell mechanisms and thus strengthen the conclusions we draw on the T cell dynamics.</p>
<p><b><u>Transition and replication of transitional effector cells happens in Lymph node before entering the blood</u></b></p> <p>The model assumes that the recruited transitional effector cells are former <i>Mtb.</i>-specific naïve CD4+ T cells that have clonally expanded within the <i>lymph node</i> and exited into the blood stream. Under this assumption, transitional effector cells do not replicate in this model. The rate of naïve CD4+ T cell clonal expansion</p>	<p>To incorporate replication of transitional effector cells into the model, a parameter <math>R_E</math> would be applied which would determine the rate at which replication occurs, dependent on the current transitional effector cell count.</p>

changes with time dependent on stimulation from innate processes and antigen presence [44] so could be considered to be incorporated into $\delta$ .	
--	--

**Table S10. Main assumptions of the model and implications on challenging these assumptions**

## **Chapter 6. Discussion & Conclusion**

Decision making in vaccine development employs relatively antiquated methods compared to the methods employed for drug development. As such, developers may be discarding vaccine candidates and wasting considerable resources. This failure to utilise modern methods may be, in part, due to the complexities in measuring a biomarker of vaccine efficacy and defining the dynamics of the immune system, but also simply represents a failure to harness quantitative expertise into vaccine development. In this thesis, I take the initial step to explore the potential utility of PK/PD methods for vaccine development, which I define as vaccine Immunostimulation/Immunodynamic (IS/ID) modelling.

The strengths, weaknesses and implications of the work outlined in the separate chapters of this thesis are discussed in the associated publications. Here I outline strengths, weaknesses, implications and future work of the thesis as a whole.

### **Summary of findings**

I aimed to apply mathematical modelling to IFN- $\gamma$  responses following vaccination with TB vaccine, BCG, to establish if differences in response dynamics were due to population covariates in humans and macaques. Secondly, I aimed to use these results to determine which macaque subpopulation best represented human responses. In addition, we generated data on IFN- $\gamma$  responses in mice after receiving varying doses of novel TB vaccine H56+IC31 and mathematically determined the shape of the dose-response curve at early and late time ranges. I applied IS/ID modelling to the longitudinal mouse responses to establish how dose affects key model parameters and to human H56/H1+IC31 clinical data, allowing me to map model parameters between species. I then predicted the IFN- $\gamma$  response dynamics for the remaining doses in humans and consequently, potentially the most immunogenic dose.

I found that BCG status in humans (baseline BCG-naïve or baseline BCG-vaccinated) was associated with differences in the peak and end response and the long-term IFN- $\gamma$  response after BCG vaccination (using simple regression methods) (paper 1). When the mathematical

model was calibrated to the BCG human data, differences in model parameters across the BCG status covariate were found; those that dictated the baseline and peak response magnitude and timing of peak. In the macaque population, differences in similar model parameters were found when the data was stratified by macaque colony of origin and Indonesian macaques had the closest immune response dynamics to the baseline BCG-naïve humans (paper 2).

A peaked curve was a better description of the mouse H56+IC31 IFN- $\gamma$  dose-response data than a saturating curve for early and late time points (paper 3). Calibrating a revaccination model to the data and mapping changes in the estimated mouse model parameters across dose group to the estimated human model parameters, I found at day 224 (a latest time point), the model-predicted median number of human IFN- $\gamma$  secreting CD4+ T cells were the highest for the dose group in the range 1-10 $\mu$ g H56/H1+500 nmol IC31. This suggests a dose of 1-10 $\mu$ g may be the most immunogenic in humans (paper 4).

## **Strengths**

The strengths of the work from each chapter are summarised as follows (see papers 1-4).

### ***Strengths of chapter 2/paper 1***

In chapter 2, I presented an analysis of the differences in key IFN- $\gamma$  immune response aspects (e.g. peak, long term responses and AUC) following BCG vaccination due to population covariates. This analysis has not been conducted before and provides valuable insights into which human population covariates do (and do not) influence these key response aspects. Thus, this work indicates in future stratification of vaccine trials to minimise variation in key BCG response aspects. The influence of monocyte to lymphocyte ratio on these responses has never been considered before.

### ***Strengths of chapter 3/paper 2***

In chapter 3, I extended the analysis from chapter 2 by applying a mathematical model to the human BCG response data and a macaque BCG dataset. This demonstrated the utility of mathematical modelling to quantify vaccine immune response dynamics and was an early example of IS/ID modelling.

Here, we used data on response to BCG after one vaccination of the licensed dose of BCG to determine the most representative macaque subpopulation for the human responses. Finding the most representative macaque model to test BCG immunogenicity is an important aspect of TB vaccine development, as BCG is regularly used as a control arm in current clinical trials. However, these results may not be generalizable to a different vaccination regimen, dose or for a new TB vaccine. It is possible that, as some new TB vaccines are BCG boosters (Figure 1.2, Table B.1 in Appendix B) and are therefore building on an existing BCG response, the most similar macaque model to human (in terms of the BCG response) may also be the most similar for these vaccines. To test this hypothesis would require the incorporation of new data on new TB vaccines. Despite this, our primary aim in chapter 3 was to apply novel mathematical modelling methods to the response data to quantify the dynamic *trends* of the data over time to statistically determine which macaque model should be selected to represent human responses. This is an improvement on the historical methods of preclinical/clinical comparisons, where qualitative observations, point estimates or summary measures such as AUC are used. As these methods rely on the absolute values of the response data, they are limited by sampling consistency. For example, sampling times in the macaque data differed across within and between macaque subpopulations (and between macaques and humans) and showed high variability over time. I would like to re-emphasize that our conclusions to chapter 3 are not that we have predicted which macaque model is the “winning” macaque model for TB vaccine development, only a macaque model that has the most similar responses to BCG as a subpopulation of humans. Other response factors are very important and should be considered in combination. For example, the natural susceptibility and pathology similarities, which are known to differ between macaque subpopulations [193, 205-207].

Although my model was a highly simplified version of the complexities of the immune system the model described the data well even for the small macaque sample sizes. A key strength

in using a simple model for translational purposes is that, providing the mathematical model is appropriate to all species, translating mechanism of response is simply mapping between model parameters. Such model-based allometric scaling is used in practice in PK/PD to scale drug dynamics between animals and humans [265] but has never before been used in vaccines. I presented a first example of vaccine model-based allometric scaling between macaques and humans.

### ***Strengths of chapter 4/paper 3***

In chapter 4, I successfully generated an intensive time course of IFN- $\gamma$  response data to vaccination where AUC and peak analysis showed a trend toward higher responses over time in the lower doses than in the higher doses. By using mathematical curve fitting, I showed definitively, that the IFN- $\gamma$  dose-response follows a peaked shape instead of the commonly assumed saturation shape for multiple time ranges. This level of quantitative analysis of vaccine dose response curves and the change in dose response shape over time has never been conducted before.

### ***Strengths of chapter 5/paper 4***

The final work in chapter 5 presents the first example of the allometric relationship between vaccine immune dynamics between mice and humans through the mapping of estimated model parameters between the two species. I was able to provide a guide of the most immunogenic dose in humans, based on mouse IFN- $\gamma$  responses. This predicted dose range in humans has recently been corroborated by preliminary empirical results from the phase 1/2a clinical dose ranging study of H56 + 500 nmol IC31 (ClinicalTrials.gov no. NCT01865487) (unpublished, personal communication, Thomas Scriba), where developers have decided to use 5  $\mu$ g H56+IC31 in future clinical trials, rather than 50  $\mu$ g in previous trials. These modelling methods mirrors techniques incorporated in PK/PD modelling for drug development and have never been used before for this purpose in vaccine development.

Again, although my model was simple, it was a good description of the mouse dose group and human data and produced biological meaningful results. Due to data sample size, I was

required to constrain aspects of the model parameterization (i.e. fixing the standard deviations of the estimated model parameters) and data (i.e. grouping dose). Despite this, my choice of constraints provided an optimal balance between obtaining identifiable model parameterisations and providing sufficient information on vaccine responses to achieve my aims.

Overall strengths of the thesis are as follows.

### ***Novel mathematical modelling methods***

My work proposed a new field of science: a mathematical and statistical modelling framework for accelerating vaccine development. My work incorporated methods to quantify biological *mechanism* using mathematical models, which, to my knowledge, has never been directly integrated into the areas of vaccine development I focused on here, especially in determining optimum vaccine dose. Using biological mechanistic models to describing longitudinal data has the advantage over a purely statistical description as data on known biological parameters of the model across species can aid in more effective allometric translation of vaccine responses. We can also make new biological inference using mechanistic models by calibrating them to responses by subpopulation (e.g. dose grouping) and IS/ID models can be generalised to describe similar response for other vaccines (e.g. T cell mediated vaccines for cancer). Purely statistical description is an effective tool for describing and comparing the *shape* of longitudinal data. However, this does not take into account the underlying biological mechanism that produced that dataset and as such, may not as generalizable for other subpopulations or vaccines. Additionally, integration of further biological complexity with the provision of more immunological data is intuitive for mechanistic modelling compared to statistical modelling. There is a new recognition of the need for mathematical modelling to accelerate vaccine development [185, 344], and I believe I present the first steps in achieving this for TB vaccines.

### ***IS/ID mathematical model based on known CD4+ T cell dynamics***

I spent considerable time developing the model alongside experts to ensure a simple model that provided insight into the IFN- $\gamma$  immune response. The IS/ID model in this thesis assumes a linear immune pathway once vaccination is administered, i.e. effector responses are initiated once antigen presentation and naïve T cell differentiation has occurred, they then deplete and transition to a memory phenotype. Once memory cells experience exposure to antigen again (revaccination), they revert to effector phenotype. This is an acknowledged pathway for CD4<sup>+</sup> T cells; central memory CD4<sup>+</sup> T cells have been shown to have developed directly from effector cells [327-329]. I chose this pathway after consideration of the literature on TB vaccine immune responses. However, an alternative model has been suggested, whereby effector and central memory cells are initiated simultaneously after vaccination [81, 83, 330]. This could be another possibility for the model.

I chose the terminology “Transitional Effector Memory” to coincide the terminology used by current TB vaccine developers. Sharpe et al use the term Transitional Effector Memory to describe activated, non-lymphoid homing (measured by low expression of CC47 marker) in a recent study of BCG vaccination in macaques. These cells were detected early on after vaccination with BCG in macaques and correlated with IFN- $\gamma$  levels, both of which declined over time [345]. However, other authors may suggest the terms “Transitional Effector” or “Activated Effector” [346] or “Cells with Effector Functionality” [347] as a more appropriate name for the assumed the short-lived, activated cells in my model. While I agree these definitions would also be appropriate for the IS/ID model, I wanted to take into account the possibility that the IFN- $\gamma$  producing CD4<sup>+</sup> T cells initially recruited into the IS/ID model may have already been primed by NTM. This would suggest that any cell in the IS/ID model system may already be a “memory” cell type. Soares et. al. state that excessive stimulation of CD4<sup>+</sup> T cells by antigen is likely to lead to an effector memory type response [327]. Considering the age of the participants we use in this thesis, is likely that they will have been persistently exposed to NTMs, which are known to elicit a mycobacterial specific IFN- $\gamma$  response in vaccination studies [320, 348].

I also use the terminology “Resting Central Memory” (CM). Soares et. al. and Sharpe et. al. show that after BCG vaccination, CM cells (measured by low expression of CD4<sup>+</sup>5RA and high expression of CCR7 [327] and high expression of CD28 and CCR7 [345]) were present in the later stages [327, 345] and that these cells transitioned from effector-type activated cells and

expressed high levels of Bcl-2, an anti-apoptotic marker indicating long-life [327]. It is generally acknowledged, however, that CM cells, produce predominantly IL-2 [83] and less IFN- $\gamma$  than their effector counterparts, however, there is evidence to suggest that they still produce IFN- $\gamma$  even at low levels [327, 349, 350]. The terminology for this group could potentially be framed as “Resting Long-Lived Memory” cells.

In conclusion, there may be debate around the immune cell terminology used in the IS/ID in this thesis, however I believe the characteristics of the cells in the model and the transitions between them should receive the focus, i.e. short versus long lived, active versus resting. It is acknowledged also that the dynamics and terminology for CD4+ T cells in TB research is still an area of great investigation and discoveries into this field are current and changing. With this in mind, my model was designed to clearly communicate with my intended *current* collaborators and future revisions of the IS/ID model will take into account any shifting terminology in the field.

### ***Insights into new biological mechanism***

During the process of development and parameterisation of the IS/ID model, valuable discussion around model structure led to interesting questions around vaccine immune response biology and mechanism. For example, in the case of the revaccination model, are there important differences in “reactivated” Transitional Effector Memory (TEM) cells due to revaccination compared to those following primary vaccination? i.e. would two compartments, TEM<sub>primary</sub> and a TEM<sub>revaccination</sub>, be a more accurate representation of revaccination biology? However, without data on these mechanisms (and on the cell groups they apply to) it would not be possible to add these to the model. This raises further questions around the data availability; what data would I need to parameterise this and do the tools exist to be able to collect such data? This thesis and further IS/ID modelling of vaccine immune responses may be a catalyst to new discovery around biological mechanism and laboratory assays.

### ***Mitigation of potential risks***

Conducting novel science such as this thesis comes with risk and I worked hard to mitigate any risks I felt would jeopardise producing meaningful results. One of the biggest risks we faced was the potential of the H56+IC31 multi-dose mouse data to be uninformative, which would have not allowed me to complete the predictive dose modelling in chapter 5. To reduce this risk, we had early interactions with colleagues at SSI who had previously produced informative data with H56+IC31 in mice. Secondly, we doubled the ELISPOT plates for every time point testing two incubation times; 24 and 48 hours providing two avenues for results (see paper 3). Finally, we regularly read the ELISPOT plates to monitor the results and check for anomalies. Risks were also involved in developing the model and calibrating it to the data. I needed to ensure my results were precise given the model structure and data sample sizes. To achieve this with the data I had available, required using a simple IS/ID model (with a maximum of two compartments). These models are easily communicable, which in the context of this thesis is vital as I aimed to introduce mathematical modelling to an environment where it is not regularly used. Another benefit to these methods is the ability to easily adapt model structure, essential for integrating further biological complexity.

### ***The use of the Nonlinear Mixed Effects Modelling framework***

I used the method of NLMEM to calibrate my model to the longitudinal data in chapters 3 and 5. In a survey of PK/PD modelling between 2002 and 2004, 92% of studies used NLMEM as the parameter estimation method [283]. However, other methods of parameter estimation are available. Naïve pooled analysis assumes all data comes from the same individual and while the model parameters can be estimated, any variation in response is ignored, which in my case is not appropriate. In a two-stage approach, each individual's model prediction is made and summary statistics on the mean parameters are made. Both of these methods require each individual to have extensively sampled and balanced data in order to make valuable predictions [351, 352]. Additionally, alternative algorithms to estimate the parameters within the NLMEM framework are available. NONMEM [353] is acknowledged as one of the first NLMEM software developed for PK/PD analysis and uses the First Order (FO) and First Order Conditional Estimation (FOCE) algorithms [354]. FO and FOCE methods use simplification of the likelihood equation to estimate the parameters [281]. I used Monolix to estimate the parameters [318] which in comparison, is a new software and utilises a more

exact method of parameter estimation - the SAEM algorithm. SAEM has shown to be robust and accurate even for sparse data [355], more so than other methods (FO and FOCE). However, computation time is longer due to the complexity of the method [356, 357]. There are benefits and drawbacks to all NLMEM methods depending on the data and model; the superiority of one method compared to another has never been shown definitively [352] .

## **Weaknesses & Challenges**

### ***Weaknesses of chapter 2/paper 1***

In chapter 2, although I did show differences in key IFN- $\gamma$  immune response aspects (e.g. peak, long term responses and AUC), the fundamental biological mechanisms driving these differences were not explored. However, chapter 2 was considered a preliminary analysis of the human BCG response and the describing underlying mechanism using an IS/ID model was the aim of chapter 3.

### ***Weaknesses of chapter 3/paper 2***

In chapter 3, IFN- $\gamma$  responses in a macaque population were available. However, the sample sizes of the macaque colony subpopulations were variable. With these smaller sample sizes model parameterization and validation were less reliable than for the larger groups; the estimated model parameters were more uncertain. Nevertheless, conventional vaccine studies in macaques are often limited to 6-9 per group due to space and cost. These smaller macaque experiments are then used to inform clinical vaccine trials, making the small sample sizes used here, more representative of current vaccine development. The uncertainty I experienced for these small groups highlights the need for larger sample sizes and could be used to push the vaccine development field to increase sample numbers to reduce response uncertainty.

It may appear that the closeness of the baseline response (in the model, the parameter  $TEM_0$ ) could be considered the sole indicator of which macaque subpopulation should be “chosen”. However, the goodness of fit (BIC) of the macaque subpopulation model predictions to the

baseline BCG-naïve human population data (figure 4, paper 2) are not ordered the same as the absolute difference in magnitude of baseline response between the macaque subpopulations and the baseline BCG-naïve human population, (i.e. baseline  $TEM_0$  value closeness ranking were 1. (closest to baseline BCG-naïve human  $TEM_0$  value) Indonesian cynomologus, 2. Indian rhesus, 3. Chinese cynomologus, 4. Mauritian cynomologus whereas the goodness of fit statistic in Figure 4 rankings were: 1. (best fit) Indonesian cynomologus, 2. Indian rhesus, 3. Mauritian cynomologus, 4. Chinese cynomologus). This suggests that the baseline response is not necessarily the best indicator of similarity between macaque and human responses and overall dynamics should be considered.

In chapter 3, I gave the first example of the application of my IS/ID model to vaccine immune responses. As discussed, a strength of my IS/ID model is its simplicity. However, in order to make a simple model, key assumptions around the immunological mechanism were made, as such, some immunological detail had to be omitted. For example, I assumed a nonlinear non-mechanistic equation for rate parameter,  $\delta$ , to represent T cell stimulation, attributed to innate cell processes. However,  $\delta$  is not supported by innate response data and therefore does not represent a specific group of cells or cytokines. Consequently, there is no direct biological interpretation of the  $\delta$  rate parameters. Variation in vaccine immune responses can be large across different ages and populations, possibly attributed to underlying differences in genetics or exposure rates. Where demographic data was available, I tested for differential IFN- $\gamma$  responses across human and animal subpopulations. Data on geographical location of participants was not available in chapter 3 (I did not have access to longitudinal responses in the African participants) so I could not determine differences in IFN- $\gamma$  dynamics by geography. In chapter 3, I stratified the macaque results by colony of origin, but no other population covariates. Data is available in these macaques on age and this is intended as further work. In summary, limited data constricted the conclusions I could make around immune response dynamics (the IS/ID model structure) and how they varied across the population.

### ***Weaknesses of chapter 4/paper 3***

In chapter 4, my aim was to generate H56 multi-dose data that would provide sufficient longitudinal data for the IS/ID model calibration. Dose concentration feasibility and animal

cost limited the size of the study. A wide range of doses were chosen to “capture” a wide response range which we believed would provide adequate information on the full dose response curve. We successfully predicted a most immunogenic dose by fitting a peaked curve to the dose response data (paper 3). However, there was uncertainty associated with these predictions which was potentially due to a lack of response information between dose 0 and 0.1  $\mu\text{g}$ , which would provide information on the increase of the peaked curve. As a result, I could not fully capture the H56+IC31 dose response curve as the dosing was weighted towards the higher end of the curve. Despite this, I showed a definitive decline in the dose-response at the higher dose range (approximately after dose 1  $\mu\text{g}$  H56+IC31) and found that the probable most immunogenic dose is lower than the minimum dose currently used. I suggest further H56+IC31 dose testing in mice to establish the curve between 0 and 0.1  $\mu\text{g}$  H56+IC31.

Additionally, in chapter 4, I chose sampling times that would potentially capture the peak of response between primary and revaccination, after revaccination and a long-term response based on previous H56-series response data. Based on the vaccination times (day 0 and 15) we concentrated our sampling between vaccination times and shortly after revaccination to try and ensure that the peak responses were captured. Our experiment design led to informative results of the IFN- $\gamma$  dynamics by dose in chapter 5. Nevertheless, it is possible that the experiment design could be improved. For example, sampling points were more extensively between primary and revaccination than after revaccination (5 and 4 time points, respectively). It is possible that redistribution of these sampling points (potentially weighted to later time points) may provide a more informative model calibration. Additionally, redistributing the mice such that there were more mice per dose and less doses may have provided a better model fit. Model-based optimisation techniques are used in drug development to establish the optimal experiment by systematically simulating and analysing different designs. The goal is to maximise information on response dynamics using the minimal resources [358, 359]. We did not have the capacity to use such methods to find an optimal experiment design in this thesis, but this is an aim of future work.

#### ***Weaknesses of chapter 5/paper 4***

In chapter 5, the data on human demographics such as age, gender and ethnicity was not available for the H1 trial. The small sample size in this human dataset also meant I was forced to fix the majority of the model parameters to achieve an identifiable model parameterisation. As a result, information on the variation in response dynamics, especially by population covariate, was limited. In chapter 5, I relied on vaccine dose allometry to create the mapping from mouse to human response. In drugs, the systemic nature of their effect allows for dose scaling to be based on animal body weight [360]. It is generally acknowledged that vaccine dose allometric scaling does not benefit from precision gained in drug scaling [360, 361]. This may be due to the complexity in the immune response elicited by vaccination which relies on complex interactions that behave nonlinearly over time and across multiple biological scales (e.g. molecular to cellular to whole systems). I assumed a dose allometric scaling factor of ten between mouse and human, based on published data by the developers of H56 [230, 234, 235] (I also considered the scaling factor 3.33 in a sensitivity analysis). However, this scaling factor has not yet been substantiated as without an established relationship of dose to efficacy in humans, this scaling is difficult to verify. As mentioned previously, for other TB vaccines the dose scaling is variable; a scaling factor is assumed to be ten times from mouse to human for BCG [241, 242], 100 times for MVA 85A [213, 241] and 0.5 for VPM1002 [241, 243]. I also assumed that the scaling factor was linear with respect to dose i.e. the scaling factor of ten could be used to predict the dose value of all dose groups in humans. Current hypotheses suggest that a nonlinear relationship may be more accurate i.e. decreasing as dose decreases (personal communication, Thomas Evans MD). However, there is currently no evidence to support this. In conclusion, the H-series dose scaling factor between mouse and human is currently vastly under researched. It is vital that further predictions of human immune responses using IS/ID modelling should be supported by more in depth vaccine dose allometric evaluations.

There were some overall limitations and challenges to this thesis as a whole.

***The use of IFN- $\gamma$  as the sole marker of vaccine immunogenicity and the model as a systemic blood model***

Throughout the thesis, I chose the sole use of IFN- $\gamma$  as an indicator of TB vaccine immune response. This was guided by the data available to me during the project. This choice of TB response marker has been a longstanding limitation in the TB vaccine field as there is conflicting data on the protective ability of IFN- $\gamma$  on its own. A protective TB vaccine immune response is more likely to be a combination of cytokines or cell types [144]. For example, work by Andersen et al. showed that polyfunctional T cell responses emitting combinations of IFN- $\gamma$ , TNF- $\alpha$  and IL-2 after vaccination with H1+CAF01 were well sustained over long-term timelines; protective and maintained post-challenge with *Mtb*. [223]. Similar results were found after vaccination with TB vaccine MVA85A [362]. The combination of these cytokines secreted by the CD4+ T cells during an immune response to TB vaccination may alter the function of the cell [92], for example, it has been shown that when cells lose polyfunctionality and produce predominantly IFN- $\gamma$  they are close to “exhaustion” [363]. Therefore, omission of data on these cytokines may have implications for my model parameterisation, i.e. for the above example, the cell death rate parameter in the model (both chapter 3 and 5 models) may be affected. The nature of T cell cytokine secretion may also be dose dependent; it is plausible that the low IFN- $\gamma$  response observed for high doses (in chapters 4 and 5) could be a result of cells being removed quickly from the model due to exhaustion or that a higher dose induces CD4+ T cells secreting cytokines other than IFN- $\gamma$  that the ELISPOT assay cannot detect. In summary, the nature of the response for any TB vaccine dose cannot be fully characterised with only IFN- $\gamma$  data. To fully establish an effective immune response in the case of TB vaccines requires comparison of immune response against bacteria count measures. I did not collect this data in the thesis, as it was not viable for me to do so. I acknowledge that the mixed evidence that IFN- $\gamma$  levels correlate with protection in humans [135-137] and macaques [193] is a limitation for the results in chapters 2 and 3. However, I felt that previous evidence showing the correlation of bacteria counts and H-series vaccination IFN- $\gamma$  response (i.e. lower bacteria count for low doses) in small animals [217, 224] was sufficient to justify the results in chapters 4 and 5. Further to this, as my model represents IFN- $\gamma$  secreting CD4+ T cells measured using the ELISPOT assay in PBMC in humans and macaques, and splenocytes in the mouse, it is a generalisation of vaccine immunogenicity, homogeneously mixed in the blood. However, TB immune activity is mainly focused around the lungs and draining lymph nodes [37]. For ethical and logistical reasons, blood is the most viable measure of TB vaccine immunogenicity in humans, therefore, it is vital that its ability to accurately reflect localised

TB immune responses is understood. This is a current area of TB research with mixed support [92, 364]. However, even though the immune marker (and assay choice) have been subject to criticism throughout the thesis and as such presented here as limitations, in the current TB vaccine pipeline, IFN- $\gamma$  and the ELISPOT assay are continually used to assess vaccine immunogenic in order to progress vaccines through development phases. With this in mind, I wanted my IS/ID model structure and output to reflect conventional immunogenicity measures used in TB vaccine development. This meant using IFN- $\gamma$  as the sole marker of vaccine immunogenicity and a systemic blood model. In conclusion, while this is a limitation of this thesis, it is driven by a limitation of the TB vaccine development field.

### ***Omission of important subpopulations***

Two of the most prioritized human subpopulations in TB research are those who have latent TB infection (LTBI) and/or HIV positive. TB clinical trials are commonly stratified by these two covariates. Data was not available on HIV positive individuals during the project timeline. Even though data was available on LTBI status in both the H1 and H56 clinical trials, I did not include this covariate to analyse in this thesis. This was due to little information on the influence of these LTBI on the precise immune mechanism and dose response [240]. Analysing responses from across further subpopulations would be essential in future work. Although I included subpopulations where data were available, the implication of not testing for subpopulation differences is non-generalizable results.

### **Implications**

Each chapter in the thesis has specific implications for different aspects of vaccine development (see papers 1-4). In paper 1 and 2, I showed the BCG vaccination status (baseline naïve or vaccinated) has an impact on IFN- $\gamma$  responses to BCG vaccination, further supporting that stratification by the covariate is important in further TB vaccine research. Paper 2 also implies that the colony of origin of macaque used to represent humans in further BCG (and potentially new TB vaccine) research should be carefully considered and mathematical modelling as a translational tool can inform which macaque colony to select. Results by Langermans et al. [207] and Sharpe et. al. [206] showed a significant difference in IFN- $\gamma$

responses (after BCG vaccination and *Mtb.* challenge, respectively) between macaques due to colony of origin. However, to my knowledge, no mechanistic and statistical comparison from macaque to human BCG response, as presented here, has been published. Paper 3 suggests that lower doses than previously explored in mice using very similar vaccines [217, 219, 233, 338, 365], would be preferential for further study, a result supported by previous work in H4 + IC31 vaccine [217]. Finally, in paper 4, using the data in paper 3 and modelling predictions, my results imply that previous H-series clinical trials are over-dosing and in terms of an IFN- $\gamma$  response, the dose should be reduced in further research. Previous empirical evidence [221, 232] and recent results (ClinicalTrials.gov no. NCT01865487) (unpublished, personal communication, Thomas Scriba), on the H-series vaccines supports this finding, where smaller doses were found to be equally or more immunogenic than larger doses.

***Mathematical modelling as a tool to accelerate vaccine development and eventual reduction animal and human exposure in testing phases***

Collectively, the results of the thesis imply that mathematical modelling may be a useful tool to accelerate vaccine development. I believe IS/ID modelling should be integrated into not only the early stages of animal experimentation, but used to inform clinical trial design in the same way PK/PD is an established tool in drug development. More specifically, further incorporation of mathematical modelling to vaccine development could help vaccine development move towards reduction in laboratory animals [10] for pre-clinical vaccine testing by focussing more on *in silico* than empirical experimentation (in line with the aims of the National Centre for the Replacement, Refinement and Reduction of Animals in Research (NC3R's)). However, in the preliminary stages of incorporating IS/ID modelling into preclinical research, extensive pre-clinical data would have to be gathered to calibrate and make inferences on IS/ID models (e.g. for paper 3). Following this, these results can be used to iteratively decrease the number of animals needed to design new experiments to test dose or vaccination regimen. Additionally, it is plausible that parameter estimation from one T cell mediated vaccine, maybe used as prior information for further IS/ID modelling work on other T cell mediated vaccines, thus reducing the number of animals required for development. Similarly, employing simulation based methods to predict vaccine clinical trial outcomes using models can also reduce exposure to humans in clinical trials (in terms of dose amount and

required trial sample sizes). My work also implies that, if modelling is to be incorporated into vaccine development, a shift in the way vaccine immunogenicity data is collected may have to occur. As modelling methods are not regularly used in the development of vaccines, data sufficient to populate models is not routinely collected. As such, further discussion around adaptation of current pre-clinical procedures to accommodate modelling should be a first step in incorporating IS/ID in vaccine development. Finally, common to modelling to inform policies in any arena, cross discipline learning and understanding of what models can do (and importantly, what they can't) are essential in the understanding of how IS/ID modelling can aid in vaccine development.

### **Future work**

The strengths, weaknesses and implications of this thesis highlight further questions that could lead to future work.

### ***Validation of the modelling predictions***

The results I produced in paper 4 have been corroborated by a phase 1/2a empirical study that ran parallel to the PhD measuring immunogenicity of varying H56 dose. These results are not yet published, but we have confirmation that the lowest dose 5ug was chosen, which falls within the range of the predictions I made in paper 4. This has been a promising validation of IS/ID modelling predictions as a legitimate tool for TB vaccine development.

Although we did not predict dose-dependent H56+IC31 efficacy in this work, the logical progression to this is to conduct a clinical efficacy trial to test this dose prediction in a healthy, BCG vaccinated population. Animal challenge studies could also be conducted alongside further IS/ID modelling to verify model predictions.

### ***Incorporation of important subpopulations***

Future IS/ID modelling work should consider the effects further human subpopulations have on immune responses to TB vaccination, prioritizing those with LTBI and HIV positive. Other

human population covariates to consider may include; age (infant, adolescent or elderly)[366, 367], sex [368], geographic location [165], and those that contribute to immunosuppression such as smoking [369], diabetes status [103] or helminth infection [107] as these have been shown to be risk factors for *Mtb.* infection or TB disease. Care must be taken when incorporating these covariates due to the affect they may have on the nature of the IFN- $\gamma$  response to *Mtb.* infection; elements of the current model may have to be amended. A literature review would be required to determine this. In line of the aims of the thesis, including more data on different human subpopulations would enable me to establish:

- *Appropriate animal models potentially for each subpopulation*
- *Differential dosing by subpopulation.* Based on our work in chapter 5, it could be possible that vaccine dose may have to be altered for different human subpopulations. For example, HIV+ participants, whose T cell counts may be depleted compared to HIV- participants, may require lower doses of the vaccine.

Further work should include additional data on animal subpopulations. It has been shown that animal age [370], sex [371] and in the case of mice, strain [372] could result in differential immune response to vaccination.

### ***Modelling to explore vaccination regimen and adjuvant dose***

In chapter 5, the data selected from the H56/H1+IC31 trials were from a two vaccination regimen. This regimen was used to inform the design of the mouse experiment outlined in chapter 4. However, in the H56 trial [232] and upcoming trials H56 (not yet published), an additional vaccination was given, i.e. a three vaccination regimen, two months apart (data after third vaccination was excluded from my analysis in order to pool with the H1 data). More generally, the regimens of the current TB vaccines in the pipeline vary, some with one vaccination (mostly the BCG replacement vaccines) and some with three (in the case of the boost vaccines). The timings between vaccination vary too, from 2 weeks to 4 months apart (see background section). Considering that the majority of the TB vaccines in the pipeline target a similar immunological response, should vaccination regimens differ as much? Current methods to determine regimen are conducted empirically in early clinical phases (1/2a) in vaccine development [239, 373-375]. In contrast, drug regimen is regularly explored and

optimised using model-based simulation based on early response data. With this in mind, IS/ID modelling could be used to explore the effects of timing of a third vaccination, providing insight into the opportune time to boost vaccine responses, which can then be empirically verified. Not only this, the effects of changing dose *within* a vaccine regimen could be assessed, i.e. escalate (or deescalate) dose between vaccinations. In recent studies with the H4 vaccine, the effects of changing adjuvant dose alongside antigen dose were assessed [222]. The combination of three adjuvant and four antigen doses were tested here in 100 men and women over two trial sites, incurring considerable cost. To test more combinations of adjuvant and antigen(s) clinically, would require a large, expensive multi-dimensional factorial design trial. Again, IS/ID modelling could be used to simulate and explore a wide range of adjuvant and antigen dose combinations.

All the developmental variables discussed; population covariates, vaccine design, vaccination timing, variable antigen dosing within a regimen and adjuvant dose could be combined into a multi-dimensional simulated trial based on early data, to more effectively explore and narrow this space before trials ever began. This would be advantageous to the vaccine development community as it would save the vast resources required to achieve this empirically.

### ***Modelling to exploring more complex immune systems with further data***

It has already been suggested that a protective TB vaccines immune response is likely to be a combination of cytokines or cells types and not solely an IFN- $\gamma$  response [144]. The roles of CD8+ T cells and B cells in TB vaccine responses are less defined, but are believed to play an important role [77, 376, 377]. As mentioned, the non-mechanistic nature of the parameter  $\delta$  in my model, highlights the need for incorporation of innate cell data as the nature of the vaccine in the study (e.g. live replicating, adjuvanted or viral vector) or population covariates may affect the innate cell processes. The complex interaction of cytokines and cells mean a more advanced, “network” model, consisting of multiple separate, yet connected models would be the next evolution of the IS/ID model to represent TB vaccine immune responses. Calibration of this model would require a large amount of data on multiple cytokines and cell measures that are achievable with existing tools [378]. However, such data may not exist in the longitudinal form required, therefore this thesis serves as a starting point for discussion

on the collection of vaccine immune response markers in vaccine studies. It is important to note, as more complexity is added; the potential for differences between species immunology may arise which would be problematic when translating responses from animal to human. Discussion between preclinical and clinical vaccinologists and modellers at all stages of development would be vital to overcome this. This work should be considered the first step in a “complete” translational vaccine performance framework.

### ***Modelling to increase confidence in most immunogenic dose***

The work in chapter 4 outlined my findings when multi-doses of H56+IC31 were given to mice and corresponding IFN- $\gamma$  response followed over time. Statistical curves fitted to the dose-response data enabled me to predict the most immunogenic dose at varying time points. To gain confidence in this most immunogenic dose prediction, further dose experiments in mice should be conducted. This provides an opportunity to use modelling methods to design an optimal mouse experiment, the aim of which would be to gain the most confidence around most immunogenic dose using the least mice as possible. I have conducted preliminary work towards this aim by simulating new experiment scenarios and assessing the impact on the confidence interval bounds (see appendix E for an outline of this work). In summary, by simulating IFN- $\gamma$  response of mice based on the multi-dose data generated in paper 3, I was able to establish an experimental design whereby I increased confidence in the most immunogenic dose prediction using “optimal” arrangement of the *in silico* mouse responses. Similar work could be conducted on the uncertainty surrounding BCG response prediction due to the small macaque sample sizes (chapter 3) to provide vaccine developers with adequate macaque sample sizes for confident response predictions to translate to humans. To further this analysis, advanced simulation-based trial optimisation methods developed for drug trials, should be utilised [358, 359] and the results empirically verified. While using these methods to design optimised pre-clinical experiments would aid in better defining a most immunogenic dose range to take into early clinical trials, the objective is to apply them in optimising clinical trials. My ultimate aim of future work is to use modelling to design a vaccine clinical trial to test vaccine dose efficacy using the minimum number of participants, thus limiting unnecessary exposure and reducing trial costs. These trials can then be clinically

validated. This work is beyond the scope of the thesis, but I believe I have made vital first steps in working towards this aim.

### ***Application of IS/ID modelling to diseases other than TB***

Here I have explored the use of modelling to accelerate vaccine development in TB, but IS/ID modelling, like PK/PD modelling, is a framework that can be applied to vaccine development for other diseases. As an example of an opportunity for IS/ID modelling to potentially accelerate vaccine development is in yellow fever where the licensed vaccine dose has been challenged. As mentioned previously, after shortages of the yellow fever vaccine, 17DD, were reported and due to recent yellow fever outbreaks in Africa [379], dose fractionation studies were conducted. The results of these studies show a lower dose (ranging from one fifth [246] to one tenth [244, 380]) was found to be as protective (measured using a known antibody correlate) as the current higher licensed dose [244, 246, 379, 380]. Dose fractionation studies for the yellow fever vaccine are ongoing. I believe that IS/ID modelling could have been an effective tool, incorporated during preclinical and early clinical development of this vaccine, to prioritise the lower, equally as protective 17DD dose. Had this been the case, wasted resources and money may have been saved and the vaccine better distributed. As future work, I intend to embark on a grant project to investigate this. This will require response data on varying doses of 17DD in animals and humans, and a new mathematical model to represent the antibody response. However, predictions could be easily validated due to the known antibody correlate of protection for yellow fever.

Whether TB or yellow fever vaccines, the generalized steps to integrate modelling into vaccine development are outlined below, (a scheme of the steps is in Figure 6.1):

1. An immunogenic vaccine is developed and a wide range of doses are tested in mice or other small animal models to establish an initial approximate dose response curve. An aim here is to find the minimum and maximum doses that provide the bounds of the dose response curve (within the constraints of the manufacturing process and ability of the assay to assess the dose). Of note, if applicable, this process should be repeated for a range of adjuvant doses (i.e. the dose response curve should be assumed the same shape or magnitude across adjuvant).

2. Mechanistic mathematical modelling techniques (IS/ID) are applied to estimate the parameters that describe the underlying dynamics of the initial animal-derived dose response relationship. Historical data from similar platforms could be used as guidance. The modeller then determines the experimental design to yield the maximum information on the dose response curve, given limitations on animal number, ability to achieve the desired concentrations of the product, and cost. For example, the modeller and developer then develop a further study to asymptotically approach the best dose, using methods to select both the doses to be studied and the number of animals per group. Pre-defined desired confidence intervals can be used to determine the groups and group numbers.
3. The IS/ID model is fit to human response data on limited doses (maybe just one) and the animal IS/ID model parameters are mapped to human parameters for the equivalent dose. Equivalent dose is based on allometric dose scaling based on historical data from similar platforms or products. The mapping is used to predict the *theoretical* human dose response relationship.
4. A selection of doses is chosen to most rapidly define the extremes of the human response based on this theoretical prediction. As in step 1, the aim is to define an approximate shape and the confidence bounds of the dose response curve (depending on the variability of the immune response measurement(s) chosen), using a limited number of human subjects per arm.
5. IS/ID modelling is applied using the phase 1 data to predict the dose response relationship as a guide for a limited number of further doses to be tested, either in an adaptive fashion in Phase 1 or incorporated into a future study. A dose-response surrogate that can be assessed in essential real-time and an unblinded assessment team are needed.
6. This data is then fed back into the model (step 5) to gain understanding of the confidence intervals around the chosen doses. As further human data is collected, the IS/ID model is refined, used to hone best dose and to design next phase trials.

***Further steps to incorporate IS/ID modelling into vaccine development***

Compared to drug development, vaccine development faces different challenges. From a developmental perspective, there are different expectations from vaccine to drug development industry and regulators; model-based vaccine development is not an established method in the vaccine development world. Vaccines are based on empirical evidence and that is where focus remains, historically and at present. Breaking through this expectation will be the next step to fully integrating mathematical modelling into vaccine development. I suggest the following actions.

1. A collaborative group of interested parties from academia, biotech, large vaccine manufacturers, regulators, governmental and non-governmental agencies must be established to aid communication, data access and development of methodology. The first meeting of such a group of individuals occurred in May 2015 at the headquarters of TB vaccine developers Aeras (Rockville, MD), where a multidisciplinary team met to discuss the current state of vaccine dose finding and the potential for mathematical modelling to assist in this arena. It was concluded at this meeting that modelling was a promising step forward in vaccine development.
2. Incentives, such as large data packages and a commitment by vaccine developers, need to be applied to encourage modellers with experience in drug dosing to move to vaccine studies, which has a potentially greater impact on human health than any other treatment intervention. Linking to existing modelling consortia such as the TB Modelling and Analysis Consortium and International Society of Pharmacometrics would also facilitate access to modelling expertise.
3. In drug development, modellers use all available (relevant and standardized) data to refine the understanding of PK/PD findings throughout the product development process. This has historically had a great influence on trial design; generating sufficient data to enable informative modelling. Therefore, modellers should be involved throughout the entire vaccine development process, even before initiating the earliest animal studies, to help narrow the design space and predict optimal outcomes at each step.
4. Vaccine funding agencies should be encouraged to consider head to head studies in which conventional methods for selecting vaccine dose are used in parallel with the

outlined modelling techniques, to better understand the impact on speed of development, number of participants exposed and cost of vaccine design.

## **Conclusion**

This thesis has demonstrated the utility of mathematical modelling to compare animal models to the humans they aim to represent; quantify vaccine immune response dynamics and predict vaccine dose relationship across species. I believe future work on IS/ID modelling to include data on more complex immune response networks and different animal and human subpopulations is entirely feasible and would establish IS/ID modelling as a legitimate tool to accelerate vaccine development.

**1**

Immunogenic vaccine developed and wide range of doses tested in small animals

**2**

$\frac{dy}{dt} = \alpha xy - x^2 \dots$

Immunostimulation/Immunodynamic (IS/ID) modeling used to predict dose-response relationship

**3**

$\alpha, \beta, \lambda \dots$

Allometric scaling translates animal to human IS/ID model parameters for the equivalent dose

$\frac{dy}{dt} = \alpha xy - x^2 \dots$

Use IS/ID model to predict *theoretical* human dose response based on allometrically scaled model parameters

**4**

First-in-man phase I trial using "best" doses from from theoretical IS/ID predicted dose response relationship

**5**

$\frac{dy}{dt} = \alpha xy - x^2 \dots$

Use IS/ID modeling to predict the dose response curve based on the existing human data

Select two additional doses that will be studied in more detail

**6**

Use existing human data to continue to refine the model, best dose prediction and suggest new trial design

Figure 6.1. Schema depicting the steps required to incorporate vaccine Immunostimulation (IS) /Immunodynamic (ID) modeling into vaccine development. [Graphics included credited to: The Noun Project <https://thenounproject.com/>]

## References

- [1] Han S. Clinical vaccine development. *Clinical and experimental vaccine research*. 2015;4:46-53.
- [2] Riedel S. Edward Jenner and the history of smallpox and vaccination. *Proc (Bayl Univ Med Cent)*. 2005;18:21-5.
- [3] Plotkin SA, Plotkin SL. The development of vaccines: how the past led to the future. *Nat Rev Microbiol*. 2011;9:889-93.
- [4] Siegrist CA. *Vaccine Immunology*. Elsevier; 2008. p. 17-36.
- [5] Kaufmann SH, McElrath MJ, Lewis DJ, Del Giudice G. Challenges and responses in human vaccine development. *Curr Opin Immunol*. 2014;28:18-26.
- [6] Barker L, Hessel L, Walker B. Rational approach to selection and clinical development of TB vaccine candidates. *Tuberculosis*. 2012;92 Suppl 1:S25-9.
- [7] Dickson M, Gagnon JP. The cost of new drug discovery and development. *Discovery medicine*. 2004;4:172-9.
- [8] Kanesa-athan N, Shaw A, Stoddard JJ, Vernon TM. Ensuring the optimal safety of licensed vaccines: a perspective of the vaccine research, development, and manufacturing companies. *Pediatrics*. 2011;127 Suppl 1:S16-22.
- [9] Gerdts V, Wilson HL, Meurens F, van Drunen Littel-van den Hurk S, Wilson D, Walker S, et al. Large animal models for vaccine development and testing. *ILAR J*. 2015;56:53-62.
- [10] Tanner R, McShane H. Replacing, reducing and refining the use of animals in tuberculosis vaccine research. *ALTEX*. 2016.
- [11] Flynn JL, Capuano SV, Croix D, Pawar S, Myers A, Zinovik A, et al. Non-human primates: a model for tuberculosis research. *Tuberculosis (Edinb)*. 2003;83:116-8.
- [12] Rehli M. Of mice and men: species variations of Toll-like receptor expression. *Trends Immunol*. 2002;23:375-8.
- [13] Nathanson N, Mathieson BJ. Biological considerations in the development of a human immunodeficiency virus vaccine. *J Infect Dis*. 2000;182:579-89.
- [14] Graham BS, Mascola JR. Lessons from failure--preparing for future HIV-1 vaccine efficacy trials. *J Infect Dis*. 2005;191:647-9.
- [15] Christe KL, McChesney MB, Spinner A, Rosenthal AN, Allen PC, Valverde CR, et al. Comparative efficacy of a canine distemper-measles and a standard measles vaccine for immunization of rhesus macaques (*Macaca mulatta*). *Comp Med*. 2002;52:467-72.
- [16] Guirakhoo F, Pugachev K, Zhang Z, Myers G, Levenbook I, Draper K, et al. Safety and efficacy of chimeric yellow fever-dengue virus tetravalent vaccine formulations in nonhuman primates. *J Virol*. 2004;78:4761-75.
- [17] Lefevre EA, Carr BV, Inman CF, Prentice H, Brown IH, Brookes SM, et al. Immune responses in pigs vaccinated with adjuvanted and non-adjuvanted A(H1N1)pdm/09 influenza vaccines used in human immunization programmes. *PLoS One*. 2012;7:e32400.
- [18] Endsley JJ, Waters WR, Palmer MV, Nonnecke BJ, Thacker TC, Jacobs WR, Jr., et al. The calf model of immunity for development of a vaccine against tuberculosis. *Vet Immunol Immunopathol*. 2009;128:199-204.
- [19] De Bont J, Vercruyse J, Grzych JM, Meeus PF, Capron A. Potential of a recombinant *Schistosoma bovis*-derived glutathione S-transferase to protect cattle against experimental and natural *S. mattheei* infection. *Parasitology*. 1997;115 ( Pt 3):249-55.
- [20] Sow FB, Gallup JM, Olivier A, Krishnan S, Patera AC, Suzich J, et al. Respiratory syncytial virus is associated with an inflammatory response in lungs and architectural remodeling of lung-draining lymph nodes of newborn lambs. *Am J Physiol Lung Cell Mol Physiol*. 2011;300:L12-24.
- [21] Leroux-Roels G, Bonanni P, Tantawichien T, Zepp F. Vaccine development. *Understanding Modern Vaccines: Perspectives in Vaccinology*. 2011;1:115-50.

- [22] Seok J, Warren HS, Cuenca AG, Mindrinos MN, Baker HV, Xu W, et al. Genomic responses in mouse models poorly mimic human inflammatory diseases. *Proc Natl Acad Sci U S A*. 2013;110:3507-12.
- [23] Mestas J, Hughes CC. Of mice and not men: differences between mouse and human immunology. *J Immunol*. 2004;172:2731-8.
- [24] Langhorne J, Buffet P, Galinski M, Good M, Harty J, Leroy D, et al. The relevance of non-human primate and rodent malaria models for humans. *Malar J*. 2011;10:23.
- [25] Hokey DA, Ginsberg A. The current state of tuberculosis vaccines. *Hum Vaccin Immunother*. 2013;9:2142-6.
- [26] Christen U, Hintermann E. An Update on Animal Models of Autoimmune Hepatitis: Are we There Yet? *Curr Pharm Des*. 2015;21:2391-400.
- [27] Plotkin SA, Orenstein WA, Offit PA. *Vaccines*. 6 ed: Saunders; 2013.
- [28] Little SF, Webster WM, Norris SL, Andrews GP. Evaluation of an anti-rPA IgG ELISA for measuring the antibody response in mice. *Biologicals*. 2004;32:62-9.
- [29] Semenova VA, Schiffer J, Steward-Clark E, Soroka S, Schmidt DS, Brawner MM, et al. Validation and long term performance characteristics of a quantitative enzyme linked immunosorbent assay (ELISA) for human anti-PA IgG. *J Immunol Methods*. 2012;376:97-107.
- [30] Orme IM. Vaccine development for tuberculosis: current progress. *Drugs*. 2013;73:1015-24.
- [31] Shingleton A. Allometry: The Study of Biological Scaling. *Nature Education Knowledge*. 2010;3:2.
- [32] WHO. *Global Tuberculosis Report 2016*. World Health Organization; 2016. p. 1-201.
- [33] Nations U. *Sustainable Development Goals*.
- [34] Uplekar M, Raviglione M. WHO's End TB Strategy: From stopping to ending the global TB epidemic. *Indian J Tuberc*. 2015;62:196-9.
- [35] Fletcher HA, Schragger L. TB vaccine development and the End TB Strategy: importance and current status. *Transactions of the Royal Society of Tropical Medicine and Hygiene*. 2016;110:212-8.
- [36] Barry CE, 3rd, Boshoff HI, Dartois V, Dick T, Ehrst S, Flynn J, et al. The spectrum of latent tuberculosis: rethinking the biology and intervention strategies. *Nat Rev Microbiol*. 2009;7:845-55.
- [37] O'Garra A, Redford PS, McNab FW, Bloom CI, Wilkinson RJ, Berry MP. The immune response in tuberculosis. *Annu Rev Immunol*. 2013;31:475-527.
- [38] Corbett EL, Watt CJ, Walker N, Maher D, Williams BG, Raviglione MC, et al. The growing burden of tuberculosis: global trends and interactions with the HIV epidemic. *Arch Intern Med*. 2003;163:1009-21.
- [39] Turner RD, Bothamley GH. Cough and the Transmission of Tuberculosis. *Journal of Infectious Diseases*. 2015;211:1367-72.
- [40] Fennelly KP, Jones-Lopez EC, Ayakaka I, Kim S, Menyha H, Kirenga B, et al. Variability of infectious aerosols produced during coughing by patients with pulmonary tuberculosis. *Am J Respir Crit Care Med*. 2012;186:450-7.
- [41] Ypma RJ, Altes HK, van Soolingen D, Wallinga J, van Ballegooijen WM. A sign of superspreading in tuberculosis: highly skewed distribution of genotypic cluster sizes. *Epidemiology*. 2013;24:395-400.
- [42] Sompayrac L. *How the Immune System Works*. 4 ed. Chichester: John Wiley & Sons Ltd; 2012.
- [43] Playfair JHL, Chain BM. *Immunology at a glance*. 9th ed. Oxford: Wiley-Blackwell; 2009.
- [44] Abbas A, Lichtman A, Pillai S. *Cellular and Molecular Immunology*. 8 ed: Elsevier Saunders; 2015.
- [45] Middleton AM, Chadwick MV, Nicholson AG, Dewar A, Groger RK, Brown EJ, et al. Interaction of *Mycobacterium tuberculosis* with human respiratory mucosa. *Tuberculosis*. 2002;82:69-78.
- [46] Lerner TR, Borel S, Gutierrez MG. The innate immune response in human tuberculosis. *Cell Microbiol*. 2015;17:1277-85.
- [47] Sia JK, Georgieva M, Rengarajan J. Innate Immune Defenses in Human Tuberculosis: An Overview of the Interactions between *Mycobacterium tuberculosis* and Innate Immune Cells. *J Immunol Res*. 2015;2015:747543.

- [48] Eum SY, Kong JH, Hong MS, Lee YJ, Kim JH, Hwang SH, et al. Neutrophils are the predominant infected phagocytic cells in the airways of patients with active pulmonary TB. *Chest*. 2010;137:122-8.
- [49] Wolf AJ, Linas B, Trevejo-Nunez GJ, Kincaid E, Tamura T, Takatsu K, et al. Mycobacterium tuberculosis infects dendritic cells with high frequency and impairs their function in vivo. *J Immunol*. 2007;179:2509-19.
- [50] Espert L, Beaumelle B, Vergne I. Autophagy in Mycobacterium tuberculosis and HIV infections. *Frontiers in cellular and infection microbiology*. 2015;5:49.
- [51] Gutierrez MG, Master SS, Singh SB, Taylor GA, Colombo MI, Deretic V. Autophagy is a defense mechanism inhibiting BCG and Mycobacterium tuberculosis survival in infected macrophages. *Cell*. 2004;119:753-66.
- [52] Behar SM, Martin CJ, Booty MG, Nishimura T, Zhao X, Gan HX, et al. Apoptosis is an innate defense function of macrophages against Mycobacterium tuberculosis. *Mucosal immunology*. 2011;4:279-87.
- [53] Marino S, Pawar S, Fuller CL, Reinhart TA, Flynn JL, Kirschner DE. Dendritic cell trafficking and antigen presentation in the human immune response to Mycobacterium tuberculosis. *J Immunol*. 2004;173:494-506.
- [54] Cooper AM, Khader SA. The role of cytokines in the initiation, expansion, and control of cellular immunity to tuberculosis. *Immunol Rev*. 2008;226:191-204.
- [55] Flynn JL, Chan J. Immunology of tuberculosis. *Annu Rev Immunol*. 2001;19:93-129.
- [56] Flynn JL, Goldstein MM, Triebold KJ, Koller B, Bloom BR. Major histocompatibility complex class I-restricted T cells are required for resistance to Mycobacterium tuberculosis infection. *Proc Natl Acad Sci U S A*. 1992;89:12013-7.
- [57] Chackerian AA, Perera TV, Behar SM. Gamma interferon-producing CD4+ T lymphocytes in the lung correlate with resistance to infection with Mycobacterium tuberculosis. *Infection and immunity*. 2001;69:2666-74.
- [58] Kaufmann SH. Fact and fiction in tuberculosis vaccine research: 10 years later. *Lancet Infect Dis*. 2011;11:633-40.
- [59] Lertmemongkolchai G, Cai G, Hunter CA, Bancroft GJ. Bystander activation of CD8+ T cells contributes to the rapid production of IFN-gamma in response to bacterial pathogens. *J Immunol*. 2001;166:1097-105.
- [60] Sud D, Bigbee C, Flynn JL, Kirschner DE. Contribution of CD8+ T cells to control of Mycobacterium tuberculosis infection. *J Immunol*. 2006;176:4296-314.
- [61] van Pinxteren LA, Cassidy JP, Smedegaard BH, Agger EM, Andersen P. Control of latent Mycobacterium tuberculosis infection is dependent on CD8 T cells. *Eur J Immunol*. 2000;30:3689-98.
- [62] Kamath AB, Woodworth J, Xiong X, Taylor C, Weng Y, Behar SM. Cytolytic CD8+ T cells recognizing CFP10 are recruited to the lung after Mycobacterium tuberculosis infection. *J Exp Med*. 2004;200:1479-89.
- [63] Serbina NV, Lazarevic V, Flynn JL. CD4(+) T cells are required for the development of cytotoxic CD8(+) T cells during Mycobacterium tuberculosis infection. *J Immunol*. 2001;167:6991-7000.
- [64] Flynn JL, Chan J, Triebold KJ, Dalton DK, Stewart TA, Bloom BR. An essential role for interferon gamma in resistance to Mycobacterium tuberculosis infection. *The Journal of experimental medicine*. 1993;178:2249-54.
- [65] Lammas DA, Casanova JL, Kumararatne DS. Clinical consequences of defects in the IL-12-dependent interferon-gamma (IFN-gamma) pathway. *Clin Exp Immunol*. 2000;121:417-25.
- [66] Jouanguy E, Doffinger R, Dupuis S, Pallier A, Altare F, Casanova JL. IL-12 and IFN-gamma in host defense against mycobacteria and salmonella in mice and men. *Curr Opin Immunol*. 1999;11:346-51.
- [67] Bean AG, Roach DR, Briscoe H, France MP, Korner H, Sedgwick JD, et al. Structural deficiencies in granuloma formation in TNF gene-targeted mice underlie the heightened susceptibility to aerosol Mycobacterium tuberculosis infection, which is not compensated for by lymphotoxin. *J Immunol*. 1999;162:3504-11.

- [68] Flynn JL, Goldstein MM, Chan J, Triebold KJ, Pfeffer K, Lowenstein CJ, et al. Tumor necrosis factor- $\alpha$  is required in the protective immune response against *Mycobacterium tuberculosis* in mice. *Immunity*. 1995;2:561-72.
- [69] Lin PL, Flynn JL. CD8 T cells and *Mycobacterium tuberculosis* infection. *Semin Immunopathol*. 2015;37:239-49.
- [70] Redford PS, Murray PJ, O'Garra A. The role of IL-10 in immune regulation during *M. tuberculosis* infection. *Mucosal immunology*. 2011;4:261-70.
- [71] Hirsch CS, Rojas R, Wu M, Toossi Z. *Mycobacterium tuberculosis* Induces Expansion of Foxp3 Positive CD4 T-cells with a Regulatory Profile in Tuberculin Non-sensitized Healthy Subjects: Implications for Effective Immunization against TB. *J Clin Cell Immunol*. 2016;7.
- [72] Larson RP, Shafiani S, Urdahl KB. Foxp3(+) regulatory T cells in tuberculosis. *Adv Exp Med Biol*. 2013;783:165-80.
- [73] Abebe F, Bjune G. The protective role of antibody responses during *Mycobacterium tuberculosis* infection. *Clin Exp Immunol*. 2009;157:235-43.
- [74] Meraviglia S, El Daker S, Dieli F, Martini F, Martino A.  $\gamma\delta$  T cells cross-link innate and adaptive immunity in *Mycobacterium tuberculosis* infection. *Clin Dev Immunol*. 2011;2011:587315.
- [75] Maglione PJ, Chan J. How B cells shape the immune response against *Mycobacterium tuberculosis*. *Eur J Immunol*. 2009;39:676-86.
- [76] Gold MC, Napier RJ, Lewinsohn DM. MR1-restricted mucosal associated invariant T (MAIT) cells in the immune response to *Mycobacterium tuberculosis*. *Immunological reviews*. 2015;264:154-66.
- [77] Sebina I, Cliff JM, Smith SG, Nogaro S, Webb EL, Riley EM, et al. Long-lived memory B-cell responses following BCG vaccination. *PloS one*. 2012;7:e51381.
- [78] Kononova TE, Urazova OI, Novitskii VV, Churina EG, Kolobovnikova YV, Ignatov MV, et al. Functional activity of Th-17 lymphocytes in pulmonary tuberculosis. *Bull Exp Biol Med*. 2014;156:743-5.
- [79] Kirman JR, Henao-Tamayo MI, Agger EM. The Memory Immune Response to Tuberculosis. *Microbiol Spectr*. 2016;4.
- [80] Sallusto F, Lanzavecchia A, Araki K, Ahmed R. From vaccines to memory and back. *Immunity*. 2010;33:451-63.
- [81] Kaech SM, Wherry EJ, Ahmed R. Effector and memory T-cell differentiation: implications for vaccine development. *Nat Rev Immunol*. 2002;2:251-62.
- [82] Pepper M, Jenkins MK. Origins of CD4(+) effector and central memory T cells. *Nat Immunol*. 2011;12:467-71.
- [83] Seder RA, Darrah PA, Roederer M. T-cell quality in memory and protection: implications for vaccine design. *Nature reviews Immunology*. 2008;8:247-58.
- [84] Esser MT, Marchese RD, Kierstead LS, Tussey LG, Wang F, Chirmule N, et al. Memory T cells and vaccines. *Vaccine*. 2003;21:419-30.
- [85] Andersen P, Smedegaard B. CD4(+) T-cell subsets that mediate immunological memory to *Mycobacterium tuberculosis* infection in mice. *Infect Immun*. 2000;68:621-9.
- [86] Kipnis A, Irwin S, Izzo AA, Basaraba RJ, Orme IM. Memory T lymphocytes generated by *Mycobacterium bovis* BCG vaccination reside within a CD4<sup>+</sup> CD44<sup>lo</sup> CD62 ligand<sup>hi</sup> population. *Infection and immunity*. 2005;73:7759-64.
- [87] Orme IM. The Achilles heel of BCG. *Tuberculosis (Edinb)*. 2010;90:329-32.
- [88] McShane H. Tuberculosis vaccines: beyond bacille Calmette-Guerin. *Philos Trans R Soc Lond B Biol Sci*. 2011;366:2782-9.
- [89] Connor LM, Harvie MC, Rich FJ, Quinn KM, Brinkmann V, Le Gros G, et al. A key role for lung-resident memory lymphocytes in protective immune responses after BCG vaccination. *Eur J Immunol*. 2010;40:2482-92.
- [90] Ramakrishnan L. Revisiting the role of the granuloma in tuberculosis. *Nat Rev Immunol*. 2012;12:352-66.

- [91] Lin PL, Ford CB, Coleman MT, Myers AJ, Gawande R, Ioerger T, et al. Sterilization of granulomas is common in active and latent tuberculosis despite within-host variability in bacterial killing. *Nat Med*. 2014;20:75-9.
- [92] Gideon HP, Phuah J, Myers AJ, Bryson BD, Rodgers MA, Coleman MT, et al. Variability in tuberculosis granuloma T cell responses exists, but a balance of pro- and anti-inflammatory cytokines is associated with sterilization. *PLoS Pathog*. 2015;11:e1004603.
- [93] Narasimhan P, Wood J, Macintyre CR, Mathai D. Risk factors for tuberculosis. *Pulm Med*. 2013;2013:828939.
- [94] Espinal MA, Perez EN, Baez J, Henriquez L, Fernandez K, Lopez M, et al. Infectiousness of *Mycobacterium tuberculosis* in HIV-1-infected patients with tuberculosis: a prospective study. *Lancet*. 2000;355:275-80.
- [95] Classen CN, Warren R, Richardson M, Hauman JH, Gie RP, Ellis JH, et al. Impact of social interactions in the community on the transmission of tuberculosis in a high incidence area. *Thorax*. 1999;54:136-40.
- [96] Morrison J, Pai M, Hopewell PC. Tuberculosis and latent tuberculosis infection in close contacts of people with pulmonary tuberculosis in low-income and middle-income countries: a systematic review and meta-analysis. *Lancet Infect Dis*. 2008;8:359-68.
- [97] Yates TA, Khan PY, Knight GM, Taylor JG, McHugh TD, Lipman M, et al. The transmission of *Mycobacterium tuberculosis* in high burden settings. *The Lancet infectious diseases*. 2016;16:227-38.
- [98] Baussano I, Williams BG, Nunn P, Beggiato M, Fedeli U, Scano F. Tuberculosis incidence in prisons: a systematic review. *PLoS medicine*. 2010;7:e1000381.
- [99] McCreesh N, Faghmous I, Looker C, Dodd PJ, Plumb ID, Shanaube K, et al. Coverage of clinic-based TB screening in South Africa may be low in key risk groups. *Public Health Action*. 2016;6:19-21.
- [100] Lonroth K, Williams BG, Stadlin S, Jaramillo E, Dye C. Alcohol use as a risk factor for tuberculosis - a systematic review. *BMC Public Health*. 2008;8:289.
- [101] Walker NF, Meintjes G, Wilkinson RJ. HIV-1 and the immune response to TB. *Future Virol*. 2013;8:57-80.
- [102] Patel NR, Swan K, Li X, Tachado SD, Koziel H. Impaired M. tuberculosis-mediated apoptosis in alveolar macrophages from HIV+ persons: potential role of IL-10 and BCL-3. *J Leukoc Biol*. 2009;86:53-60.
- [103] Stevenson CR, Critchley JA, Forouhi NG, Roglic G, Williams BG, Dye C, et al. Diabetes and the risk of tuberculosis: a neglected threat to public health? *Chronic Illn*. 2007;3:228-45.
- [104] Stalenhoef JE, Alisjahbana B, Nelwan EJ, van der Ven-Jongekrijg J, Ottenhoff TH, van der Meer JW, et al. The role of interferon-gamma in the increased tuberculosis risk in type 2 diabetes mellitus. *Eur J Clin Microbiol Infect Dis*. 2008;27:97-103.
- [105] Delamaire M, Maugeudre D, Moreno M, Le Goff MC, Allannic H, Genetet B. Impaired leucocyte functions in diabetic patients. *Diabet Med*. 1997;14:29-34.
- [106] Babu S, Nutman TB. Helminth-Tuberculosis Co-infection: An Immunologic Perspective. *Trends Immunol*. 2016;37:597-607.
- [107] Elias D, Akuffo H, Thors C, Pawlowski A, Britton S. Low dose chronic *Schistosoma mansoni* infection increases susceptibility to *Mycobacterium bovis* BCG infection in mice. *Clin Exp Immunol*. 2005;139:398-404.
- [108] Naranbhai V, Hill AV, Abdool Karim SS, Naidoo K, Abdool Karim Q, Warimwe GM, et al. Ratio of monocytes to lymphocytes in peripheral blood identifies adults at risk of incident tuberculosis among HIV-infected adults initiating antiretroviral therapy. *J Infect Dis*. 2014;209:500-9.
- [109] Naranbhai V, Kim S, Fletcher H, Cotton MF, Violari A, Mitchell C, et al. The association between the ratio of monocytes:lymphocytes at age 3 months and risk of tuberculosis (TB) in the first two years of life. *BMC Med*. 2014;12:1-6.

- [110] Naranbhai V, Moodley D, Chipato T, Stranix-Chibanda L, Nakabaiito C, Kamateeka M, et al. The association between the ratio of monocytes: lymphocytes and risk of tuberculosis among HIV-infected postpartum women. *J Acquir Immune Defic Syndr*. 2014;67:573-5.
- [111] Rhodes SJ, Knight GM, Fielding K, Scriba TJ, Pathan AA, McShane H, et al. Individual-level factors associated with variation in mycobacterial-specific immune response: Gender and previous BCG vaccination status. *Tuberculosis (Edinb)*. 2016;96:37-43.
- [112] Marais BJ. Childhood tuberculosis: epidemiology and natural history of disease. *Indian J Pediatr*. 2011;78:321-7.
- [113] Rajagopalan S. Tuberculosis in Older Adults. *Clin Geriatr Med*. 2016;32:479-91.
- [114] Marion CR, High KP. Tuberculosis in Older Adults. In: Norman D, Yoshikawa T, editors. *Infectious Disease in the Aging*: Humana Press; 2009. p. 97-110.
- [115] Lonroth K, Jaramillo E, Williams BG, Dye C, Raviglione M. Drivers of tuberculosis epidemics: the role of risk factors and social determinants. *Soc Sci Med*. 2009;68:2240-6.
- [116] Cegielski JP, Arab L, Cornoni-Huntley J. Nutritional risk factors for tuberculosis among adults in the United States, 1971-1992. *Am J Epidemiol*. 2012;176:409-22.
- [117] Hoang T, Agger EM, Cassidy JP, Christensen JP, Andersen P. Protein energy malnutrition during vaccination has limited influence on vaccine efficacy but abolishes immunity if administered during *Mycobacterium tuberculosis* infection. *Infect Immun*. 2015;83:2118-26.
- [118] Bates MN, Khalakdina A, Pai M, Chang L, Lessa F, Smith KR. Risk of tuberculosis from exposure to tobacco smoke: a systematic review and meta-analysis. *Arch Intern Med*. 2007;167:335-42.
- [119] Lin HH, Ezzati M, Murray M. Tobacco smoke, indoor air pollution and tuberculosis: a systematic review and meta-analysis. *PLoS Med*. 2007;4:e20.
- [120] Lonroth K, Williams BG, Cegielski P, Dye C. A consistent log-linear relationship between tuberculosis incidence and body mass index. *International journal of epidemiology*. 2010;39:149-55.
- [121] Chandra RK. Nutrition and the immune system: an introduction. *The American journal of clinical nutrition*. 1997;66:460S-3S.
- [122] Cegielski JP, McMurray DN. The relationship between malnutrition and tuberculosis: evidence from studies in humans and experimental animals. *Int J Tuberc Lung Dis*. 2004;8:286-98.
- [123] Abba K, Sudarsanam TD, Grobler L, Volmink J. Nutritional supplements for people being treated for active tuberculosis. *The Cochrane database of systematic reviews*. 2008:CD006086.
- [124] Szabo G. Alcohol's contribution to compromised immunity. *Alcohol Health Res World*. 1997;21:30-41.
- [125] Houtmeyers E, Gosselink R, Gayan-Ramirez G, Decramer M. Regulation of mucociliary clearance in health and disease. *Eur Respir J*. 1999;13:1177-88.
- [126] Wang H, Yu M, Ochani M, Amella CA, Tanovic M, Susarla S, et al. Nicotinic acetylcholine receptor alpha7 subunit is an essential regulator of inflammation. *Nature*. 2003;421:384-8.
- [127] Hanekom WA, Dockrell HM, Ottenhoff TH, Doherty TM, Fletcher H, McShane H, et al. Immunological outcomes of new tuberculosis vaccine trials: WHO panel recommendations. *PLoS Med*. 2008;5:e145.
- [128] Liew FY, Millott S, Parkinson C, Palmer RM, Moncada S. Macrophage killing of *Leishmania* parasite in vivo is mediated by nitric oxide from L-arginine. *J Immunol*. 1990;144:4794-7.
- [129] Cooper AM, Dalton DK, Stewart TA, Griffin JP, Russell DG, Orme IM. Disseminated tuberculosis in interferon gamma gene-disrupted mice. *The Journal of experimental medicine*. 1993;178:2243-7.
- [130] Dalton DK, Pitts-Meek S, Keshav S, Figari IS, Bradley A, Stewart TA. Multiple defects of immune cell function in mice with disrupted interferon-gamma genes. *Science*. 1993;259:1739-42.
- [131] Kamijo R, Shapiro D, Gerecitano J, Le J, Bosland M, Vilcek J. *Mycobacterium bovis* infection of mice lacking receptors for interferon-gamma or for transcription factor IRF-1. *J Interferon Res*. 1994;14:281-2.
- [132] Jouanguy E, Altare F, Lamhamedi S, Revy P, Emile JF, Newport M, et al. Interferon-gamma-receptor deficiency in an infant with fatal bacille Calmette-Guerin infection. *The New England journal of medicine*. 1996;335:1956-61.

- [133] Newport MJ, Huxley CM, Huston S, Hawrylowicz CM, Oostra BA, Williamson R, et al. A mutation in the interferon-gamma-receptor gene and susceptibility to mycobacterial infection. *The New England journal of medicine*. 1996;335:1941-9.
- [134] Kaufmann SH. Envisioning future strategies for vaccination against tuberculosis. *Nat Rev Immunol*. 2006;6:699-704.
- [135] Mittrucker HW, Steinhoff U, Kohler A, Krause M, Lazar D, Mex P, et al. Poor correlation between BCG vaccination-induced T cell responses and protection against tuberculosis. *Proc Natl Acad Sci U S A*. 2007;104:12434-9.
- [136] Kagina BM, Abel B, Scriba TJ, Hughes EJ, Keyser A, Soares A, et al. Specific T cell frequency and cytokine expression profile do not correlate with protection against tuberculosis after bacillus Calmette-Guerin vaccination of newborns. *Am J Respir Crit Care Med*. 2010;182:1073-9.
- [137] Fletcher HA, Snowden MA, Landry B, Rida W, Satti I, Harris SA, et al. T-cell activation is an immune correlate of risk in BCG vaccinated infants. *Nat Commun*. 2016;7:11290.
- [138] Fletcher HA. Correlates of immune protection from tuberculosis. *Curr Mol Med*. 2007;7:319-25.
- [139] Smith SG, Zelmer A, Blitz R, Fletcher HA, Dockrell HM. Polyfunctional CD4 T-cells correlate with in vitro mycobacterial growth inhibition following *Mycobacterium bovis* BCG-vaccination of infants. *Vaccine*. 2016;34:5298-305.
- [140] Cooper AM. Cell-mediated immune responses in tuberculosis. *Annual review of immunology*. 2009;27:393-422.
- [141] Smith SG, Lalor MK, Gorak-Stolinska P, Blitz R, Beveridge NE, Worth A, et al. *Mycobacterium tuberculosis* PPD-induced immune biomarkers measurable in vitro following BCG vaccination of UK adolescents by multiplex bead array and intracellular cytokine staining. *BMC Immunol*. 2010;11:35.
- [142] Abebe F. Is interferon-gamma the right marker for bacille Calmette-Guerin-induced immune protection? The missing link in our understanding of tuberculosis immunology. *Clin Exp Immunol*. 2012;169:213-9.
- [143] Lalor MK, Smith SG, Floyd S, Gorak-Stolinska P, Weir RE, Blitz R, et al. Complex cytokine profiles induced by BCG vaccination in UK infants. *Vaccine*. 2010;28:1635-41.
- [144] Petruccioli E, Scriba TJ, Petrone L, Hatherill M, Cirillo DM, Joosten SA, et al. Correlates of tuberculosis risk: predictive biomarkers for progression to active tuberculosis. *Eur Respir J*. 2016;48:1751-63.
- [145] Lyadova IV, Oberdorf S, Kapina MA, Apt AS, Swain SL, Sayles PC. CD4 T cells producing IFN-gamma in the lungs of mice challenged with mycobacteria express a CD27-negative phenotype. *Clinical and experimental immunology*. 2004;138:21-9.
- [146] Takenami I, Finkmoore B, Machado A, Jr., Emodi K, Riley LW, Arruda S. Levels of interferon-gamma increase after treatment for latent tuberculosis infection in a high-transmission setting. *Pulm Med*. 2012;2012:757152.
- [147] White AD, Sarfas C, West K, Sibley LS, Wareham AS, Clark S, et al. Evaluation of the Immunogenicity of *Mycobacterium bovis* BCG Delivered by Aerosol to the Lungs of Macaques. *Clin Vaccine Immunol*. 2015;22:992-1003.
- [148] Abu-Raddad LJ, Sabatelli L, Achterberg JT, Sugimoto JD, Longini IM, Jr., Dye C, et al. Epidemiological benefits of more-effective tuberculosis vaccines, drugs, and diagnostics. *Proceedings of the National Academy of Sciences of the United States of America*. 2009;106:13980-5.
- [149] Dye C, Glaziou P, Floyd K, Raviglione M. Prospects for tuberculosis elimination. *Annu Rev Public Health*. 2013;34:271-86.
- [150] Harris RC, Sumner T, Knight GM, White RG. Systematic review of mathematical models exploring the epidemiological impact of future TB vaccines. *Hum Vaccin Immunother*. 2016;12:2813-32.
- [151] Dye C. Tuberculosis 2000-2010: control, but not elimination. *Int J Tuberc Lung Dis*. 2000;4:S146-52.

- [152] Lietman T, Blower SM. Potential impact of tuberculosis vaccines as epidemic control agents. *Clin Infect Dis*. 2000;30 Suppl 3:S316-22.
- [153] Ottenhoff TH, Kaufmann SH. Vaccines against tuberculosis: where are we and where do we need to go? *PLoS Pathog*. 2012;8:e1002607.
- [154] Kaufmann SH. EFIS lecture. Immune response to tuberculosis: How to control the most successful pathogen on earth. *Immunology letters*. 2016;175:50-7.
- [155] Fletcher HA. Sleeping Beauty and the Story of the Bacille Calmette-Guerin Vaccine. *MBio*. 2016;7.
- [156] Behr MA, Wilson MA, Gill WP, Salamon H, Schoolnik GK, Rane S, et al. Comparative genomics of BCG vaccines by whole-genome DNA microarray. *Science*. 1999;284:1520-3.
- [157] Trunz BB, Fine P, Dye C. Effect of BCG vaccination on childhood tuberculous meningitis and miliary tuberculosis worldwide: a meta-analysis and assessment of cost-effectiveness. *Lancet*. 2006;367:1173-80.
- [158] WHO. Global Tuberculosis Report 2013. World Health Organization; 2013. p. 1-306.
- [159] Ferguson RG, Simes AB. BCG vaccination of Indian infants in Saskatchewan. *Tubercle*. 1949;30:5-11.
- [160] Aronson JD. Protective vaccination against tuberculosis with special reference to BCG vaccination. *Am Rev Tuberc*. 1948;58:255-81.
- [161] B.C.G. AND vole bacillus vaccines in the prevention of tuberculosis in adolescents; first (progress) report to the Medical Research Council by their Tuberculosis Vaccines Clinical Trials Committee. *Br Med J*. 1956;1:413-27.
- [162] Trial of BCG vaccines in south India for tuberculosis prevention: first report--Tuberculosis Prevention Trial. *Bull World Health Organ*. 1979;57:819-27.
- [163] Palmer CE, Shaw LW, Comstock GW. Community trials of BCG vaccination. *Am Rev Tuberc*. 1958;77:877-907.
- [164] Shaw LW. Field studies on immunization against tuberculosis. I. Tuberculin allergy following BCG vaccination of school children in Muscogee County, Georgia. *Public Health Rep*. 1951;66:1415-6.
- [165] Mangtani P, Abubakar I, Ariti C, Beynon R, Pimpin L, Fine PE, et al. Protection by BCG vaccine against tuberculosis: a systematic review of randomized controlled trials. *Clin Infect Dis*. 2014;58:470-80.
- [166] Hur YG, Gorak-Stolinska P, Lalor MK, Mvula H, Floyd S, Raynes J, et al. Factors affecting immunogenicity of BCG in infants, a study in Malawi, The Gambia and the UK. *BMC Infect Dis*. 2014;14:184.
- [167] Hoefsloot W, van Ingen J, Andrejak C, Angeby K, Bauriaud R, Bemer P, et al. The geographic diversity of nontuberculous mycobacteria isolated from pulmonary samples: an NTM-NET collaborative study. *Eur Respir J*. 2013;42:1604-13.
- [168] Palmer CE, Long MW. Effects of infection with atypical mycobacteria on BCG vaccination and tuberculosis. *Am Rev Respir Dis*. 1966;94:553-68.
- [169] Wilson ME, Fineberg HV, Colditz GA. Geographic latitude and the efficacy of bacillus Calmette-Guerin vaccine. *Clin Infect Dis*. 1995;20:982-91.
- [170] Kwan CK, Ernst JD. HIV and tuberculosis: a deadly human syndemic. *Clin Microbiol Rev*. 2011;24:351-76.
- [171] Mansoor N, Scriba TJ, de Kock M, Tameris M, Abel B, Keyser A, et al. HIV-1 infection in infants severely impairs the immune response induced by Bacille Calmette-Guerin vaccine. *J Infect Dis*. 2009;199:982-90.
- [172] Hijikata M, Matsushita I, Hang NT, Maeda S, Thuong PH, Tam DB, et al. Age-dependent association of mannose-binding lectin polymorphisms with the development of pulmonary tuberculosis in Viet Nam. *Hum Immunol*. 2014.
- [173] Brewer TF, Colditz GA. Relationship between bacille Calmette-Guerin (BCG) strains and the efficacy of BCG vaccine in the prevention of tuberculosis. *Clin Infect Dis*. 1995;20:126-35.

- [174] McShane H. Developing an improved vaccine against tuberculosis. *Expert Rev Vaccines*. 2004;3:299-306.
- [175] Evans TG, Schragger L, Thole J. Status of vaccine research and development of vaccines for tuberculosis. *Vaccine*. 2016;34:2911-4.
- [176] McShane H, Hill A. Prime-boost immunisation strategies for tuberculosis. *Microbes Infect*. 2005;7:962-7.
- [177] Clem AS. Fundamentals of vaccine immunology. *J Glob Infect Dis*. 2011;3:73-8.
- [178] Brock I, Weldingh K, Leyten EM, Arend SM, Ravn P, Andersen P. Specific T-cell epitopes for immunoassay-based diagnosis of *Mycobacterium tuberculosis* infection. *J Clin Microbiol*. 2004;42:2379-87.
- [179] Schellack C, Prinz K, Egyed A, Fritz JH, Wittmann B, Ginzler M, et al. IC31, a novel adjuvant signaling via TLR9, induces potent cellular and humoral immune responses. *Vaccine*. 2006;24:5461-72.
- [180] Lingnau K, Riedl K, von Gabain A. IC31 and IC30, novel types of vaccine adjuvant based on peptide delivery systems. *Expert Rev Vaccines*. 2007;6:741-6.
- [181] van Dissel JT, Joosten SA, Hoff ST, Soonawala D, Prins C, Hokey DA, et al. A novel liposomal adjuvant system, CAF01, promotes long-lived *Mycobacterium tuberculosis*-specific T-cell responses in human. *Vaccine*. 2014;32:7098-107.
- [182] Holten-Andersen L, Doherty TM, Korsholm KS, Andersen P. Combination of the cationic surfactant dimethyl dioctadecyl ammonium bromide and synthetic mycobacterial cord factor as an efficient adjuvant for tuberculosis subunit vaccines. *Infect Immun*. 2004;72:1608-17.
- [183] Black GF, Weir RE, Floyd S, Bliss L, Warndorff DK, Crampin AC, et al. BCG-induced increase in interferon-gamma response to mycobacterial antigens and efficacy of BCG vaccination in Malawi and the UK: two randomised controlled studies. *Lancet*. 2002;359:1393-401.
- [184] Diel R, Goletti D, Ferrara G, Bothamley G, Cirillo D, Kampmann B, et al. Interferon-gamma release assays for the diagnosis of latent *Mycobacterium tuberculosis* infection: a systematic review and meta-analysis. *Eur Respir J*. 2011;37:88-99.
- [185] Cardona PJ, Williams A. Experimental animal modelling for TB vaccine development. *Int J Infect Dis*. 2017;56:268-73.
- [186] Lin S, Lin Y, Nery JR, Urich MA, Breschi A, Davis CA, et al. Comparison of the transcriptional landscapes between human and mouse tissues. *Proc Natl Acad Sci U S A*. 2014;111:17224-9.
- [187] Leist M, Hartung T. Inflammatory findings on species extrapolations: humans are definitely no 70-kg mice. *ALTEX*. 2013;30:227-30.
- [188] Cardona PJ. The Progress of Therapeutic Vaccination with Regard to Tuberculosis. *Front Microbiol*. 2016;7:1536.
- [189] Apt A, Kramnik I. Man and mouse TB: contradictions and solutions. *Tuberculosis (Edinb)*. 2009;89:195-8.
- [190] Guirado E, Gordillo S, Gil O, Diaz J, Tapia G, Vilaplana C, et al. Intragranulomatous necrosis in pulmonary granulomas is not related to resistance against *Mycobacterium tuberculosis* infection in experimental murine models induced by aerosol. *Int J Exp Pathol*. 2006;87:139-49.
- [191] Cardona PJ, Gordillo S, Diaz J, Tapia G, Amat I, Pallares A, et al. Widespread bronchogenic dissemination makes DBA/2 mice more susceptible than C57BL/6 mice to experimental aerosol infection with *Mycobacterium tuberculosis*. *Infect Immun*. 2003;71:5845-54.
- [192] Lasco TM, Turner OC, Cassone L, Sugawara I, Yamada H, McMurray DN, et al. Rapid accumulation of eosinophils in lung lesions in guinea pigs infected with *Mycobacterium tuberculosis*. *Infect Immun*. 2004;72:1147-9.
- [193] Flynn JL, Gideon HP, Mattila JT, Lin PL. Immunology studies in non-human primate models of tuberculosis. *Immunological reviews*. 2015;264:60-73.
- [194] Carlsson HE, Schapiro SJ, Farah I, Hau J. Use of primates in research: a global overview. *Am J Primatol*. 2004;63:225-37.

- [195] Gormus BJ, Blanchard JL, Alvarez XH, Didier PJ. Evidence for a rhesus monkey model of asymptomatic tuberculosis. *J Med Primatol*. 2004;33:134-45.
- [196] Capuano SV, 3rd, Croix DA, Pawar S, Zinovik A, Myers A, Lin PL, et al. Experimental *Mycobacterium tuberculosis* infection of cynomolgus macaques closely resembles the various manifestations of human *M. tuberculosis* infection. *Infection and immunity*. 2003;71:5831-44.
- [197] Pena JC, Ho WZ. Monkey models of tuberculosis: lessons learned. *Infect Immun*. 2015;83:852-62.
- [198] Kaushal D, Mehra S, Didier PJ, Lackner AA. The non-human primate model of tuberculosis. *J Med Primatol*. 2012;41:191-201.
- [199] Scanga CA, Flynn JL. Modeling tuberculosis in nonhuman primates. *Cold Spring Harb Perspect Med*. 2014;4:a018564.
- [200] Rhodes SJ, Sarfas C, Knight GM, White A, Pathan AA, McShane H, et al. Predicting IFN-gamma responses after BCG vaccination in humans from macaques: A proof-of-concept study of Immunostimulation/Immunodynamic modelling methods. *Clin Vaccine Immunol*. 2017.
- [201] Barclay WR, Anacker RL, Brehmer W, Leif W, Ribic E. Aerosol-Induced Tuberculosis in Subhuman Primates and the Course of the Disease After Intravenous BCG Vaccination. *Infect Immun*. 1970;2:574-82.
- [202] Janicki BW, Good RC, Minden P, Affronti LF, Hymes WF. Immune responses in rhesus monkeys after bacillus Calmette-Guerin vaccination and aerosol challenge with *Mycobacterium tuberculosis*. *Am Rev Respir Dis*. 1973;107:359-66.
- [203] Reed SG, Coler RN, Dalemans W, Tan EV, DeLa Cruz EC, Basaraba RJ, et al. Defined tuberculosis vaccine, Mtb72F/AS02A, evidence of protection in cynomolgus monkeys. *Proc Natl Acad Sci U S A*. 2009;106:2301-6.
- [204] Kaushal D, Foreman TW, Gautam US, Alvarez X, Adekambi T, Rangel-Moreno J, et al. Mucosal vaccination with attenuated *Mycobacterium tuberculosis* induces strong central memory responses and protects against tuberculosis. *Nat Commun*. 2015;6:8533.
- [205] Sharpe SA, Eschelbach E, Basaraba RJ, Gleeson F, Hall GA, McIntyre A, et al. Determination of lesion volume by MRI and stereology in a macaque model of tuberculosis. *Tuberculosis (Edinb)*. 2009;89:405-16.
- [206] Sharpe S, White A, Gleeson F, McIntyre A, Smyth D, Clark S, et al. Ultra low dose aerosol challenge with *Mycobacterium tuberculosis* leads to divergent outcomes in rhesus and cynomolgus macaques. *Tuberculosis (Edinb)*. 2016;96:1-12.
- [207] Langermans JA, Andersen P, van Soolingen D, Vervenne RA, Frost PA, van der Laan T, et al. Divergent effect of bacillus Calmette-Guerin (BCG) vaccination on *Mycobacterium tuberculosis* infection in highly related macaque species: implications for primate models in tuberculosis vaccine research. *Proceedings of the National Academy of Sciences of the United States of America*. 2001;98:11497-502.
- [208] Kanthaswamy S, Ng J, Satkoski Trask J, George DA, Kou AJ, Hoffman LN, et al. The genetic composition of populations of cynomolgus macaques (*Macaca fascicularis*) used in biomedical research. *J Med Primatol*. 2013;42:120-31.
- [209] Javed S, Marsay L, Wareham A, Lewandowski KS, Williams A, Dennis MJ, et al. Temporal Expression of Peripheral Blood Leukocyte Biomarkers in a *Macaca fascicularis* Infection Model of Tuberculosis; Comparison with Human Datasets and Analysis with Parametric/Non-parametric Tools for Improved Diagnostic Biomarker Identification. *PLoS One*. 2016;11:e0154320.
- [210] Hanekom W, Johnston P, Kaplan G, Karp C, Shackelton L, Stuart L, et al. Revision of the Bill & Melinda Gates Foundation TB vaccine strategy - 2014. 2014.
- [211] Hawkrigde T, Scriba TJ, Gelderbloem S, Smit E, Tameris M, Moyo S, et al. Safety and immunogenicity of a new tuberculosis vaccine, MVA85A, in healthy adults in South Africa. *J Infect Dis*. 2008;198:544-52.

- [212] Whelan KT, Pathan AA, Sander CR, Fletcher HA, Poulton I, Alder NC, et al. Safety and immunogenicity of boosting BCG vaccinated subjects with BCG: comparison with boosting with a new TB vaccine, MVA85A. *PLoS One*. 2009;4:e5934.
- [213] Tameris MD, Hatherill M, Landry BS, Scriba TJ, Snowden MA, Lockhart S, et al. Safety and efficacy of MVA85A, a new tuberculosis vaccine, in infants previously vaccinated with BCG: a randomised, placebo-controlled phase 2b trial. *Lancet*. 2013;381:1021-8.
- [214] Ndiaye BP, Thienemann F, Ota M, Landry BS, Camara M, Dieye S, et al. Safety, immunogenicity, and efficacy of the candidate tuberculosis vaccine MVA85A in healthy adults infected with HIV-1: a randomised, placebo-controlled, phase 2 trial. *Lancet Respir Med*. 2015;3:190-200.
- [215] Orr MT, Ireton GC, Beebe EA, Huang PW, Reese VA, Argilla D, et al. Immune subdominant antigens as vaccine candidates against *Mycobacterium tuberculosis*. *J Immunol*. 2014;193:2911-8.
- [216] Stylianou E, Griffiths KL, Poyntz HC, Harrington-Kandt R, Dicks MD, Stockdale L, et al. Improvement of BCG protective efficacy with a novel chimpanzee adenovirus and a modified vaccinia Ankara virus both expressing Ag85A. *Vaccine*. 2015;33:6800-8.
- [217] Aagaard C, Hoang TT, Izzo A, Billeskov R, Troudt J, Arnett K, et al. Protection and polyfunctional T cells induced by Ag85B-TB10.4/IC31 against *Mycobacterium tuberculosis* is highly dependent on the antigen dose. *PLoS One*. 2009;4:e5930.
- [218] Skeiky YA, Dietrich J, Lasco TM, Stagliano K, Dheenadhayalan V, Goetz MA, et al. Non-clinical efficacy and safety of HyVac4:IC31 vaccine administered in a BCG prime-boost regimen. *Vaccine*. 2010;28:1084-93.
- [219] Hoang T, Aagaard C, Dietrich J, Cassidy JP, Dolganov G, Schoolnik GK, et al. ESAT-6 (EsxA) and TB10.4 (EsxH) based vaccines for pre- and post-exposure tuberculosis vaccination. *PLoS One*. 2013;8:e80579.
- [220] Dietrich J, Aagaard C, Leah R, Olsen AW, Stryhn A, Doherty TM, et al. Exchanging ESAT6 with TB10.4 in an Ag85B fusion molecule-based tuberculosis subunit vaccine: efficient protection and ESAT6-based sensitive monitoring of vaccine efficacy. *J Immunol*. 2005;174:6332-9.
- [221] Geldenhuys H, Mearns H, Miles DJ, Tameris M, Hokey D, Shi Z, et al. The tuberculosis vaccine H4:IC31 is safe and induces a persistent polyfunctional CD4 T cell response in South African adults: A randomized controlled trial. *Vaccine*. 2015;33:3592-9.
- [222] Norrby M, Vesikari T, Lindqvist L, Maeurer M, Ahmed R, Mahdavifar S, et al. Safety and immunogenicity of the novel H4:IC31 tuberculosis vaccine candidate in BCG-vaccinated adults: Two phase I dose escalation trials. *Vaccine*. 2017.
- [223] Lindenstrom T, Agger EM, Korsholm KS, Darrach PA, Aagaard C, Seder RA, et al. Tuberculosis subunit vaccination provides long-term protective immunity characterized by multifunctional CD4 memory T cells. *J Immunol*. 2009;182:8047-55.
- [224] Weinrich Olsen A, van Pinxteren LA, Meng Okkels L, Birk Rasmussen P, Andersen P. Protection of mice with a tuberculosis subunit vaccine based on a fusion protein of antigen 85b and esat-6. *Infection and immunity*. 2001;69:2773-8.
- [225] Olsen AW, Williams A, Okkels LM, Hatch G, Andersen P. Protective effect of a tuberculosis subunit vaccine based on a fusion of antigen 85B and ESAT-6 in the aerosol guinea pig model. *Infect Immun*. 2004;72:6148-50.
- [226] Langermans JA, Doherty TM, Vervenne RA, van der Laan T, Lyashchenko K, Greenwald R, et al. Protection of macaques against *Mycobacterium tuberculosis* infection by a subunit vaccine based on a fusion protein of antigen 85B and ESAT-6. *Vaccine*. 2005;23:2740-50.
- [227] van Dissel JT, Soonawala D, Joosten SA, Prins C, Arend SM, Bang P, et al. Ag85B-ESAT-6 adjuvanted with IC31(R) promotes strong and long-lived *Mycobacterium tuberculosis* specific T cell responses in volunteers with previous BCG vaccination or tuberculosis infection. *Vaccine*. 2011;29:2100-9.
- [228] van Dissel JT, Arend SM, Prins C, Bang P, Tingskov PN, Lingnau K, et al. Ag85B-ESAT-6 adjuvanted with IC31 promotes strong and long-lived *Mycobacterium tuberculosis* specific T cell responses in naive human volunteers. *Vaccine*. 2010;28:3571-81.

- [229] Lenz N, Schindler T, Kagina BM, Zhang JD, Lukindo T, Mpina M, et al. Antiviral Innate Immune Activation in HIV-Infected Adults Negatively Affects H1/IC31-Induced Vaccine-Specific Memory CD4+ T Cells. *Clin Vaccine Immunol*. 2015;22:688-96.
- [230] Reither K, Katsoulis L, Beattie T, Gardiner N, Lenz N, Said K, et al. Safety and Immunogenicity of H1/IC31(R), an Adjuvanted TB Subunit Vaccine, in HIV-Infected Adults with CD4+ Lymphocyte Counts Greater than 350 cells/mm<sup>3</sup>: A Phase II, Multi-Centre, Double-Blind, Randomized, Placebo-Controlled Trial. *PLoS One*. 2014;9:e114602.
- [231] Lin PL, Dietrich J, Tan E, Abalos RM, Burgos J, Bigbee C, et al. The multistage vaccine H56 boosts the effects of BCG to protect cynomolgus macaques against active tuberculosis and reactivation of latent *Mycobacterium tuberculosis* infection. *J Clin Invest*. 2012;122:303-14.
- [232] Luabeya AK, Kagina BM, Tameris MD, Geldenhuys H, Hoff ST, Shi Z, et al. First-in-human trial of the post-exposure tuberculosis vaccine H56:IC31 in *Mycobacterium tuberculosis* infected and non-infected healthy adults. *Vaccine*. 2015;33:4130-40.
- [233] Elvang T, Christensen JP, Billeskov R, Thi Kim Thanh Hoang T, Holst P, Thomsen AR, et al. CD4 and CD8 T cell responses to the *M. tuberculosis* Ag85B-TB10.4 promoted by adjuvanted subunit, adenovector or heterologous prime boost vaccination. *PLoS One*. 2009;4:e5139.
- [234] Knudsen NP, Olsen A, Buonsanti C, Follmann F, Zhang Y, Coler RN, et al. Different human vaccine adjuvants promote distinct antigen-independent immunological signatures tailored to different pathogens. *Sci Rep*. 2016;6:19570.
- [235] Billeskov R, Tan EV, Cang M, Abalos RM, Burgos J, Pedersen BV, et al. Testing the H56 Vaccine Delivered in 4 Different Adjuvants as a BCG-Booster in a Non-Human Primate Model of Tuberculosis. *PLoS One*. 2016;11:e0161217.
- [236] Ruhwald M, Agger EM, Hoff ST, Andersen P. H1- and H56- subunit vaccines against TB - an overview of the clinical development. *Eur Respir J*. 2014;44.
- [237] Evans TG, McElrath MJ, Matthews T, Montefiori D, Weinhold K, Wolff M, et al. QS-21 promotes an adjuvant effect allowing for reduced antigen dose during HIV-1 envelope subunit immunization in humans. *Vaccine*. 2001;19:2080-91.
- [238] Regules JA, Cicatelli SB, Bennett JW, Paolino KM, Twomey PS, Moon JE, et al. Fractional Third and Fourth Dose of RTS,S/AS01 Malaria Candidate Vaccine: A Phase 2a Controlled Human Malaria Parasite Infection and Immunogenicity Study. *J Infect Dis*. 2016;214:762-71.
- [239] Nassim C, Christensen S, Henry D, Holmes S, Hohenboken M, Kanasa-Thanan N. Identification of Antigen and Adjuvant Doses Resulting in Optimal Immunogenicity and Antibody Persistence up to One Year After Immunization with a Pandemic A/H1N1 Influenza Vaccine in Children 3 to < 9 Years of Age. *The Pediatric infectious disease journal*. 2012.
- [240] Moguche AO, Musvosvi M, Penn-Nicholson A, Plumlee CR, Mearns H, Geldenhuys H, et al. Antigen Availability Shapes T Cell Differentiation and Function during Tuberculosis. *Cell Host Microbe*. 2017;21:695-706 e5.
- [241] Tchilian EZ, Desel C, Forbes EK, Bandermann S, Sander CR, Hill AV, et al. Immunogenicity and protective efficacy of prime-boost regimens with recombinant (delta)ureC hly+ *Mycobacterium bovis* BCG and modified vaccinia virus ankara expressing *M. tuberculosis* antigen 85A against murine tuberculosis. *Infect Immun*. 2009;77:622-31.
- [242] Fletcher HA, Tanner R, Wallis RS, Meyer J, Manjaly ZR, Harris S, et al. Inhibition of mycobacterial growth in vitro following primary but not secondary vaccination with *Mycobacterium bovis* BCG. *Clin Vaccine Immunol*. 2013;20:1683-9.
- [243] Loxton AG, Knaul JK, Grode L, Gutschmidt A, Meller C, Eisele B, et al. Safety and Immunogenicity of the Recombinant *Mycobacterium bovis* BCG Vaccine VPM1002 in HIV-Unexposed Newborn Infants in South Africa. *Clin Vaccine Immunol*. 2017;24.
- [244] Campi-Azevedo AC, de Almeida Estevam P, Coelho-Dos-Reis JG, Peruhype-Magalhaes V, Villela-Rezende G, Quaresma PF, et al. Subdoses of 17DD yellow fever vaccine elicit equivalent virological/immunological kinetics timeline. *BMC Infect Dis*. 2014;14:391.

- [245] Wu JT, Peak CM, Leung GM, Lipsitch M. Fractional dosing of yellow fever vaccine to extend supply: a modelling study. *Lancet*. 2016;388:2904-11.
- [246] Roukens AH, Vossen AC, Bredenbeek PJ, van Dissel JT, Visser LG. Intradermally administered yellow fever vaccine at reduced dose induces a protective immune response: a randomized controlled non-inferiority trial. *PLoS One*. 2008;3:e1993.
- [247] Barrett JS, Fossler MJ, Cadieu KD, Gastonguay MR. Pharmacometrics: a multidisciplinary field to facilitate critical thinking in drug development and translational research settings. *Journal of clinical pharmacology*. 2008;48:632-49.
- [248] Gastonguay M. MI-210: Essentials of Population PKPD Modeling and Simulation - Course Notes. Metrum Institute.
- [249] Wright DF, Winter HR, Duffull SB. Understanding the time course of pharmacological effect: a PKPD approach. *Br J Clin Pharmacol*. 2011;71:815-23.
- [250] Mould DR, Upton RN. Basic concepts in population modeling, simulation, and model-based drug development. *CPT Pharmacometrics Syst Pharmacol*. 2012;1:e6.
- [251] Kimko H, Pinheiro J. Model-Based Clinical Drug Development in the Past, Present & Future: a Commentary. *Br J Clin Pharmacol*. 2014.
- [252] Lavielle M. *Mixed Effects Models for the Population Approach: Models, Tasks, Methods and Tools*: Chapman & Hall; 2015.
- [253] Kimko HC, Reece SS, Holford NH, Peck CC. Prediction of the outcome of a phase 3 clinical trial of an antischizophrenic agent (quetiapine fumarate) by simulation with a population pharmacokinetic and pharmacodynamic model. *Clin Pharmacol Ther*. 2000;68:568-77.
- [254] Sheiner LB. Learning versus confirming in clinical drug development. *Clin Pharmacol Ther*. 1997;61:275-91.
- [255] EMA. EFPIA-EMA Modelling and Simulation Workshop Report. 2012.
- [256] Holford NH, Kimko HC, Monteleone JP, Peck CC. Simulation of clinical trials. *Annual review of pharmacology and toxicology*. 2000;40:209-34.
- [257] Zhang L, Pfister M, Meibohm B. Concepts and challenges in quantitative pharmacology and model-based drug development. *AAPS J*. 2008;10:552-9.
- [258] Stone JA, Banfield C, Pfister M, Tannenbaum S, Allerheiligen S, Wetherington JD, et al. Model-based drug development survey finds pharmacometrics impacting decision making in the pharmaceutical industry. *J Clin Pharmacol*. 2010;50:20S-30S.
- [259] Garnett C, Gobburu JV, Lee J. Contribution of Modeling and Simulation in the Regulatory Review and Decision-Making: U.S. FDA Perspective. In: Kimko H, Peck CC, editors. *Clinical Trial Simulations*: Springer; 2010. p. 37-57.
- [260] FDA. FDA Critical Path Initiative. 2004.
- [261] EMA. 2016 Activity report of the Modelling and simulation working group (MSWG). 2016.
- [262] West GB, Brown JH, Enquist BJ. A general model for the origin of allometric scaling laws in biology. *Science*. 1997;276:122-6.
- [263] Boxenbaum H. Interspecies scaling, allometry, physiological time, and the ground plan of pharmacokinetics. *J Pharmacokinet Biopharm*. 1982;10:201-27.
- [264] Mahmood I, Balian JD. The pharmacokinetic principles behind scaling from preclinical results to phase I protocols. *Clinical pharmacokinetics*. 1999;36:1-11.
- [265] Knibbe CA, Zuideveld KP, Aarts LP, Kuks PF, Danhof M. Allometric relationships between the pharmacokinetics of propofol in rats, children and adults. *Br J Clin Pharmacol*. 2005;59:705-11.
- [266] Amantana A, Chen Y, Tyavanagimatt SR, Jones KF, Jordan R, Chinsangaram J, et al. Pharmacokinetics and interspecies allometric scaling of ST-246, an oral antiviral therapeutic for treatment of orthopoxvirus infection. *PloS one*. 2013;8:e61514.
- [267] Wilkins JJ, Langdon G, McIlhannon H, Pillai G, Smith PJ, Simonsson US. Variability in the population pharmacokinetics of isoniazid in South African tuberculosis patients. *Br J Clin Pharmacol*. 2011;72:51-62.

- [268] Katsube T, Yano Y, Wajima T, Yamano Y, Takano M. Pharmacokinetic/pharmacodynamic modeling and simulation to determine effective dosage regimens for doripenem. *J Pharm Sci.* 2010;99:2483-91.
- [269] Westfall PH, Tsai K, Ogenstad S, Tomoiaga A, Moseley S, Lu Y. Clinical trials simulation: a statistical approach. *J Biopharm Stat.* 2008;18:611-30.
- [270] Pienaar E, Dartois V, Linderman JJ, Kirschner DE. In silico evaluation and exploration of antibiotic tuberculosis treatment regimens. *BMC Syst Biol.* 2015;9:79.
- [271] Zhu M, Starke JR, Burman WJ, Steiner P, Stambaugh JJ, Ashkin D, et al. Population pharmacokinetic modeling of pyrazinamide in children and adults with tuberculosis. *Pharmacotherapy.* 2002;22:686-95.
- [272] Milan Segovia RC, Dominguez Ramirez AM, Jung Cook H, Magana Aquino M, Vigna Perez M, Brundage RC, et al. Population pharmacokinetics of rifampicin in Mexican patients with tuberculosis. *J Clin Pharm Ther.* 2013;38:56-61.
- [273] Hamberg AK, Dahl ML, Barban M, Scordo MG, Wadelius M, Pengo V, et al. A PK-PD model for predicting the impact of age, CYP2C9, and VKORC1 genotype on individualization of warfarin therapy. *Clin Pharmacol Ther.* 2007;81:529-38.
- [274] Goncalves BP, Pett H, Tiono AB, Murry D, Sirima S, Niemi M, et al. Age, weight, and CYP2D6 genotype are major determinants of primaquine pharmacokinetics in African children. *Antimicrob Agents Chemother.* 2017.
- [275] Addy C, Tatosian DA, Glasgow XS, Iii IN, Sisk CM, Kauh EA, et al. Effects of Age, Sex, and Obesity on the Single-Dose Pharmacokinetics of Omarigliptin in Healthy Subjects. *Clin Pharmacol Drug Dev.* 2016;5:374-82.
- [276] Sime FB, Roberts MS, Roberts JA. Optimization of dosing regimens and dosing in special populations. *Clinical microbiology and infection : the official publication of the European Society of Clinical Microbiology and Infectious Diseases.* 2015;21:886-93.
- [277] Conti R, Veenstra DL, Armstrong K, Lesko LJ, Grosse SD. Personalized medicine and genomics: challenges and opportunities in assessing effectiveness, cost-effectiveness, and future research priorities. *Med Decis Making.* 2010;30:328-40.
- [278] Ogilvie LA, Wierling C, Kessler T, Lehrach H, Lange BM. Predictive Modeling of Drug Treatment in the Area of Personalized Medicine. *Cancer Inform.* 2015;14:95-103.
- [279] Ballesta A, Zhou Q, Zhang X, Lv H, Gallo JM. Multiscale design of cell-type-specific pharmacokinetic/pharmacodynamic models for personalized medicine: application to temozolomide in brain tumors. *CPT Pharmacometrics Syst Pharmacol.* 2014;3:e112.
- [280] Mould DR, Upton RN. Basic concepts in population modeling, simulation, and model-based drug development-part 2: introduction to pharmacokinetic modeling methods. *CPT Pharmacometrics Syst Pharmacol.* 2013;2:e38.
- [281] Upton RN, Mould DR. Basic concepts in population modeling, simulation, and model-based drug development: part 3-introduction to pharmacodynamic modeling methods. *CPT Pharmacometrics Syst Pharmacol.* 2014;3:e88.
- [282] Vynnycky E, White RG. *Introduction to Infectious Disease Modelling*: Oxford University Press; 2010.
- [283] Dartois C, Brendel K, Comets E, Laffont CM, Laveille C, Tranchand B, et al. Overview of model-building strategies in population PK/PD analyses: 2002-2004 literature survey. *Br J Clin Pharmacol.* 2007;64:603-12.
- [284] Davidian M. Non-linear mixed-effects models. In: Fitzmaurice M, Davidian M, Verbeke G, Molenberghs G, editors. *Longitudinal Data Analysis*: Chapman & Hall/CRC Press; 2009. p. 107-41.
- [285] Bonate PL. *Nonlinear Mixed Effects Models: Theory. Pharmacokinetic-Pharmacodynamic Modeling and Simulation.* 2 ed: Springer US; 2011. p. 233-301.
- [286] Le D, Miller JD, Ganusov VV. Mathematical modeling provides kinetic details of the human immune response to vaccination. *Front Cell Infect Microbiol.* 2014;4:177.
- [287] De Boer RJ, Perelson AS. Quantifying T lymphocyte turnover. *J Theor Biol.* 2013;327:45-87.

- [288] Antia R, Koella JC, Perrot V. Models of the within-host dynamics of persistent mycobacterial infections. *Proc Biol Sci.* 1996;263:257-63.
- [289] Wigginton JE, Kirschner D. A model to predict cell-mediated immune regulatory mechanisms during human infection with *Mycobacterium tuberculosis*. *J Immunol.* 2001;166:1951-67.
- [290] Gammack D, Doering CR, Kirschner DE. Macrophage response to *Mycobacterium tuberculosis* infection. *Journal of mathematical biology.* 2004;48:218-42.
- [291] Marino S, Kirschner DE. The human immune response to *Mycobacterium tuberculosis* in lung and lymph node. *J Theor Biol.* 2004;227:463-86.
- [292] Marino S, Myers A, Flynn JL, Kirschner DE. TNF and IL-10 are major factors in modulation of the phagocytic cell environment in lung and lymph node in tuberculosis: a next-generation two-compartmental model. *J Theor Biol.* 2010;265:586-98.
- [293] Marino S, Sud D, Plessner H, Lin PL, Chan J, Flynn JL, et al. Differences in reactivation of tuberculosis induced from anti-TNF treatments are based on bioavailability in granulomatous tissue. *PLoS computational biology.* 2007;3:1909-24.
- [294] Clarelli F, Natalini R. A pressure model of immune response to mycobacterium tuberculosis infection in several space dimensions. *Math Biosci Eng.* 2010;7:277-300.
- [295] Ibarguen-Mondragon E, Esteva L, Chavez-Galan L. A mathematical model for cellular immunology of tuberculosis. *Math Biosci Eng.* 2011;8:973-86.
- [296] Lalande L, Bourguignon L, Maire P, Goutelle S. Mathematical modeling and systems pharmacology of tuberculosis: Isoniazid as a case study. *J Theor Biol.* 2016;399:43-52.
- [297] Hao W, Schlesinger LS, Friedman A. Modeling Granulomas in Response to Infection in the Lung. *PLoS One.* 2016;11:e0148738.
- [298] Segovia-Juarez JL, Ganguli S, Kirschner D. Identifying control mechanisms of granuloma formation during *M. tuberculosis* infection using an agent-based model. *J Theor Biol.* 2004;231:357-76.
- [299] Bru A, Cardona PJ. Mathematical modeling of tuberculosis bacillary counts and cellular populations in the organs of infected mice. *PLoS One.* 2010;5:e12985.
- [300] Fallahi-Sichani M, Kirschner DE, Linderman JJ. NF-kappaB Signaling Dynamics Play a Key Role in Infection Control in Tuberculosis. *Front Physiol.* 2012;3:170.
- [301] Datta M, Via LE, Chen W, Baish JW, Xu L, Barry CE, 3rd, et al. Mathematical Model of Oxygen Transport in Tuberculosis Granulomas. *Ann Biomed Eng.* 2016;44:863-72.
- [302] Kirschner D. Dynamics of co-infection with *M. Tuberculosis* and HIV-1. *Theor Popul Biol.* 1999;55:94-109.
- [303] Ray JC, Wang J, Chan J, Kirschner DE. The timing of TNF and IFN-gamma signaling affects macrophage activation strategies during *Mycobacterium tuberculosis* infection. *J Theor Biol.* 2008;252:24-38.
- [304] Alavez-Ramirez J, Castellanos JR, Esteva L, Flores JA, Fuentes-Allen JL, Garcia-Ramos G, et al. Within-host population dynamics of antibiotic-resistant *M. tuberculosis*. *Math Med Biol.* 2007;24:35-56.
- [305] Magombedze G, Mulder N. A mathematical representation of the development of *Mycobacterium tuberculosis* active, latent and dormant stages. *J Theor Biol.* 2012;292:44-59.
- [306] Pedruzzi G, Rao KV, Chatterjee S. Mathematical model of mycobacterium-host interaction describes physiology of persistence. *J Theor Biol.* 2015;376:105-17.
- [307] Chisholm RH, Tanaka MM. The emergence of latent infection in the early evolution of *Mycobacterium tuberculosis*. *Proc Biol Sci.* 2016;283.
- [308] McDaniel MM, Krishna N, Handagama WG, Eda S, Ganusov VV. Quantifying Limits on Replication, Death, and Quiescence of *Mycobacterium tuberculosis* in Mice. *Front Microbiol.* 2016;7:862.
- [309] Lyons MA, Reisfeld B, Yang RS, Lenaerts AJ. A physiologically based pharmacokinetic model of rifampin in mice. *Antimicrob Agents Chemother.* 2013;57:1763-71.

- [310] Lyons MA, Lenaerts AJ. Computational pharmacokinetics/pharmacodynamics of rifampin in a mouse tuberculosis infection model. *J Pharmacokinet Pharmacodyn*. 2015;42:375-89.
- [311] Jayaram R, Gaonkar S, Kaur P, Suresh BL, Mahesh BN, Jayashree R, et al. Pharmacokinetics-pharmacodynamics of rifampin in an aerosol infection model of tuberculosis. *Antimicrobial agents and chemotherapy*. 2003;47:2118-24.
- [312] Bruzzese T, Rimaroli C, Bonabello A, Mozzi G, Ajay S, Cooverj ND. Pharmacokinetics and tissue distribution of rifametane, a new 3-azinomethyl-rifamycin derivative, in several animal species. *Arzneimittelforschung*. 2000;50:60-71.
- [313] Binda G, Domenichini E, Gottardi A, Orlandi B, Ortelli E, Pacini B, et al. Rifampicin, a general review. *Arzneimittelforschung*. 1971;21:1907-77.
- [314] Day J, Schlesinger LS, Friedman A. Tuberculosis research: going forward with a powerful "translational systems biology" approach. *Tuberculosis (Edinb)*. 2010;90:7-8.
- [315] Dalmia N, Ramsay AJ. Prime-boost approaches to tuberculosis vaccine development. *Expert Rev Vaccines*. 2012;11:1221-33.
- [316] Macallan DC, Borghans JA, Asquith B. Human T Cell Memory: A Dynamic View. *Vaccines (Basel)*. 2017;5.
- [317] Gong C, Linderman JJ, Kirschner D. Harnessing the heterogeneity of T cell differentiation fate to fine-tune generation of effector and memory T cells. *Front Immunol*. 2014;5:57.
- [318] Monolix: Users Guide. 4.3.3 ed2014.
- [319] Pathan AA, Sander CR, Fletcher HA, Poulton I, Alder NC, Beveridge NE, et al. Boosting BCG with recombinant modified vaccinia ankara expressing antigen 85A: different boosting intervals and implications for efficacy trials. *PLoS One*. 2007;2:e1052.
- [320] McShane H, Pathan AA, Sander CR, Keating SM, Gilbert SC, Huygen K, et al. Recombinant modified vaccinia virus Ankara expressing antigen 85A boosts BCG-primed and naturally acquired antimycobacterial immunity in humans. *Nat Med*. 2004;10:1240-4.
- [321] Raftery A. Bayesian Model Selection in Social Research. *Sociological Methodology*. 1995;25:111-63.
- [322] R. R: A Language and Environment. In: Team DC, editor. Vienna, Austria: R Foundation for Statistical Computing (<http://www.r-project.org/>); 2005.
- [323] Flynn JL. Immunology of tuberculosis and implications in vaccine development. *Tuberculosis (Edinb)*. 2004;84:93-101.
- [324] Mayer-Barber KD, Andrade BB, Oland SD, Amaral EP, Barber DL, Gonzales J, et al. Host-directed therapy of tuberculosis based on interleukin-1 and type I interferon crosstalk. *Nature*. 2014;511:99-103.
- [325] Macallan DC, Asquith B, Irvine AJ, Wallace DL, Worth A, Ghattas H, et al. Measurement and modeling of human T cell kinetics. *Eur J Immunol*. 2003;33:2316-26.
- [326] Homann D, Teyton L, Oldstone MB. Differential regulation of antiviral T-cell immunity results in stable CD8+ but declining CD4+ T-cell memory. *Nat Med*. 2001;7:913-9.
- [327] Soares AP, Kwong Chung CK, Choice T, Hughes EJ, Jacobs G, van Rensburg EJ, et al. Longitudinal changes in CD4(+) T-cell memory responses induced by BCG vaccination of newborns. *J Infect Dis*. 2013;207:1084-94.
- [328] Harrington LE, Janowski KM, Oliver JR, Zajac AJ, Weaver CT. Memory CD4 T cells emerge from effector T-cell progenitors. *Nature*. 2008;452:356-60.
- [329] Hu H, Huston G, Duso D, Lepak N, Roman E, Swain SL. CD4(+) T cell effectors can become memory cells with high efficiency and without further division. *Nat Immunol*. 2001;2:705-10.
- [330] Restifo NP, Gattinoni L. Lineage relationship of effector and memory T cells. *Curr Opin Immunol*. 2013;25:556-63.
- [331] Aagaard CS, Hoang TT, Vingsbo-Lundberg C, Dietrich J, Andersen P. Quality and vaccine efficacy of CD4+ T cell responses directed to dominant and subdominant epitopes in ESAT-6 from *Mycobacterium tuberculosis*. *J Immunol*. 2009;183:2659-68.

- [332] Felmlee MA, Morris ME, Mager DE. Mechanism-based pharmacodynamic modeling. *Methods in molecular biology*. 2012;929:583-600.
- [333] Kelley CT. *Iterative Methods for Optimization*: Society for Industrial and Applied Mathematics; 1999.
- [334] Motulsky HJ, Christopoulos A. *Fitting models to biological data using linear and nonlinear regression. A practical guide to curve fitting*. San Diego, CA: Oxford University Press, USA; 2003.
- [335] Cavanaugh JE. Unifying the derivations for the Akaike and corrected Akaike information criteria. *Statistics and Probability Letters*. 1997;33:201-8.
- [336] Burnham KP, Anderson DR. *Multimodel Inference: Understanding AIC and BIC in Model Selection*. *Sociological Methods and Research*. 2004;33:261-304.
- [337] Rhodes SJ, Zelmer A, Knight GM, Prabowo SA, Stockdale L, Evans TG, et al. The TB vaccine H56+IC31 dose-response curve is peaked not saturating: Data generation for new mathematical modelling methods to inform vaccine dose decisions. *Vaccine*. 2016;34:6285-91.
- [338] Aagaard C, Hoang T, Dietrich J, Cardona PJ, Izzo A, Dolganov G, et al. A multistage tuberculosis vaccine that confers efficient protection before and after exposure. *Nat Med*. 2011;17:189-94.
- [339] Lalvani A, Pathan AA, McShane H, Wilkinson RJ, Latif M, Conlon CP, et al. Rapid detection of *Mycobacterium tuberculosis* infection by enumeration of antigen-specific T cells. *Am J Respir Crit Care Med*. 2001;163:824-8.
- [340] Henriksen-Lacey M, Christensen D, Bramwell VW, Lindenstrom T, Agger EM, Andersen P, et al. Liposomal cationic charge and antigen adsorption are important properties for the efficient deposition of antigen at the injection site and ability of the vaccine to induce a CMI response. *J Control Release*. 2010;145:102-8.
- [341] Sprent J, Basten A. Circulating T and B lymphocytes of the mouse. II. Lifespan. *Cell Immunol*. 1973;7:40-59.
- [342] Hao W, Crouser ED, Friedman A. Mathematical model of sarcoidosis. *Proc Natl Acad Sci U S A*. 2014;111:16065-70.
- [343] Tough DF, Sprent J. Life span of naive and memory T cells. *Stem Cells*. 1995;13:242-9.
- [344] Castiglione F, Liso A. The role of computational models of the immune system in designing vaccination strategies. *Immunopharmacol Immunotoxicol*. 2005;27:417-32.
- [345] Sharpe S, White A, Sarfas C, Sibley L, Gleeson F, McIntyre A, et al. Alternative BCG delivery strategies improve protection against *Mycobacterium tuberculosis* in non-human primates: Protection associated with mycobacterial antigen-specific CD4 effector memory T-cell populations. *Tuberculosis (Edinb)*. 2016;101:174-90.
- [346] Lanzavecchia A, Sallusto F. Dynamics of T lymphocyte responses: intermediates, effectors, and memory cells. *Science*. 2000;290:92-7.
- [347] Lindenstrom T, Knudsen NP, Agger EM, Andersen P. Control of chronic mycobacterium tuberculosis infection by CD4 KLRG1- IL-2-secreting central memory cells. *J Immunol*. 2013;190:6311-9.
- [348] Weir RE, Fine PE, Nazareth B, Floyd S, Black GF, King E, et al. Interferon-gamma and skin test responses of schoolchildren in southeast England to purified protein derivatives from *Mycobacterium tuberculosis* and other species of mycobacteria. *Clin Exp Immunol*. 2003;134:285-94.
- [349] Adekambi T, Ibegbu CC, Kalokhe AS, Yu T, Ray SM, Rengarajan J. Distinct effector memory CD4+ T cell signatures in latent *Mycobacterium tuberculosis* infection, BCG vaccination and clinically resolved tuberculosis. *PLoS One*. 2012;7:e36046.
- [350] Dong C, Martinez G. T cells: The usual subsets. *Nature Reviews Immunology*; 2010.
- [351] Jelliffe R, Schumitzky A, Van Guilder M. Population pharmacokinetics/pharmacodynamics modeling: parametric and nonparametric methods. *Ther Drug Monit*. 2000;22:354-65.
- [352] Kiang TK, Sherwin CM, Spigarelli MG, Ensom MH. *Fundamentals of Population Pharmacokinetic Modelling : Modelling and Software*. *Clin Pharmacokinet*. 2012;51:515-25.

- [353] Beal S, Sheiner LB, Boeckmann A, Bauer RJ. NONMEM User's Guides. Ellicott City, MD, USA: Icon Development Solutions; 2009.
- [354] Wang Y. Derivation of various NONMEM estimation methods. *J Pharmacokinet Pharmacodyn*. 2007;34:575-93.
- [355] Chan PL, Jacqmin P, Lavielle M, McFadyen L, Weatherley B. The use of the SAEM algorithm in MONOLIX software for estimation of population pharmacokinetic-pharmacodynamic-viral dynamics parameters of maraviroc in asymptomatic HIV subjects. *J Pharmacokinet Pharmacodyn*. 2011;38:41-61.
- [356] Bauer RJ, Guzy S, Ng C. A survey of population analysis methods and software for complex pharmacokinetic and pharmacodynamic models with examples. *AAPS J*. 2007;9:E60-83.
- [357] Dartois C, Lemenuel-Diot A, Laveille C, Tranchand B, Tod M, Girard P. Evaluation of uncertainty parameters estimated by different population PK software and methods. *J Pharmacokinet Pharmacodyn*. 2007;34:289-311.
- [358] Mentre F, Dubruc C, Thenot JP. Population pharmacokinetic analysis and optimization of the experimental design for mizolastine solution in children. *J Pharmacokinet Pharmacodyn*. 2001;28:299-319.
- [359] Retout S, Mentre F. Optimization of individual and population designs using Splus. *J Pharmacokinet Pharmacodyn*. 2003;30:417-43.
- [360] Sullivan M. Moving candidate vaccines into development from research: lessons from HIV. *Immunology and cell biology*. 2009;87:366-70.
- [361] FDA. Considerations for the Design of Early-Phase Clinical Trials of Cellular and Gene Therapy Products: Guidance for Industry. In: Services USDoHaH, editor.: Office of Communication, Outreach and Development (OCOD); 2015.
- [362] Beveridge NE, Price DA, Casazza JP, Pathan AA, Sander CR, Asher TE, et al. Immunisation with BCG and recombinant MVA85A induces long-lasting, polyfunctional Mycobacterium tuberculosis-specific CD4+ memory T lymphocyte populations. *Eur J Immunol*. 2007;37:3089-100.
- [363] Wherry EJ. T cell exhaustion. *Nat Immunol*. 2011;12:492-9.
- [364] Cliff JM, Kaufmann SH, McShane H, van Helden P, O'Garra A. The human immune response to tuberculosis and its treatment: a view from the blood. *Immunol Rev*. 2015;264:88-102.
- [365] Ciabattini A, Prota G, Christensen D, Andersen P, Pozzi G, Medaglini D. Characterization of the Antigen-Specific CD4(+) T Cell Response Induced by Prime-Boost Strategies with CAF01 and CpG Adjuvants Administered by the Intranasal and Subcutaneous Routes. *Frontiers in immunology*. 2015;6:430.
- [366] Giefing-Kroll C, Berger P, Lepperdinger G, Grubeck-Loebenstien B. How sex and age affect immune responses, susceptibility to infections, and response to vaccination. *Aging Cell*. 2015;14:309-21.
- [367] Mawa PA, Nkurunungi G, Egesa M, Webb EL, Smith SG, Kizindo R, et al. The impact of maternal infection with Mycobacterium tuberculosis on the infant response to bacille Calmette-Guerin immunization. *Philosophical transactions of the Royal Society of London Series B, Biological sciences*. 2015;370.
- [368] Furman D. Sexual dimorphism in immunity: improving our understanding of vaccine immune responses in men. *Expert Rev Vaccines*. 2015;14:461-71.
- [369] Garmendia J, Morey P, Bengoechea JA. Impact of cigarette smoke exposure on host-bacterial pathogen interactions. *Eur Respir J*. 2012;39:467-77.
- [370] McShane H, Williams A. A review of preclinical animal models utilised for TB vaccine evaluation in the context of recent human efficacy data. *Tuberculosis (Edinb)*. 2014;94:105-10.
- [371] Klein SL, Jedlicka A, Pekosz A. The Xs and Y of immune responses to viral vaccines. *The Lancet infectious diseases*. 2010;10:338-49.
- [372] Daugelat S, Ladel CH, Kaufmann SH. Influence of mouse strain and vaccine viability on T-cell responses induced by Mycobacterium bovis bacillus Calmette-Guerin. *Infect Immun*. 1995;63:2033-40.

- [373] Kester KE, McKinney DA, Tornieporth N, Ockenhouse CF, Heppner DG, Hall T, et al. Efficacy of recombinant circumsporozoite protein vaccine regimens against experimental *Plasmodium falciparum* malaria. *The Journal of infectious diseases*. 2001;183:640-7.
- [374] Hadler SC, de Monzon MA, Lugo DR, Perez M. Effect of timing of hepatitis B vaccine doses on response to vaccine in Yucpa Indians. *Vaccine*. 1989;7:106-10.
- [375] Belshe RB, Frey SE, Graham I, Mulligan MJ, Edupuganti S, Jackson LA, et al. Safety and immunogenicity of influenza A H5 subunit vaccines: effect of vaccine schedule and antigenic variant. *The Journal of infectious diseases*. 2011;203:666-73.
- [376] Brookes RH, Pathan AA, McShane H, Hensmann M, Price DA, Hill AV. CD8+ T cell-mediated suppression of intracellular *Mycobacterium tuberculosis* growth in activated human macrophages. *Eur J Immunol*. 2003;33:3293-302.
- [377] Achkar JM, Chan J, Casadevall A. B cells and antibodies in the defense against *Mycobacterium tuberculosis* infection. *Immunol Rev*. 2015;264:167-81.
- [378] Smith SG, Smits K, Joosten SA, van Meijgaarden KE, Satti I, Fletcher HA, et al. Intracellular Cytokine Staining and Flow Cytometry: Considerations for Application in Clinical Trials of Novel Tuberculosis Vaccines. *PLoS one*. 2015;10:e0138042.
- [379] WHO. Fractional dose yellow fever vaccine as a dose-sparing option for outbreak response. WHO, Geneva: WHO; 2016.
- [380] Martins RM, Maia Mde L, Farias RH, Camacho LA, Freire MS, Galler R, et al. 17DD yellow fever vaccine: a double blind, randomized clinical trial of immunogenicity and safety on a dose-response study. *Human vaccines & immunotherapeutics*. 2013;9:879-88.

## Appendices

### **Appendix A. Paper 5: Dose finding for new vaccines: the role for immunostimulation/immunodynamic modelling**

The contents of paper 5 were a joint contribution between Dr Thomas Evans and myself. Due to his experience in the field, Dr Thomas Evans provided the rationale for the paper and contributed to writing the background and rationale to the text. I aggregated the data for the figures, wrote the technical aspects of the text and incorporated Dr Evans text. Gwen Knight, Richard White and Denise Kirschner reviewed the paper. The participants of the workshop entitled “*Modelling does responses following vaccination*” held on Friday, May 29th 2015 at the headquarters of TB vaccine developers Aeras (Rockville, MD) reviewed the paper.

Registry  
T: +44(0)20 7299 4646  
F: +44(0)20 7299 4656  
E: registry@lshtm.ac.uk

## RESEARCH PAPER COVER SHEET

PLEASE NOTE THAT A COVER SHEET MUST BE COMPLETED FOR EACH RESEARCH PAPER INCLUDED IN A THESIS.

### SECTION A – Student Details

Student	Sophie Rhodes
Principal Supervisor	Richard White
Thesis Title	The development of a mathematical modelling framework to translate TB vaccine response between species and predict the most immunogenic dose in humans using animal data

*If the Research Paper has previously been published please complete Section B, if not please move to Section C*

### SECTION B – Paper already published

Where was the work published?			
When was the work published?			
If the work was published prior to registration for your research degree, give a brief rationale for its inclusion			
Have you retained the copyright for the work?*	Choose an item.	Was the work subject to academic peer review?	Choose an item.

\*If yes, please attach evidence of retention. If no, or if the work is being included in its published format, please attach evidence of permission from the copyright holder (publisher or other author) to include this work.

### SECTION C – Prepared for publication, but not yet published

Where is the work intended to be published?	Vaccine
Please list the paper's authors in the intended authorship order:	Sophie J. Rhodes, Gwenan M. Knight, Denise Kirshcner, Richard G. White, Thomas G. Evans
Stage of publication	<b>Submitted</b>

### SECTION D – Multi-authored work

For multi-authored work, give full details of your role in the research included in the paper and in the preparation of the paper. (Attach a further sheet if necessary)	See next page
--	---------------

Student Signature: \_\_\_\_\_



Date: 13/6/17

Supervisor Signature: \_\_\_\_\_



Date: 13/6/17

## **Dose finding for new vaccines: the role for immunostimulation/immunodynamic modelling**

Authors: Sophie J. Rhodes<sup>a\*</sup>, Gwenan M. Knight<sup>a,b</sup>, Denise E. Kirschner<sup>c</sup>, Richard G. White<sup>a+</sup>, Thomas G. Evans<sup>d+</sup>

\* Corresponding author

+ joint senior authors

Institutions:

<sup>a</sup> TB Modelling Group, CMMID, TB Centre, London School of Hygiene and Tropical Medicine, UK

<sup>b</sup> National Institute for Health Research Health Protection Research Unit in Healthcare Associated Infection and Antimicrobial Resistance, Imperial College London, UK

<sup>c</sup> University of Michigan Medical School, Ann Arbor, MI, USA

<sup>d</sup> TomegaVax, Portland, Oregon, USA

## **Abstract**

Vaccine dosing decision making employs relatively antiquated methods compared to the methods employed for drug dosing decision making. As such, we may be discarding vaccine candidates and wasting considerable resources. This failure to use modern methods may, in part, be due to the complexities in measuring a biomarker of vaccine efficacy and defining the dynamics of the immune system, but also simply represents a failure to harness quantitative expertise into vaccine development. We challenge this status quo by translating the mathematical frameworks used for drug dosing to optimise vaccine dosing decision making, which we define as immunostimulation/immunodynamic modelling.

## Introduction to vaccine dose

Vaccines are one of the most important public health discoveries and are the most cost-efficient intervention known in medicine [1]. Both the pipeline and business rationale for new vaccines are strong [2]. However, taking a vaccine from discovery to licensure can cost in the region of US\$0.8 billion [3]. With these enormous costs, there is intense pressure to make well-informed decisions at each stage of the development process; mistakes are expensive and delays can waste precious time that could save lives. Finding optimal *vaccine dose amounts* (hereafter dose), as well as *identifying appropriate regimens*, are key factors in reaching maximal vaccine efficacy at the requisite safety level. Ideally, we would gain the most accurate information regarding vaccine efficacy if we tested a wide range of doses in humans; however, we are constrained by clinical, ethical, historical, and financial concerns. Instead, we currently estimate effective human doses based on responses in small animal models in which we are able to test large dose ranges over short timeframes. The key challenge is then to accurately translate vaccine responses from these animal studies to humans, as the relationships are still not fully characterized, and fraught with issues of not only scale, but physiological differences between species. Therefore, it is common in later stage vaccine studies to allow the momentum of clinical development, despite a lack of clear understanding of immune response kinetics, to drive selection of a dose that has not been thoroughly evaluated.

So, the question remains: how can we more effectively and systematically identify an optimal vaccine dose? Surprisingly, the definitive text on vaccine development does not include strategies for dose finding [4] and there is limited regulatory guidance on dose-finding methodologies from licensing organizations such as the FDA [5]. Authoritative reviews of the recently approved RTSS-S malaria vaccine from WHO and the developer make no mention of the confidence of the selection of dose (even after extensive analysis of regimen), despite previous data which calls the certainty of dose selection into question [6, 7]. In fact, prior to a recent submission the confidence intervals concerning the selection of the “right dose” have not been stated.

The world of drug development faced similar questions, yet is far more advanced in the use of systematic methods for dose optimization. This can be attributed partly to the use of pharmacometrics: mechanistic mathematical models that describe within host drug dynamics (pharmacokinetics/pharmacodynamics (PK/PD), see Table 1: Mathematical/quantitative methods technical glossary, for definition).

In the drug development world, the recognition for the need for quantitative analysis to assess drug dose happened 40+ years ago and moved forward with little knowledge of data (and software) requirements. Now, the large pharmaceutical industry has decades of effort applying quantitative analysis to improve dose selection for small molecule drugs. There is no such parallel used for vaccine dosing, which may be due to the diversity and complexity of immune responses measured or a lack of appreciation of potential tools. Vaccine development is now in a position (40 years later) to borrow from the experiences, expertise and technical utilities of model-based drug development, which we believe will vastly accelerate effective vaccine development.

Our aim is to launch a new field for to applying quantitative methods to improve vaccine dose decision-making and ultimately vaccine discovery: immunostimulation/immunodynamic (IS/ID) modelling. We present discussion on existing complexities around dose determination for vaccines; techniques used in the drug development field; how these techniques might be applied to vaccine studies, and how these studies would be advanced if such a path were taken.

### **Complexities between vaccine dose and response**

The immune response required for protection against a disease relies on complex interactions that behave nonlinearly over time and across multiple biological scales (e.g. molecular to cellular to whole systems). In addition, the variation in immune responses to vaccination can be large across different ages and populations, possibly attributed to underlying differences in genetics or exposure rates. Assays and protocols for measuring immune response, as well as the chosen biomarkers, may also vary in usage and dynamic range across populations.

Such complexity can present enormous challenges in the early stages of vaccine development. For example, while having access to an agreed biological marker of protective response is beneficial, vaccine development is often moved forward without such a marker, and it is not until later that efficacy evaluations are determined [8]. Nonetheless, during product development dose decisions must be made, regardless of the developer's faith in the biomarker to demonstrate efficacy. As such, our goal here is not to discuss the actual surrogates of vaccine efficacy, but how to apply a quantitative, systematic framework to increase the likelihood of selecting an optimal dose, once a surrogate is chosen.

A key assumption in the development of new vaccines is an often presupposed relationship between dose and host response: historically the sigmoidal, saturation curve (usually on a logarithmic axis) has reigned supreme (Figure 1A) [9, 10]. This assumes that a minimum vaccine dose can be found that gives no host response, that there is a window of vaccine doses where the response rapidly escalates and that there is a clear response plateau above a certain dose threshold. The goal of vaccine development has then been to increase the dose until the response plateau is reached and assume the highest, safe dose is optimal (with some margin of error to allow for host variation).

However, this "classic" sigmoidal response curve is now being challenged by data from newer vaccine platforms (Figure 1B-D). For example, a trial of a gp120 vaccine in alum for HIV-1 infection in humans, as compared to the same protein formulated with QS-21, revealed that the surrogate response (at the time this was binding and homologous virus neutralization) at a dose of 30  $\mu\text{g}$  was equivalent to that of 300  $\mu\text{g}$  of the same vaccine in alum. A further study with 0.5, 3, and 30  $\mu\text{g}$  of the vaccine, revealed no decrease in response (Figure 1B) [11, 12]. Functional assays showed a peak response at the lowest dose which was 1,000 fold lower than that observed when alum was used as an adjuvant. Thus, neither the lower bound nor the curve of the dose response relationship has ever been established (which may or may not be sigmoidal), due to an inability to accurately dilute the vaccine.

Figure 1C outlines a dose response curve for the surrogate Tuberculosis (TB) protection measure, IFN- $\gamma$  level, in mice receiving a candidate vaccine of fusion protein H56 in the IC31 adjuvant system [13]. When responses were tested two weeks after vaccination, the IFN- $\gamma$

response was higher at lower doses suggesting a lower dose is optimal. These early animal dose response data are reflected in the preliminary human dose response curve [14]. To note, responses taken at such early time points may not represent the memory response, which could be indicative of long-lasting immunity. However, this information is not regularly recorded.

Figure 1D shows our overall experience with a human adenovirus (Ad35) vaccine, in which antigen-specific CD4+ and CD8+ T cell cytokine responses are not congruent, exhibiting maximum responses at different vaccine doses and highlighting the limitations of achievable dose concentrations [15, 16]. Thus, dose response studies will need to be defined by choosing one of the cellular responses as primary, or by a pre-determined ratio of the two.

These unexpected dose response curves have not been adequately acknowledged nor explored for vaccine development and dosing. Additionally, the influence of varying vaccine composition (i.e. antigen and adjuvant formulations) may result in differing dose response curves, for example, the inverted U-shaped response [17, 18] described in Fig 1C. To test all combinations of adjuvant and antigen(s) clinically, requires a large, expensive multi-dimensional factorial design trial. A mathematical and computational modelling framework would have the capability to more effectively explore and narrow this space before trials ever began.

### **Vaccine dose finding: current methods and comparison to drug dose optimization**

Current methods for finding optimal vaccine dose are purely empirical [4]. Typically, a “low” dose in mice or other small animals is chosen and increased by half log increments until the maximum plateau in response is met. This dose range is then scaled up and applied in larger animals and humans. However, no formal assessment of vaccine allometric scaling (see Table 1 for definition) has been undertaken for vaccine development; vaccine induced immune mechanisms and how they differ with species are not considered in this scaling. This may be problematic as the immune response between animals and humans appears to range between none with some protein formulations to nearly 500-fold scaling with DNA (from microgram in the mouse to milligrams in man [19]). Once the starting dose has been

established in humans, it is then increased incrementally until a “maximal” safe dose, which is defined by predetermined safety criteria, is achieved.

This empirical methodology means human trials often progress with a pre-defined limited number of doses. Ultimately, vaccine dose decisions are being made without a complete understanding of the confidence intervals for the full range of the dose response curve. In drug development, the determination of optimal dose is based on more quantitative approaches: model-based PK/PD determinations and allometry, and toxicology bounds.

Animal experiments are first conducted to determine the exposure and half-life of the active drug components in the relevant regions of the body. Mathematical models are then applied to this data to predict doses that generate the desired PK/PD outcome. By applying allometric scaling to the model parameters, in conjunction with the effects of variation in metabolic pathway across species, an estimation of the doses needed to obtain similar exposure in humans is then derived. Following this, the PK/PD modeler can then postulate appropriate doses to be used in initial clinical studies to estimate the dose response relationship based on acceptable toxicity. As more data becomes available, PK/PD models can be used iteratively to refine these estimates, aiding in a reduction of the total number of subjects required to establish the desired confidence intervals, thus minimizing potential harm. As an example, modelling was able to tease through the different doses and protocols to derive optimal values for TB drug treatments, which previously had never been formally compared[20]. In classic drug trials, toxicology boundaries are established, in healthy volunteers, by quickly determining the maximally tolerated dose (MTD). For example, in oncology, drug safety bounds are established through iterative *learning and confirming*; by applying the “3+3 design” [21] or continual reassessment methodology [22].

In summary, as modelling is not performed for vaccines, nor is allometric scaling for vaccines well understood, both our vaccine trials and final doses are prone to be sub-optimal.

**Immunostimulation (IS) /immunodynamic (ID) modelling: Mathematical modelling for improved vaccine dose decision making**

Our proposal for using mathematical modelling to inform vaccine dose finding is based on the approach used in drug development. Utilizing pre-clinical dose and toxicology information and the method we term vaccine immunostimulation (IS) /immunodynamic (ID) modelling (an analogue of the established PK/PD modelling), we aim to translate dose response relationships from animals to humans. The proposed steps to achieve this aim, outlined in Figure 2, are as follows:

7. An immunogenic vaccine is developed and a wide range of doses are tested in mice or best-other-animal model to establish an initial approximate dose response curve. An aim here is to find the minimum and maximum doses that provide the bounds of the dose response curve (within the constraints of the manufacturing process and ability of the assay to assess the dose). Of note, each new adjuvant formulation of a given antigen combination should be considered a unique entity.
8. Mechanistic mathematical modelling techniques (IS/ID) are applied to estimate the parameters that describe the underlying dynamics of the initial animal-derived dose response relationship. Historical data from similar platforms could be used as guidance. The modeler then determines the experimental design to yield the maximum information on the dose response curve, given limitations on animal number, ability to achieve the desired concentrations of the product, and cost. For example, the modeler and developer then develop a further study to asymptotically approach the best dose, using methods to select both the doses to be studied and the number of animals per group. Pre-defined desired confidence intervals can be used to determine the groups and group numbers.
9. Allometric scaling based on historical data from similar platforms or products is used to translate the IS/ID model parameters from animal to human and thus predict the *theoretical* human dose response relationship.
10. A selection of doses is chosen to most rapidly define the extremes of the response based on this theoretical prediction. As in step 1, the aim is to define an approximate shape and the confidence bounds of the dose response curve (depending on the variability of the immune response measurement(s) chosen), using a limited number of human subjects per arm.
11. IS/ID modelling is applied using the phase 1 data to predict the dose response relationship as a guide for a limited number of further doses to be tested, either in an

adaptive fashion in Phase 1 or incorporated into a future study. A dose-response surrogate that can be assessed in essential real-time and an unblinded assessment team are needed.

12. This data is then fed back into the model (step 5) to gain understanding of the confidence intervals around the chosen doses. As further human data is collected, the IS/ID model is refined, used to hone best dose and to design next phase trials.

IS/ID modelling requires the use of not only statistical models, but *mechanistic* mathematical models that yield an understanding of the underlying mechanics of the immune response (refer to Table 1 for distinction between statistical and mathematical modelling). At present this mechanistic modelling for vaccines is in its infancy, but approaches are now underway with B cells and antibodies (however, not yet for dose) [23].

Mathematical modelling can also be further incorporated into the Phase 2 clinical development stage by borrowing techniques used outside the public health field. For example, Evolutionary Operation uses modelling to continually evolve trial design by perturbing model parameters and assessing effects on model outcome [24, 25]. Modelling can then inform trial designs likely to produce a given result whilst minimizing the number of participants exposed to the product. These trial designs can then be clinically verified.

Difficulties can be anticipated when predicting response confidence intervals due to between-patient response variability. However, methods from drug PK/PD analysis are readily available to address such variability; for example, nonlinear mixed effects modelling (NLMEM or machine learning) is an established statistical framework to characterize the variation within and between individual responses in a population (see Table 1).

Another major concern for vaccine developers is the ability to formulate a wide enough range of doses needed to adequately assess the dose response relationship. Additionally, assays for measuring the dose of the vaccine, or chosen immune response surrogate may potentially be unreliable at high or very small doses. These issues need to be taken into consideration when initiating the design of dosing studies.

## **Next steps for implementation**

How can we implement vaccine dose modelling? First, we believe that a collaborative group of interested parties from academia, biotech, large vaccine manufacturers, regulators, governmental and non-governmental agencies must be established to aid communication, data access and development of methodology. The first meeting of such a group of individuals occurred in May 2015 at the headquarters of TB vaccine developers Aeras (Rockville, MD), where a multidisciplinary team met to discuss the current state of vaccine dose finding and the potential for mathematical modelling to assist in this arena.

Second, we need to apply incentives, such as large data packages and a commitment by vaccine developers, to encourage modelers with experience in drug dosing to move to vaccine studies, which has a potentially greater impact on human health than any other treatment intervention. Linking to existing modelling consortia such as the TB Modelling and Analysis Consortium and International Society of Pharmacometrics would also facilitate access to modelling expertise. We believe that the vaccine regulatory bodies have also lacked critical evaluations of vaccine product dose selection, and that agencies such as FDA should encourage modelers to move from the drug side of the agency into vaccines. Thus, the motivation and investments must come from both bottom up and top down.

Third, modelers need to be involved throughout the entire vaccine development process, even before initiating the earliest animal studies, to help narrow the design space and predict optimal outcomes at each step. In drug development, modelers use all available (relevant and standardized) data to refine the understanding of PK/PD findings throughout the product development process. This has historically had a great influence on trial design; generating sufficient data to enable informative modelling. First steps to include modelling into vaccine development are under way in TB research. We conducted an intensive animal vaccine multi-dose study of a candidate TB vaccine (presently in phase 2) designed by a modeler specifically to generate data for dose response finding using translational IS/ID methods. IS/ID modelling was applied to determine the dose-response curve and shows a definitive n-shape for multiple time points after vaccination and that the predicted best dose is likely to be lower than previously investigated (manuscript under review). Preliminary work has been

conducted to *simulate* further responses (based on this empirical data) to obtain optimal dosing cohorts and narrow the confidence interval around predicted best dose. Additionally, we are now also developing a IS/ID mechanistic model of the dose-dependent induction of memory, effector, and regulatory T cell subsets (as per [26, 27]) to translate best dose from mouse to human.

Fourth, we recommend the creation of large shared data platforms through large-scale collaborative efforts with multinational pharmaceutical companies; platforms such as the Critical Path Institute already exist in drug development. Creating a parallel venture in vaccine development would help achieve the aim of attracting modelers as well as maximizing information on vaccine allometric scaling information and model parameterization.

Finally, we encourage the NIH and other vaccine funding agencies to consider head to head studies in which conventional methods for selecting vaccine dose are used in parallel with the outlined modelling techniques, to better understand the impact on speed of development, number of participants exposed and cost of vaccine design.

### **Summary**

In summary, the field of vaccine dosing determination remains in an undeveloped state compared to its far more advanced drug counterpart, due to a lack of a formal quantitative methodology, approach and assessment. This may, in part, be due to complex and incompletely understood vaccine immune responses, but also simply a failure to harness quantitative expertise into vaccine research. To move forward, we need to work collaboratively to design more effective pre-clinical experiments and adapt existing mathematical frameworks to determine how to systematically identify optimal vaccine dose. We challenge this status quo by translating the mathematical frameworks used for drug dosing to optimize vaccine dosing decision making, and to launch the field of immunostimulation/immunodynamic modelling.

### *Acknowledgements*

We would like to thank the attendees of the *Modelling does responses following vaccination* workshop held on Friday, May 29th 2015 at the headquarters of TB vaccine developers Aeras (Rockville, MD), namely, P. Heaton, S. Kern, J. Cox, D. Kaslow, S. Ciupe, K. Kester, R. Small, V. Sinha, J. Yu, D. Zak, M. Davenport, M. White, W. Dewé, I. Troconiz. Their expert input has greatly informed this discussion. Additionally, we would like to thank our colleagues at Statens Serum Institut for access to immunogenicity data for the H56+IC31 vaccine in mice.

### *Funding*

SR is supported by a LSHTM studentship funded by Aeras. GK is funded by the National Institute for Health Research Health Protection Research Unit (NIHR HPRU) in Healthcare Associated Infection and Antimicrobial Resistance at Imperial College London in partnership with Public Health England (PHE). The views expressed are those of the author(s) and not necessarily those of the NHS, the NIHR, the Department of Health or Public Health England. RGW is funded the UK Medical Research Council (MRC) and the UK Department for International Development (DFID) under the MRC/DFID Concordat agreement that is also part of the EDCTP2 programme supported by the European Union (MR/J005088/1), the Bill and Melinda Gates Foundation (TB Modelling and Analysis Consortium: OPP1084276) and UNITAID (4214-LSHTM-Sept15; PO #8477-0-600).

### *Additional Information*

#### *Author contributions*

SR and TE wrote the main manuscript text. TE provided the data for Figure 1 and SR prepared Figures 1 and 2 and wrote Table 1. All authors (SR, GK, DK, RW, TE) reviewed the manuscript.

Description of mathematical approach	Application/Examples
<p><b>Mathematical modelling:</b> The use of mathematical language to mimic the mechanisms of a naturally occurring system [28].</p>	<p>The most commonly used models in mathematical biology are “compartmental models” that use ordinary differential equations to capture the flow into and out of specified “compartments” believed to reflect the important parts or sub-populations of the system. For example, in infectious disease modelling, to describe the spread of a pathogen within a population, the compartments of susceptible, infected and recovered are used (see case studies in [29]). The additional complexity of math models, vs. statistical models, yields potentially improved understanding of the mechanistic relationships between variables.</p>
<p><b>Statistical modelling:</b> A model concerned with identifying the probability distributions of data in order to make inferences on tendencies in the dataset. Models that attempt to quantify the relationship between independent and outcome (dependent) variables.</p>	<p>Data can be modeled by common parametric continuous distributions such as the Gaussian and Gamma, or Poisson for considering frequency of events in time. Regression analysis and splines describe the relationship between variables.</p>
<p><b>Pharmacokinetics (PK):</b> What the body does to the drug, i.e. the concentration of drug in the body (as it is absorbed and eliminated) over time [30].</p> <p><b>Pharmacodynamics (PD):</b> What the drug does to the body, i.e. how the “effect” of the drug (e.g. in the blood) changes with the concentration of the drug in the body [30].</p> <p><b>PKPD modelling (AKA pharmacometric modelling):</b> The use of a mathematical model (e.g. compartmental, <math>E_{max}</math> equation) to describe the PK and PD mechanisms related to a drug in the host [31].</p> <p><b>Nonlinear Mixed Effects Modelling (NLMEM):</b> A statistical framework in which a pharmacometric mathematical model is placed in order to quantify the variability in the model parameters across a population. Software such as NONMEM[32], Monolix [33] , WinBUGs [34], Adapt [35] have been developed specifically for NLMEM analysis.</p> <p><b>Pharmacometric population modelling approach:</b> The use of pharmacometric and statistical modelling (NLMEM) to quantify differences in individual drug responses across a population and what population characteristics can be attributed to causing these differences.</p>	<p>The pharmacometric population modelling approach has been widely accepted and applied in drug development[36] in areas such as:</p> <ul style="list-style-type: none"> <li>▪ <u>Early “first-in-man” dose selection:</u> Extrapolation of preclinical efficacy and safety data to early-stage clinical trials using physiological based PK (PBPK) models to make predictions of the full time course of PK mechanisms [37].</li> <li>▪ <u>Identifying important subpopulations:</u> Identification of which covariates in a population provide an explanation of the nature of PK variability in drug responses. As a consequence, dosage/regimens may be optimized or “personalized” for these populations.</li> <li>▪ <u>Designing and optimizing studies in later stages:</u> Testing dose escalation [38] and regimen for designing proof of concept studies and optimizing sampling design. In addition, aiding in designing or simulating confirmatory studies; “Learning and confirming” [39].</li> </ul>

<p><b>Allometric scaling:</b> The quantifiable relationship between animal body size and characteristic, e.g. the physiological relationship between animal size and metabolism or life span. Scaling can be used to compare animal characteristics over time, as the animal grows (ontogenetic allometry) or within a species population (static allometry) or between species (evolutionary allometry)[40].</p>	<p>In humans, allometric scaling is applied to common PK parameters such as volume of distribution, absorption and clearance by using the host's weight, (e.g. for the drug Isoniazid e.g.[41]). Translational studies between species (nonhuman to human) compare PK parameters by using power equations relating the parameter to body weight[42-44] to scale between species. For examples see [45, 46].</p>
---	---

**Table 1. Mathematical/quantitative methods technical glossary**

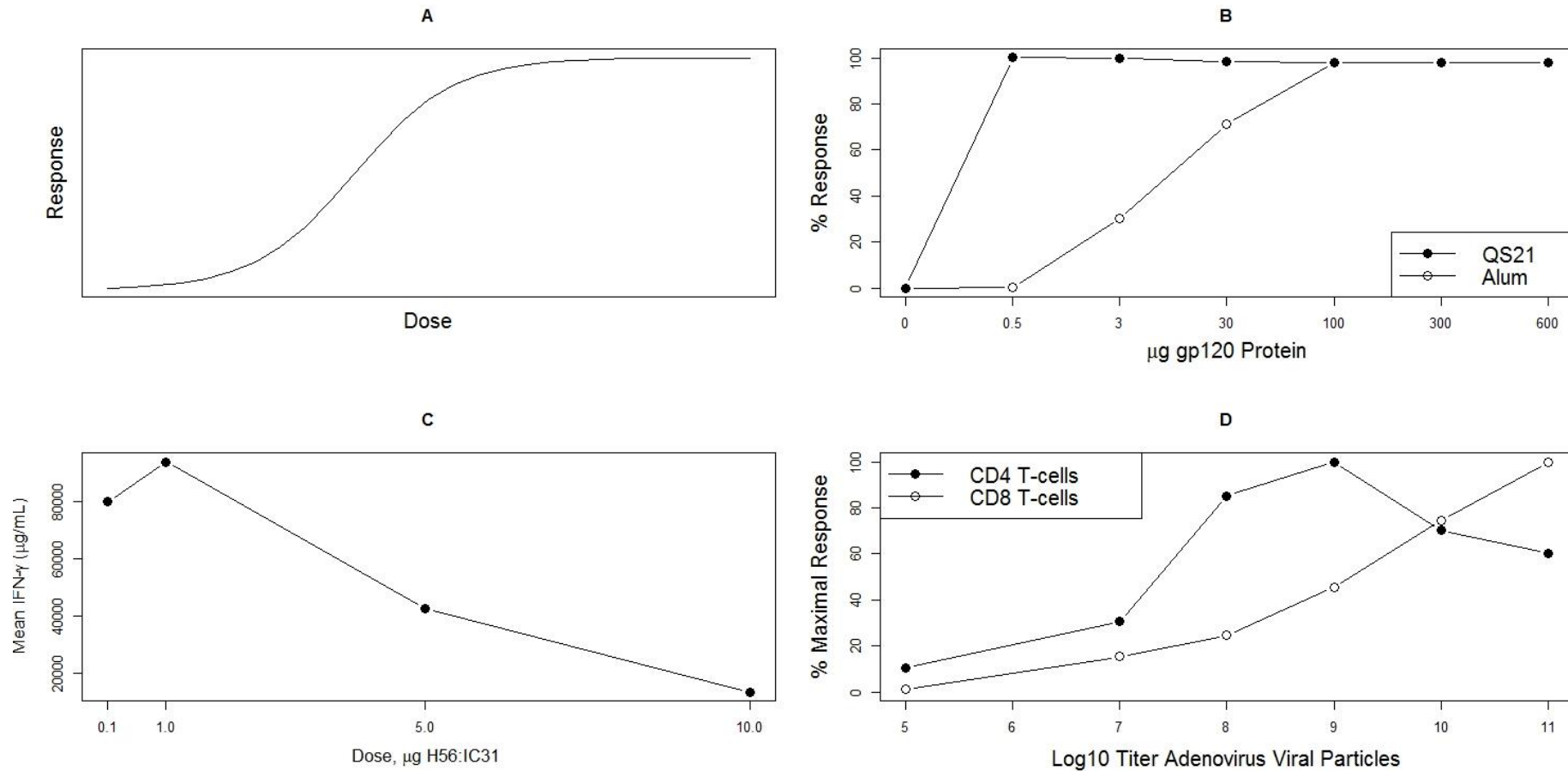


**Figure 1. Dose response curves for vaccines showing relationships between dose and the corresponding host response.** (A) Demonstration of a theoretical sigmoidal dose response curve. (B) Results of two independent studies of a HIV-1 gp120 vaccine using either alum or QS-21 and graphically depicted as percent of the maximal response of antibody titers (either oligomeric binding or neutralizing). (C) Dose-response curve of two-week IFN-gamma levels emitted by CD4+ T-cells in splenocytes of mice that received the candidate TB vaccine of fusion protein H56 in the IC-31 adjuvant system. Median values from 6 mice per dose are shown. The differences in response at each dose are significantly different ( $p < 0.05$ ). (D) A dose-response combined parameter for cytokine producing T cells induced by an Ad35 vaccine based on studies conducted in mice, rhesus macaques, and humans. CD4+ T cells are induced and maximal at lower doses and CD8+ T cell responses continue to increase with dose. Both the ability to make a more concentrated stock and toxicity at the highest dose limited further dose finding in humans.

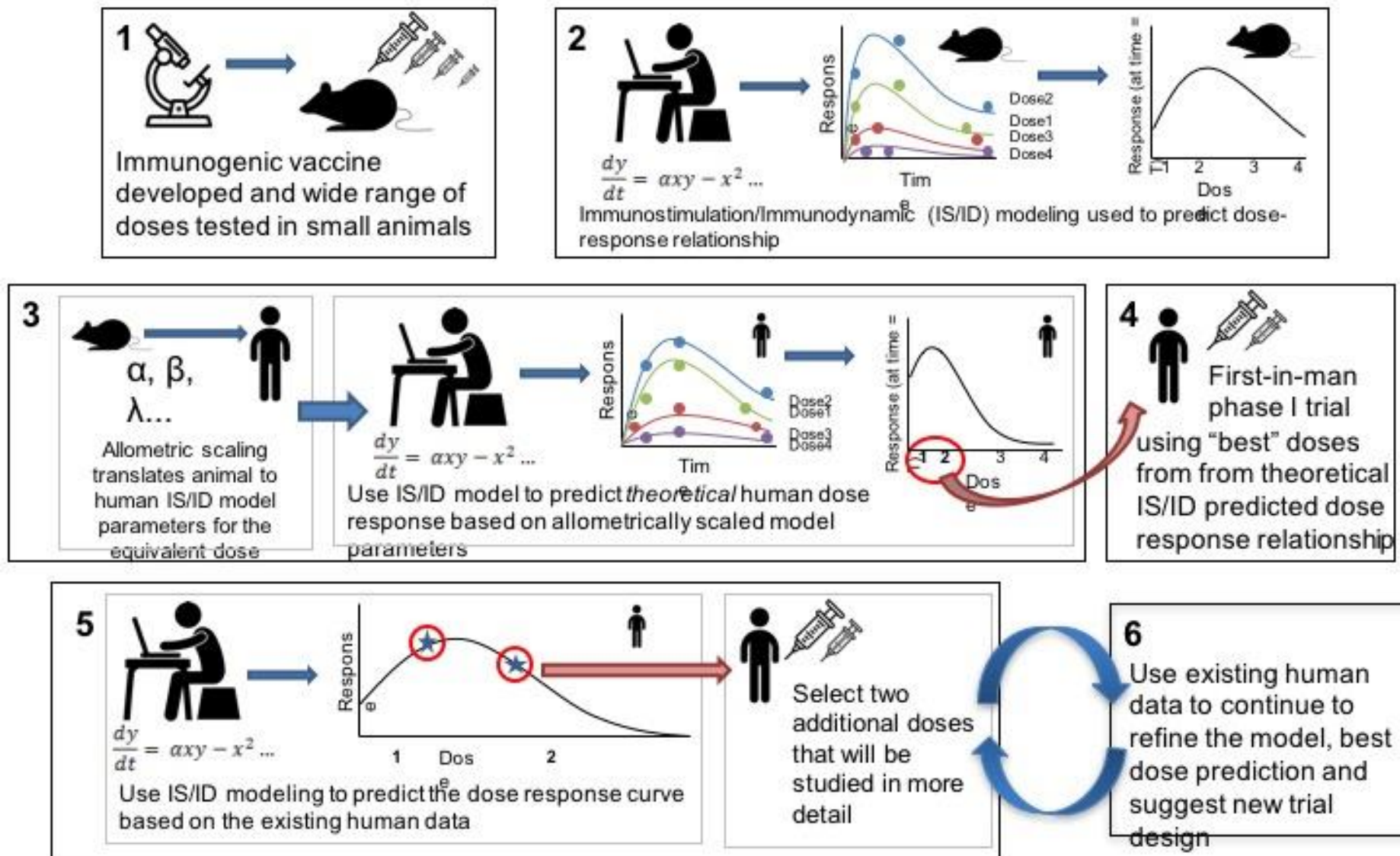


Figure 2. Schema depicting the steps required to incorporate immunostimulation (IS) /immunodynamic (ID) modeling into vaccine development. [Graphics included credited to The Noun Project <https://thenounproject.com/>]

## Paper 5: References

- [1] Han S. Clinical vaccine development. *Clinical and experimental vaccine research*. 2015;4:46-53.
- [2] Kaufmann SH, McElrath MJ, Lewis DJ, Del Giudice G. Challenges and responses in human vaccine development. *Current opinion in immunology*. 2014;28:18-26.
- [3] Dickson M, Gagnon JP. The cost of new drug discovery and development. *Discovery medicine*. 2004;4:172-9.
- [4] Plotkin SA, Orenstein WA, Offit PA. *Vaccines*. 6 ed: Saunders; 2013.
- [5] White AD, Sarfas C, West K, Sibley LS, Wareham AS, Clark S, et al. Evaluation of the Immunogenicity of Mycobacterium bovis BCG Delivered by Aerosol to the Lungs of Macaques. *Clinical and vaccine immunology : CVI*. 2015;22:992-1003.
- [6] JTEG. Background paper on the RTS,S/AS01 Malaria vaccine. Geneva, Switzerland: WHO; 2015.
- [7] Stoute JA, Slaoui M, Heppner DG, Momin P, Kester KE, Desmons P, et al. A preliminary evaluation of a recombinant circumsporozoite protein vaccine against Plasmodium falciparum malaria. *RTS,S Malaria Vaccine Evaluation Group. The New England journal of medicine*. 1997;336:86-91.
- [8] Plotkin SA. Vaccines: correlates of vaccine-induced immunity. *Clinical infectious diseases : an official publication of the Infectious Diseases Society of America*. 2008;47:401-9.
- [9] Little SF, Webster WM, Norris SL, Andrews GP. Evaluation of an anti-rPA IgG ELISA for measuring the antibody response in mice. *Biologicals : journal of the International Association of Biological Standardization*. 2004;32:62-9.
- [10] Semenova VA, Schiffer J, Steward-Clark E, Soroka S, Schmidt DS, Brawner MM, et al. Validation and long term performance characteristics of a quantitative enzyme linked immunosorbent assay (ELISA) for human anti-PA IgG. *Journal of immunological methods*. 2012;376:97-107.
- [11] Shibata R, Peterson M, Good J. Effect of adjuvant QS21 on antibody response by rgp120 vaccines. 13th International AIDS Conference. Durban, ZA2000.
- [12] Evans TG, McElrath MJ, Matthews T, Montefiori D, Weinhold K, Wolff M, et al. QS-21 promotes an adjuvant effect allowing for reduced antigen dose during HIV-1 envelope subunit immunization in humans. *Vaccine*. 2001;19:2080-91.
- [13] Lingnau K, Riedl K, von Gabain A. IC31 and IC30, novel types of vaccine adjuvant based on peptide delivery systems. *Expert review of vaccines*. 2007;6:741-6.
- [14] Geldenhuys H, Mearns H, Miles DJ, Tameris M, Hokey D, Shi Z, et al. The tuberculosis vaccine H4:IC31 is safe and induces a persistent polyfunctional CD4+T cell response in South African adults: A randomized controlled trial. *Vaccine*. 2015;33:3592-9.
- [15] Kagina BM, Tameris MD, Geldenhuys H, Hatherill M, Abel B, Hussey GD, et al. The novel tuberculosis vaccine, AERAS-402, is safe in healthy infants previously vaccinated with BCG, and induces dose-dependent CD4+and CD8T cell responses. *Vaccine*. 2014;32:5908-17.
- [16] Tameris M, Hokey DA, Nduba V, Sacarlal J, Laher F, Kiringa G, et al. A double-blind, randomised, placebo-controlled, dose-finding trial of the novel tuberculosis vaccine AERAS-402, an adenovirus-vectored fusion protein, in healthy, BCG-vaccinated infants. *Vaccine*. 2015;33:2944-54.

- [17] Spellberg BJ, Ibrahim AS, Avenissian V, Filler SG, Myers CL, Fu Y, et al. The anti-Candida albicans vaccine composed of the recombinant N terminus of Als1p reduces fungal burden and improves survival in both immunocompetent and immunocompromised mice. *Infection and immunity*. 2005;73:6191-3.
- [18] Parish CR. Immune response to chemically modified flagellin. I. Induction of antibody tolerance to flagellin by acetoacetylated derivatives of the protein. *The Journal of experimental medicine*. 1971;134:1-20.
- [19] Smith LR, Wloch MK, Chaplin JA, Gerber M, Rolland AP. Clinical Development of a Cytomegalovirus DNA Vaccine: From Product Concept to Pivotal Phase 3 Trial. *Vaccines*. 2013;1:398-414.
- [20] Pienaar E, Dartois V, Linderman JJ, Kirschner DE. In silico evaluation and exploration of antibiotic tuberculosis treatment regimens. *BMC systems biology*. 2015;9:79.
- [21] Storer BE. An evaluation of phase I clinical trial designs in the continuous dose-response setting. *Statistics in medicine*. 2001;20:2399-408.
- [22] O'Quigley J, Pepe M, Fisher L. Continual reassessment method: a practical design for phase 1 clinical trials in cancer. *Biometrics*. 1990;46:33-48.
- [23] Wang S, Mata-Fink J, Kriegsman B, Hanson M, Irvine DJ, Eisen HN, et al. Manipulating the selection forces during affinity maturation to generate cross-reactive HIV antibodies. *Cell*. 2015;160:785-97.
- [24] Spendley W, Hext GR, Himsworth FR. Sequential Application of Simplex Designs in Optimisation and Evolutionary Operation. *Technometrics*. 1962;4:441-61.
- [25] Box GEP. Evolutionary Operation: A Method for Increasing Industrial Productivity. *Journal of the Royal Statistical Society Series C (Applied Statistics)*. 1957;6:81-101.
- [26] Seder RA, Darrah PA, Roederer M. T-cell quality in memory and protection: implications for vaccine design. *Nature reviews Immunology*. 2008;8:247-58.
- [27] Foulds KE, Wu CY, Seder RA. Th1 memory: implications for vaccine development. *Immunological reviews*. 2006;211:58-66.
- [28] Berry J, Houston K. *Mathematical Modelling*. London: Edward Arnold; 1995.
- [29] Vynnycky E, White RG. *Introduction to Infectious Disease Modelling*. 1 ed: Oxford University Press; 2010.
- [30] Wright DF, Winter HR, Duffull SB. Understanding the time course of pharmacological effect: a PKPD approach. *British journal of clinical pharmacology*. 2011;71:815-23.
- [31] Mould DR, Upton RN. Basic concepts in population modeling, simulation, and model-based drug development. *CPT: pharmacometrics & systems pharmacology*. 2012;1:e6.
- [32] Beal S, Sheiner LB, Boeckmann A, Bauer RJ. *NONMEM User's Guides*. Ellicott City, MD, USA: Icon Development Solutions; 2009.
- [33] *Monolix: Users Guide*. 4.3.3 ed2014.
- [34] Lunn DJ, Thomas A, Best N, Spiegelhalter D. WinBUGS -- a Bayesian modelling framework: concepts, structure, and extensibility. *Statistics and Computing*. 2000;10:325--37.
- [35] D'Argenio DZ, Schumitzky A, Wang X. *Adapt 5 User's Guide: Pharmacokinetic/Pharmacodynamic Systems Analysis Software*. Los Angeles: Biomedical Simulations Resource; 2009.
- [36] Stone JA, Banfield C, Pfister M, Tannenbaum S, Allerheiligen S, Wetherington JD, et al. Model-based drug development survey finds pharmacometrics impacting decision making in the pharmaceutical industry. *Journal of clinical pharmacology*. 2010;50:20S-30S.

- [37] Kimko H, Pinheiro J. Model-Based Clinical Drug Development in the Past, Present & Future: a Commentary. *British journal of clinical pharmacology*. 2014.
- [38] Katsube T, Yano Y, Wajima T, Yamano Y, Takano M. Pharmacokinetic/pharmacodynamic modeling and simulation to determine effective dosage regimens for doripenem. *Journal of pharmaceutical sciences*. 2010;99:2483-91.
- [39] Sheiner LB. Learning versus confirming in clinical drug development. *Clinical pharmacology and therapeutics*. 1997;61:275-91.
- [40] Shingleton A. Allometry: The Study of Biological Scaling. *Nature Education Knowledge*. 2010;3:2.
- [41] Wilkins JJ, Langdon G, McIlleron H, Pillai G, Smith PJ, Simonsson US. Variability in the population pharmacokinetics of isoniazid in South African tuberculosis patients. *British journal of clinical pharmacology*. 2011;72:51-62.
- [42] West GB, Brown JH, Enquist BJ. A general model for the origin of allometric scaling laws in biology. *Science*. 1997;276:122-6.
- [43] Boxenbaum H. Interspecies scaling, allometry, physiological time, and the ground plan of pharmacokinetics. *Journal of pharmacokinetics and biopharmaceutics*. 1982;10:201-27.
- [44] Mahmood I, Balian JD. The pharmacokinetic principles behind scaling from preclinical results to phase I protocols. *Clinical pharmacokinetics*. 1999;36:1-11.
- [45] Knibbe CA, Zuideveld KP, Aarts LP, Kuks PF, Danhof M. Allometric relationships between the pharmacokinetics of propofol in rats, children and adults. *British journal of clinical pharmacology*. 2005;59:705-11.
- [46] Amantana A, Chen Y, Tyavanagimatt SR, Jones KF, Jordan R, Chinsangaram J, et al. Pharmacokinetics and interspecies allometric scaling of ST-246, an oral antiviral therapeutic for treatment of orthopoxvirus infection. *PloS one*. 2013;8:e61514.

## Appendix B. Additional Background

### New TB Vaccines

A brief description of each vaccine candidate follows based information from the WHO 2016 TB report [1] .

There are three types [2] of new candidate: whole cell vaccine, viral vectored subunit vaccine and adjuvant protein subunit vaccine. New candidate TB vaccines are also categorised into two strategies: to replace BCG or to boost on previous BCG immune responses [3]. A booster vaccine works by building upon the immunity induced by previous vaccination [4]. A BCG booster vaccine would be administered following BCG vaccination either during infancy or adolescence [5]. In the current pipeline, most of the whole cell vaccines are designed to replace BCG and the subunit vaccines are predominantly used as BCG boosters.

#### 1. *Whole cell vaccines*

Whole cell vaccines utilize the whole BCG or *Mtb.* cell to promote an immune response, however the bacteria maybe killed or altered to reduce virulence [15, 44]. Whole cell vaccines in TB development are an attractive option they induce a wide, diverse immune response, including cellular and humoral responses [69]. Whole cell BCG vaccines aim to improve upon current BCG by either adding antigens for example those present in the *Mtb.* bacilli and not in current BCG strains, by enhancing antigens already expressed by BCG, or by removing BCG genes thought to be associated with immune evasion [70, 85]. Some whole cell vaccines are also designed to target populations where BCG is known to be unsafe, such as children infected with HIV [206].

##### a. MTBVAC

MTBVAC is a live *Mtb.* strain attenuated with deletions of the *Mtb.* virulence genes, *phoP* and *fadD26* [1]. MTBVAC was developed by the University of Zaragoza (Spain), Biofabri (Spain) and Institut Pasteur (France). A phase 1, dose-ranging trial in healthy adults was conducted to compare immunogenicity to BCG vaccination (clinicaltrials.gov NCT02013245). Each participant was given a single vaccination at the beginning of the trial. A phase 1 trial of

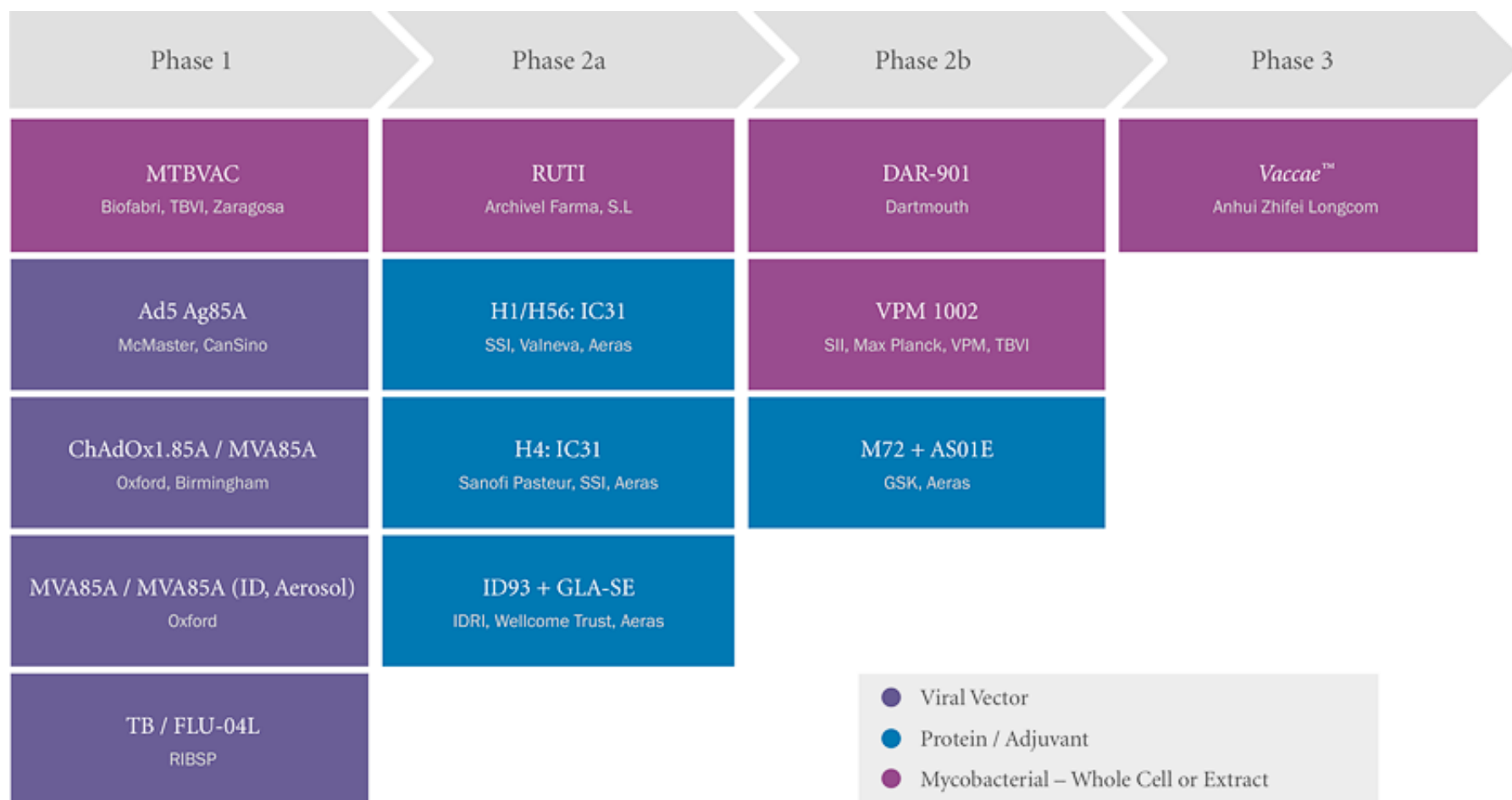
MTBVAC in infants, administered as a BCG replacement, is ongoing (clinicaltrials.gov NCT02729571).

b. DAR-901

The DAR-901 vaccine, developed by Dartmouth (USA) and Aeras (TB vaccine developers (USA)) is a heat inactivated, NTM whole cell vaccine. It is designed as a BCG booster vaccine. It has already been shown to be effective in a phase 3 trial in Tanzania in HIV positive, BCG primed population [11]. Currently, DAR-901 is a phase 2b trial in BCG vaccinated adolescents in which participants receive only one vaccination of DAR-901 at the beginning of the trial (clinicaltrials.gov NCT02712424).

c. RUTI

RUTI is made of non-live, fragmented and detoxified *Mtb.* bacteria [12], developed by Archivel Farma (Spain). RUTI is as an immunotherapeutic vaccine, which is given in conjunction with antibiotic therapy with the aim of shortening treatment times. A dose-ranging Phase II trial in HIV positive and negative participants who also received one month of Isoniazid treatment



Please note: Information is self-reported by vaccine sponsors.

*Revised on October 7, 2016*

**Figure 1.2 (repeated here) 2015 developmental pipeline for new TB vaccines by Aeras, TB vaccine developers (permission to use granted 15/6/17 see appendix B for e-mail correspondence)**

in South Africa was completed recently (clinicaltrials.gov NCT01136161). Two vaccinations of RUTI were administered, one at the beginning of the trial, the second, one month later.

d. VPM 1002

The VPM 1002 vaccine is a live, recombinant BCG vaccine, originally developed at the Max Planck Institute of Infection Biology (Germany). VPM 1002 is the only recombinant BCG vaccine in the pipeline, developed to enhance BCG. This is achieved by adding to BCG, in this case, the insertion of listeriolysin, which aids to enhance cross priming of CD8 T cells [13]. A phase 2b trial is currently being conducted to assess the safety and immunogenicity of VPM 1002 in HIV infected and uninfected infants in South Africa (clinicaltrials.gov NCT02391415). VPM1002 is given once at the beginning of the trial.

e. Vaccae

The Vaccae vaccine is a NTM developed by the pharmaceutical company Anhui Zhifei Longcom (China) [2]. Vaccae is the only TB vaccine in the pipeline to be in phase 3 and has been licensed as a therapeutic vaccine to help shorten TB drug regimens in those with drug-susceptible TB. The current phase 3 Vaccae trial is being conducted to assess the efficacy and safety in preventing TB disease in LTBI participants (measured using a PPD skin test). Participants are given, in total, six vaccinations with Vaccae intradermally (every two weeks) (clinicaltrials.gov NCT01979900).

2. *Subunit vaccines*

The remaining vaccines in the TB vaccine pipeline are subunit vaccines. Broadly speaking, a subunit vaccine extracts antigens from a pathogen deemed the “best” at stimulating the required immune response [7]. Subunit vaccines are potentially safer to use in a broad population (i.e. those whose are immunocompromised) than a whole cell vaccine, by only containing fragments of the pathogen [14]. However, identifying appropriate antigens for a subunit vaccine is challenging and multiple antigens may have to be investigated and combined to develop a vaccine that generates a robust, long-lasting immune response [14].

In TB vaccine pipeline, antigens that contribute to *Mtb.* virulence, the strength of bacteria’s structure or allow for the bacteria to enter immune response cells have been identified for

candidate subunit vaccines. These are outlined in Table B.1. The subunit vaccines in the pipeline combine them in different combinations. Alongside the antigen, a delivery system is required to prolong exposure to the antigen to generate a strong response (delivery system) or heighten the response once it is created (immunomodulatory) [15].

<b>Antigen</b>	<b>Description</b>
Ag85A, Ag85B	<i>Mtb.</i> antigens 85A and 85B are proteins associated with <i>Mtb.</i> cell wall maintenance [16, 17]. Both antigens have been shown to induce a substantial protective immunity against aerosol <i>Mtb.</i> challenge in mice [18, 19], guinea pigs [20] and macaques [21].
ESAT-6, Rv3619, Rv3620	<i>Mtb.</i> antigen ESAT-6 is an early-stage protein that mediates the entry of mycobacteria into cells [22]. ESAT-6 is well recognized in TB patients [23, 24]. In mice vaccinated with an ESAT-6 subunit vaccine, strong ESAT-6-specific T cell responses were seen that resulted in protective immunity to <i>Mtb.</i> challenge at the same level as that provide by BCG [25, 26]. <i>Mtb.</i> antigen Rv3620 and Rv3619 are ESAT-6 like proteins associated with <i>Mtb.</i> virulence [27, 28]. IFN- $\gamma$ , IL-12 and IgG responses are heightened to Rv3620 and Rv3619 stimulation in mice [29].
Rv2660c, Rv1813	The late stage antigens Rv2660c and Rv1813 are secreted by <i>Mtb.</i> bacilli during latent infection in order for the bacteria to adapt to hostile conditions produced by the hosts immune response [30, 31]. Rv2660c is selectively recognized by latently infected individuals as compared to individuals with active pulmonary TB [32, 33]. Strong CD4+and CD8 T cell responses were observed after stimulation with Rv1813 in mice [34].
TB10.4	The TB10.4 antigen is associated with virulence of <i>Mtb.</i> [35]. TB10.4 induces the largest and broadest immune responses in T cells from TB patients as compared to those of BCG-vaccinated and non vaccinated individuals [36, 37]. In mice, the administration of TB10.4 was shown to induce Th1 responses which were associated with protection against <i>Mtb.</i> infection [38].
Rv2608	Rv2608 is a surface-associated cell wall protein of the <i>Mtb.</i> PPE family

	[39] which provoke Th1 responses and confer protection against <i>Mtb.</i> challenge in mice [40].
Mtb32A	<i>Mtb.</i> antigen 32a is thought to be associated with bacteria metabolism and respiration, which could be associated with bacterial latency. Mtb32a is a BCG derived antigen [41]. Mtb32a based vaccines, reduced the bacterial burden significantly in the lungs of all mice after challenge [42].
Mtb39A	<i>Mtb.</i> antigen 39A is known to be important for cell wall maintenance and cell wall processes [43]. Strong IFN- $\gamma$ T cell responses were seen in PBMC after stimulation with Mtb39A in humans [44]. Mice immunized with Mtb39A showed a decrease in bacterial load after challenge [44].
<b>Adjuvant</b>	<b>Description</b>
IC31	Developed by Valneva, IC31 is a delivery adjuvant consists of a cationic peptide and the TLR9 agonist ODN1a [45] capable of inducing strong cellular and humoral responses [46].
CAF01	SSI proprietary liposomal adjuvant CAF01, consists of DDA (a cationic peptide), the delivery system and TBD (a mycobacterial cord factor) an immunomodulator is able to effectively develop Th1 responses [47, 48].
GLA-SE	The GLA-SE adjuvant which contains a synthetic TLR4 agonist, Glucopyranosyl Lipid Adjuvant (GLA), an immunomodulator, formulated in oil-in-water emulsion (delivery) [49]. GLA-SE provokes strong Th1 responses [50].
AS01E	The adjuvant AS01E, developed by GSK, is a liposome-based adjuvant containing the immunomodulators, 3-O-desacyl-4'-monophosphoryl lipid A (MPL), and saponin QS-21 [51]. It is safe and provides strong immune responses to <i>Mtb.</i> antigens [51, 52].

**Table B.1 Antigenic components and adjuvants for TB subunit vaccines.**

## 2.1 Virus-vectored subunit vaccines

### a. Ad5Ag85A

Ad5Ag85A is an adenovirus serotype 5 vector expressing *Mtb.* antigen Ag85A, which has been developed by McMaster University (Canada). A phase 1 trial, assessing safety and

immunogenicity of two doses of Ad5Ag85A in BCG vaccinated and BCG naïve healthy participants was found to be safe and able to stimulate polyfunctional T cell responses after one vaccination [53]. The [clinicaltrials.gov](https://clinicaltrials.gov) number for this trial is NCT00800670, however according to this website, the trial was terminated after the low dose participants were enrolled. A safety and immunogenicity phase 1 dose-ranging study of the aerosol administration of this vaccine is currently underway ([clinicaltrials.gov](https://clinicaltrials.gov) NCT02337270).

b. MVA85A/MVA85A

MVA85A is an attenuated vaccinia-vectored vaccine candidate expressing *Mtb.* antigen Ag85A designed as a booster vaccine for BCG, developed at the University of Oxford (UK). MVA85A has previously progressed through to phase 2b where it was given to BCG vaccinated infants in South Africa [54] and HIV positive adults in South Africa and Senegal [55] (see below for more details on these studies). In those trials, MVA85A was administered intradermally. In the current pipeline, aerosolized MVA85A has been administered to BCG vaccinated adults in the UK in a phase 1 trial ([clinicaltrials.gov](https://clinicaltrials.gov) NCT01497769). Compared to the phase 1 intradermal trial, aerosolized MVA85A induces a stronger CD4+ T cell response [56]. Another phase 1 trial is being conducted to assess the safety and immunogenicity of aerosolized MVA85A in LTBI participants and compare against the intradermal injection ([clinicaltrials.gov](https://clinicaltrials.gov) NCT02532036). In both clinical trials, one dose of MVA85A was given (either aerosolized or intradermally) with a simultaneous boost of placebo (either aerosolized or intradermally) in order to blind the experiments.

c. ChAdOx1.85A/MVA85A

ChAdOx1.85A is a simian adenovirus expressing *Mtb.* antigen Ag85A, which was developed at the University of Oxford as a BCG booster. A phase 1 clinical trial in BCG vaccination adults is currently being conducted to assess safety and immunogenicity of ChAdOx1.85A, administered alone and with a boost of MVA85A ([clinicaltrials.gov](https://clinicaltrials.gov) NCT01829490). Participants receive either one intramuscular vaccination of ChAdOx1.85A or one vaccination of ChAdOx1.85A at the beginning of the trial with a boost of MVA85A 2 months later or two vaccinations of ChAdOx1.85A 1 month apart followed by a boost with MVA85A after 4 months.

d. TB/FLU-04L

TB/FLU-04 L is an influenza virus-vectored vaccine that has been developed by the Research Institute on Influenza (Russia). *Mtb.* antigens Ag85A and ESAT-6 are expressed by the influenza virus strain H1N1. A phase 1 trial in BCG vaccinated, LTBI negative adults has recently been completed (clinicaltrials.gov NCT02501421). Participants were given two vaccinations of the same dose, intranasally, 3 weeks apart.

*2.2 Adjuvanted protein subunit vaccines*

Adjuvanted protein subunit vaccines are a combination of antigenic proteins combined with an adjuvant, a delivery system used to enhance or prolong vaccine antigen exposure to the immune response (adjuvant delivery system) or aid the host response by co-stimulating key immune cells (immunomodulatory) [15]. Table B.1 describes the adjuvants in use in the TB vaccine pipeline.

a. ID93 + GLA-SE

The protein vaccine ID93 is comprised of antigens Rv2608, Rv3619, Rv3620 and Rv1813 (Table B.1) and adjuvanted with GLA-SE. ID93 + GLA-SE was developed by the Infectious Disease Research Institute (USA) and Aeras (USA). ID93 + GLA-SE is currently in a phase 2a trial in South Africa for HIV-negative participants who have completed TB disease treatment (Clinicaltrials.gov NCT02465216). In this trial, participants receive either low or high dose of antigen in combination with low or high dose of the adjuvant at the beginning of the trial and two months later.

b. M72 + AS01E

M72 is protein adjuvant vaccine adjuvanted with AS01E developed by GlaxoSmithKline pharmaceuticals and Aeras (USA). It is comprised of antigens 32A and 39A (Table B.1). A phase 2b trial is currently being conducted with M72 + AS01E in HIV negative, LTBI negative participants in South Africa, Kenya and Zambia. Participants receive two vaccinations of the same dose of M72+AS01E at the beginning of the trial and one month later. The primary endpoint of this trial is to assess efficacy against TB disease, secondary endpoints are safety and immunogenicity (Clinicaltrials.gov NCT01755598).

## Simple PK Model Example

A simple example to demonstrate a PK model is to look at the pharmacokinetics of the drug Theophylline, used to treat respiratory diseases such as chronic obstructive pulmonary disease and asthma [57]. The data in figure B.1 show the concentration of theophylline collected repeatedly over 24 hours for 12 individuals (longitudinal data). There is obvious variation in the sample as some individuals' responses peak lower than others, etc.

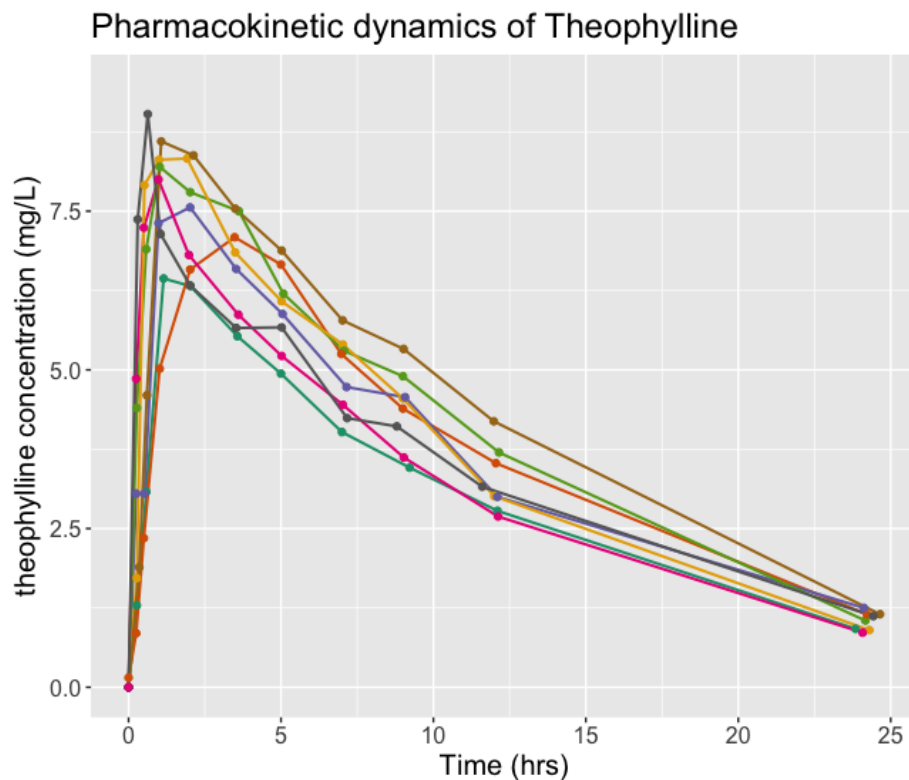


Figure B.1. Data open access in R from the nlme package – data collected from study by Upton et al for example PK modelling in NONMEM (Boeckmann, A. J., Sheiner, L. B. and Beal, S. L. (1994), NONMEM Users Guide: Part V, NONMEM Project Group, University of California, San Francisco.)

To calibrate the model to the individuals data and quantify the variation in the responses, complex statistical frameworks are applied, known as NLME statistics [58-60].

The mathematical most commonly used to describe this PK data is a one compartmental model describing the absorption and elimination over a volume of the drug after a dose has been administered. The following equation describes this mathematically:

$$\frac{Dose * k_a}{Volume(k_a - k_e)} (e^{-k_e * time} - e^{-k_a * time})$$

where  $k_a$  and  $k_e$  are the rates of theophylline absorption and elimination, respectively. To calibrate the model to the individual's data and quantify the variation in the responses, complex statistical frameworks are applied, known as NLME statistics (see below). Figure B.2 shows the results when this method is used to calibrate the model to the data. With this fit, we can then determine how the parameters of the model vary across the 12 individuals.

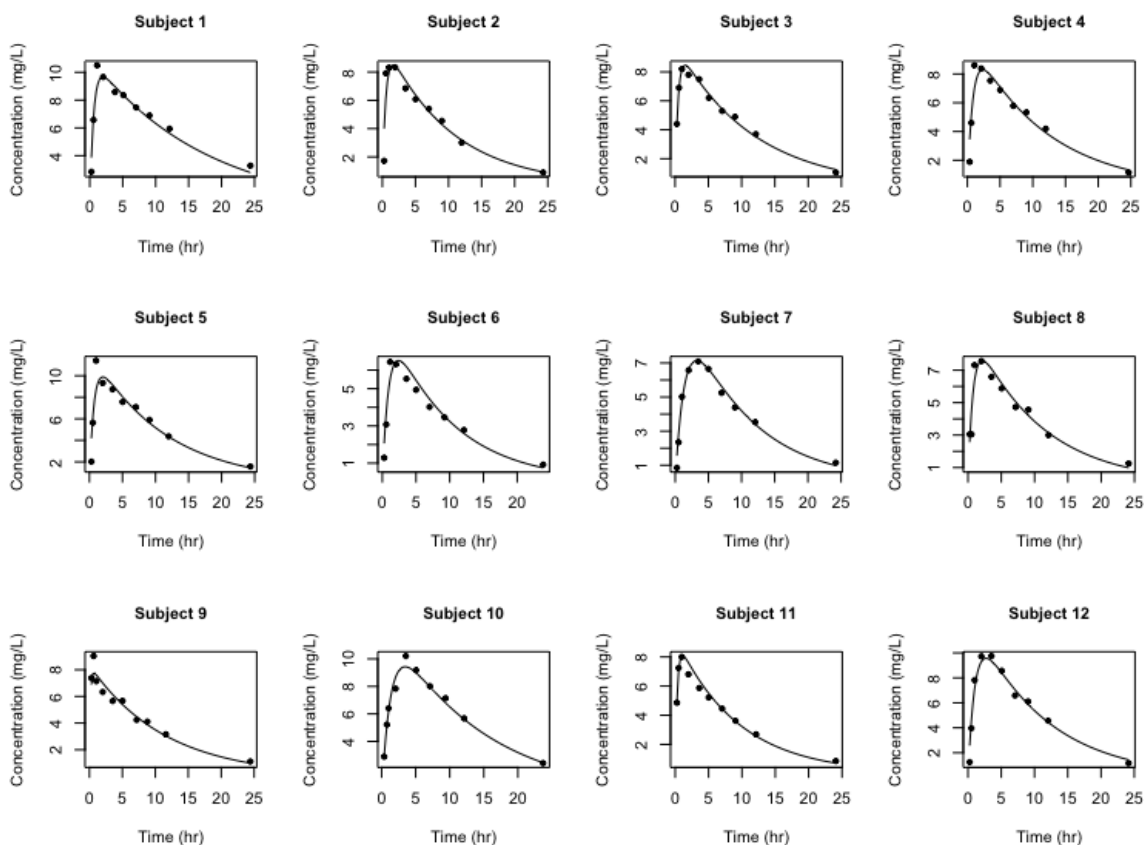


**Figure B.2. Individual fits for the 12 individual theophylline concentration data of the one compartmental model with first order absorption and linear elimination using the nlme package in R.**

### NLMEM: methods, implementation and diagnostics

### ***NLMEM framework overview and parameter estimation methods***

The objective of NLMEM is to estimate the “best” model parameterisation to describe the data. Once this is achieved we can then make inferences around the population and individual response dynamics. To conduct NLMEM for a population the following is required:

1. **Longitudinal response data.** It is advantageous to have extensively sampled data as possible, and data does not need to be uniformly sampled over sub-populations.
2. **Population covariate data.** If applicable to modelling aims.
3. **A mathematical model.** The assumed underlying biological mechanism of the data is incorporated into the mathematical model to calibrate to the data (see literature review).
4. **Statistical models to account for individual responses.** To account for the following two levels of variation, the NLMEM framework statistical model requires two components:
  1. The proposed distribution of the model parameters from the population typical response to account for individual responses over time.
  2. The relationship between the error of the data from the mathematical model prediction, known as the residual error, on an individual level of time (assumed to be the same distribution for each individual). A fundamental assumption to NLMEM (and general linear regression) is that the residual errors are normally distributed. However, the variation of the normal distribution may be more exaggerated depending on the magnitude of the data itself (heteroscedastic variation). As such, the purpose of the residual error model is to transform potential heteroscedastic variation to normal (homoscedastic) variation around the model prediction.
5. **An Objective Function (OF).** To quantify the goodness of fit of the model prediction (with a specific set of parameters) to the data, a measure is required, this is known as the objective function (OF). We use a likelihood based method as the OF in NLMEM. Briefly, the likelihood assesses the likelihood of the model prediction under a chosen parameter set, to have predicted the observed data [61]. A model parameterisation that produces a higher likelihood OF value is seen as more probable to have produce the data. The aim

then is to find the parameter set with that produces the maximum likelihood OF value, known as the Maximum Likelihood Estimator (MLE). To calculate the OF over all individual model predictions in a population requires the product of all OFs for those individuals. As the likelihood OF values are probabilities and as such, can be small values ( $\ll 1$  in some cases) finding a product of these values over all individuals can be computationally difficult. As a standard practise, and for computational ease, we use -2 times the sum of the log of the likelihood (LL) when calculating the multiple likelihood OF's over all individuals in a population, a.k.a. the deviance. If we use the deviance as our objective function we now aim to minimise this value instead of maximise (for derivation see [62, 63]). As we assume the residual errors of the data to the model prediction is normally distributed, we base the likelihood OF on the normal distribution equation (see [62] and [63] for derivation of normal LL equation).

## **6. An algorithm to estimate the “best” model (mathematical and statistical) parameters**

The idea of NLMEM is to work through parameter sets (population typical parameters, the variation on the parameters needed to account for all individuals and the residual error parameters) to find the “best” set. In terms of the OF (-2LL), this is the parameter set that minimizes the -2LL value. NLMEM uses a one-stage approach where both population typical and the variation of the parameters to account for the individual's data are estimated simultaneously. As mentioned previously, we are using a hierarchical model, the individual parameters are related to the population typical parameters by a distribution with the population typical parameters as the mean and an unknown variation (which we aim to estimate). Another way to consider our problem is: to find the best population typical parameter values for our longitudinal data from multiple individuals by looking at the probability of the parameter values to produce such data (likelihood), has an intermediary step – the unknown individual parameters. To achieve our aim of minimise the -2LL with respect to the unknown population typical parameters, we need to incorporate the individual parameters into the likelihood OF. As we don't know what these individual parameters are, we have to assess the -2LL of all possible individual parameter values. To achieve this use a “marginal” likelihood, (marginal as we are effectively marginalising out the potential

individual parameter values). Formally put, the likelihood for finding the population typical parameters is (taken from [62]):

$$\mathcal{L}_y(\theta) \propto p(\mathbf{y}|\theta) = \int p(\mathbf{y}, \boldsymbol{\psi}|\theta) d\boldsymbol{\psi}$$

Where  $L$  is the likelihood of the data given the population parameters,  $y$  represents the observed data (for all individuals and time points),  $\theta$  are the vector of population parameters, and  $\boldsymbol{\psi}$  the vector of individual parameters. A marginal likelihood OF is common when trying to solve a maximizing (or minimizing) likelihood problem for a certain unknown parameter (here, population typical model parameters) with a “latent” or “nuisance” variable (in our case the individual parameters). To minimise this OF, requires solving integrals over the possible values of the population deviation to cover the individual parameters. This is not possible to do analytically in most PK/PD modelling exercises so a numerical integration estimation method is usually employed. We have chosen to use an estimation method known as Stochastic Approximation to the Expectation Maximisation (SAEM) algorithm. We use the software Monolix [64, 65] to implement this method. It is important to note, however that this is not the only estimation method used in PK/PD, but we only consider this one in this project.

## 7. Software to estimate parameter values using the estimation algorithm (SAEM)

We do not go into technical detail of the SAEM algorithm, but a brief description is outlined as follows.

1. A starting value for the population typical parameters and variance is given by the user.
2. Individual parameter values are simulated out from a conditional distribution that combines the initial guess of the population parameters and variances and the observed data – essentially combining a prior of the population parameters and the data resulting in individual parameters that lie in between the two (see [62] for technical explanation of this distribution).
3. The likelihood value given those individual parameters is calculated.

4. The individual parameters are then combined and used as the distribution of the new population parameter estimates.
5. The new population parameters is used to simulate another round of individual parameters based on the conditional distribution as in step 2.
6. The likelihood of the data given these individual parameters is calculated and compare to the previous likelihood value (from previous population parameter estimate). The population parameters that maximises (or minimises in the case of -2LL) the likelihood compared to the previous population parameter is taken (essentially starting a Markov Chain) - honing in on the distribution that best describes the population mean and variance (the parameters we wish to estimate). The individual parameters from each iteration are “stored” to generate as much information as possible on the best population parameters.
7. Iterations selecting a population parameter set and simulating out the individual parameters continue until a satisfactory convergence (assessed using a threshold value of the difference in likelihood value between each iteration) is met.
8. Once satisfactory population parameters are found (step 7), individual parameters are simulated to represent the individuals in the population. These individual parameter values can be used as a preliminary assessment of the influence of population covariates, i.e. using statistical tests to establish differences in these estimated parameters between covariate strata.

For a more in-depth and technical explanation see [62, 65] and an informative video on a simple SAEM algorithm implementation can be found at <http://wiki.webpopix.org/images/2/20/saem.mp4>.

We choose Monolix and SAEM because it has been shown to be a robust and powerful method for estimation in population PK/PD modelling [65-69]. In this project, members on the advisory panel with experience in PKPD (Dr Steven Kern (BMGF), Dr Jeremie Guedj (INSERM)) who recommend this software and expertise in how to use it was available throughout the project.

### 8. A covariate model structure.

A way of incorporating population covariates to establish if parameter estimates are significantly different between subpopulations and what these values are (parameter-covariate relationship are outlined in the main papers and corresponding supplementary material). A systematic way of finding the appropriate covariate model is needed: here we use a forward addition method and the LRT to assess model performance (exact methods for covariate analysis outlined in the main papers).

#### ***NLMEM Implementation in Monolix***

Table B.2 outlines the requirements in order to implement a NLMEM analysis in Monolix.

Requirement	Description						
Dataset	Data on the longitudinal responses over time with covariate information in csv format. Each line in the dataset should contain an ID (which will be the same for one subject in repeated measures data for all times), time and response value minimum. Values for the covariate for the subject ID should be repeated for each line.						
Mathematical model	The mathematical model to represent the responses over time should be coded in the MlxTran framework in order for Monolix to use for the estimation. Guides to the MLXtran language can be found at <a href="http://mlxtran.lixoft.com/mlxtran-user-guide/">http://mlxtran.lixoft.com/mlxtran-user-guide/</a> . An example of the code used to for the BCG vaccination model in paper 2 can be found below.						
Initial guesses of the population parameters	Visual inspection of the model prediction compared to the data is good to establish a starting point for the parameter estimation algorithm. This can be done in Monolix or in R.						
Residual error model	<p>The residual error (RE) model is applied to account for discrepancies between the observed data and the model prediction. The assumption in NLMEM is that the REs are normally distributed, but may be dependent on the magnitude of the response (i.e. it is intuitive that the error may be higher for higher values of the response than for lower values). Three common models are outlined in the table below. We only concentrate on these three models in our fitting as they are generally considered to reflect lab assay variability patterns [59]. Alternatives are outlined in [59].</p> <table border="1"> <thead> <tr> <th>Error model</th> <th>Model equation</th> <th>Description</th> </tr> </thead> <tbody> <tr> <td>Constant</td> <td><math>Y = f+a*e</math></td> <td>Constant residual error variance from the model prediction, f</td> </tr> </tbody> </table>	Error model	Model equation	Description	Constant	$Y = f+a*e$	Constant residual error variance from the model prediction, f
Error model	Model equation	Description					
Constant	$Y = f+a*e$	Constant residual error variance from the model prediction, f					

	Proportional	$Y = f + b \cdot f \cdot e$	Proportional residual error variance when we believe the variance is proportional to the model prediction, $f$
	Combined	$Y = f + (a + b \cdot f) \cdot e$	A combination of constant and proportional residual error variances
<p><b>where <math>Y = \text{data point}</math>, <math>f = \text{model prediction}</math>, <math>a, b = \text{scalars to be determined during parameter estimation process}</math>, <math>e = \text{Normally distributed random variable } N(0,1)</math>.</b></p> <p>To establish which RE model is best, we used the inbuilt model comparison tool in Monolix. Here, for a specific model parameterisation different RE models are tested (the three above) and the one with the lowest goodness of fit values is chosen to represent the RE.</p>			
Covariance model	It is important to test if the random effects (the variation) of the model parameters are co-dependent, i.e. correlated. We tested if any combination of our parameters were correlated across the population with the inbuilt Monolix tool.		
Covariate model	In both paper 2 and 4, establishing the appropriate covariate model is an aim of the work, so methods to do this are outlined in the respective papers – explanation of procedure to include covariates and the covariate-parameter relationship is outlined in the supplementary of the papers.		
Distribution of the individual parameters	As it is common in PK/PD modelling for data to follow a lognormal distribution and to ensure positivity of estimated individual model parameters [59, 70], we used a lognormal distribution to represent the distribution of the individual mathematical model parameters.		

**Table B.2. Requirements for implementation of NLMEM in Monolix software.**

The outlined requirements are concerned with the models (mathematical and statistical) used in the NLMEM framework, which are dependent on the data and model in question. Requirements for the execution of the SAEM estimation algorithm were kept at default values outlined in see [64].

Example MlxTran code for T cell model used in paper 2:

```
<MODEL>
DESCRIPTION:
Model for one vaccination BCG: Human/Macaque
[LONGITUDINAL]
INPUT:
parameter = [E0, k,h,L,m,p]
```

EQUATION:

$t_0 = 0$

$E_0 = E_0$

$M_0 = 0$

$d1 = L \cdot (1/\text{factorial}(k-1))$        $d2 = 1/(h^k)$        $d3 = t^{(k-1)}$        $d4 = \exp(-t/h)$

$d = d1 \cdot d2 \cdot d3 \cdot d4$

$\text{ddt}_E = d - p \cdot m \cdot E - (1-p) \cdot m \cdot E$

$\text{ddt}_M = (1-p) \cdot m \cdot E$

Total = E + M

odeType = stiff

OUTPUT:

output = Total

### ***Diagnostics to assess parameter estimation results***

To evaluate the estimated model parameters, we use the following diagnostics:

1. **Goodness of fit measures.** The  $-2 \cdot \text{LogLikelihood}$  value evaluated at the estimated model parameter values gives an indication of the goodness of fit of the model parameterisation. On its own, it is not meaningful, however it can be used to compare across model parameterisations (strictly nested models) on the same dataset where a lower value indicates a better fit [60]. We use the Likelihood ratio test (LRT) to compare our nested models in this work, following the chi squared distribution with the appropriate degrees of freedom [62]. For non-nested mechanistic and statistical model comparisons, we predominantly use the Bayesian Information Criterion (BIC) [71]. The BIC is an extension to the  $-2 \cdot \text{LogLikelihood}$  OF that accounts for the complexity of the model i.e.:

$$BIC = -2 * LL + \text{Log}(n) * k$$

where LL is the LogLikelihood, n is the number of data points and k, the number of estimated model parameters. A complex mathematical model with an equivalent  $-2LL$  to a simpler model, is penalised for its complexity and as such, the BIC is inflated, indicating a worse model fit [72].

2. **Estimated model parameter precision.** We use the relative standard error (RSE) of the estimated parameters as an indication of the precision of the estimated model parameters. The RSE is the standard deviation of the error from the best estimated parameter value. Technically speaking, the RSE describes the surface of the OF local to the parameter at the predicted best value: a sharply peaked function will give few values that

could be considered “best” and consequently, a low RSE, a flat, broad surface would give many “best” values and a high RSE, see [73] for technical explanation. The RSE is SE/estimated parameter value. We consider a RSE value of <30% to be an acceptable value, indicating an identifiable model parameter estimate [58].

3. **Graphical Plots.** We use two main graphical diagnostic plots for the main papers:

a. *Visual Predictive Check (VPC) plot*

The visual predictive check plot (VPC) is a simulation based diagnostic tool for assessing the appropriateness of the proposed mathematical model to describe the empirical data. This is done by comparing data simulated using the model and estimated population mean parameters and associated variances, to the empirical data distribution [62]. To construct the VPC, the mathematical model is calibrated to the dataset in question and the resulting estimated parameters and associated variances are used to simulate a theoretical population dataset, equivalent to the size of the population in question. This procedure is repeated 500 times and key percentiles (e.g. the 10<sup>th</sup>, 50<sup>th</sup> and 90<sup>th</sup> percentiles) of each simulated population dataset are recorded and the ranges of these percentiles are plotted. If the model is appropriate to represent the data, when the observed percentiles are plotted alongside the VPC, they should fall in the bounds of the simulated percentile ranges. These plots are common as a diagnostic tool in PK/PD modelling and have been suggested as the most efficient plots to assess a NLMEM parameter estimation [74]. The plots are produced by Monolix as a standard output and are included in the paper or supplementary in this format.

b. *Parameter prediction plot*

The parameter prediction plots show the prediction of the mathematical model for the estimated population parameters compared to the median of the data (the population typical response) and the distribution of the model predictions due to the estimated parameter variation (to cover the population spread of the data, usually the 10<sup>th</sup> to 90<sup>th</sup> percentile or the 25<sup>th</sup> to 75<sup>th</sup>). Plots included in the work are either Monolix standard outputs (those with pink percentile bands) or manually produced in R (included in the main papers 2 and 4).

We add the following diagnostic plots in the supplementary of each paper or in the appendix corresponding to the papers chapter:

*c. Observed versus predicted data plots*

In these plots, the observed data is plotted against the predicted value on a population and individual level. Plots where the observed and predicted values are similar should show a diagonal distribution along a line of unity (i.e. if the prediction is the same as observed value that point will lie on the diagonal line extending from the origin of the plot).

*d. Residual plots*

The (weighed) residuals of the model prediction to the data are plotted here. This plot allows us to check if the residuals are normally distributed. Ideally, residuals should lie uniformly on either side of the mean, within approximately 2 SDs either side, corresponding to the 5% and 95% percentiles. Residuals can be plotted against i. time and ii. population predictions. Any bias in these plots suggests a mathematical model errors (if bias in i.) or residual model errors (if bias in ii.). We include the Monolix standard output of these plots

***NLMEM software background***

NONlinear Mixed Effects Modelling (NONMEM) is acknowledged to be the first software developed for PK/PD modelling [60]. Developed in 1984, NONMEM could efficiently estimate PK parameters to even sparse data, paving the way for MBDD for the first time. After NONMEM was released, other software were developed with new methods for parameter estimation and improvements on user-friendly operation [60]. Table B.3 outlines the main software for PK/PD modelling.

Name	Method of parameter estimation
NONMEM [75]	First order approximation, First order conditional estimation [76], SAEM
WinBUGs[77]	Markov Chain Monte Carlo (MCMC)
Monolix [64]	Stochastic Approximation to Expectation Maximisation (SAEM)
Pheonix NLME [78]	nonparametric population pharmacokinetic modelling (NPEM)
S-Adapt Adapt[79]	Monte Carlo Expectation Maximisation

**Table B.3. Main software used in PK/PD modelling and their methods of parameter estimation.**

## TB immune response mathematical modelling: literature review results

No	First Author, year	Aims	Cells/Cytokines	Bacteria	Model type	# of compartments	Data	Disease Outcome Measure	Interventions	Main results
1	Antia [80] (1996)	Construct a simple model to explore how mycobacteria interacts with host immune response giving rise to observed patterns of infection	T cells (non-specific)	In active and dormant states	ODE	3	Used to Parameterize model	Extracellular bacteria increased to high levels	-	<p>Two mechanisms for bacteria to persist: slow replication or dormant stage.</p> <p>With only slow replication, successful persistence is dependent on inoculum size – the smaller the better.</p> <p>Successful persistence may result in bac proliferation as T cells will become exhausted in the long run and die.</p>
2	Kirschner [81] (1999)	1. Explore the impact of Mycobacterium tuberculosis, the	Activated CD4/CD8T, MCs HIV viral population	Bac population (not specified inter or ex bac)	ODE	4	Used to Parameterize model	Extracellular bacteria increased to high levels	TB treatment affecting the Bac growth rate (non-specific drug)	T- cell populations were lower in the presence of both <i>Mtb.</i> and HIV than in the case of infection with HIV alone.

		<p>bacteria that causes TB, on the HIV-infected immune system using a mathematical model.</p> <p>2. Explore the effect of TB treatment on co-infection</p>								<p>Viral load and <i>Mtb.</i> population are higher in the co-infected cases, than the single-pathogen infection cases.</p> <p>T-cell counts do improve over a short period of time after treatment initiation. Suggesting, treatment of TB in HIV-infected individuals can have a profound effect on their progression to AIDS.</p> <p>A TB drug that suppresses bacterial growth, as opposed to enhancing the bacterial death rate, will likely be more effective.</p>
3	Wigginton [82] (2001)	<p>1. Build human IR model characterizing cellular and cytokine</p>	<p>MCS (R, I, A): CD4TC (0,1 &amp; 2): IL-4, IL-10, IFN-<math>\gamma</math> &amp; IL-12</p>	In & Ex: infect only MCS	ODE	4 biological components, 12 compartments.	Used to Parameterize model	Extracellular bacteria increased to high levels	cytokine D&D experiments.	<p>All disease states achievable. IFN-<math>\gamma</math> present but low during latency - controlled by IL-10. Enhanced during active disease. Increased IFN-<math>\gamma</math> causes excessive tissue damage. Deletion of IFN-<math>\gamma</math></p>

		behaviour during <i>Mtb</i> infection. 2. Investigate which cytokines/IR behaviour are most important for reducing bac load.								causes rapid progression to active disease.
4	Gammack [83] (2003)	1. Build a model to investigate early immune response dynamics 2. Determine which conditions the bacteria population decreases.	MCs (R & I): Chemokine fMET-Leu-Phe (from bac)	In & Ex: Infect MCs.	Spatial PDE (diffusion eqns)	4 variables. I MCs can: phagocytose & kill, phagocytose but not kill, cannot phagocytose or kill with diff params	Used to Parameterize model	Extracellular bacteria increased to high levels	Change params: rate of phagocytosis, rate of intracellular killing and intracellular Bac growth.	MCs become saturated and ineffective if Bac growth too fast of phagocytosis too slow: uncontrolled granuloma. No steady state was found which could indicate adaptive response is essential.

5	Marino [84] (2004)	1. Build human IR model characterizing cellular and cytokine behaviour during <i>Mtb</i> infection in lung and DLN. 2. Investigate which cytokines/IR behaviour are most important for different disease stages.	Lung: MCs (R, I & A) DLN: DC (I & M):  Lung: CD4TC (0,1 & 2), DLN: CD4TC (0, 1):  Lung: IL-4, IL-10, IFN- $\gamma$ , IL-12 DLN: IL-12	In & Ex: infect only macrophages	ODE	DLN: 3 components, 3 compartments. Intermediate blood stage for TC migration.	Used to Parameterize model	Extracellular bacteria increased to high levels	Treatment effects introduced by increasing amount of IDC.	All disease states achievable. IFN- $\gamma$ levels are regulated by IL-10 during latency - levels are 3 fold higher than active disease - activated MCs important for latency. Decreasing activation rate by IFN- $\gamma$ is strong indicator of active disease.
6	Marino & Pawar [85] (2004)	1. Use an existing model (replication of Marino and K 2004) to explore how altering model	Lung: MCs (R, I & A) DLN: DC (I & M):  Lung: CD4TC (0,1 & 2), DLN: CD4TC (0, 1):	In & Ex: infect only MCs	ODE	DLN: 3 components, 3 compartments. Intermediate blood stage for	Used to Parameterize model and results of model output compared to published data (not	Extracellular bacteria increased to high levels	Cytokine D&D experiments.	All disease states achievable. Activated macs important for latency. DC and T-cell trafficking rates alter disease status between latent and active disease.

		parameters effects disease outcome.	Lung: IL-4, IL-10, IFN- $\gamma$ , IL-12 DLN: IL-12			TC migration.	fitted to data) – mouse data			
7	Segovia-Juarez [86] (2004)	1. Create an ABM representing the process of infection and granuloma formation. 2. identify mechanisms important for granuloma formation and control	MCS (discrete): TCs (discrete): Chemokines (continuous)	Infect and replicate in MCS.	ABM	-	Used to Parameterize model	Extracellular bacteria increased to high levels - bacteria count within the granuloma - absence of infected macrophages	Sensitivity analysis provides 3 separate outcomes: clearance, small controlled granuloma, large necrotic granuloma.	Factors that significantly affect granuloma outcome: increase in chemokine diffusion increases gran size, arrival time of TCs, # of TCs, ability to activate MCS.
8	Sud [87] (2006)	1. Use a mathematical model to simulate knock-out experiments in <i>Mt.b</i> infection. 2. Explore role of CD8TCs in	MCS (R, I, A): CD4TC (0,1 & 2), CD8TC (0, cyt & Effector): IL-4, IL-10, IFN- $\gamma$ , IL-12 & TNF	In & Ex: infect only macrophages	ODE	5 biological components, 16 compartment.	Used to Parameterize model	Extracellular bacteria increased to high levels	D & D experiments. Vaccination simulated by increasing memory TCs (longer half-life of cell) at initial introduction	All disease states achievable. INF-g important, but not sufficient to control infection. Both subsets of CD8 important but disease controlled without. Vaccination - most effective combo: CD4TC1 and cyto CD8TC most

		<i>Mtb.</i> infection							of <i>Mtb.</i> (CD4, CD8)	effective memory combo to have to clear.
9	Alavez-Ramirez [88] (2006)	1. build a model to represent the effects of antimicrobial drugs on a drug resistant and sensitive bac population.	Incorporated into a "immune system effectiveness" rate	Resistant or Sensitive states	ODE	4: Sensitive, resistant to 1, resistant to 2 and resistant to 1 & 2 drugs.	Used to Parameterize model	progression of bacteria toward antibiotic resistance	Two antimicrobial drug treatments for LTB (INH & RIF) - affect killing of sensitive Bac parameter	If drug treatment cannot eliminate sensitive bac, resistance persists, similar to if no treatment applied, depending on bac fitness. Two drugs are more likely to keep drug resist strains under control.
10	Marino & Sud [89] (2007)	1. Use mathematical model to characterize the role of TNF and effect of anti-TNF drugs on reactivation.	MCs (R, I, A): CD4TC (0,1 & 2), CD8TC (0, cyt & Effector): IL-4, IL-10, IFN- $\gamma$ , IL-12 & TNF	In & Ex: infect only MCs	ODE	5 biological components, 16 compartment.	Used to Parameterize model	Extracellular bacteria increased to high levels	D&D experiments. VCT of anti-TNF treatments - post-exposure treatment scenario.	Small amounts of TNF required for latency - high in active, but not as much as IFN- $\gamma$ . Low bioavailability (amount of TNF available in granuloma) for treatment is most likely to cause reactivation.
11	Ray [90] (2008)	Build a model to represent the	MCs	MC activation components	ODE	9 proteins involved in activation, 1 bacteria	Used to Parameterize model	NO levels producing by macrophages	Perturbation of params using LHCS	If IFN- $\gamma$ and TNF signals come before infection, NOS levels are impaired - killing not as effective.

		intracellular mechanisms of MC activation		– see [90] for list						
12	Marino & Myers [91] (2010)	1. Build a human lung and DLN model to identify mechanisms for disease control focusing on pro and anti inflammatory cytokines	Lung: MCs (R, I, AA, CA), DCs (I & M) DLN: Same as lung:  Lung: CD4TCs (precursor 1, 1) CD8TC(cyto, effector) DLN: Same as lung plus naive CD4, naive CD8:  Lung: TNF, IFN- $\gamma$ , IL-12, IL-10 DLN: Same as lung	Bac loads measured from mice.	ODE	2 sections: Lung : 14 compartments, DLN : 18 compartments	Model calibrated to data - nonlinear least squares with Latin Hypercube Sampling (LHS) of the model parameters - mouse data	Extracellular bacteria increased to high levels	D&D of TNF, IFN- $\gamma$ , IL-10	TNF very important for Mac and DC recruitment, but not anti or pro inflammatory phenotype. IL-10 important in balancing pro/anti inflammation response in lungs.
13	Clarelli [92] (2010)	1. Describe the innate immune response following	MCs (R, I):  Chemoattractant	move via diffusion, reproduce and killed by MCs.	Spatial PDE (diffusion eqns)	-	Used to Parameterize model	Extracellular bacteria increased to high levels	Perturbations of equation rates to determine stability of	Established a critical value for the killing efficiency parameter (for distinct # of MCs) between which bacteria load explodes or

		an <i>Mtb.</i> infection.								solution. "weak" and "strong" immune response introduced	dies out; more MCs, less efficiency needed.
14	Ahlers [93] (2010)	Exclude – HIV model TB mentioned, but no explicit TB model									
15	Bru [94] (2010)	1. Create a model that can explain the dynamics of the onset of granuloma formation	Generic Chemokines, MC (alive (R, I) or dead (necrotic, apoptosed), foamy), DC, innate lymph, T cell (alive or dead)	Only grow in MC, after threshold MC necrotic – bac become extracell.	ABM	-	Model calibrated to data - mouse data	Extracellular bacteria increased to high levels - bacteria count with the granuloma	"tolerance" level – defined by the chemokine threshold (above which a new cell is attracted neighbour square in model) Reinfection	Chemokine levels and distribution determine the formation of granulomas A higher apoptosis rate increases the ability to control bacteria growth Decrease in duplication time is advantageous to the bacilli Differing inoculum size has varying outcome in for high and low host tolerance level	
16	Ibarguen-Mondragon [95] (2011)	1. Build a model of the dynamics of <i>Mtb.</i> infection to the	MC (R,I): TC	one population of Bac. Infect MCs	ODE	4: MC (R,I), T, Bac	Used to Parameterize model	Extracellular bacteria increased to high levels	Infection rate of MCs only parameter changed.	Altering infection rate of RMCs led to extinction ( $R_0 < 1$ ), a latency state ( $R_0 = 1.25$ ) and active ( $R_0 = 12.5$ )	

		minimum level biologically viable and determine thresholds for disease progression								
17	Fallahi-Sichani [96] (2012)	1. Build a mathematical model of the granuloma to explore the affects of NF-kB (encodes TNF) on immune response to <i>Mtb</i> .	MC (R,I,A): Th (effector, cyto): TNF, NF-kB pathway - see [96] for list	Infect and replicate in MCs. Replication outside MCs is slower than inside.	ABM [86] & ODEs (intra cell).	2 for ODE	Used to Parameterize model	Extracellular bacteria increased to high levels - bacteria count within the granuloma - granuloma size and amount of diseased tissue – absence of TNF- $\alpha$	Manipulation of the NF-kB signalling pathway to simulate treatment that decreases inactivation rate of pathway	Sensitive balance between slow and fast NF-KB pathway signal parameters to control for over-activated MCs (inflammation) leading to damage or granuloma breakdown, resulting in disease (slow rates of inactivation of pathway lead to damage).
18	Magombe dze [97] (2012)	1. Model to represent <i>Mtb</i> . progression from active to latent to dormant stages	No immune response cell groups or cyto/chemokines considered	Active replicating Bac, latent bac (slow replication) and dormant bac (no replication)	ODE	8 in total: 3 bac (active, latent, dormant), nutrient, oxygen and NO comp, gene	Used to Parameterize model - mouse data	Persistence of the active <i>Mtb</i> . bacteria	Different bacteria stress conditions produced by different immune	

						expression of latent and dormant bac			response scenarios.	
19	Lyons & Lenaerts [98] (2013)	<p>PBPK/PD model, to more efficiently determine the in vivo multidrug dose</p> <p>-response relationships new anti-TB combination regimens in mice</p>	No immune response cells	No bacteria	ODE	Rifampin amounts moving through 12 compartments of the mouse physiology (lung, brain, gut, etc.) (PK)	Model calibrated to data - Bayesian Markov chain Monte Carlo (MCMC) procedures - mouse data		Different doses of rifampin	<p>Model predictions for rifampin concentrations in plasma, liver, kidneys, and lungs, following oral administration, fit well to experimental data from multiple studies.</p> <p>Model is a starting point for the integration of rifampin pharmacokinetics in mice into a larger mathematical framework, including the immune response to <i>Mtb.</i> infection</p>
20	Zheng [99] (2014)	<p>Exclude – population level model of natural history of TB – Susceptible, Latent, Infected model</p> <p>Measure of persistence of <i>Mtb.</i> in a population and investigate how well <i>Mtb.</i> can persist as a function of the latent period</p>								

21	Pedruzzi [100] (2015)	Aimed to describe the role of iron homeostasis, lipids metabolism and the innate immune response, in terms of NO. Which factors enable or hamper persistent infection?	MCS – static environment for bac (no dynamics)	Bac load in MCS, Iron, Lipid, NO concentrations in cells	ODE	4	Used to Parameterize model	Persistence of the active <i>Mtb.</i> bacteria	Parameter sensitivity analysis to assess the stability of the system (bac growth or containment) under different parameter values (bio conditions)	Model was sensitive to parameter governing the infection induced NO production – small perturbations changed dynamics from stable controlled Bac counts to unstable, increasing bac counts.  For bacteria to survive, the parameter governing bacs effect on iron production should be dampened.
22	Lyons & Lenaerts [101] (2015)	1. Physiologically based PK/PD model for rifampin in <i>Mtb.</i> infected mice, including a population model for the host-immune	MCS, CD4&CD8T, IL2, IL12, IFN- $\gamma$ , IL10	Bac in lung, ex, or in MC's (activated or infected MC's), Bac is killed by immune response and concentration of drug in lungs from the PBPK model (see Lyons &	ODE	8 – 3 bac, 3 MC's. 2 T	Model calibrated to data - Bayesian Markov chain Monte Carlo (MCMC) procedures - mouse data	Extracellular bacteria increased to high levels	Dose fractionation study	Model fit well to PK data for RIF and bacteria counts in mice for multiple doses.

		response to infection.  2. Calibration to data on rifampin in mice.		Lenaerts [98] (2013))		brain, gut, etc.) (PK)				
23	Datta [102] (2016)	Theoretical model of oxygen diffusion and consumption in TB granulomas	-	-	Spatial PDE (diffusion eqns)	Oxygen diffusion equations over layers of a spherical granuloma	Used to Parameterize model – rabbit data	Oxygen levels inside the granuloma and granuloma size	Assessment of size of granuloma and relationship of necrotic and hypoxic radii inside granuloma	<p>Only the larger granulomas (radius &gt; 0.2 mm) can achieve a necrotic (no oxygen – bac death) core.</p> <p>Hypoxic (deprived of adequate oxygen – altered bac metabolism) and necrotic radii increase dramatically with increasing granuloma size for smaller granulomas (radius &lt; 0.6 mm), but then more gradually for larger granulomas (radius &gt; 0.6 mm).</p> <p>An approximate analytical solution was able to predict the size of hypoxic and necrotic regions in agreement with</p>

										experimental results from the animal model.
24	Hao [103] (2016)	<p>The evolution of a granuloma model of TB (once formed)</p> <p>Q: Does the reduction in granuloma volume depend on the immune response, and does the reduction in granuloma volume depend on the time when the treatment began?</p>	<p>MCs (normal, alternative activated), infected MC's, Th1, Th2, DCs, Naïve CD4T, IL-2, IL-12, TNF-<math>\alpha</math>, IL-10, IL-13, IFN-<math>\gamma</math>, a and B, IL-1B.</p> <p>Radius of gran, dynamic boundary conds</p>	<p>Intercellular or extracellular Bac</p>	<p>Spatial PDE (diffusion eqns)</p>	<p>10 cells+bac</p>	<p>Used to Parameterize model</p>	<p>Extracellular bacteria increased to high levels - bacteria count within the granuloma - granuloma size and amount of diseased tissue</p>	<p>"Immune strength" - parameter representing influx of adaptive cells</p> <p>IL-10 antibody treatment</p>	<p>As immune strength increases, the radius of the granuloma increases and bac load decreases – too strong and pro-inflammatory causes tissue damage.</p> <p>The sooner treatment is started, the more effective the loss of bac (both types) – a lower immune strength and early treatment is best (compared to high immune strength) (<i>although result reported in abstract contradicts main text?</i>)</p>

25	6. Lalande [104] (2016)	<p>Develop a mathematical model describing time course of TB infection and its early treatment by Isoniazid in human lung.</p> <p>Test dose regimens</p>	<p>Cell model taken from Marino [84] (2004) &amp; Wigginton [82] (2001) (see above)</p> <p>PK model of INH distribution in plasma, alveolar cells and lung lining fluid</p>	<p>ODE of effect of immune response cells and INH on bacteria (ex and int) population</p>	ODE	21	Model calibrated to data	Extracellular bacteria increased to high levels	Different doses of INH, 19, 37, 75, 150, 300 600 mg in one regimen	<p>Adequately reproduced properties of the early bactericidal activity of INH observed in TB patients.</p> <p>Bacteria kill curves simulated with the model reproduced</p> <p>the biphasic killing effect of INH and the predicted declines in extracellular bacteria were comparable to clinical data.</p> <p>The first phase was driven by the drug effect. Second phase, while drug pharmacology still influenced bacteria kill, dynamics of infected macrophages also influenced.</p>
26	Zhou [105] (2016)	<p>Exclude – review on diseases due to poverty, not specifically TB and no new models</p> <p>Modelling is mentioned but mostly in context of flu (H7N9)</p>								

27	Chisholm [106] (2016)	Introduce a model of <i>Mtb</i> states (active or latent) to illuminate the conditions under which latency can emerge as an evolutionarily stable strategy for <i>Mtb.</i> survival.	Immune response cells do not explicitly feature. Infection does not protect and immunity is considered not to affect host susceptibility in the long run. The more likely the pathogen to become latent affects the host recovery rate – i.e. more latency means less bacterial killing by immune response and thus	A active or L latent <i>Mtb</i> infection compartments	ABM,ODE	2 for ODE (active and latent <i>Mtb.</i> populations)	Used to Parameterize model	Persistence of the active <i>Mtb.</i> bacteria	Host recovery rate is changed and R0 assessed as a result to determine if latency in these cases is beneficial	<p><i>“Latency is an optimal evolutionary strategy for pathogens when the gain from reducing the recovery rate outweighs the disadvantage of losing transmission opportunities.”</i></p> <p>[106]</p>
----	-----------------------	--	---	--	---------	---	----------------------------	--	--	---

			lower host recovery.							
28	Wallis [107] (2016)	Exclude – not immune response models but summary of three population level models								
		<ol style="list-style-type: none"> <li>1. Looking at innate response resistance in miners</li> <li>2. Looking at “relapse” after anti-TNF treatment</li> <li>3. Statistical model analysing risk of relapse in person undergoing treatment</li> </ol>								
29	McDaniel [108] (2016)	mathematical modeling to investigate the rates of <i>Mtb.</i> replication and death during infection in mice	No immune response cells modelled	bacteria that are plasmid bearing or plasmid free – replication and death or go into a quiescent state	ODE	2 or 4 (quiescent)	Model calibrated to data - multiple linear regressions to data for different time ranges - mouse data	Persistence of the active <i>Mtb.</i> bacteria	Different replication and death rates modelled for different time periods, no explicit intervention	<p>Model with only early changes in rates had lower AIC indicating that replication and death rate slows there is no diff in replication and death rate after approx. 2 months</p> <p>The majority of bacterial cells must be replicating in the chronic phase of infection to explain the data – not the conventional hypothesis of non-replicating <i>Mtb.</i> in chronic phase</p>
30	Rhodes [109] (2017)	Exclude – My paper 2 (chapter 3) included in thesis								

**Table B.4. Results of TB immune response modelling literature review. Abbreviations: MC – Macrophage, I – Infected, A – Activated, R – Resting, D&D – Depletion and Deletion, DC – Dendritic cells, Ma – Mature, Im – Immature, CD4TC – CD4+ T-cell, (0,1,2 – phenotypes), CD8+ T-cell, EC – Effector cell, Bac – Bacteria, In –**

Intracellular, Ex- Extracellular, ODE – Ordinary Differential Equation, Gran – Granuloma, LHCS – latin hypercube sampling sensitivity analysis, DLN – draining lymph node, LTB – latent TB, INH – Isoniazid, RIF – Rifampin, IR – Immune Response, *Mtb.* – Mycobacterium Tuberculosis, Params – parameters, BAL – Bronchoalveolar lavage, VCT – Virtual clinical trial.

## Permission for Figure use in Chapter 1

Figure 1.1

Dear Sophie,

Thank you for your request for permission to reprint and reproduce certain WHO copyrighted material.

On behalf of the World Health Organization, we are pleased to authorize your request to reproduce the WHO materials as detailed in the form below, subject to the terms and conditions of the non-exclusive licence below.

We thank you for your interest in WHO published materials and good luck with your project.

Kind regards,  
Catalina

Catalina GRADIN  
Technical Assistant  
WHO Press

Strategy, Policy and Information Department

World Health Organization

The license can be provided if requested.

Figure 1.2

Hi Sophie,

Dara asked me to reach out to you about the TB vaccine pipeline. You are welcome to use it – and I've attached the latest version here. Please make sure the disclaimer about information being self-reported is included, and let me know if I can help with anything else.

Thanks,

Jennie

Jennie Willson

Manager, Strategic Communications, External Affairs

Phone: 301-547-2867

Email: [jwillson@aeras.org](mailto:jwillson@aeras.org)

Advancing Tuberculosis Vaccines for the World

[www.aeras.org](http://www.aeras.org) | @aerasglobaltb

## **Appendix C. Supplementary Material for paper 2 (chapter 3)**

The following are from the supplementary material for paper 2 in chapter 3. The table numbers follow from the supplementary outlined in chapter 3.

### **Additional Results**

#### *Diagnostic plots*

Additional diagnostic plots for analysis 1 can be found in S4-S7.

Figure S4 shows the residual plots for the macaque total cell predictions in analysis 1. The residuals seem to be normally distributed, although the IWRES by time and the prediction pdf (bottom row) show slight model under prediction. This is most apparent at time points 84 and 112. However, this may be a result of the large variation in the data between time points (particularly for day 84 and 112), which the model is unable to accommodate. Figure S5 shows the residual plots for the human total cell predictions in analysis 1. Residual error in this case seem to approximate a normal distribution, however there appears to be slight under prediction by the model, particularly at day 0 and 28 (IWRES plot, top row). Despite this, the VPC in Figure 2, paper 2, indicates that the model is still an adequate prediction of the data, for both species. The observed versus predicted response plots in Figure S6 also reflect the discrepancy between data and model total cell predictions for population (left column) and individual (right column) data for A. macaques and B. humans.

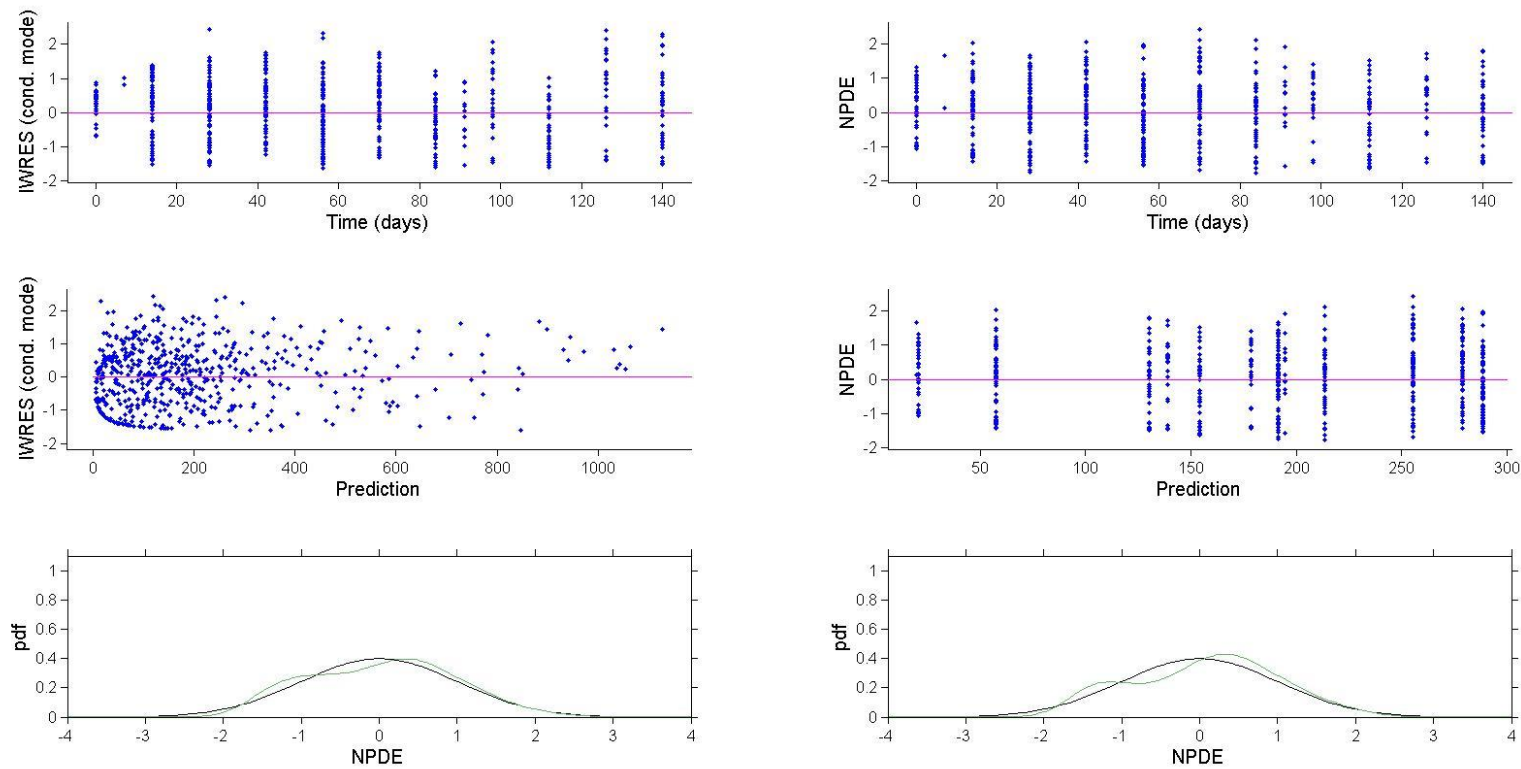


**Figure S4.** Residual (difference between data and total cells as predicted by the model) plots for macaque predicted total responses. The first row shows the individual weighted residuals (IWRES) and normalised prediction distribution errors (NPDE) using simulated individual parameters against time. The second row shows the residual error against the prediction. The bottom rows show the distribution of the residuals compared to a Gaussian pdf curve so assess the normality of the residuals.

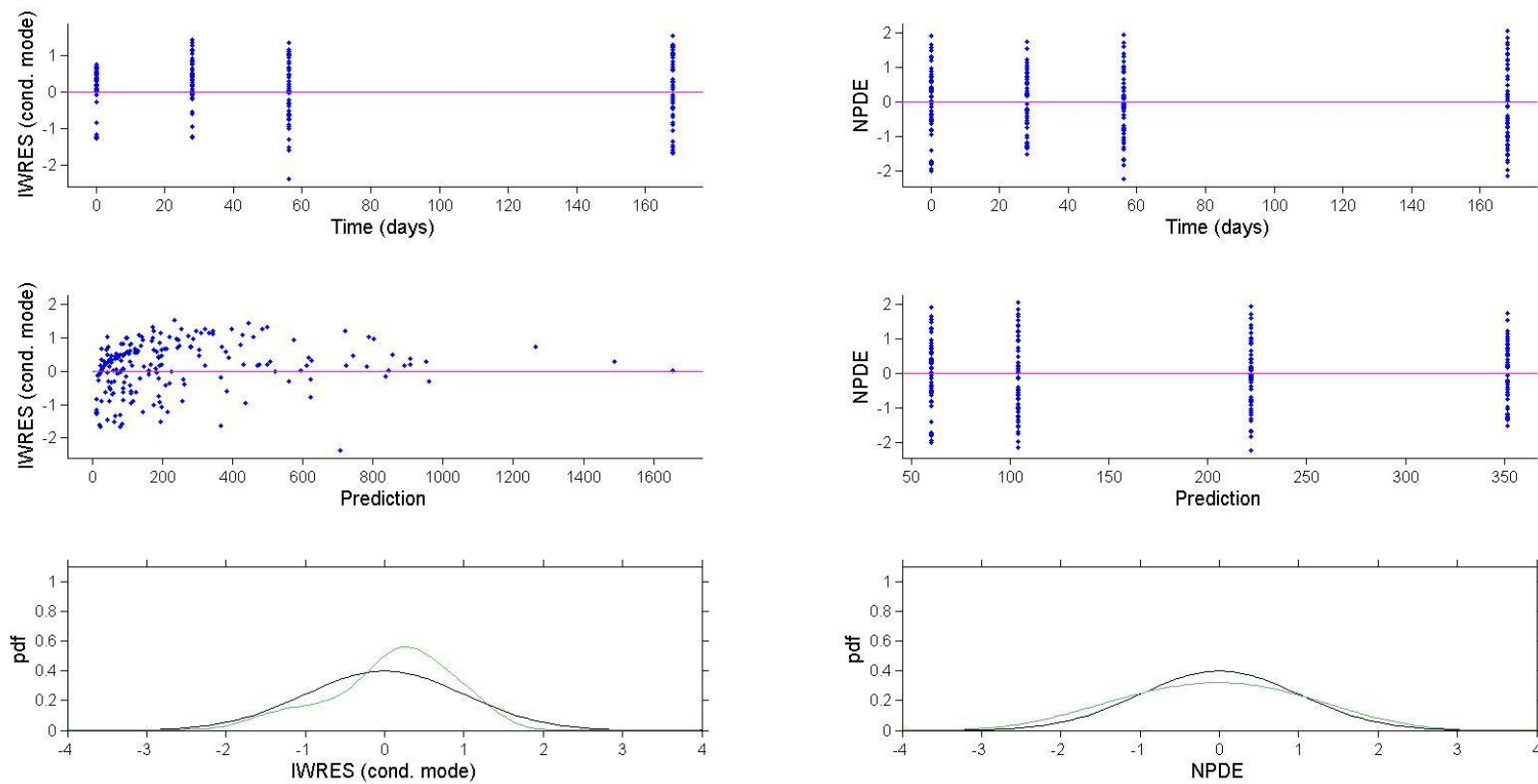


**Figure S5. Residual (difference between data and total cells as predicted by the model) plots for human predicted total responses. The first row shows the individual weighted residuals (IWRES) and normalised prediction distribution errors (NPDE) using simulated individual parameters against time. The second row shows the residual error against the prediction. The bottom rows show the distribution of the residuals compared to a Gaussian pdf curve so assess the normality of the residuals.**

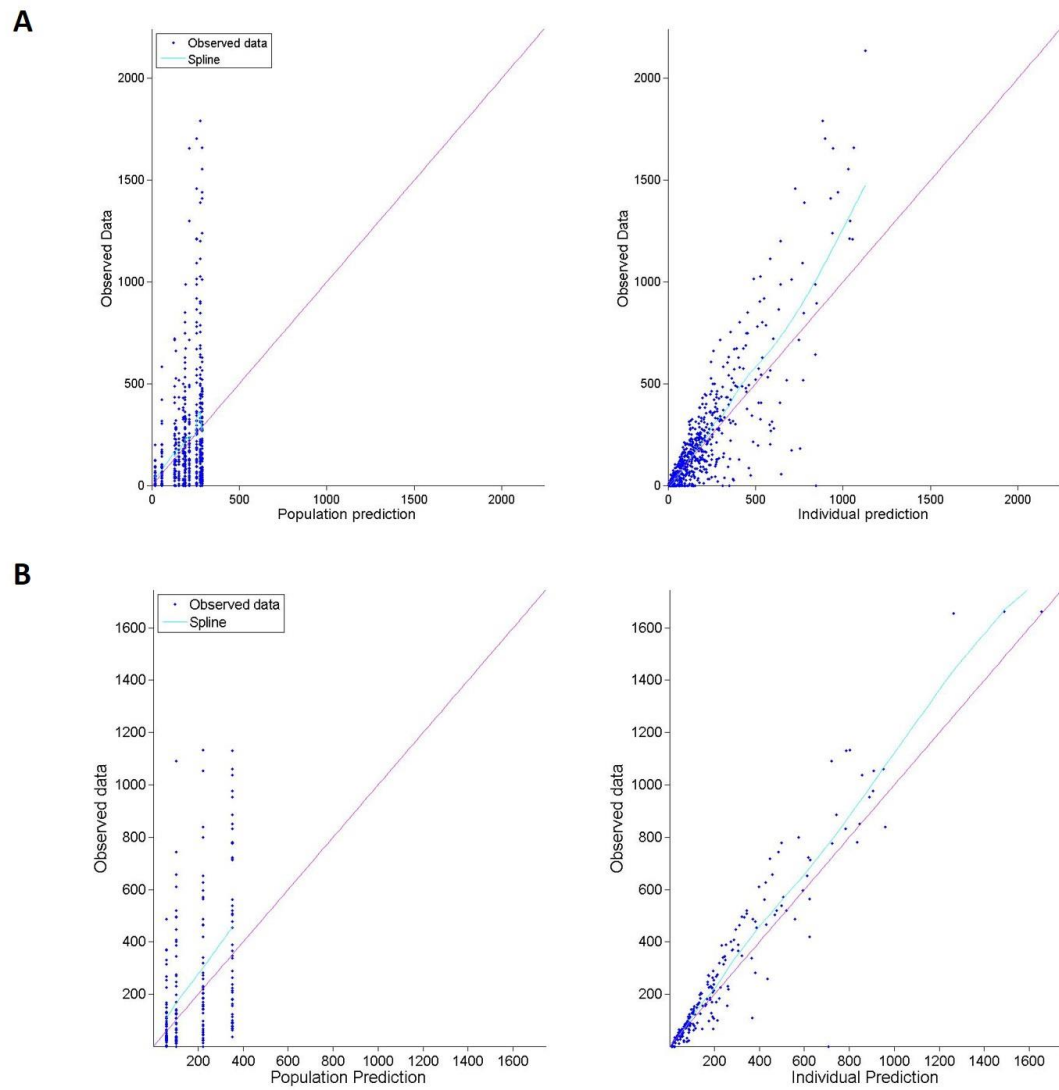


**Figure S6. Empirical data versus predicted total IFN- $\gamma$  responses for A. macaques and B. humans**

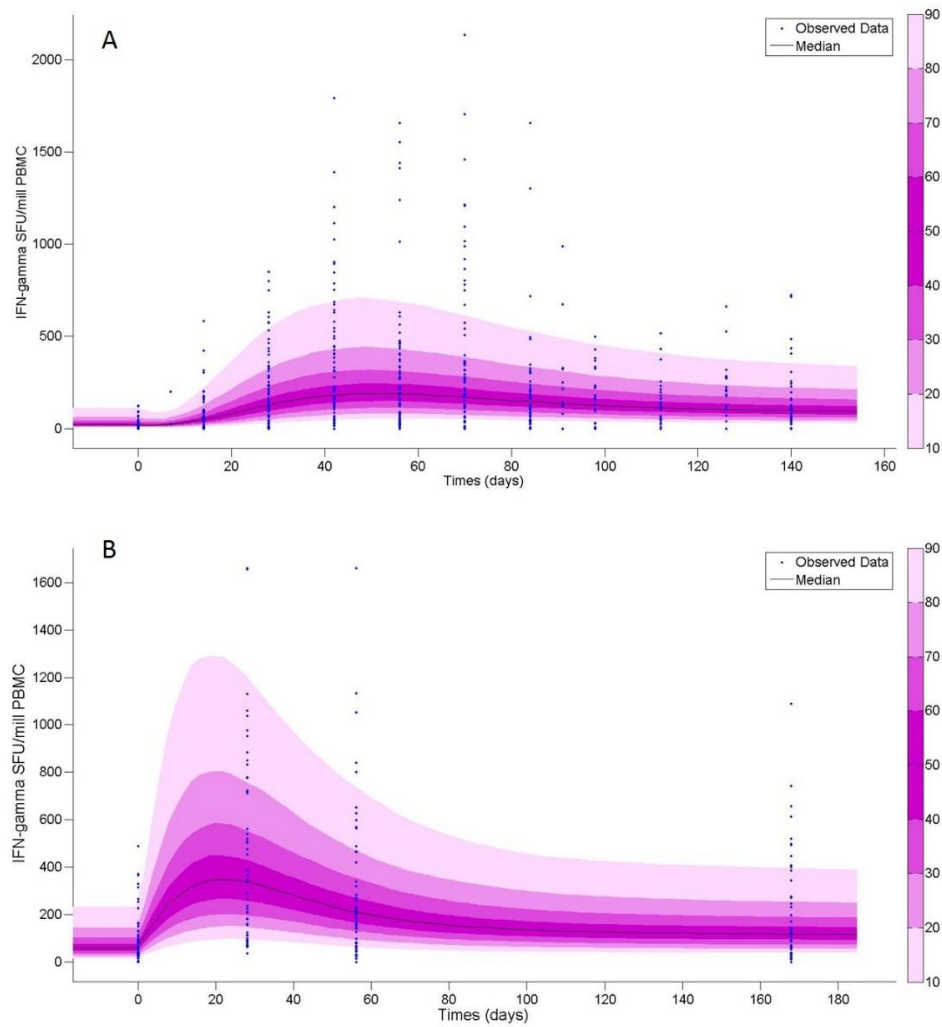


**Figure S7. Prediction distribution plot for A. macaques and B. humans. The black points represent the empirical data. The bands represent the 10<sup>th</sup> to 90<sup>th</sup> percentiles of the theoretical predictions using the estimated population parameters and associated variation for analysis 1 (Table 1, paper 2). The black line shows the median total cell response prediction**

### *Diagnostic plots*

Additional diagnostic plots for the macaque and human subpopulation-models can be found in Figures S15-S18.

Figures S15 and S16 show the accuracy of the model predictions for the macaque covariate model. Although the residuals are close to normally distributed (Figure S15), the Mauritian and Chinese cynomolgus macaque parameter sets over predict for higher IFN- $\gamma$  responses (Figure S16). This could potentially be due to small colony populations. The Indian rhesus and Indonesian cynomolgus macaque predictions better describe the data. The VPC plots (Figure S13 see chapter 3 supplementary) show that, although the simulated percentile bands are wide for the Chinese, Indonesian and Mauritian cynomolgus macaques due to reduction in population size for these colonies, the empirical percentiles still fall (aside from variation between time points in the data) within the simulated bands.

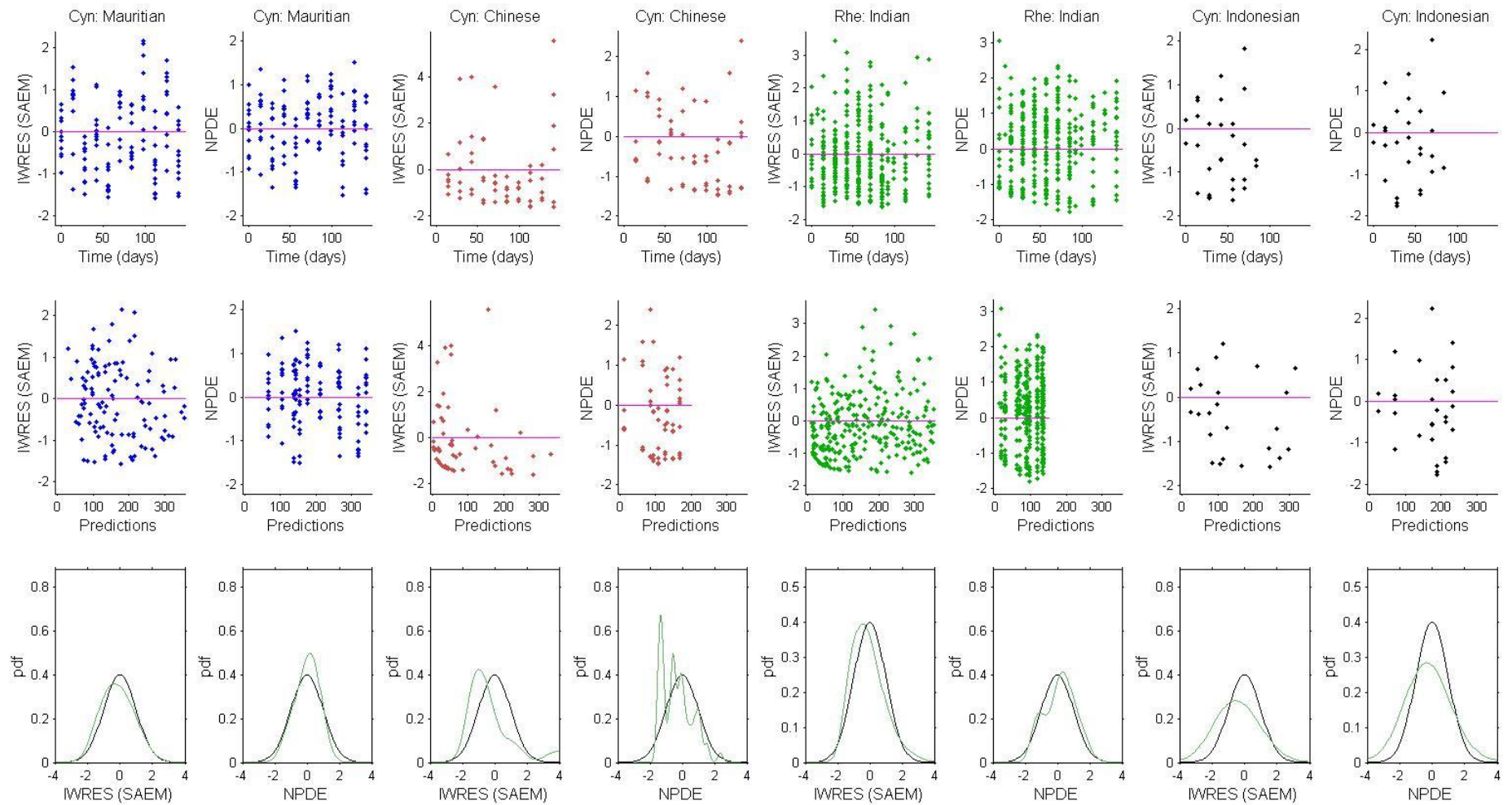


**Figure S15. Residual (difference between data and total cells as predicted by the model) plots for macaque predicted total responses stratified by colony. The first row shows the individual weighted residuals (IWRES) and normalised prediction distribution errors (NPDE) using simulated individual parameters against time. The second**

row shows the residual error against the prediction. The bottom rows shows the distribution of the residuals compared to a Gaussian pdf curve so assess the normality of the residuals

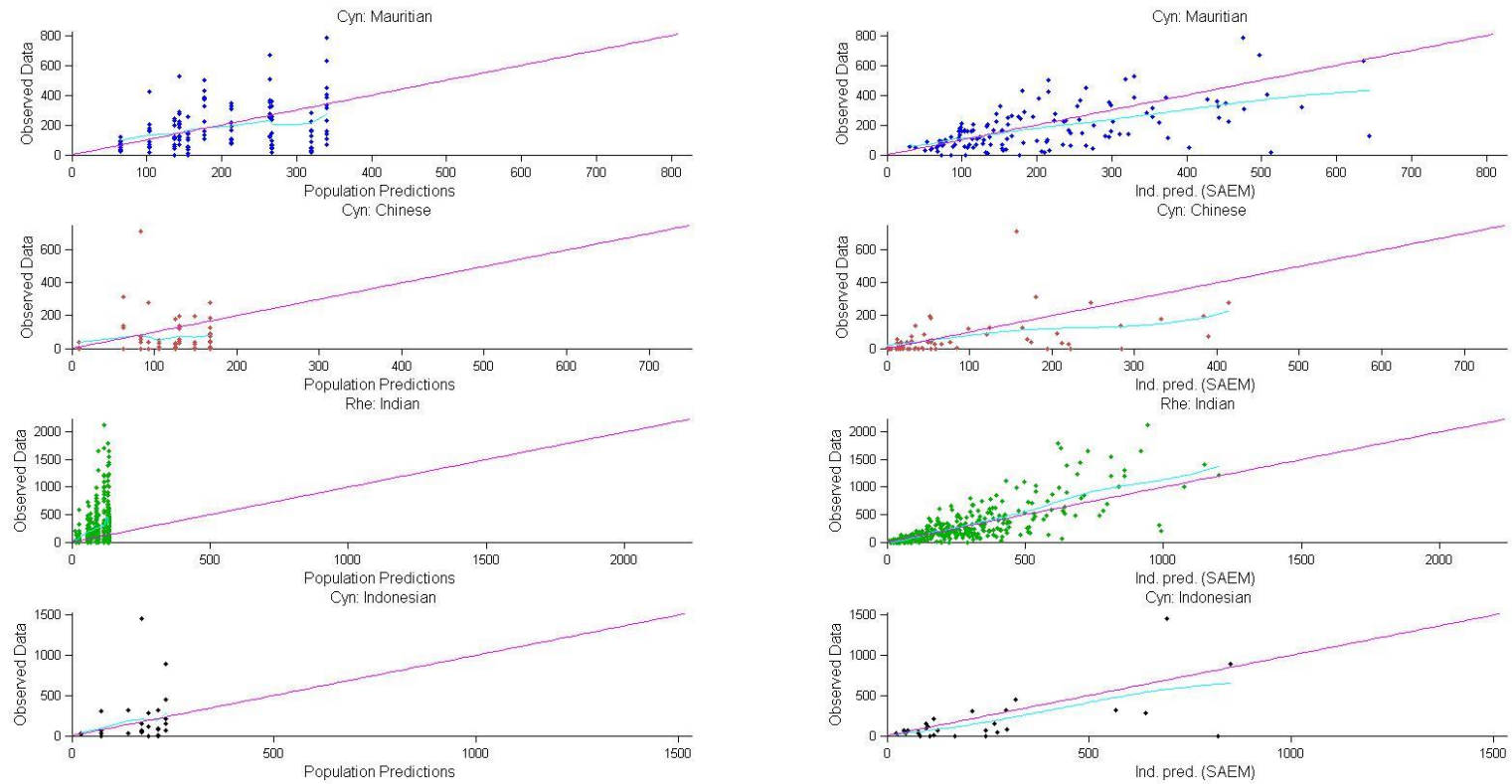


Figure S16. Macaque observed versus predicted IFN- $\gamma$  total responses stratified by colony

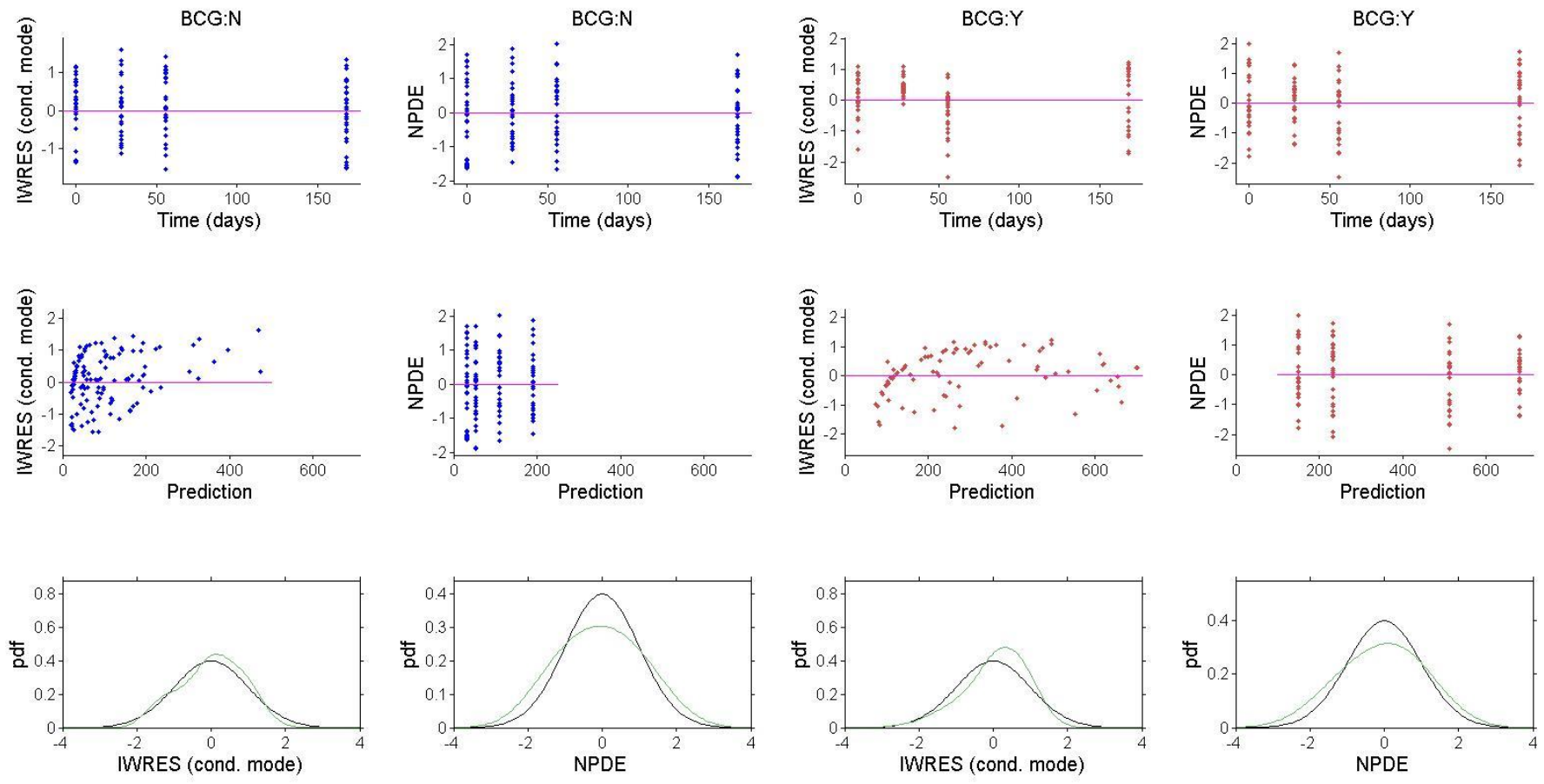


Figure S17. Residual (difference between data and total cells as predicted by the model) plots for human predicted total responses stratified by BCG status. The first row shows the individual weighted residuals (IWRES) and normalised prediction distribution errors (NPDE) using simulated individual parameters against time. The second row shows the residual error against the prediction. The bottom rows shows the distribution of the residuals compared to a Gaussian pdf curve so assess the normality of the residuals

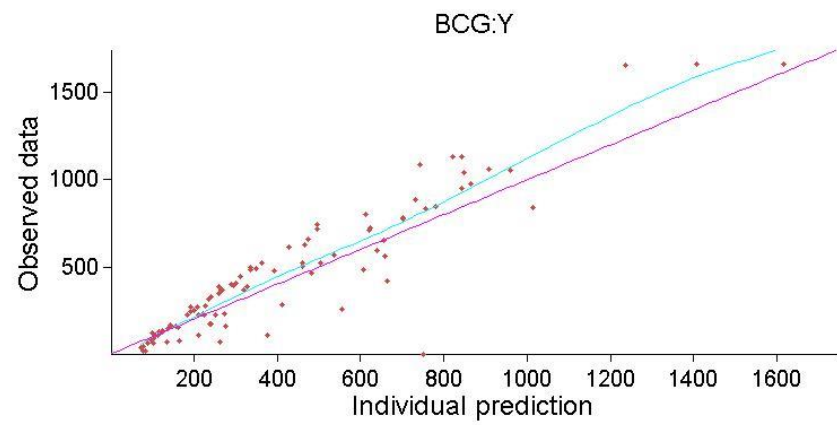
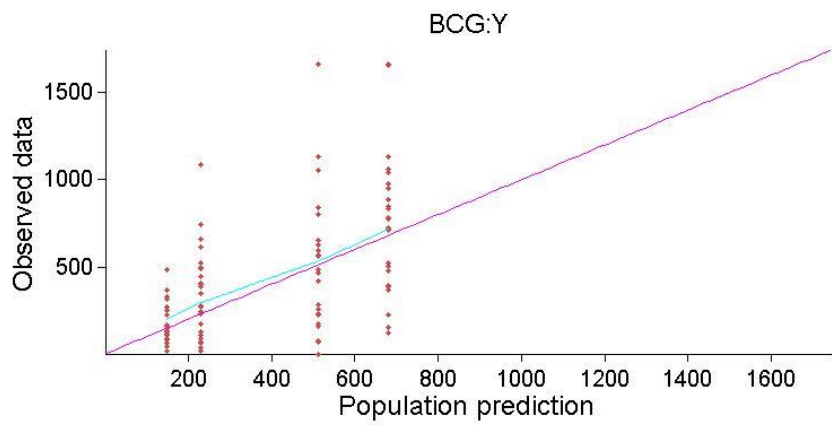
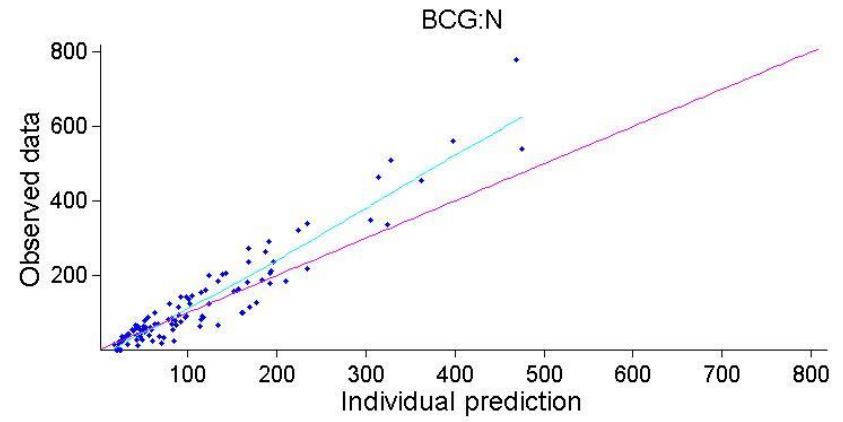
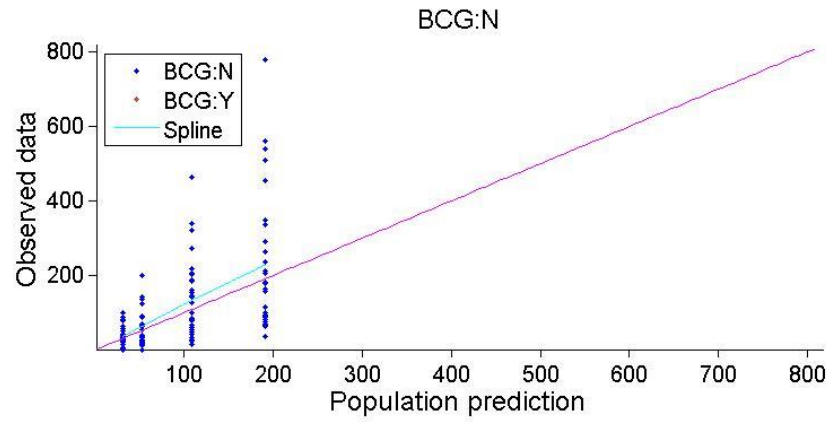


Figure S18. Human observed versus predicted IFN- $\gamma$  responses stratified by BCG status

Figures S17 and S18 show the accuracy of the model predictions for the human covariate model. For the human subpopulations of BCG status, the residuals are close to normally distributed (Figure S17), however both BCG: Y and BCG: N parameter sets under predict the higher IFN- $\gamma$  responses, more so for the BCG: N predictions (Figure S18). Despite this, the VPC plots (Figure S14, see chapter 3 supplementary) show that, the empirical percentiles still fall within the simulated bands.

### Analysis 3: Which macaque subpopulations best predicted immune responses in different human subpopulations?

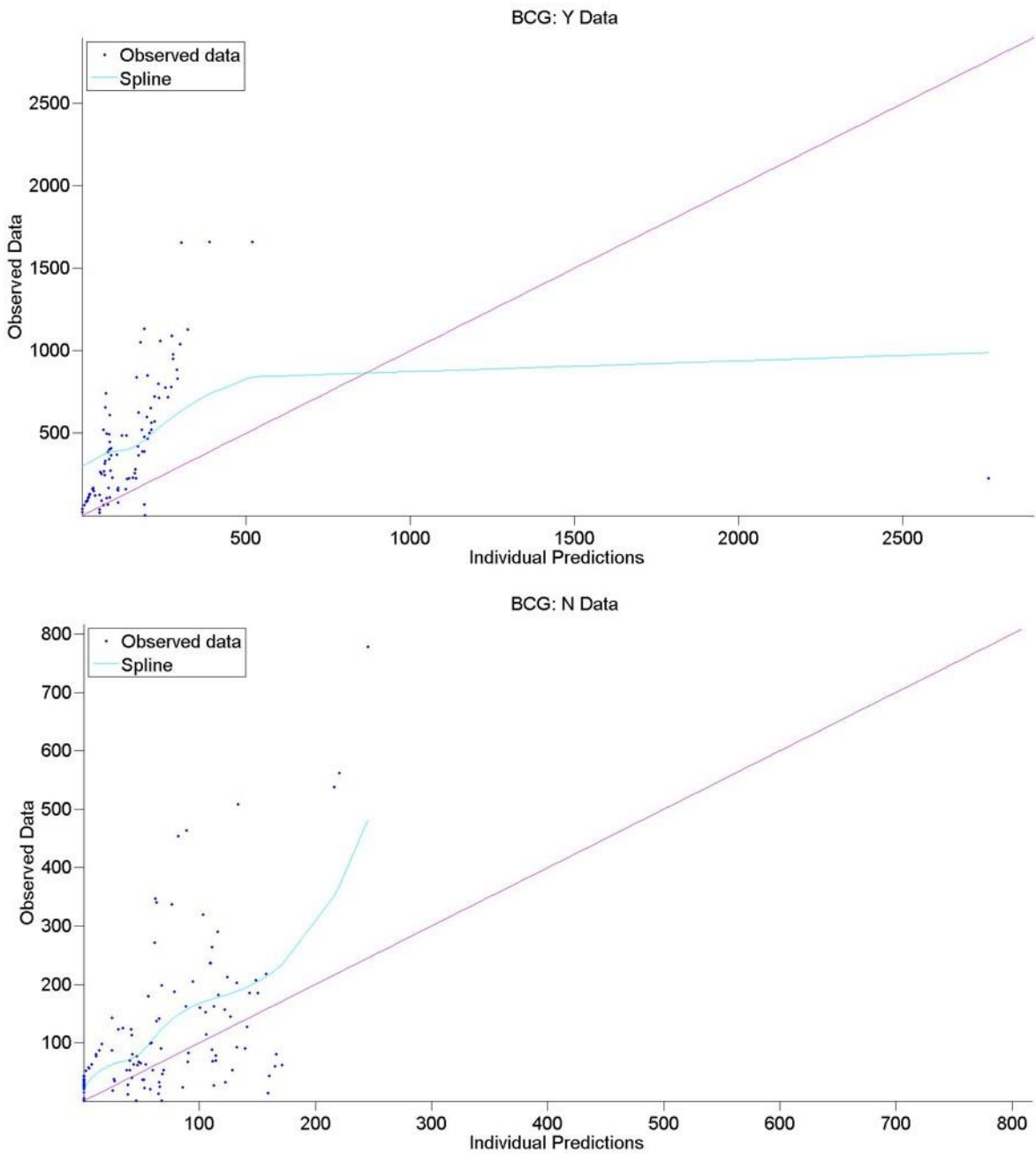
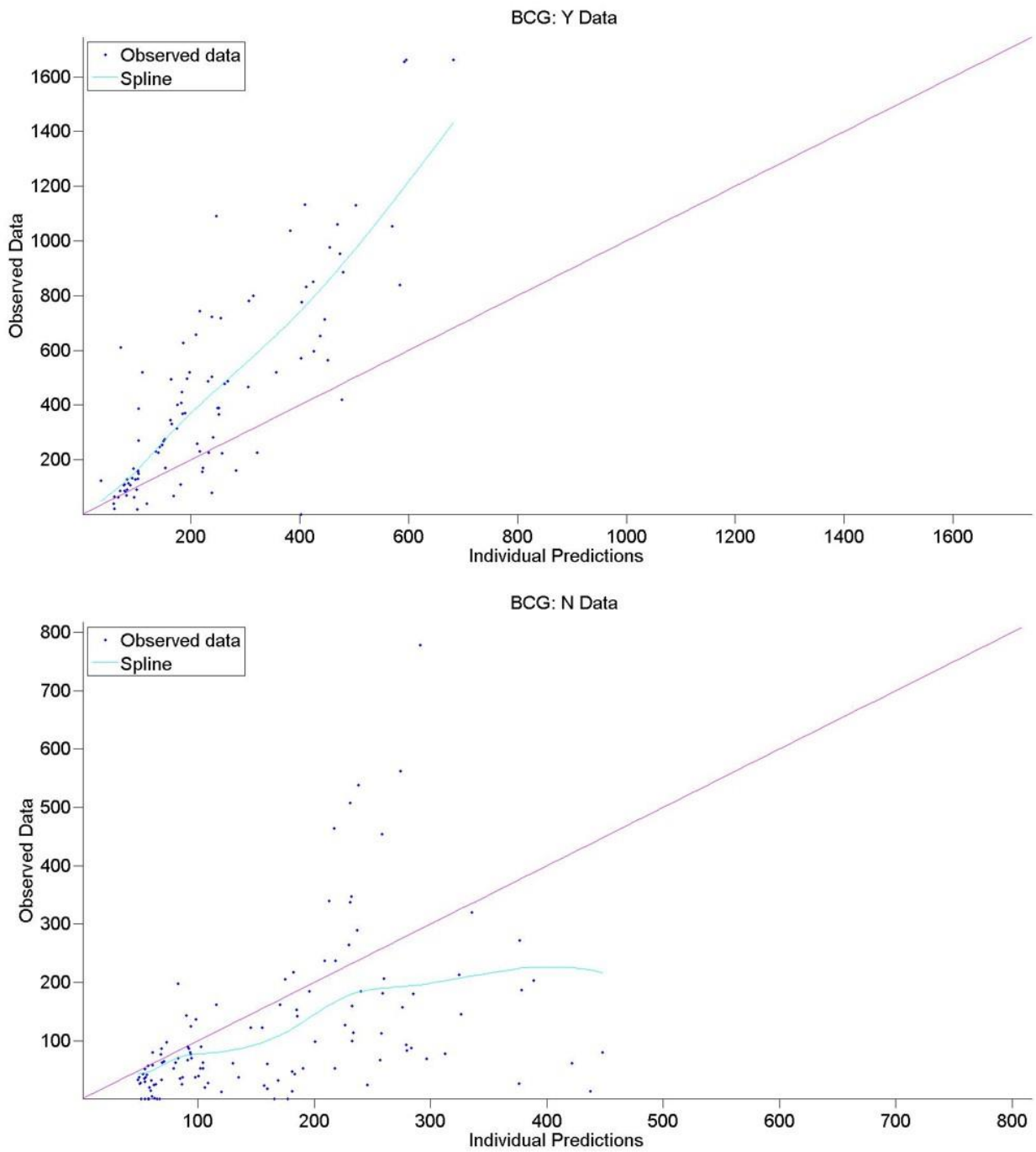
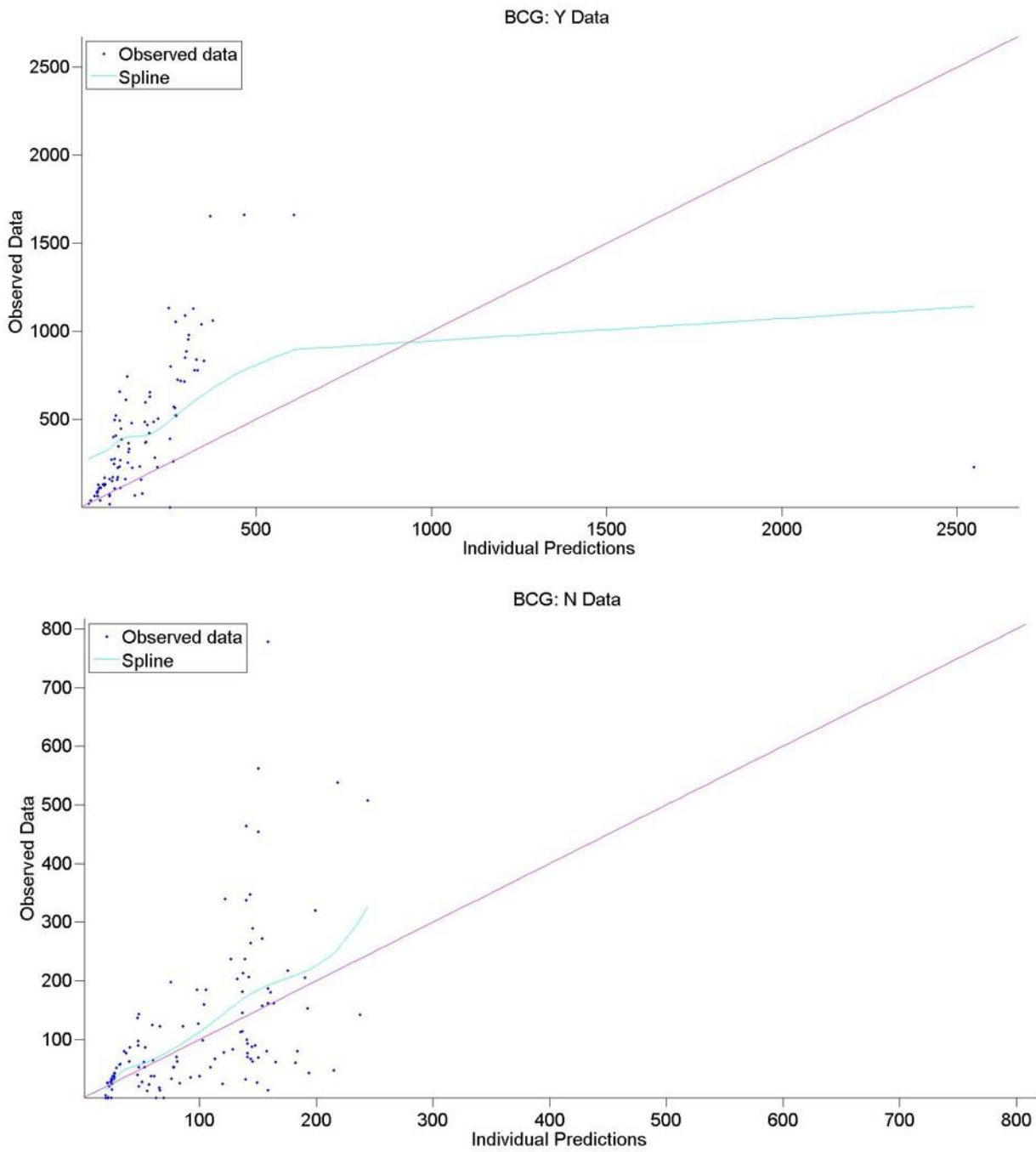


Figure S25. Individual empirical data versus individual prediction for macaque estimated subpopulation-model parameters fit to human BCG: Y data (top) and BCG: N data (bottom) for Chinese cynomolgus macaques.



**Figure S26. Individual empirical data versus individual prediction for macaque estimated subpopulation-model parameters fit to the human BCG: Y data (top) and BCG: N data (bottom) for Mauritian cynomolgus macaques.**



**Figure S27. Individual empirical data versus individual prediction for macaque estimated subpopulation-model parameters fit to the human BCG: Y data (top) and BCG: N data (bottom) for Indonesian cynomolgus macaques.**

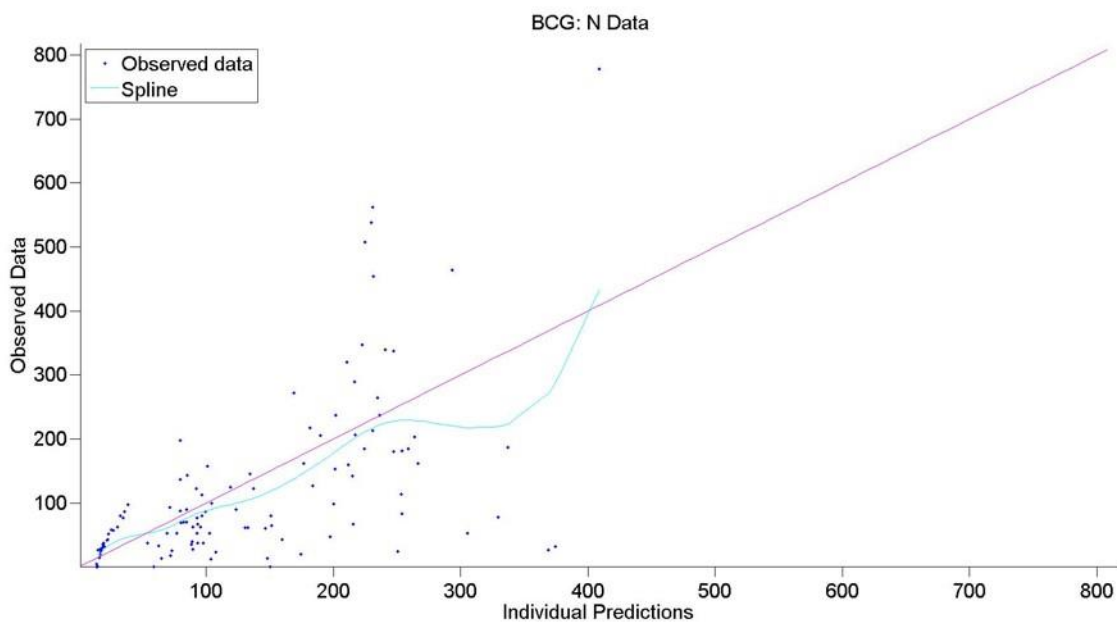
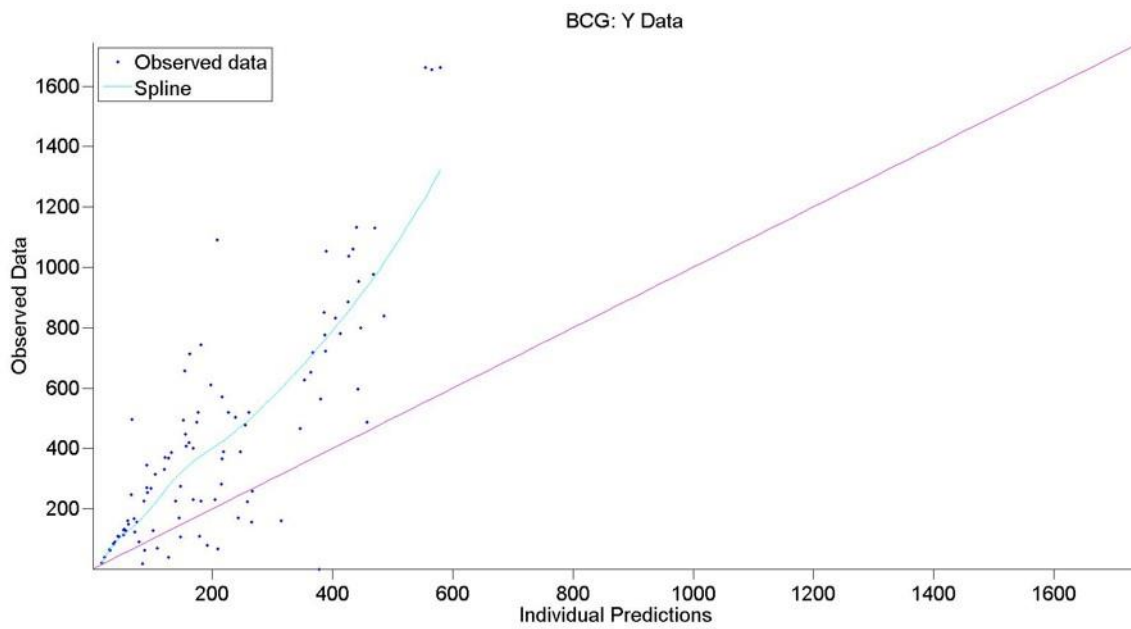


**Figure S28. Individual empirical data versus individual prediction for macaque estimated subpopulation-model parameters fit to the human BCG: Y data (top) and BCG: N data (bottom) for Indian rhesus macaques**

## Appendix D. Supplementary Material for paper 3 (chapter 4)

LONDON  
SCHOOL of  
HYGIENE  
& TROPICAL  
MEDICINE



### Proposal of H56+IC31 vaccine mouse immunogenicity experiment for mathematical modelling project

#### Contents

1. Rationale for H56+IC31 vaccine mouse immunogenicity experiment
2. H-series clinical trial summary
3. Outline of mouse experiment
  - a. Design
  - b. Costing

## **1. Rationale for H56+IC31 vaccine mouse immunogenicity experiment**

### Rationale for mouse experiment

We aim firstly, to use mathematical models to describe the immune response following vaccination with novel TB vaccines in the H-series in mice and humans and secondly, to compare estimated model parameters across species and predict dose-dependent immune responses in humans based on mouse data. The vaccines under consideration are H56 and H1, both adjuvanted with IC31. The cytokine IFN- $\gamma$  will be used as the immune response read out. Clinical data is available, providing adequate time points for modelling, but data in the mouse has been less extensively sampled. This experiment will address this gap.

### Aim of mouse experiment

To conduct an experiment in mice to provide data matched to the clinical trial regimen and extend the same regimen to different dose concentrations.

## **2. H series clinical trials summary**

The H series vaccines are currently in phases 1 of clinical development. Data on H-series vaccination given to health, BCG-vaccinated participants is taken from two clinical trials. Table D.1 summarises the clinical trials available for the modelling project from the two vaccines H1 and H56 all administered with the adjuvant IC31.

To summarise the data, when pooling all the vaccine trials together:

- There are a total of 18 participants included in the analysis who were not LTBI positive.
- All were BCG vaccinated at least 2 years prior to start of the trial.
- All received a dose concentration of 50  $\mu\text{g}$  of antigen with 500 nmol of IC31.

- Participants received H-series vaccination at day 0 and day 56.
- One trial administered a third H-series vaccination at a later time point, but this these data are not included in the analysis.

The IFN- $\gamma$  immune response was measured using an ELISPOT assay and measures were taken at various time points during the trials. These are outlined in table D.2.

Vaccine	Clinical trial Information					Data from Clinical trial used in our analysis					
	ClinicalTrials.gov ID/publication	Phase	Purpose of trial (taken from ClinicalTrials.gov)	Country conducted	Study arms	Study arm used	N	Response measurement times (days)	Median age (IQR)	Gender	Years since BCG
H56+IC31	NCT01967134/[110]	i	Evaluation of the Safety and immunogenicity profile of H56+IC31 administered to HIV-negative adults and without LTBI and no history or evidence of tuberculosis (TB) disease.	South Africa	4. N=8, LTBI negative, dose = 50 ug H56(+500nmol IC31), two vaccinations (day 0, 56) 5. N=8, LTBI positive, dose = 15 ug H56(+500nmol IC31), two vaccinations (day 0, 56) 6. N=9, LTBI positive, dose = 50 ug H56(+500nmol IC31), two vaccinations (day 0, 56)	1	8	0, 14, 56, 70, 112	32 (19–38)	M=4, F=4	>10 (assumed to be vaccinated at birth)
H1+IC31	NCT00929396/[111]	i	A safety and immunogenicity Phase 1 Trial with an adjuvanted TB subunit vaccine H1+IC31 (Ag85B-ESAT-6 + IC31) administered in PPD positive volunteers at 0 and 2 months	Netherlands	3. N=10, LTBI negative, BCG positive, dose= 50 ug H1(+500nmol IC31), two vaccinations (day 0, 56) 4. N=10, LTBI positive, dose= 50 ug H1(+500nmol IC31), two vaccinations (day 0, 56)	1	10	0, 7, 42, 63, 98, 224	49 (24–54)	M=7, F=3	>2

**Table D.1. Outline of the H56+IC31 and H1+IC31 phase i clinical trials and human demographics for each. Abbreviations: LTBI = Latent Tuberculosis Infection, IQR= Inter quartile range.**

Vaccine	2+ years previous	0	1	2	3	4	5	6	7	8	9	10	11	12	13	14	15	16	17	18	19	20	21	22	23	24	25	26	27	28	29	30	31	32	
H56	BCG	xH		X						XH		X					X																		
H1	BCG	xH	X					X		H	X					X																			X
Pooled (H56/H1)	BCG	xH	X	X				X		XH	X	X				X		X																	X

**Table D.2. Outline of the data available for the H series clinical trials following the criteria of previous BCG vaccination and a 2 H vaccination regimen. Number correspond to weeks. Abbreviations: X = Blood taken for ELISPOT test; H = H vaccine administered; xH = blood taken before vaccination on the same day.**

## 5. Outline of mouse experiment

### a. Design

Regimen: Based on the information from the clinical data Table D.1, it was decided that each mouse should receive two H56 vaccinations two weeks apart. This follows published mouse data with H56/H1 [112, 113].

Dosing: Doses 0, 0.1, 0.5, 1, 5, 15 µg antigen / 100 nmol IC31 will be used in this experiment. A scaling factor of 5 from the human dose [110] for the adjuvant concentration was based on SSI previous work. No adverse events are anticipated related to these vaccine dose concentration in the mouse.

Assay: An ELISPOT lab test will be used on mouse splenocytes using a 24 hour and 48 hours incubation time to test for significant differences between these two incubation times.

Experiment Design: Each arm of the experiment contains groups of mice, each group containing five mice to act as replicates. Each group will be culled and spleens removed at different time points depending on the regimen they belong to. The corresponding data generated (within the arm) will be aggregated to represent the time course of that arm:

- Regimen matched to H56 clinical time points. In the clinical trials, revaccination was given 8 weeks after primary vaccination with H-series vaccine [110], in the existing mouse experiments [112, 113], revaccination happened after 2 weeks. Using this time mapping (8 weeks human = 2 weeks mouse), the clinical ELISPOT time points were translated to the equivalent time points in the mouse. However, there were additional considerations to be applied that meant time points had to be shifted or removed, i.e:
  - Any time point that fell on a Friday was shifted to a Thursday to accommodate 24 hours needed to generate ELISPOT data (without requiring weekend work). ELISPOT tests are preferentially taken on Monday and Thursday at LSHTM.

- If any time point that fell within a day of another time point, these were removed for reduction in cost and time required to conduct two group culls in two consecutive days.

Table D.3 outlines the experiment design details, tables D.4 and D.5 outline the vaccination and culling times and table D.6 outlines dosing schedule calendar and culling time for each group of mice.

Title	Experiment to match to H series clinical vaccine regimen for modelling project
Test species	Mus musculus Balb/c x C57B1/6 (CB6F1) (F1 hybrid mouse breed)
Vaccine	H56
Number of animals	240 + 24 (10%)
Sex	Female
Administration frequency	Two H56 vaccinations at week 0 and 2.
Administration route	Subcutaneous
Dose concentrations	Doses: 0 (Dose1), 0.1 (Dose2), 0.5 (Dose3), 1 (Dose4), 5 (Dose5), 15 (Dose6) (all) / 100 nmol IC31
Study arms	Arm 1: 0 vaccinations
	Arm 2: 2 vaccinations of Dose 2
	Arm 3: 2 vaccinations of Dose 3
	Arm 4: 2 vaccinations of Dose 4
	Arm 5: 2 vaccinations of Dose 5
	Arm 6: 2 vaccinations of Dose 6
Groups per arm (mice per group)	Arm 1: 8 groups (5 per group)
	Arm 2: 8 groups (5 per group)
	Arm 3: 8 groups (5 per group)
	Arm 4: 8 groups (5 per group)
	Arm 5: 8 groups (5 per group)
	Arm 6: 8 groups (5 per group)
Length of follow-up	8 weeks (56 days)
Primary outcome measure	IFN- $\gamma$ production stimulated by protein vaccine H56 measured in the spleen by ELISPOT lab test
Assay information	ELISPOT cells to be done in duplicate, stimulated with H56, PHA (positive control) and PMA (negative control)

**Table D.3. Outline of mouse experiment design**

Week	Dose	0 H							1						2 H						3						4	5	6	7	8			
Days		1	2	3	4	5	6	7	8	9	10	11	12	13	14	15	16	17	18	19	20	21	22	23	24	25	26	27	28	29				
DOW		M	T	W	T	F	S	S	M	T	W	T	F	S	S	M	T	W	T	F	S	S	M	T	W	T	F	S	S	M	M	M	M	M
Arm 1	0				X				X			X			X			X				X						X					X	
Arm 2	0.1				X				X			X			X			X				X						X					X	
Arm 3	0.5				X				X			X			X			X				X						X					X	
Arm 4	1				X				X			X			X			X				X						X					X	
Arm 5	5				X				X			X			X			X				X						X					X	
Arm 6	15				X				X			X			X			X				X						X					X	

Table D.4. Dose = ug of H56 antigen. (H) = H56 given at this time point. X = group of 5 mice culled for ELISPOT. DOW = day of week

# January 2016

Monday	Tuesday	Wednesday	Thursday	Friday	Saturday	Sunday
				1	2	3
4	5	6	7	8	9	10
<b>First vaccination</b> AZ		30 mice spleen harvest AZ spleens harvest & ELISPOT set-up	ELISPOT SR	ELISPOT SR/SP		
11	12	13	14	15	16	17
30 mice spleen harvest AZ spleens harvest & ELISPOT set-up	ELISPOT SR/LS	30 mice spleen harvest AZ spleens harvest ELISPOT SR	ELISPOT SR	ELISPOT SR/SP		
18	19	20	21	22	23	24
30 mice spleen harvest AZ spleens harvest LS ELISPOT set-up	ELISPOT LS/SR <b>2nd vaccination</b> AZ	30 mice spleen harvest AZ spleens harvest ELISPOT SR	ELISPOT SR	ELISPOT SR/SP		
25	26	27	28	29	30	31

30 mice spleen harvest	ELISPOT	ELISPOT				
FC spleens harvest	LS	SR				
LS ELISPOT set-up						

## February 2016

Monday	Tuesday	Wednesday	Thursday	Friday	Saturday	Sunday
1	2	3	4	5	6	7
30 mice spleen harvest	ELISPOT	ELISPOT				
AZ spleens harvest	SR(?)/LS	SR				
SP cell prep						
LS ELISPOT set-up						
8	9	10	11	12	13	14
15	16	17	18	19	20	21
22	23	24	25	26	27	28
29	1					

30 mice spleen harvest	ELISPOT	ELISPOT				
AZ spleens harvest	SR/LS	SR				
LS ELISPOT set-up						

**Table D.5. Mouse experiment calendar commencing 4/1/16. AZ=Andrea Zelmer, LS= Lisa Stockdale, SP= Satria Arief Parabow, SR= Sophie Rhodes**

b. Costing

Table D.6 outlines an approximation of the costing of the two experiment regimens with regards to buying the mice and upkeep in the lab at LSHTM. Cost of upkeep is £26.50 per mouse per month and cost per mouse to buy is £22 (with a possible discount to £20, but prices below are calculated at £22). This costing assumes 4 weeks per month (not specified to any particular calendar month) and the cull day for each group is included in the stay. An additional 10% of the total mouse count is included to cover mice lost in the experiment due to events external to the experiment. Averages are used in table D.6 as duration of stay differs across mouse groups.

Total Mice	285 (+ 29)	
Timings		
	Weeks	Months
Average time from day 1 to end of trial (calculated per group)	2.86	
Total (average) time at LSHTM	2.86	0.72
Costs		
	GBP	USD
Cost per mouse per month	£26.50	
(Approx) Cost to keep mice for duration	£5,400	
Cost per mouse	£22	
Cost for Mice	£6,270	
10% additional mice to cover any loss during trial (based on 8 weeks stay)	£2,100	
(Approx.) Additional costs for lab equipment/vaccine etc....	£3,500	

(Approx.) Total Cost for Trial	£17,300	\$27,000
--------------------------------	---------	----------

**Table D.6. Average cost of upkeep and cost of buying for entire experiment**

## Appendix E. Additional Discussion

We have carried out some very preliminary, unpublished work to explore whether mathematical methods could be used to predict the 'next best' empirical experiment to most efficiently (i.e. fewer mice and/or financial cost) reduce the uncertainty on the optimal dose. We evaluated a small number of modelling scenarios. Figure E.2A shows the confidence interval (CI) for the dose-response curve for day 56 data (Figure E.1C taken from paper 3, Figure 3) calculated using monte carlo sampling methods. The estimated best dose (green vertical line) and best dose 95% CIs (blue vertical lines) was 1.4  $\mu\text{g}(\log_{10})$  (CI 0.2-3.5  $\mu\text{g}(\log_{10})$ ). The predicted effect of adding new empirical mouse data was simulated by sampling from a simple distribution, parameterized by the spread of empirical data. Figure E.2B & C shows two examples the predicted effect in reducing the uncertainty on the 'best dose', by allocating the mice to two different dosing experiments. Our preliminary results suggest, if we added five new mice to each dose (total 30 mice), the confidence intervals would narrow by 30% to (0.4, 2.7  $\mu\text{g}(\log_{10})$ ) (Figure E.2B). However, if we used the same total number of mice, but added 10 mice each on dose 1, 1.4 and 1.7  $\mu\text{g}(\log_{10})$ , we could achieve a decrease of 36% (0.4, 2.5  $\mu\text{g}(\log_{10})$ ) (Figure E.2C). Our preliminary work has suggested that a) the maximum safe dose may not be the optimal dose for maximising immune response, and that b) novel quantitative methods may have utility for improving the efficiency of experimental design for optimising vaccine dose finding.

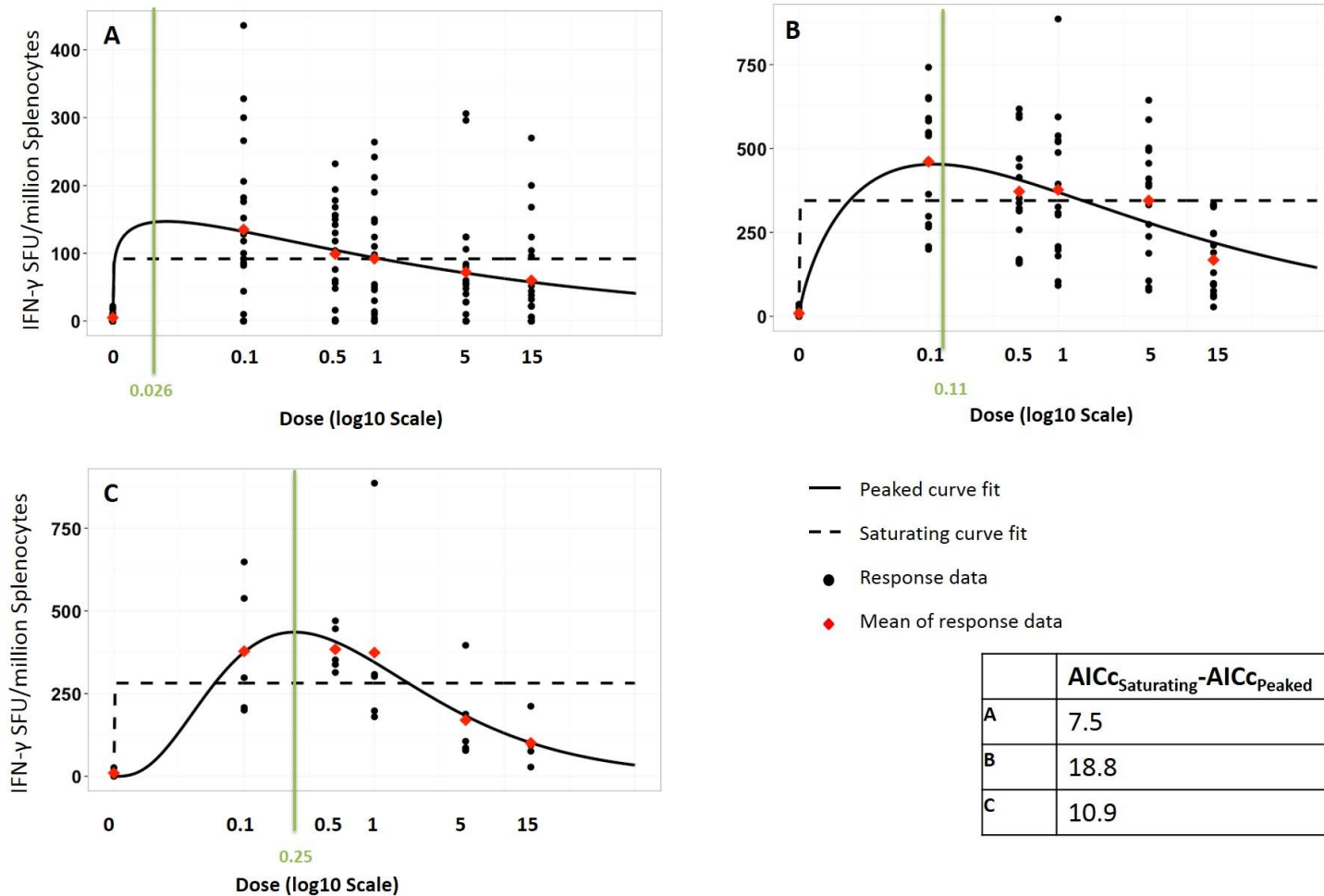


Figure E.1. (Figure taken from paper 3 [114]) Results of the dose-response curve fitting analysis for the time ranges A. between first and second vaccination (aggregated responses from days 2, 7, 9 and 14), B. post-second vaccination (days 21, 28 and 56) and C. Day 56 (last time point). Black points correspond to the number of IFN- $\gamma$  secreting CD4+ T cells from one mouse spleen in response to vaccination for the relevant time range, red diamonds show the mean of the responses, the black solid lines are the peaked (gamma) fit, the black dashed line show the saturating (sigmoidal) curve fit and the vertical green line indicated the best dose as predicted by the peaked

curve fit. The table shows the differences in AICc for A,B and C between the saturating and peaked curve fits. The x-axis is  $\log_{10}(\text{dose: } \mu\text{g H56+IC31}) + 2$  to transform the dose to a log scale and to ensure positivity, but x-axis labels show the non-logged value for clarity (to avoid infinite values, control (dose 0) is not logged).

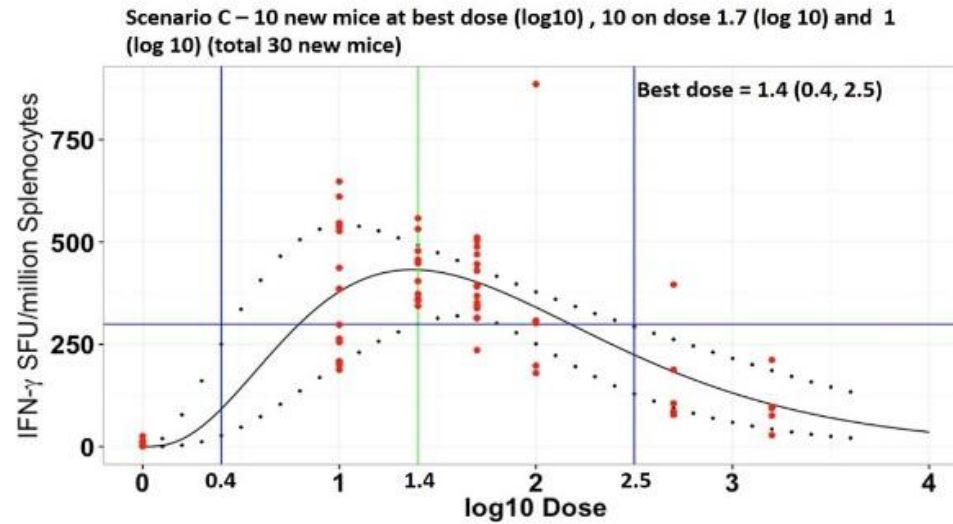
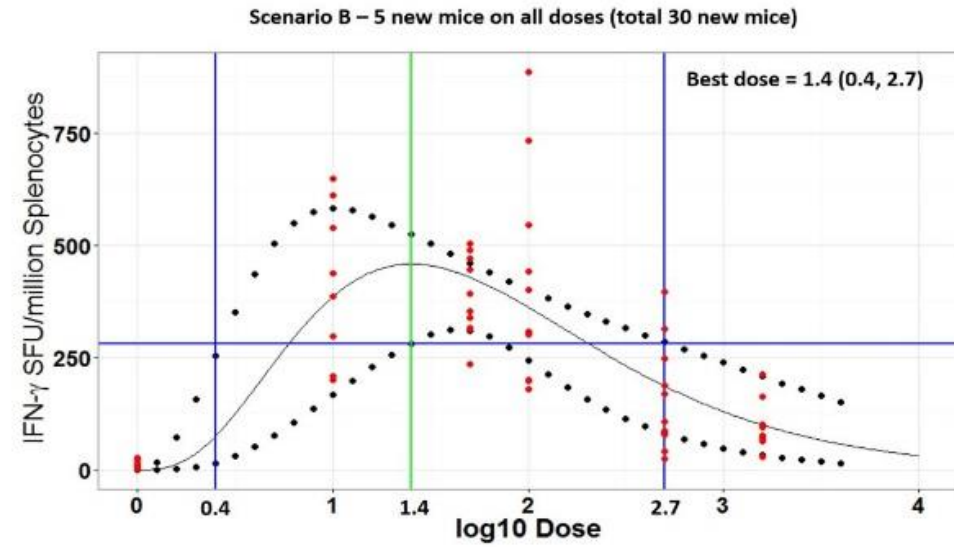
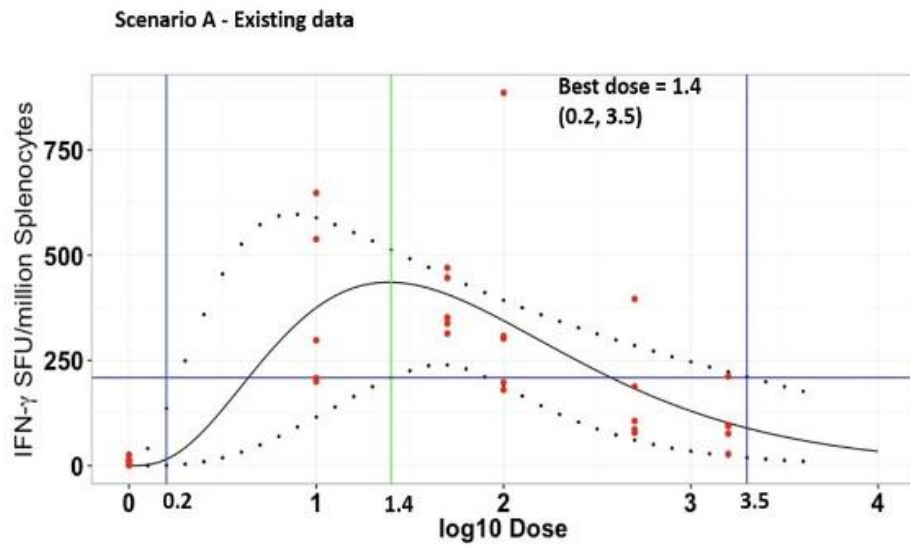


Figure E.2. Modelling to explore the predicted effects of new empirical mouse experiments on reducing uncertainty in 'best dose'. Simulated gamma-interferon secreting CD4+ T cells from the spleens of mice receiving H56+IC31 TB vaccine on the dose response confidence interval (CI) (at day 56 post first vaccination). The dotted line

represents the 95% CI using monte carlo sampling techniques, the green vertical line, the best dose as predicted by the gamma pdf curve fit to the original dose response curve data (at day 56), the blue lines, where the lower CI at best dose intersects the higher CI. Note, the curve (black line) and CI bounds (dotted line) are fit to  $\log_{10}(\text{dose}+2)$ .

## Appendix References

- [1] WHO. Global Tuberculosis Report 2016. World Health Organization; 2016. p. 1-201.
- [2] Fletcher HA, Schrager L. TB vaccine development and the End TB Strategy: importance and current status. *Transactions of the Royal Society of Tropical Medicine and Hygiene*. 2016;110:212-8.
- [3] McShane H, Hill A. Prime-boost immunisation strategies for tuberculosis. *Microbes and infection / Institut Pasteur*. 2005;7:962-7.
- [4] Clem AS. Fundamentals of vaccine immunology. *Journal of global infectious diseases*. 2011;3:73-8.
- [5] McShane H. Developing an improved vaccine against tuberculosis. *Expert review of vaccines*. 2004;3:299-306.
- [6] Abbas A, Lichtman A, Pillai S. *Cellular and Molecular Immunology*. 8 ed: Elsevier Saunders; 2015.
- [7] Plotkin SA, Orenstein WA, Offit PA. *Vaccines*. 6 ed: Saunders; 2013.
- [8] Ottenhoff TH, Kaufmann SH. Vaccines against tuberculosis: where are we and where do we need to go? *PLoS pathogens*. 2012;8:e1002607.
- [9] McShane H. Tuberculosis vaccines: beyond bacille Calmette-Guerin. *Philosophical transactions of the Royal Society of London Series B, Biological sciences*. 2011;366:2782-9.
- [10] Hesselning AC, Marais BJ, Gie RP, Schaaf HS, Fine PE, Godfrey-Faussett P, et al. The risk of disseminated Bacille Calmette-Guerin (BCG) disease in HIV-infected children. *Vaccine*. 2007;25:14-8.
- [11] von Reyn CF, Mtei L, Arbeit RD, Waddell R, Cole B, Mackenzie T, et al. Prevention of tuberculosis in Bacille Calmette-Guerin-primed, HIV-infected adults boosted with an inactivated whole-cell mycobacterial vaccine. *Aids*. 2010;24:675-85.
- [12] Cardona PJ. RUTI: a new chance to shorten the treatment of latent tuberculosis infection. *Tuberculosis*. 2006;86:273-89.
- [13] Fletcher HA. Sleeping Beauty and the Story of the Bacille Calmette-Guerin Vaccine. *mBio*. 2016;7.
- [14] WHO. Module 2: Types of vaccine and adverse reactions. *Vaccine safety basics e-learning course: WHO*; 2013.
- [15] Siegrist CA. *Vaccine Immunology*. Elsevier; 2008. p. 17-36.
- [16] Wiker HG, Harboe M. The antigen 85 complex: a major secretion product of *Mycobacterium tuberculosis*. *Microbiol Rev*. 1992;56:648-61.
- [17] Ronning DR, Vissa V, Besra GS, Belisle JT, Sacchettini JC. *Mycobacterium tuberculosis* antigen 85A and 85C structures confirm binding orientation and conserved substrate specificity. *The Journal of biological chemistry*. 2004;279:36771-7.
- [18] Prendergast KA, Counoupas C, Leotta L, Eto C, Bitter W, Winter N, et al. The Ag85B protein of the BCG vaccine facilitates macrophage uptake but is dispensable for protection against aerosol *Mycobacterium tuberculosis* infection. *Vaccine*. 2016;34:2608-15.
- [19] Goonetilleke NP, McShane H, Hannan CM, Anderson RJ, Brookes RH, Hill AV. Enhanced immunogenicity and protective efficacy against *Mycobacterium tuberculosis* of bacille Calmette-Guerin vaccine using mucosal administration and boosting with a recombinant modified vaccinia virus Ankara. *Journal of immunology*. 2003;171:1602-9.

- [20] Horwitz MA, Harth G, Dillon BJ, Maslesa-Galic S. Recombinant bacillus calmette-guerin (BCG) vaccines expressing the Mycobacterium tuberculosis 30-kDa major secretory protein induce greater protective immunity against tuberculosis than conventional BCG vaccines in a highly susceptible animal model. *Proceedings of the National Academy of Sciences of the United States of America*. 2000;97:13853-8.
- [21] Verreck FA, Vervenne RA, Kondova I, van Kralingen KW, Remarque EJ, Braskamp G, et al. MVA.85A boosting of BCG and an attenuated, *phoP* deficient *M. tuberculosis* vaccine both show protective efficacy against tuberculosis in rhesus macaques. *PloS one*. 2009;4:e5264.
- [22] Sreejit G, Ahmed A, Parveen N, Jha V, Valluri VL, Ghosh S, et al. The ESAT-6 protein of Mycobacterium tuberculosis interacts with beta-2-microglobulin (beta2M) affecting antigen presentation function of macrophage. *PLoS pathogens*. 2014;10:e1004446.
- [23] Ravn P, Demissie A, Eguale T, Wondwosson H, Lein D, Amoudy HA, et al. Human T cell responses to the ESAT-6 antigen from Mycobacterium tuberculosis. *The Journal of infectious diseases*. 1999;179:637-45.
- [24] Ulrichs T, Munk ME, Mollenkopf H, Behr-Perst S, Colangeli R, Gennaro ML, et al. Differential T cell responses to Mycobacterium tuberculosis ESAT6 in tuberculosis patients and healthy donors. *European journal of immunology*. 1998;28:3949-58.
- [25] Brandt L, Elhay M, Rosenkrands I, Lindblad EB, Andersen P. ESAT-6 subunit vaccination against Mycobacterium tuberculosis. *Infection and immunity*. 2000;68:791-5.
- [26] Pym AS, Brodin P, Majlessi L, Brosch R, Demangel C, Williams A, et al. Recombinant BCG exporting ESAT-6 confers enhanced protection against tuberculosis. *Nature medicine*. 2003;9:533-9.
- [27] Cole ST, Lew JM, Jones MJ, Kapopoulou A. TubercuList. In: *Bioinformatics Slo*, editor. 2013.
- [28] Bertholet S, Ireton GC, Ordway DJ, Windish HP, Pine SO, Kahn M, et al. A defined tuberculosis vaccine candidate boosts BCG and protects against multidrug-resistant Mycobacterium tuberculosis. *Sci Transl Med*. 2010;2:53ra74.
- [29] Mahmood A, Srivastava S, Tripathi S, Ansari MA, Owais M, Arora A. Molecular characterization of secretory proteins Rv3619c and Rv3620c from Mycobacterium tuberculosis H37Rv. *FEBS J*. 2011;278:341-53.
- [30] Yihao D, Hongyun H, Maodan T. Latency-associated protein Rv2660c of Mycobacterium tuberculosis augments expression of proinflammatory cytokines in human macrophages by interacting with TLR2. *Infect Dis (Lond)*. 2015;47:168-77.
- [31] Sherman DR, Voskuil M, Schnappinger D, Liao R, Harrell MI, Schoolnik GK. Regulation of the Mycobacterium tuberculosis hypoxic response gene encoding alpha -crystallin. *Proceedings of the National Academy of Sciences of the United States of America*. 2001;98:7534-9.
- [32] Govender L, Abel B, Hughes EJ, Scriba TJ, Kagina BM, de Kock M, et al. Higher human CD4+T cell response to novel Mycobacterium tuberculosis latency associated antigens Rv2660 and Rv2659 in latent infection compared with tuberculosis disease. *Vaccine*. 2010;29:51-7.
- [33] He H, Yang H, Deng Y. Mycobacterium tuberculosis dormancy-associated antigen of Rv2660c induces stronger immune response in latent Mycobacterium tuberculosis infection

- than that in active tuberculosis in a Chinese population. *Eur J Clin Microbiol Infect Dis*. 2015;34:1103-9.
- [34] Bertholet S, Ireton GC, Kahn M, Guderian J, Mohamath R, Stride N, et al. Identification of human T cell antigens for the development of vaccines against *Mycobacterium tuberculosis*. *Journal of immunology*. 2008;181:7948-57.
- [35] Kato-Maeda M, Rhee JT, Gingeras TR, Salamon H, Drenkow J, Smittipat N, et al. Comparing genomes within the species *Mycobacterium tuberculosis*. *Genome Res*. 2001;11:547-54.
- [36] Skjot RL, Brock I, Arend SM, Munk ME, Theisen M, Ottenhoff TH, et al. Epitope mapping of the immunodominant antigen TB10.4 and the two homologous proteins TB10.3 and TB12.9, which constitute a subfamily of the *esat-6* gene family. *Infection and immunity*. 2002;70:5446-53.
- [37] Skjot RL, Oettinger T, Rosenkrands I, Ravn P, Brock I, Jacobsen S, et al. Comparative evaluation of low-molecular-mass proteins from *Mycobacterium tuberculosis* identifies members of the ESAT-6 family as immunodominant T-cell antigens. *Infection and immunity*. 2000;68:214-20.
- [38] Hervas-Stubbs S, Majlessi L, Simsova M, Morova J, Rojas MJ, Nouze C, et al. High frequency of CD4+ T cells specific for the TB10.4 protein correlates with protection against *Mycobacterium tuberculosis* infection. *Infection and immunity*. 2006;74:3396-407.
- [39] Cole ST. Comparative and functional genomics of the *Mycobacterium tuberculosis* complex. *Microbiology*. 2002;148:2919-28.
- [40] Chaitra MG, Nayak R, Shaila MS. Modulation of immune responses in mice to recombinant antigens from PE and PPE families of proteins of *Mycobacterium tuberculosis* by the Ribi adjuvant. *Vaccine*. 2007;25:7168-76.
- [41] Begum D, Umemura M, Yahagi A, Okamoto Y, Hamada S, Oshiro K, et al. Accelerated induction of mycobacterial antigen-specific CD8+ T cells in the *Mycobacterium tuberculosis*-infected lung by subcutaneous vaccination with *Mycobacterium bovis* bacille Calmette-Guerin. *Immunology*. 2009;128:556-63.
- [42] Ahn SS, Jeon BY, Kim KS, Kwack JY, Lee EG, Park KS, et al. Mtb32 is a promising tuberculosis antigen for DNA vaccination in pre- and post-exposure mouse models. *Gene therapy*. 2012;19:570-5.
- [43] Mazandu GK, Mulder NJ. Function prediction and analysis of mycobacterium tuberculosis hypothetical proteins. *Int J Mol Sci*. 2012;13:7283-302.
- [44] Dillon DC, Alderson MR, Day CH, Lewinsohn DM, Coler R, Bement T, et al. Molecular characterization and human T-cell responses to a member of a novel *Mycobacterium tuberculosis* *mtb39* gene family. *Infection and immunity*. 1999;67:2941-50.
- [45] Lingnau K, Riedl K, von Gabain A. IC31 and IC30, novel types of vaccine adjuvant based on peptide delivery systems. *Expert review of vaccines*. 2007;6:741-6.
- [46] Schellack C, Prinz K, Egyed A, Fritz JH, Wittmann B, Ginzler M, et al. IC31, a novel adjuvant signaling via TLR9, induces potent cellular and humoral immune responses. *Vaccine*. 2006;24:5461-72.
- [47] van Dissel JT, Joosten SA, Hoff ST, Soonawala D, Prins C, Hokey DA, et al. A novel liposomal adjuvant system, CAF01, promotes long-lived *Mycobacterium tuberculosis*-specific T-cell responses in human. *Vaccine*. 2014;32:7098-107.

- [48] Holten-Andersen L, Doherty TM, Korsholm KS, Andersen P. Combination of the cationic surfactant dimethyl dioctadecyl ammonium bromide and synthetic mycobacterial cord factor as an efficient adjuvant for tuberculosis subunit vaccines. *Infection and immunity*. 2004;72:1608-17.
- [49] Dubois Cauwelaert N, Desbien AL, Hudson TE, Pine SO, Reed SG, Coler RN, et al. The TLR4 Agonist Vaccine Adjuvant, GLA-SE, Requires Canonical and Atypical Mechanisms of Action for TH1 Induction. *PloS one*. 2016;11:e0146372.
- [50] Coler RN, Bertholet S, Moutaftsi M, Guderian JA, Windish HP, Baldwin SL, et al. Development and characterization of synthetic glucopyranosyl lipid adjuvant system as a vaccine adjuvant. *PloS one*. 2011;6:e16333.
- [51] Chlibek R, Bayas JM, Collins H, de la Pinta ML, Ledent E, Mols JF, et al. Safety and immunogenicity of an AS01-adjuvanted varicella-zoster virus subunit candidate vaccine against herpes zoster in adults  $\geq 50$  years of age. *The Journal of infectious diseases*. 2013;208:1953-61.
- [52] Leroux-Roels I, Forgas S, De Boever F, Clement F, Demoitie MA, Mettens P, et al. Improved CD4(+) T cell responses to Mycobacterium tuberculosis in PPD-negative adults by M72/AS01 as compared to the M72/AS02 and Mtb72F/AS02 tuberculosis candidate vaccine formulations: a randomized trial. *Vaccine*. 2013;31:2196-206.
- [53] Smaill F, Jeyanathan M, Smieja M, Medina MF, Thantrige-Don N, Zganiacz A, et al. A human type 5 adenovirus-based tuberculosis vaccine induces robust T cell responses in humans despite preexisting anti-adenovirus immunity. *Sci Transl Med*. 2013;5:205ra134.
- [54] Tameris MD, Hatherill M, Landry BS, Scriba TJ, Snowden MA, Lockhart S, et al. Safety and efficacy of MVA85A, a new tuberculosis vaccine, in infants previously vaccinated with BCG: a randomised, placebo-controlled phase 2b trial. *Lancet*. 2013;381:1021-8.
- [55] Ndiaye BP, Thienemann F, Ota M, Landry BS, Camara M, Dieye S, et al. Safety, immunogenicity, and efficacy of the candidate tuberculosis vaccine MVA85A in healthy adults infected with HIV-1: a randomised, placebo-controlled, phase 2 trial. *The lancet Respiratory medicine*. 2015;3:190-200.
- [56] Satti I, Meyer J, Harris SA, Manjaly Thomas ZR, Griffiths K, Antrobus RD, et al. Safety and immunogenicity of a candidate tuberculosis vaccine MVA85A delivered by aerosol in BCG-vaccinated healthy adults: a phase 1, double-blind, randomised controlled trial. *The Lancet infectious diseases*. 2014;14:939-46.
- [57] BNF. Theophylline. National Institute of Health and Care Excellence.
- [58] Upton RN, Mould DR. Basic concepts in population modeling, simulation, and model-based drug development: part 3-introduction to pharmacodynamic modeling methods. *CPT: pharmacometrics & systems pharmacology*. 2014;3:e88.
- [59] Mould DR, Upton RN. Basic concepts in population modeling, simulation, and model-based drug development-part 2: introduction to pharmacokinetic modeling methods. *CPT: pharmacometrics & systems pharmacology*. 2013;2:e38.
- [60] Mould DR, Upton RN. Basic concepts in population modeling, simulation, and model-based drug development. *CPT: pharmacometrics & systems pharmacology*. 2012;1:e6.
- [61] Abba K, Sudarsanam TD, Grobler L, Volmink J. Nutritional supplements for people being treated for active tuberculosis. *The Cochrane database of systematic reviews*. 2008:CD006086.

- [62] Lavielle M. Mixed Effects Models for the Population Approach: Models, Tasks, Methods and Tools: Chapman & Hall; 2015.
- [63] Gastonguay M. MI-210: Essentials of Population PKPD Modeling and Simulation - Course Notes. Metrum Institute.
- [64] Monolix: Users Guide. 4.3.3 ed2014.
- [65] Chan PL, Jacqmin P, Lavielle M, McFadyen L, Weatherley B. The use of the SAEM algorithm in MONOLIX software for estimation of population pharmacokinetic-pharmacodynamic-viral dynamics parameters of maraviroc in asymptomatic HIV subjects. *Journal of pharmacokinetics and pharmacodynamics*. 2011;38:41-61.
- [66] Delattre M, Lavielle M. Maximum likelihood estimation in discrete mixed hidden Markov models using the SAEM algorithm. *Computational Statistics & Data Analysis*. 2012;56:2073-85.
- [67] Delyon B, Lavielle M, Moulines E. Convergence of a stochastic approximation version of the EM algorithm. *Annals of Statistics*. 1999;27:94-128.
- [68] Allasonniere S, Kuhn E, Troune A. Construction of Bayesian deformable models via a stochastic approximation algorithm: a convergence study. *Bernoulli*. 2010;16:641-78.
- [69] Kuhn E, Lavielle M. Coupling a stochastic approximation version of the EM with an MCMC procedure. *ESAIM: Probability and Statistics*. 2004:115-31.
- [70] Limpert E, Stahel W, Abbt M. Log-normal Distributions across the Sciences: Keys and Clues. *BioScience*. 2001;51:341-52.
- [71] Raftery A. Bayesian Model Selection in Social Research. *Sociological Methodology*. 1995;25:111-63.
- [72] Burnham KP, Anderson DR. Multimodel Inference: Understanding AIC and BIC in Model Selection. *Sociological Methods and Research*. 2004;33:261-304.
- [73] Davidian M. Non-linear mixed-effects models. In: Fitzmaurice M, Davidian M, Verbeke G, Molenberghs G, editors. *Longitudinal Data Analysis: Chapman & Hall/CRC Press*; 2009. p. 107-41.
- [74] Holford N. The visual predictive check - superiority to standard diagnostic (Rorschach) plots. Population Approach Group Europe. Pamplona, Spain2005.
- [75] Beal S, Sheiner LB, Boeckmann A, Bauer RJ. NONMEM User's Guides. Ellicott City, MD, USA: Icon Development Solutions; 2009.
- [76] Wang Y. Derivation of various NONMEM estimation methods. *Journal of pharmacokinetics and pharmacodynamics*. 2007;34:575-93.
- [77] Lunn DJ, Thomas A, Best N, Spiegelhalter D. WinBUGS -- a Bayesian modelling framework: concepts, structure, and extensibility. *Statistics and Computing*. 2000;10:325--37.
- [78] Certara. Phoenix WinNonlin. In: Certara, editor.2016.
- [79] D'Argenio DZ, Schumitzky A, Wang X. Adapt 5 User's Guide: Pharmacokinetic/Pharmacodynamic Systems Analysis Software. Los Angeles: Biomedical Simulations Resource; 2009.
- [80] Antia R, Koella JC, Perrot V. Models of the within-host dynamics of persistent mycobacterial infections. *Proceedings Biological sciences / The Royal Society*. 1996;263:257-63.
- [81] Kirschner D. Dynamics of co-infection with M. Tuberculosis and HIV-1. *Theor Popul Biol*. 1999;55:94-109.

- [82] Wigginton JE, Kirschner D. A model to predict cell-mediated immune regulatory mechanisms during human infection with *Mycobacterium tuberculosis*. *Journal of immunology*. 2001;166:1951-67.
- [83] Gammack D, Doering CR, Kirschner DE. Macrophage response to *Mycobacterium tuberculosis* infection. *Journal of mathematical biology*. 2004;48:218-42.
- [84] Marino S, Kirschner DE. The human immune response to *Mycobacterium tuberculosis* in lung and lymph node. *Journal of theoretical biology*. 2004;227:463-86.
- [85] Marino S, Pawar S, Fuller CL, Reinhart TA, Flynn JL, Kirschner DE. Dendritic cell trafficking and antigen presentation in the human immune response to *Mycobacterium tuberculosis*. *Journal of immunology*. 2004;173:494-506.
- [86] Segovia-Juarez JL, Ganguli S, Kirschner D. Identifying control mechanisms of granuloma formation during *M. tuberculosis* infection using an agent-based model. *Journal of theoretical biology*. 2004;231:357-76.
- [87] Sud D, Bigbee C, Flynn JL, Kirschner DE. Contribution of CD8+ T cells to control of *Mycobacterium tuberculosis* infection. *Journal of immunology*. 2006;176:4296-314.
- [88] Alavez-Ramirez J, Castellanos JR, Esteva L, Flores JA, Fuentes-Allen JL, Garcia-Ramos G, et al. Within-host population dynamics of antibiotic-resistant *M. tuberculosis*. *Mathematical medicine and biology : a journal of the IMA*. 2007;24:35-56.
- [89] Marino S, Sud D, Plessner H, Lin PL, Chan J, Flynn JL, et al. Differences in reactivation of tuberculosis induced from anti-TNF treatments are based on bioavailability in granulomatous tissue. *PLoS computational biology*. 2007;3:1909-24.
- [90] Ray JC, Wang J, Chan J, Kirschner DE. The timing of TNF and IFN- $\gamma$  signaling affects macrophage activation strategies during *Mycobacterium tuberculosis* infection. *Journal of theoretical biology*. 2008;252:24-38.
- [91] Marino S, Myers A, Flynn JL, Kirschner DE. TNF and IL-10 are major factors in modulation of the phagocytic cell environment in lung and lymph node in tuberculosis: a next-generation two-compartmental model. *Journal of theoretical biology*. 2010;265:586-98.
- [92] Clarelli F, Natalini R. A pressure model of immune response to *mycobacterium tuberculosis* infection in several space dimensions. *Mathematical biosciences and engineering : MBE*. 2010;7:277-300.
- [93] Ahlers JD, Belyakov IM. New paradigms for generating effective CD8+ T cell responses against HIV-1/AIDS. *Discovery medicine*. 2010;9:528-37.
- [94] Bru A, Cardona PJ. Mathematical modeling of tuberculosis bacillary counts and cellular populations in the organs of infected mice. *PloS one*. 2010;5:e12985.
- [95] Ibarguen-Mondragon E, Esteva L, Chavez-Galan L. A mathematical model for cellular immunology of tuberculosis. *Mathematical biosciences and engineering : MBE*. 2011;8:973-86.
- [96] Fallahi-Sichani M, Kirschner DE, Linderman JJ. NF-kappaB Signaling Dynamics Play a Key Role in Infection Control in Tuberculosis. *Frontiers in physiology*. 2012;3:170.
- [97] Magombedze G, Mulder N. A mathematical representation of the development of *Mycobacterium tuberculosis* active, latent and dormant stages. *Journal of theoretical biology*. 2012;292:44-59.
- [98] Lyons MA, Reisfeld B, Yang RS, Lenaerts AJ. A physiologically based pharmacokinetic model of rifampin in mice. *Antimicrobial agents and chemotherapy*. 2013;57:1763-71.

- [99] Zheng N, Whalen CC, Handel A. Modeling the potential impact of host population survival on the evolution of *M. tuberculosis* latency. *PloS one*. 2014;9:e105721.
- [100] Pedruzzi G, Rao KV, Chatterjee S. Mathematical model of mycobacterium-host interaction describes physiology of persistence. *Journal of theoretical biology*. 2015;376:105-17.
- [101] Lyons MA, Lenaerts AJ. Computational pharmacokinetics/pharmacodynamics of rifampin in a mouse tuberculosis infection model. *Journal of pharmacokinetics and pharmacodynamics*. 2015;42:375-89.
- [102] Datta M, Via LE, Chen W, Baish JW, Xu L, Barry CE, 3rd, et al. Mathematical Model of Oxygen Transport in Tuberculosis Granulomas. *Ann Biomed Eng*. 2016;44:863-72.
- [103] Hao W, Schlesinger LS, Friedman A. Modeling Granulomas in Response to Infection in the Lung. *PloS one*. 2016;11:e0148738.
- [104] Lalande L, Bourguignon L, Maire P, Goutelle S. Mathematical modeling and systems pharmacology of tuberculosis: Isoniazid as a case study. *Journal of theoretical biology*. 2016;399:43-52.
- [105] Zhou X, Yap P, Tanner M, Bergquist R, Utzinger J, Zhou XN. Surveillance and response systems for elimination of tropical diseases: summary of a thematic series in *Infectious Diseases of Poverty*. *Infect Dis Poverty*. 2016;5:49.
- [106] Chisholm RH, Tanaka MM. The emergence of latent infection in the early evolution of *Mycobacterium tuberculosis*. *Proceedings Biological sciences / The Royal Society*. 2016;283.
- [107] Wallis RS. Mathematical Models of Tuberculosis Reactivation and Relapse. *Frontiers in microbiology*. 2016;7:669.
- [108] McDaniel MM, Krishna N, Handagama WG, Eda S, Ganusov VV. Quantifying Limits on Replication, Death, and Quiescence of *Mycobacterium tuberculosis* in Mice. *Frontiers in microbiology*. 2016;7:862.
- [109] Rhodes SJ, Sarfas C, Knight GM, White A, Pathan AA, McShane H, et al. Predicting IFN- $\gamma$  responses after BCG vaccination in humans from macaques: A proof-of-concept study of Immunostimulation/Immunodynamic modelling methods. *Clinical and vaccine immunology : CVI*. 2017.
- [110] Luabeya AK, Kagina BM, Tameris MD, Geldenhuys H, Hoff ST, Shi Z, et al. First-in-human trial of the post-exposure tuberculosis vaccine H56:IC31 in *Mycobacterium tuberculosis* infected and non-infected healthy adults. *Vaccine*. 2015;33:4130-40.
- [111] van Dissel JT, Soonawala D, Joosten SA, Prins C, Arend SM, Bang P, et al. Ag85B-ESAT-6 adjuvanted with IC31(R) promotes strong and long-lived *Mycobacterium tuberculosis* specific T cell responses in volunteers with previous BCG vaccination or tuberculosis infection. *Vaccine*. 2011;29:2100-9.
- [112] Aagaard C, Hoang TT, Izzo A, Billeskov R, Troudt J, Arnett K, et al. Protection and polyfunctional T cells induced by Ag85B-TB10.4/IC31 against *Mycobacterium tuberculosis* is highly dependent on the antigen dose. *PloS one*. 2009;4:e5930.
- [113] Hoang T, Aagaard C, Dietrich J, Cassidy JP, Dolganov G, Schoolnik GK, et al. ESAT-6 (EsxA) and TB10.4 (EsxH) based vaccines for pre- and post-exposure tuberculosis vaccination. *PloS one*. 2013;8:e80579.
- [114] Rhodes SJ, Zelmer A, Knight GM, Prabowo SA, Stockdale L, Evans TG, et al. The TB vaccine H56+IC31 dose-response curve is peaked not saturating: Data generation for new

mathematical modelling methods to inform vaccine dose decisions. *Vaccine*. 2016;34:6285-91.